What do we learn from considering petrological processes in subduction modeling ?

Current challenges ?

Taras Gerya
undefined

Weronika Gorczyk
geologist

Manuele Faccenda
geologist

Ksenia Nikolaeva
petrologist

Yuri Mishin
chemist

Guizhi Zhu
geophysicist

Elena Sizova
petrologist

Geophysical Fluid Dynamics, D-ERDW, ETH– Zurich

http://www.GFD.ethz.ch

First 2D numerical geodynamic model

 (1970)

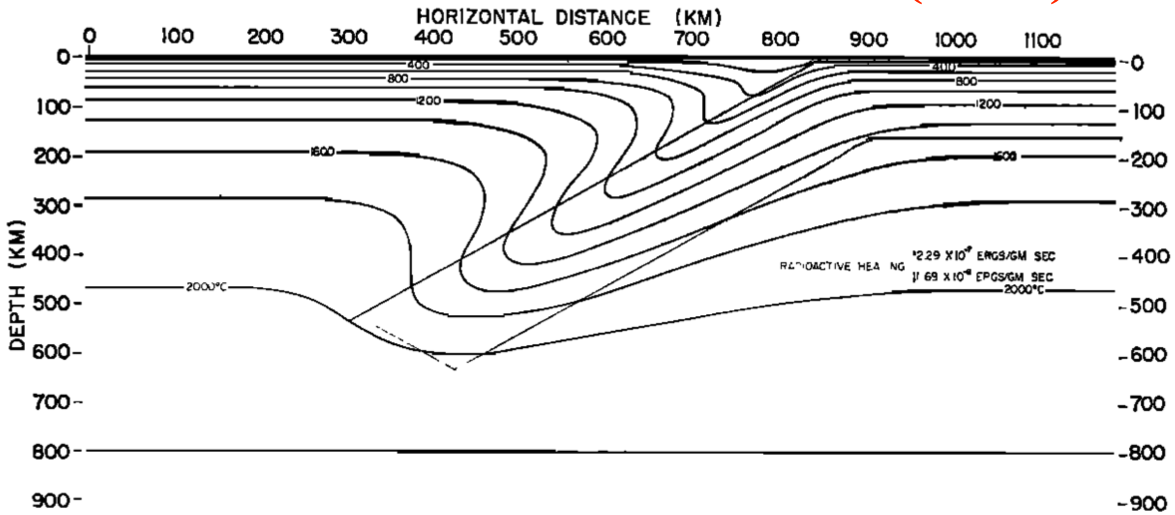

Fig. 5. Temperature regime for a spreading velocity of 1 cm/yr with conductive heat transfer only.

Introduction

The sea-floor spreading and the new global tectonic hypotheses imply the downwarping and descent of the lithosphere under island-arc regions [*Isacks et al.*, 1968]. Downwarping of the crust and upper-mantle layer into the mantle has thermal and mechanical implications and would affect observable surface-heat flux and gravity as well as seismic velocities and travel times. The question is just how sensitive are these observed variables to variations in the parameters that define the regime of a sinking crustal block. If these variables are sensitive to parameter variations, then they may be used to evaluate certain aspects of the sea-floor spreading and new global tectonic hypotheses.

Petrological processes in a subduction zone

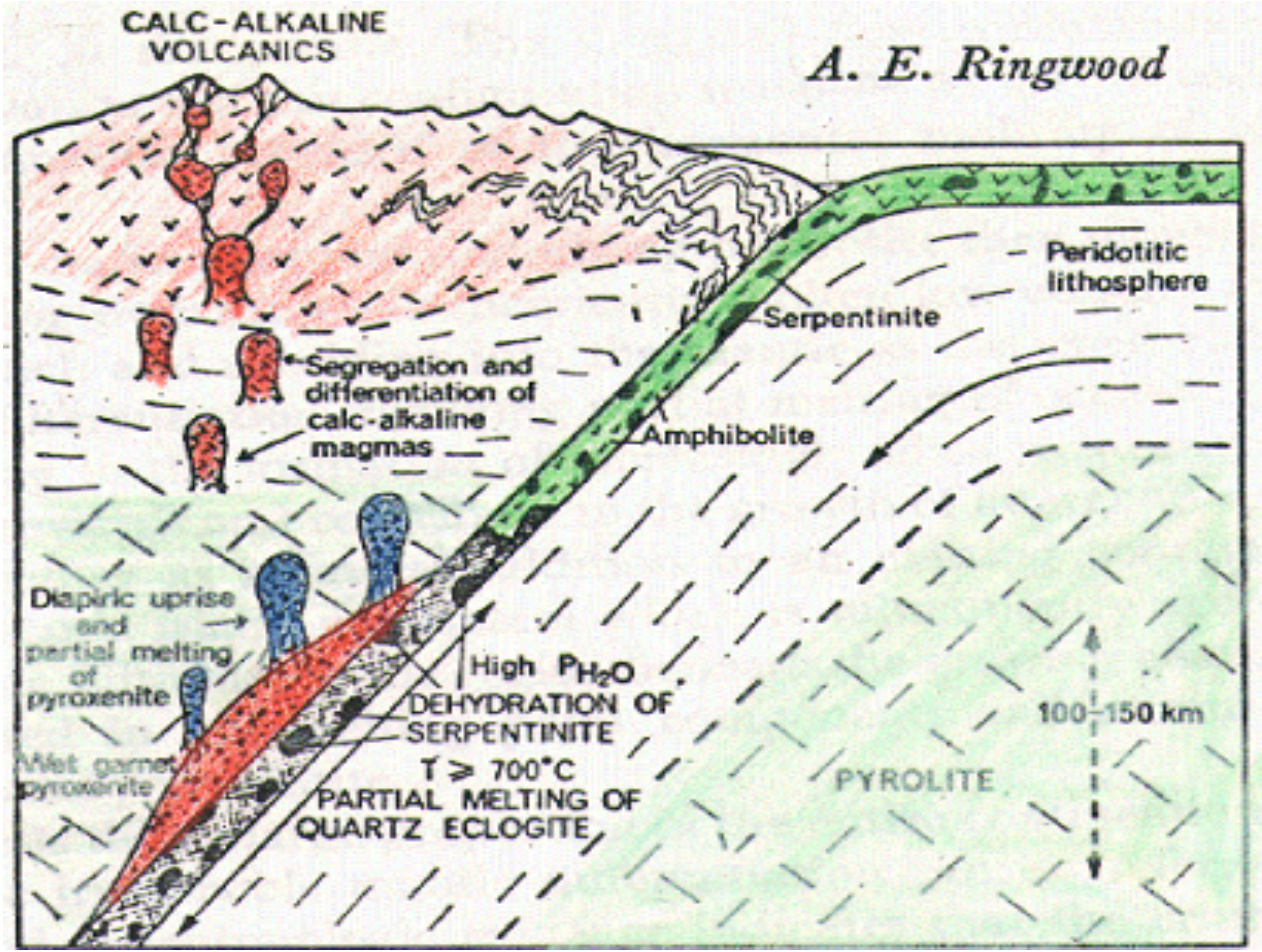

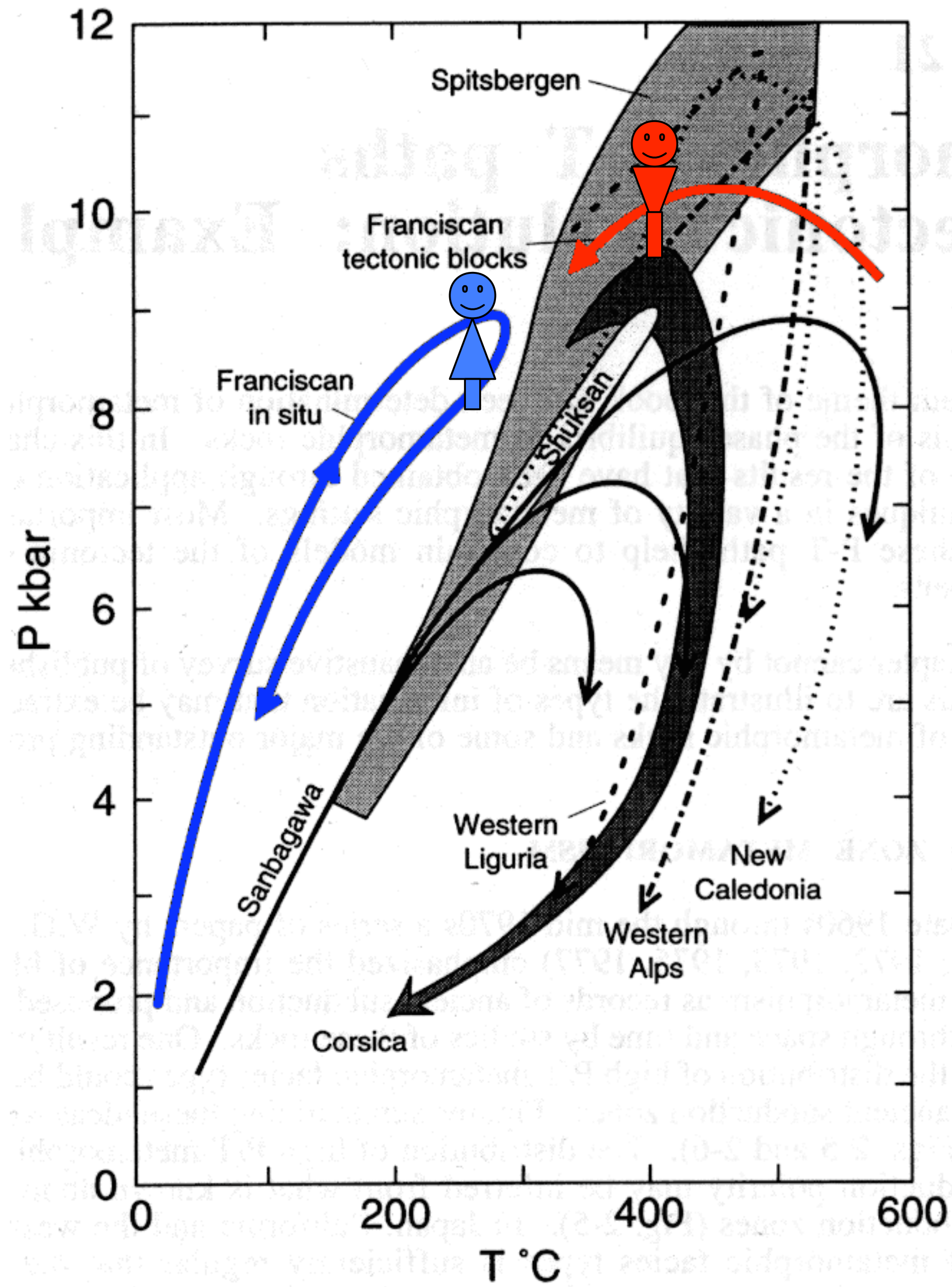

P-T paths from subduction complexes
(Ernst, 1988)

What causes contrasting P-T paths of HP rocks in the same subduction complex ?

Contrasting P-T paths:
result of continuous subduction?

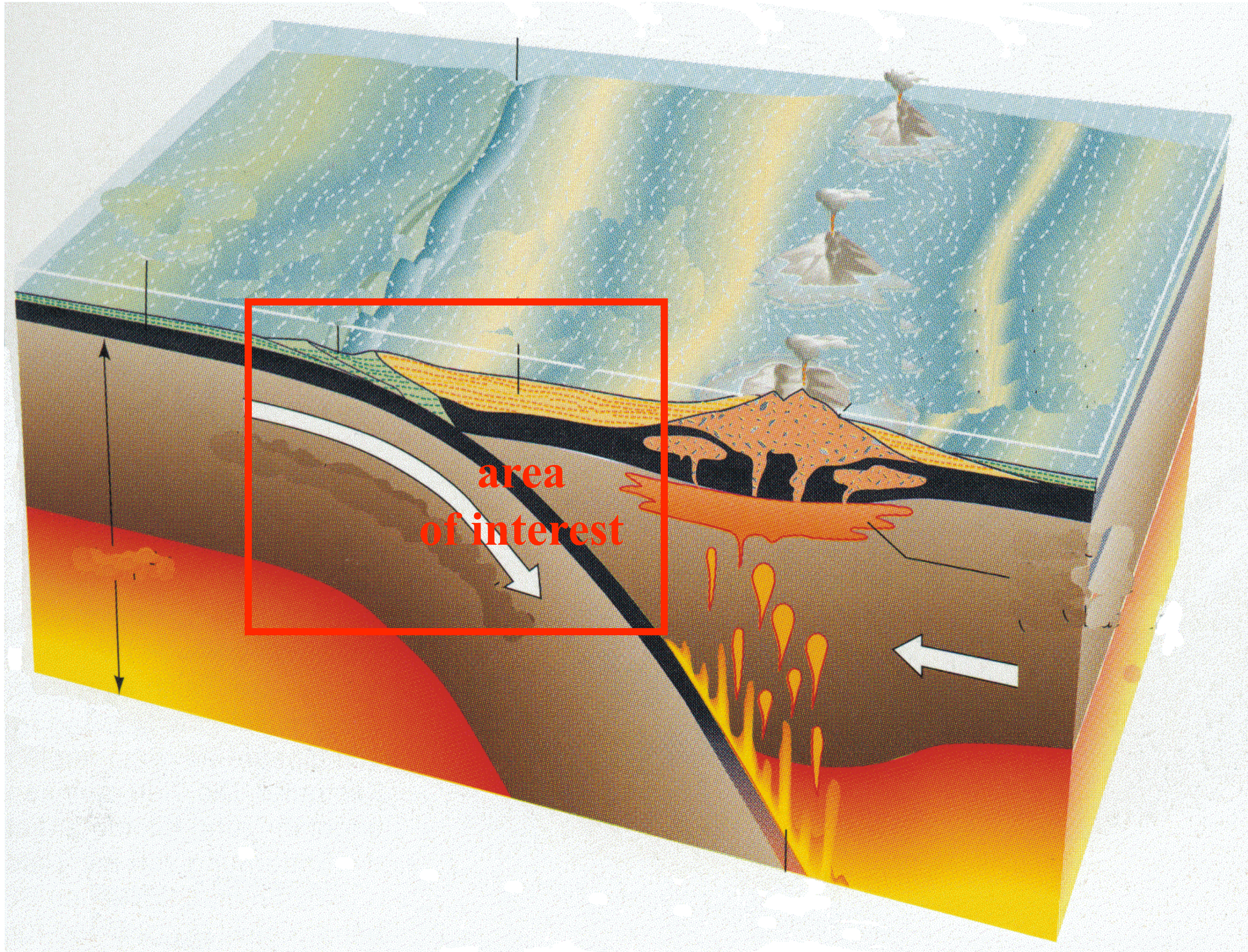

Subduction under an oceanic arc

Hydration of mantle wedge

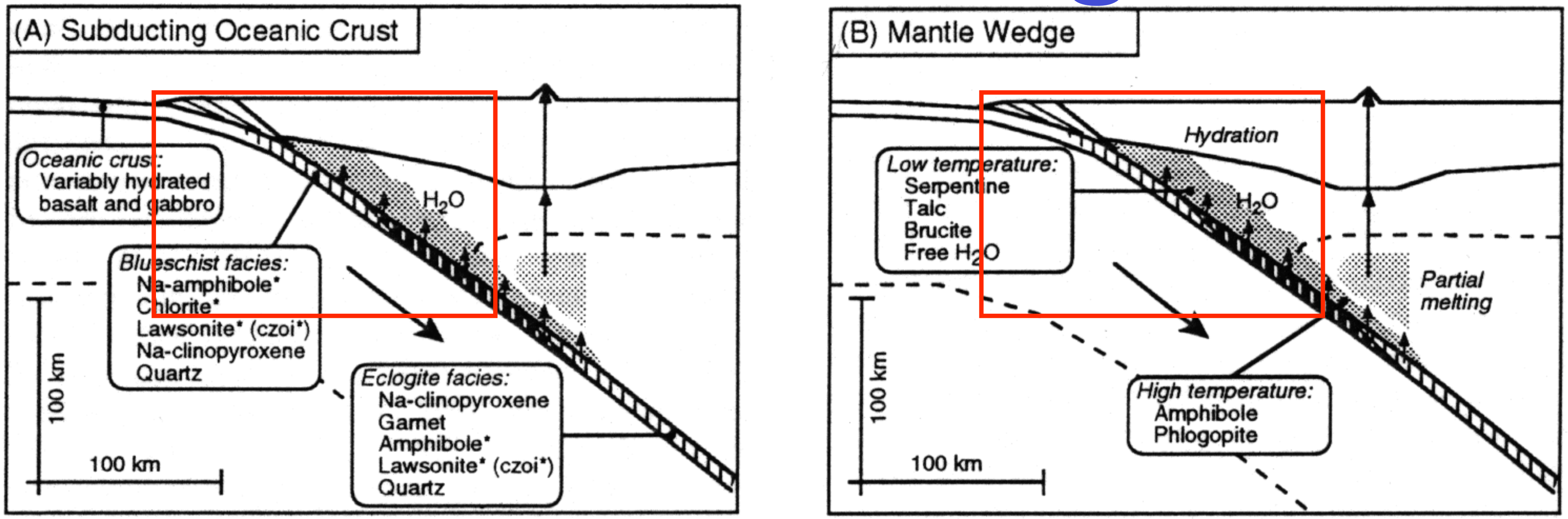

Peacock (1996)

Petrologic model of a mature subduction zone.

(A) Mineralogic changes in subducting oceanic crust. Large amounts of H_2O are released by continuous dehydration reactions that occur in subducting oceanic crust during blueschist → eclogite facies metamorphism. Proposed mineralogy of the subducting slab is shown in boxes; hydrous minerals are marked by asterisks. (B) Mineralogic changes in mantle wedge. Integrated over time, H_2O released from the subducting oceanic crust causes extensive hydration of the mantle wedge at shallow depths and adjacent to the subducting slab. Possible hydrous minerals stable at different depths are shown in boxes. Water-rich fluids that infiltrate the core of the convecting mantle wedge may trigger partial melting.

Petrological/rheological model

M.W. Schmidt, S. Poli / Earth and Planetary Science Letters 163 (1998) 361–379 369

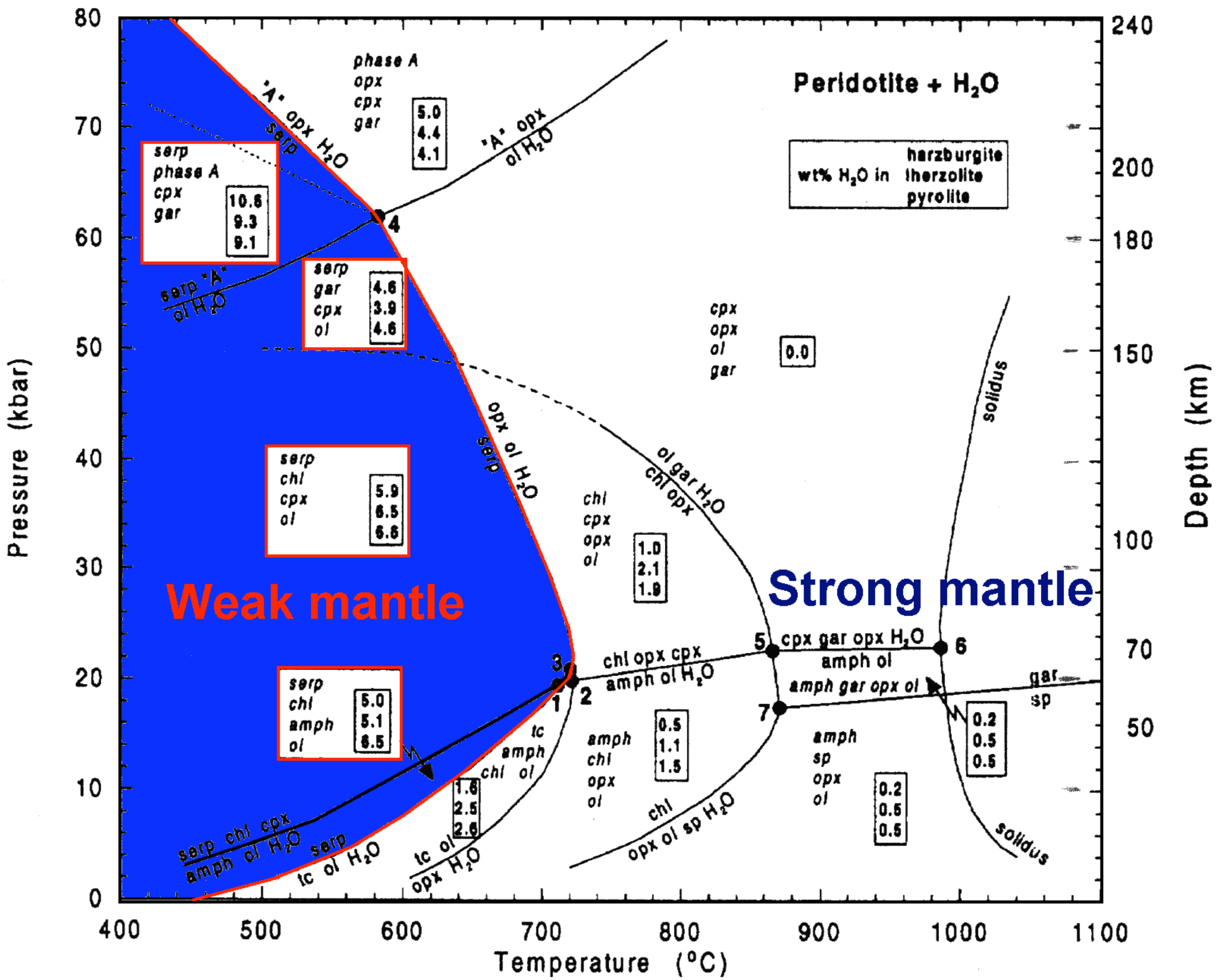

Fig. 5. Phase diagram for H_2O-saturated average mantle peridotite and maximum H_2O contents bound in hydrous phases in average peridotites. Upper value: harzburgite; middle value: lherzolite; lower value: pyrolite. The *italic* labels are assemblages in a given stability field. 'A' = phase A, *amph* = amphibole, *chl* = chlorite, *cpx* = clinopyroxene, *gar* = garnet, *ol* = olivine, *opx* = orthopyroxene, *serp* = serpentine, *sp* = spinel, *tc* = talc.

Conceptual model

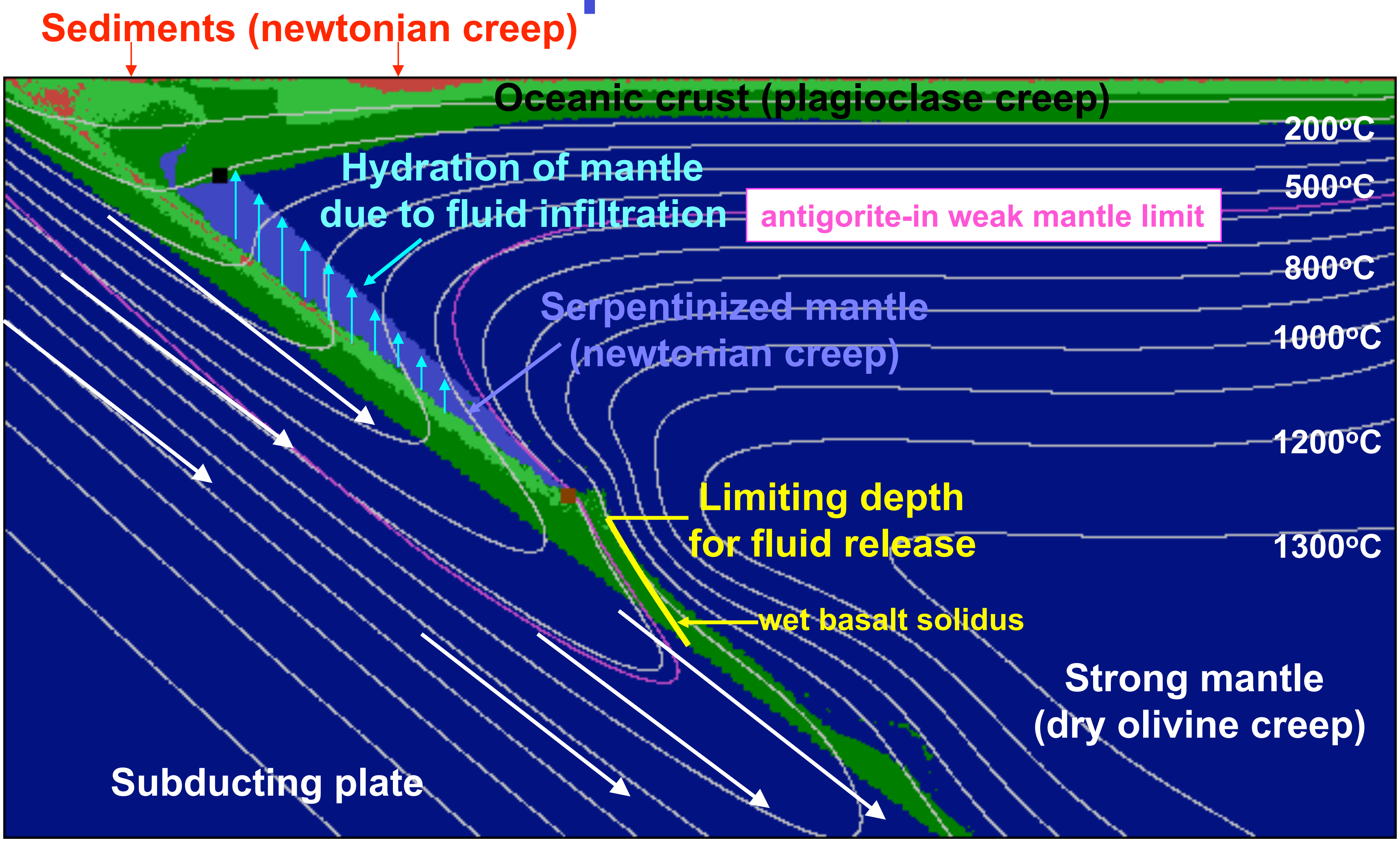

Animation
“Oceanic subduction”

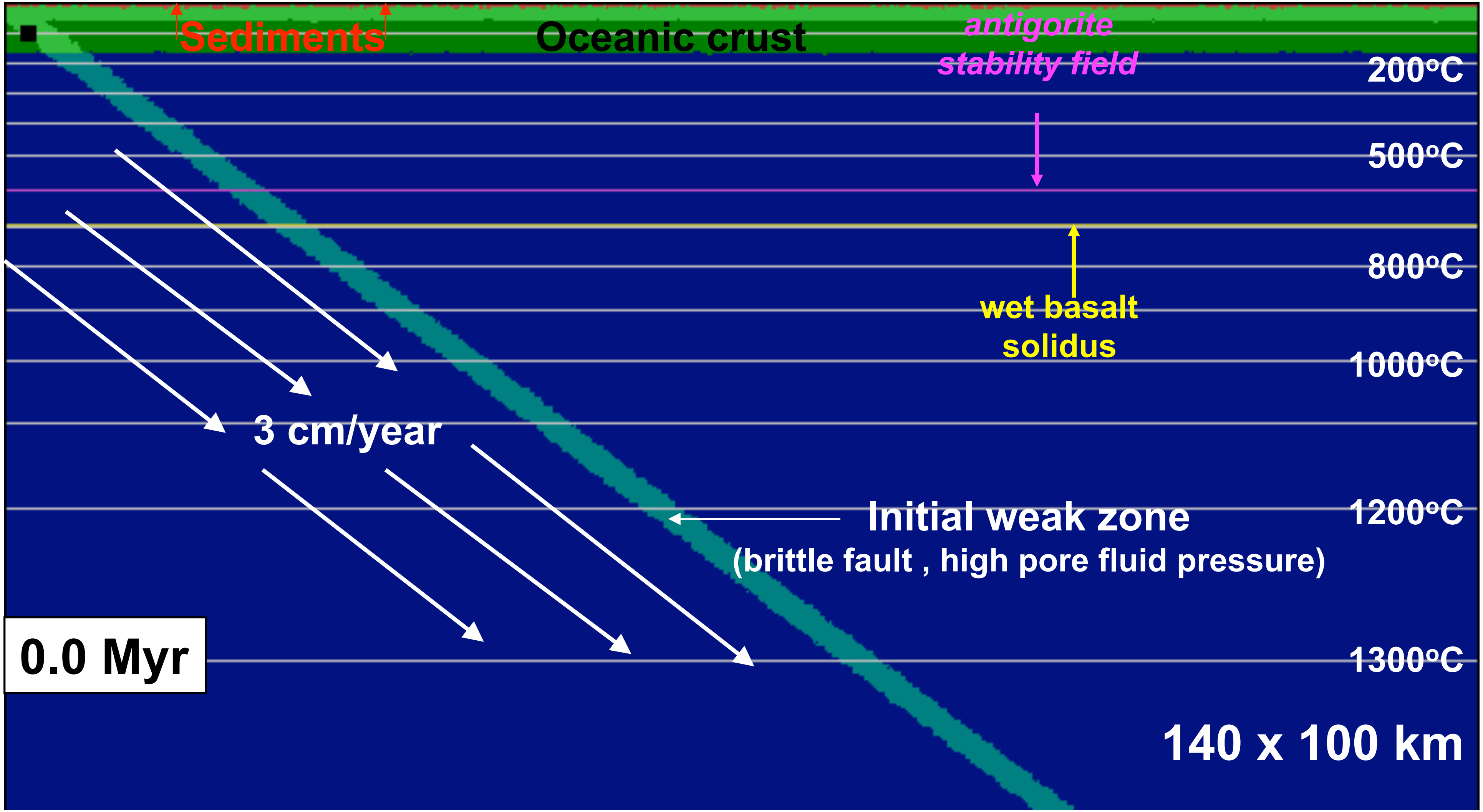

Litosphere: 40 Myr old

Subduction: rate 3 cm/year, angle 45°

Hydration of hanging wall:
max rate 2 mm/year, max depth 90 km

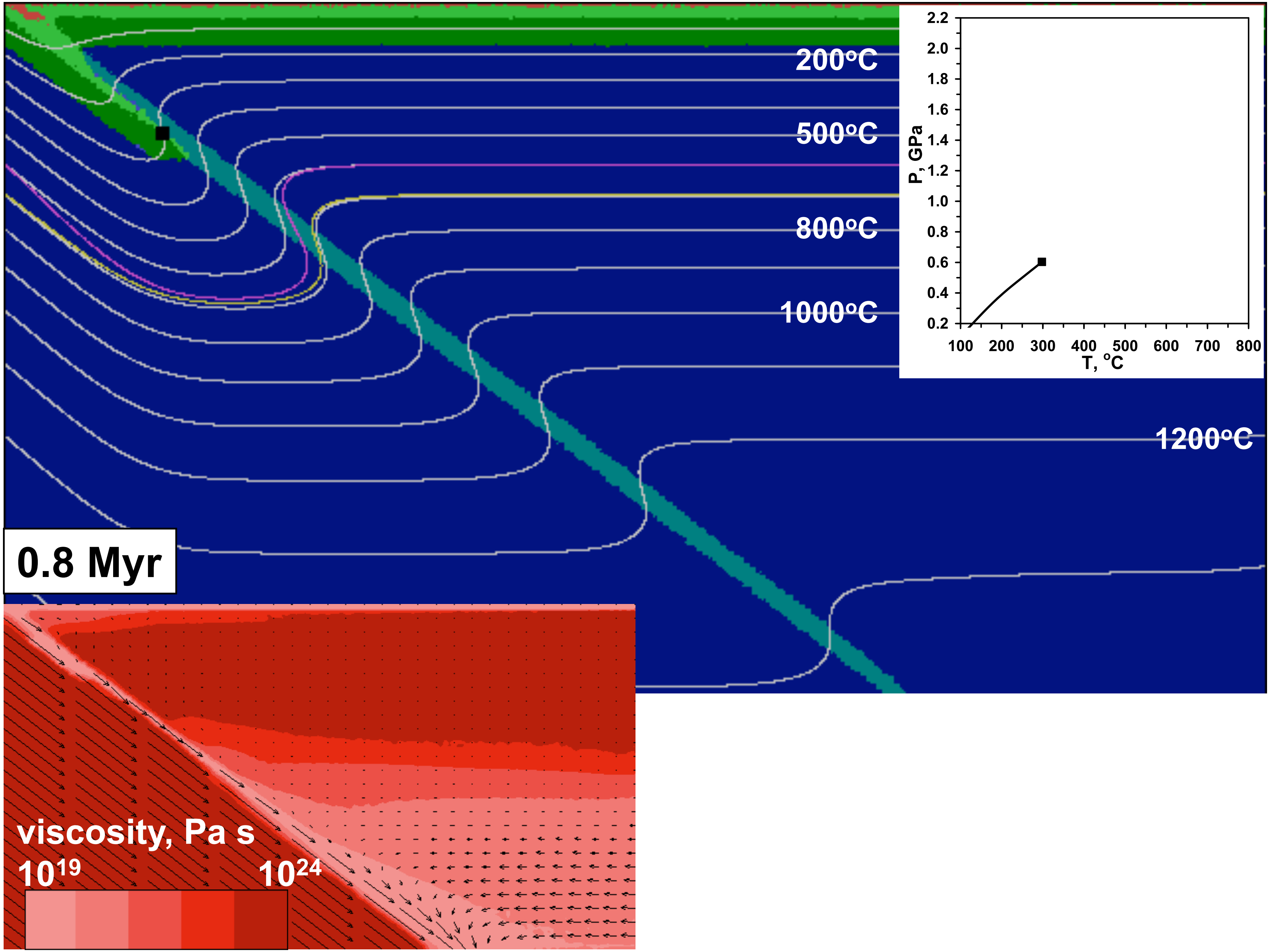

200°C
500°C
800°C
1000°C
1200°C
0.8 Myr
P, GPa
T, °C
2.2
2.0
1.8
1.6
1.4
1.2
1.0
0.8
0.6
0.4
0.2
100
200
300
400
500
600
700
800
viscosity, Pa s
10^{19}
10^{24}

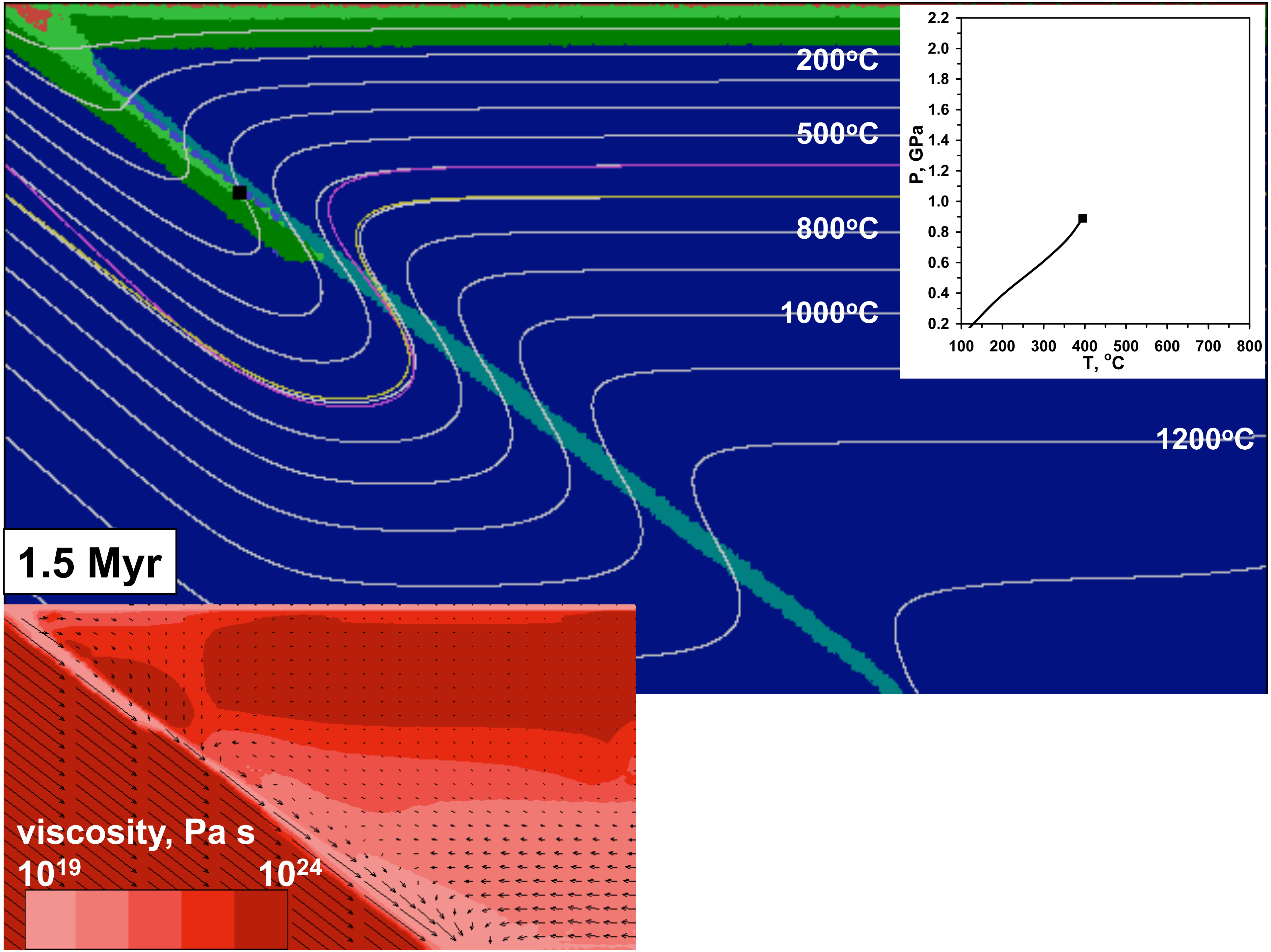

200°C
500°C
800°C
1000°C
1200°C
P, GPa
2.2
2.0
1.8
1.6
1.4
1.2
1.0
0.8
0.6
0.4
0.2
100
200
300
400
500
600
700
800
T, °C
1.5 Myr
viscosity, Pa s
10^19
10^24

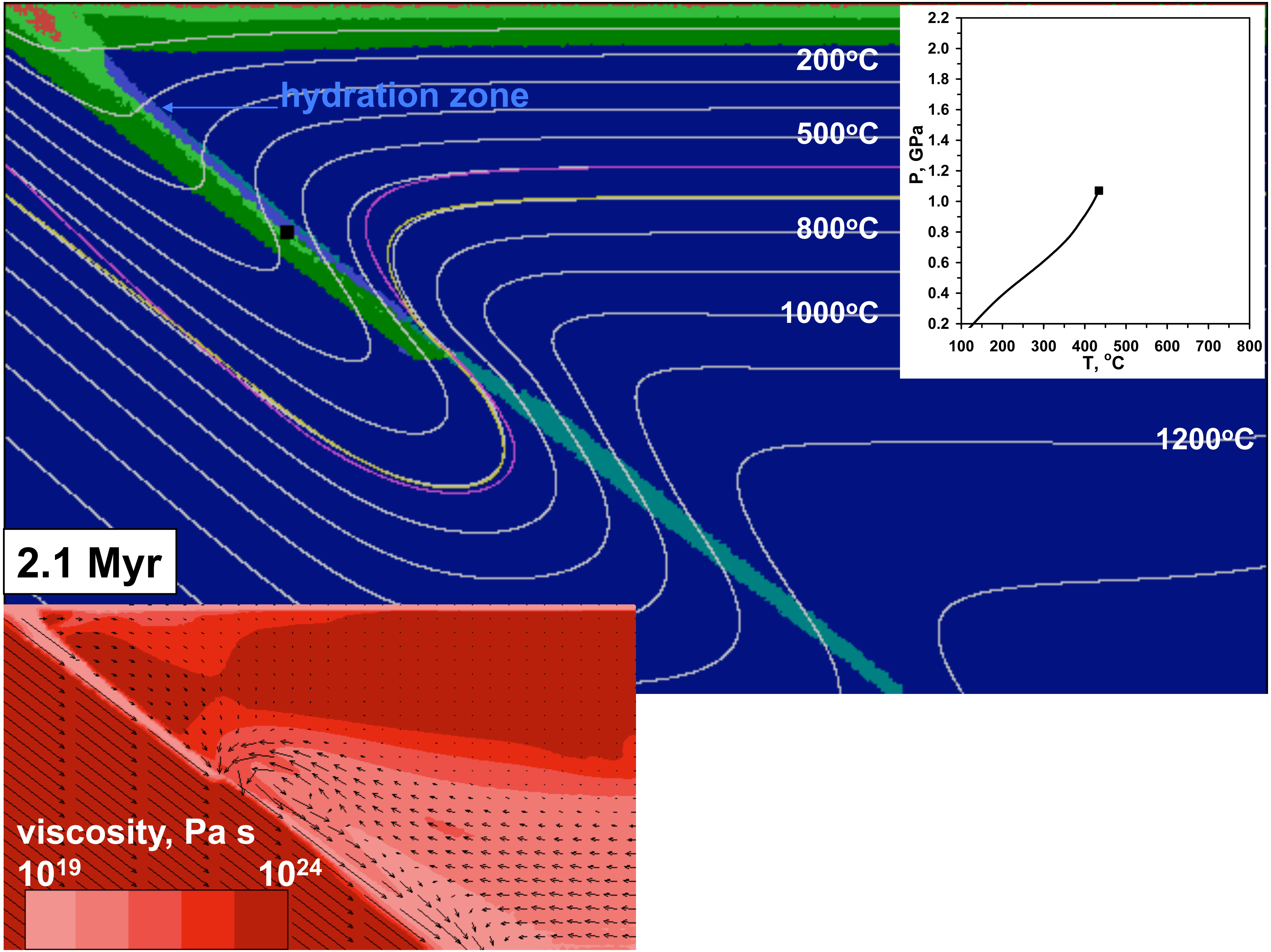

200°C
hydration zone
500°C
800°C
1000°C
1200°C
2.1 Myr
P, GPa
T, °C
viscosity, Pa s
10^19
10^24

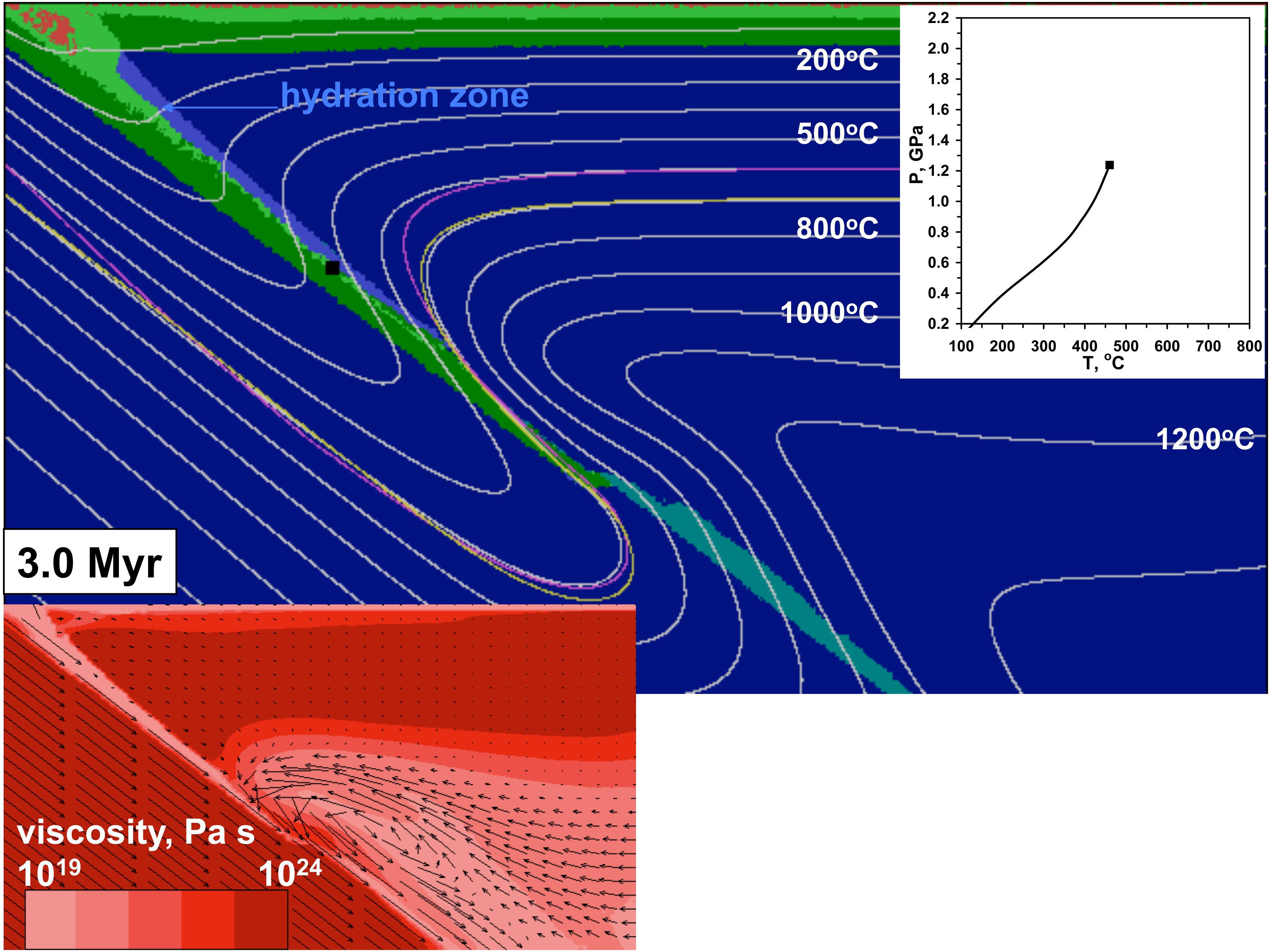

hydration zone
200°C
500°C
800°C
1000°C
1200°C
3.0 Myr
P, GPa
T, °C
2.2
2.0
1.8
1.6
1.4
1.2
1.0
0.8
0.6
0.4
0.2
100
200
300
400
500
600
700
800
viscosity, Pa s
10^{19}
10^{24}

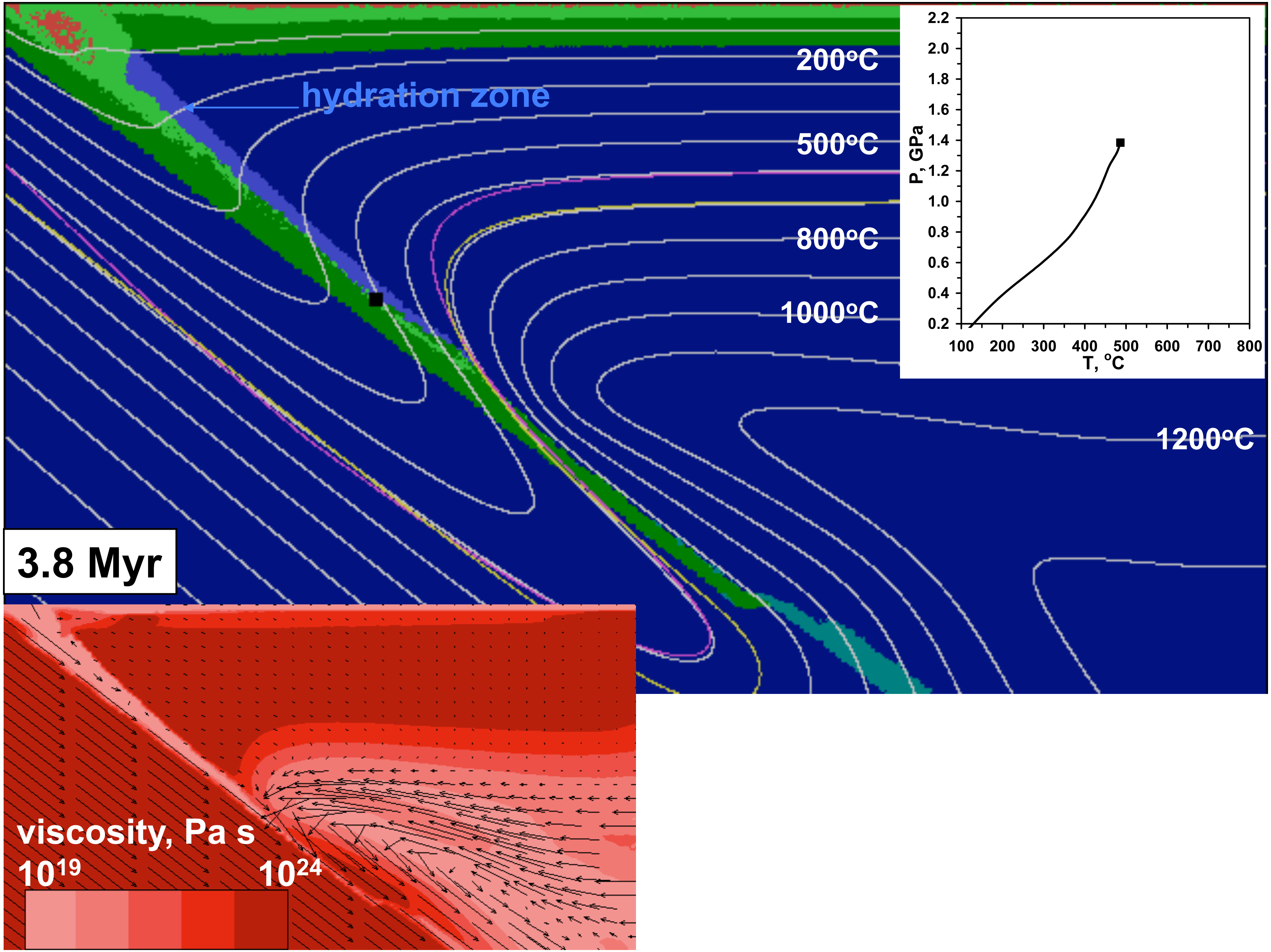
200°C
hydration zone
500°C
800°C
1000°C
1200°C
3.8 Myr
2.2
2.0
1.8
1.6
1.4
1.2
1.0
0.8
0.6
0.4
0.2
P, GPa
100
200
300
400
500
600
700
800
T, °C
viscosity, Pa s
10^{19}
10^{24}

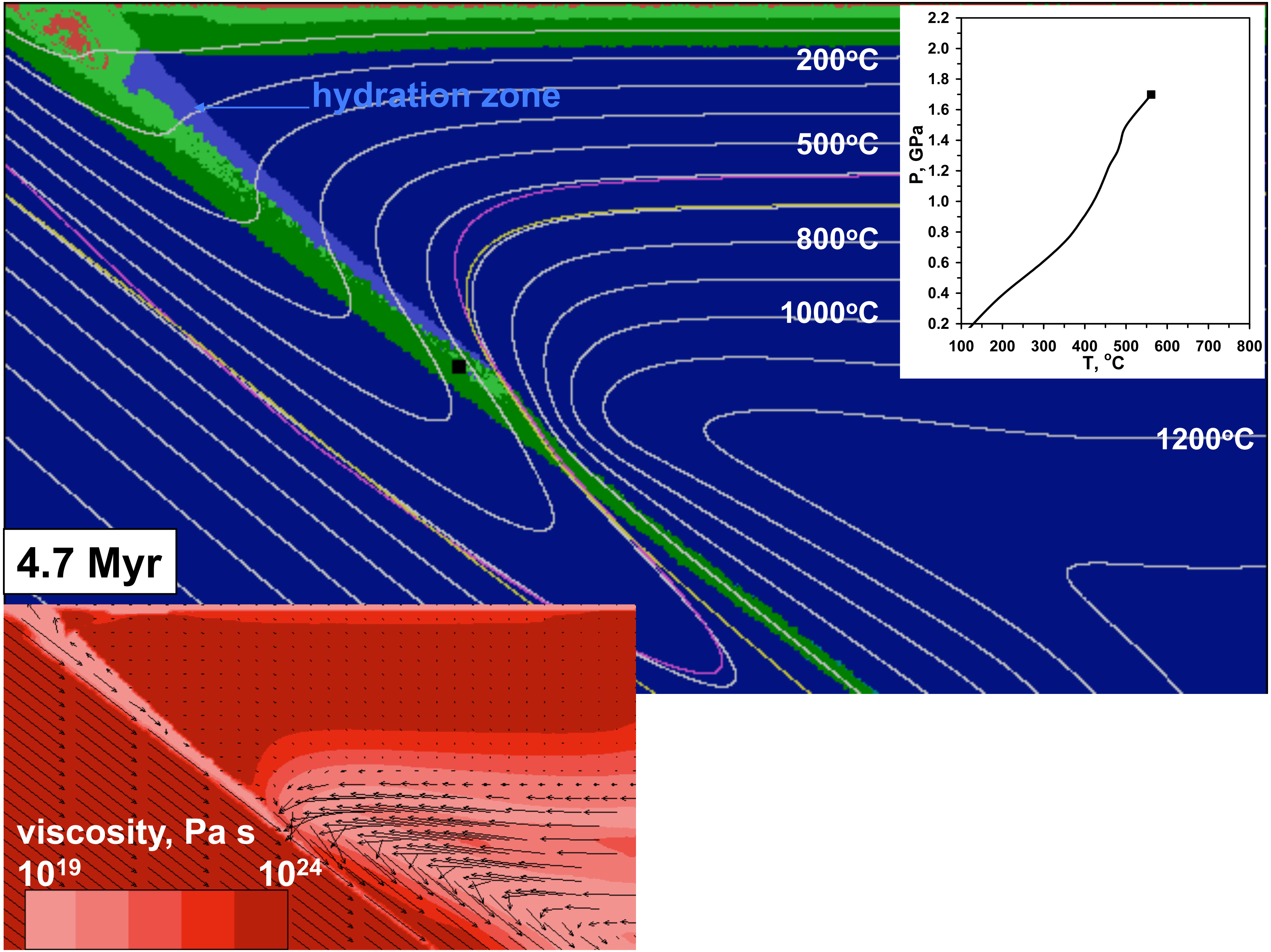

200°C
500°C
800°C
1000°C
1200°C
hydration zone
4.7 Myr
P, GPa
T, °C
2.2
2.0
1.8
1.6
1.4
1.2
1.0
0.8
0.6
0.4
0.2
100 200 300 400 500 600 700 800
viscosity, Pa s
10^{19}
10^{24}

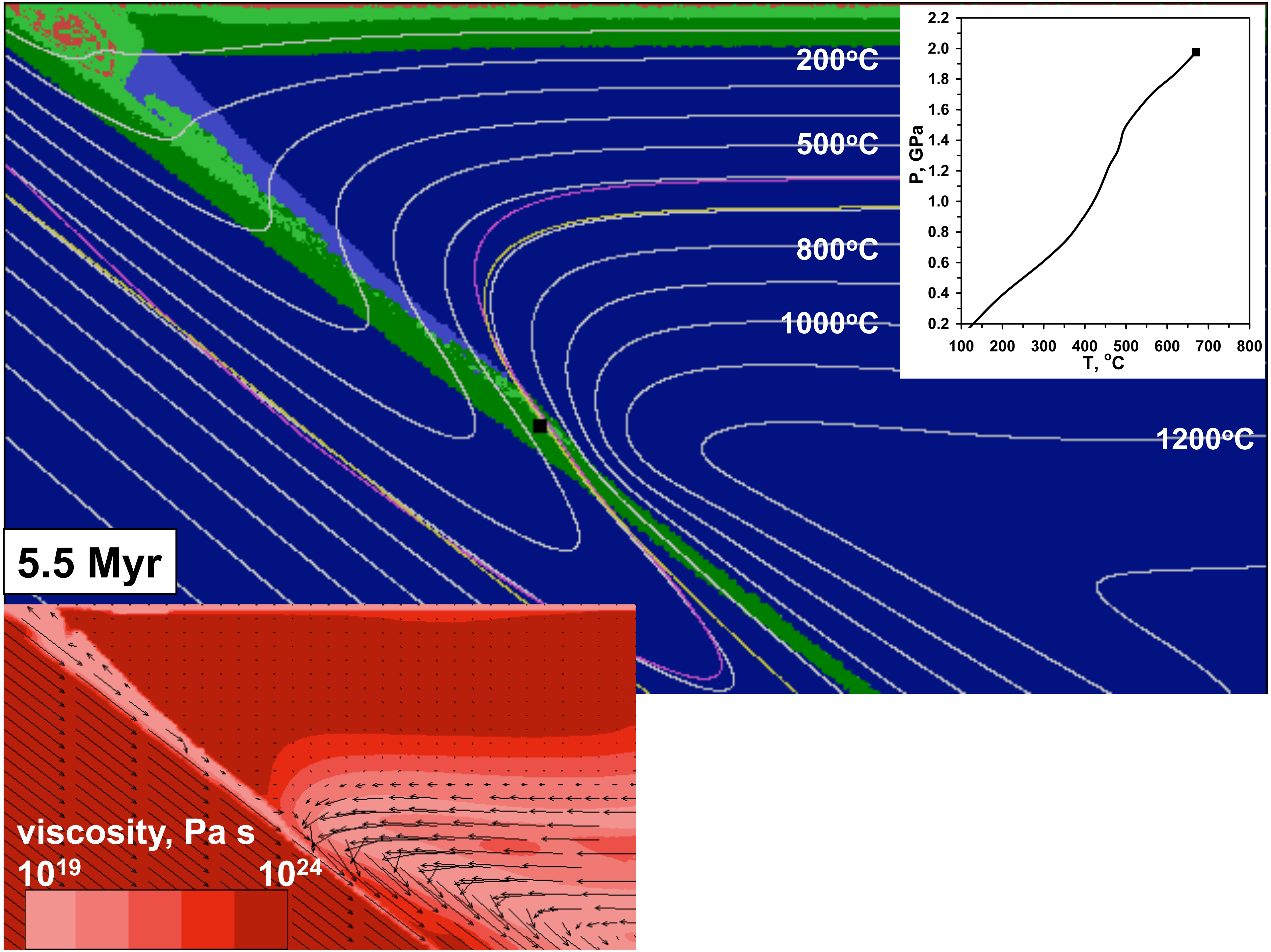
200°C
500°C
800°C
1000°C
1200°C
5.5 Myr
P, GPa
2.2
2.0
1.8
1.6
1.4
1.2
1.0
0.8
0.6
0.4
0.2
100
200
300
400
500
600
700
800
T, °C
viscosity, Pa s
10^19
10^24

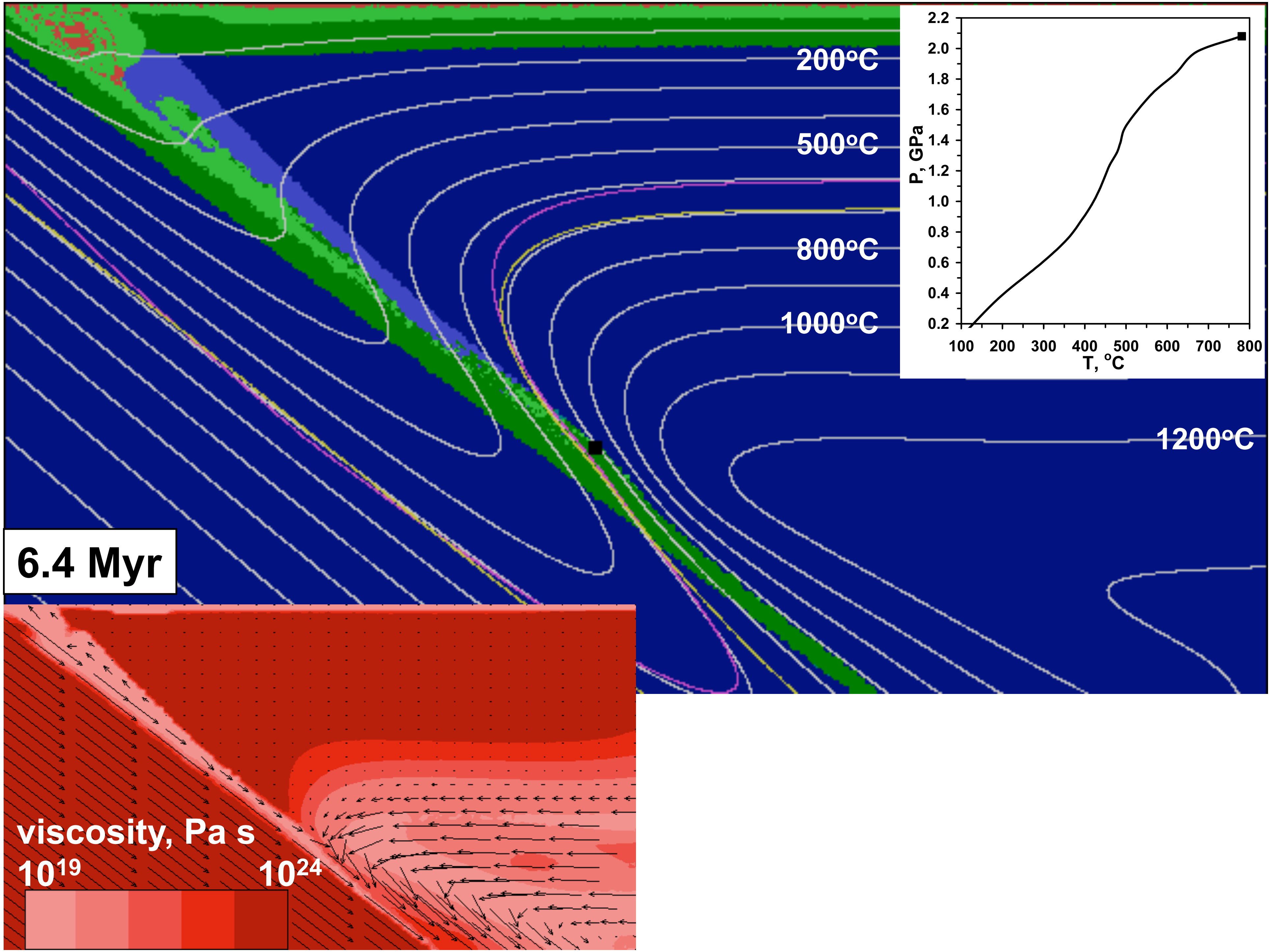

200°C
500°C
800°C
1000°C
1200°C
P, GPa
2.2
2.0
1.8
1.6
1.4
1.2
1.0
0.8
0.6
0.4
0.2
100 200 300 400 500 600 700 800
T, °C
6.4 Myr
viscosity, Pa s
10^19
10^24

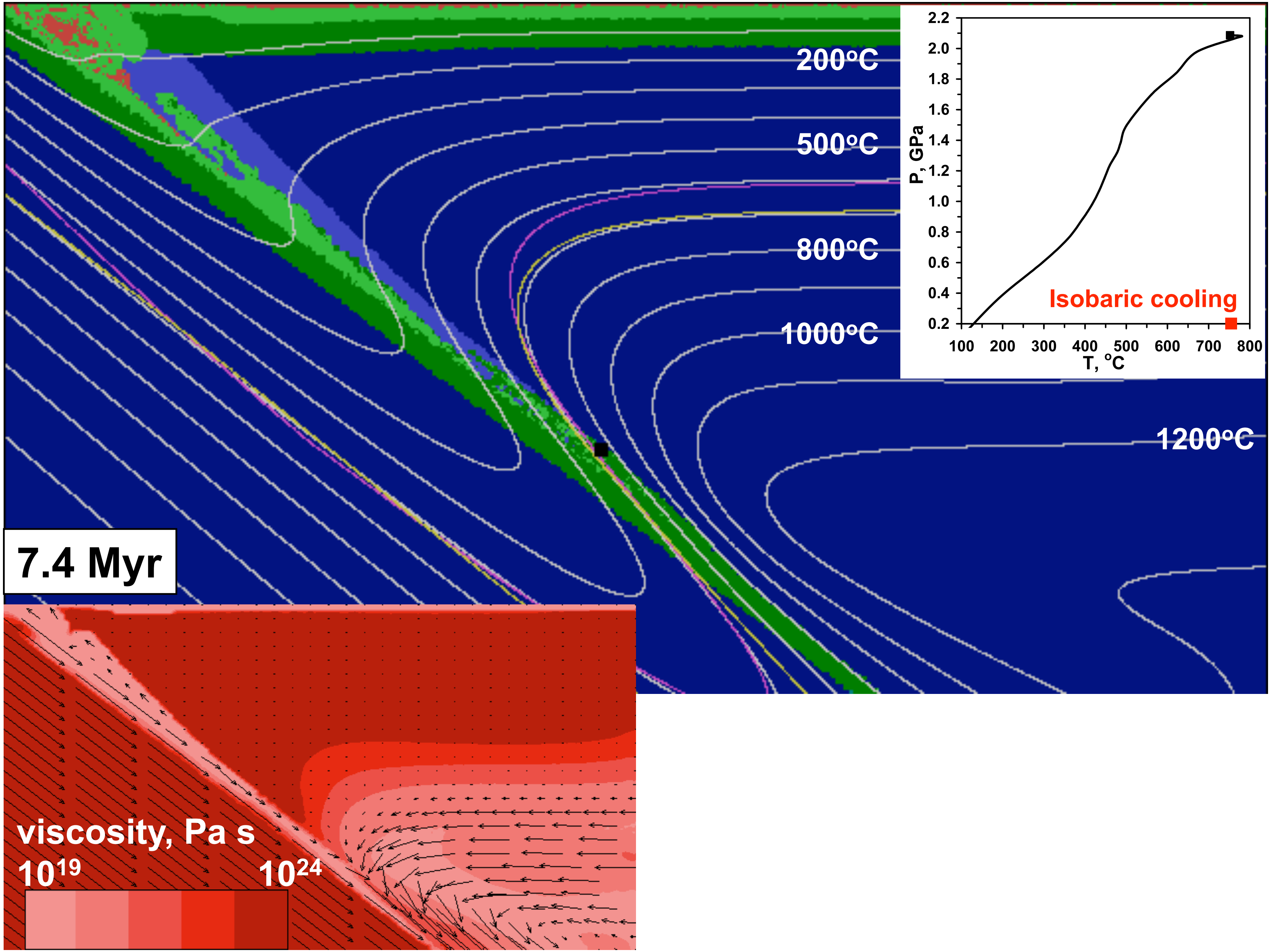

200°C
500°C
800°C
1000°C
1200°C
7.4 Myr
P, GPa
T, °C
2.2
2.0
1.8
1.6
1.4
1.2
1.0
0.8
0.6
0.4
0.2
100
200
300
400
500
600
700
800
Isobaric cooling
viscosity, Pa s
10^{19}
10^{24}

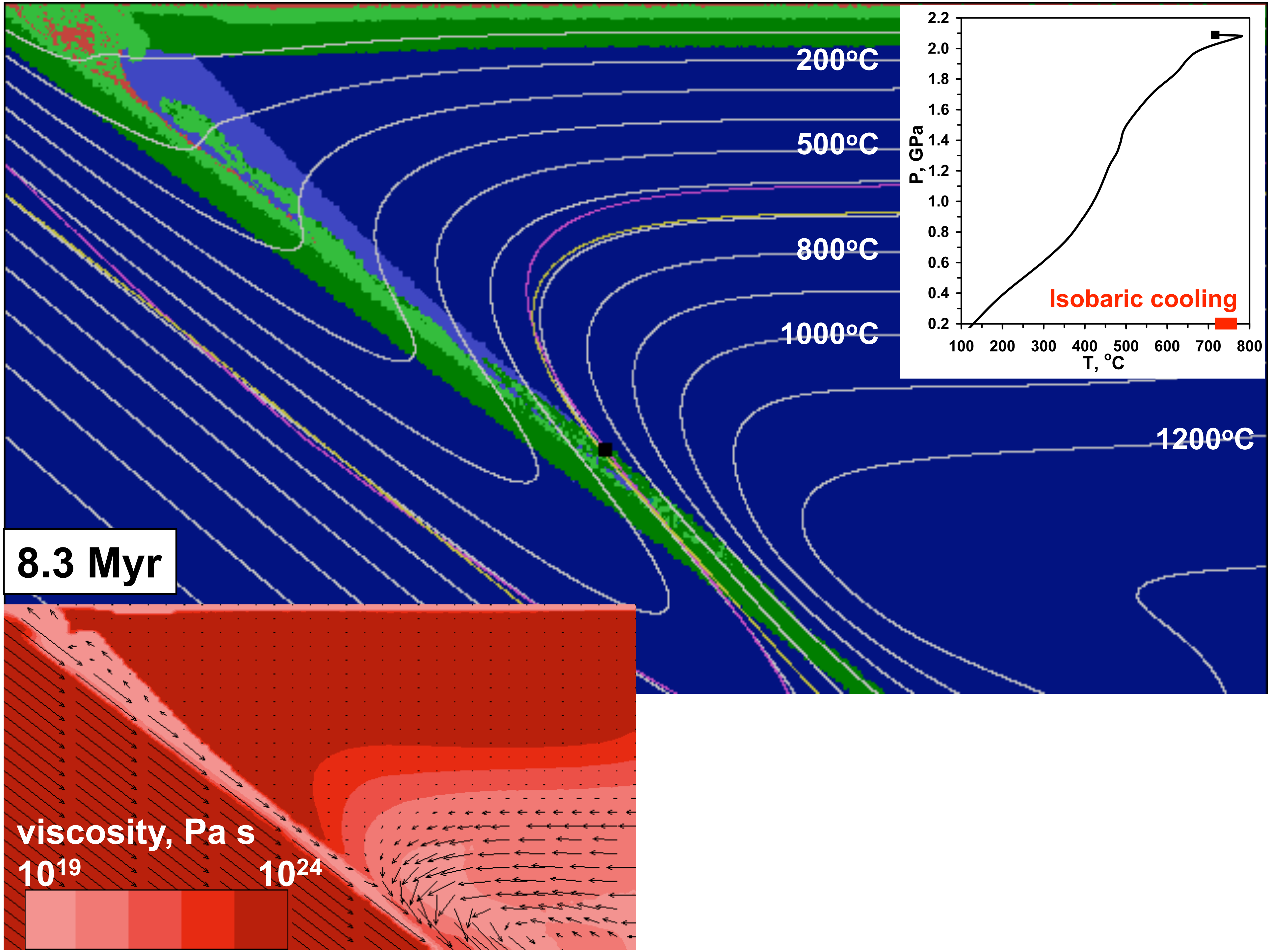

200°C
500°C
800°C
1000°C
1200°C
8.3 Myr
P, GPa
T, °C
2.2
2.0
1.8
1.6
1.4
1.2
1.0
0.8
0.6
0.4
0.2
100
200
300
400
500
600
700
800
Isobaric cooling
viscosity, Pa s
10^{19}
10^{24}

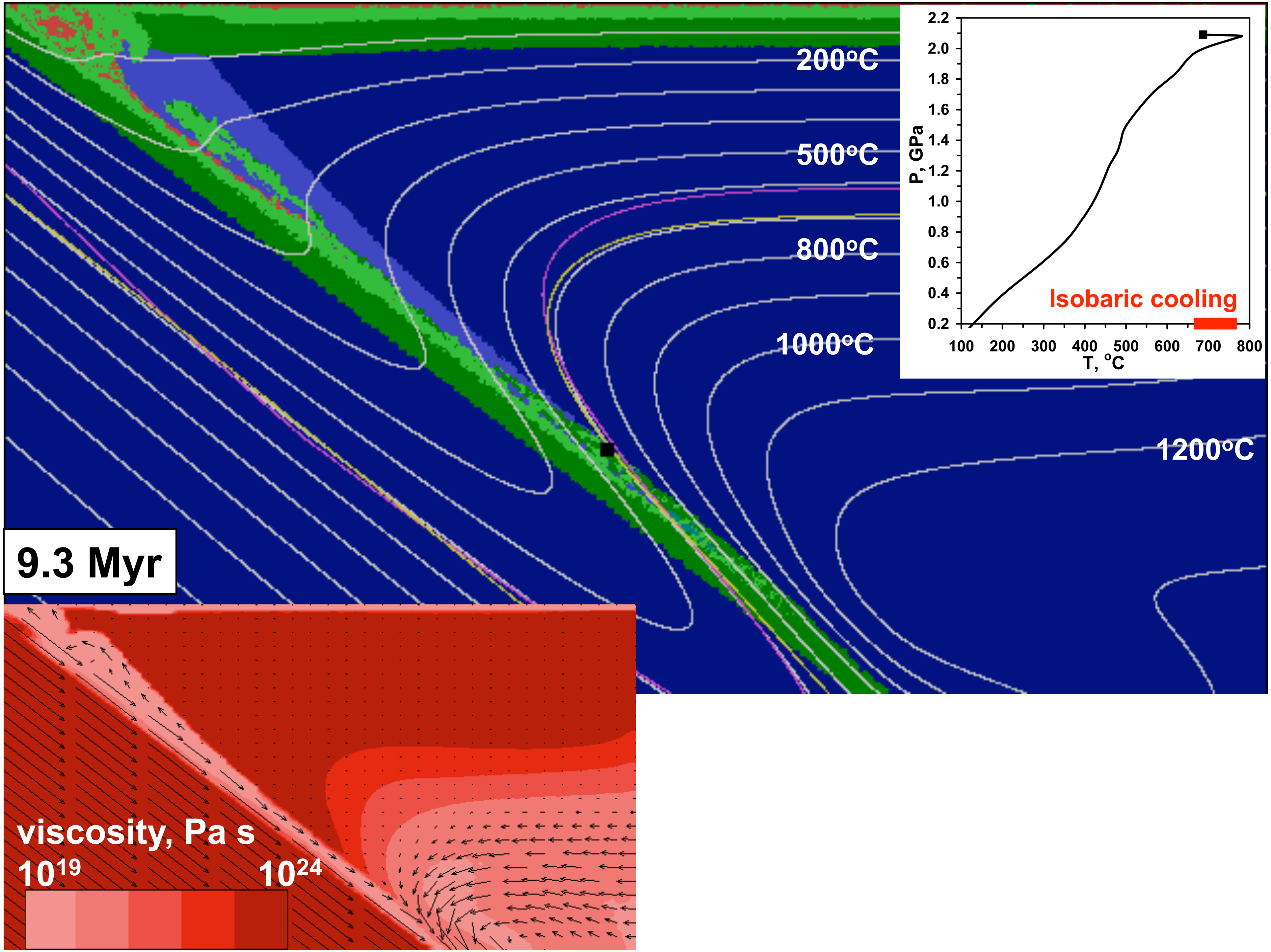

200°C
500°C
800°C
1000°C
1200°C
9.3 Myr
P, GPa
T, °C
Isobaric cooling
2.2
2.0
1.8
1.6
1.4
1.2
1.0
0.8
0.6
0.4
0.2
100
200
300
400
500
600
700
800
viscosity, Pa s
10^{19}
10^{24}

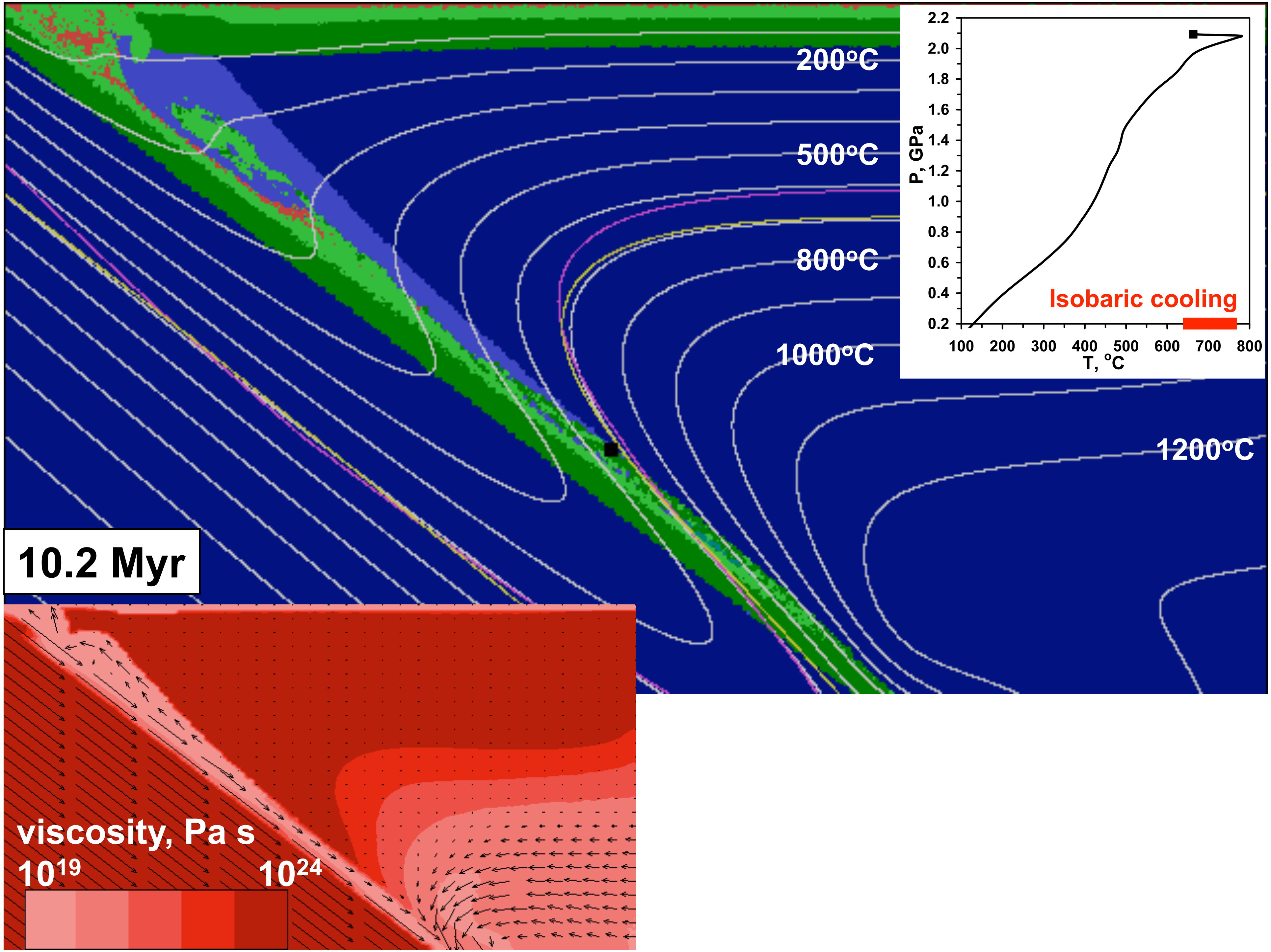

200°C
500°C
800°C
1000°C
1200°C
10.2 Myr
P, GPa
2.2
2.0
1.8
1.6
1.4
1.2
1.0
0.8
0.6
0.4
0.2
100
200
300
400
500
600
700
800
T, °C
Isobaric cooling
viscosity, Pa s
10^{19}
10^{24}

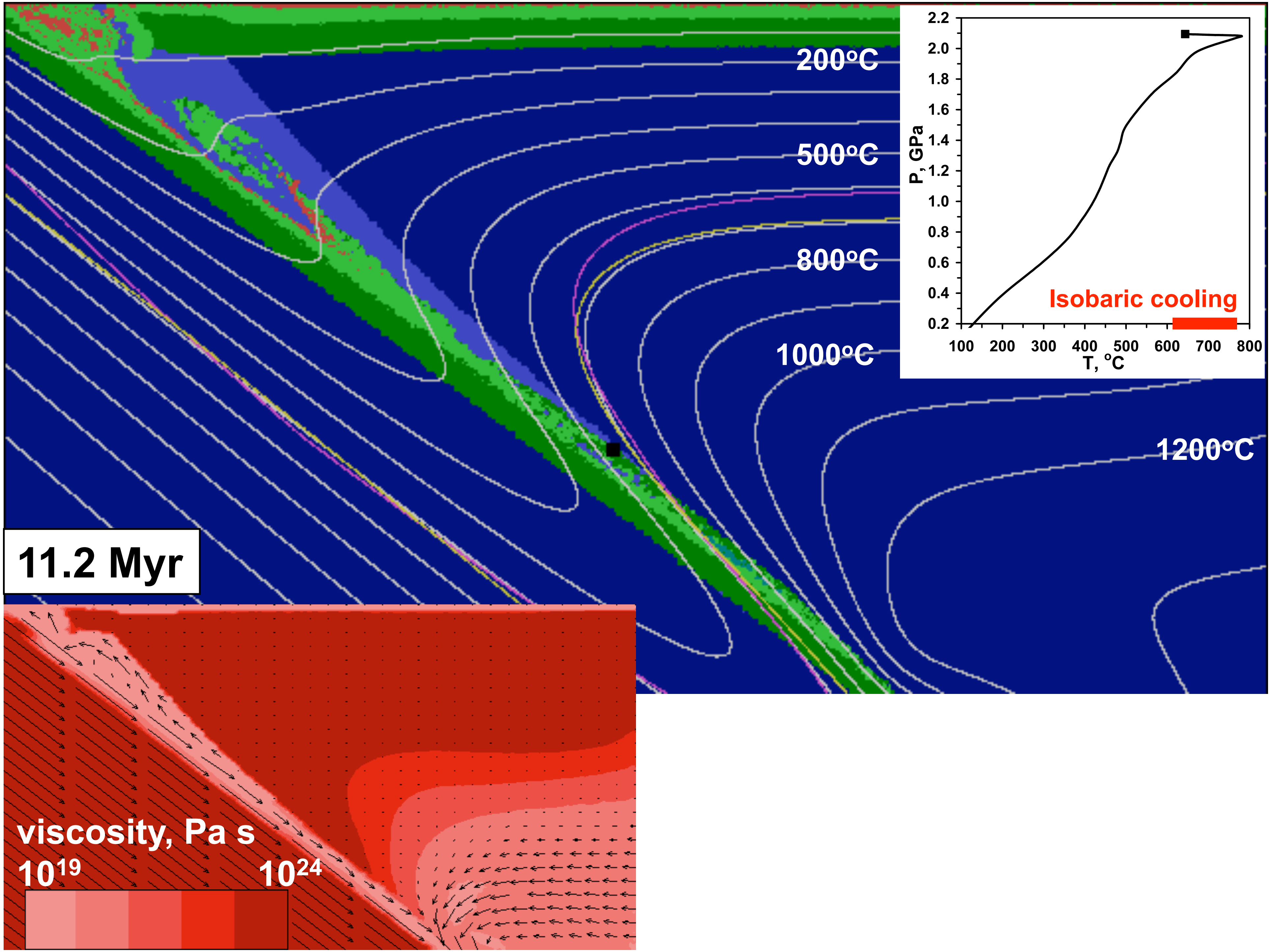

200°C
500°C
800°C
1000°C
1200°C
11.2 Myr
P, GPa
T, °C
2.2
2.0
1.8
1.6
1.4
1.2
1.0
0.8
0.6
0.4
0.2
100
200
300
400
500
600
700
800
Isobaric cooling
viscosity, Pa s
10^19
10^24

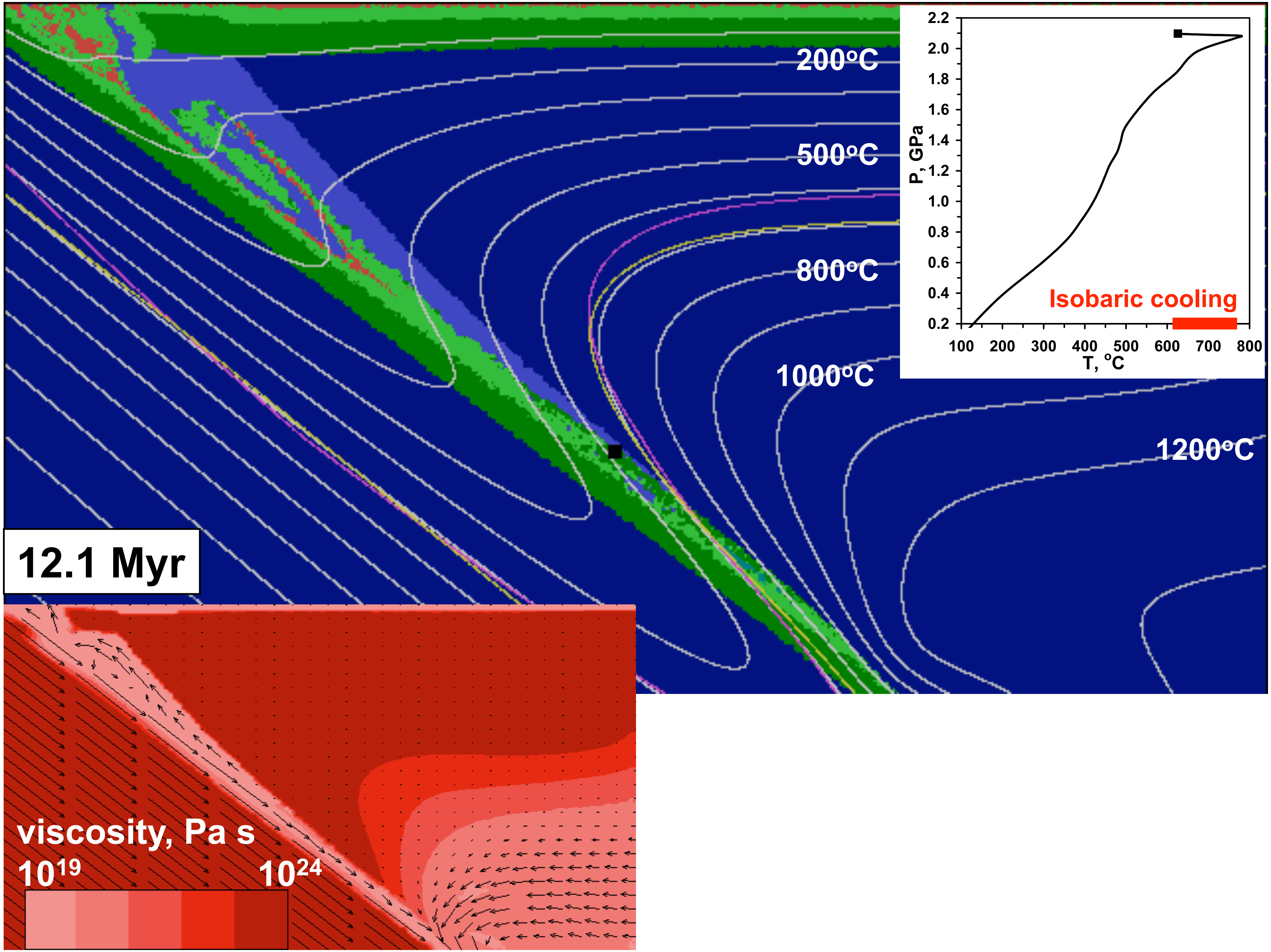

200°C
500°C
800°C
1000°C
1200°C
12.1 Myr
P, GPa
T, °C
2.2
2.0
1.8
1.6
1.4
1.2
1.0
0.8
0.6
0.4
0.2
100
200
300
400
500
600
700
800
Isobaric cooling
viscosity, Pa s
10^{19}
10^{24}

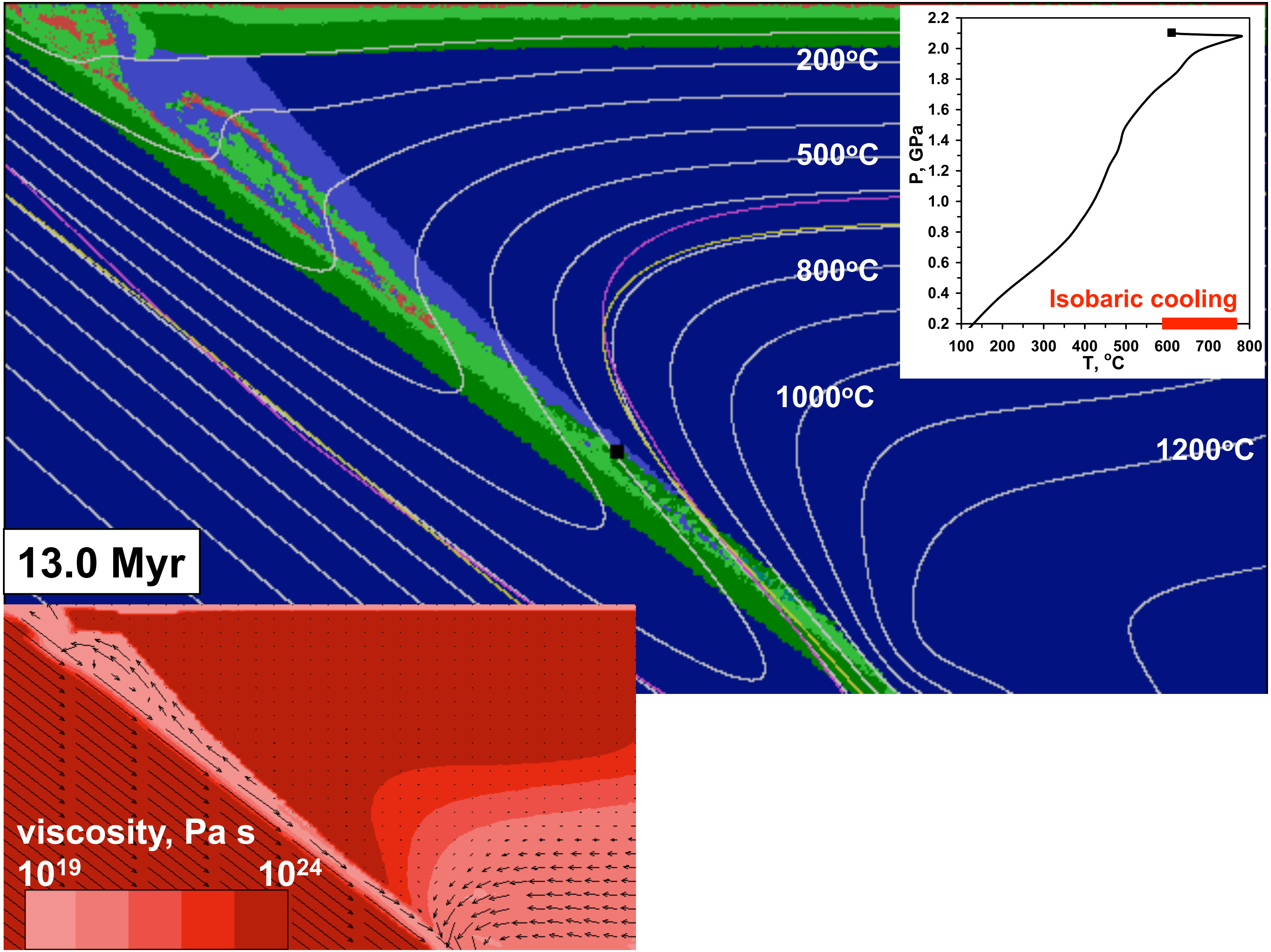

200°C
500°C
800°C
1000°C
1200°C
13.0 Myr
P, GPa
T, °C
Isobaric cooling
viscosity, Pa s
10^{19}
10^{24}

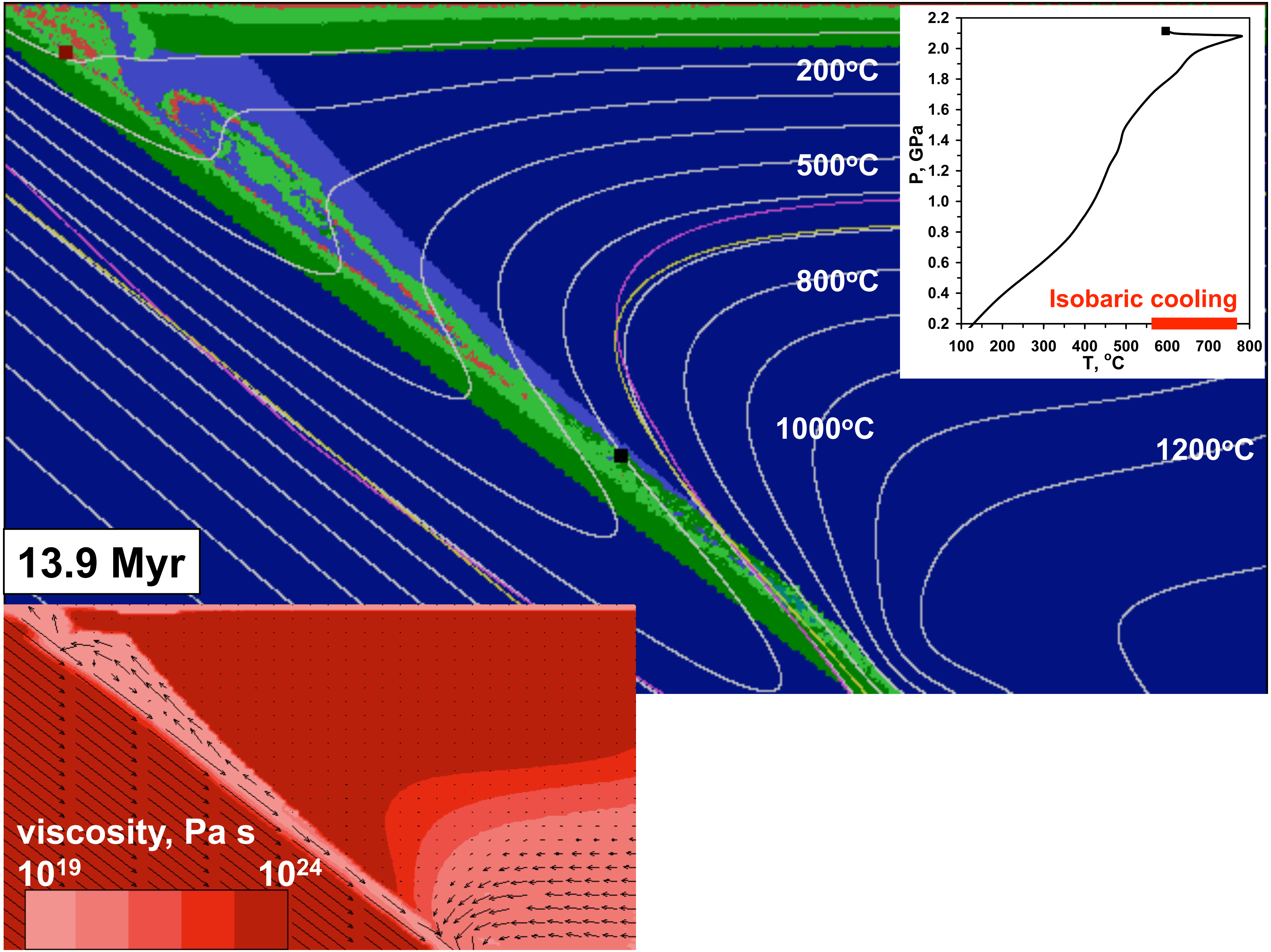
200°C
500°C
800°C
1000°C
1200°C
13.9 Myr
P, GPa
T, °C
Isobaric cooling
viscosity, Pa s
10^19
10^24

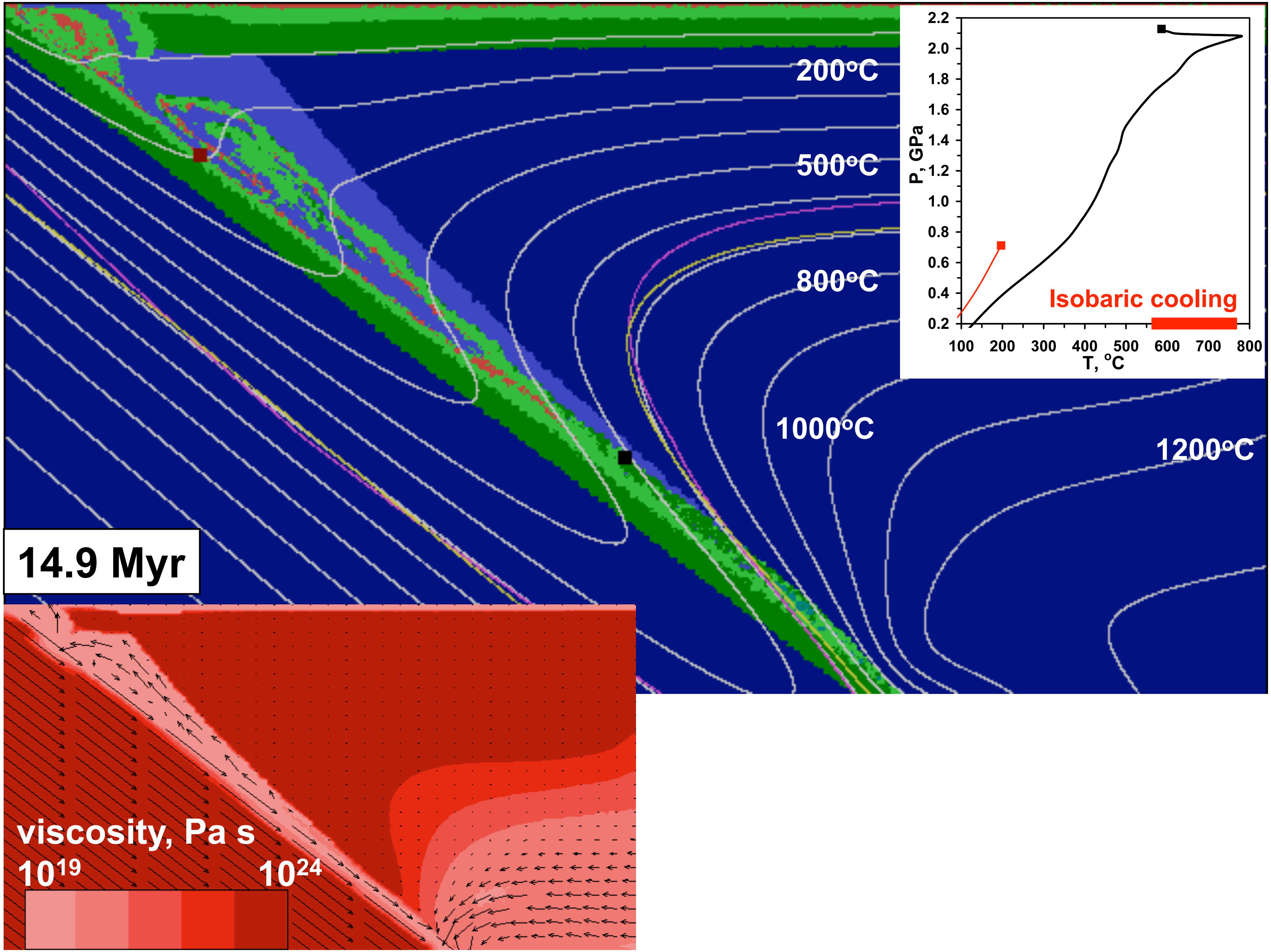

200°C
500°C
800°C
1000°C
1200°C
14.9 Myr
P, GPa
2.2
2.0
1.8
1.6
1.4
1.2
1.0
0.8
0.6
0.4
0.2
100
200
300
400
500
600
700
800
T, °C
Isobaric cooling
viscosity, Pa s
10^19
10^24

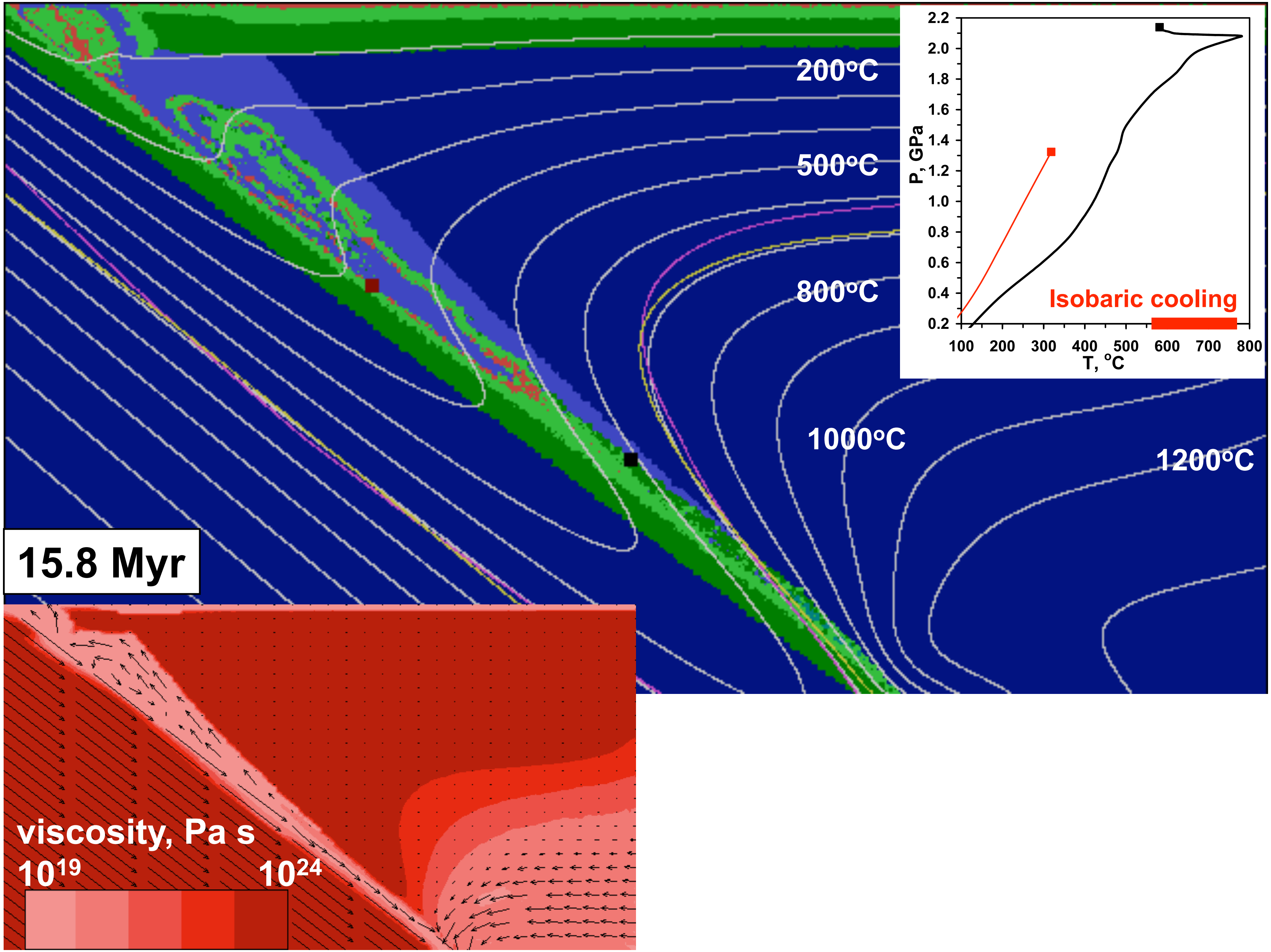

200°C
500°C
800°C
1000°C
1200°C
15.8 Myr
viscosity, Pa s
10^{19}
10^{24}
P, GPa
T, °C
Isobaric cooling
2.2
2.0
1.8
1.6
1.4
1.2
1.0
0.8
0.6
0.4
0.2
100
200
300
400
500
600
700
800

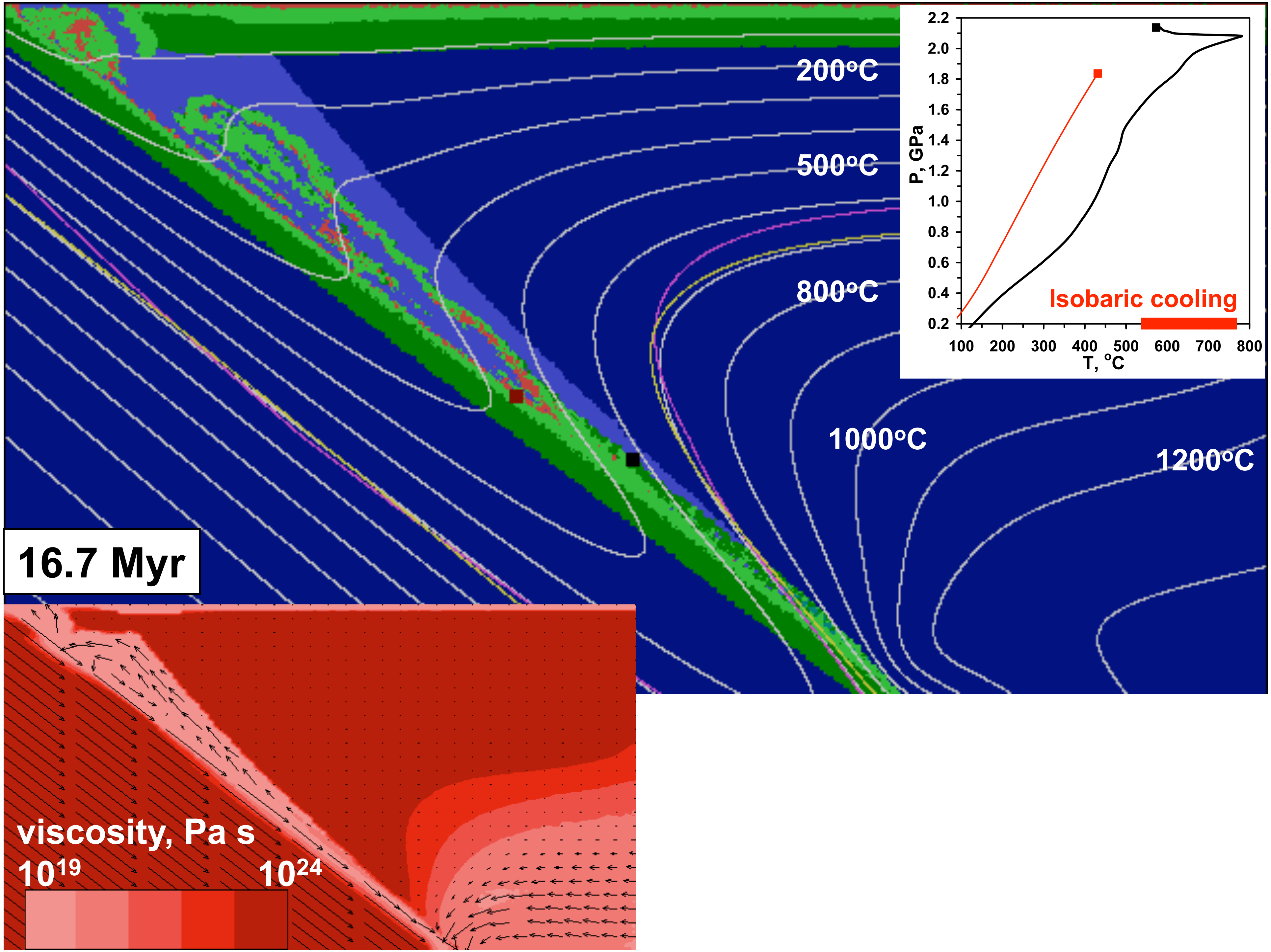

200°C
500°C
800°C
1000°C
1200°C
16.7 Myr
viscosity, Pa s
10^{19}
10^{24}
P, GPa
T, °C
Isobaric cooling
2.2
2.0
1.8
1.6
1.4
1.2
1.0
0.8
0.6
0.4
0.2
100 200 300 400 500 600 700 800

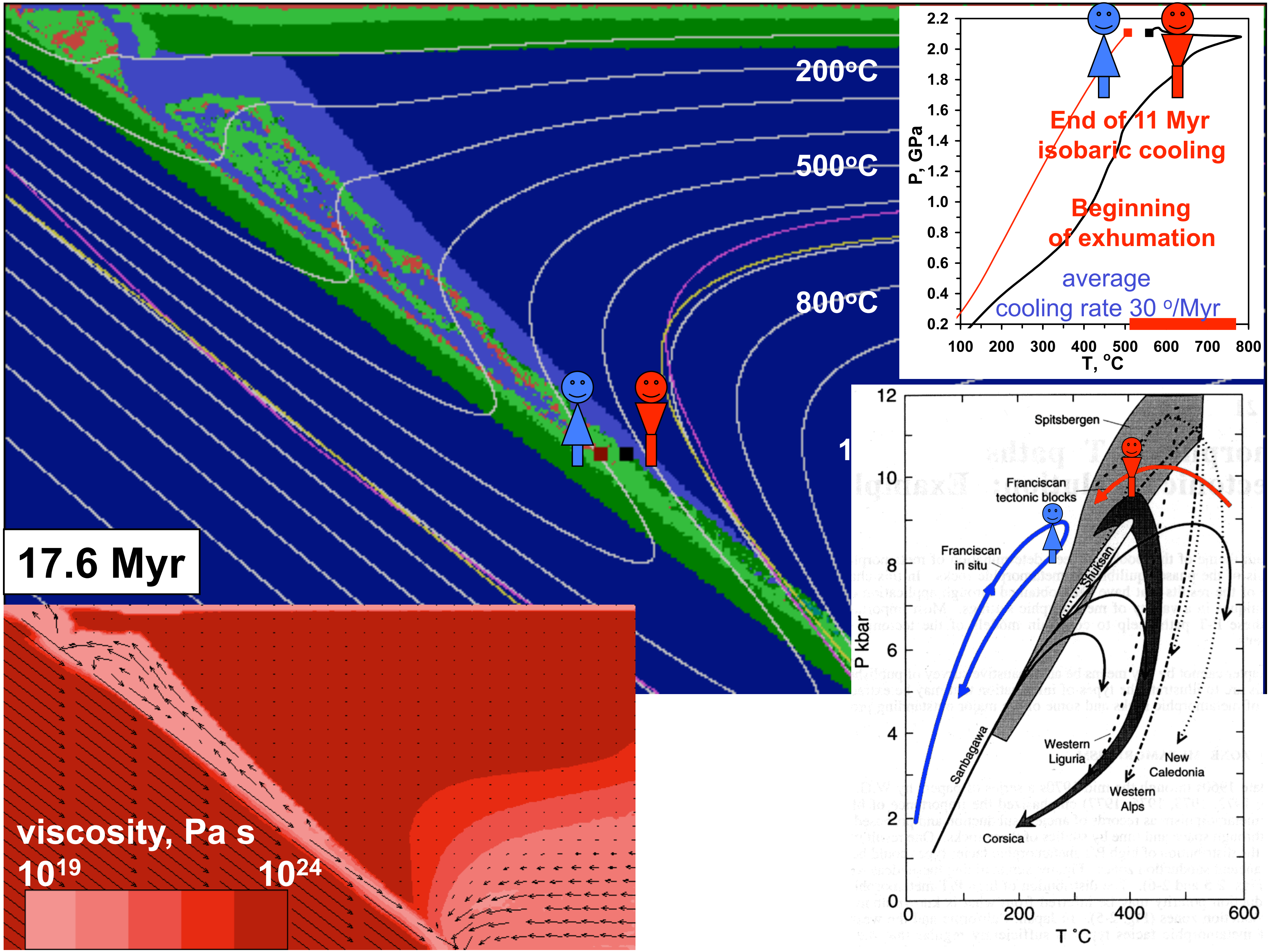

200°C
500°C
800°C
17.6 Myr
viscosity, Pa s
10^{19}
10^{24}
P, GPa
T, °C
End of 11 Myr
isobaric cooling
Beginning
of exhumation
average
cooling rate 30 °/Myr
P kbar
T °C
Spitsbergen
Franciscan
tectonic blocks
Franciscan
in situ
Shuksan
Sanbagawa
Western
Liguria
New
Caledonia
Western
Alps
Corsica

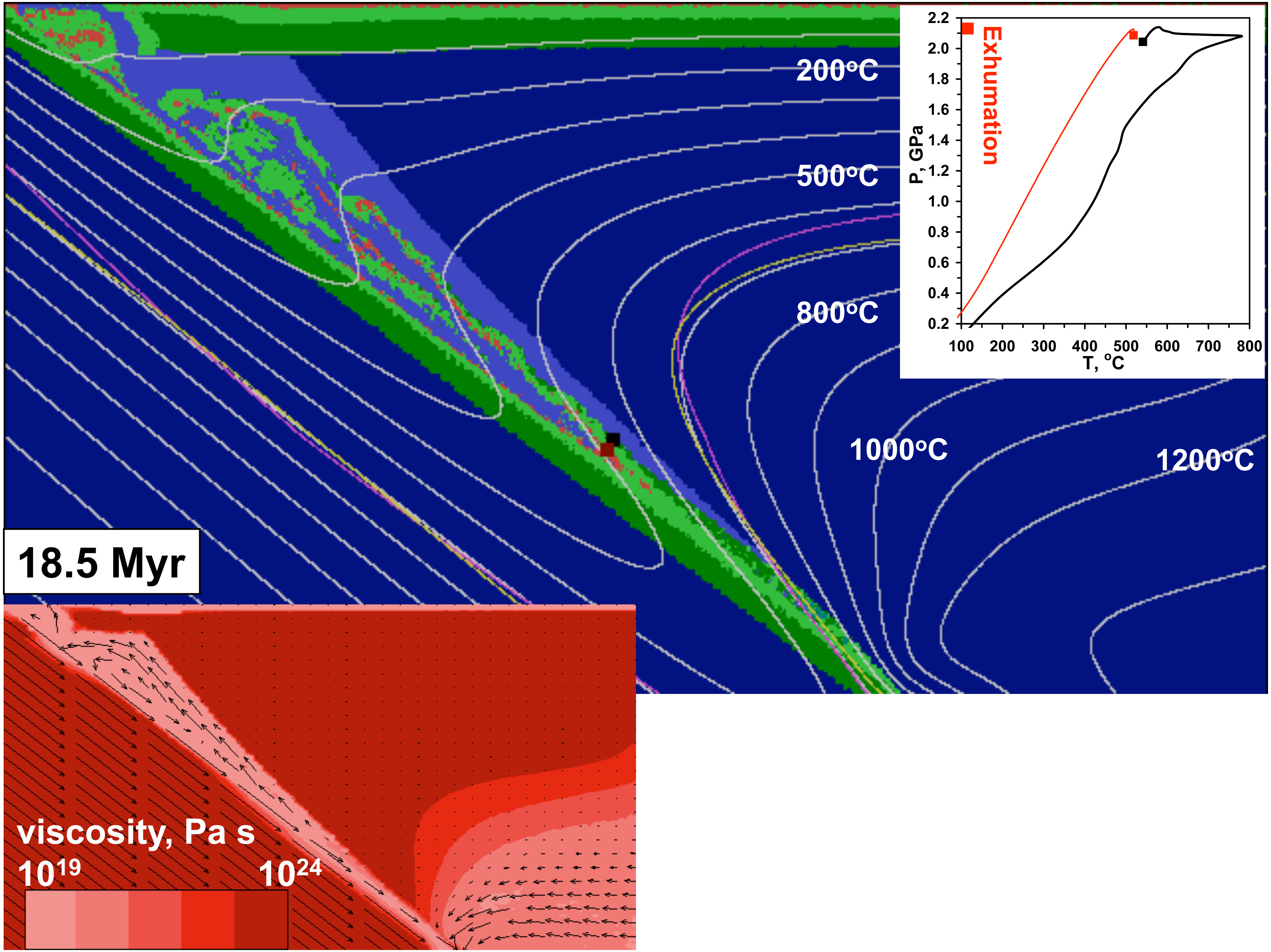

200°C
500°C
800°C
1000°C
1200°C
18.5 Myr
Exhumation
P, GPa
T, °C
viscosity, Pa s
10^{19}
10^{24}

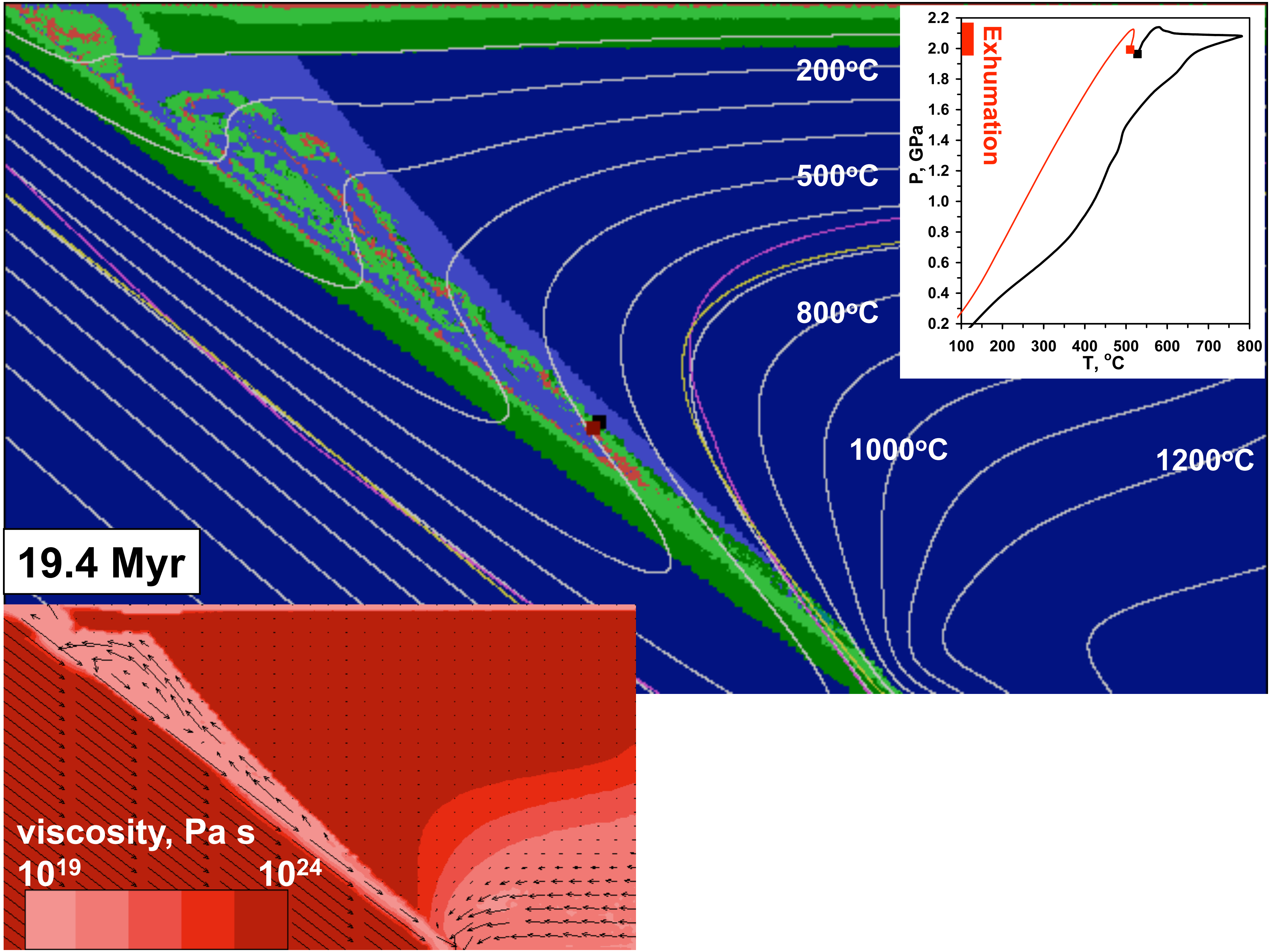
200°C
500°C
800°C
1000°C
1200°C
19.4 Myr
viscosity, Pa s
10^19
10^24
Exhumation
P, GPa
T, °C
2.2
2.0
1.8
1.6
1.4
1.2
1.0
0.8
0.6
0.4
0.2
100
200
300
400
500
600
700
800

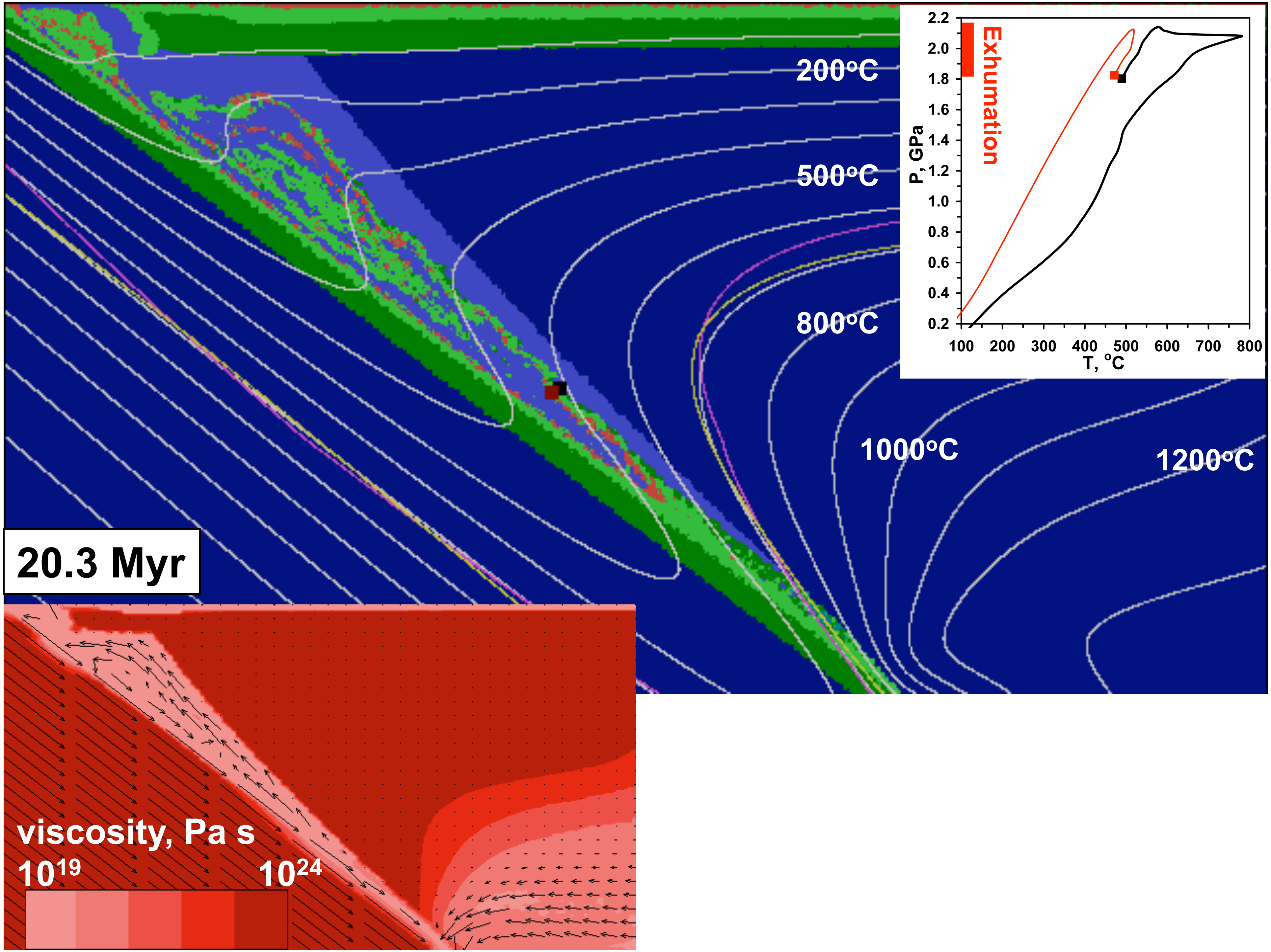

200°C
500°C
800°C
1000°C
1200°C
20.3 Myr
viscosity, Pa s
10^{19}
10^{24}
Exhumation
P, GPa
T, °C
2.2
2.0
1.8
1.6
1.4
1.2
1.0
0.8
0.6
0.4
0.2
100
200
300
400
500
600
700
800

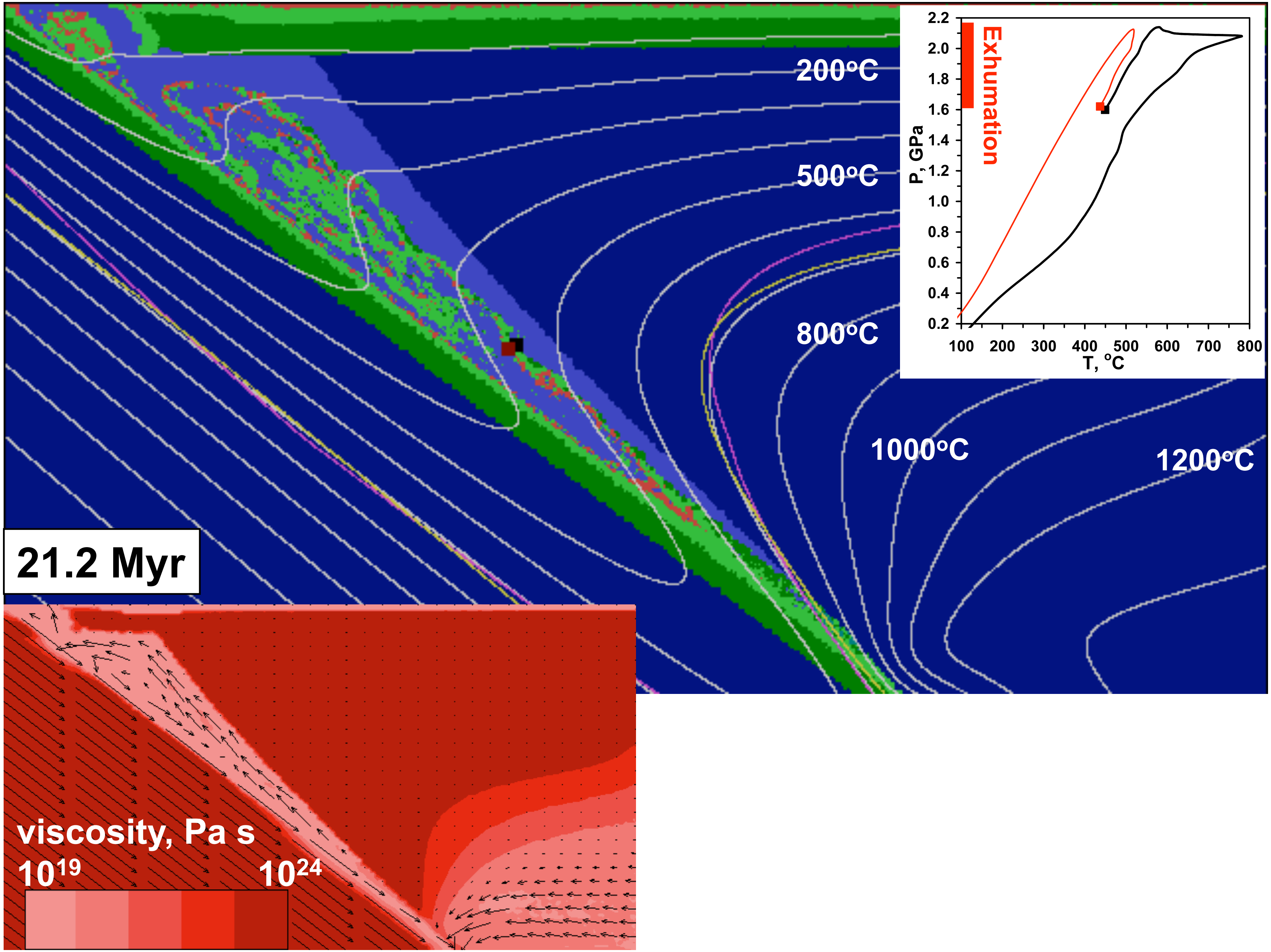

200°C
500°C
800°C
1000°C
1200°C
21.2 Myr
Exhumation
P, GPa
T, °C
viscosity, Pa s
10^{19}
10^{24}

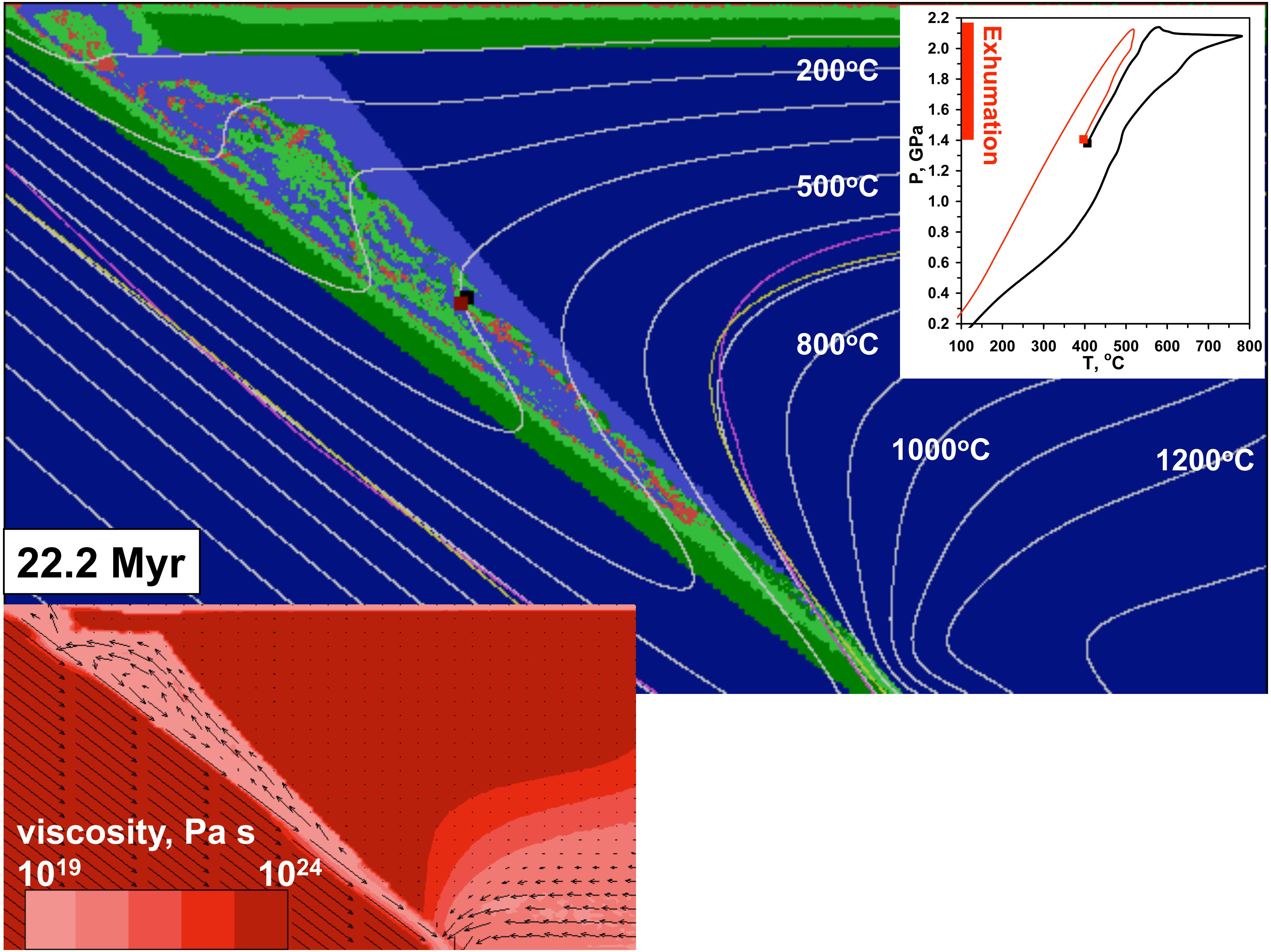

200°C
500°C
800°C
1000°C
1200°C
22.2 Myr
Exhumation
P, GPa
T, °C
2.2
2.0
1.8
1.6
1.4
1.2
1.0
0.8
0.6
0.4
0.2
100
200
300
400
500
600
700
800
viscosity, Pa s
10^19
10^24

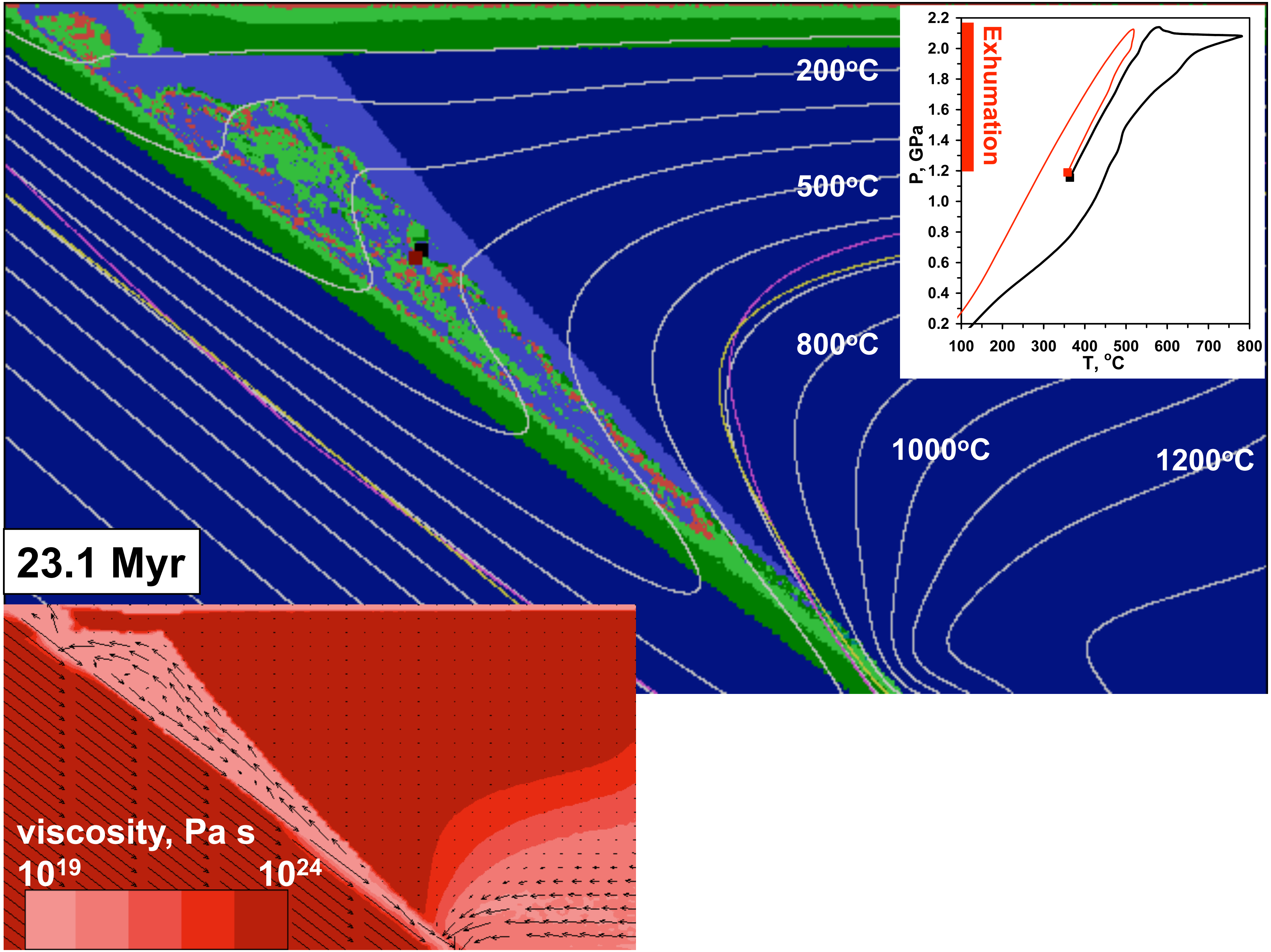

200°C
500°C
800°C
1000°C
1200°C
Exhumation
P, GPa
T, °C
2.2
2.0
1.8
1.6
1.4
1.2
1.0
0.8
0.6
0.4
0.2
100
200
300
400
500
600
700
800
23.1 Myr
viscosity, Pa s
10^{19}
10^{24}

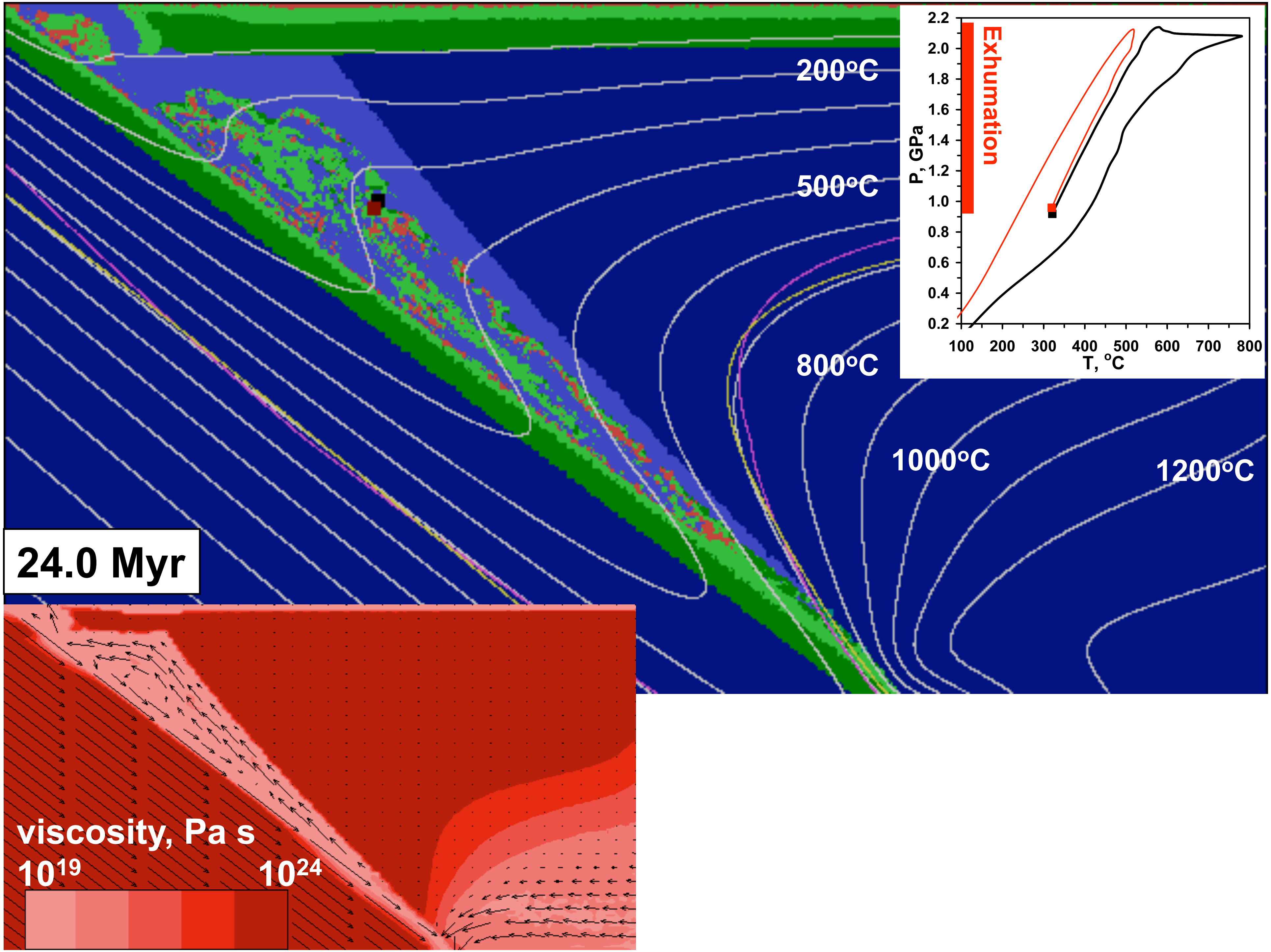
200°C
500°C
800°C
1000°C
1200°C
Exhumation
P, GPa
2.2
2.0
1.8
1.6
1.4
1.2
1.0
0.8
0.6
0.4
0.2
100
200
300
400
500
600
700
800
T, °C
24.0 Myr
viscosity, Pa s
10^19
10^24

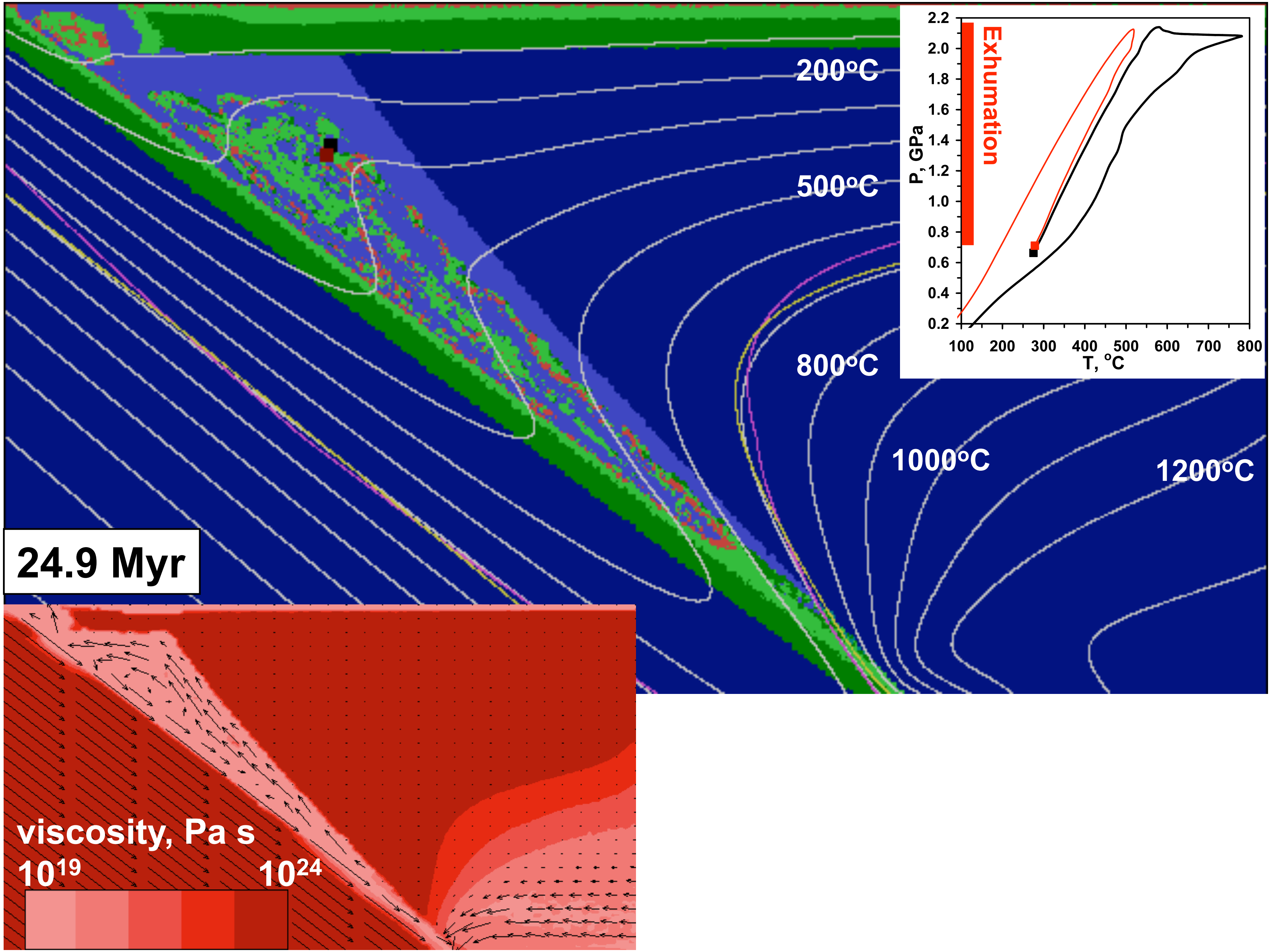

200°C
500°C
800°C
1000°C
1200°C
24.9 Myr
viscosity, Pa s
10^{19}
10^{24}
Exhumation
P, GPa
T, °C
2.2
2.0
1.8
1.6
1.4
1.2
1.0
0.8
0.6
0.4
0.2
100
200
300
400
500
600
700
800

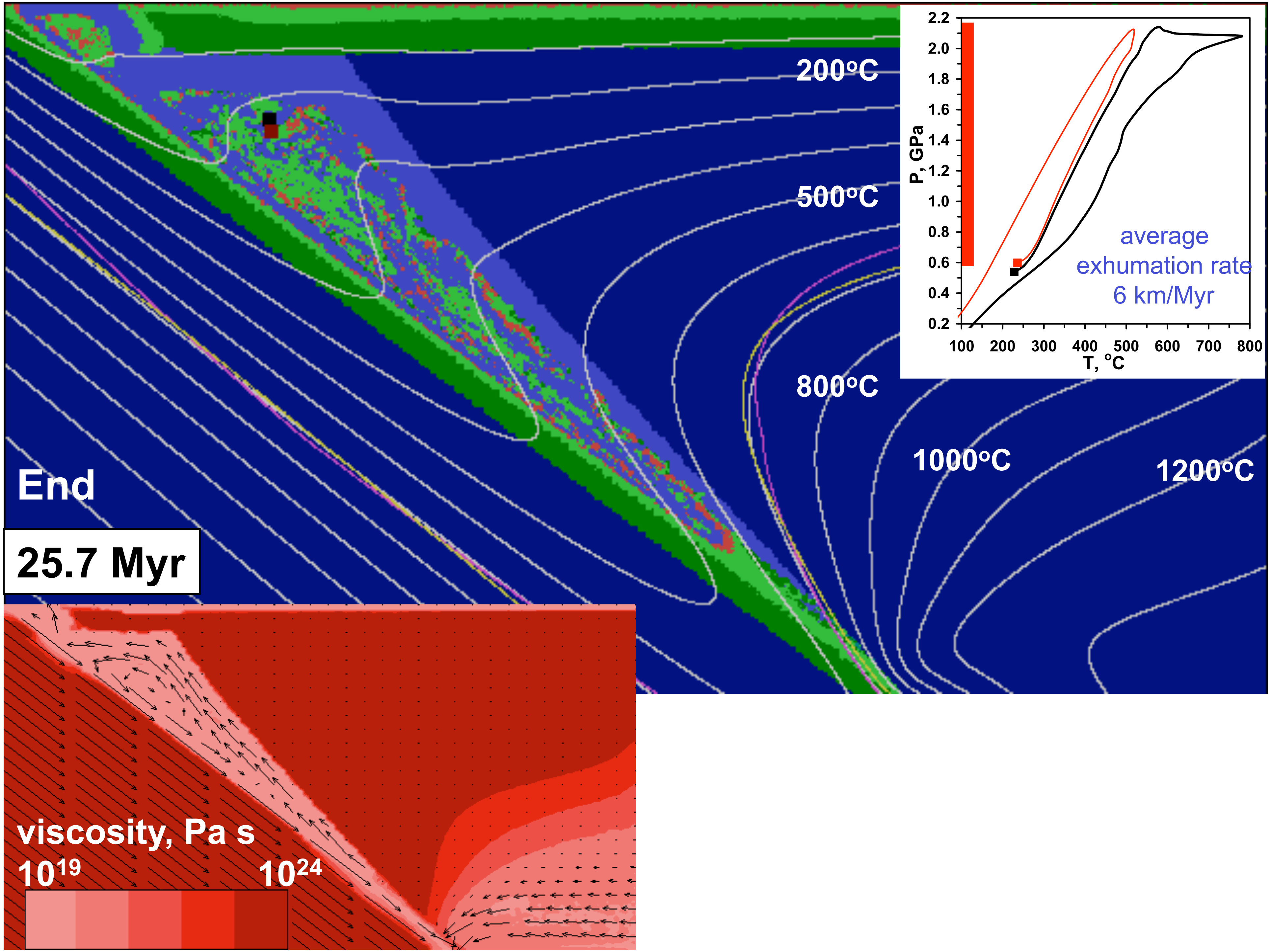

200°C
500°C
800°C
1000°C
1200°C
End
25.7 Myr
P, GPa
T, °C
average exhumation rate 6 km/Myr
viscosity, Pa s
10^19
10^24

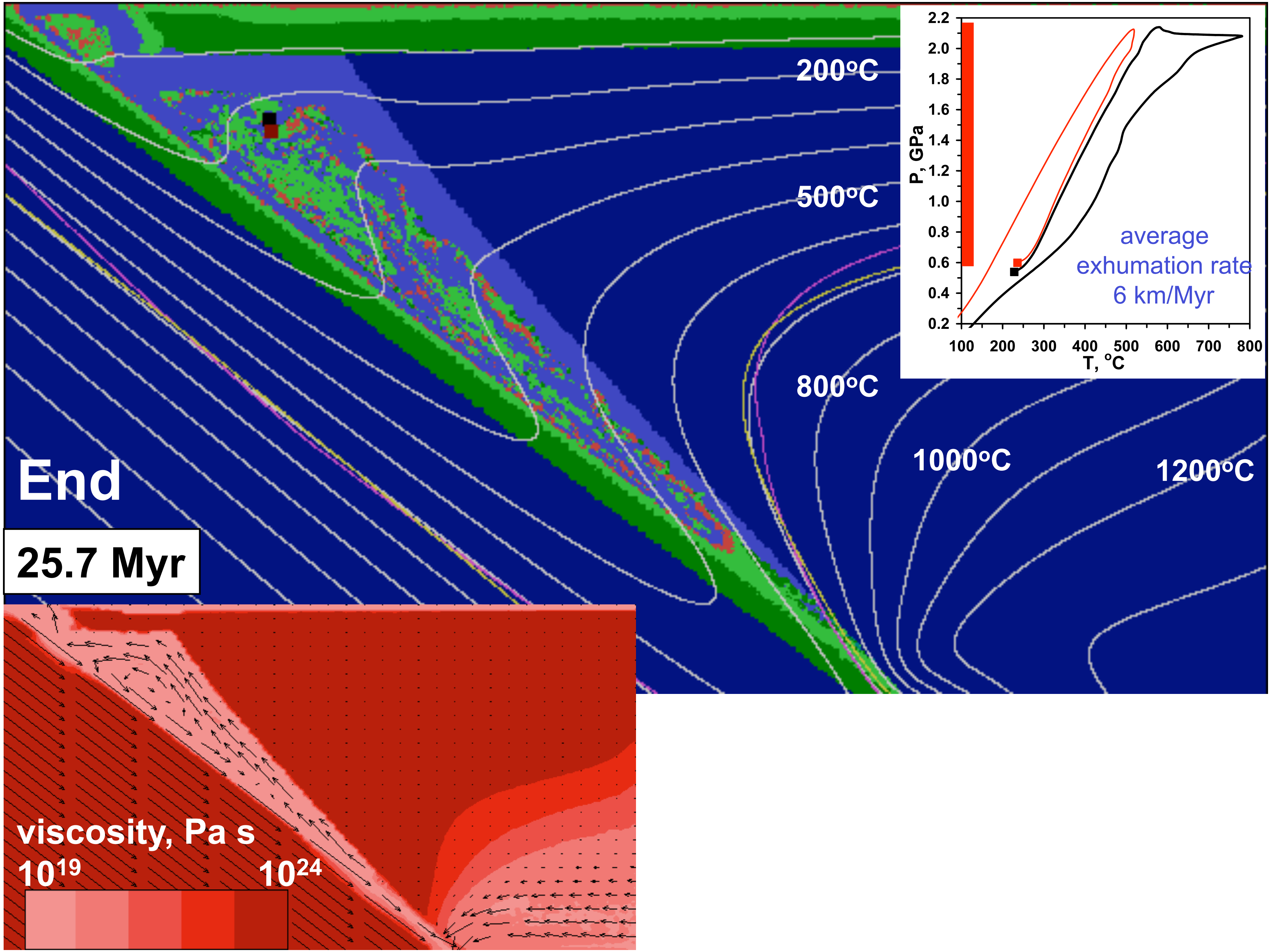
200°C
500°C
800°C
1000°C
1200°C
End
25.7 Myr
P, GPa
2.2
2.0
1.8
1.6
1.4
1.2
1.0
0.8
0.6
0.4
0.2
100
200
300
400
500
600
700
800
T, °C
average
exhumation rate
6 km/Myr
viscosity, Pa s
10^19
10^24

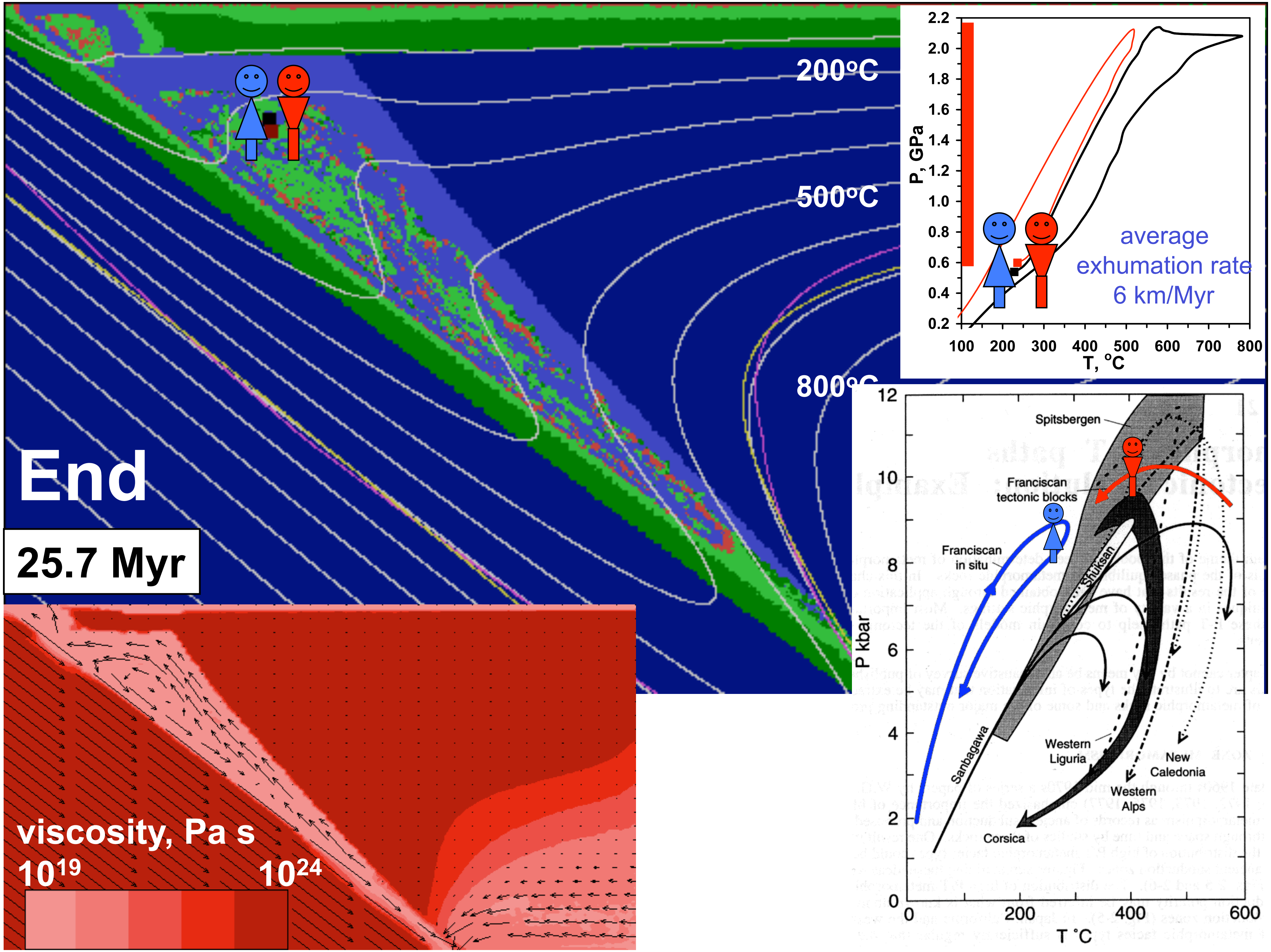

200°C
500°C
800°C
End
25.7 Myr
viscosity, Pa s
10^{19}
10^{24}
P, GPa
T, °C
average
exhumation rate
6 km/Myr
P kbar
T °C
Spitsbergen
Franciscan
tectonic blocks
Franciscan
in situ
Shuksan
Sanbagawa
Western
Liguria
New
Caledonia
Western
Alps
Corsica

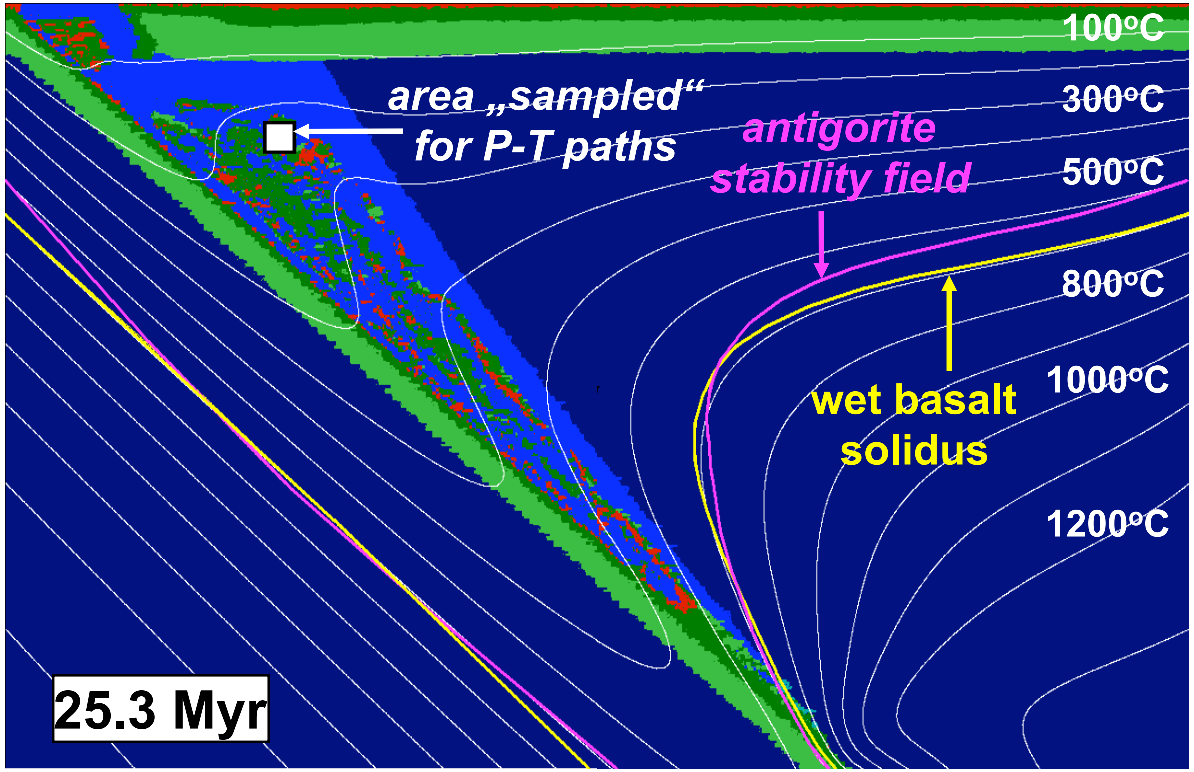

(Gerya et al., 2002, Tectonics)

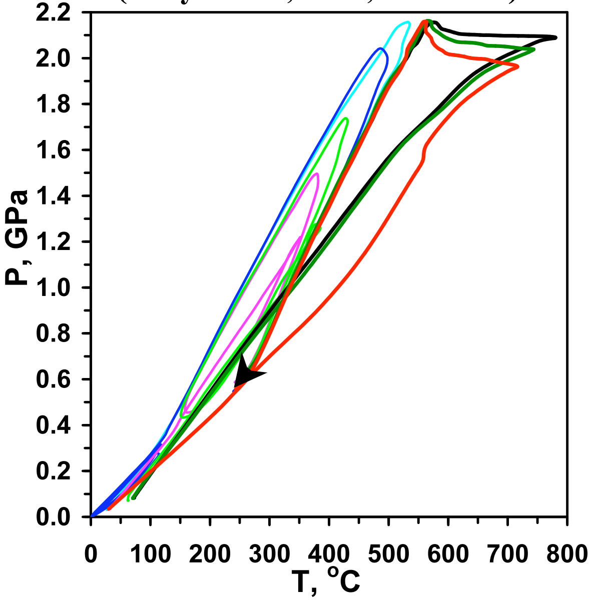

Smith et al. (1999)
Villa de Cura blueschist belt, Venezuela

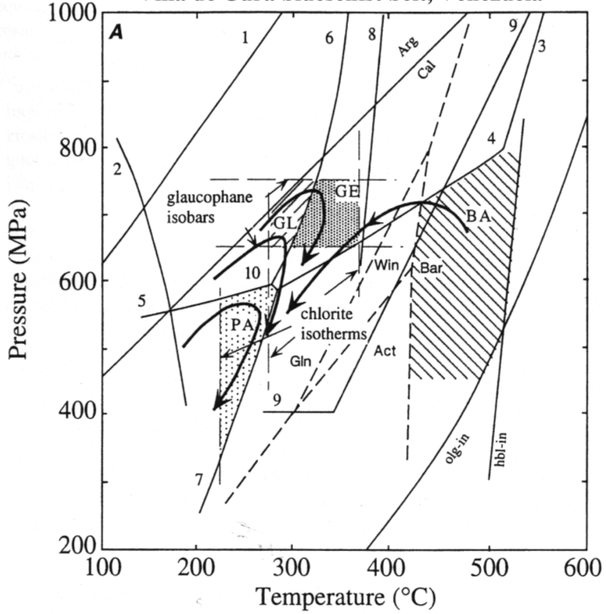

Yukon-Tanana terrane

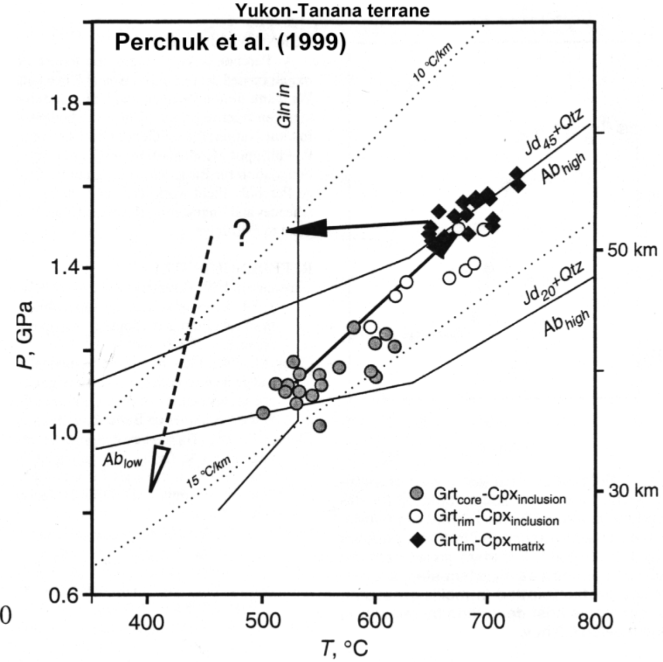

Why is subduction one-sided ?

?

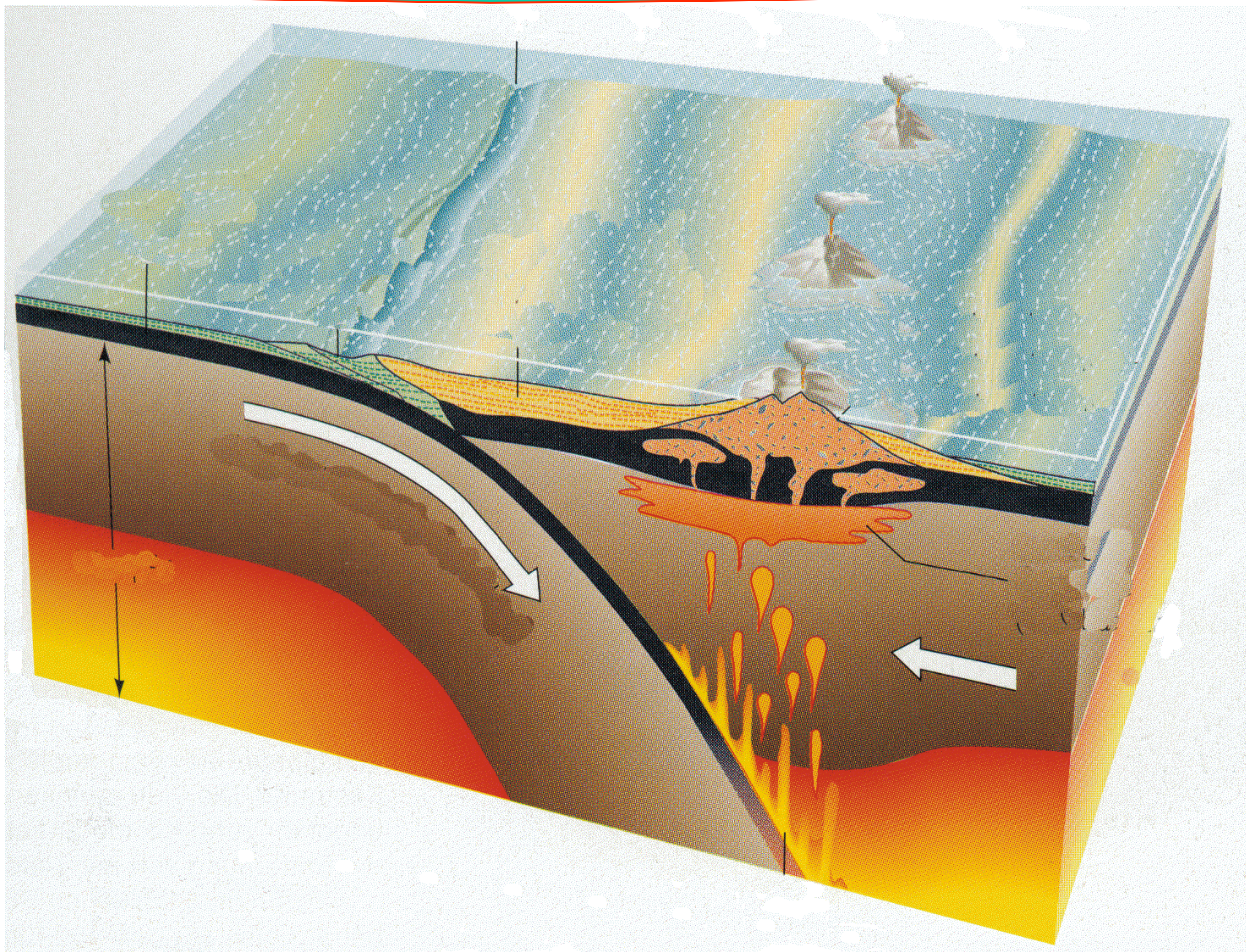

Why is subduction one-sided ?

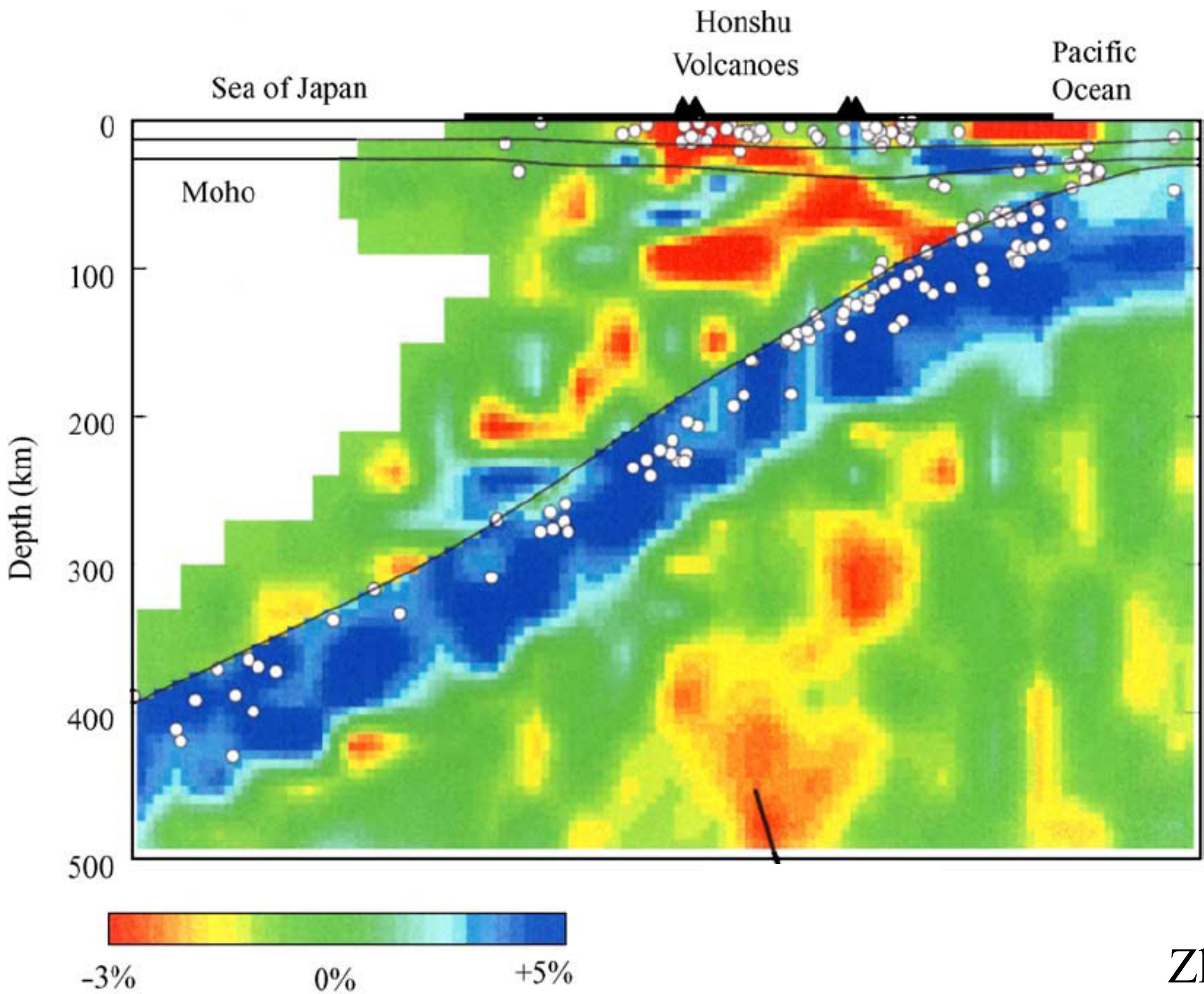

Zhao, 2004

Two-sided spontaneous numerical subduction

Tackley (1999)

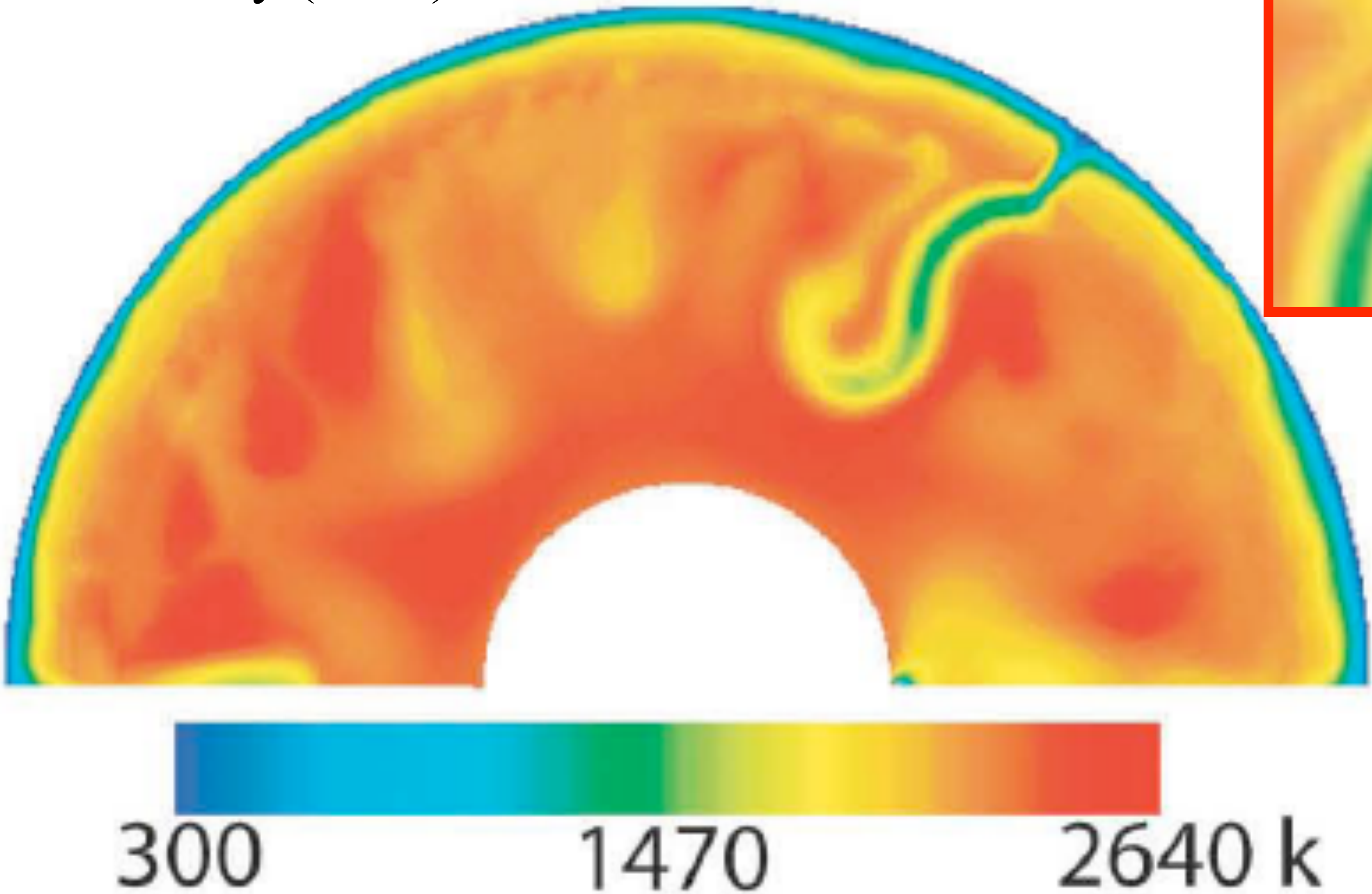

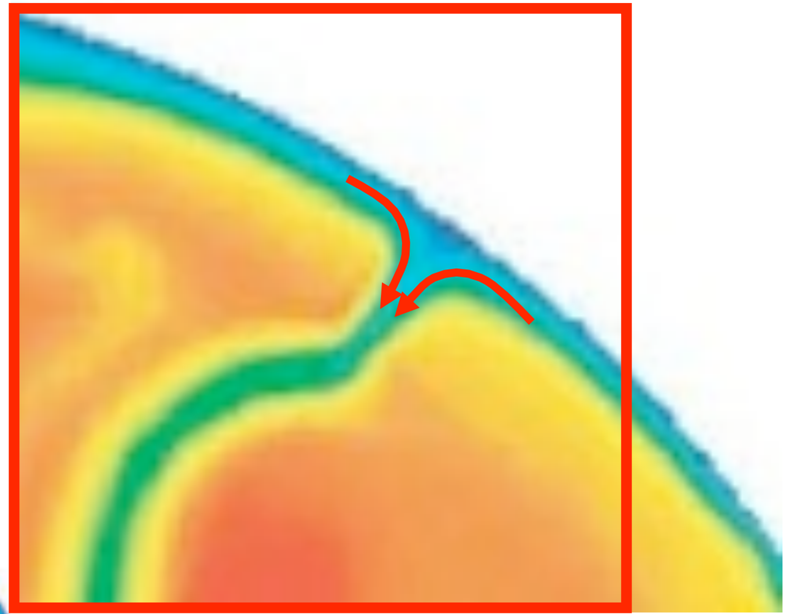

One-sided subduction

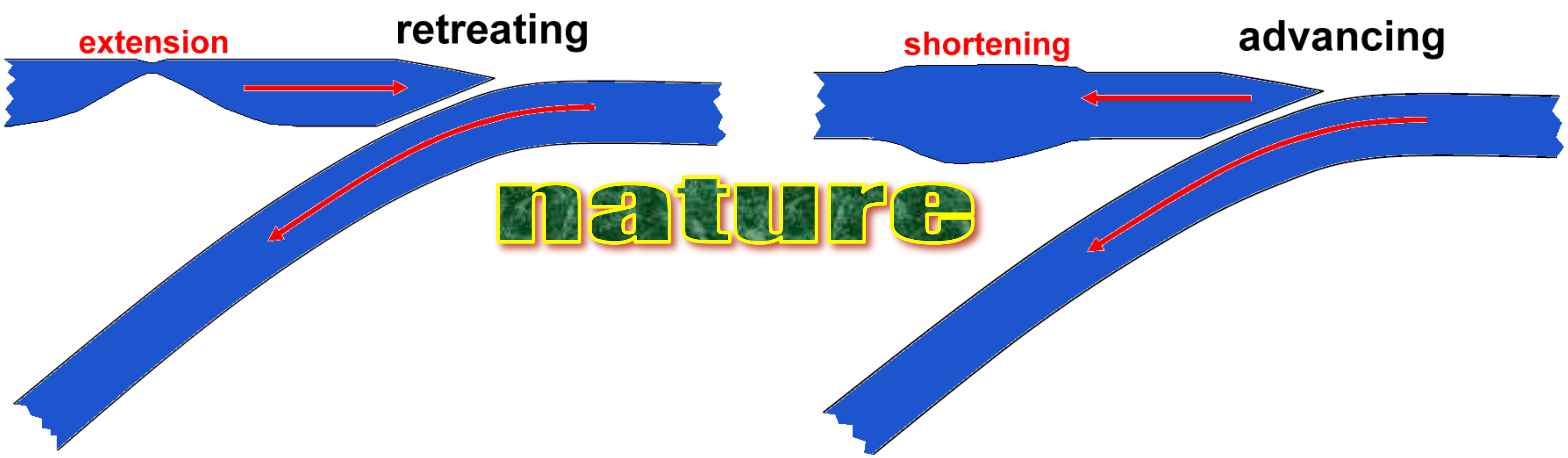

Two-sided subduction

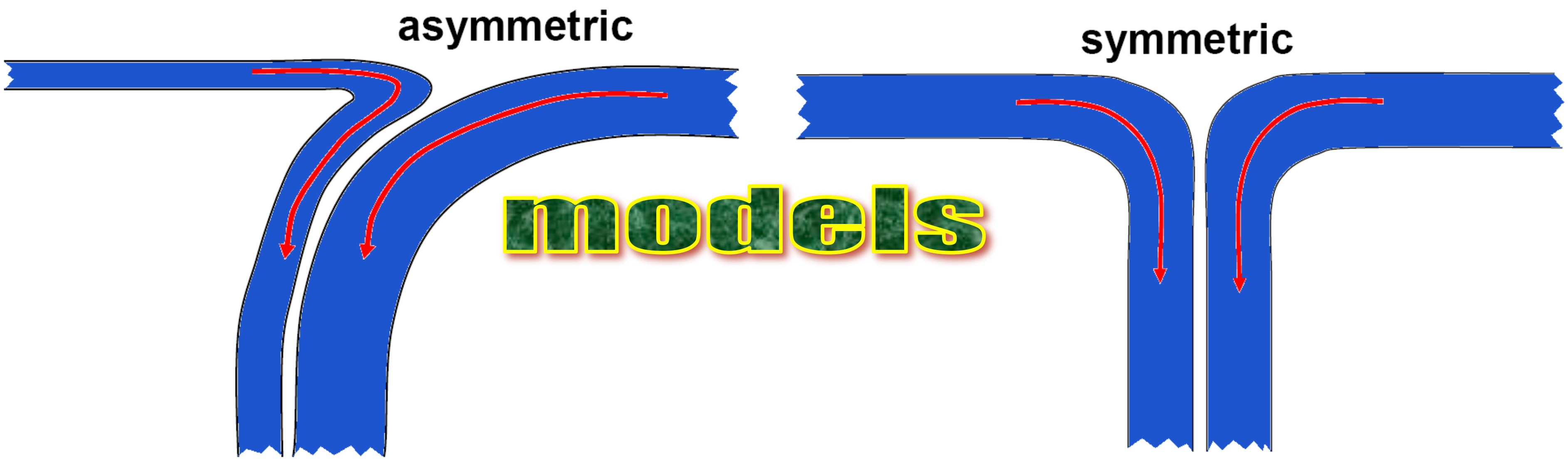

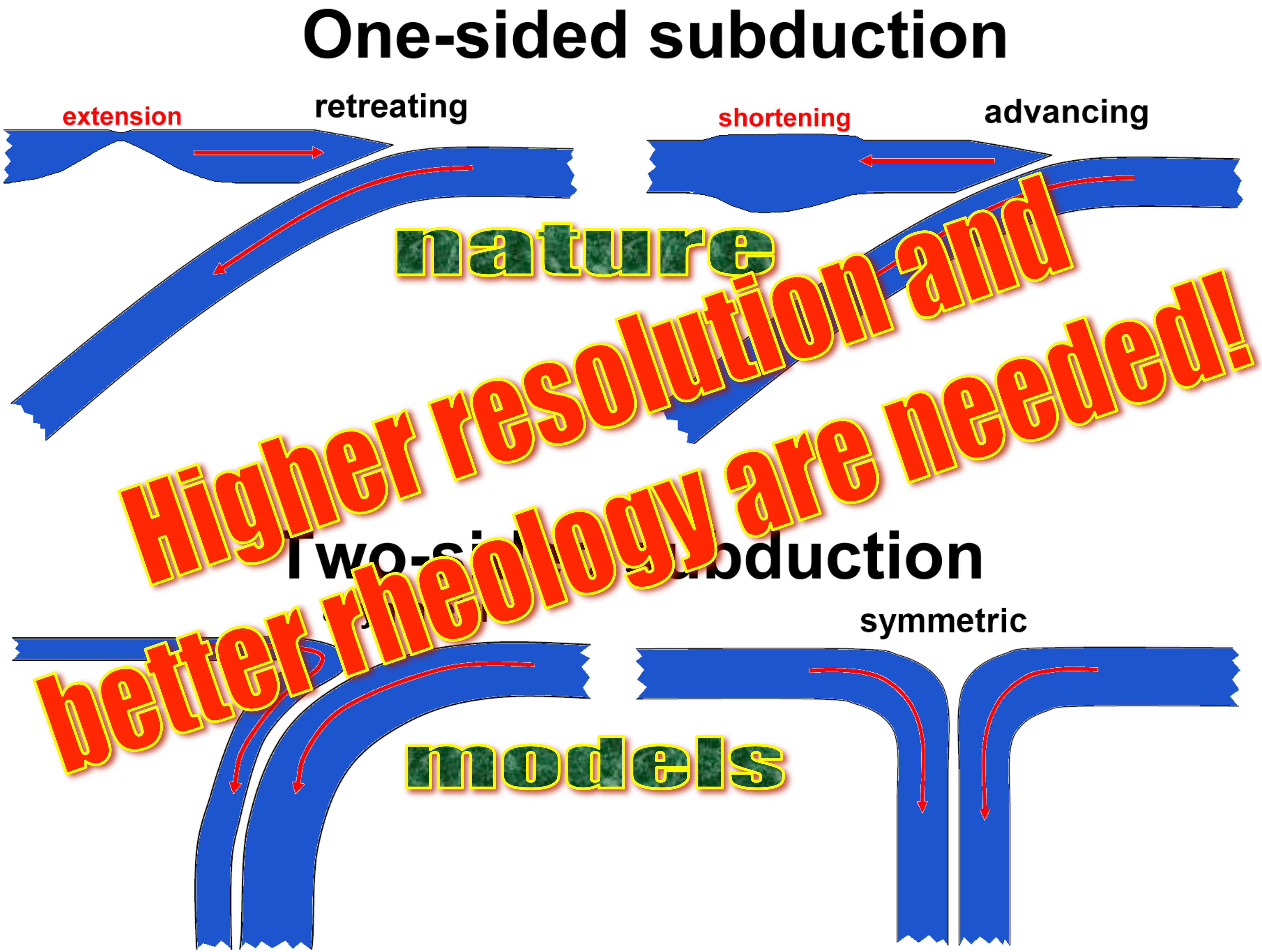
One-sided subduction
extension
retreating
shortening
advancing
nature
Higher resolution and
better rheology are needed!
symmetric
models

High resolution and viscoelastoplastic rheology are used

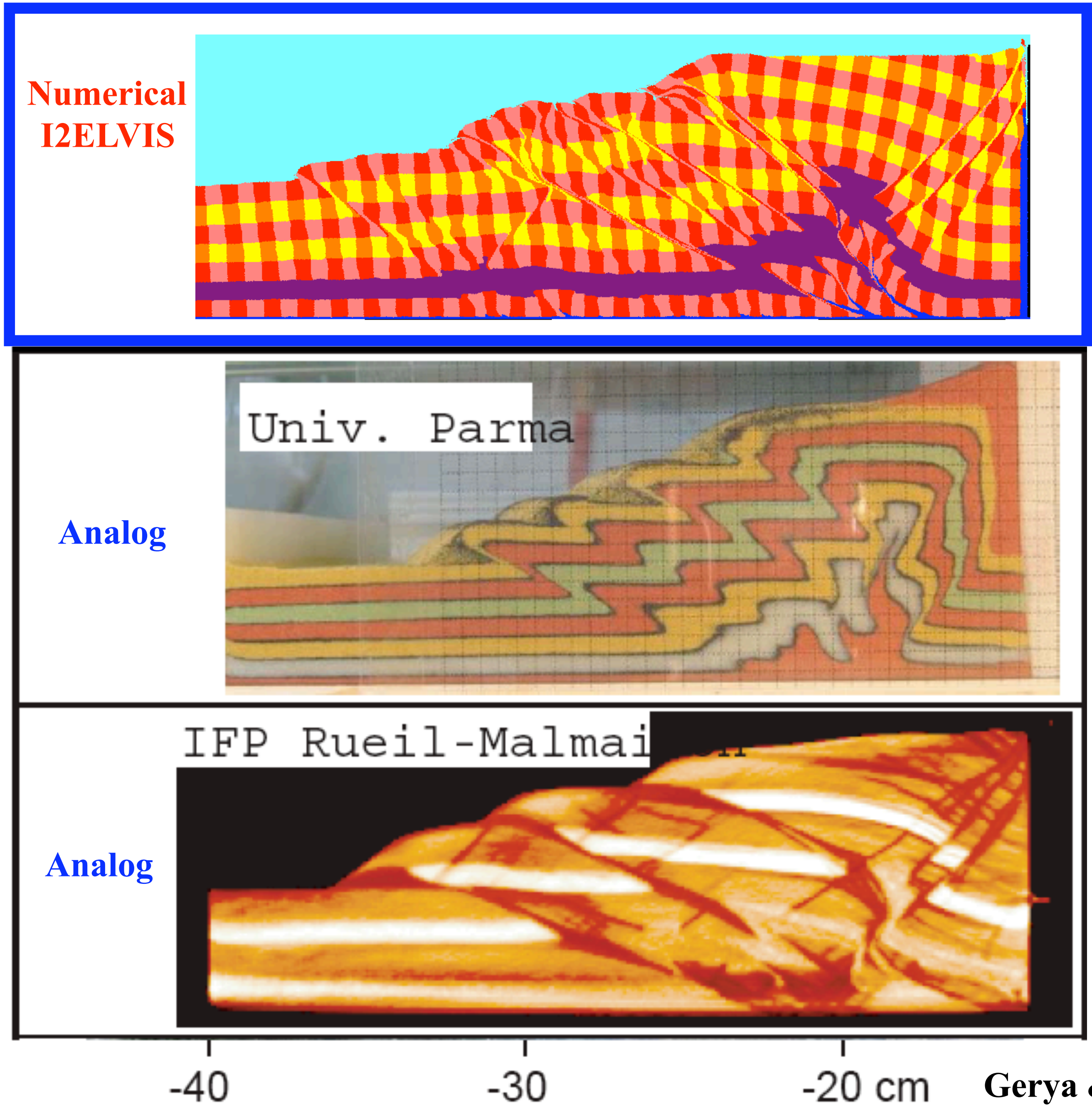

Gerya & Yuen (2007)

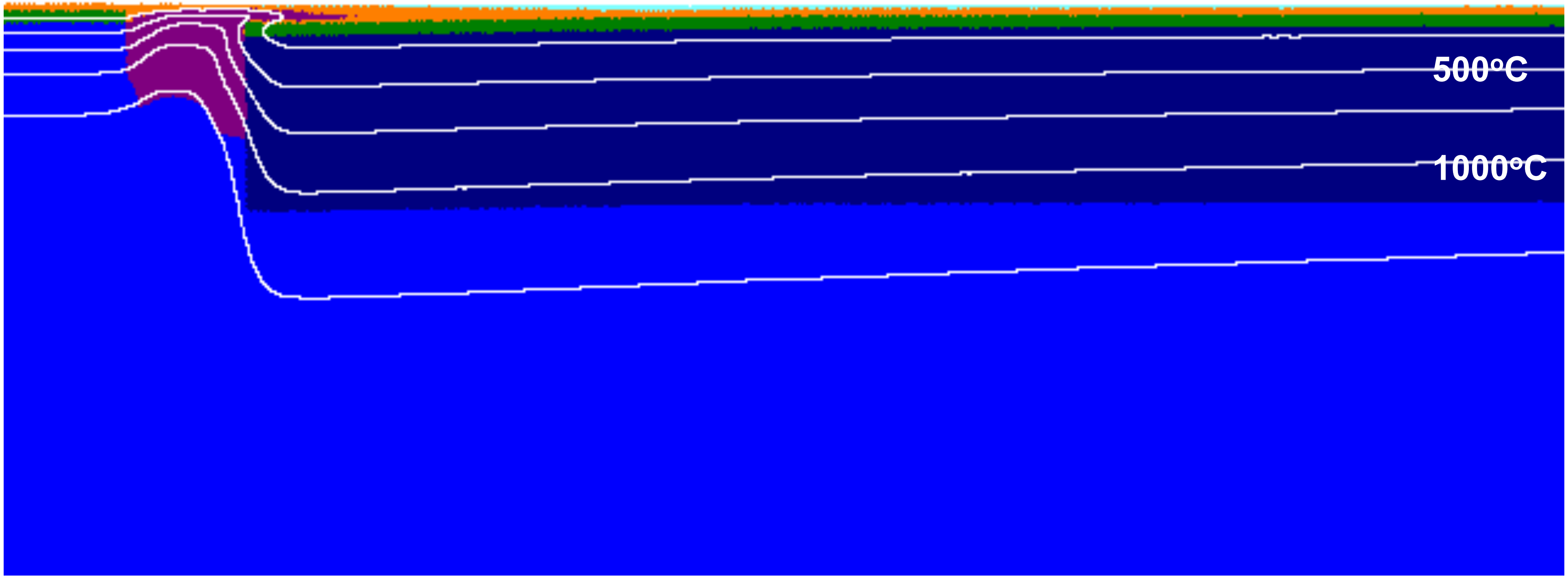

Viscoelastoplasticity is included

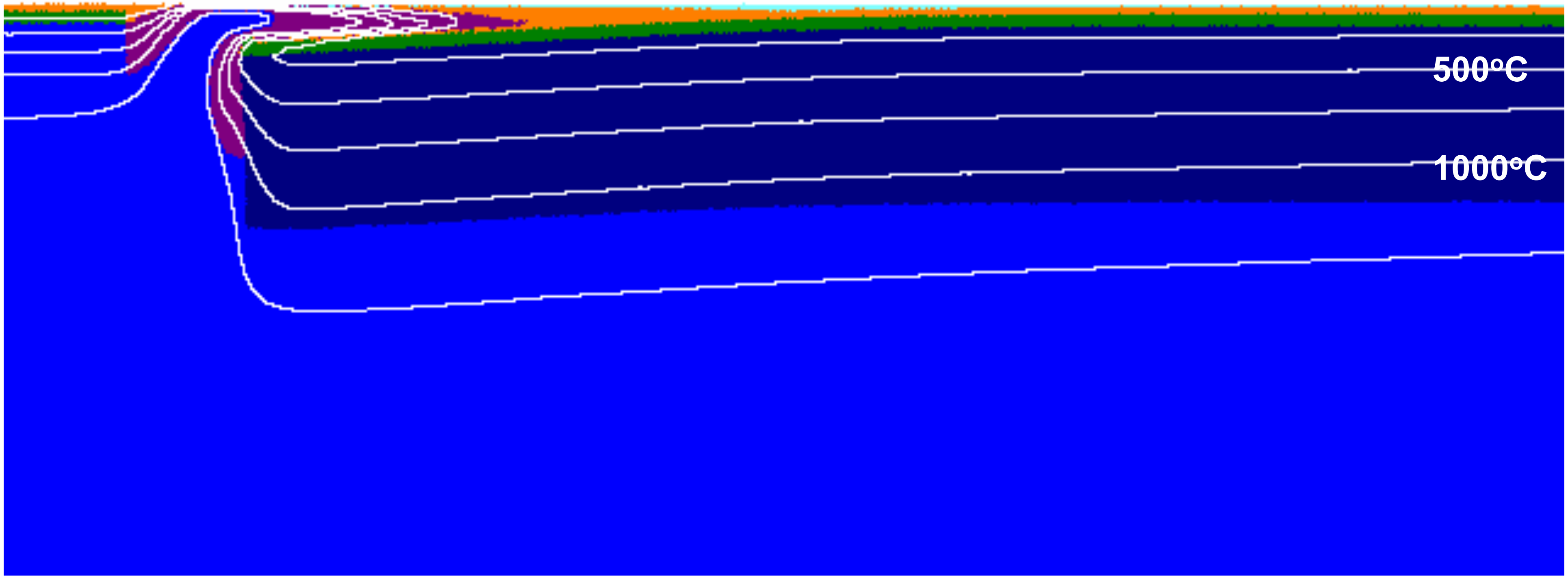
500°C
1000°C


Viscoelastoplasticity is included

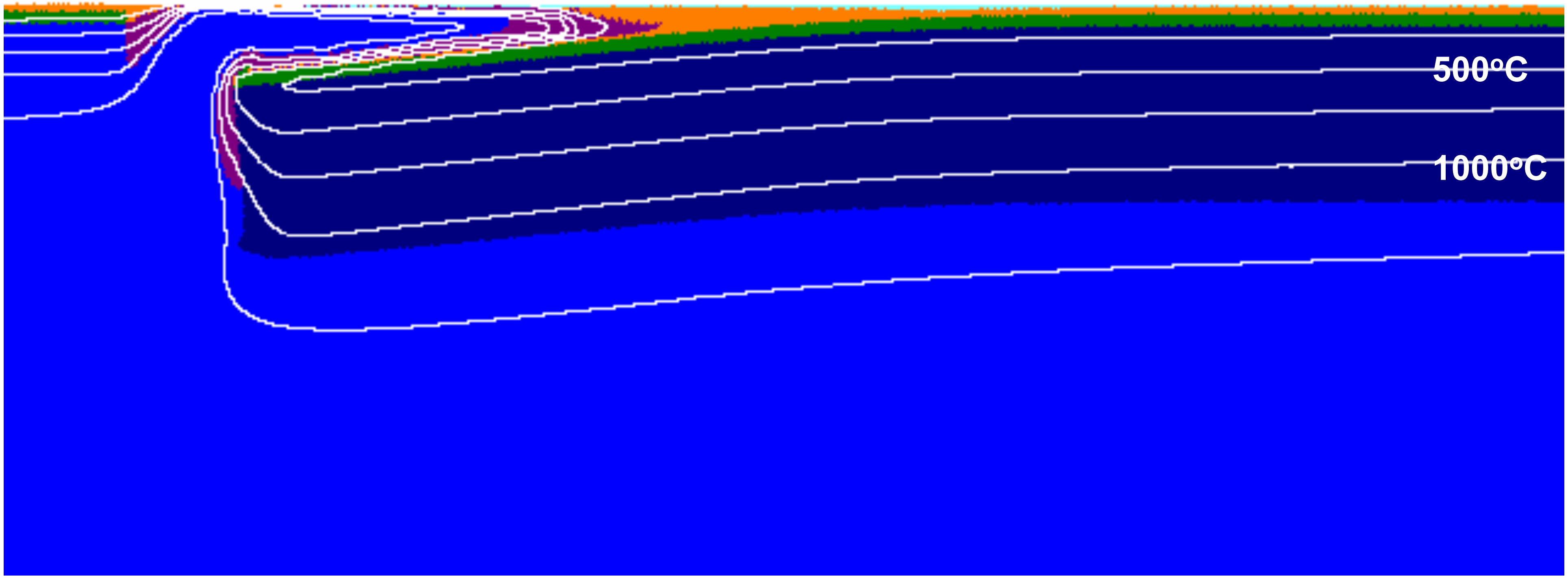
500°C
1000°C


Viscoelastoplasticity is included

Viscoelastoplasticity is included

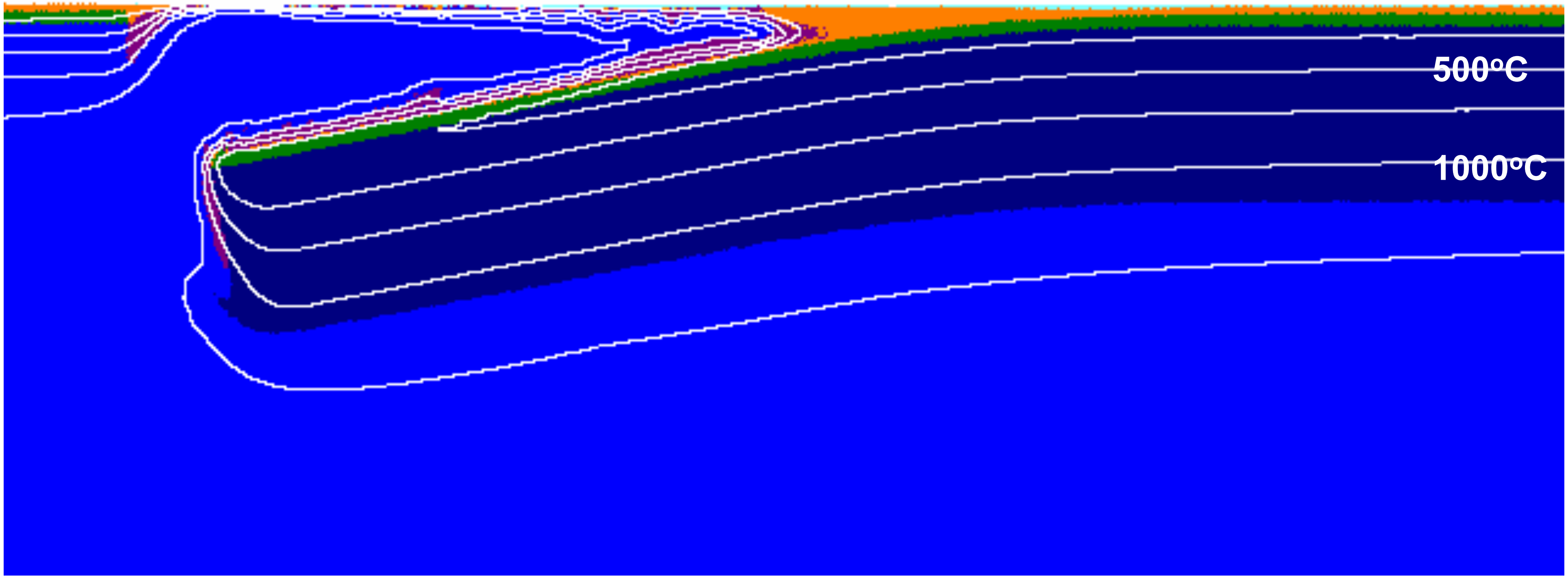
500°C
1000°C


Viscoelastoplasticity is included

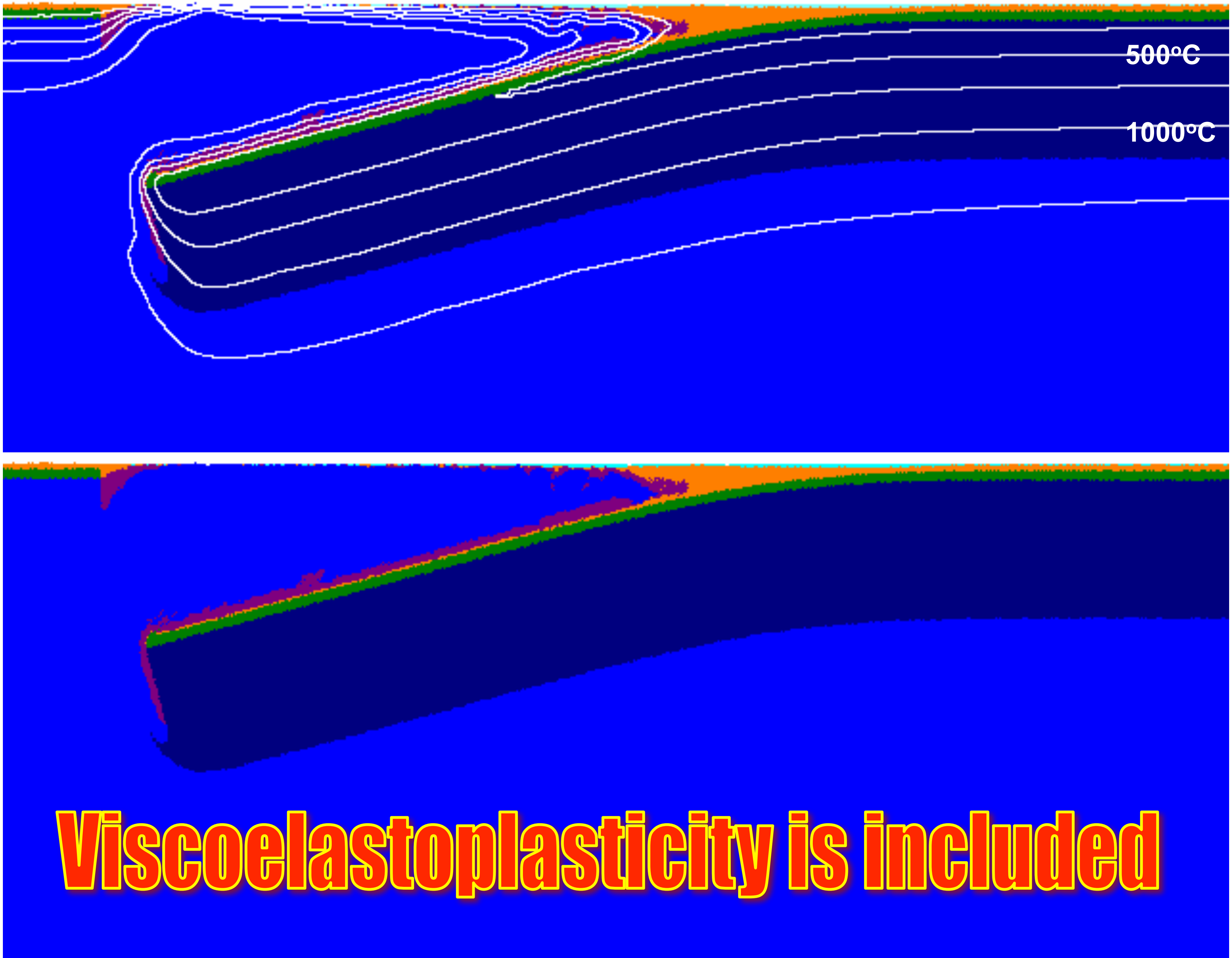
500°C
1000°C
Viscoelastoplasticity is included

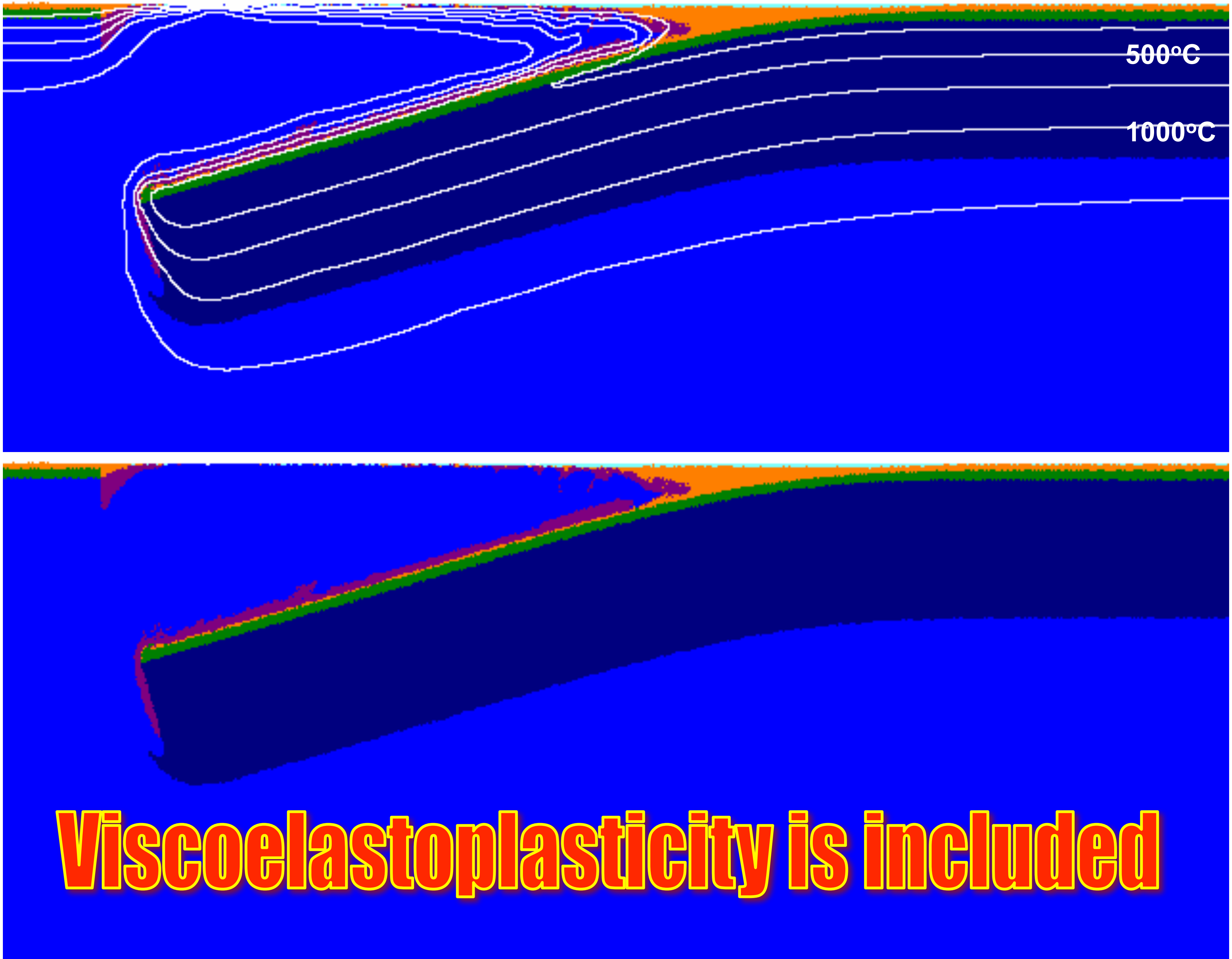

Viscoelastoplasticity is included

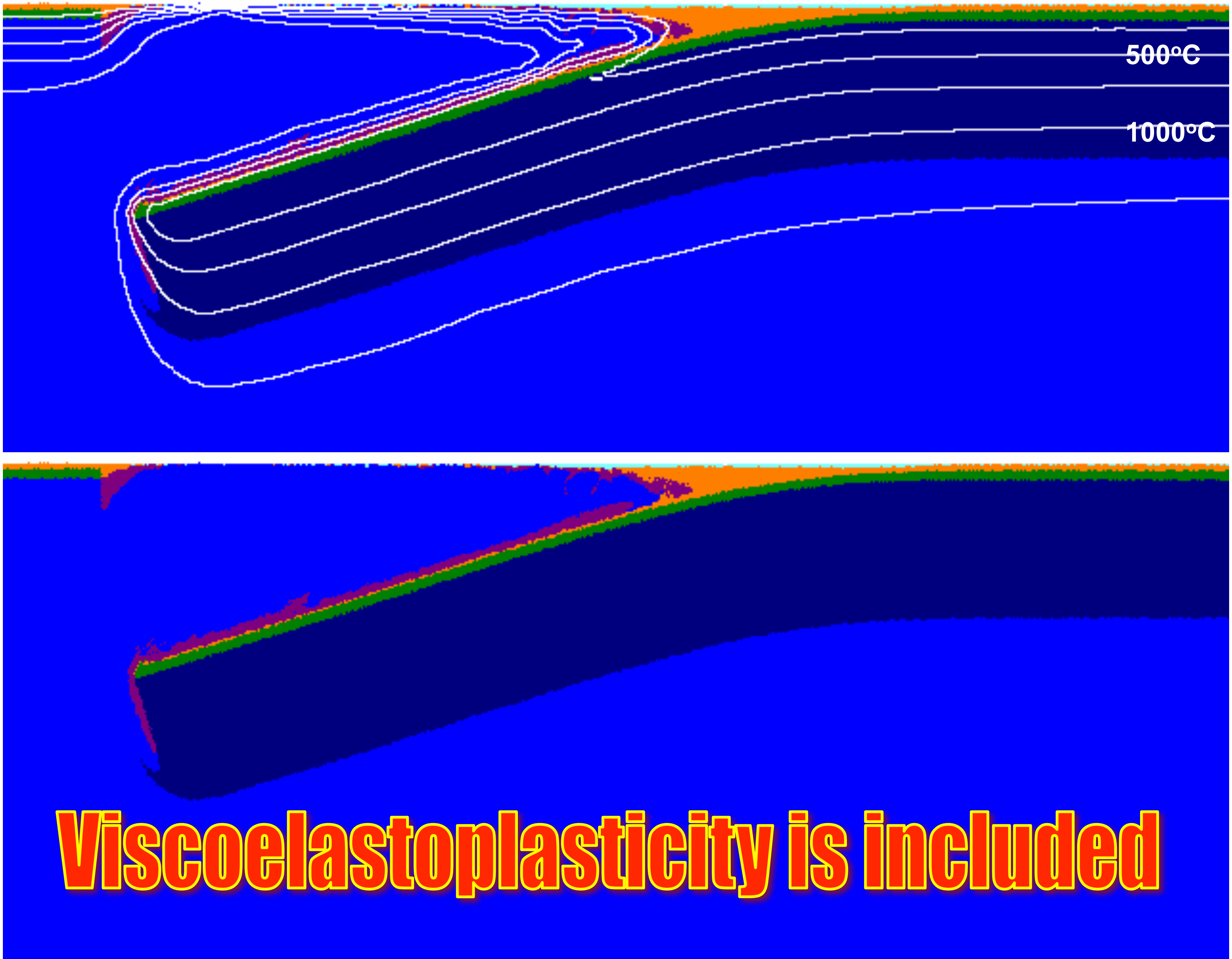

Viscoelastoplasticity is included

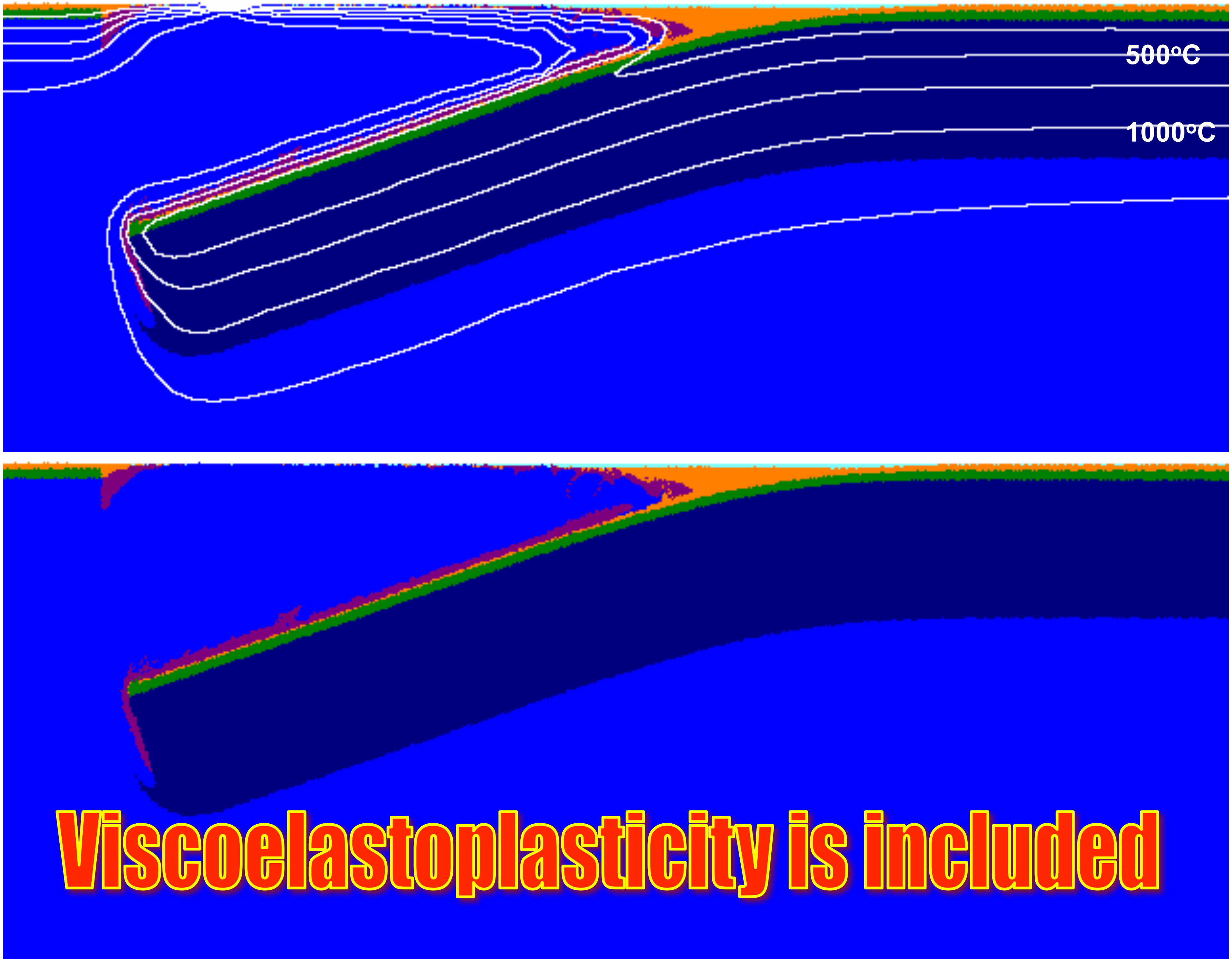
500°C
1000°C
Viscoelastoplasticity is included

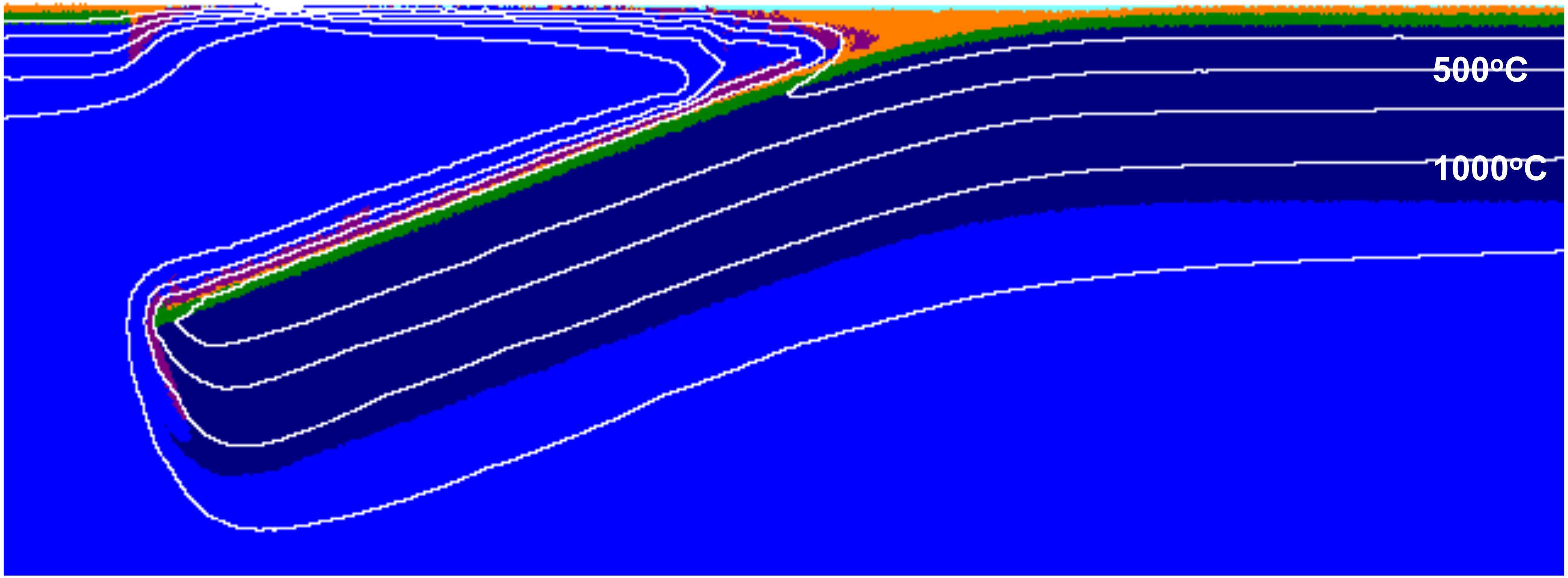
500°C
1000°C


Viscoelastoplasticity is included

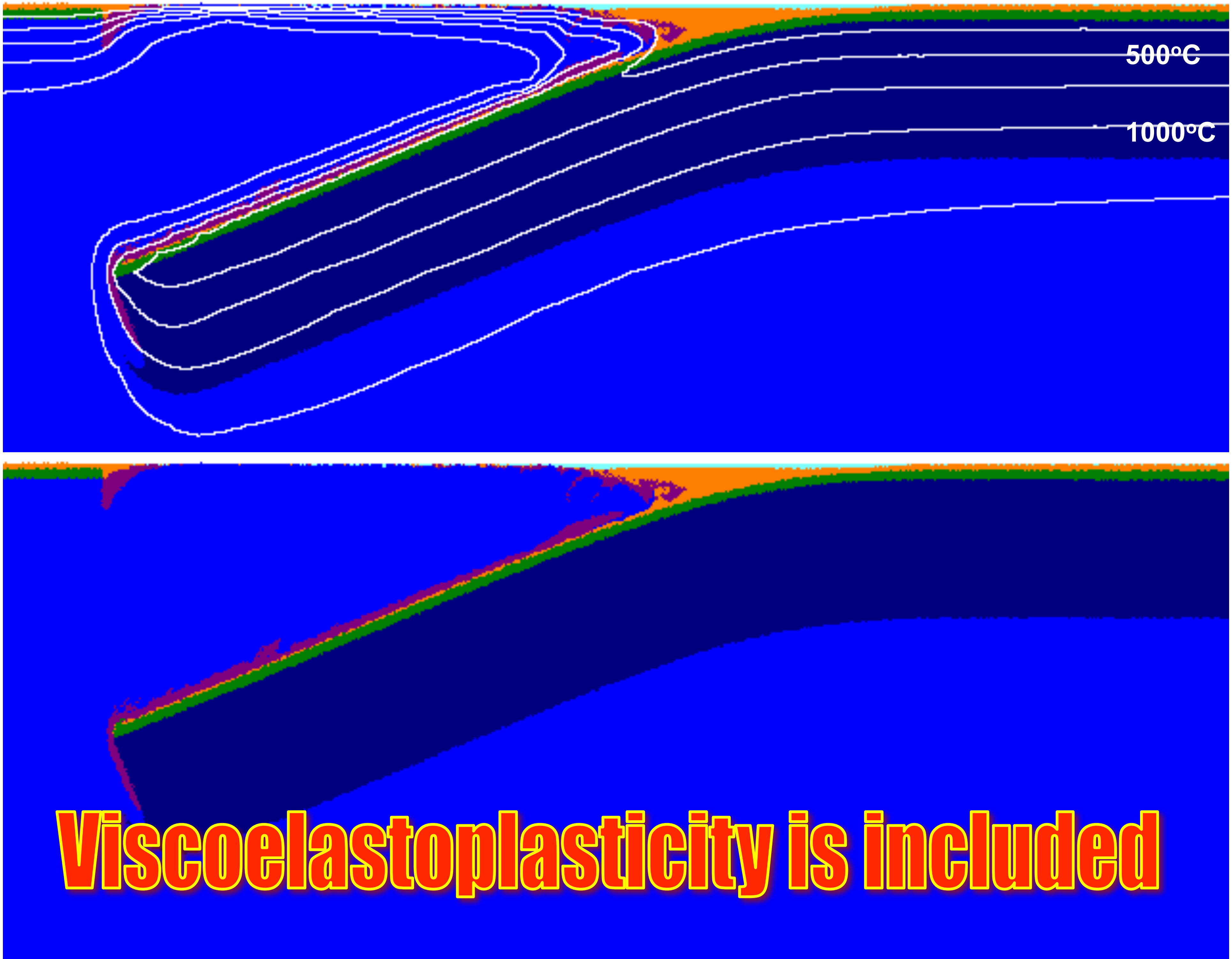

Viscoelastoplasticity is included

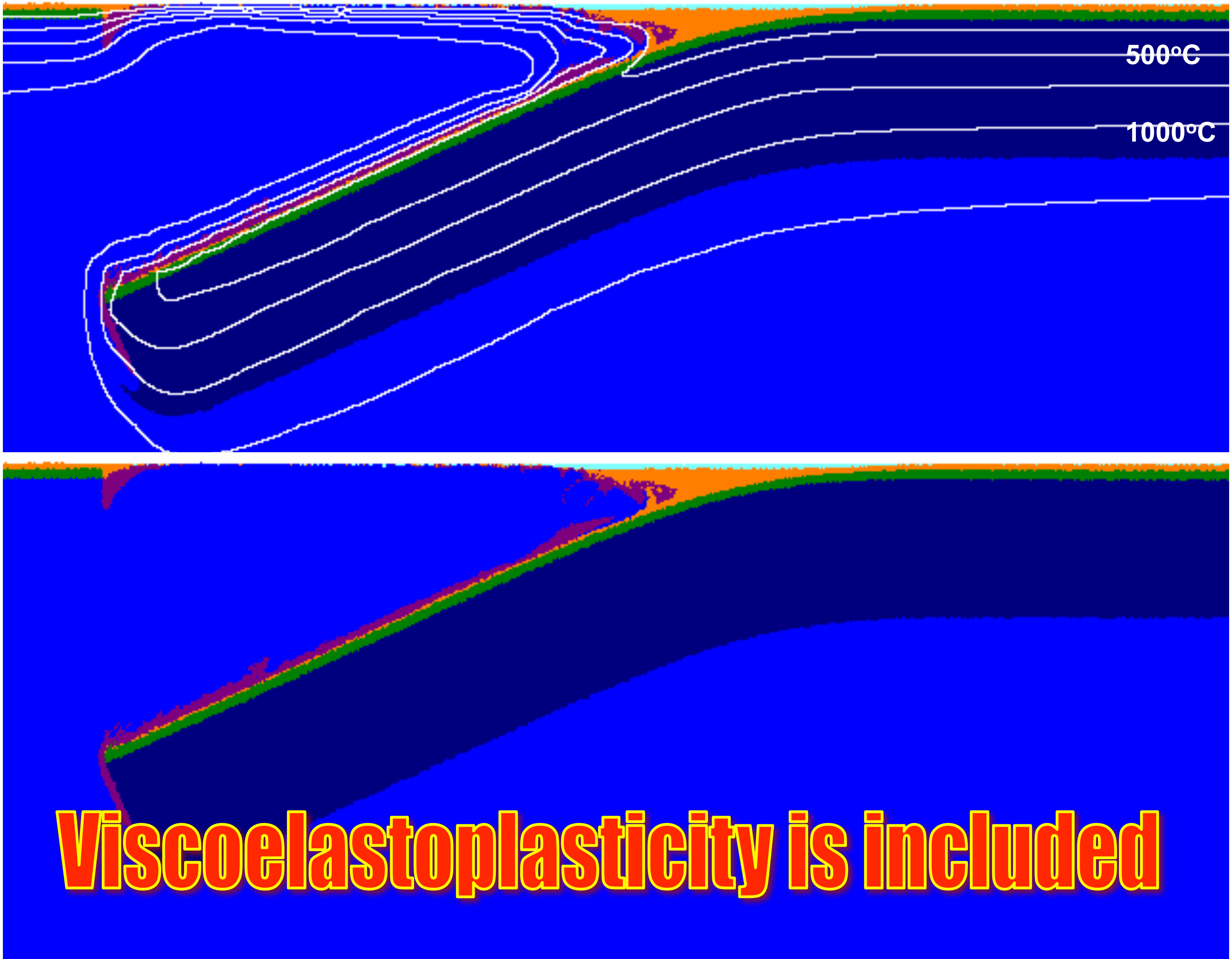
500°C
1000°C
Viscoelastoplasticity is included

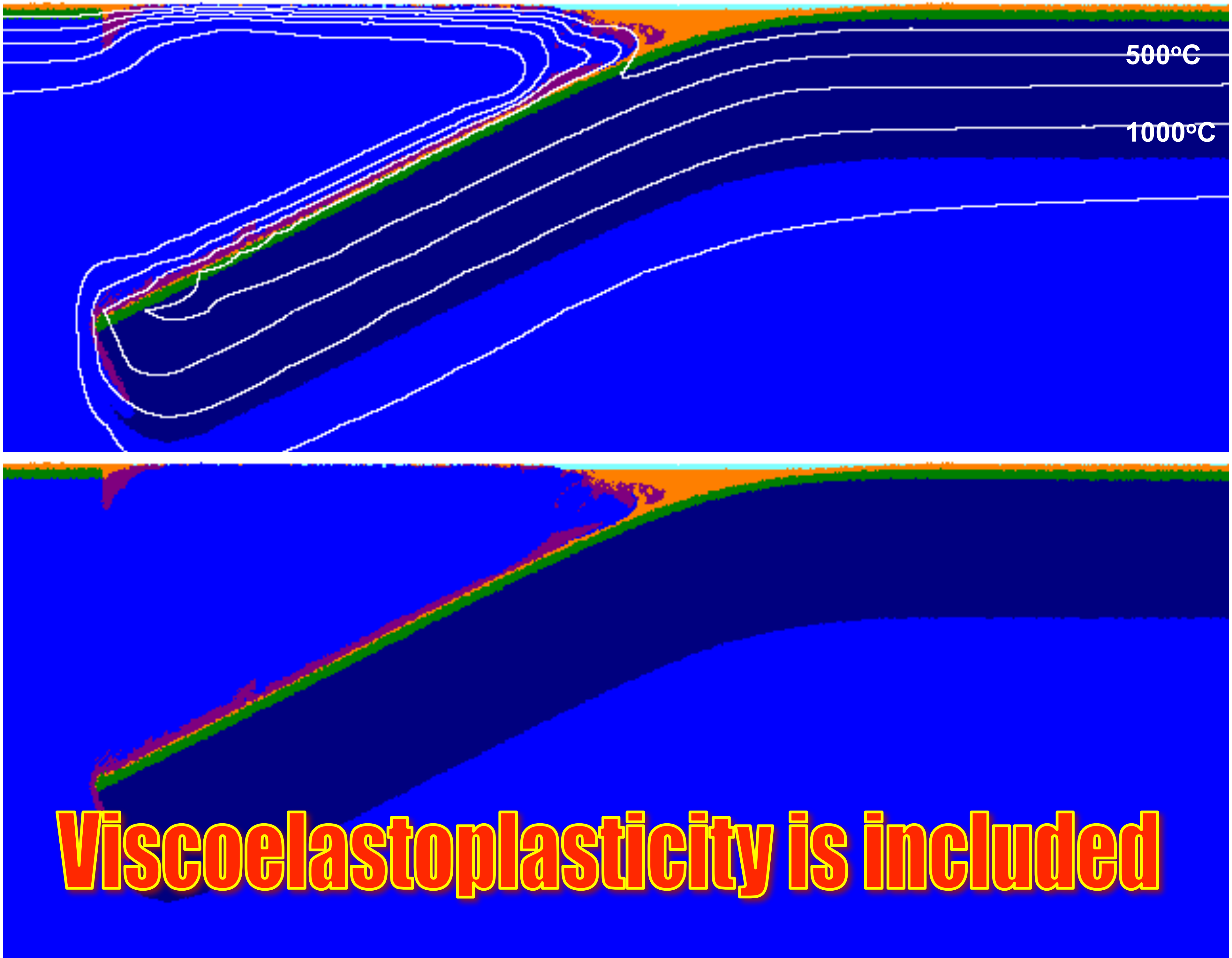
500°C
1000°C
Viscoelastoplasticity is included

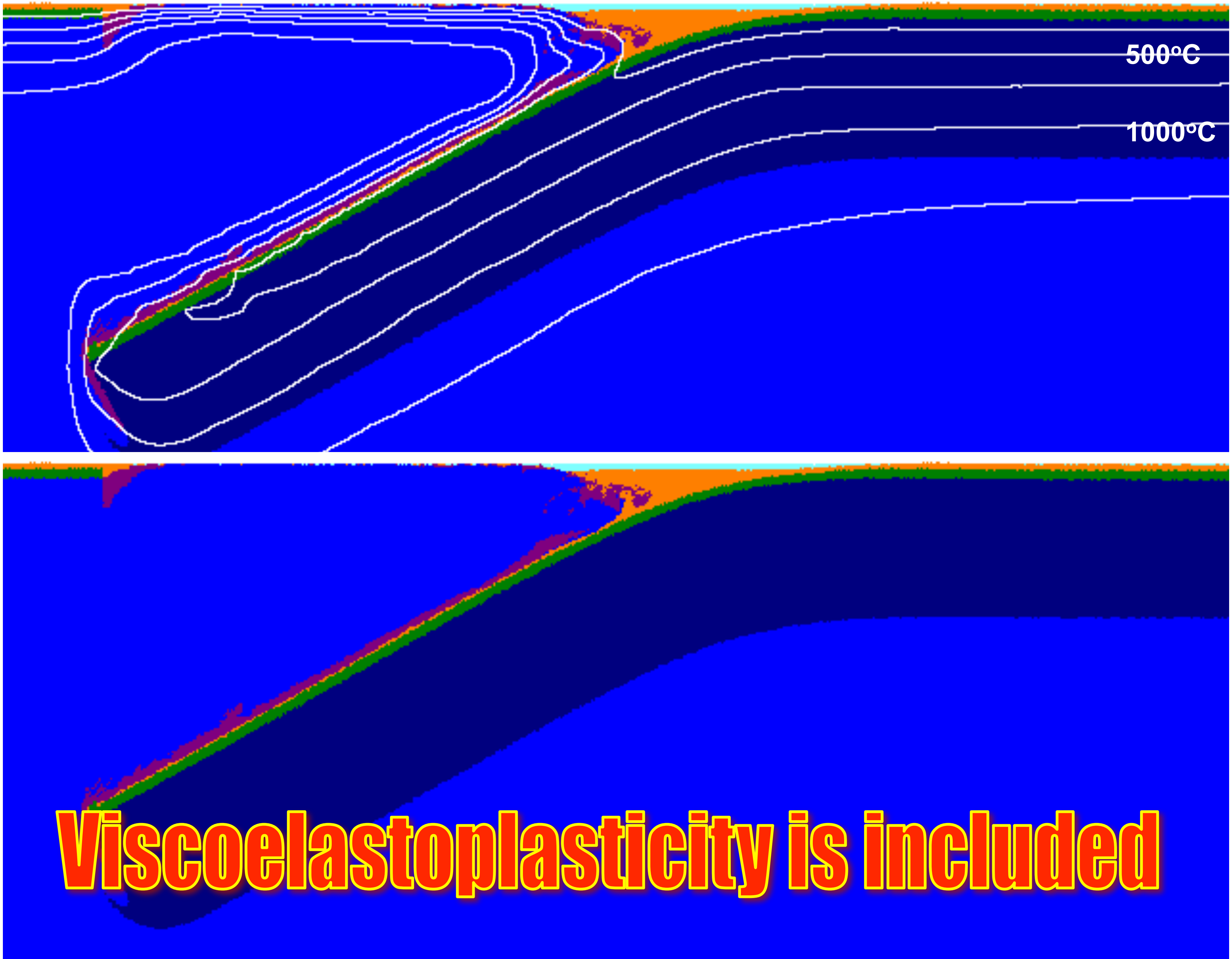
500°C
1000°C
Viscoelastoplasticity is included

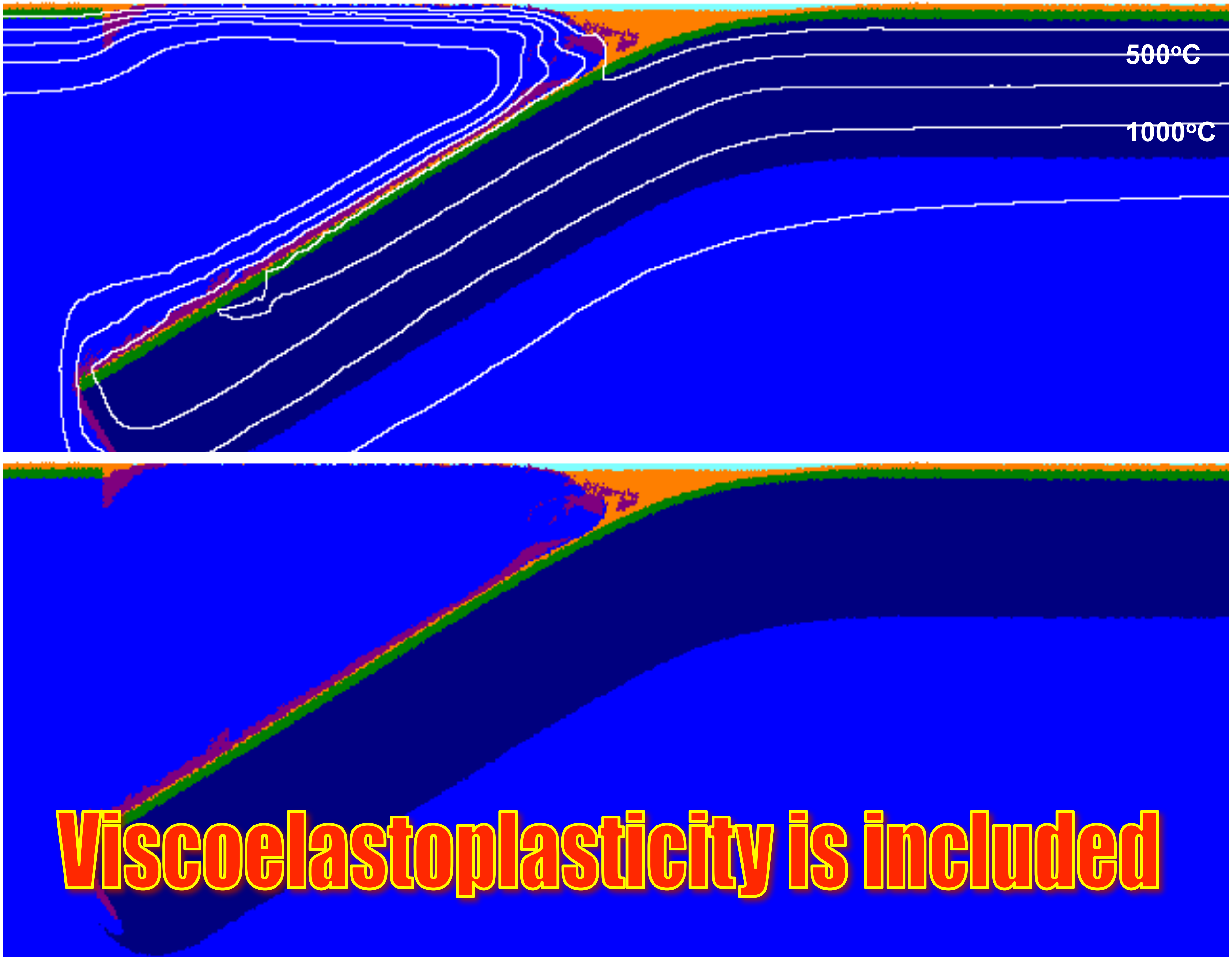

500°C
1000°C
Viscoelastoplasticity is included

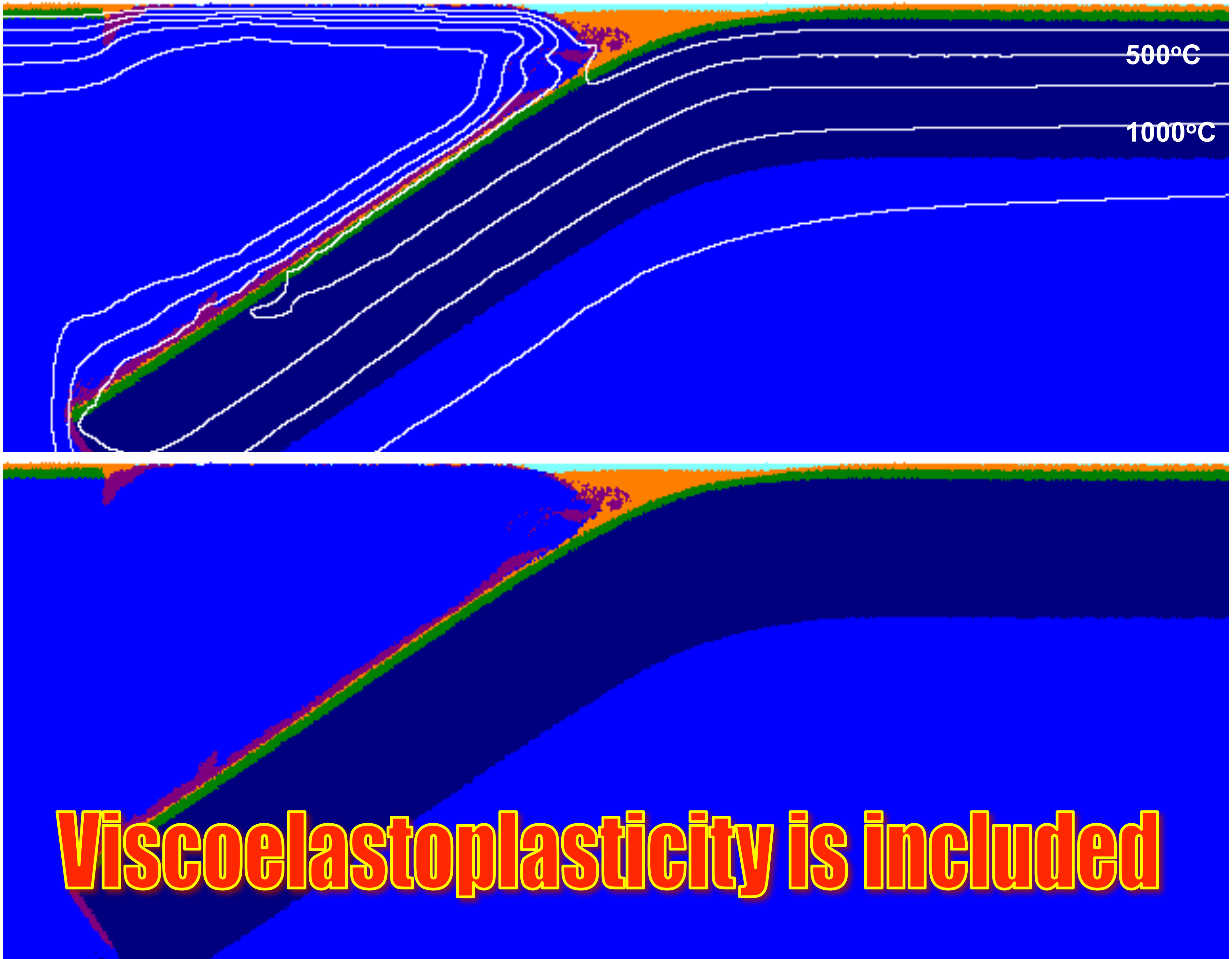

Viscoelastoplasticity is included

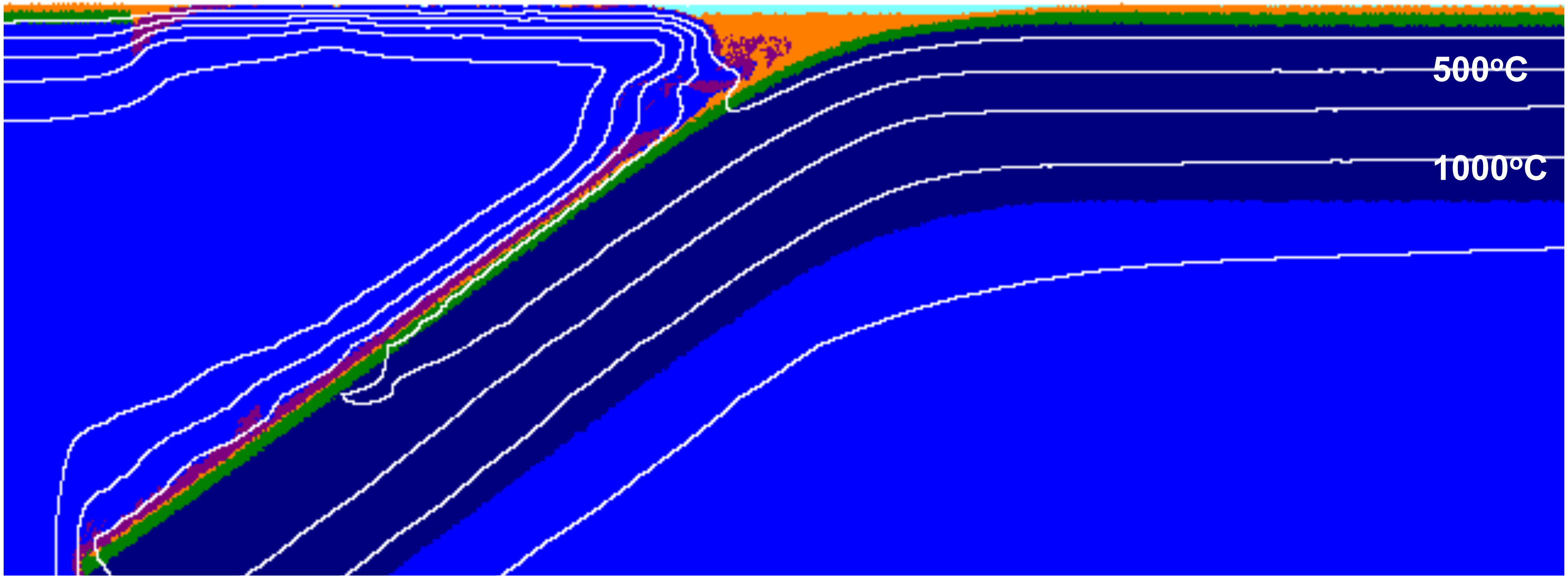
500ºC
1000ºC


Viscoelastoplasticity is included

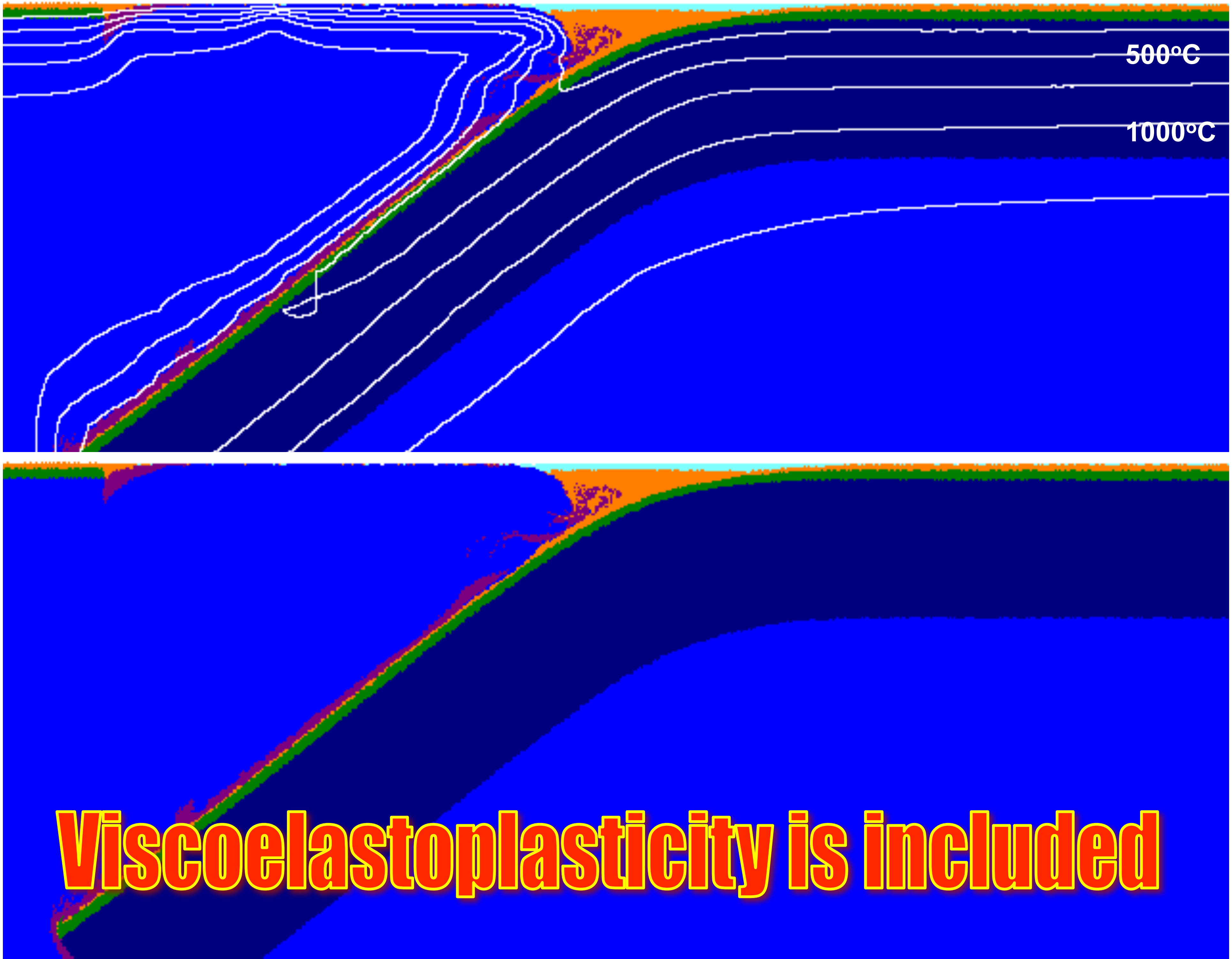
500°C
1000°C
Viscoelastoplasticity is included

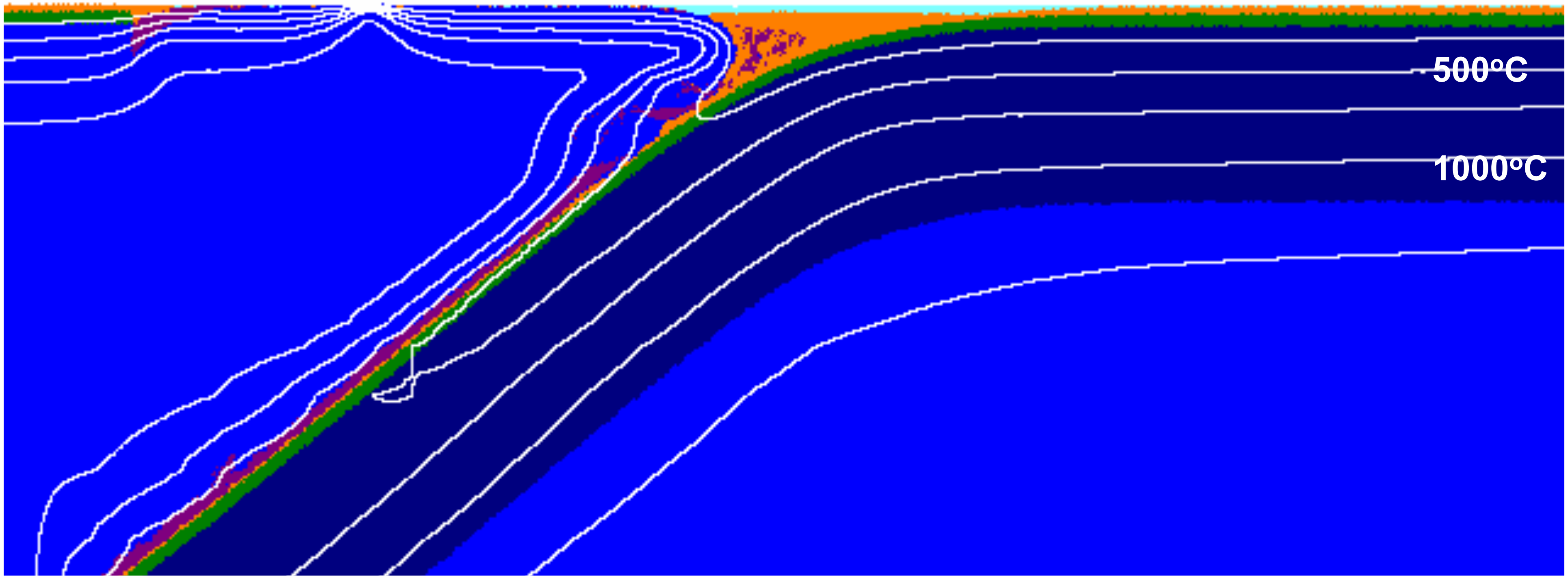

Viscoelastoplasticity is included

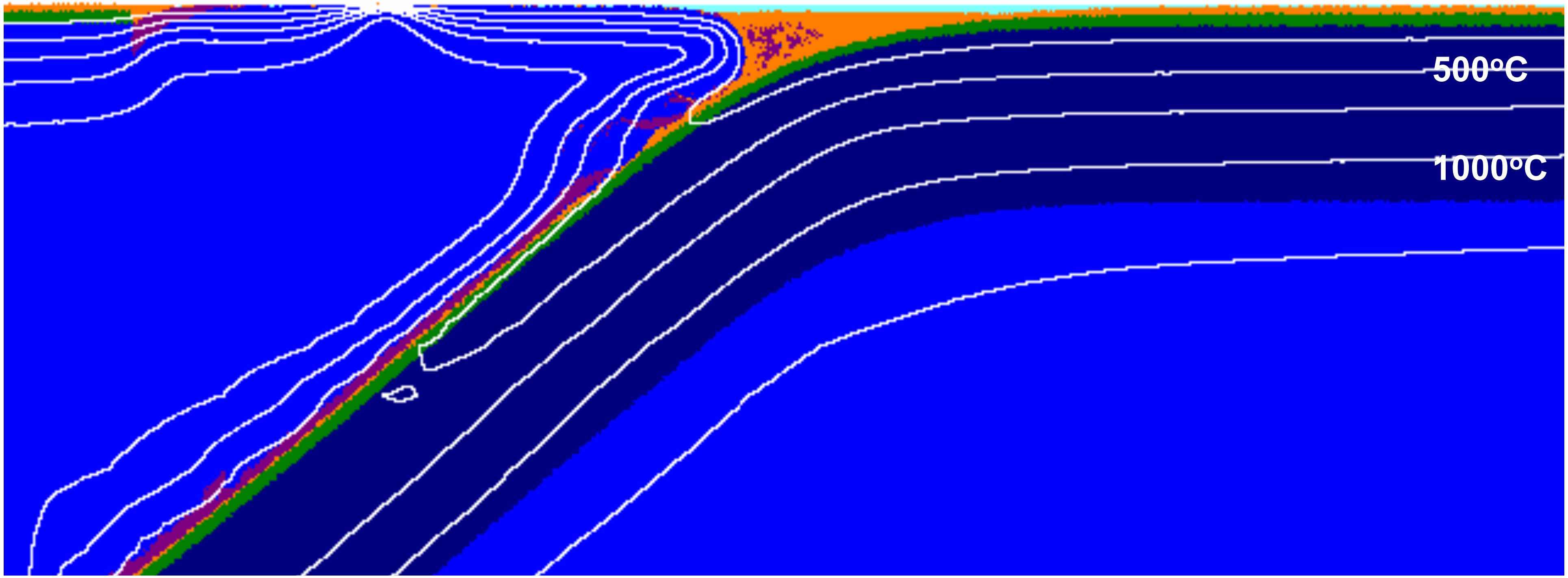
500°C
1000°C


Viscoelastoplasticity is included


500ºC
1000ºC
Viscoelastoplasticity is included

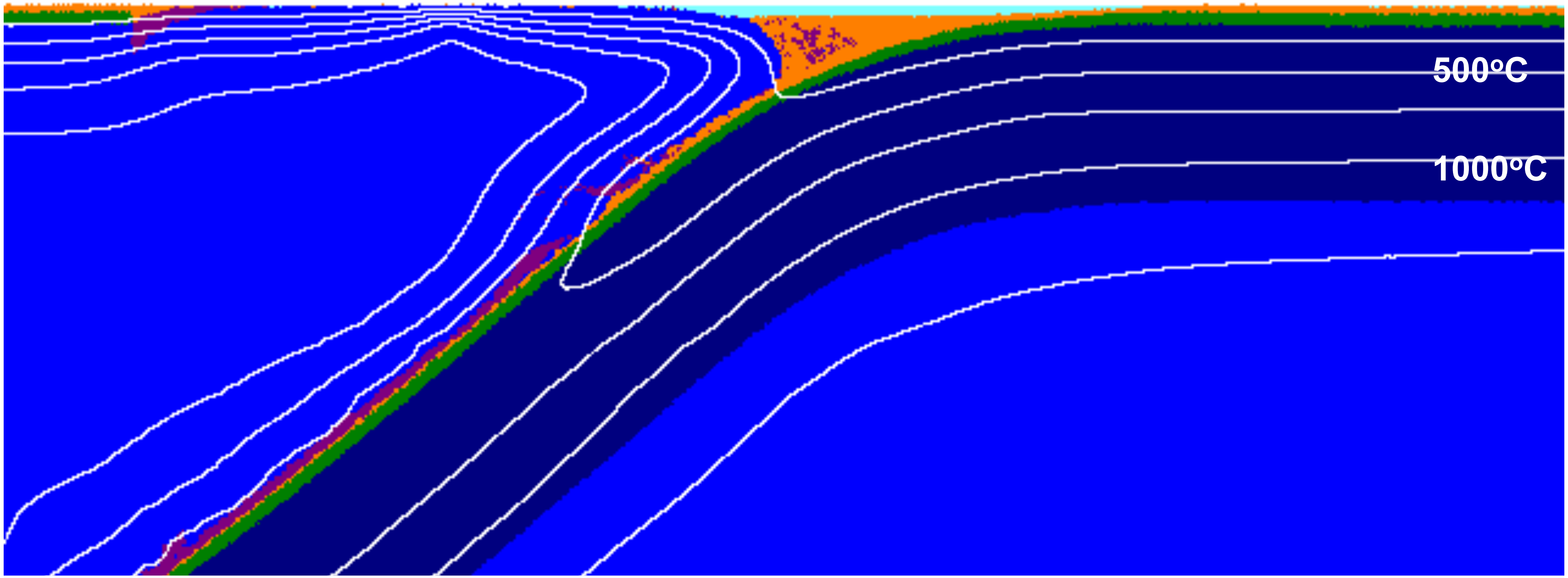
500°C
1000°C


Viscoelastoplasticity is included

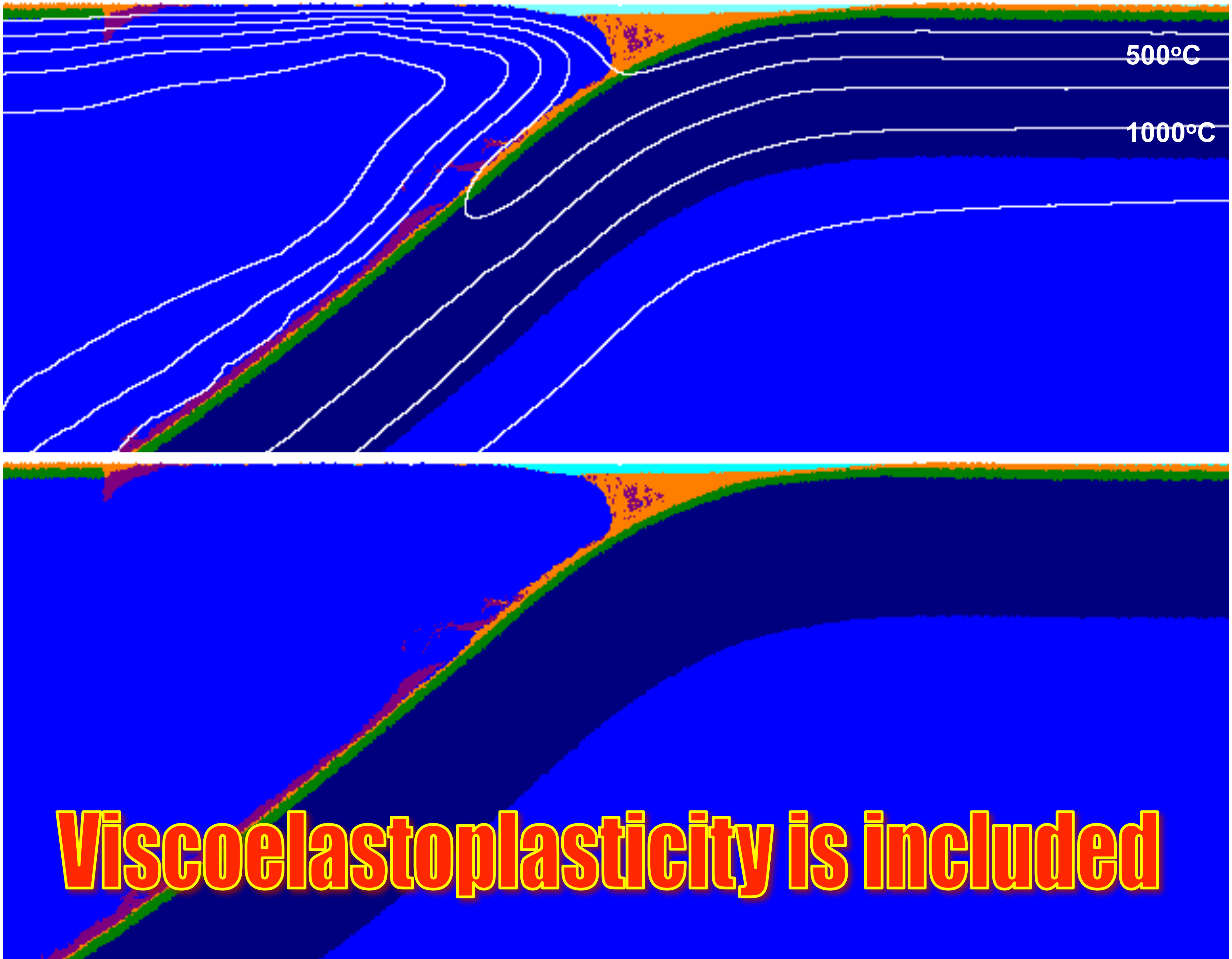

500°C
1000°C
Viscoelastoplasticity is included

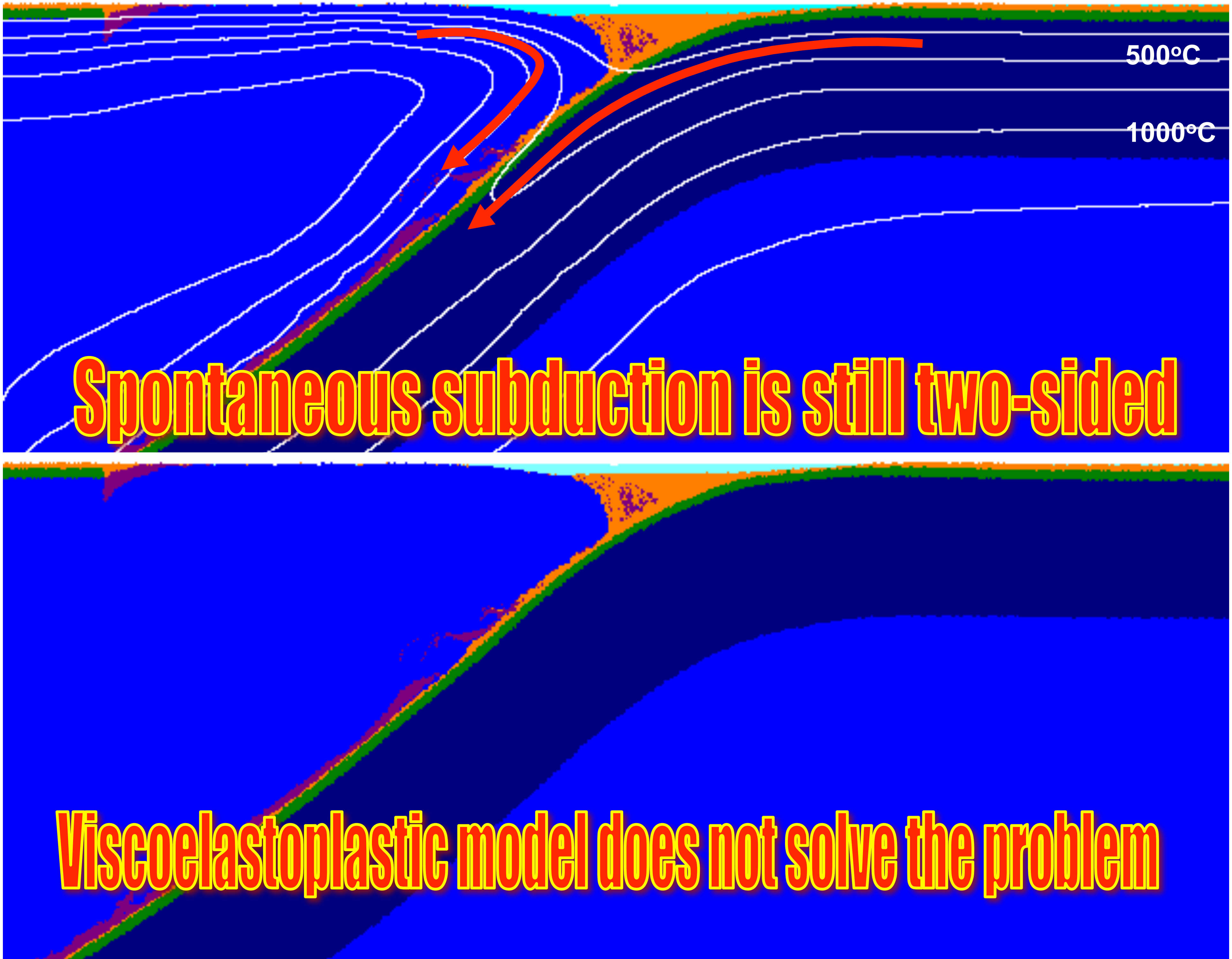

500°C
1000°C
Spontaneous subduction is still two-sided
Viscoelastoplastic model does not solve the problem

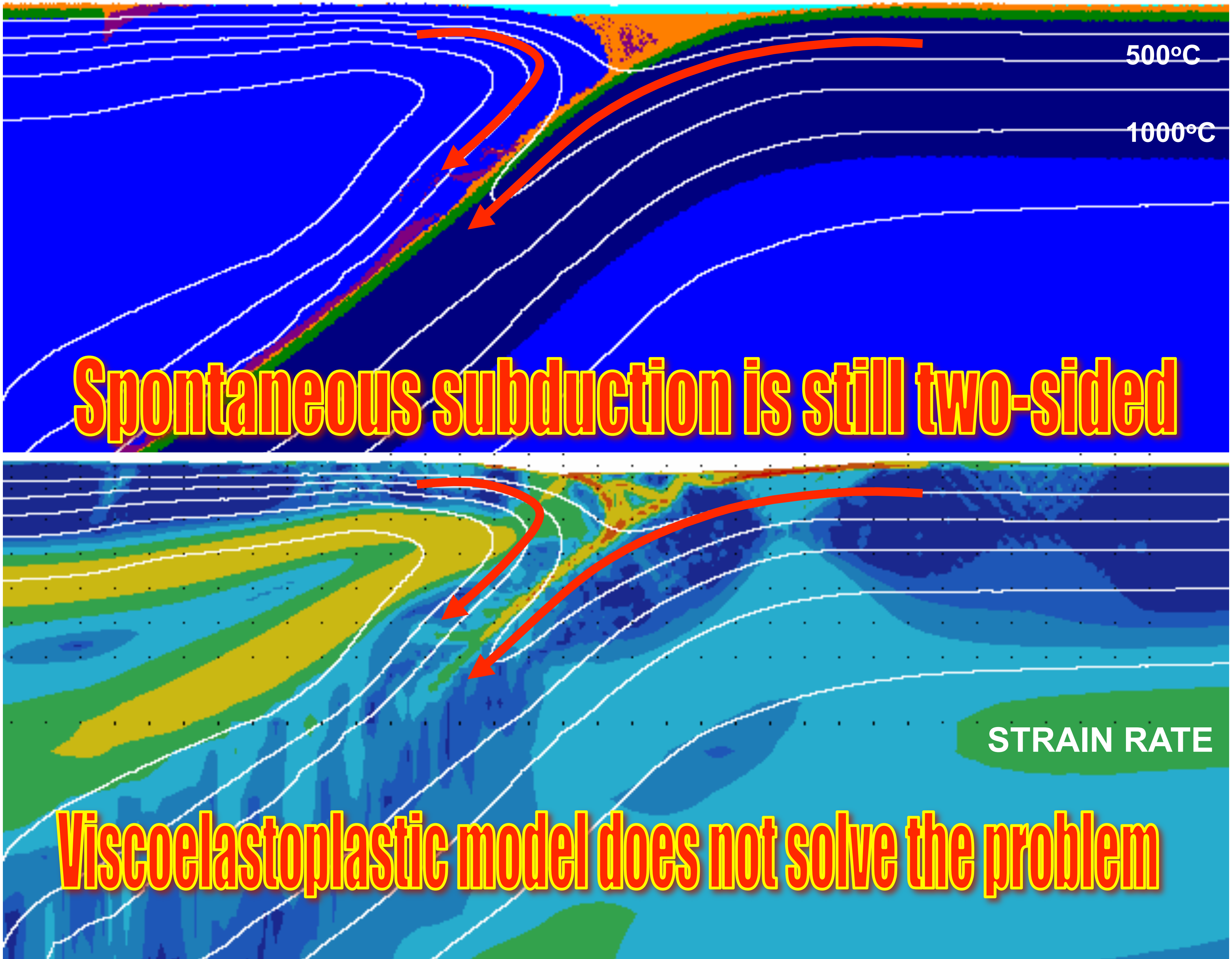

500°C
1000°C
Spontaneous subduction is still two-sided
STRAIN RATE
Viscoelastoplastic model does not solve the problem

What is forgotten ?

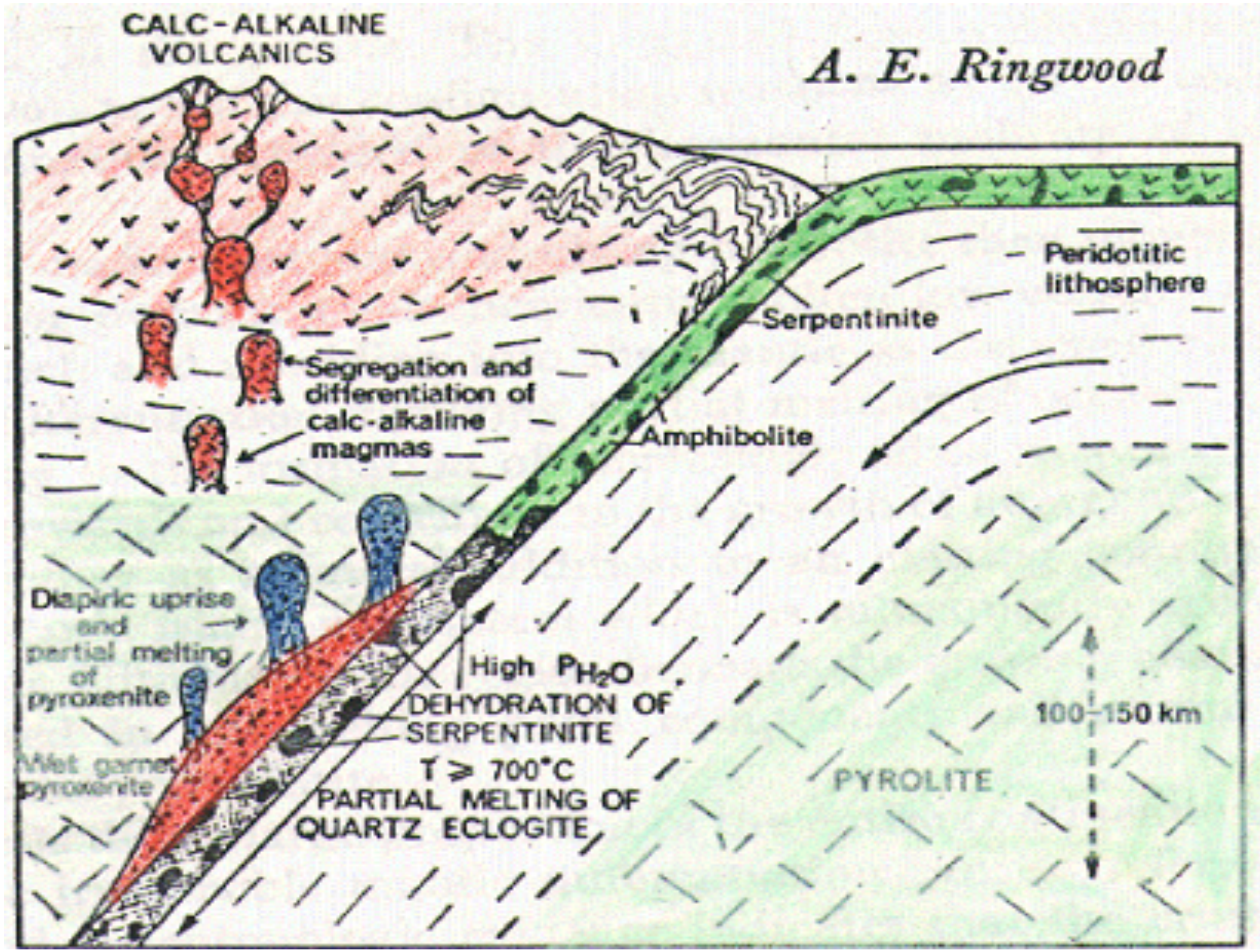

Fluids and melts!

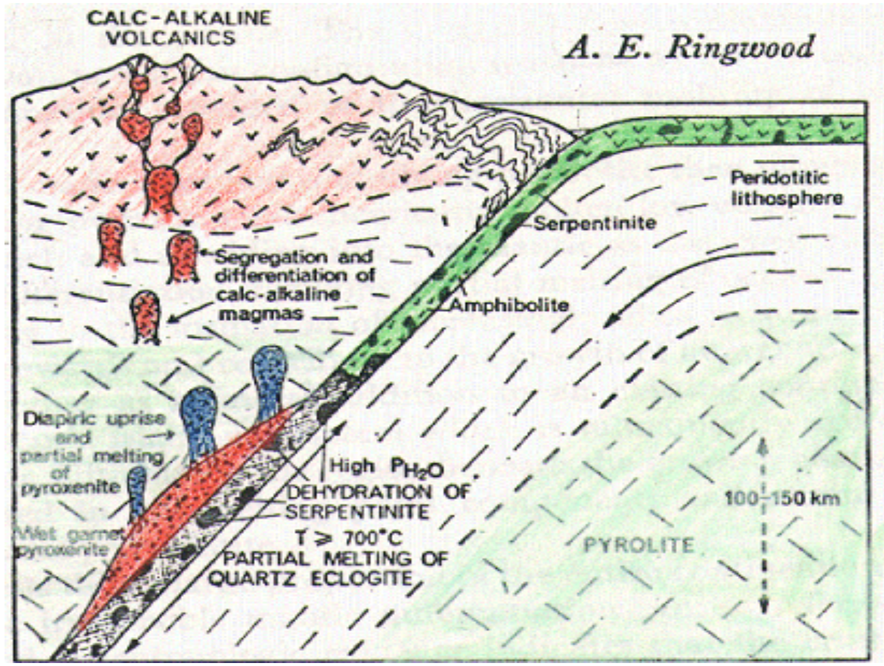

Fluids and melts

We employ a visco-elasto-plastic rheology with experimentally calibrated flow laws and elastic shear moduli computed from stable phase assemblages for each lithology (*8*). The plastic strength is taken to be dependent on pore fluid pressure P_{fluid} such that (*13*):

$$\sigma_{yield} = cos(\varphi)C + sin(\varphi)P*(1-\lambda) \quad (3)$$

(4)

Plastic strength of the crust decreases with increasing pore fluid pressure

where C is cohesion (residual strength at P=0), φ is effective internal friction angle (φ_{dry} stands for dry rocks) and $\lambda = \frac{P_{fluid}}{P_{solid}}$ is the pore fluid pressure factor, $P_{solid} = P$ corresponds to mean stress on solids.

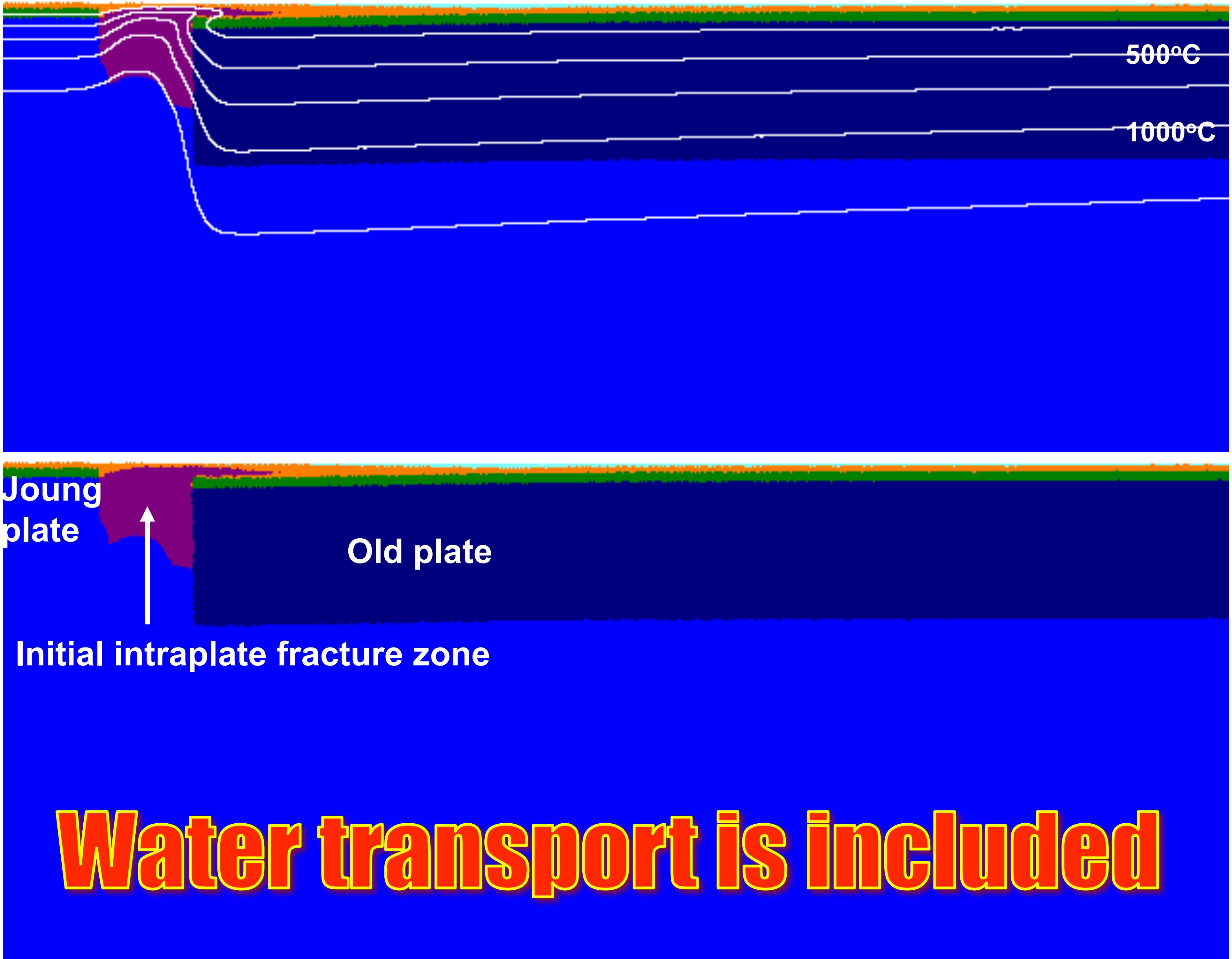
500°C
1000°C
Joung plate
Old plate
Initial intraplate fracture zone
Water transport is included

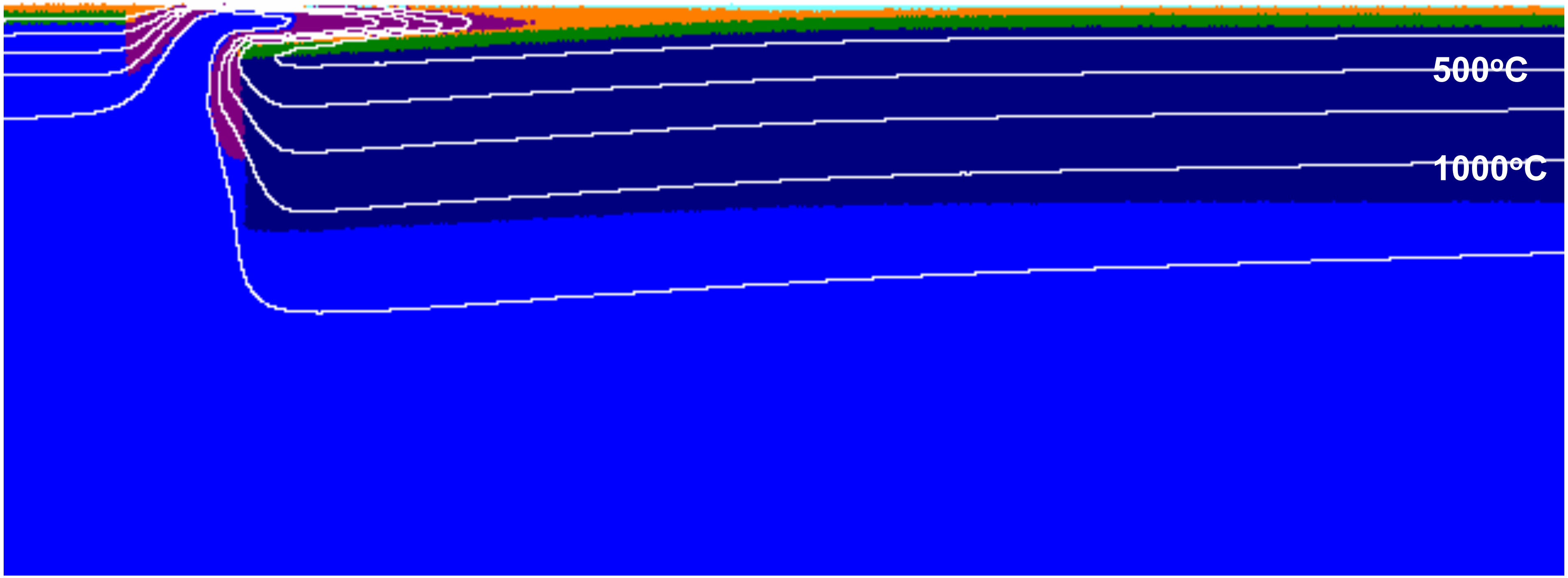
500°C
1000°C


Water transport is included

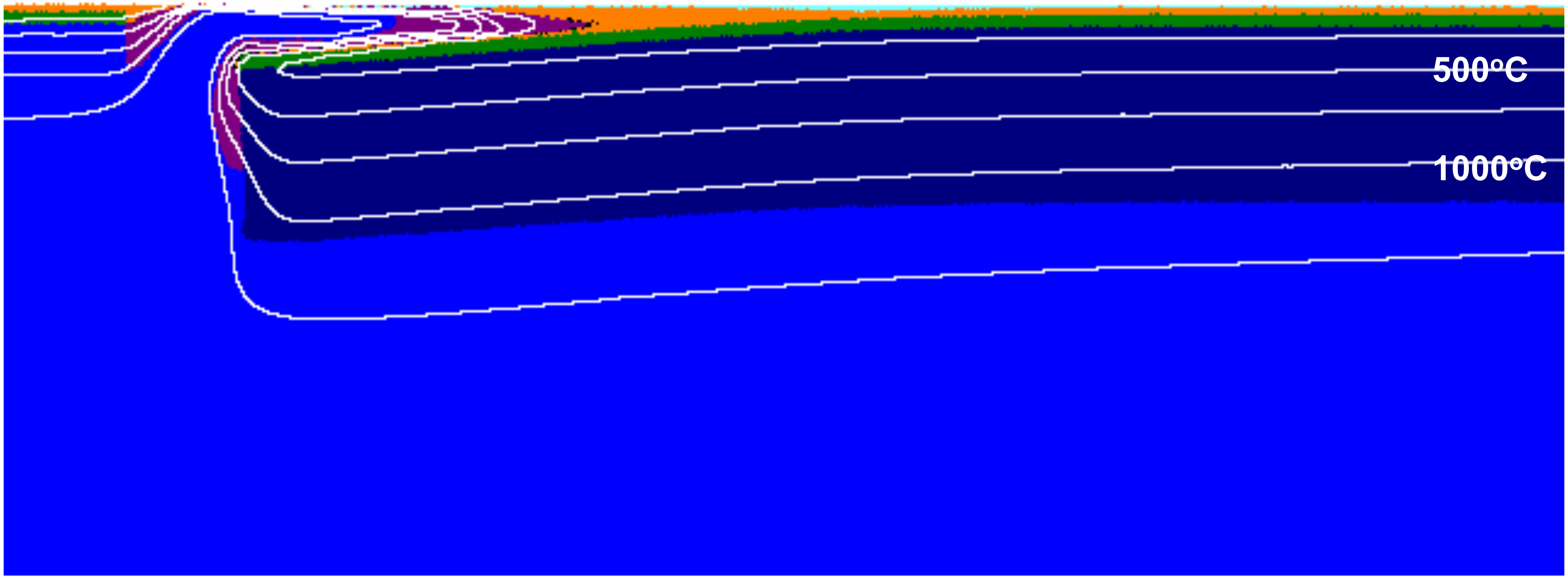

Water transport is included

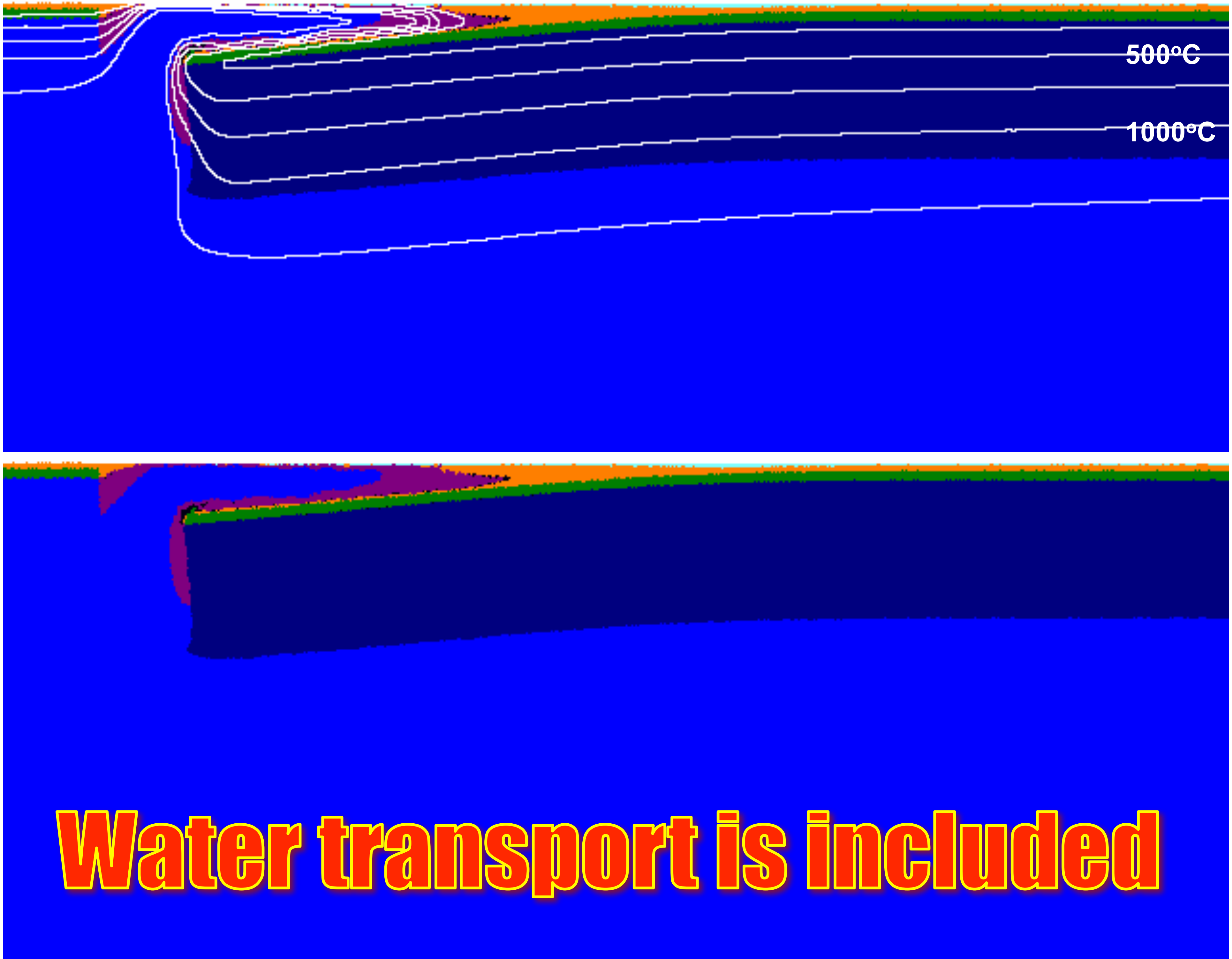
500°C
1000°C
Water transport is included

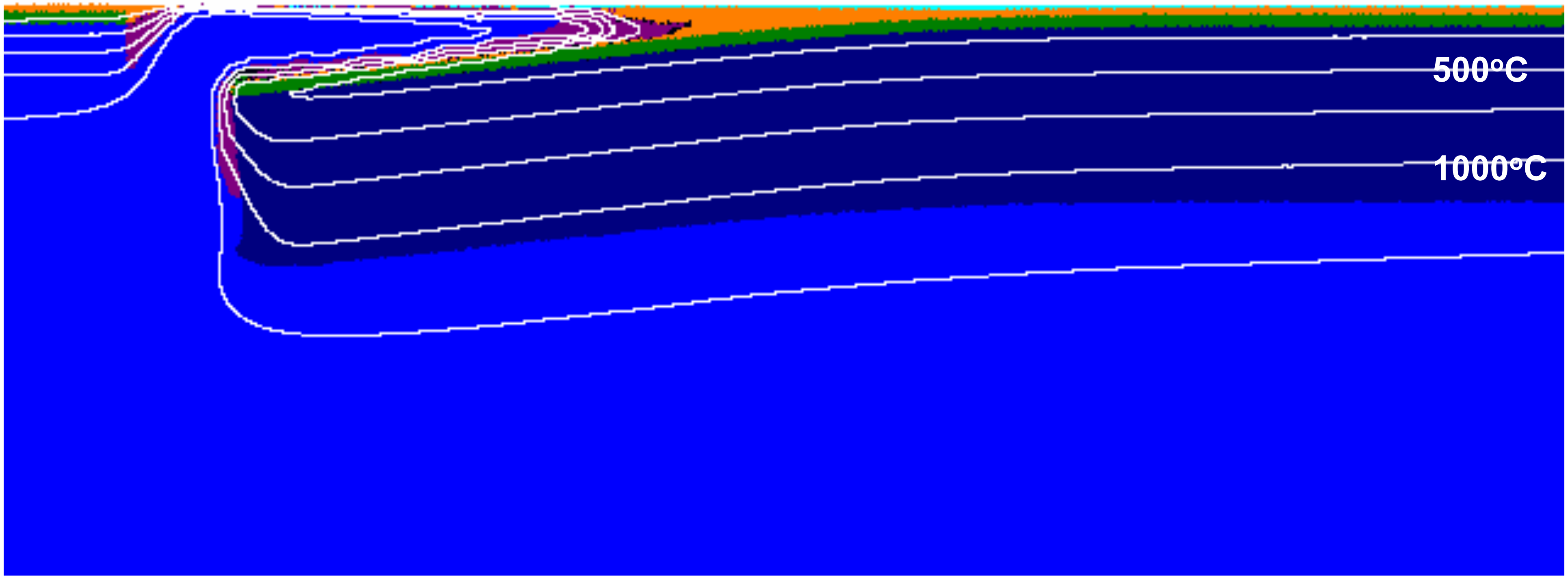
500°C
1000°C


Water transport is included

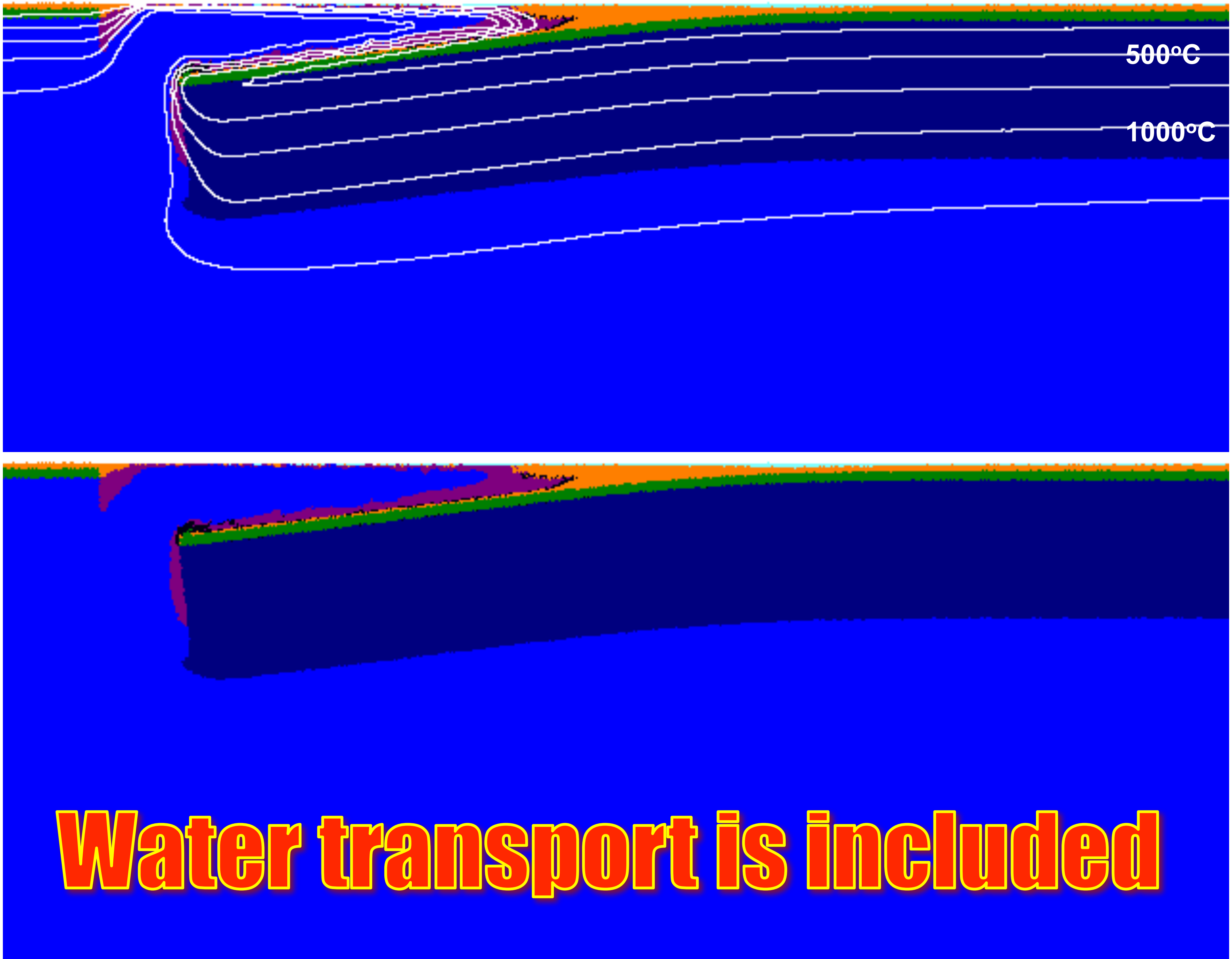
500°C
1000°C
Water transport is included

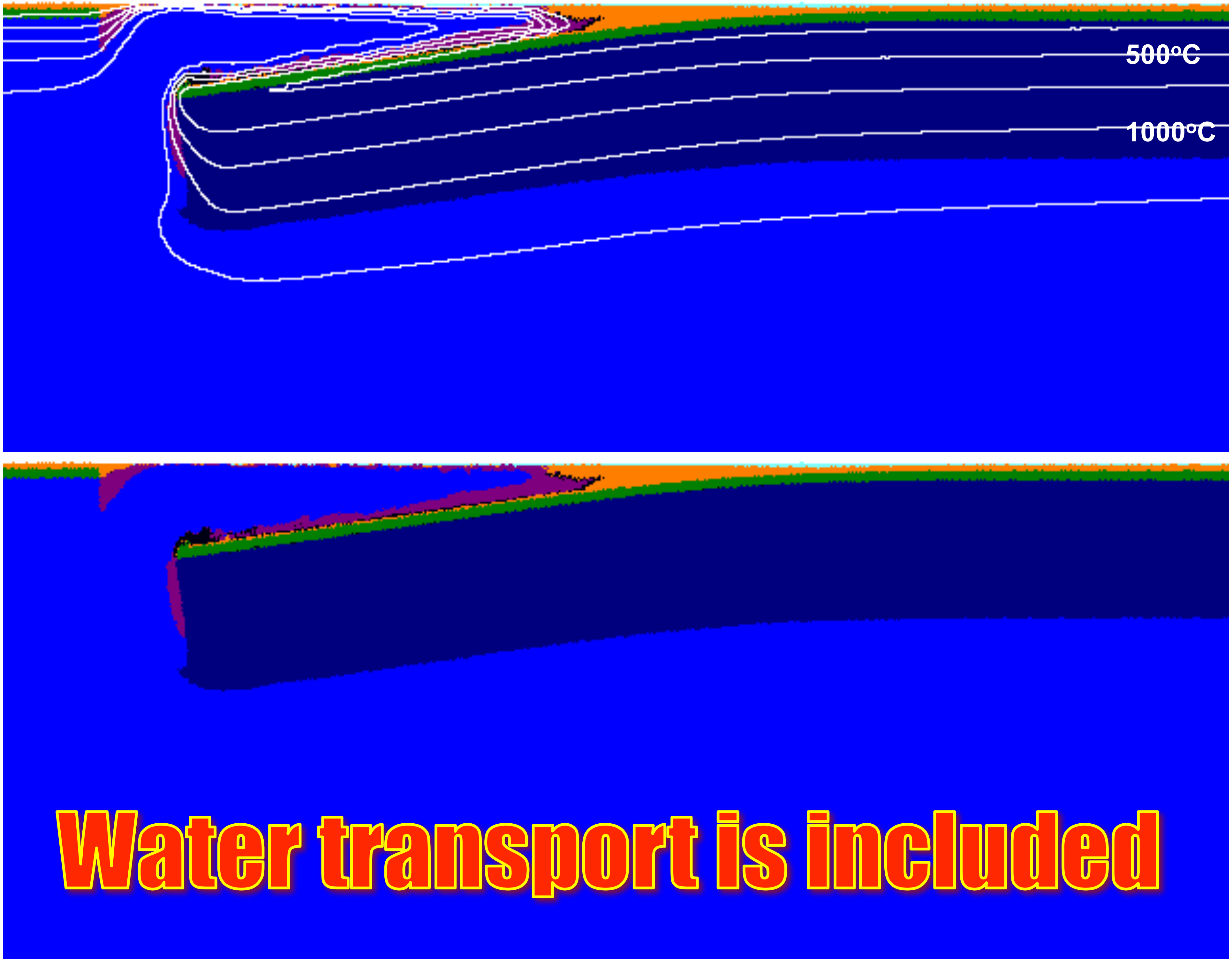

500°C
1000°C
Water transport is included

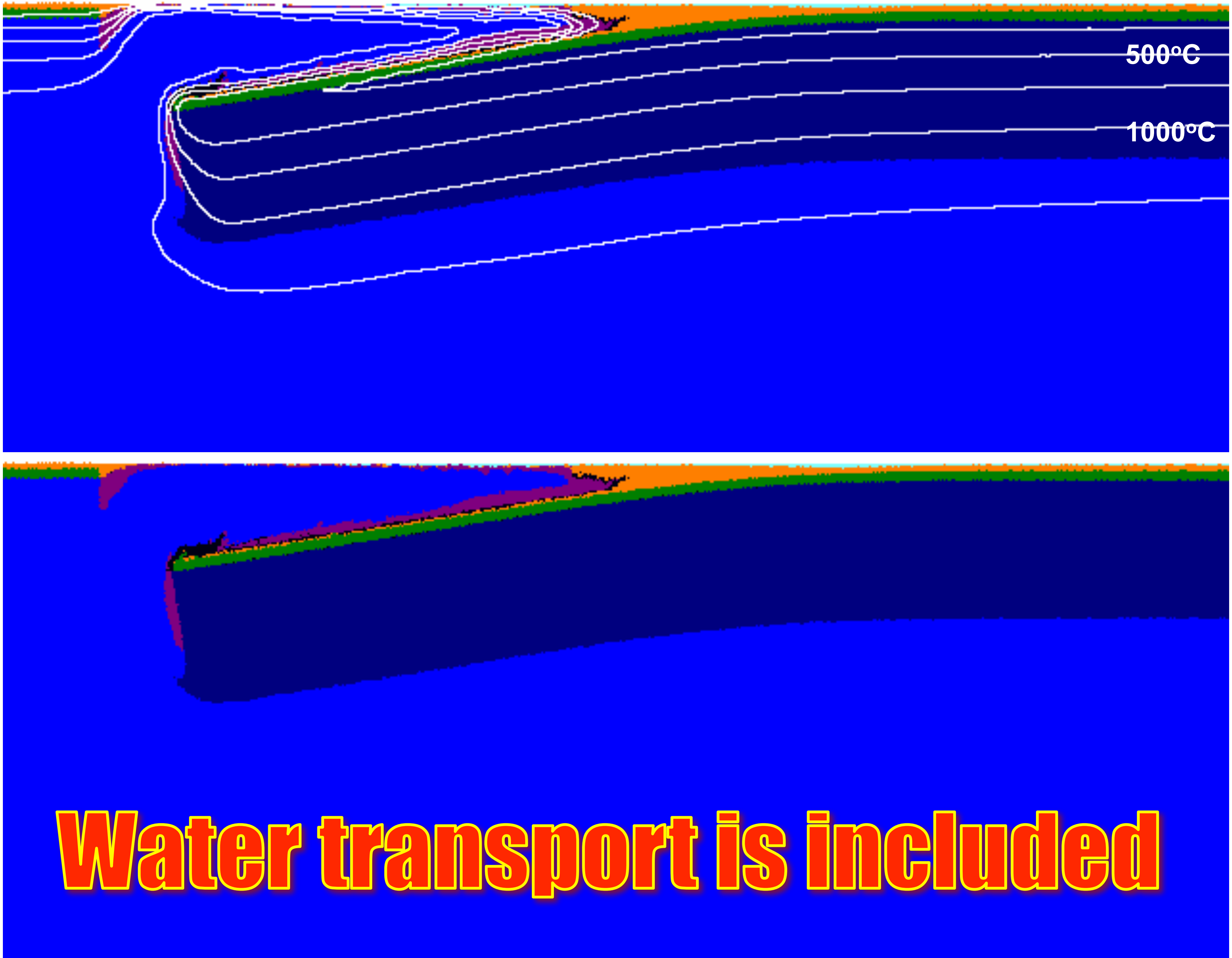
500°C
1000°C
Water transport is included

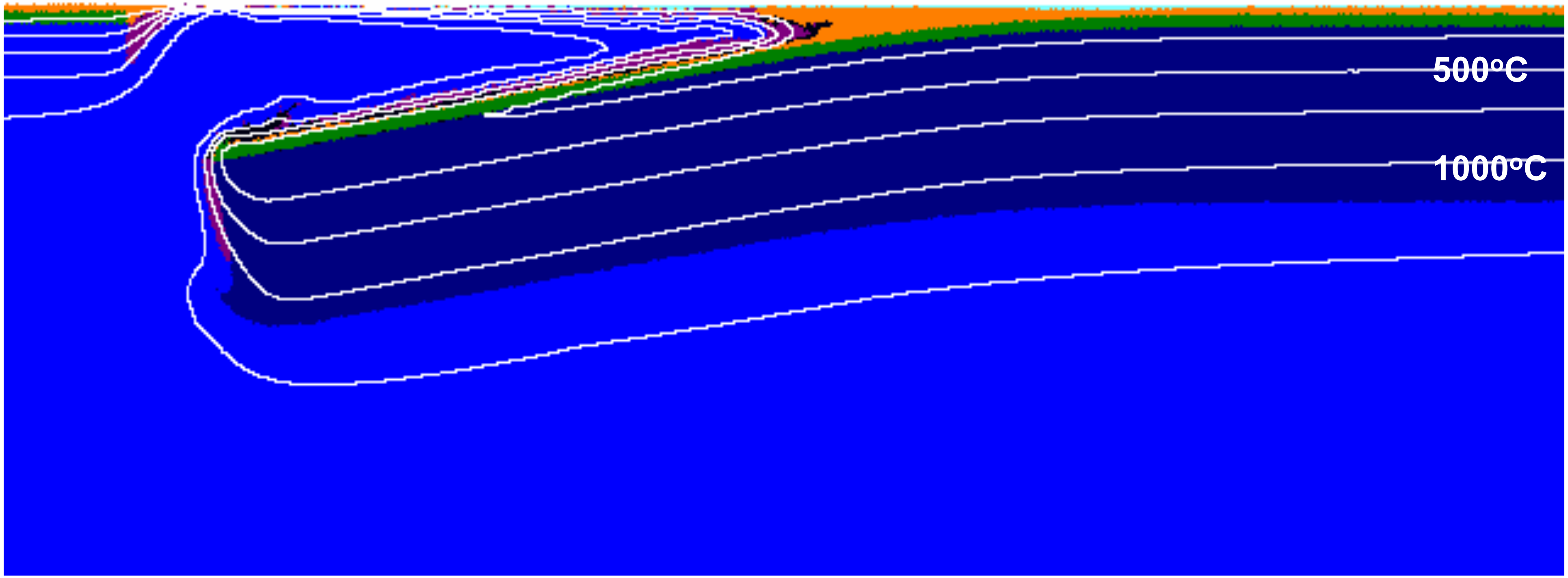
500ºC
1000ºC


Water transport is included

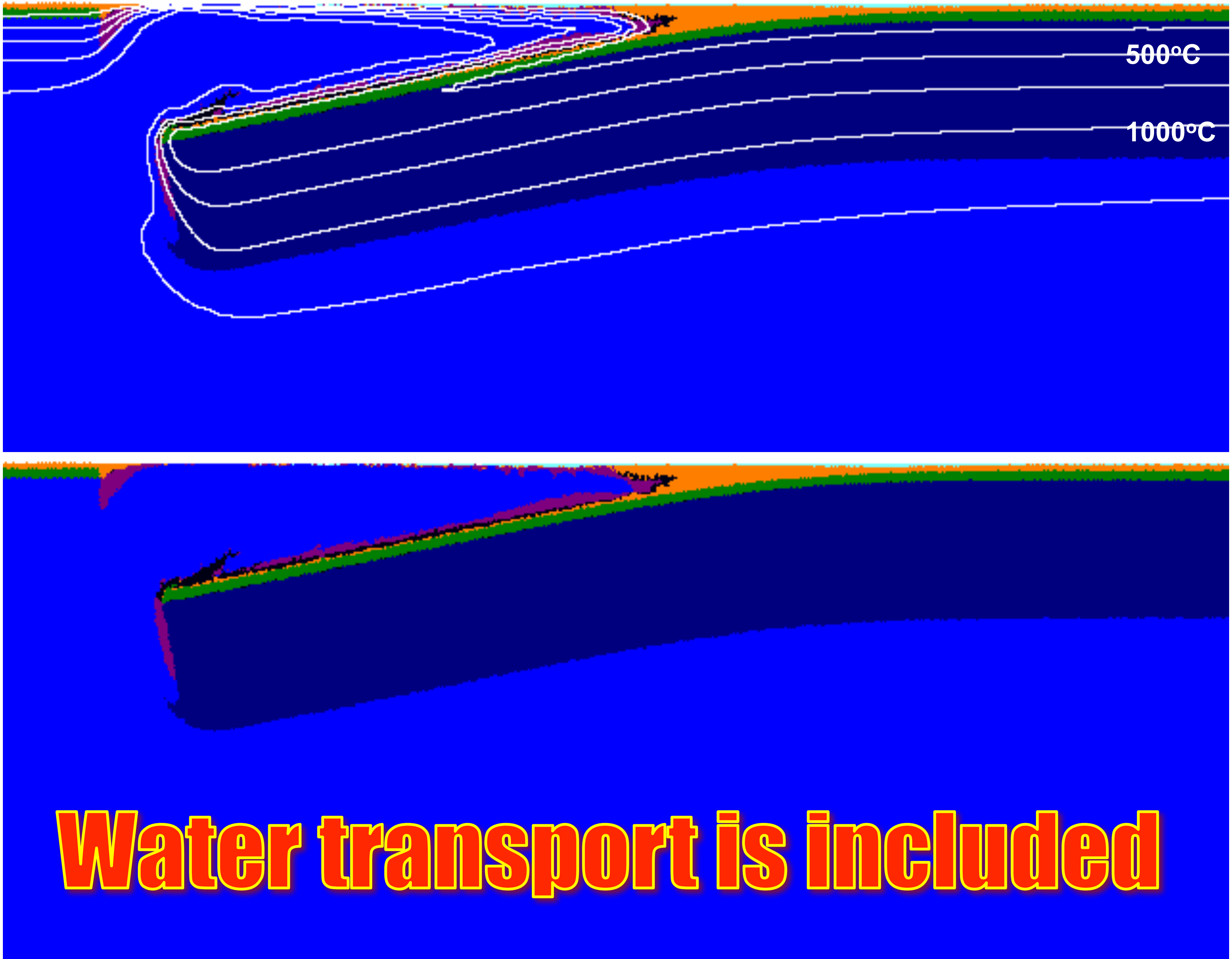

Water transport is included

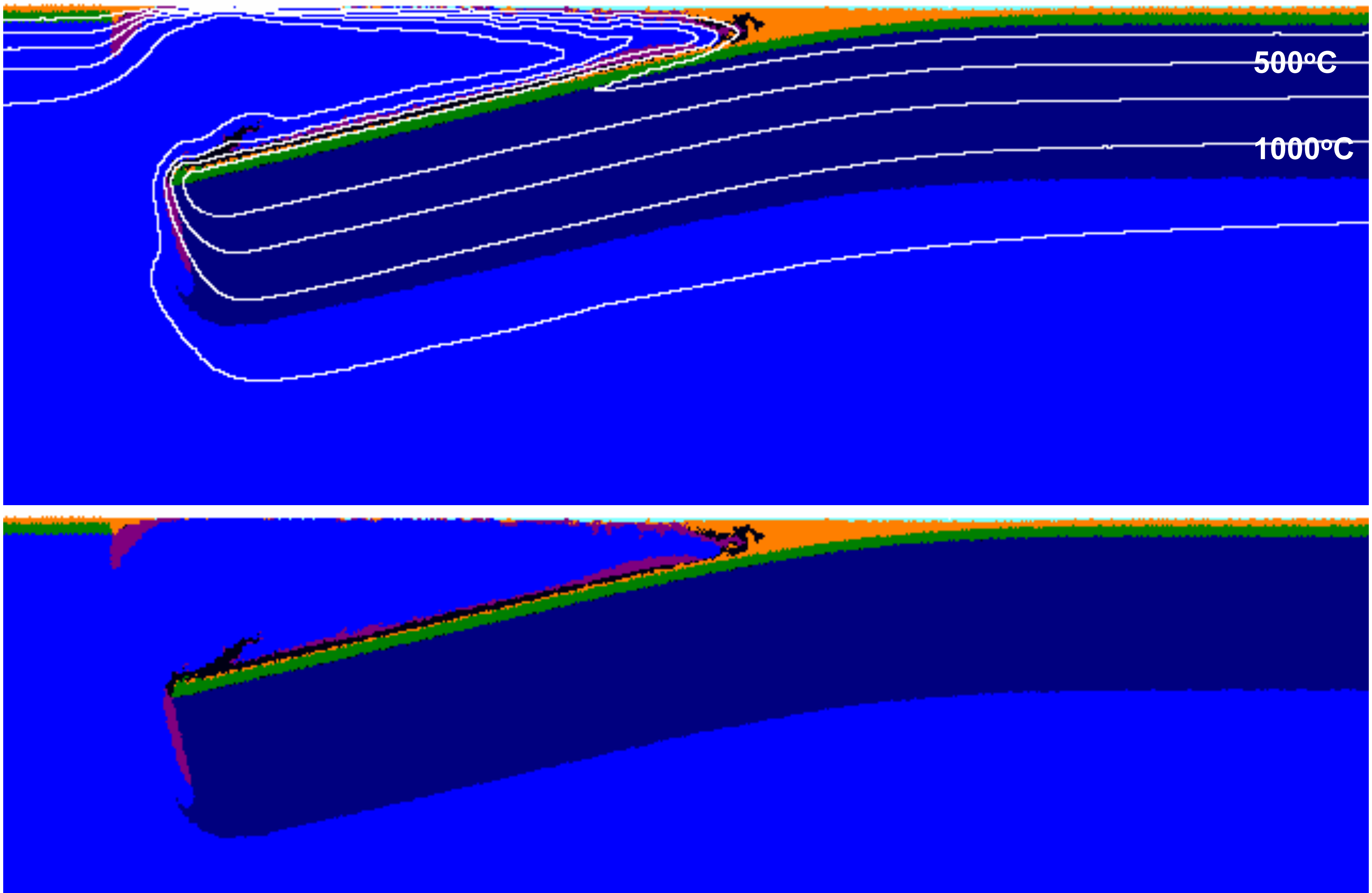

Water transport is included

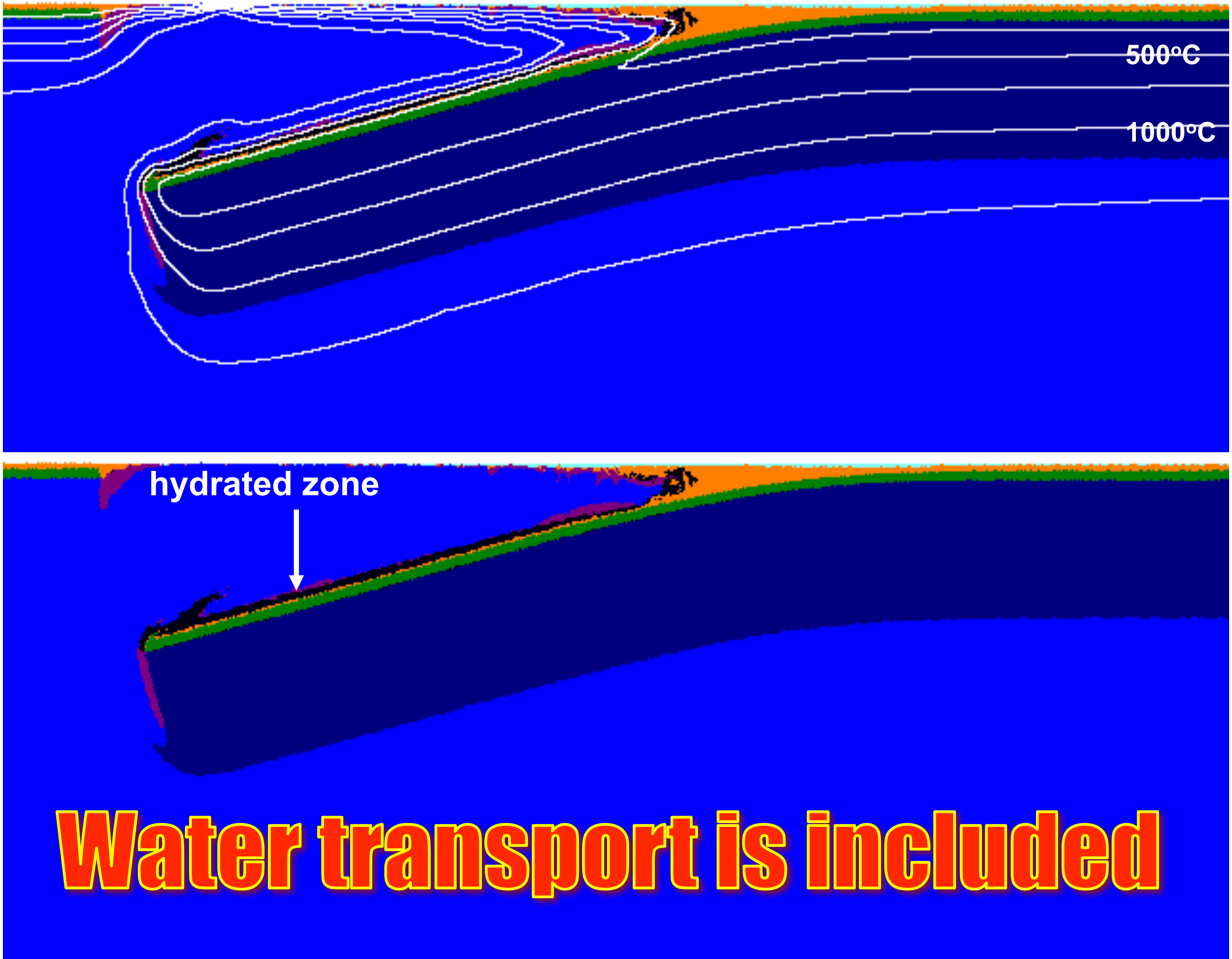
500ºC
1000ºC
hydrated zone
Water transport is included

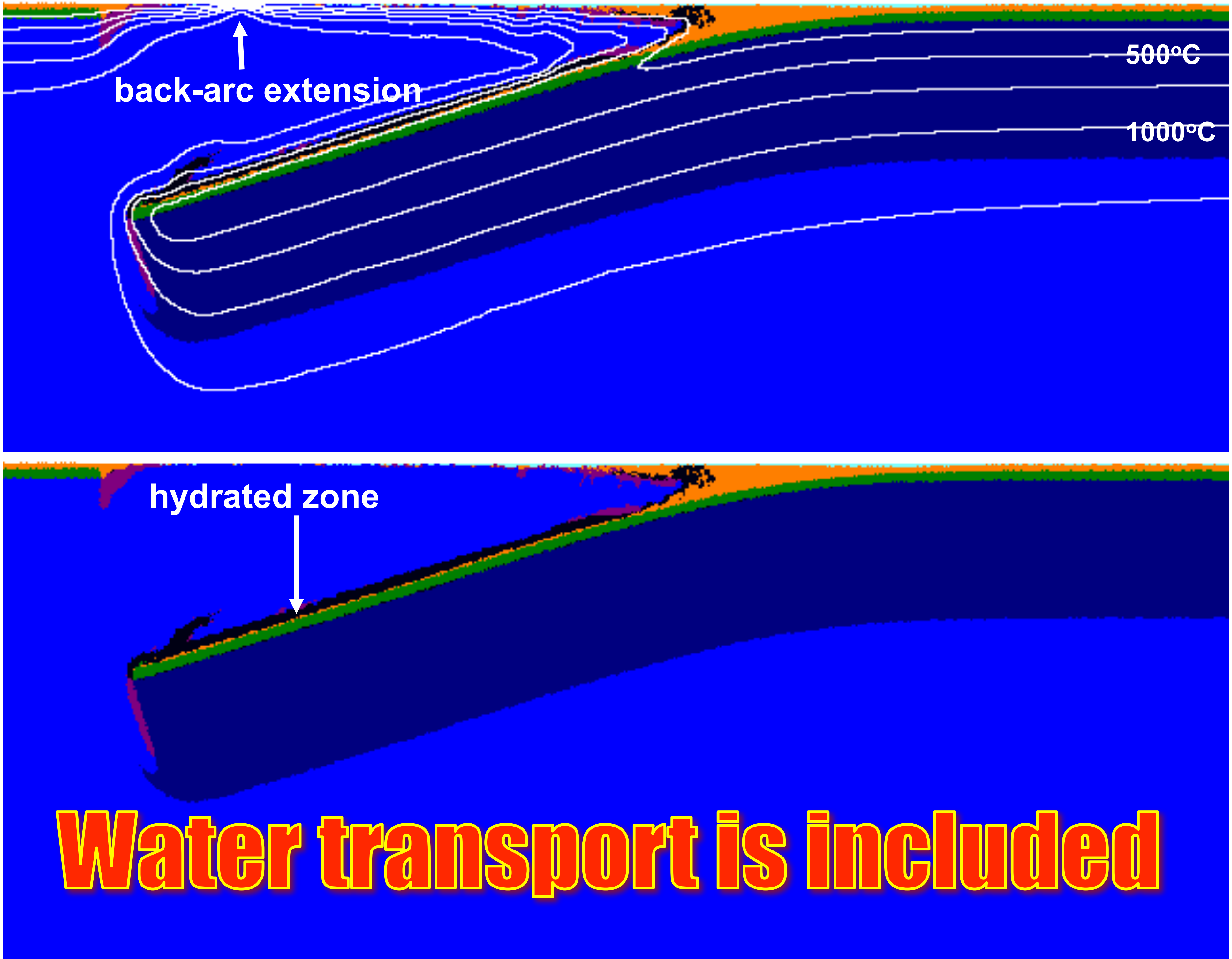

500ºC
1000ºC
back-arc extension
hydrated zone
Water transport is included

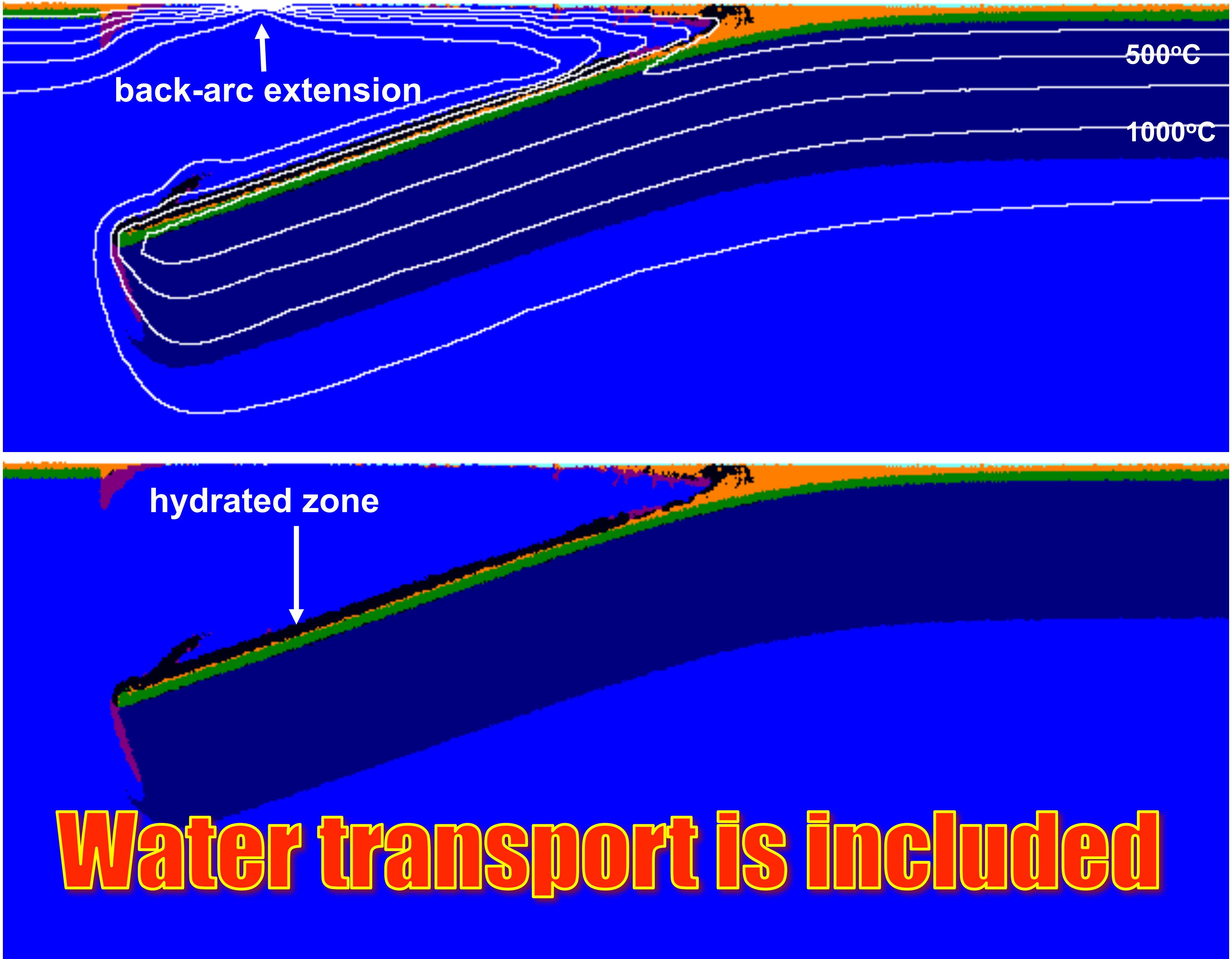
back-arc extension
500ºC
1000ºC
hydrated zone
Water transport is included

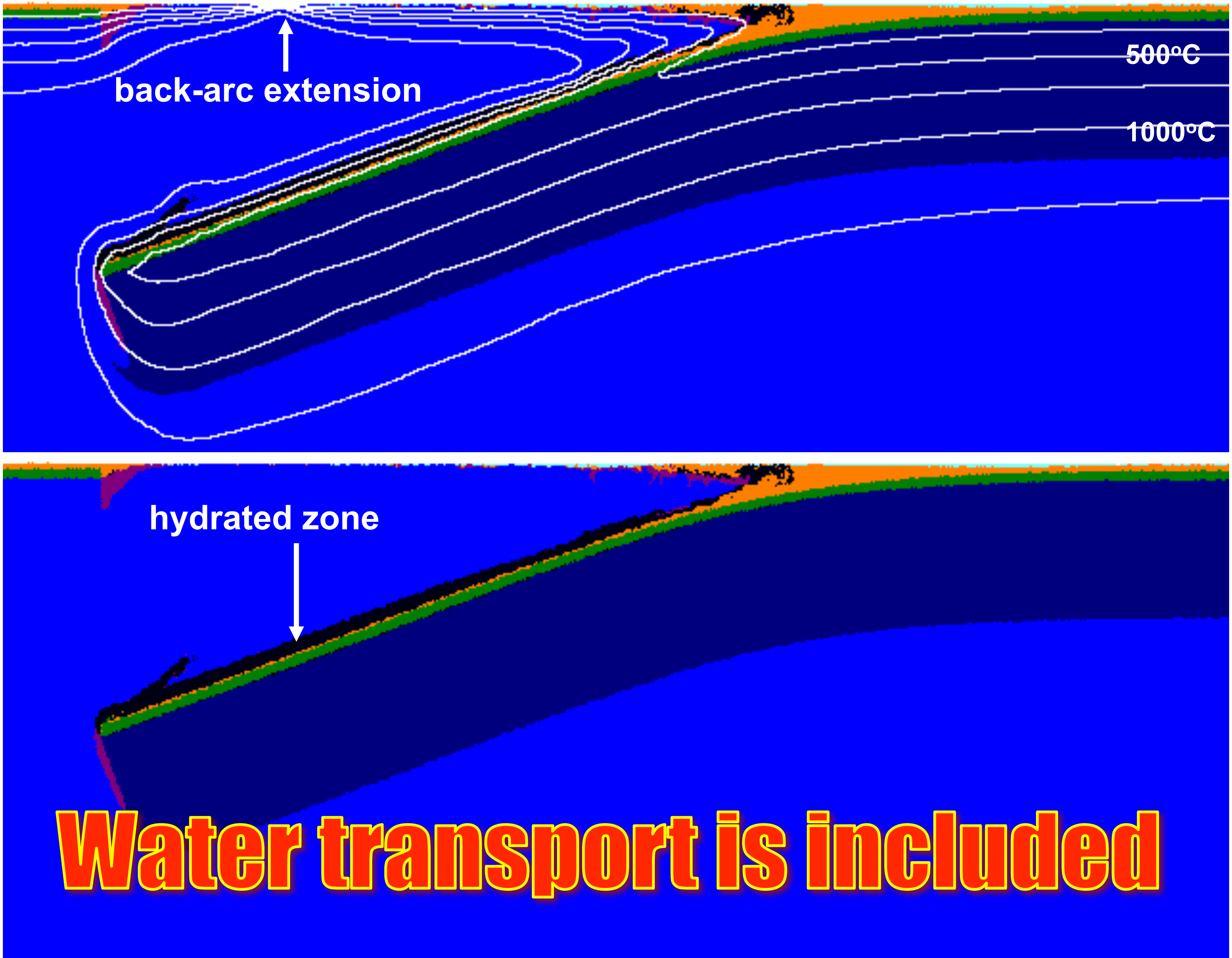
back-arc extension
500°C
1000°C
hydrated zone
Water transport is included

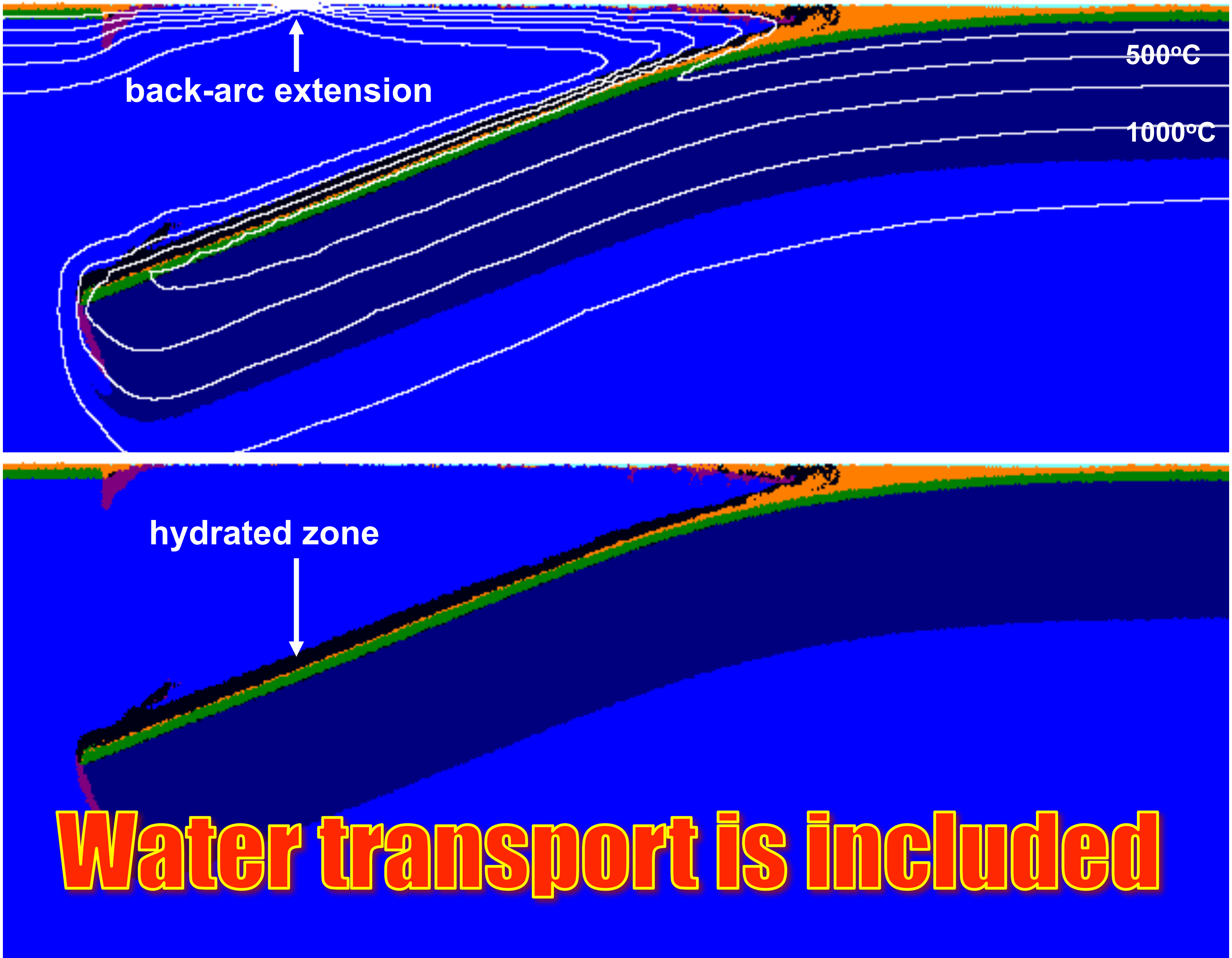
back-arc extension
500ºC
1000ºC
hydrated zone
Water transport is included

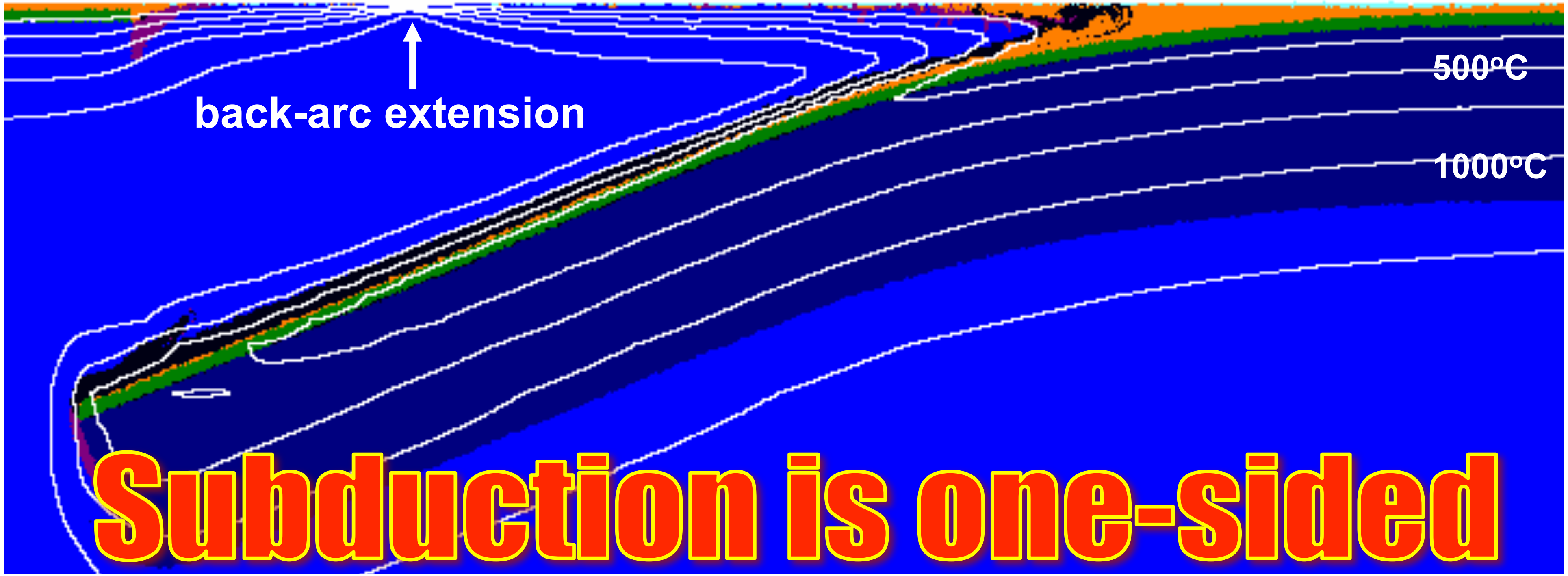
back-arc extension
500°C
1000°C
Subduction is one-sided

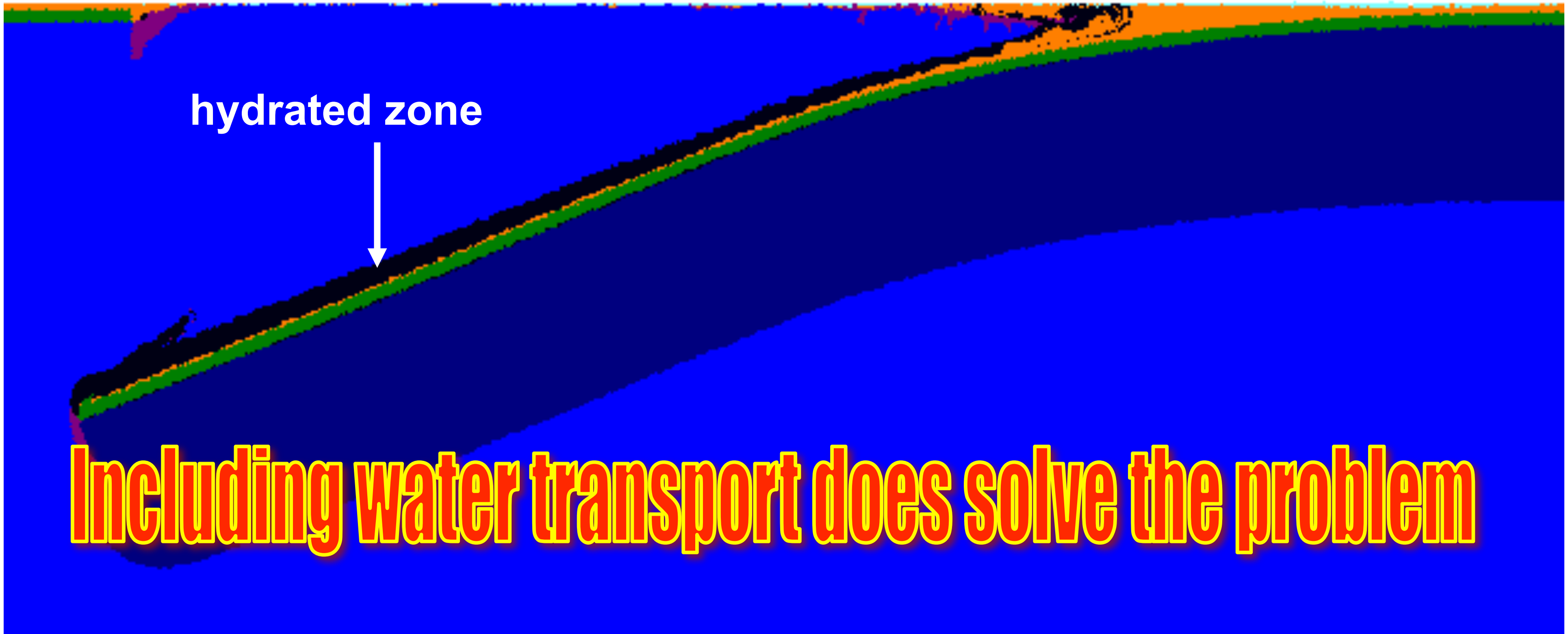
hydrated zone
Including water transport does solve the problem

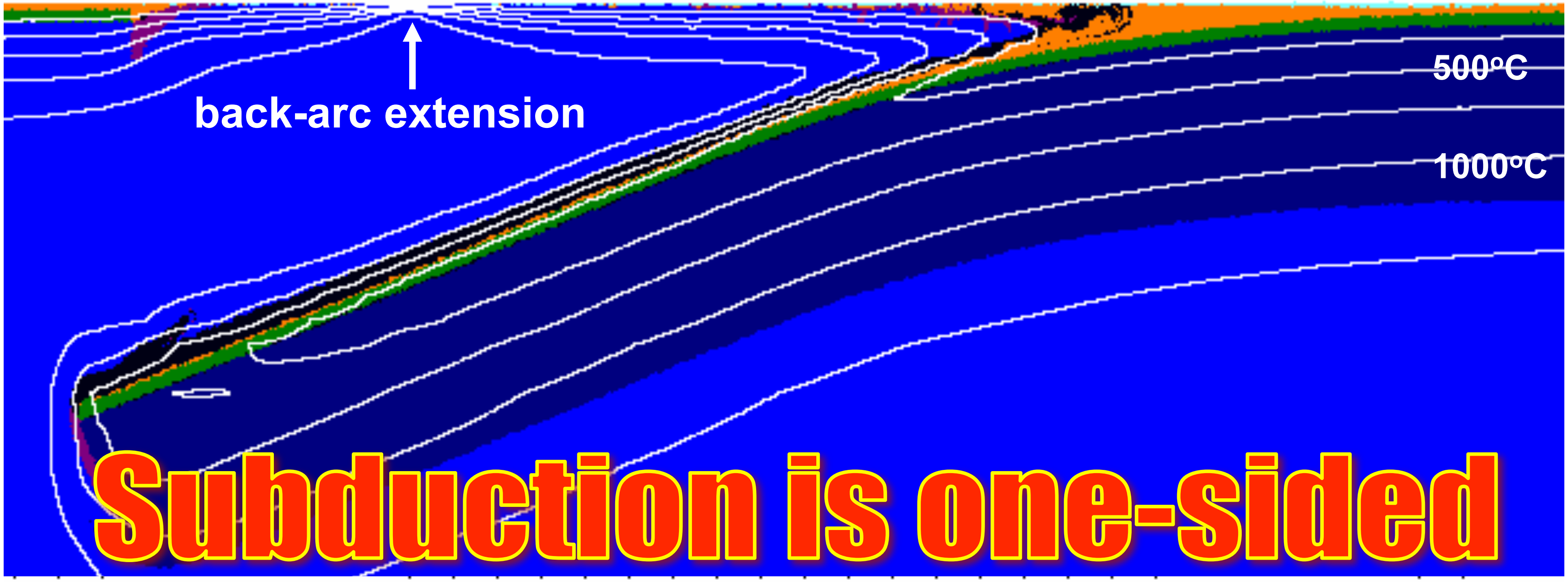
back-arc extension
500ºC
1000ºC
Subduction is one-sided

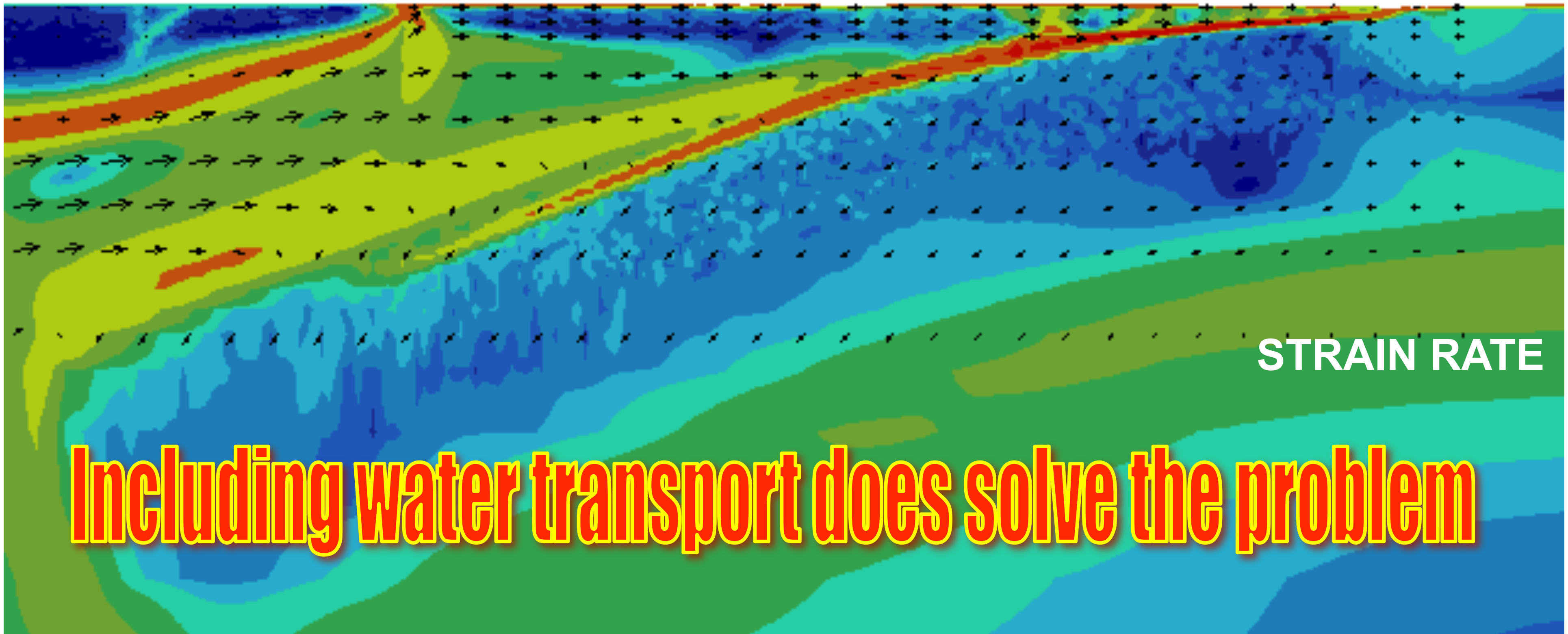
STRAIN RATE
Including water transport does solve the problem

Two subduction modes: one-sided and two-sided

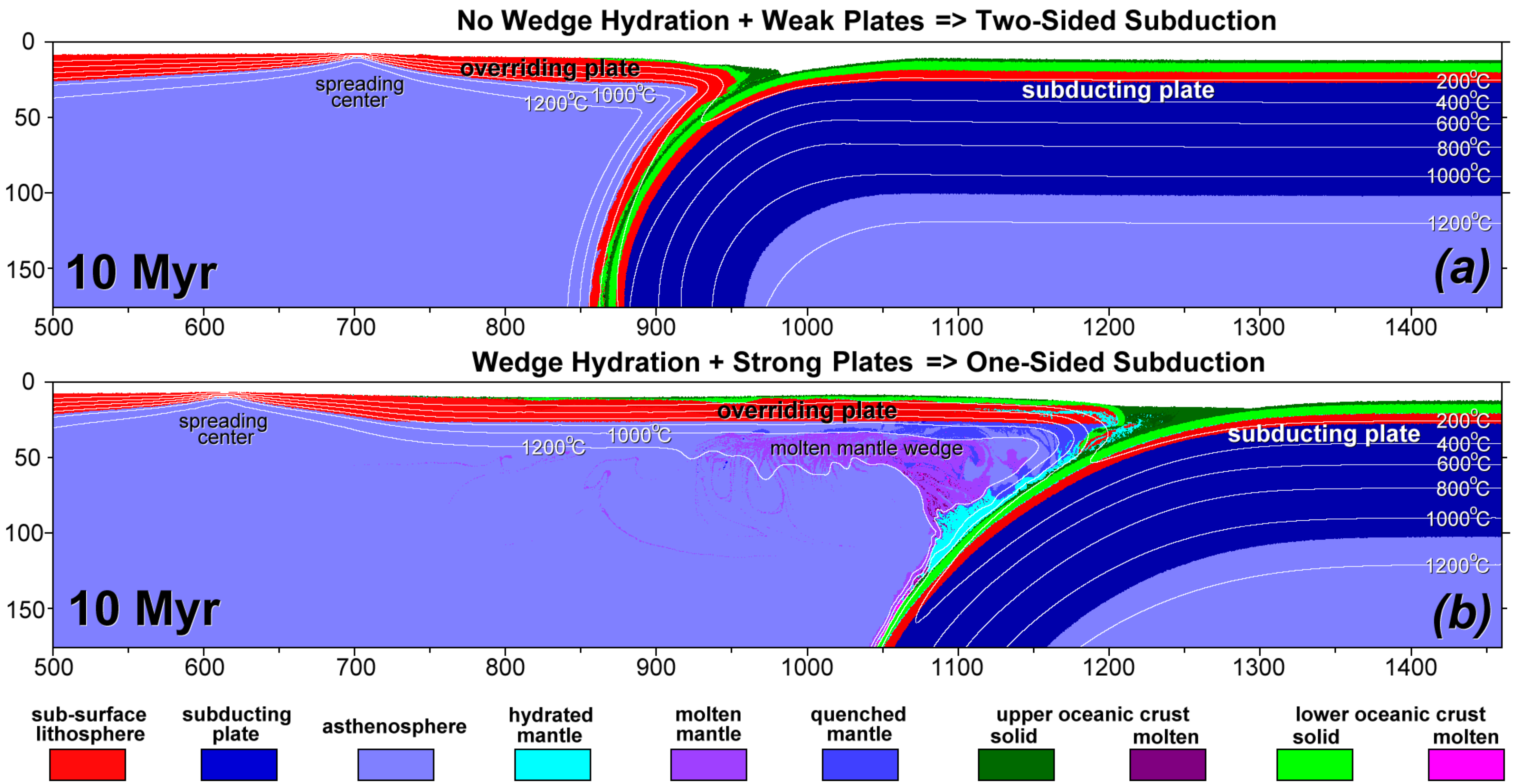

Gerya et al. (2007)

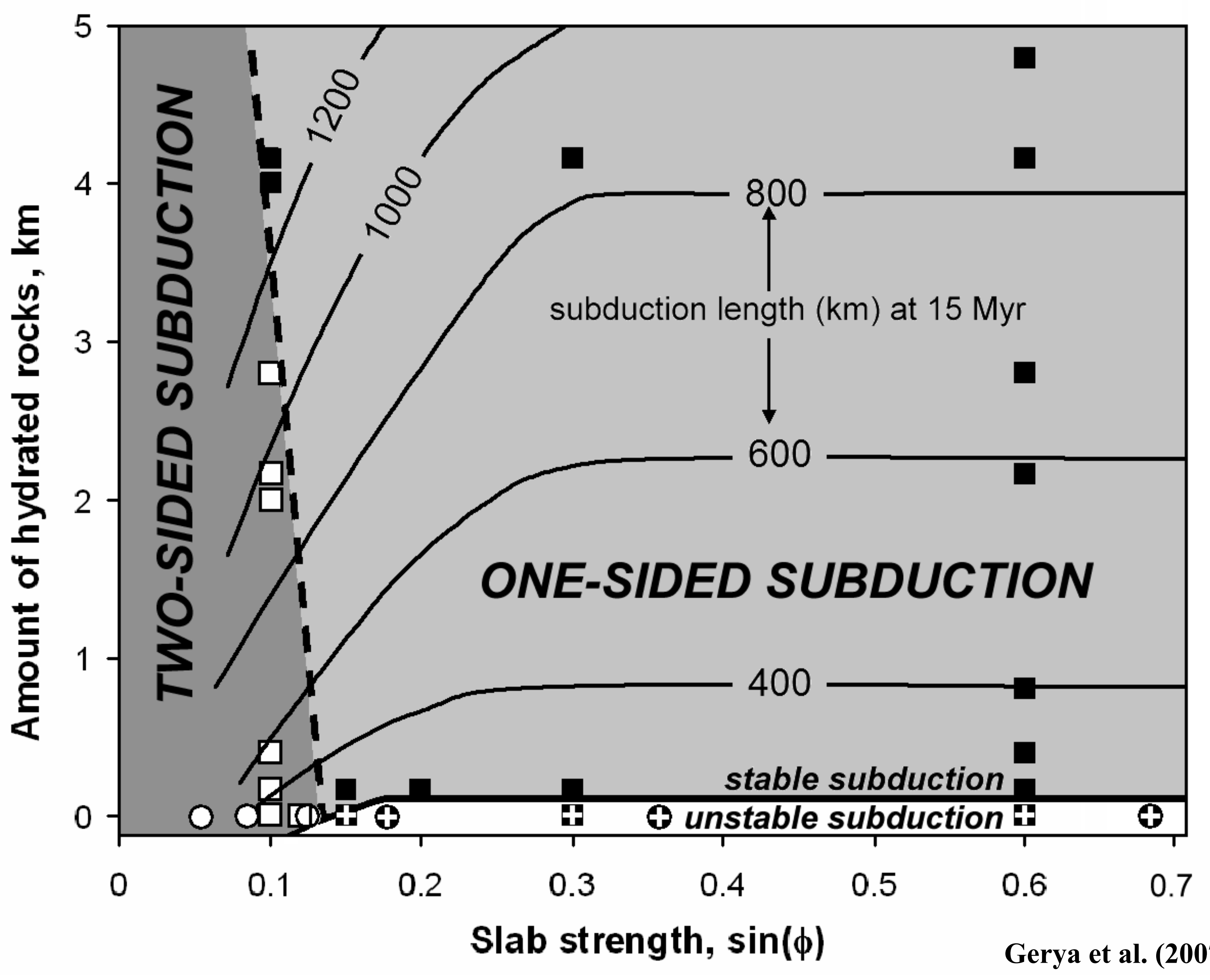

Gerya et al. (2007)

How strong slabs are indeed bending?

?

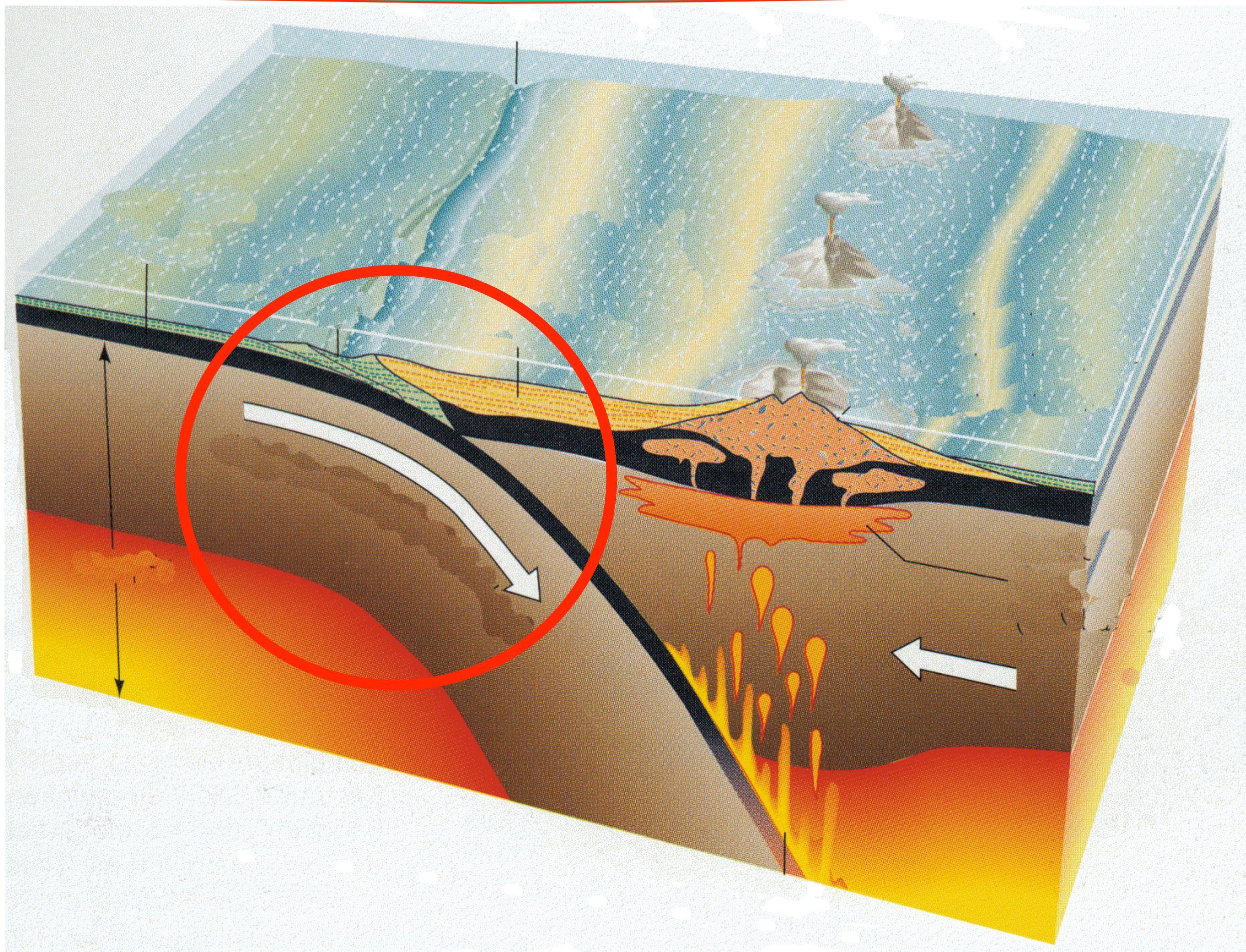

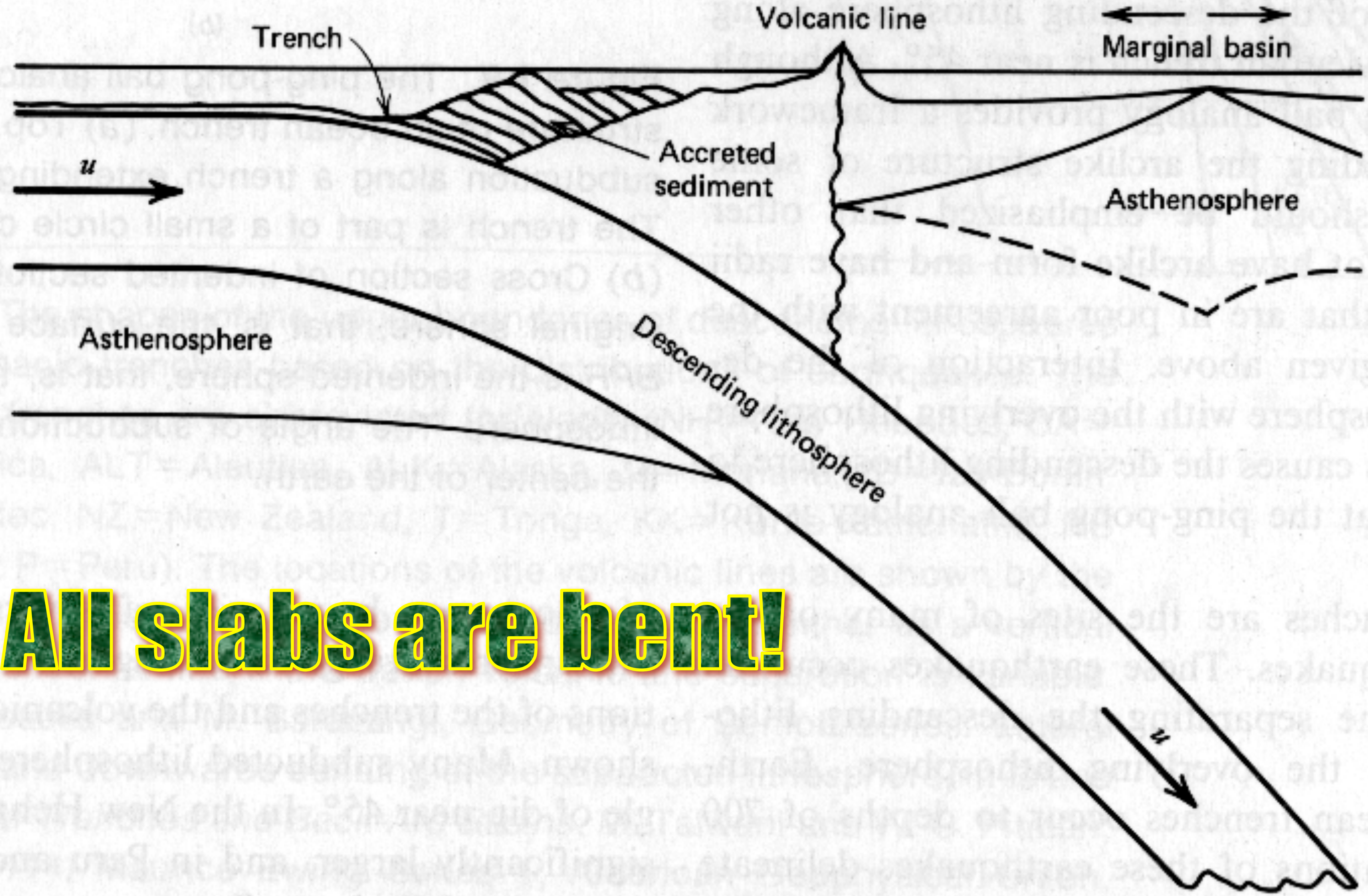

All slabs are bent!

Figure 1-8 Subduction of oceanic lithosphere at an ocean trench.
(Turcotte & Schubert, 1982)

All slabs are bent!

Subduction under
a volcanic arc / an active margin →

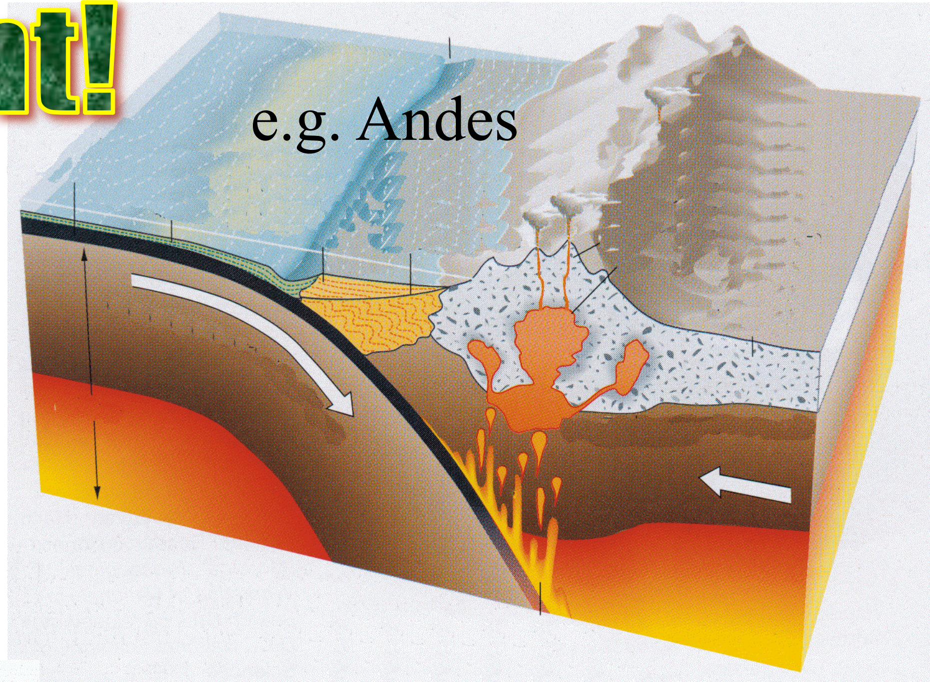

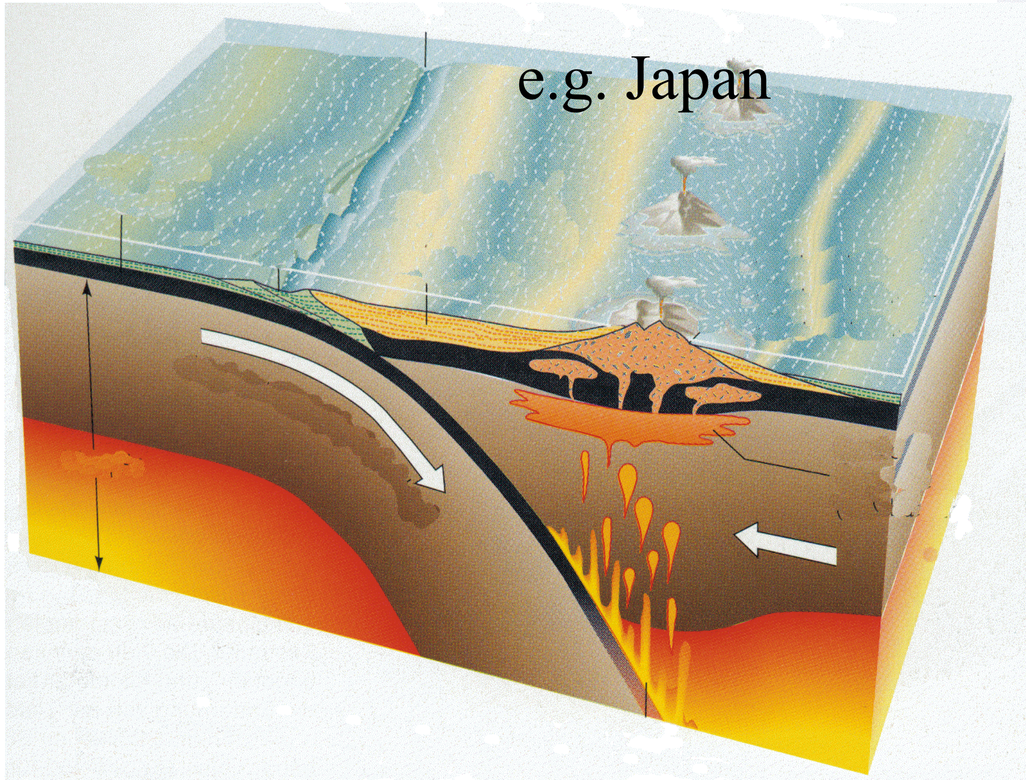

All slabs are bent!

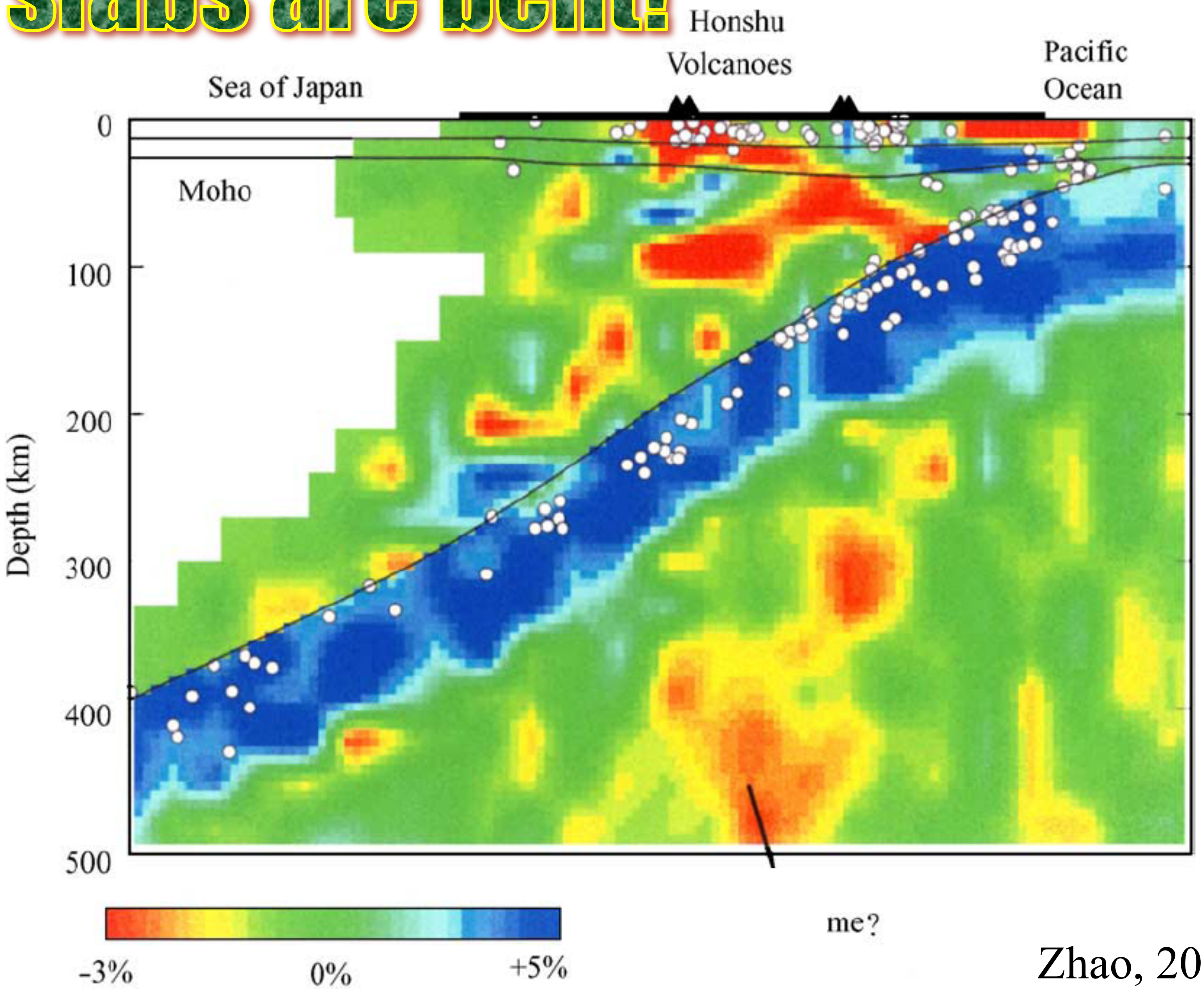

Zhao, 2004

All slabs are bent!

Turcotte & Schubert (1982)

But some slabs are bent more then the other...

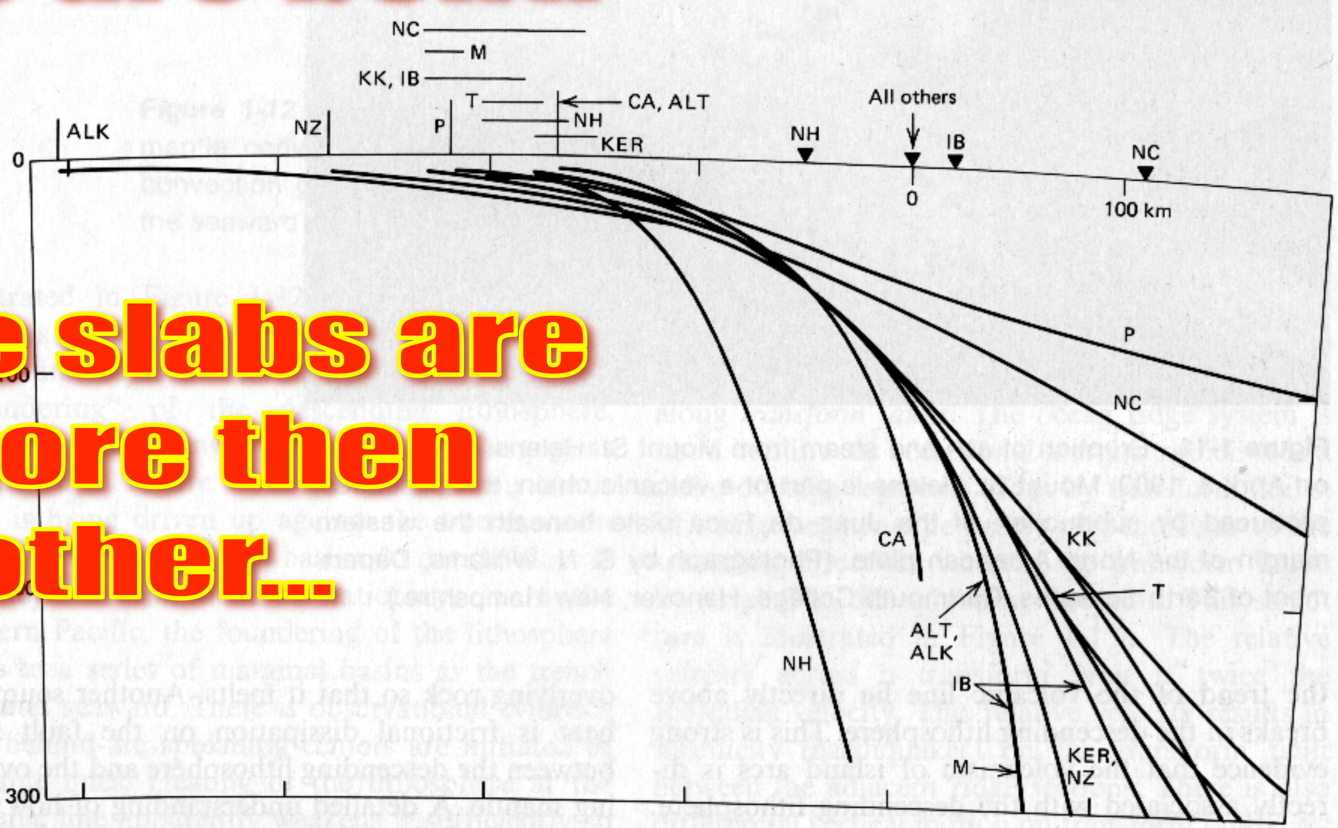

Figure 1-10 The shapes of the upper boundaries of descending lithospheres at several oceanic trenches based on the distributions of earthquakes. The names of the trenches are abbreviated for clarity (NH = New Hebrides, CA = Central America, ALT = Aleutian, ALK = Alaska, M = Mariana, IB = Izu-Bonin, KER = Kermadec, NZ = New Zealand, T = Tonga, KK = Kurile-Kamchatka, NC = North Chile, P = Peru). The locations of the volcanic lines are shown by the solid triangles. The locations of the trenches are shown either as a vertical line or as a horizontal line if the trench-volcanic line separation is variable. (From B. L. Isacks and M. Barazangi, Geometry of Benioff zones: Lateral segmentation and downwards bending of the subducted lithosphere, in *Island Arcs, Deep Sea Trenches and Back-Arc Basins*, M. Talwani and W. C. Pitman, eds., pp. 99–114, Maurice Ewing Series 1, American Geophysical Union, Washington, D.C., 1977.)

Slab bending questions

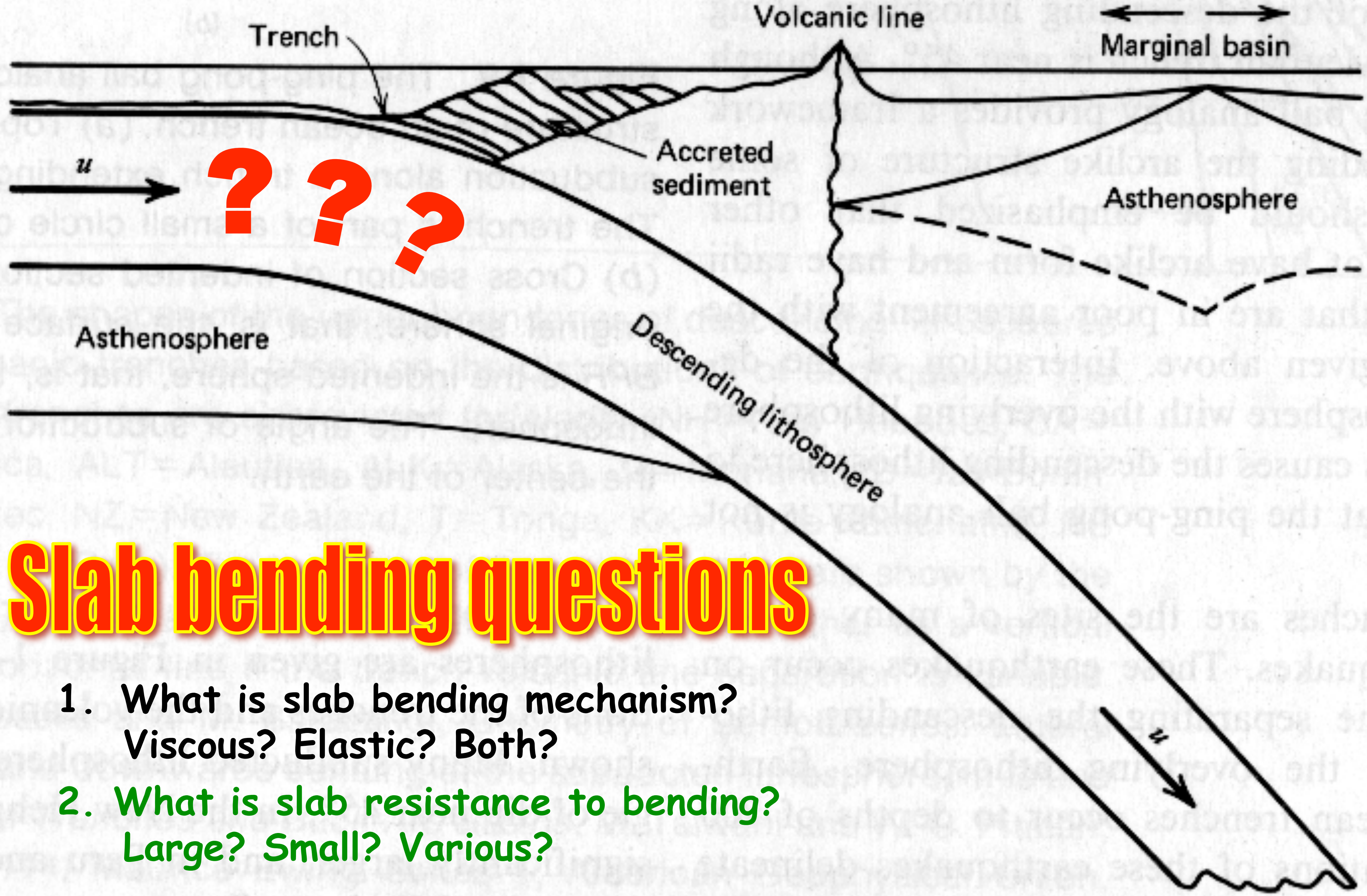

1. What is slab bending mechanism?
   Viscous? Elastic? Both?
2. What is slab resistance to bending?
   Large? Small? Various?

Figure 1-8 Subduction of oceanic lithosphere at an ocean trench.

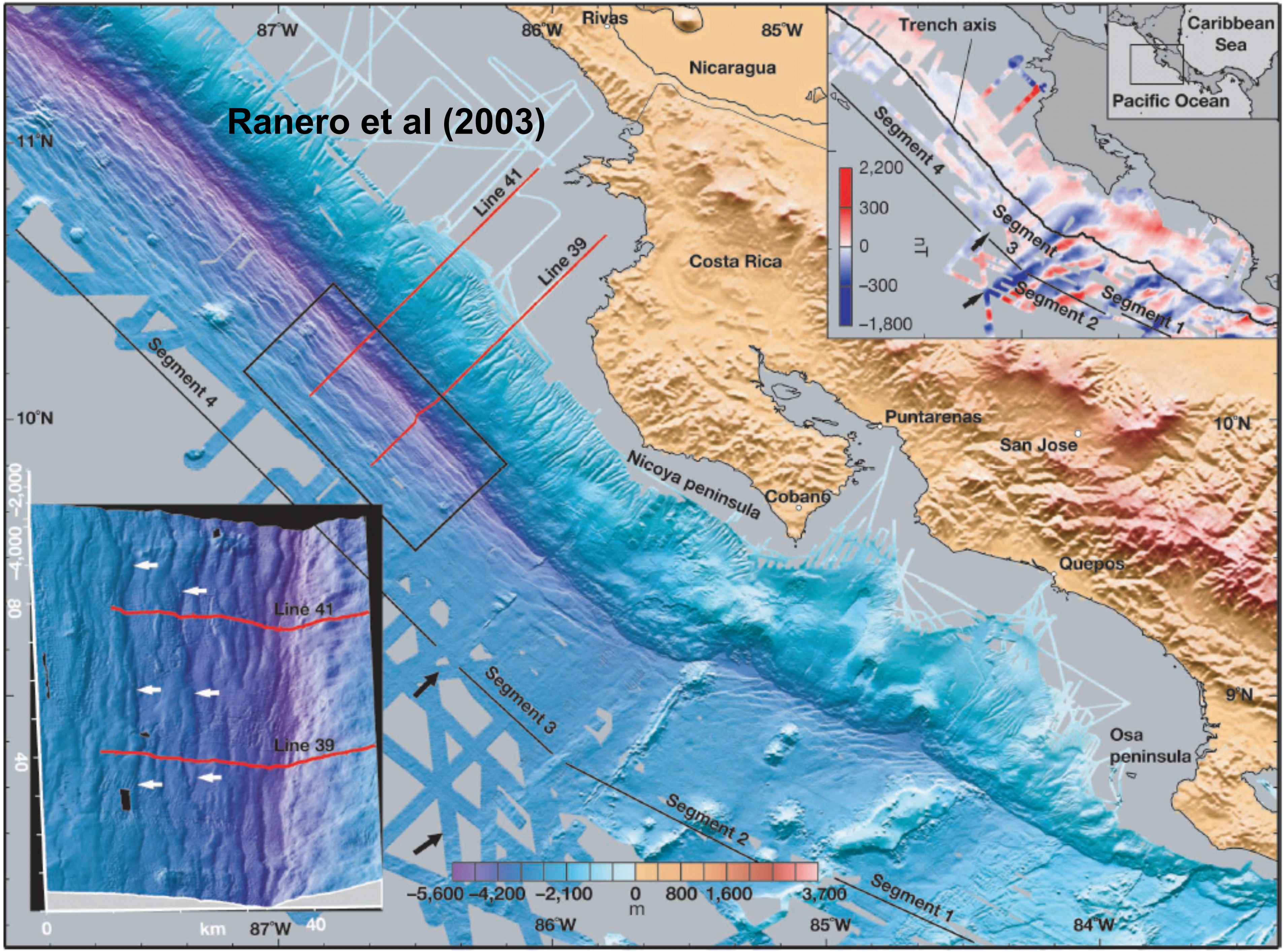

Ranero et al (2003)
87°W
86°W
85°W
84°W
Rivas
Nicaragua
Costa Rica
11°N
10°N
9°N
Line 41
Line 39
Segment 4
Segment 3
Segment 2
Segment 1
Nicoya peninsula
Cobano
Puntarenas
San Jose
Quepos
Osa peninsula
Trench axis
Caribbean Sea
Pacific Ocean
2,200
300
0
−300
−1,800
nT
−5,600 −4,200 −2,100 0 800 1,600 3,700
m
−2,000
−4,000
80
40
0
km
40

Ranero et al (2003)

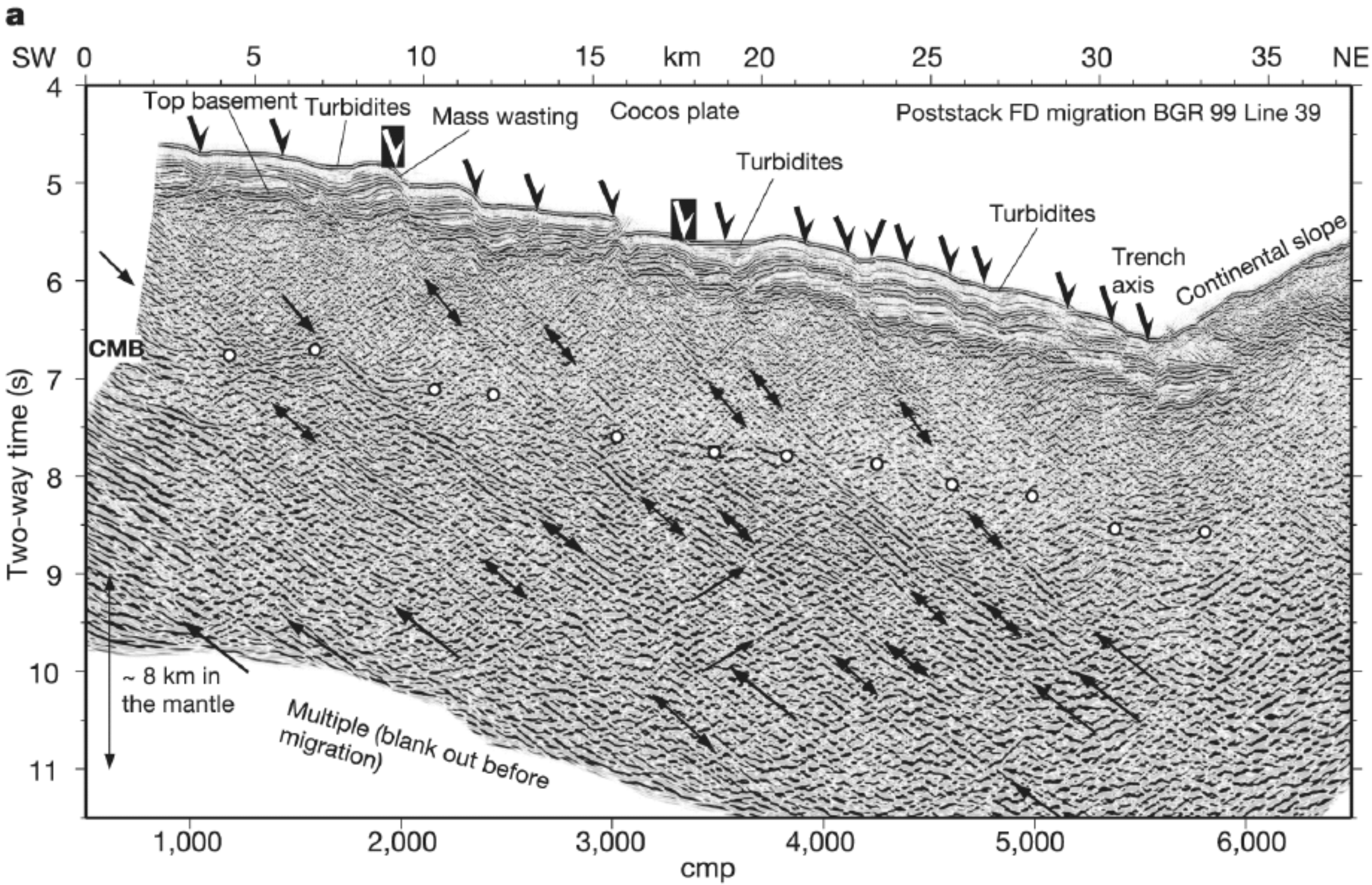

Ranero et al (2003)

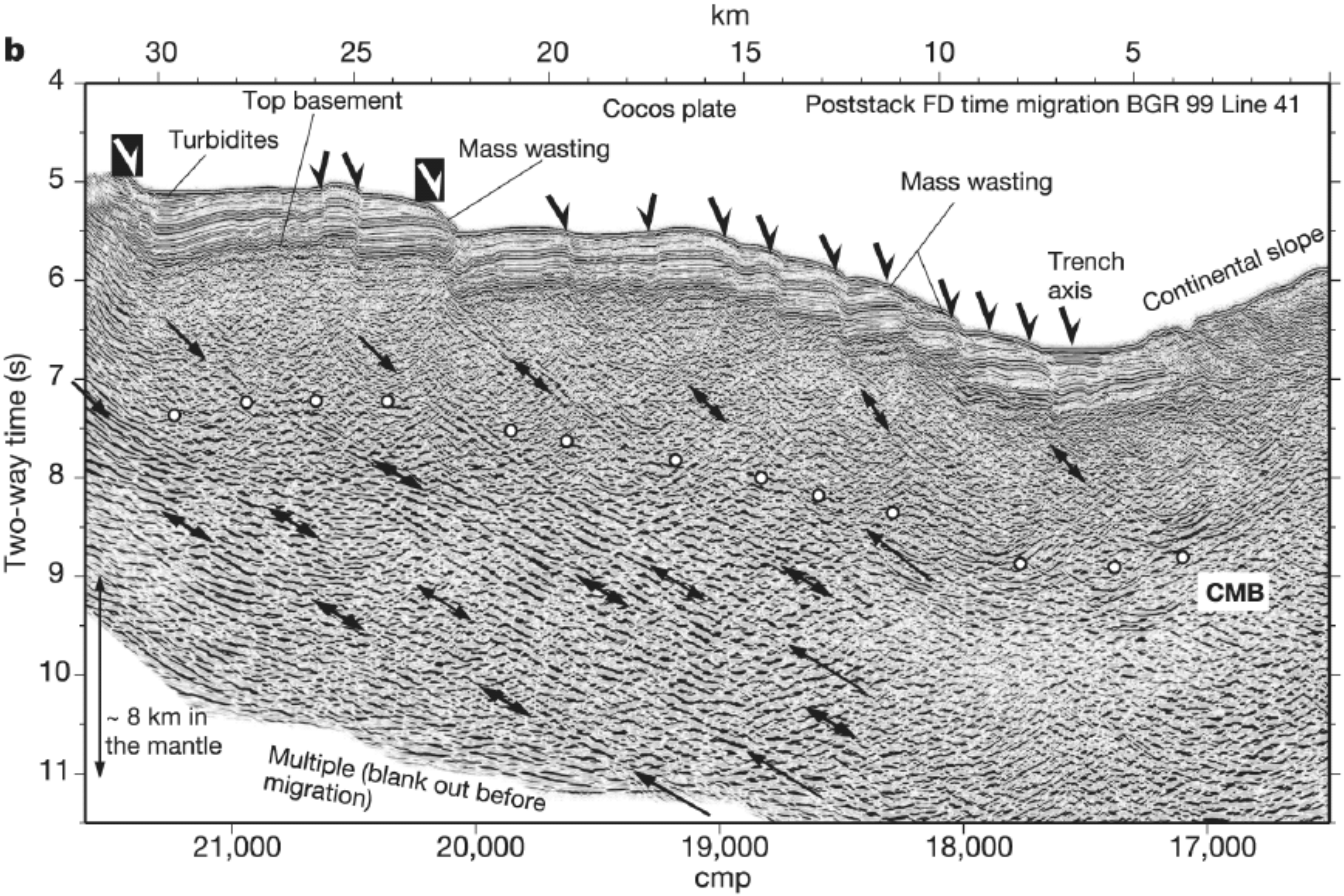

Ranero et al (2003)

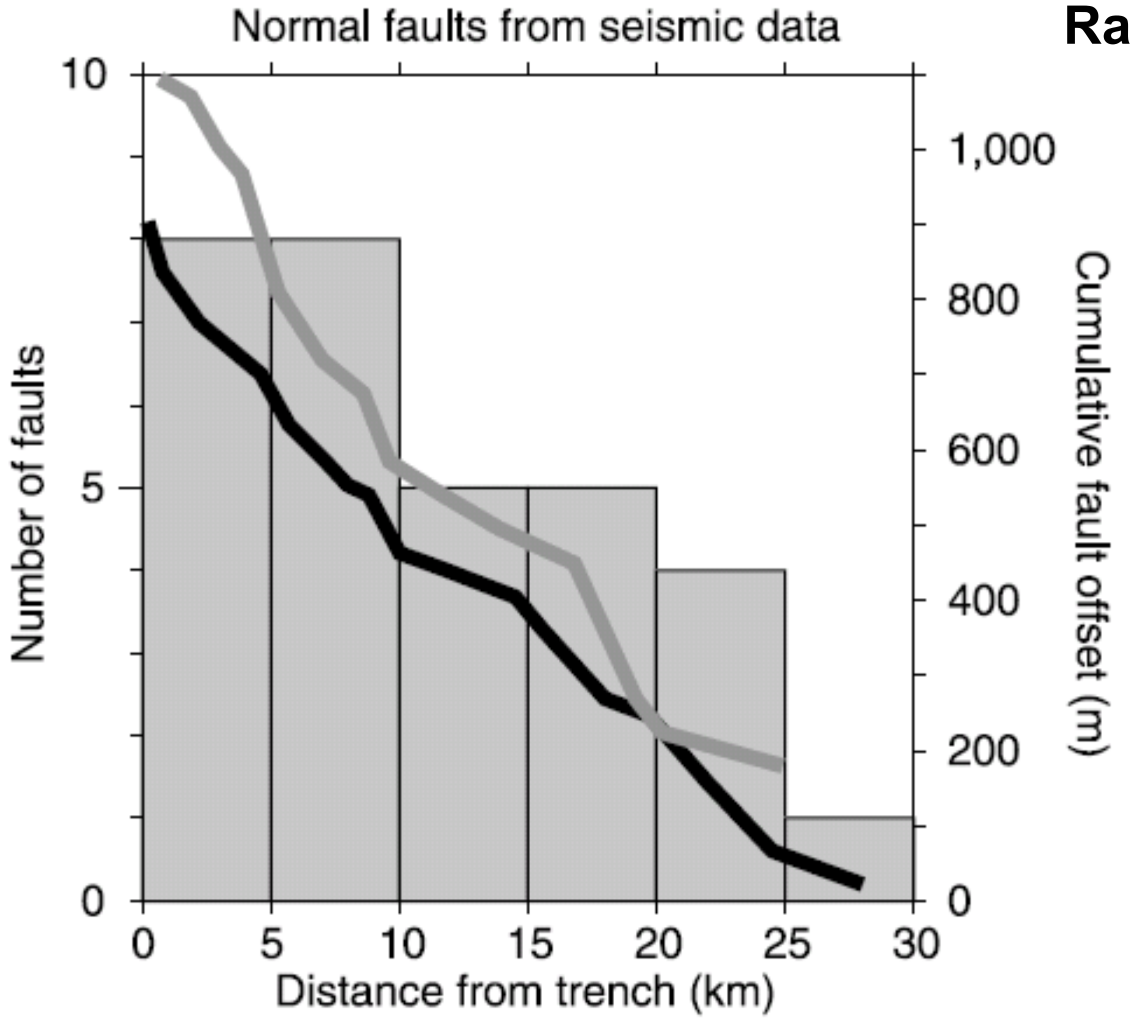

Figure 4 Histogram of fault density versus distance to the trench axis. The number of faults increases towards the axis, indicating that new faults continue to form as the plate approaches the trench axis. Lines indicate the cumulative fault offset measured at top basement for line BGR99-39 (black line) and BGR99-41 (grey line). There is a tendency to larger fault offset towards the trench.

Numerical setup

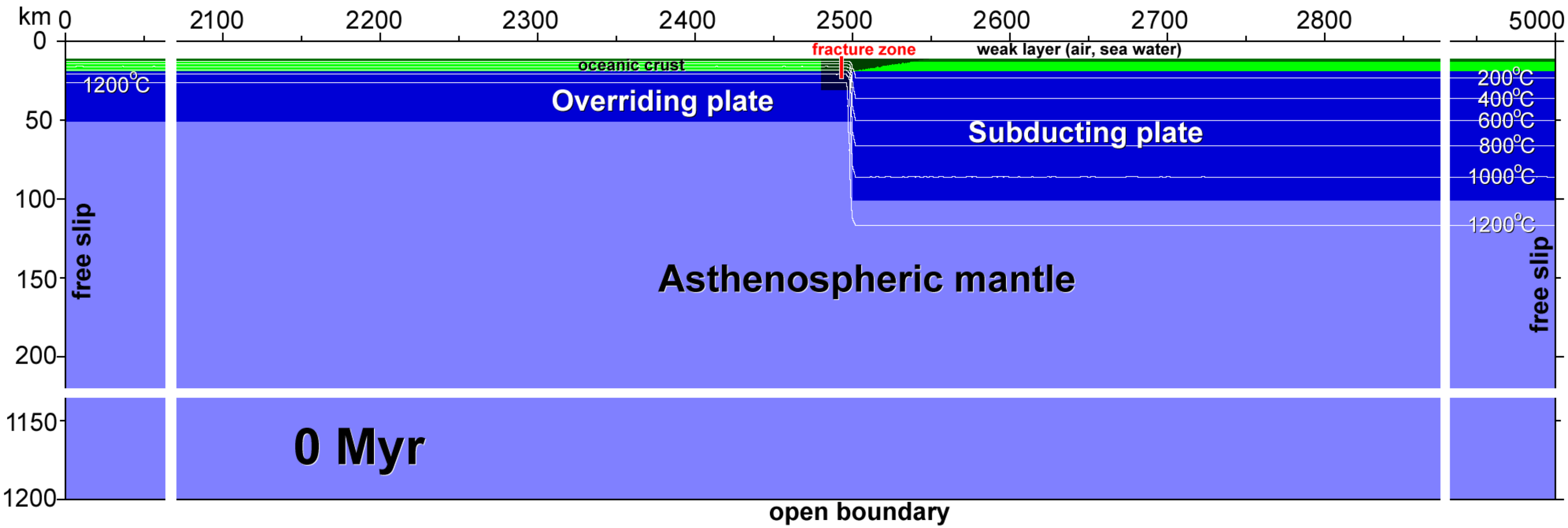

Petrological - thermomechanical numerical modeling

1. Maping of density and enthalpy in the P-T space

Gibbs free energy minimization

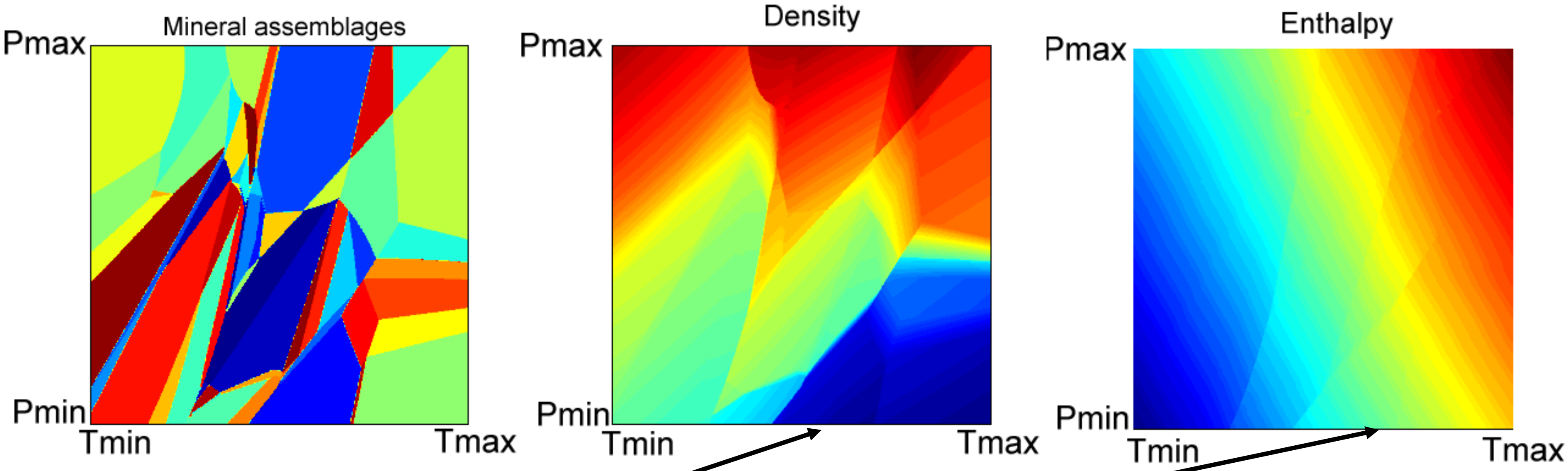

$H = H$ (***P***ressure, ***T***emperature, ***C***omposition, ***M***ineralogy)

$\rho = \rho$ (***P***ressure, ***T***emperature, ***C***omposition, ***M***ineralogy)

(Gerya et al., 2001, 2004, Connolly & Petrini, 2002, Vasiliev et al., 2004)

2. Latent heating

Latent heating is implemented via effective heat capacity (*Cp*)
and effective adiabatic heating (*Qp*)
computed numerically from the enthalpy and density maps

standard thermodynamic relations

$$Cp = (\partial H/\partial T)_P \qquad Qp = (DP/Dt)[1- \rho\,(\partial H/\partial P)_T]$$

Lagrangian temperature equation

$$\rho\, Cp(DT/Dt) = \partial(k\partial T/\partial x)/\partial x + \partial(k\partial T/\partial z)/\partial z + Qp + Q_{shear} + Q_{radioactive}$$

3. Volume changes

Volumetric effects of phase transformations
are taken into account in both the momentum and the continuity equations

Lagrangian continuity equation for compressible flow

$$D(\ln\rho)/Dt + \mathrm{div}(\underline{v}) = 0$$

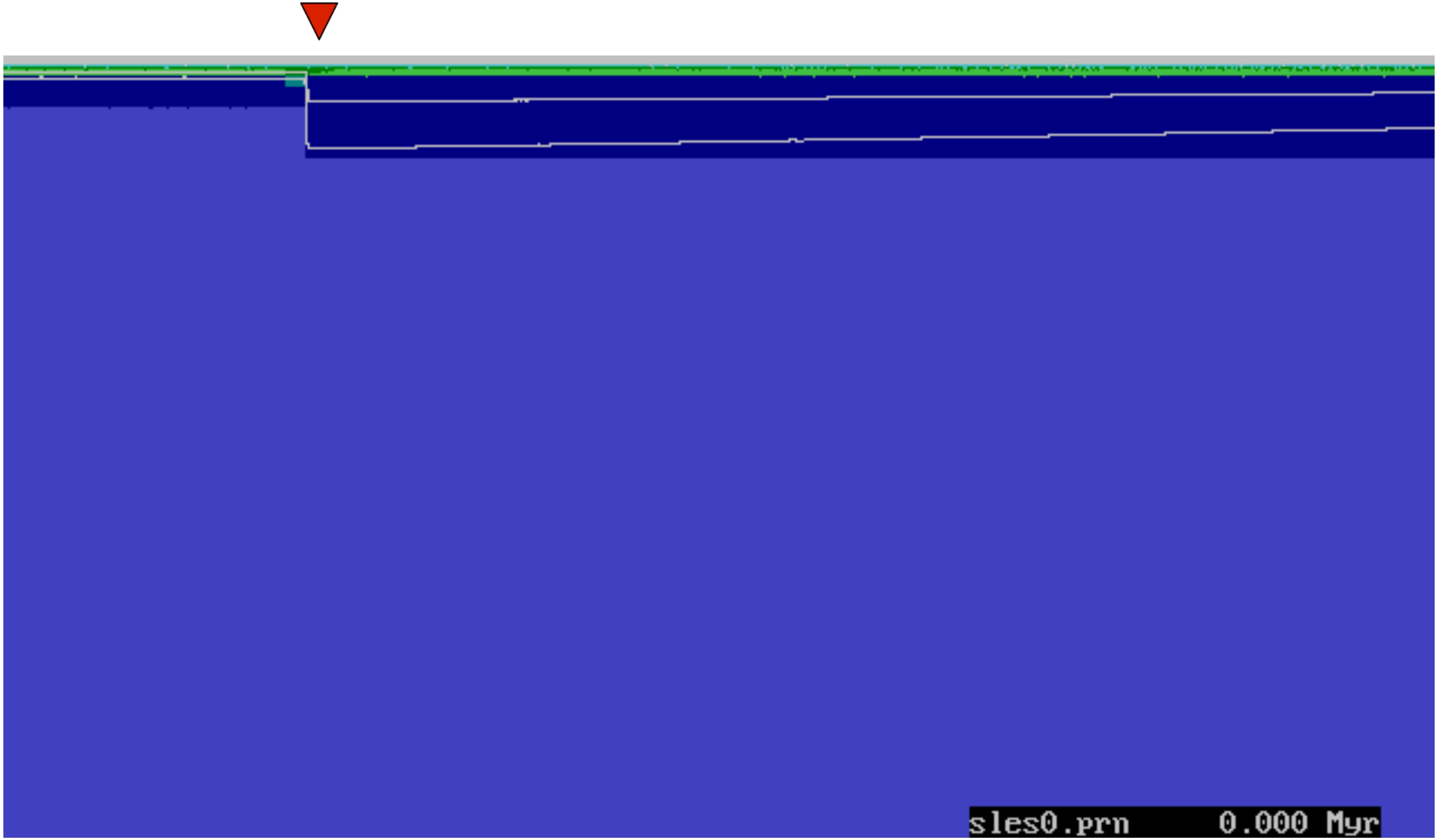
sles0.prn 0.000 Myr

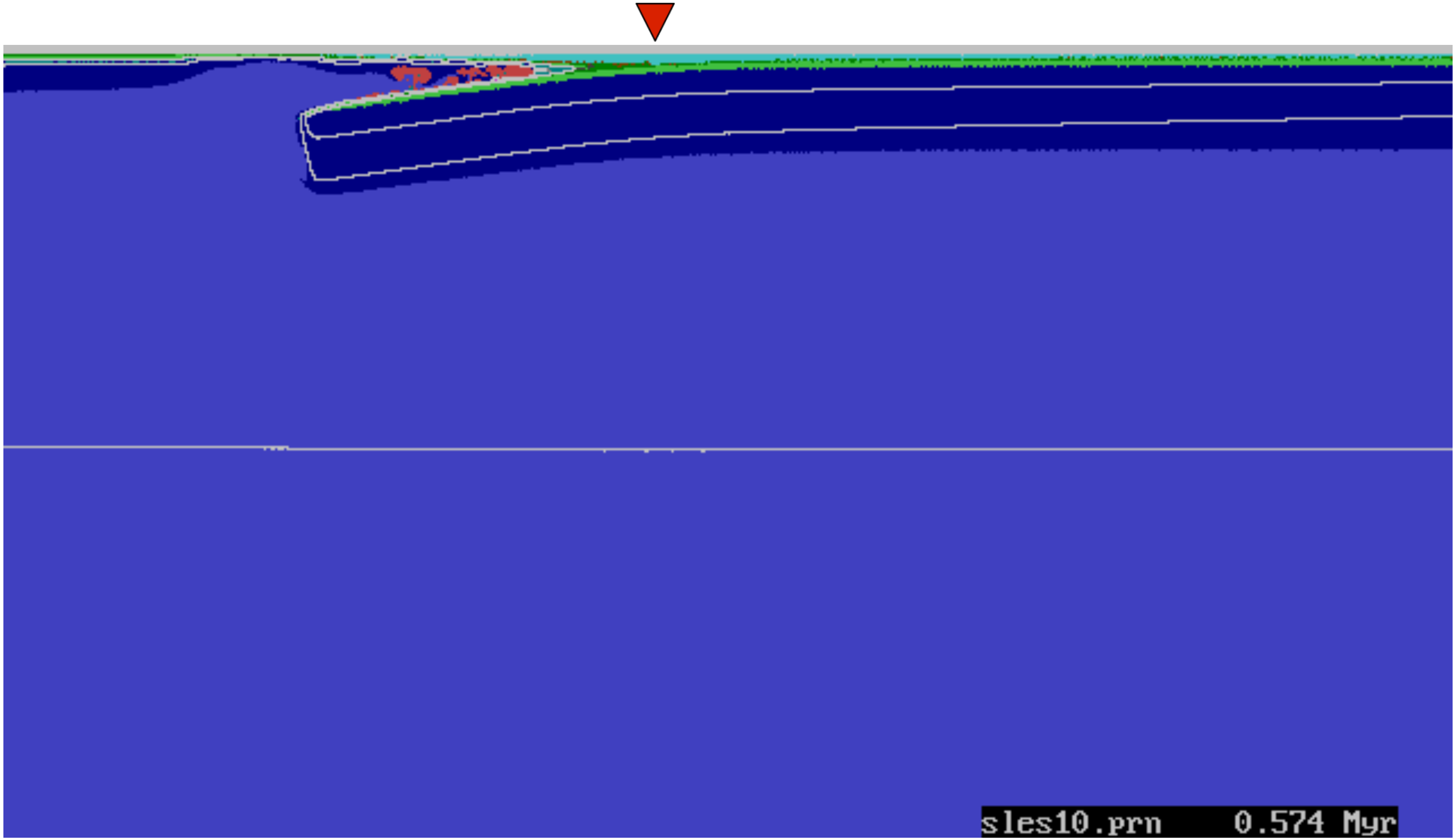
sles10.prn 0.574 Myr

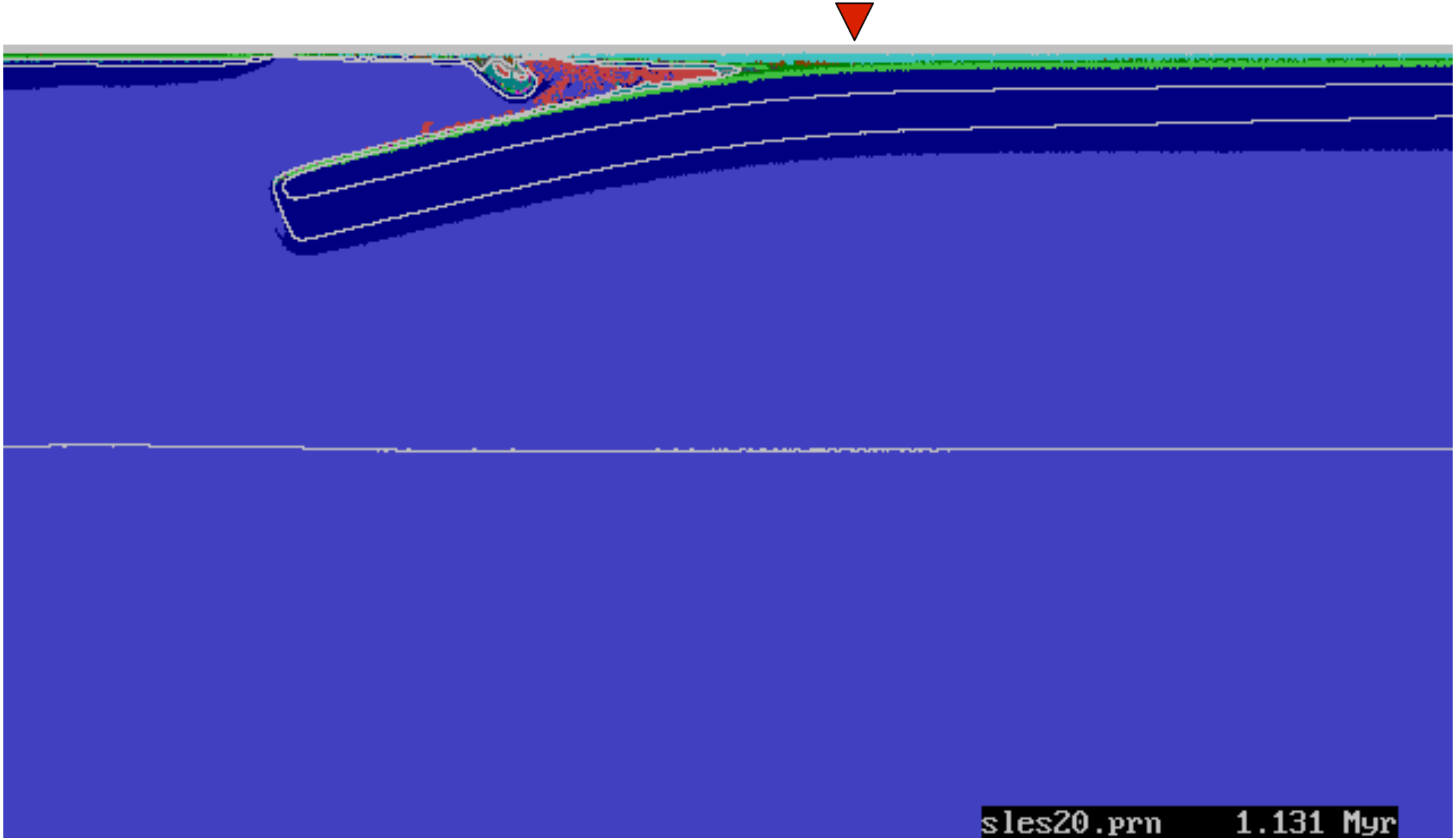
sles20.prn 1.131 Myr

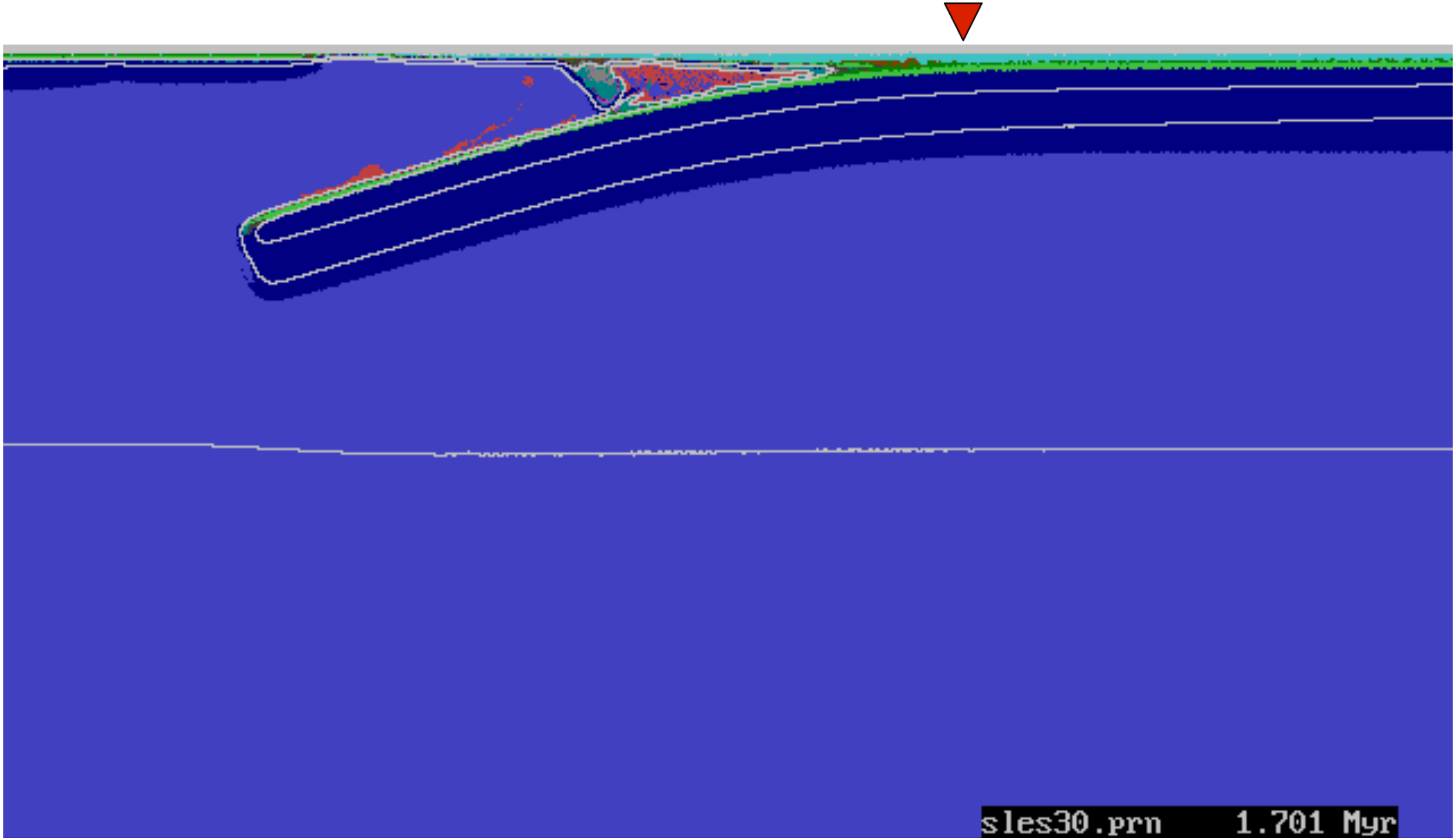
sles30.prn 1.701 Myr

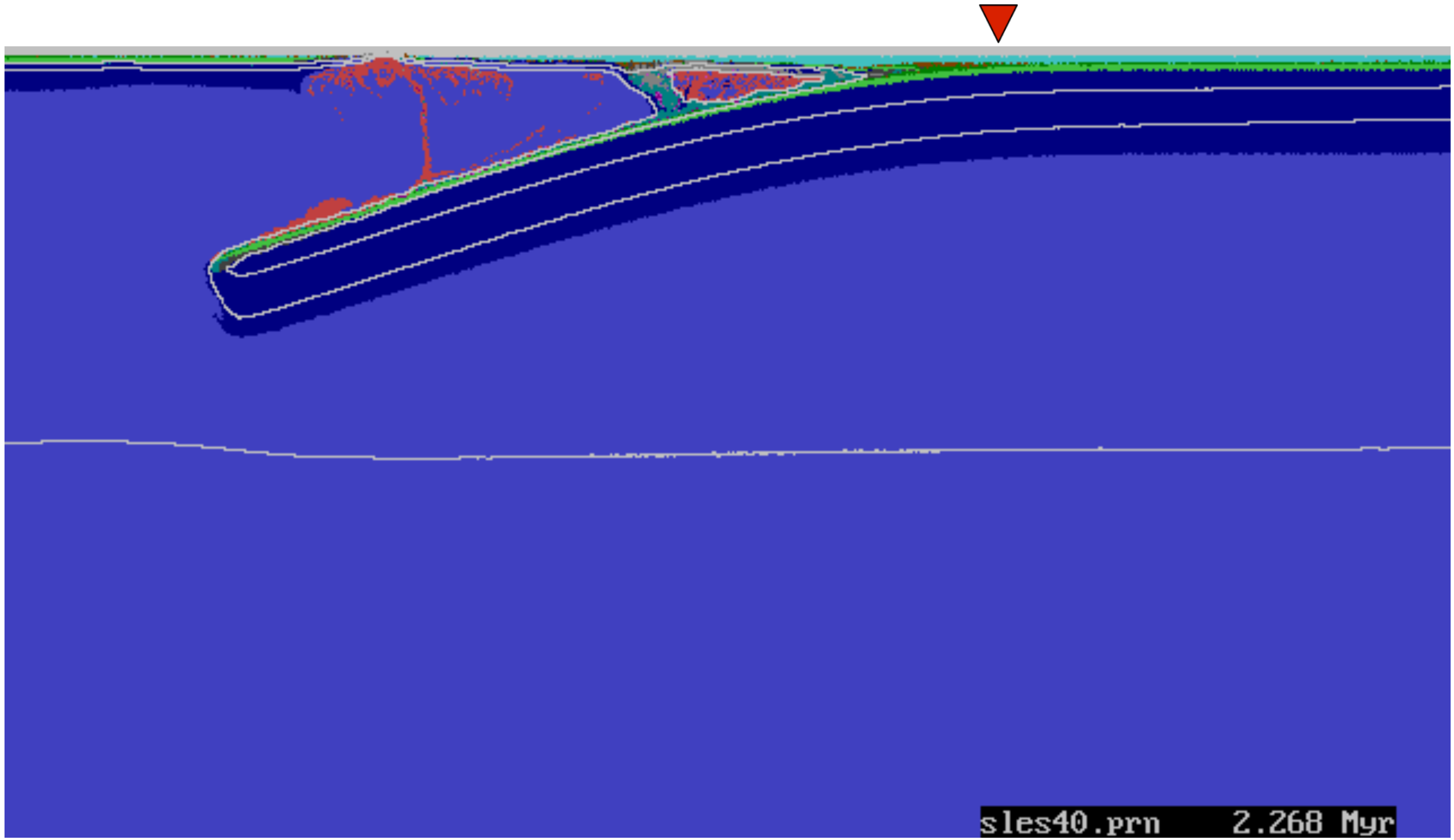
sles40.prn 2.268 Myr

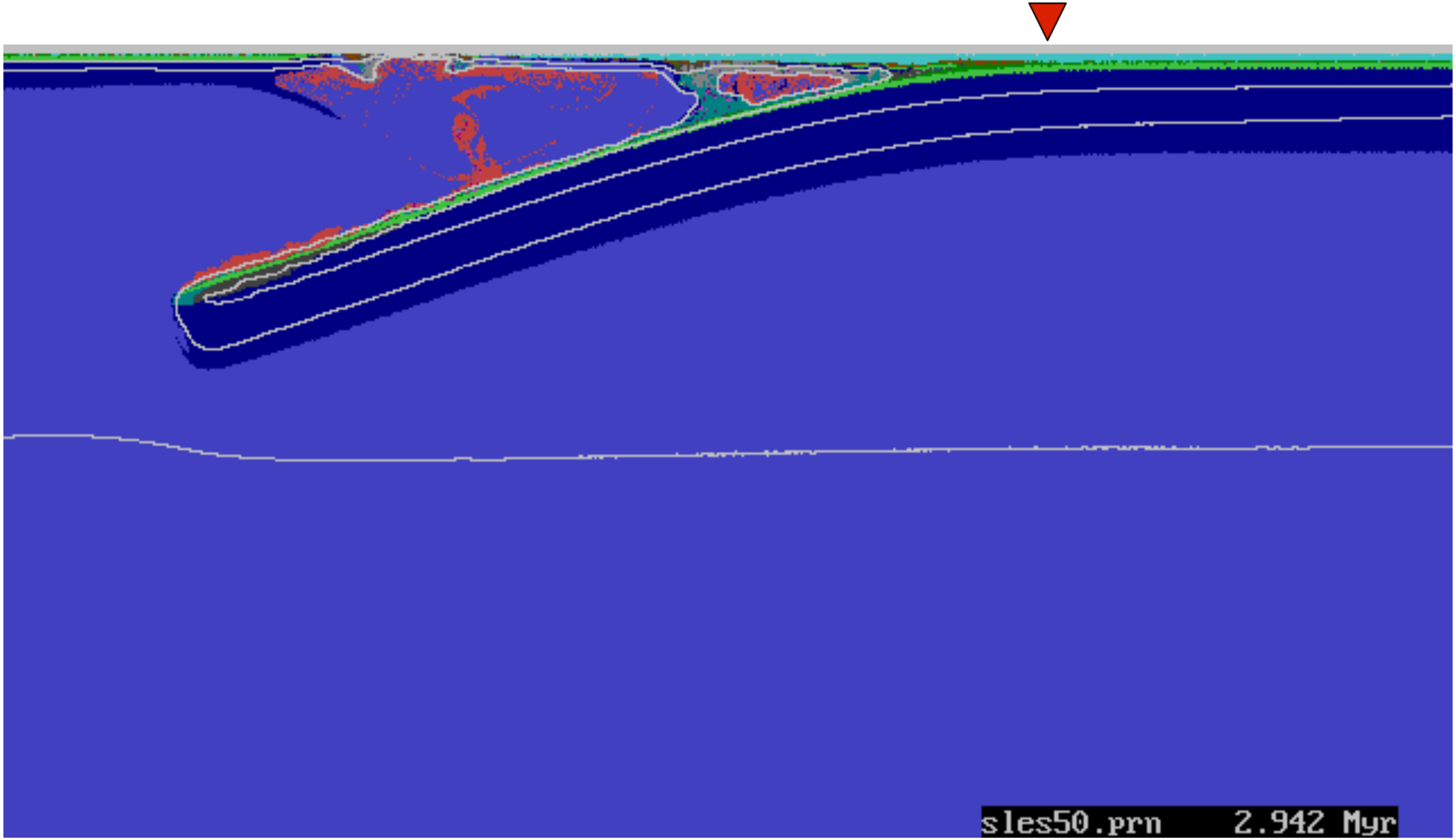
sles50.prn 2.942 Myr

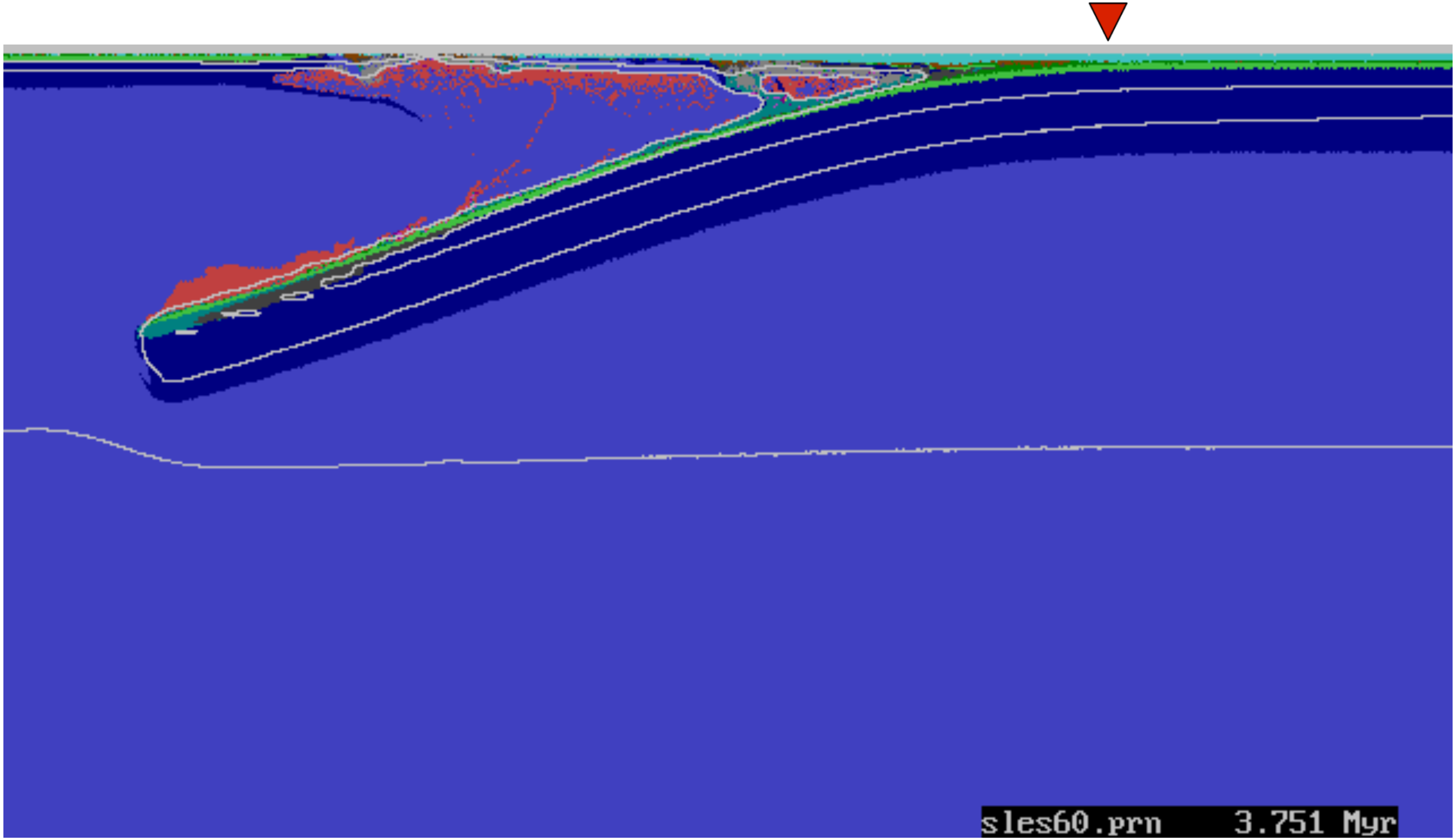
sles60.prn 3.751 Myr

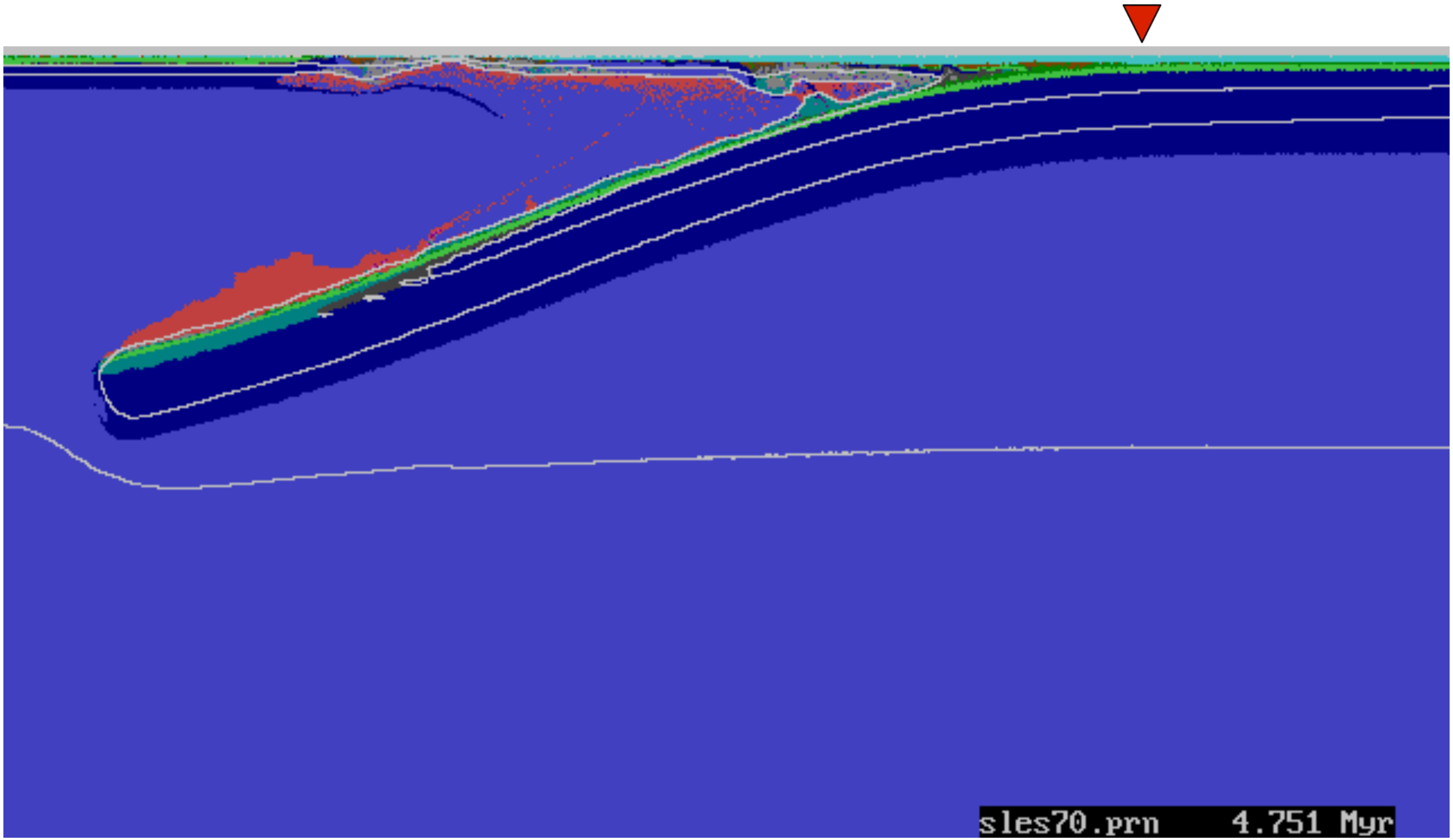
sles70.prn 4.751 Myr

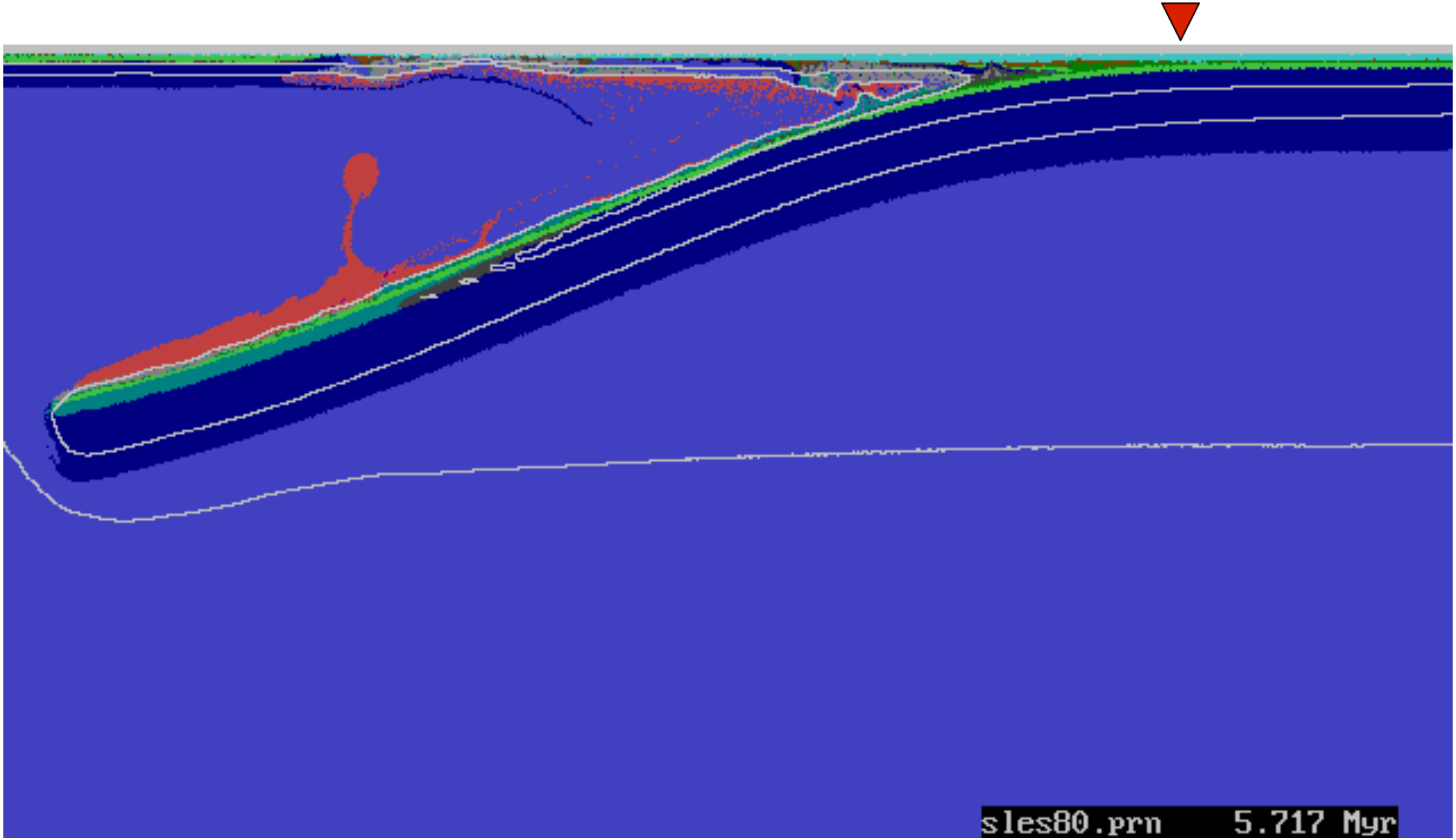
sles80.prn 5.717 Myr

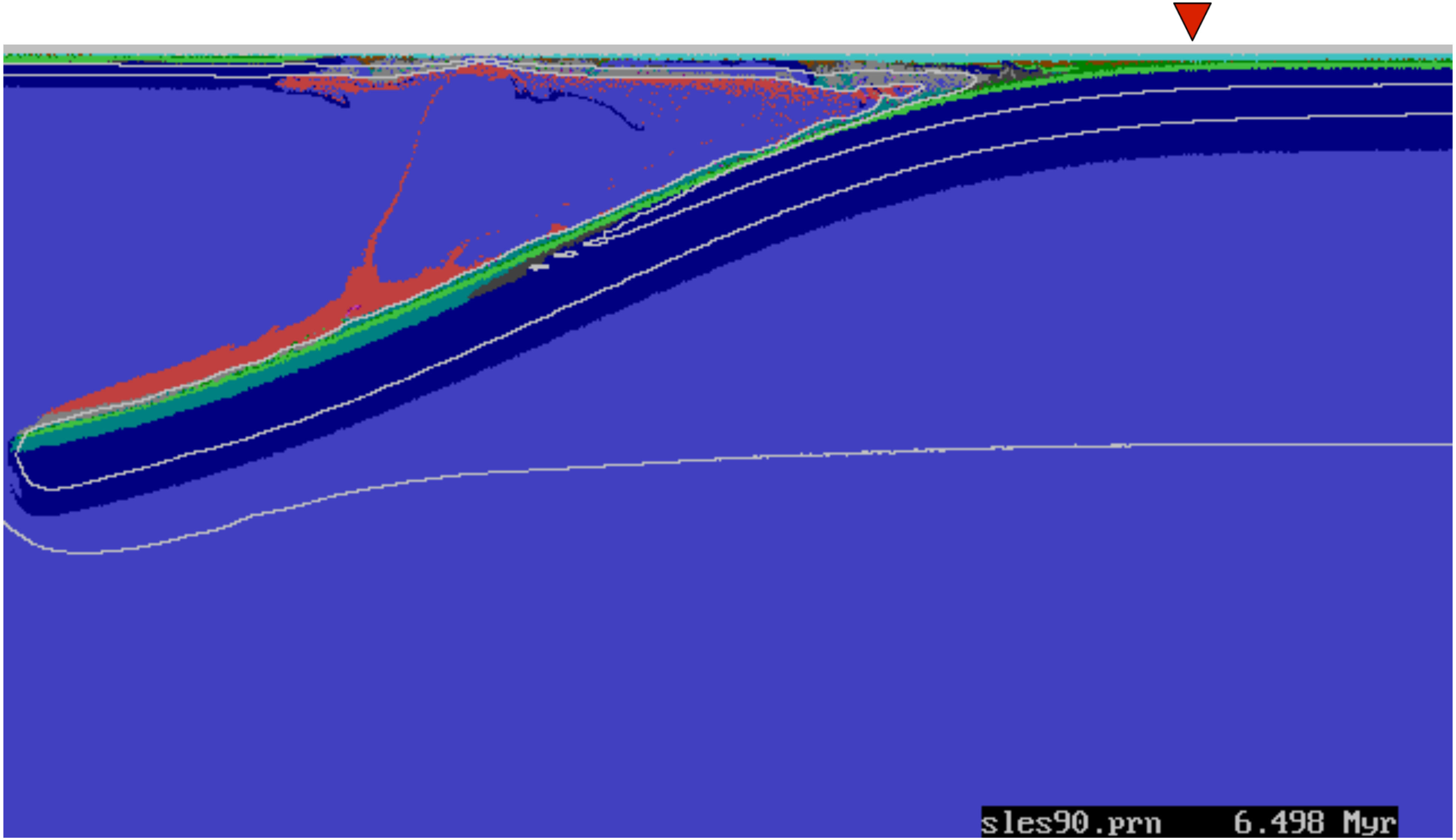
sles90.prn 6.498 Myr

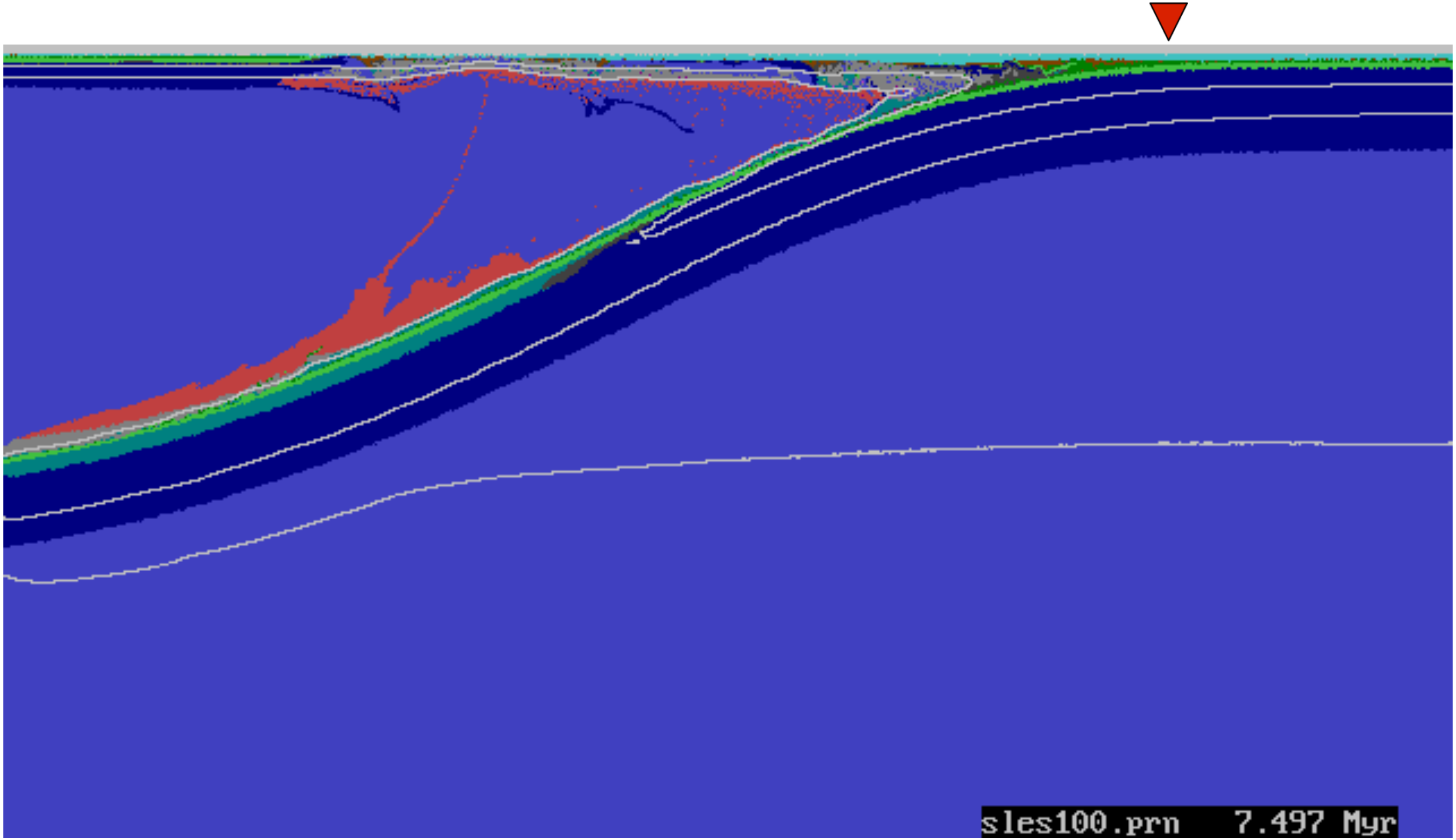
sles100.prn 7.497 Myr

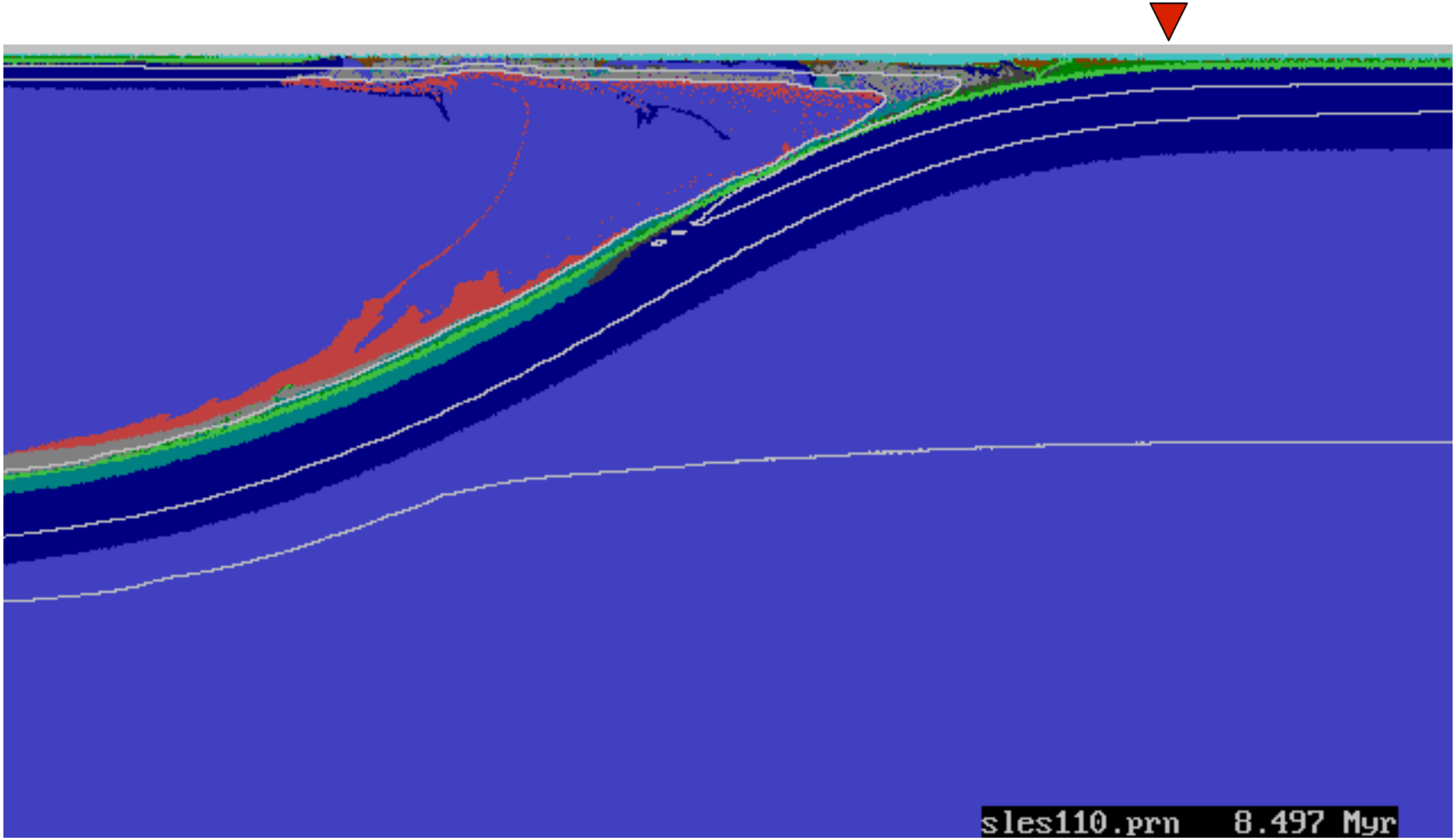
sles110.prn 8.497 Myr

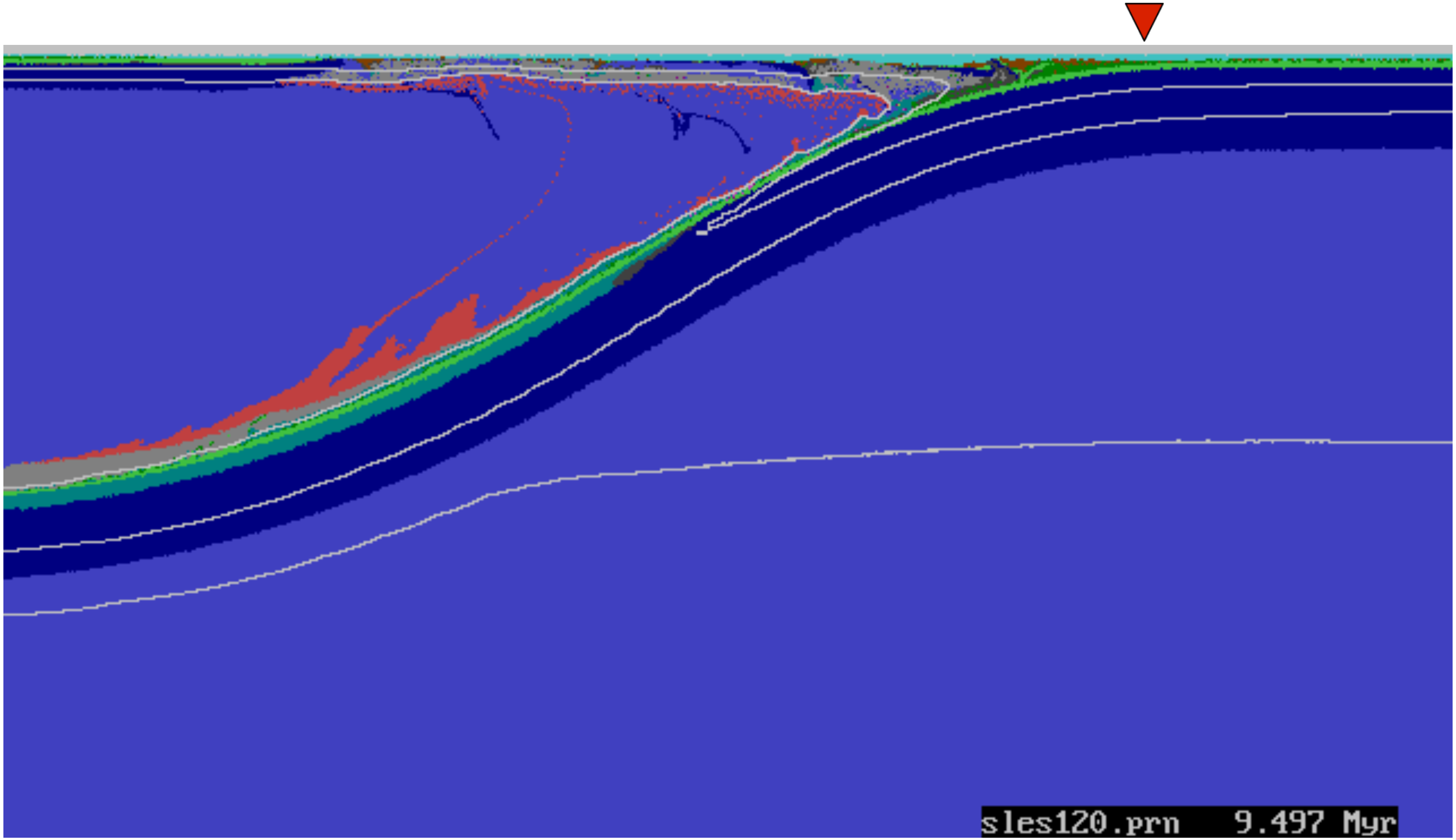
sles120.prn 9.497 Myr

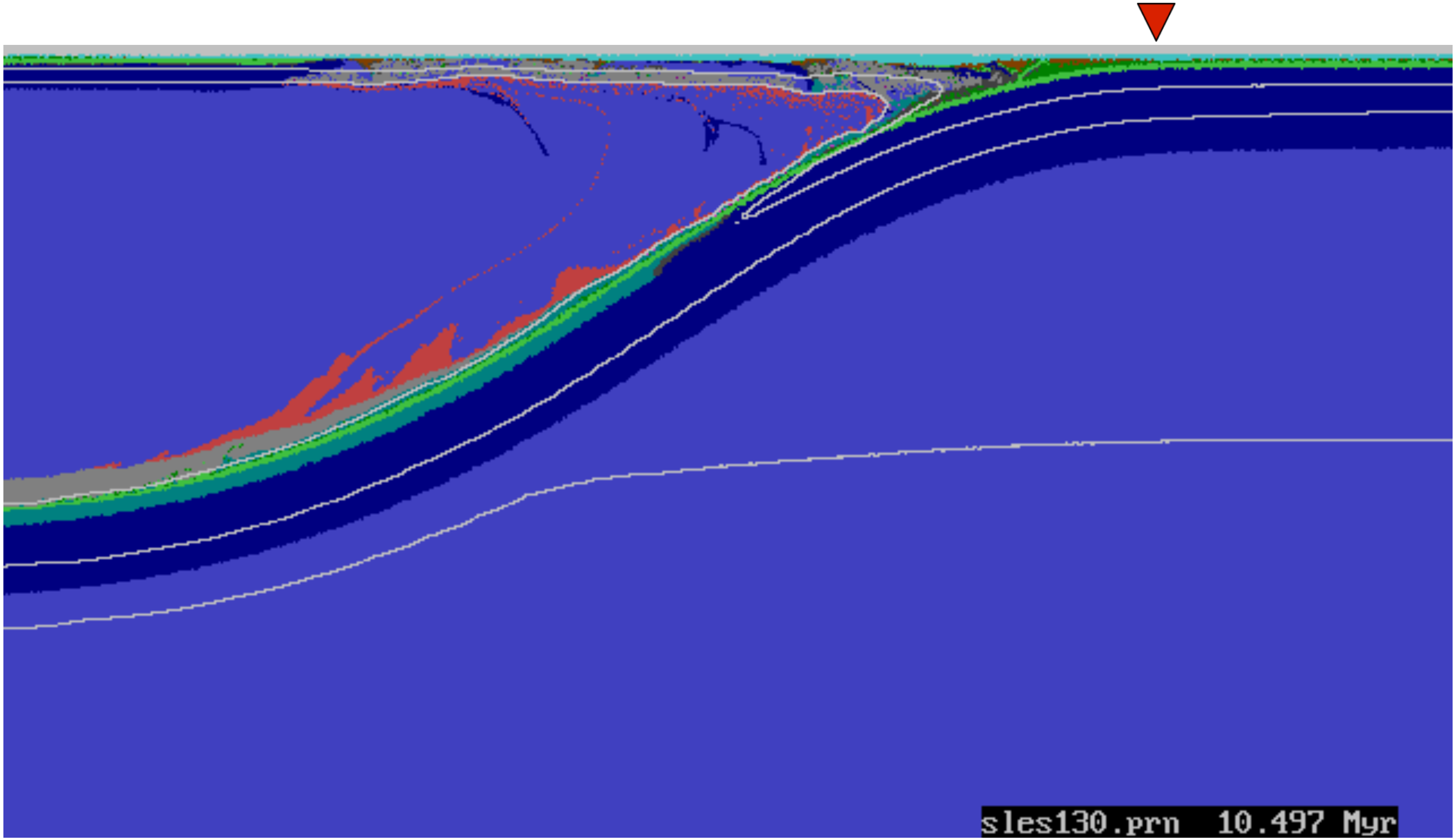
sles130.prn 10.497 Myr

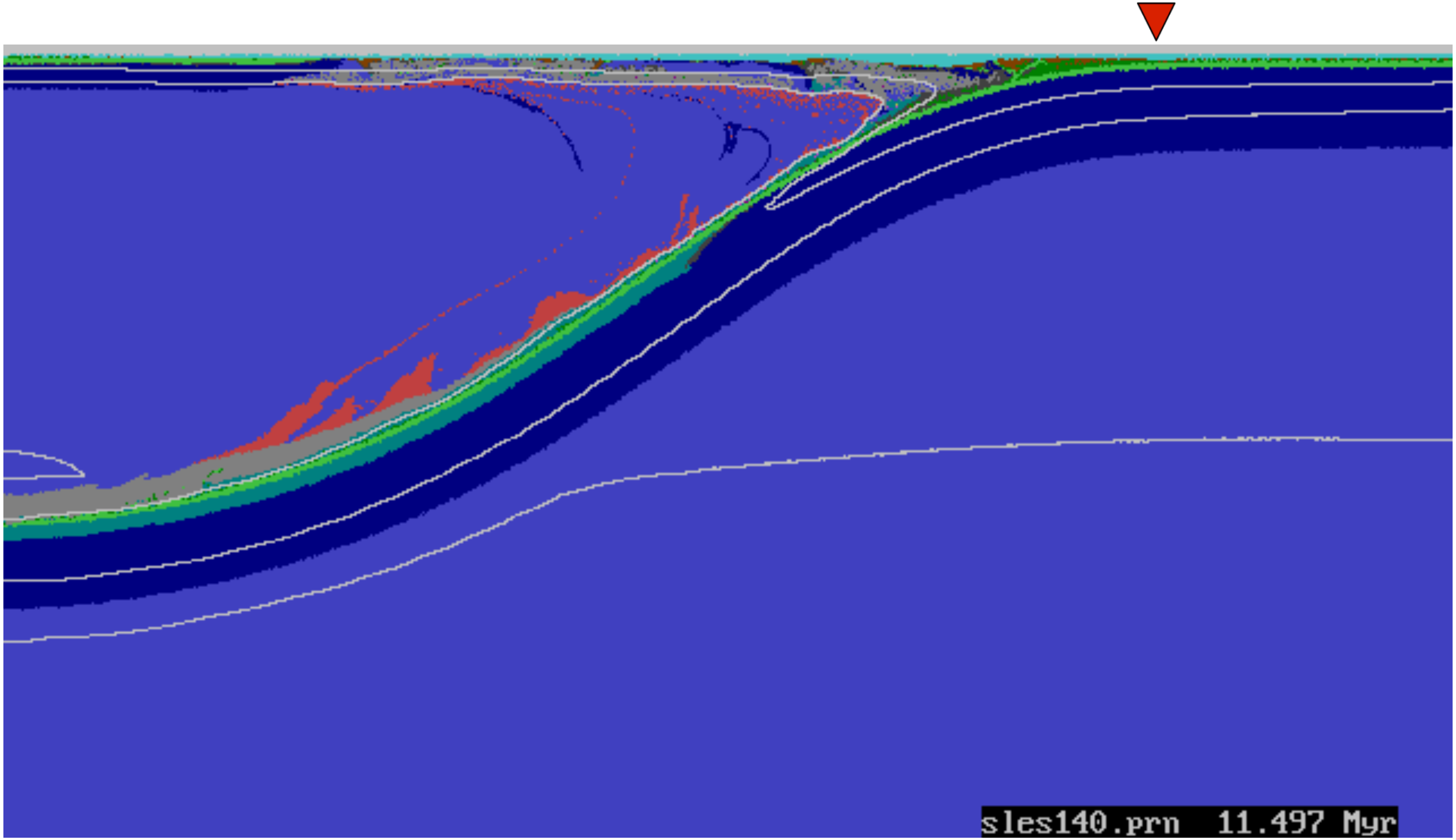
sles140.prn 11.497 Myr

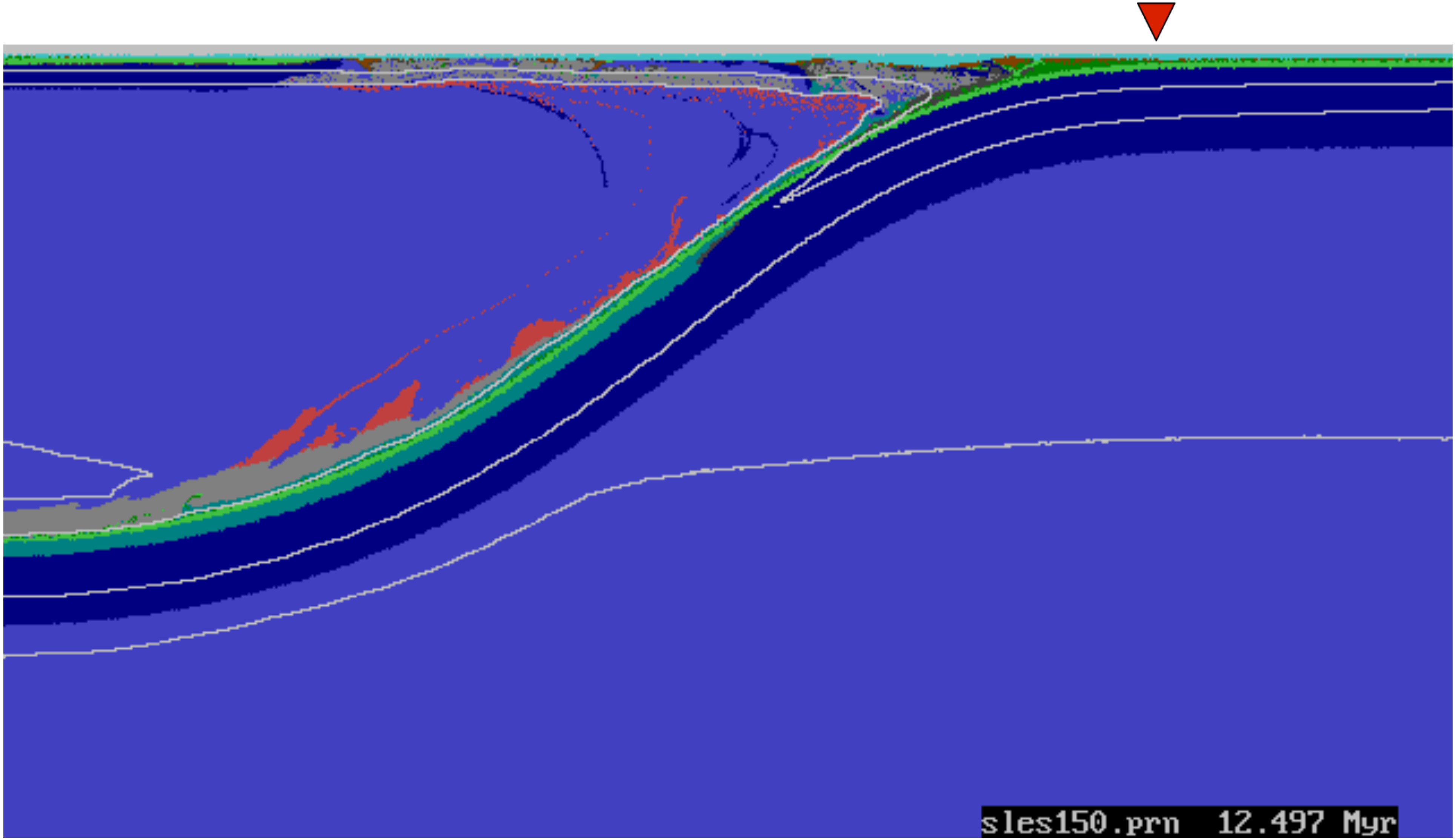
sles150.prn 12.497 Myr

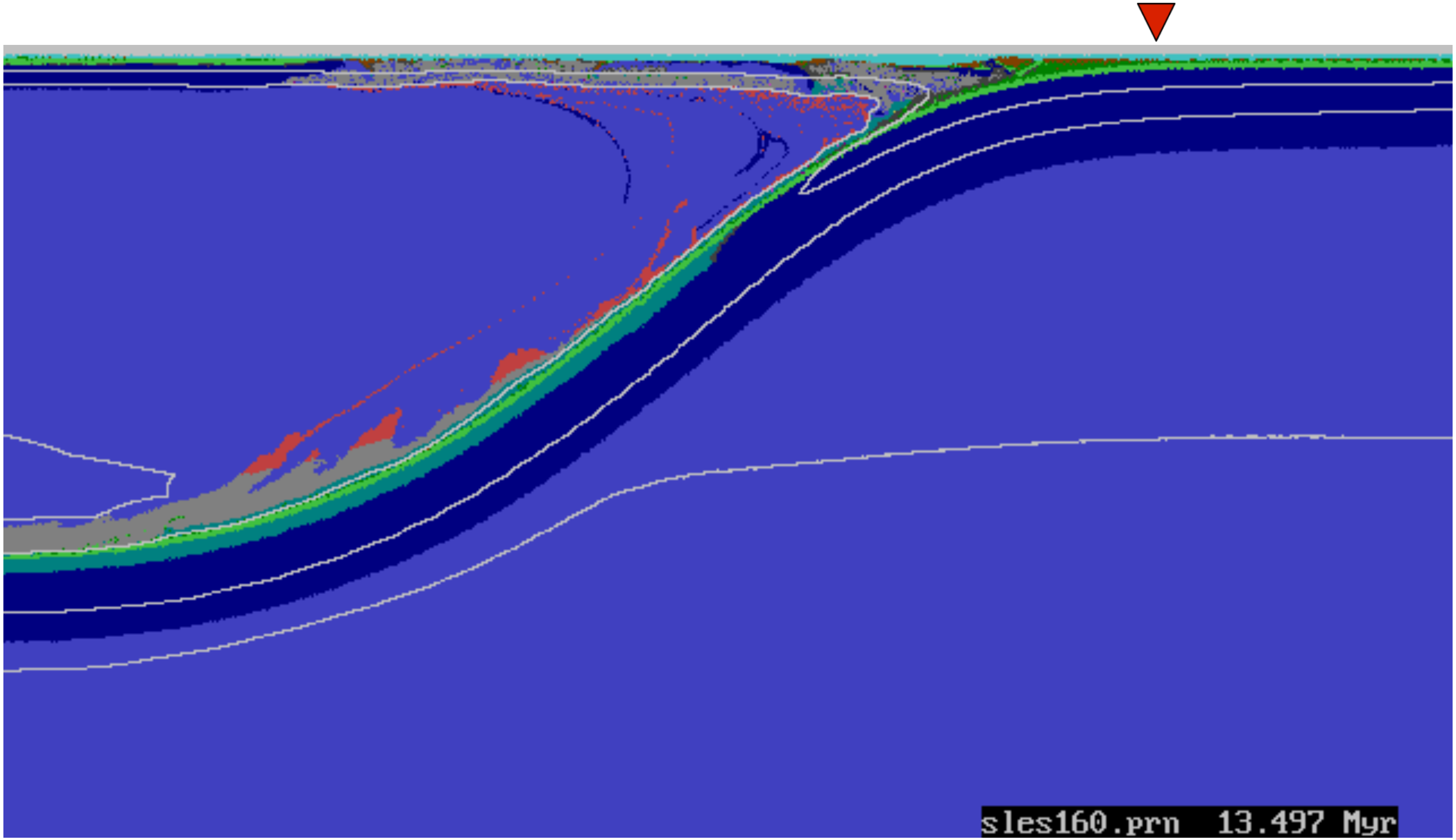
sles160.prn 13.497 Myr

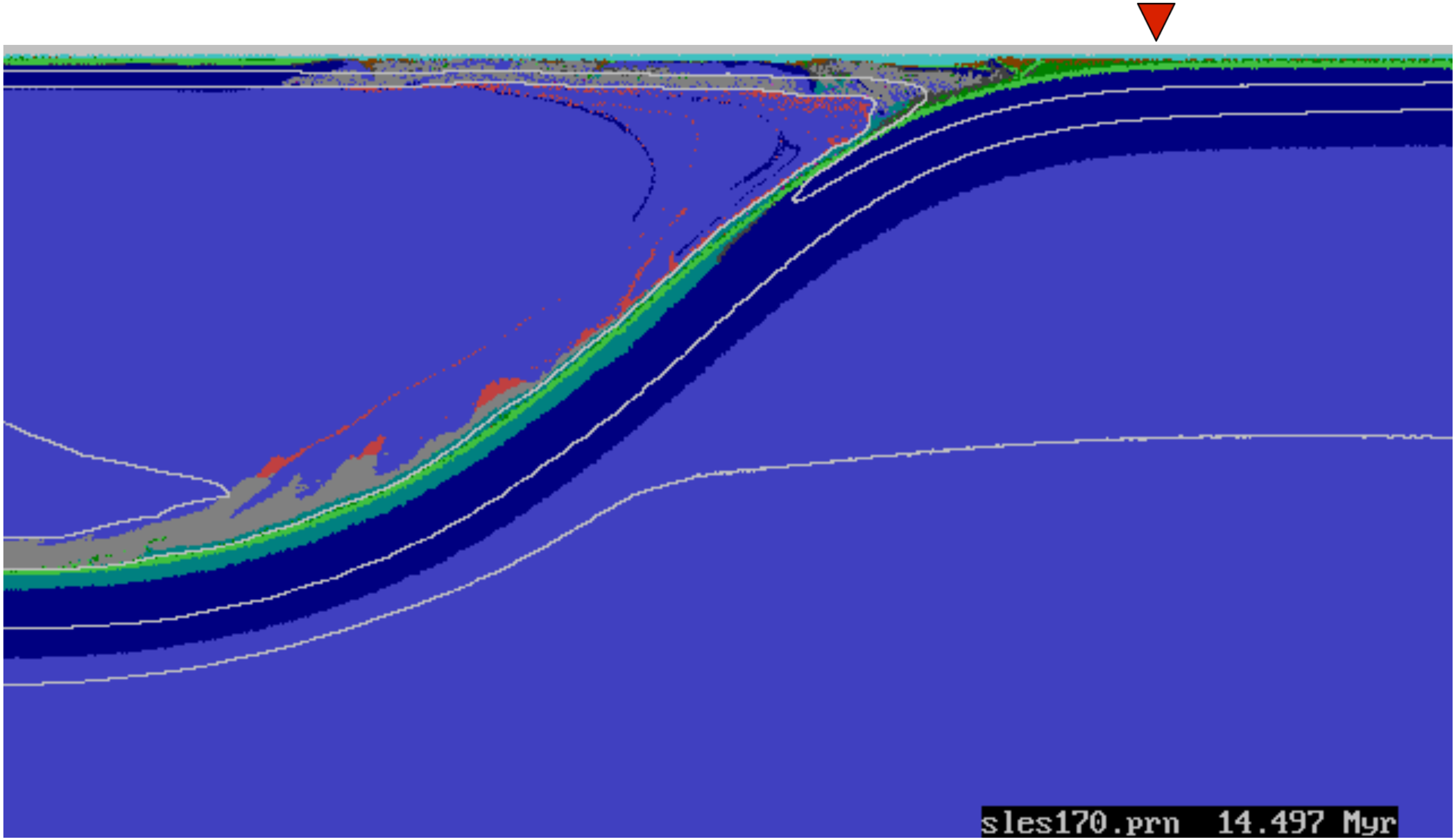
sles170.prn 14.497 Myr

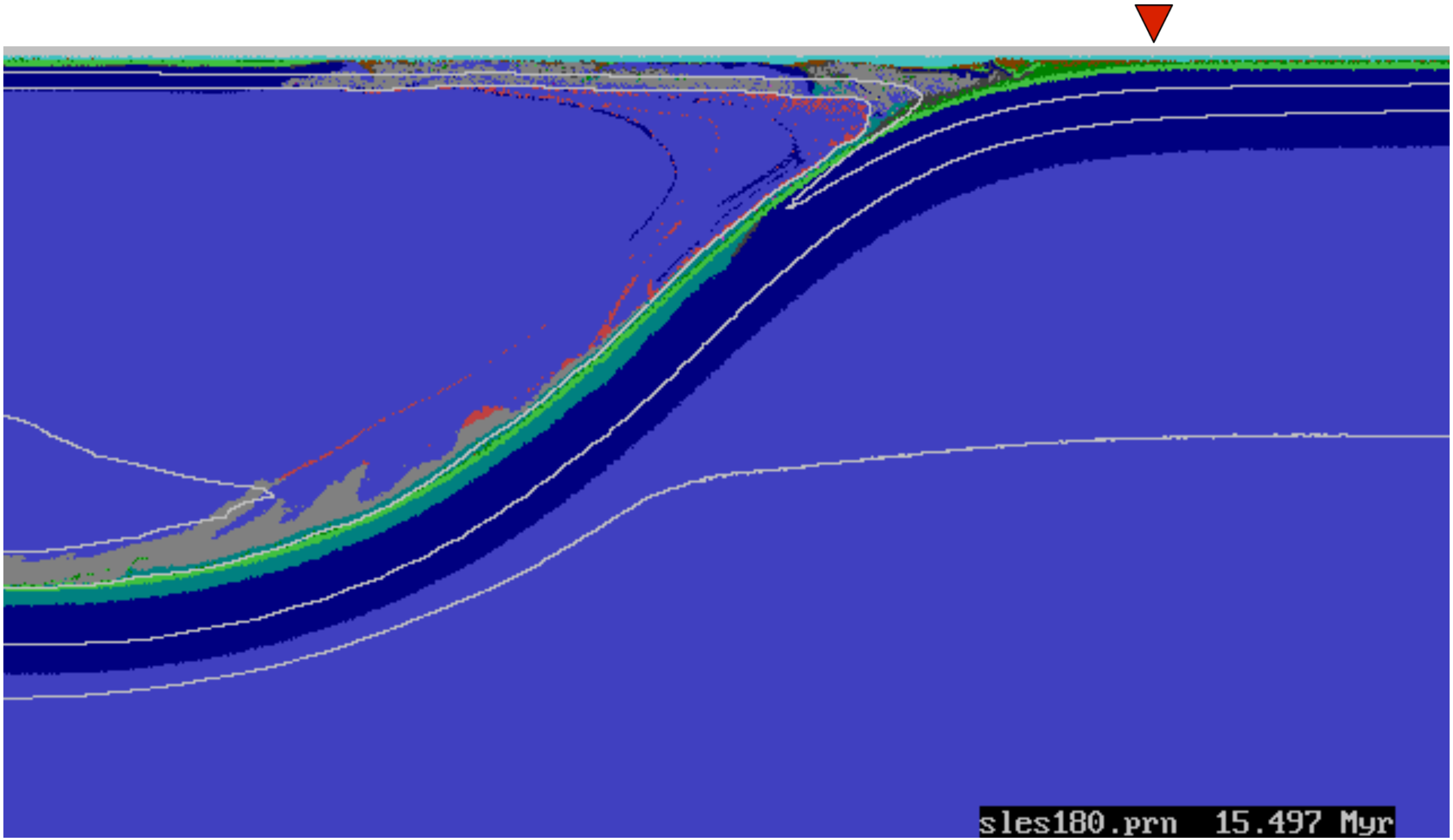
sles180.prn 15.497 Myr

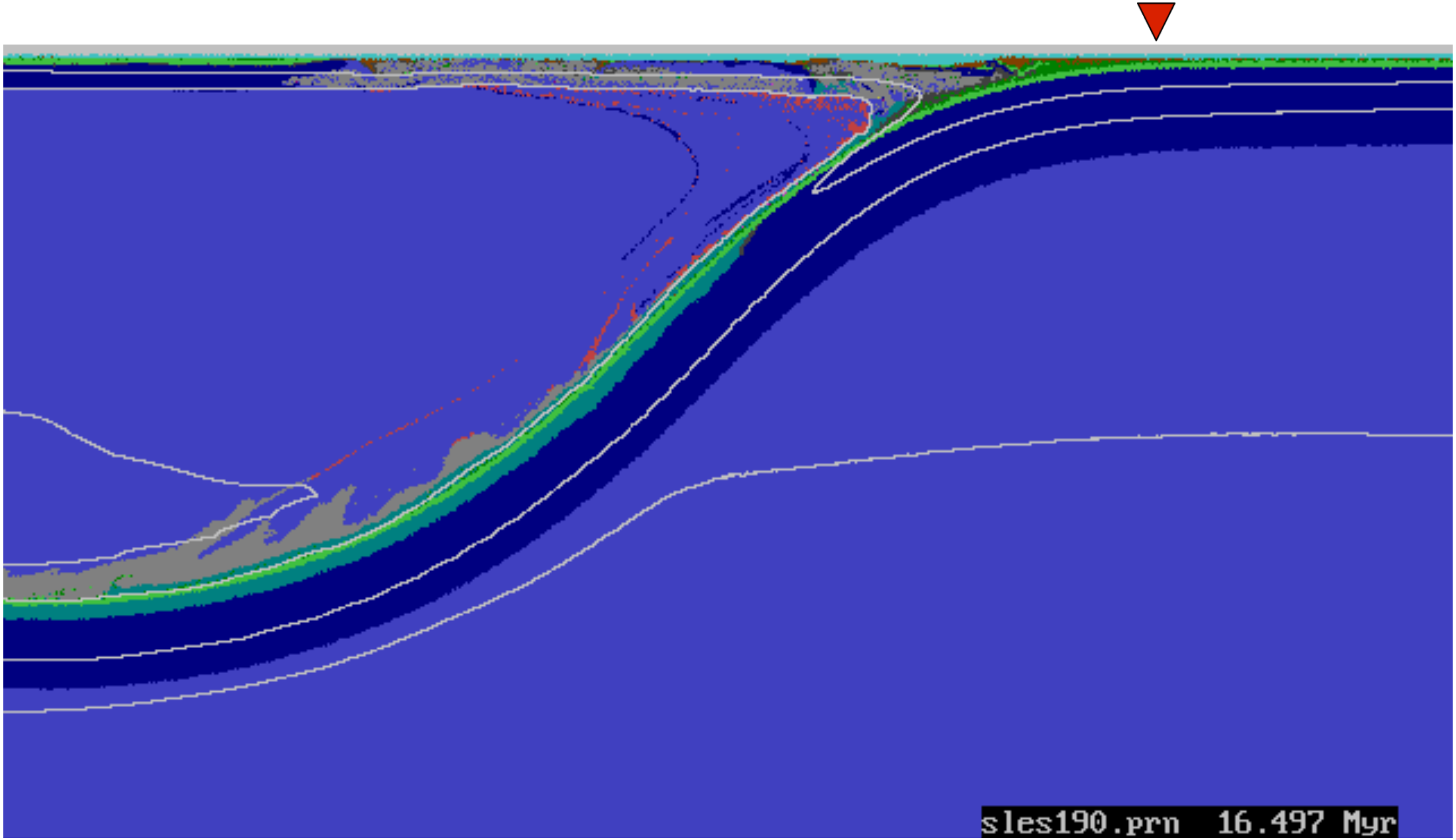
sles190.prn 16.497 Myr

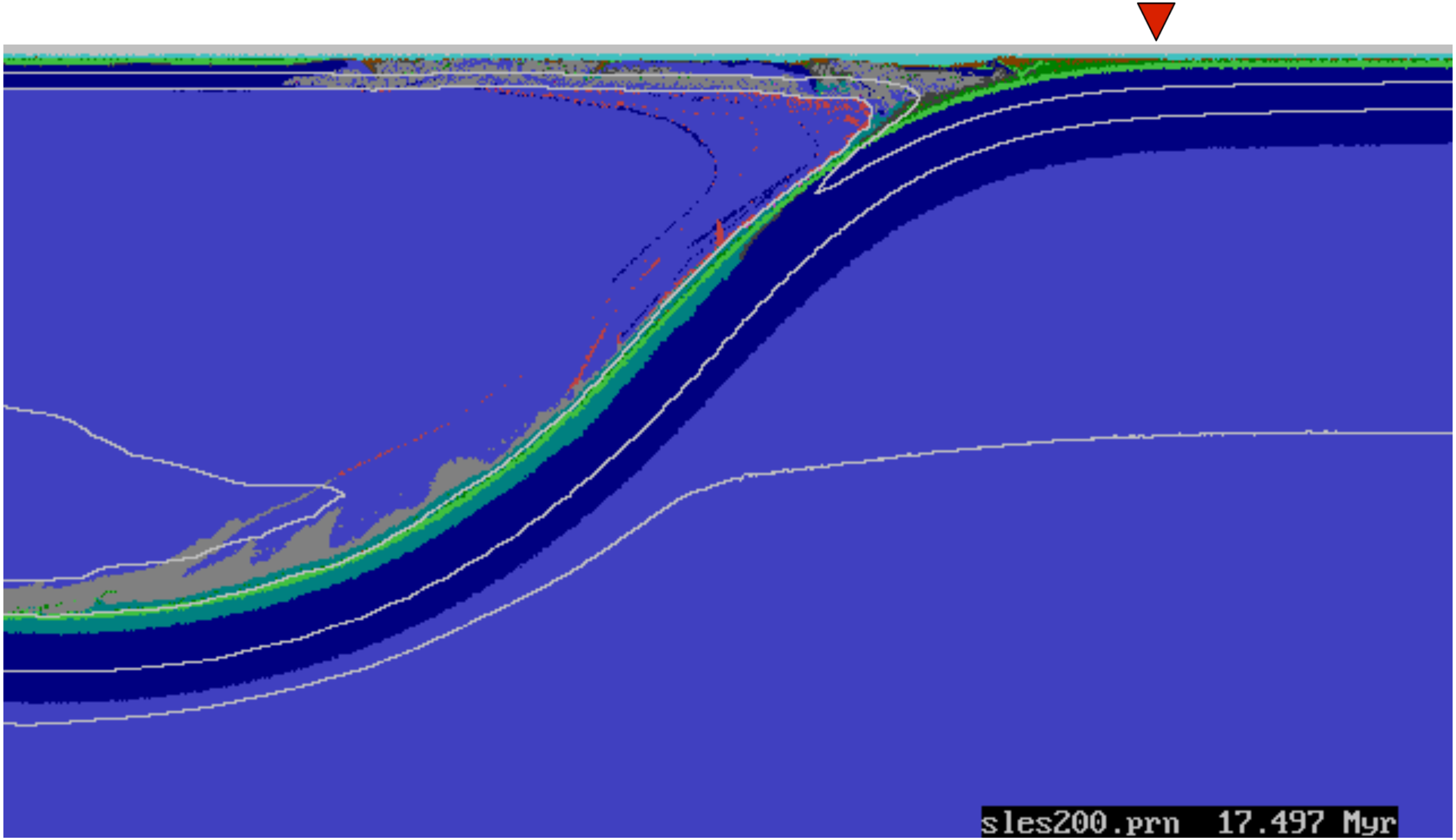
sles200.prn 17.497 Myr

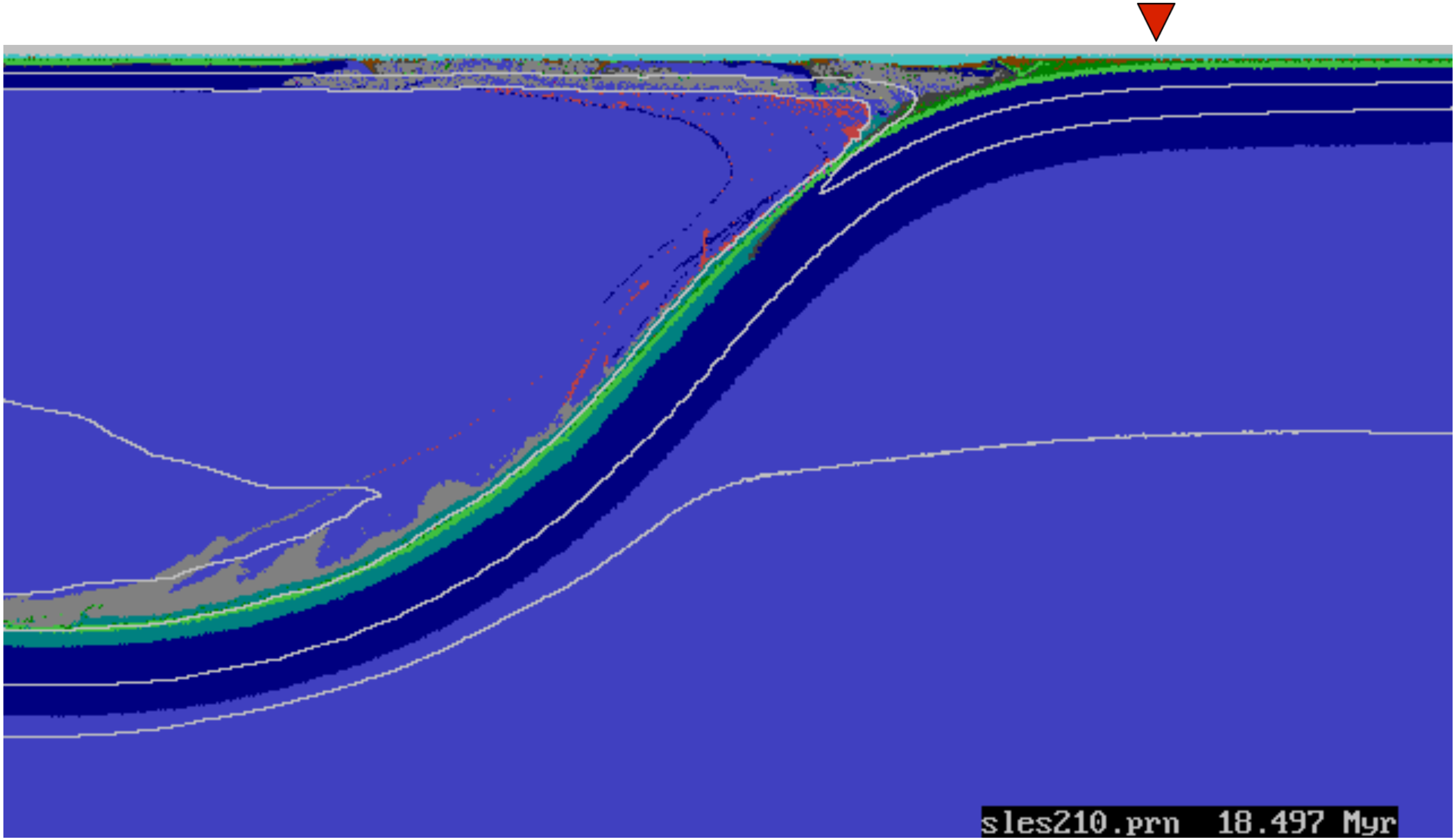
sles210.prn 18.497 Myr

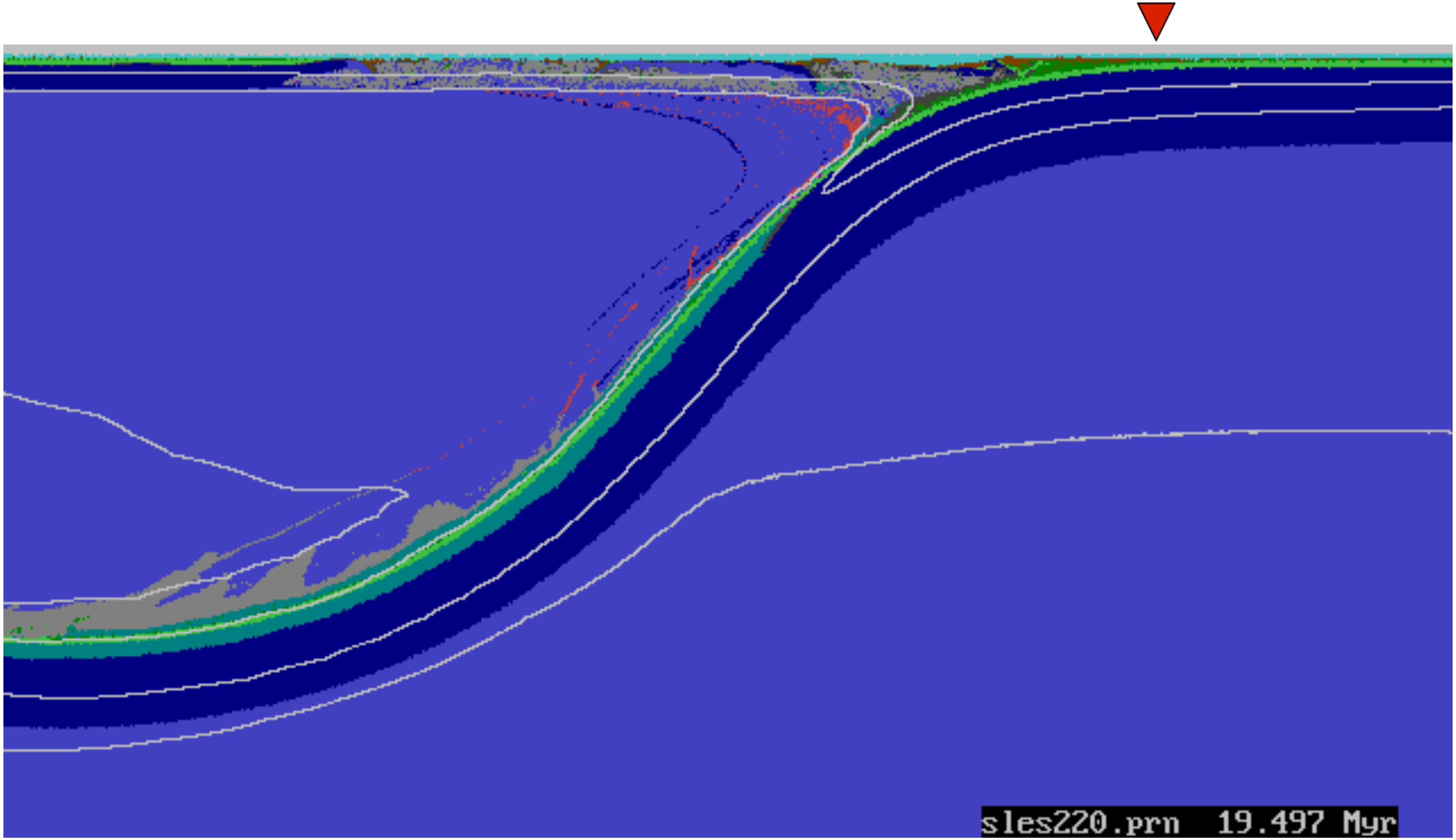
sles220.prn 19.497 Myr

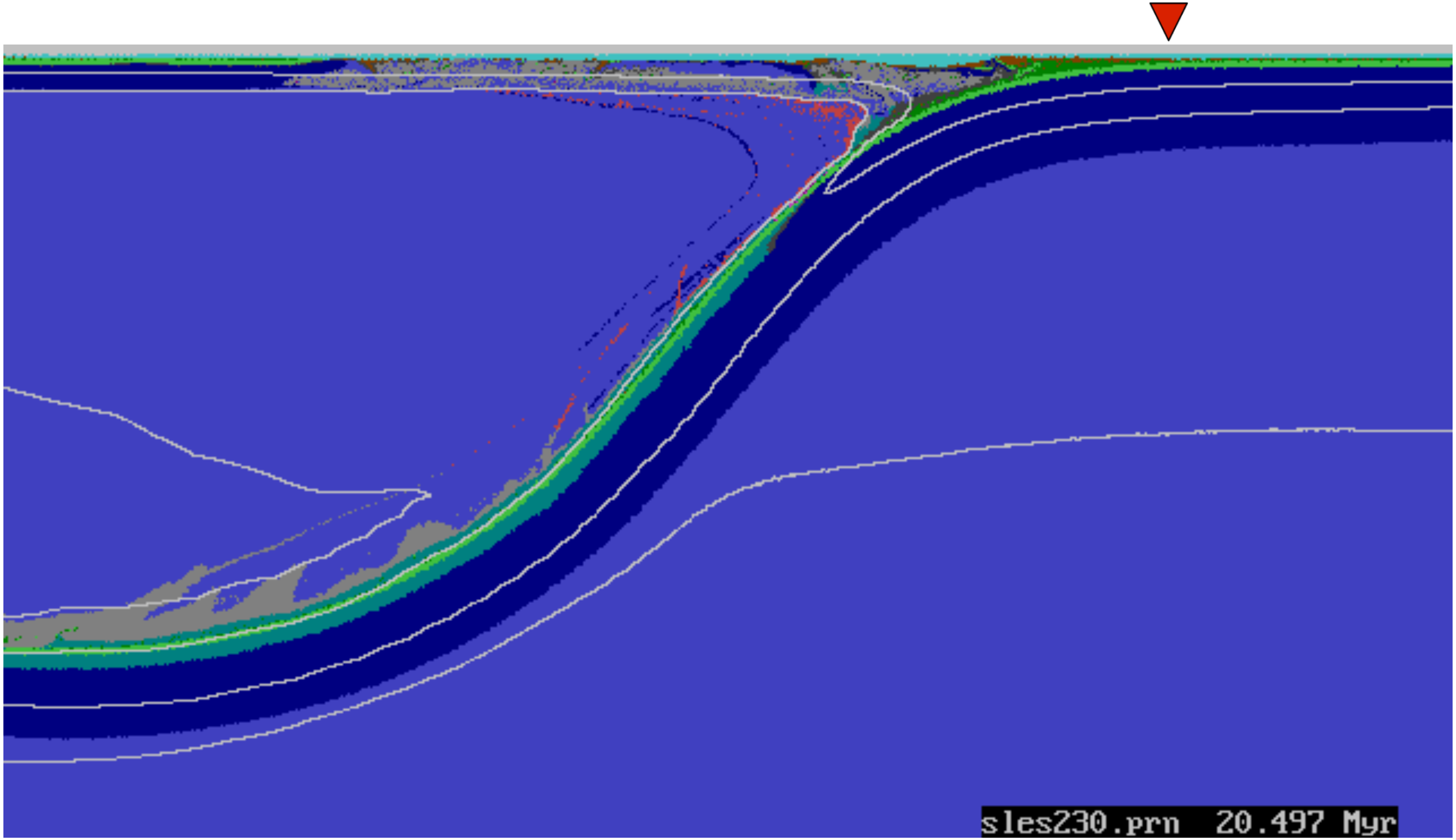
sles230.prn 20.497 Myr

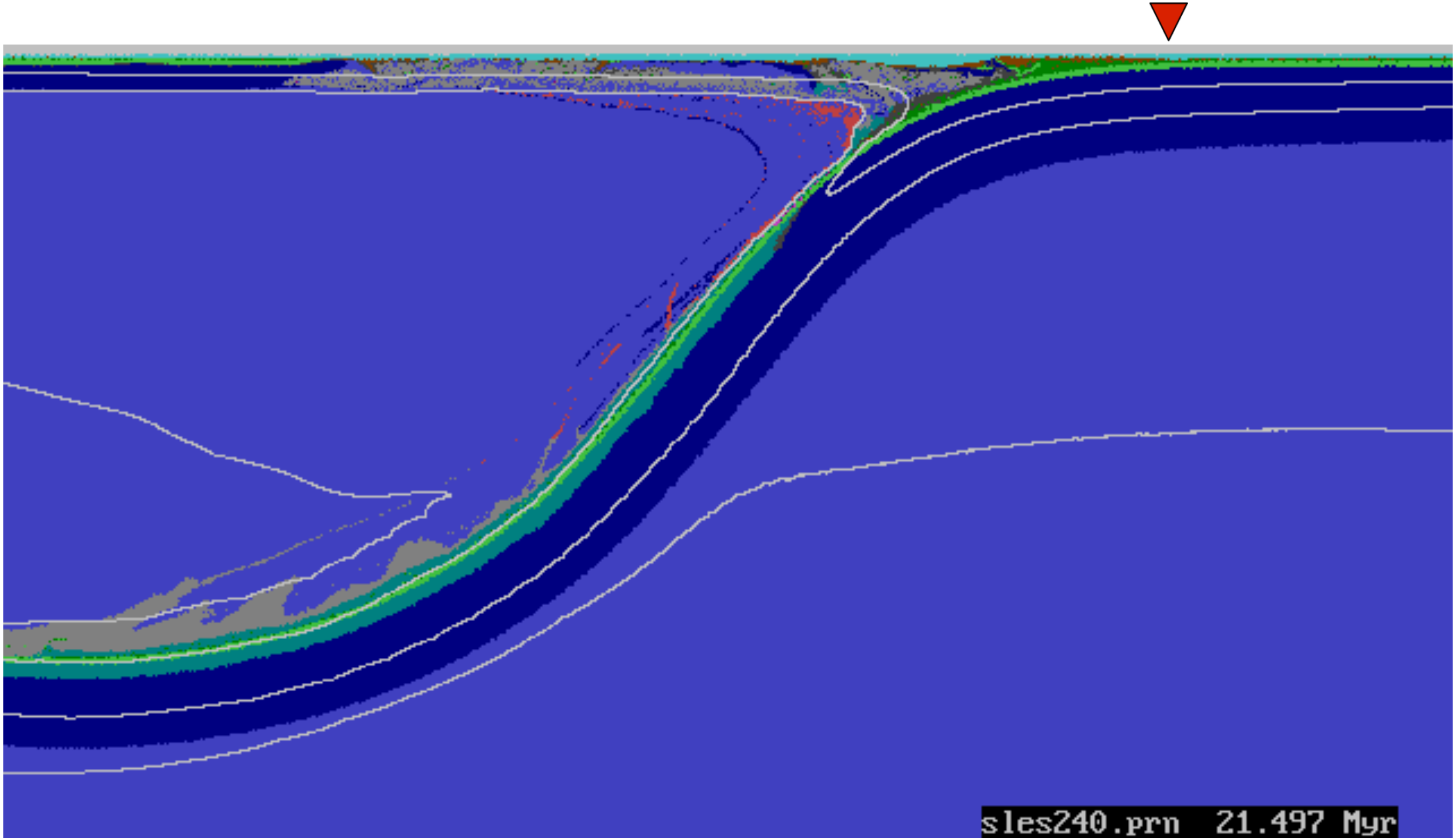
sles240.prn 21.497 Myr

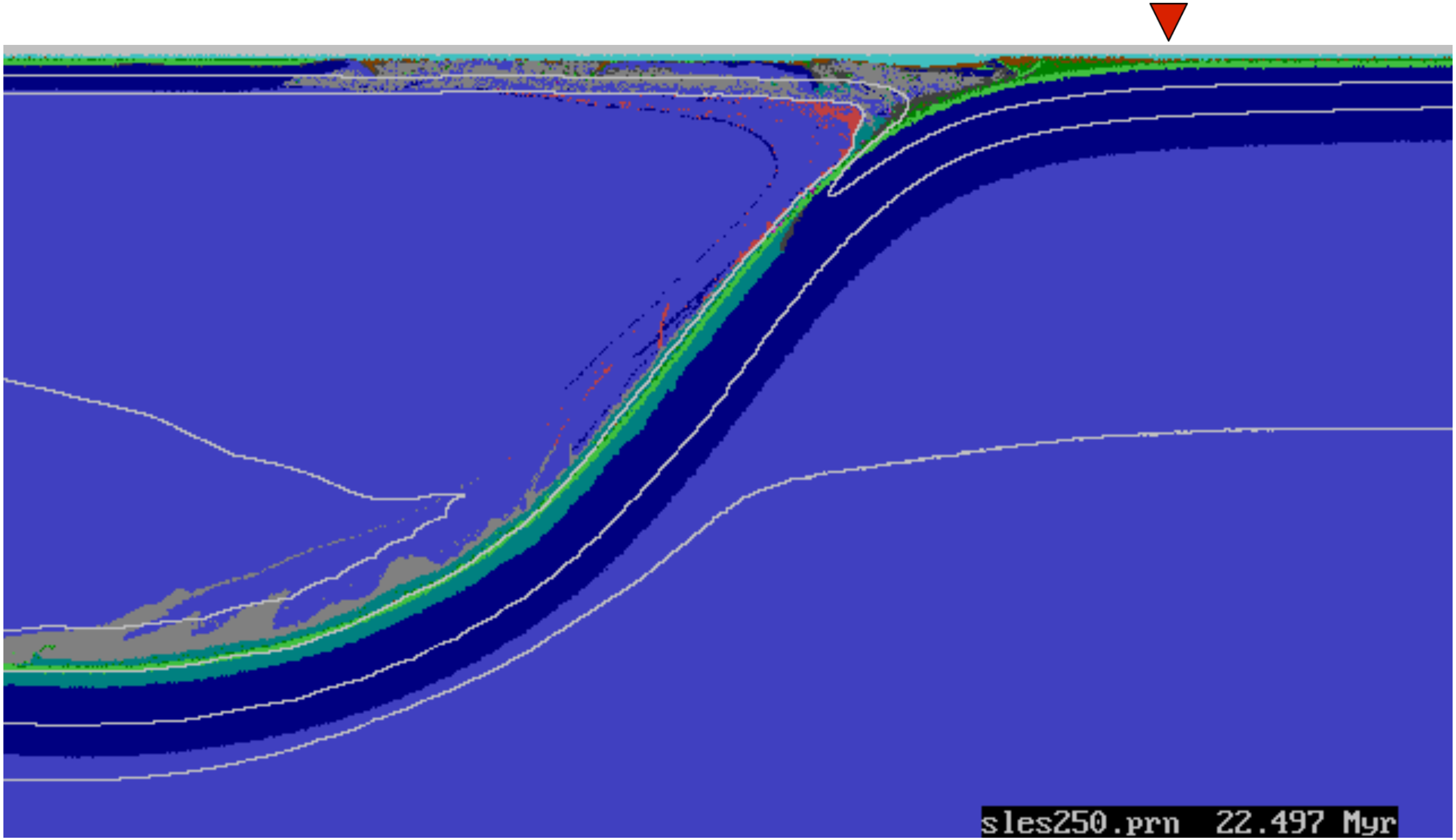
sles250.prn 22.497 Myr

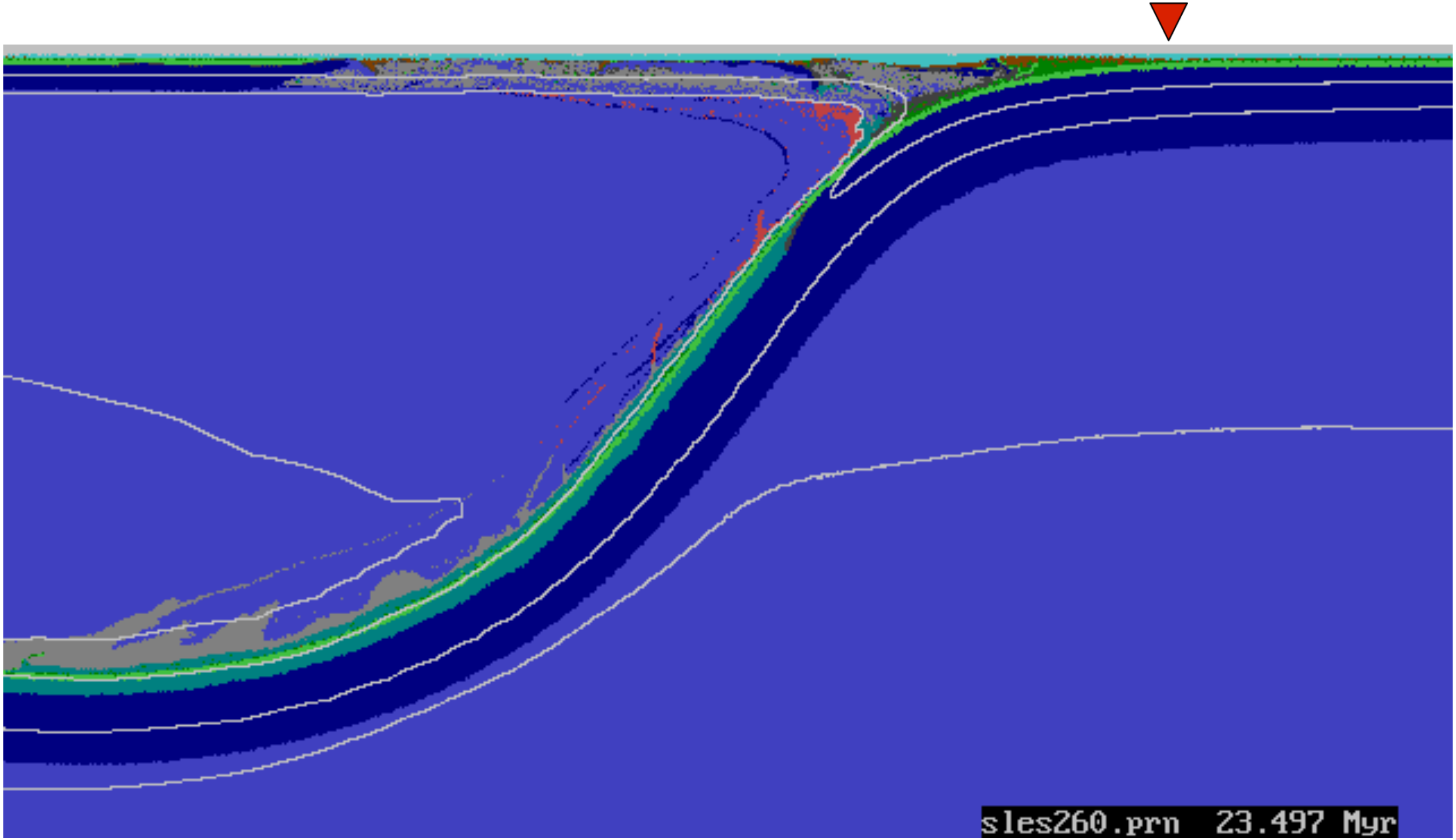
sles260.prn 23.497 Myr

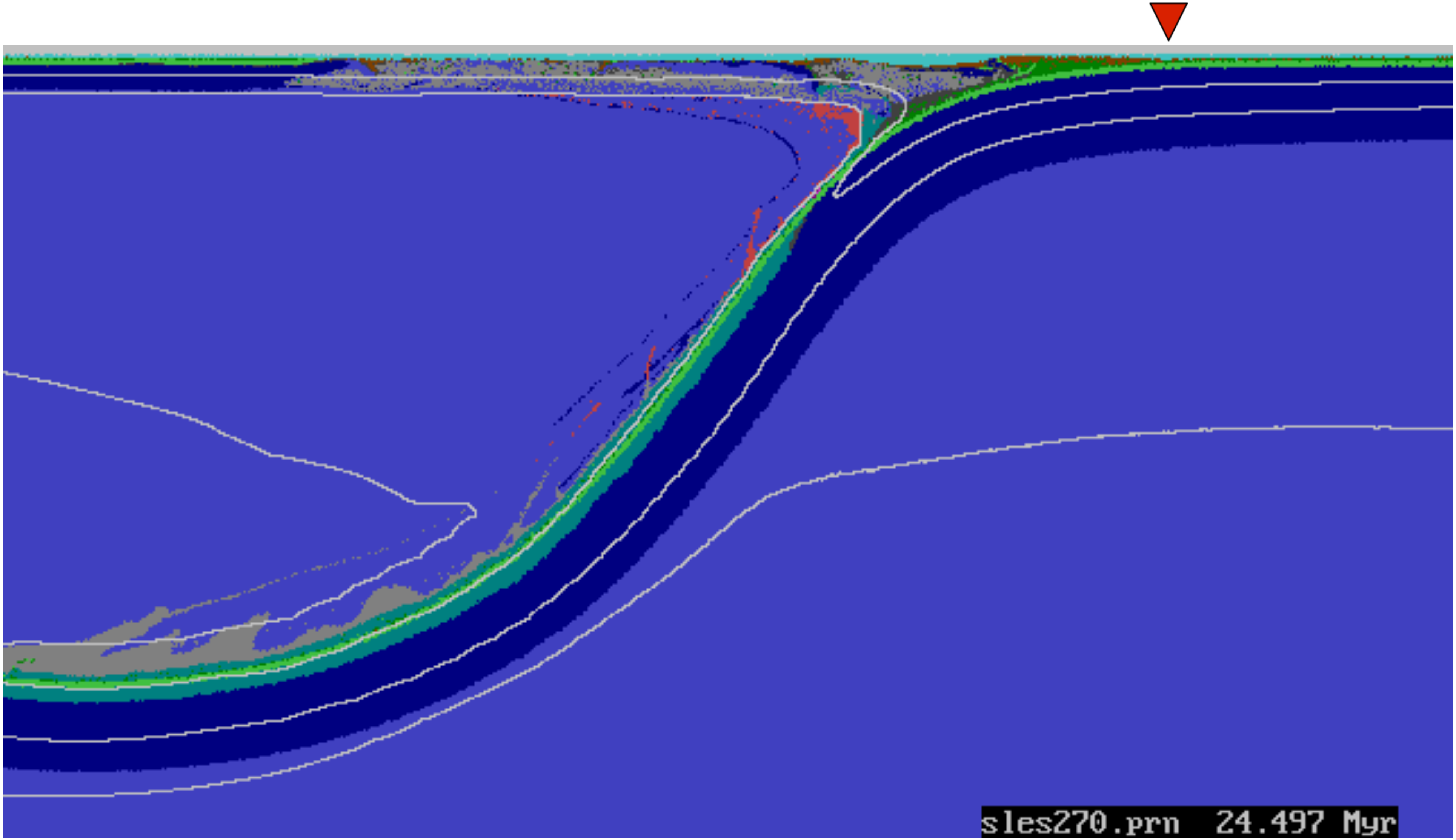
sles270.prn 24.497 Myr

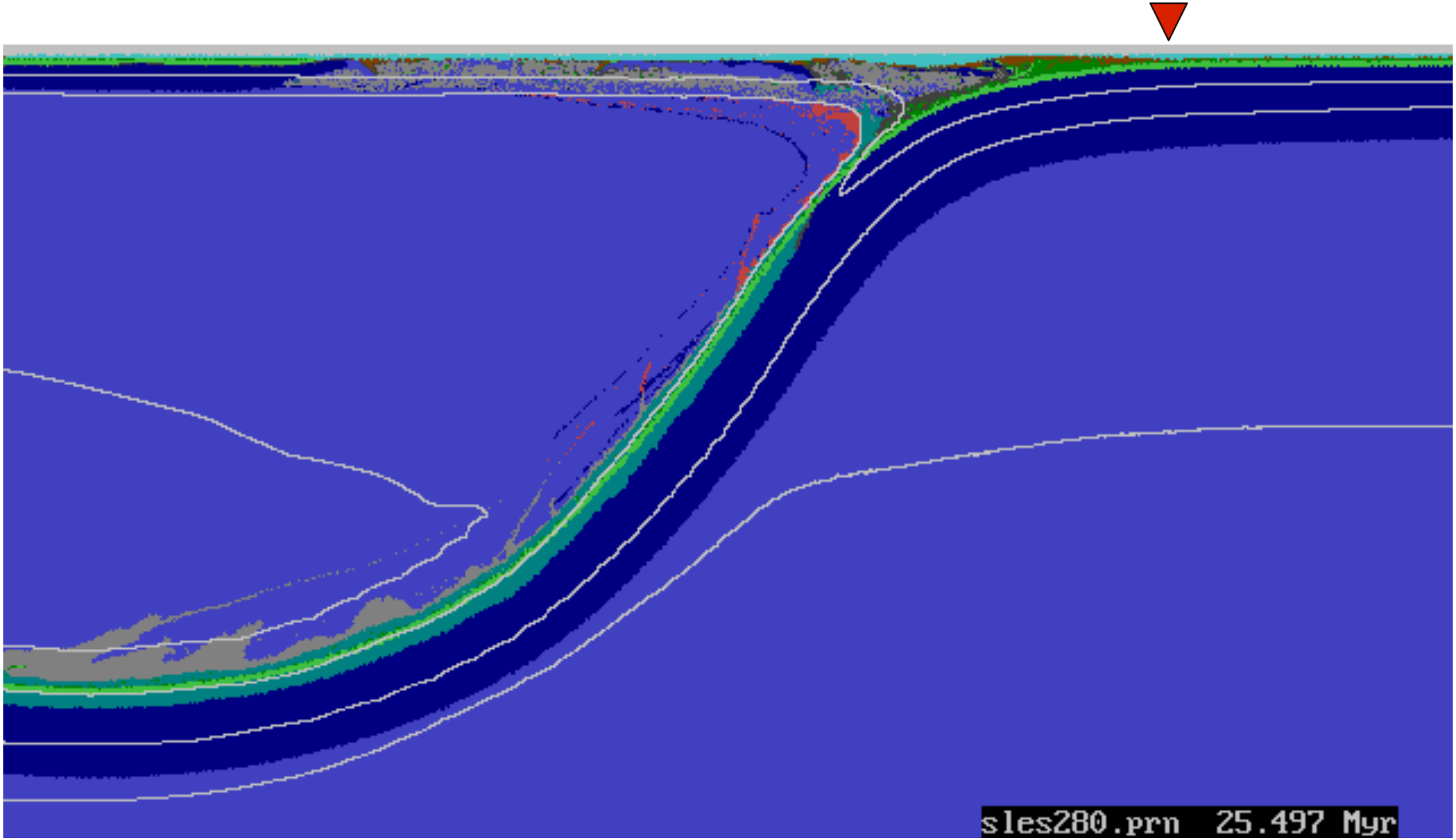
sles280.prn 25.497 Myr

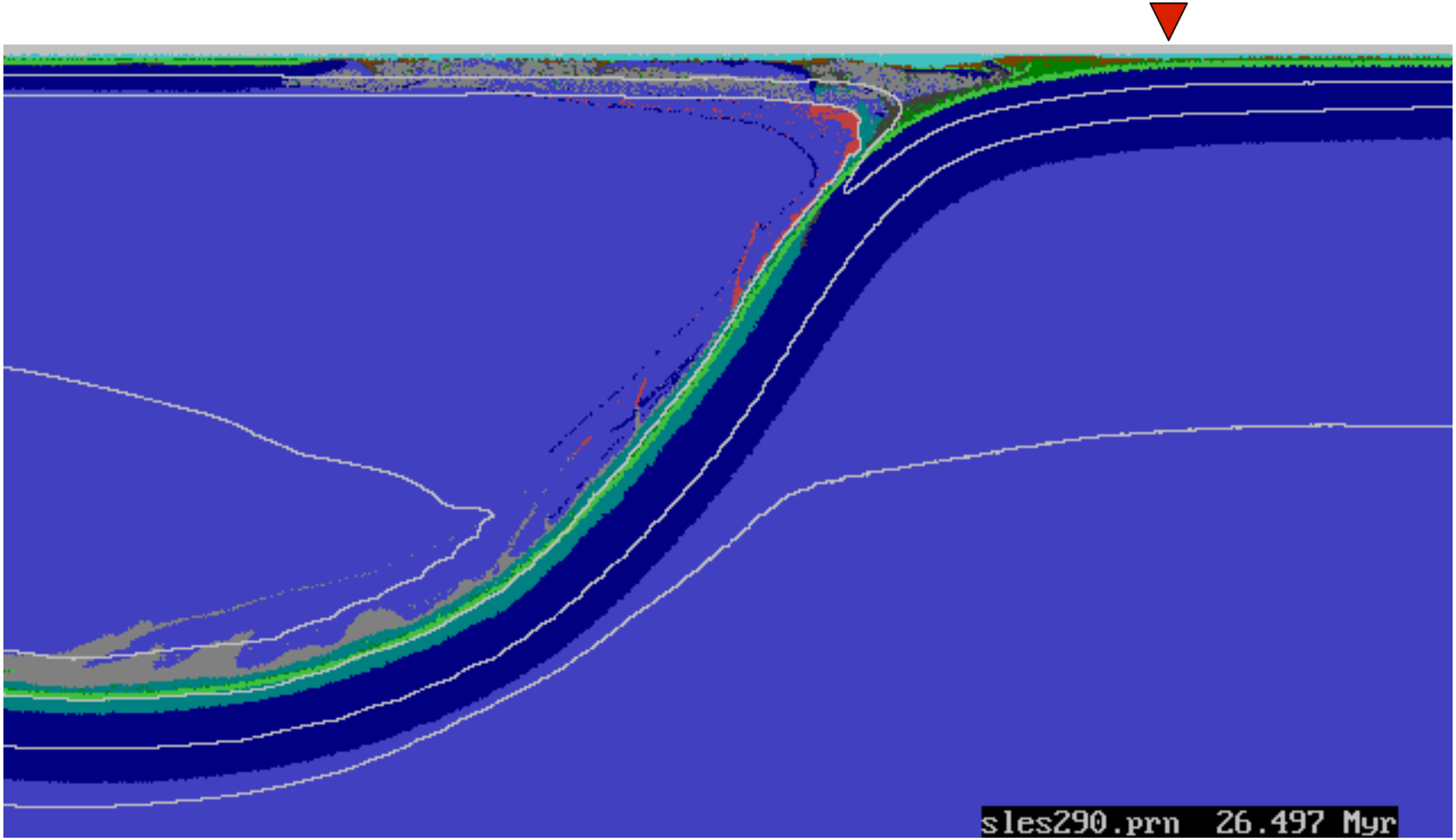
sles290.prn 26.497 Myr

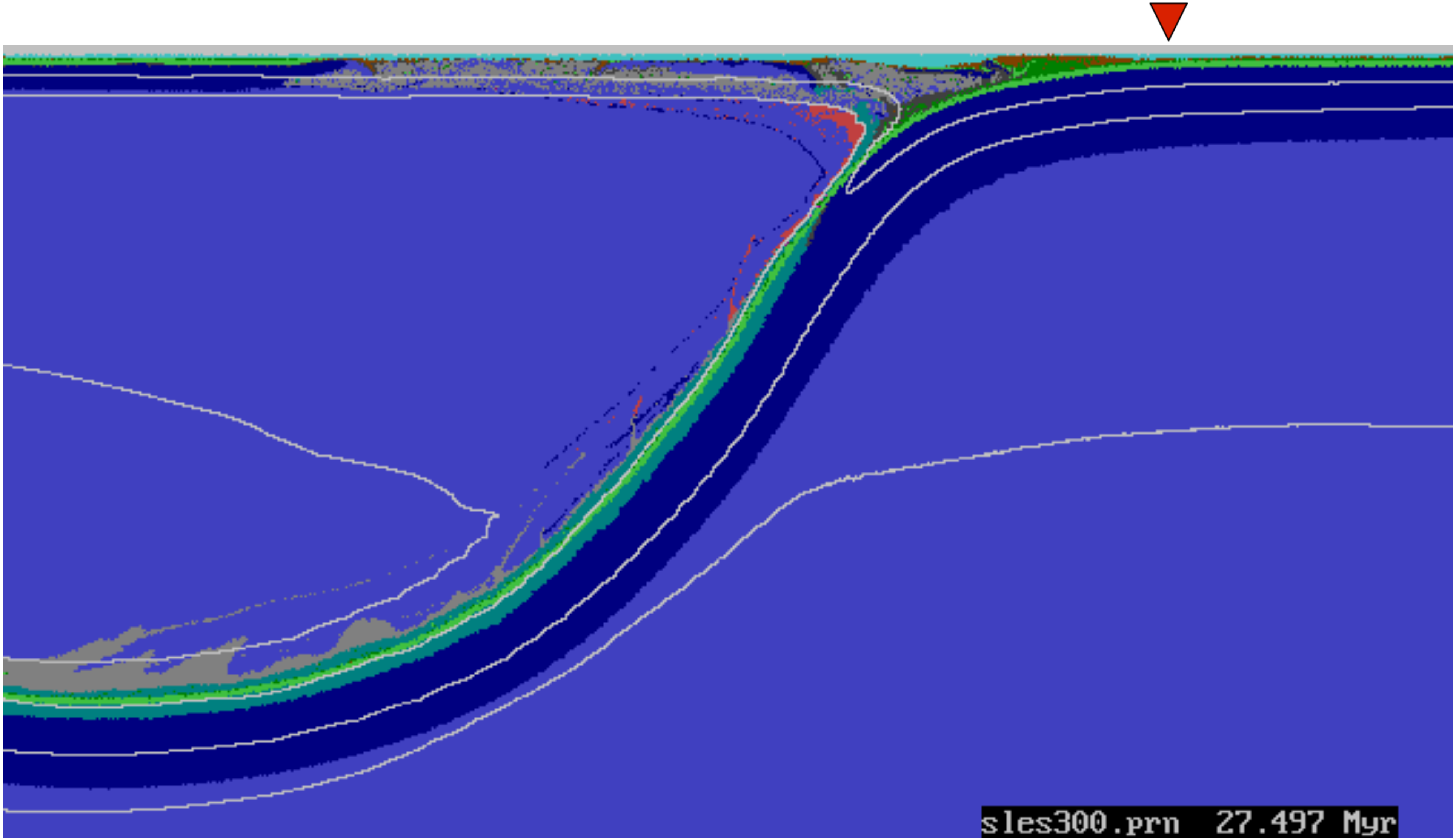
sles300.prn 27.497 Myr

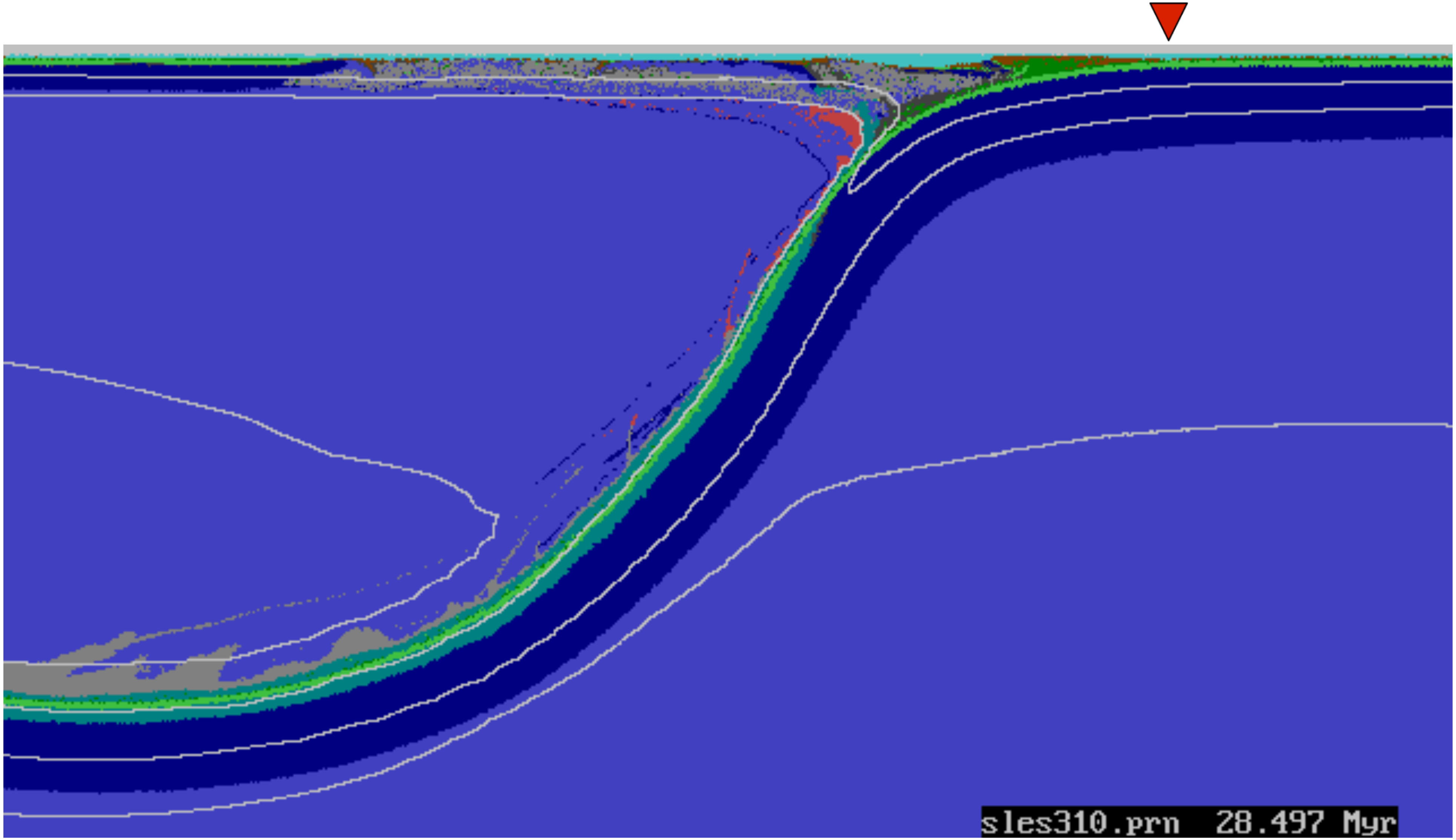
sles310.prn 28.497 Myr

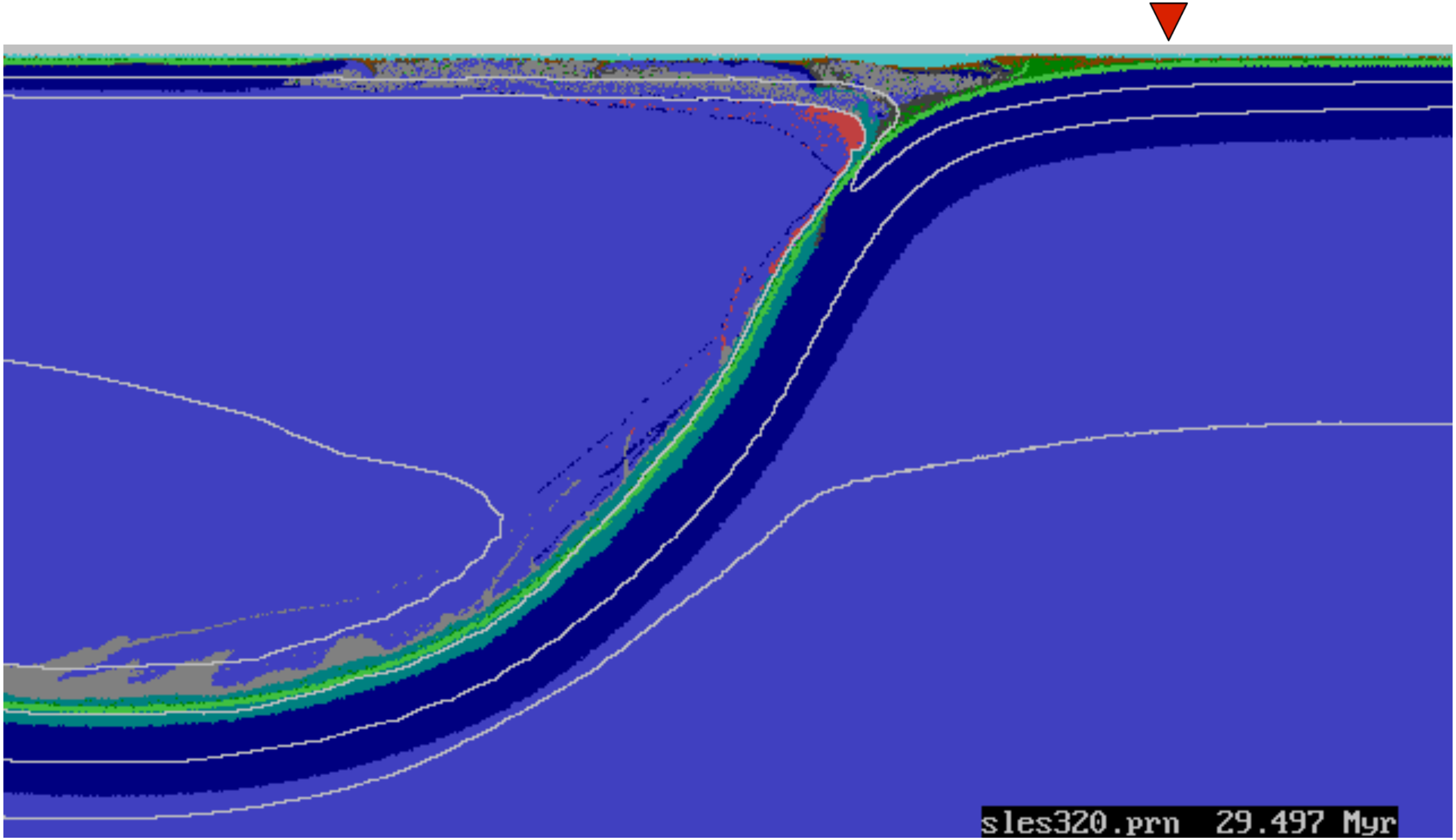
sles320.prn 29.497 Myr

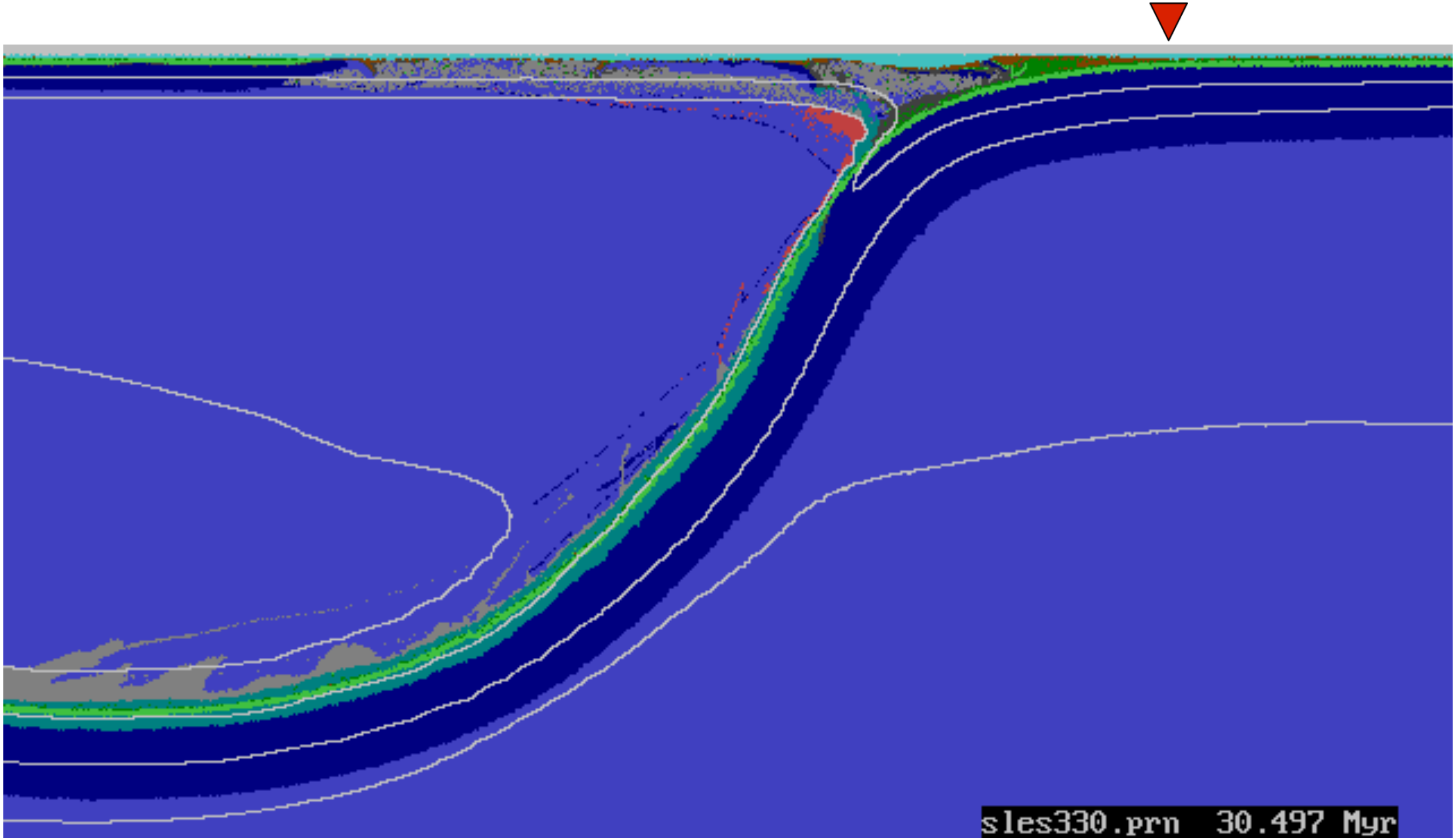

sles330.prn 30.497 Myr

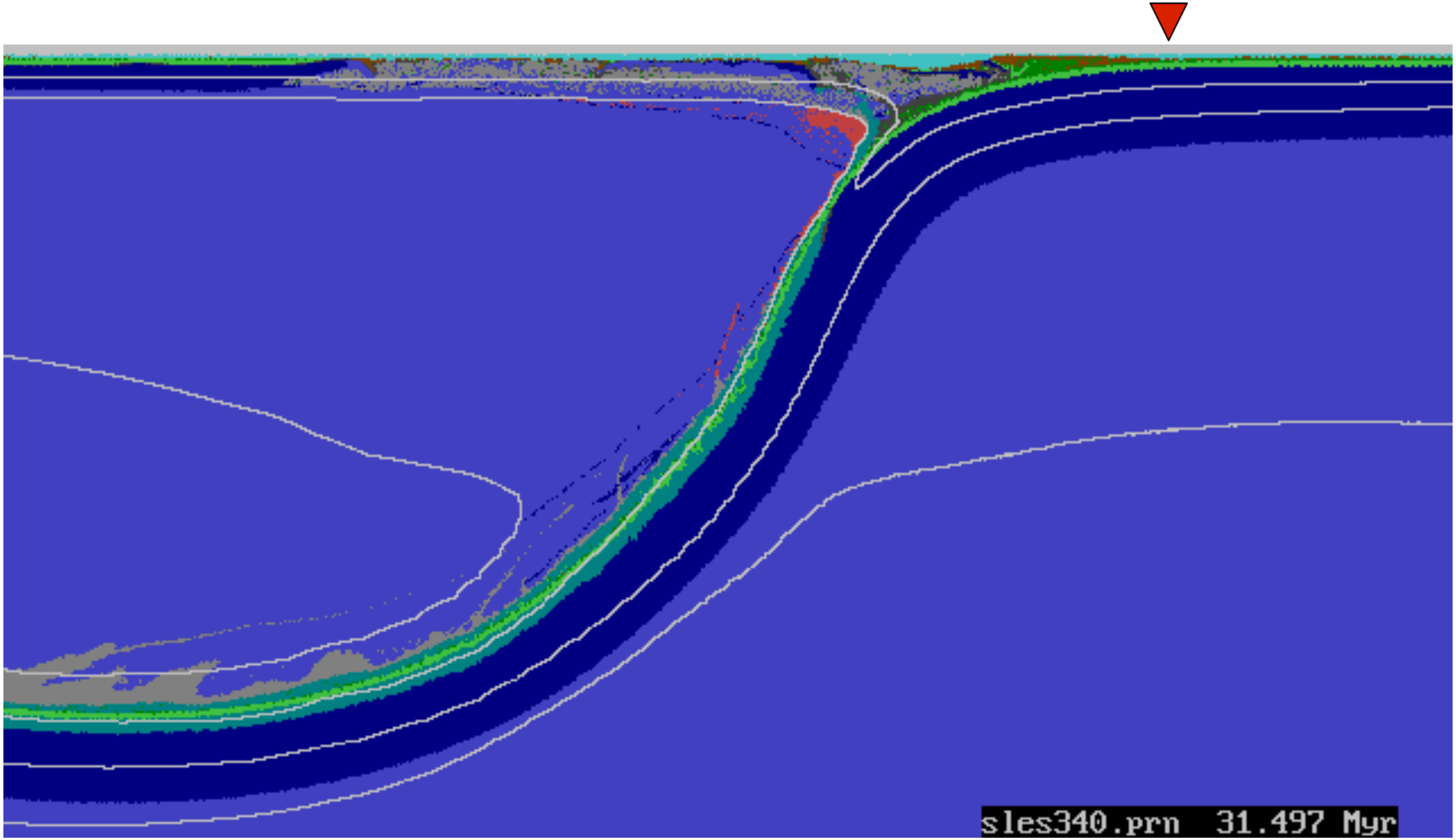
sles340.prn 31.497 Myr

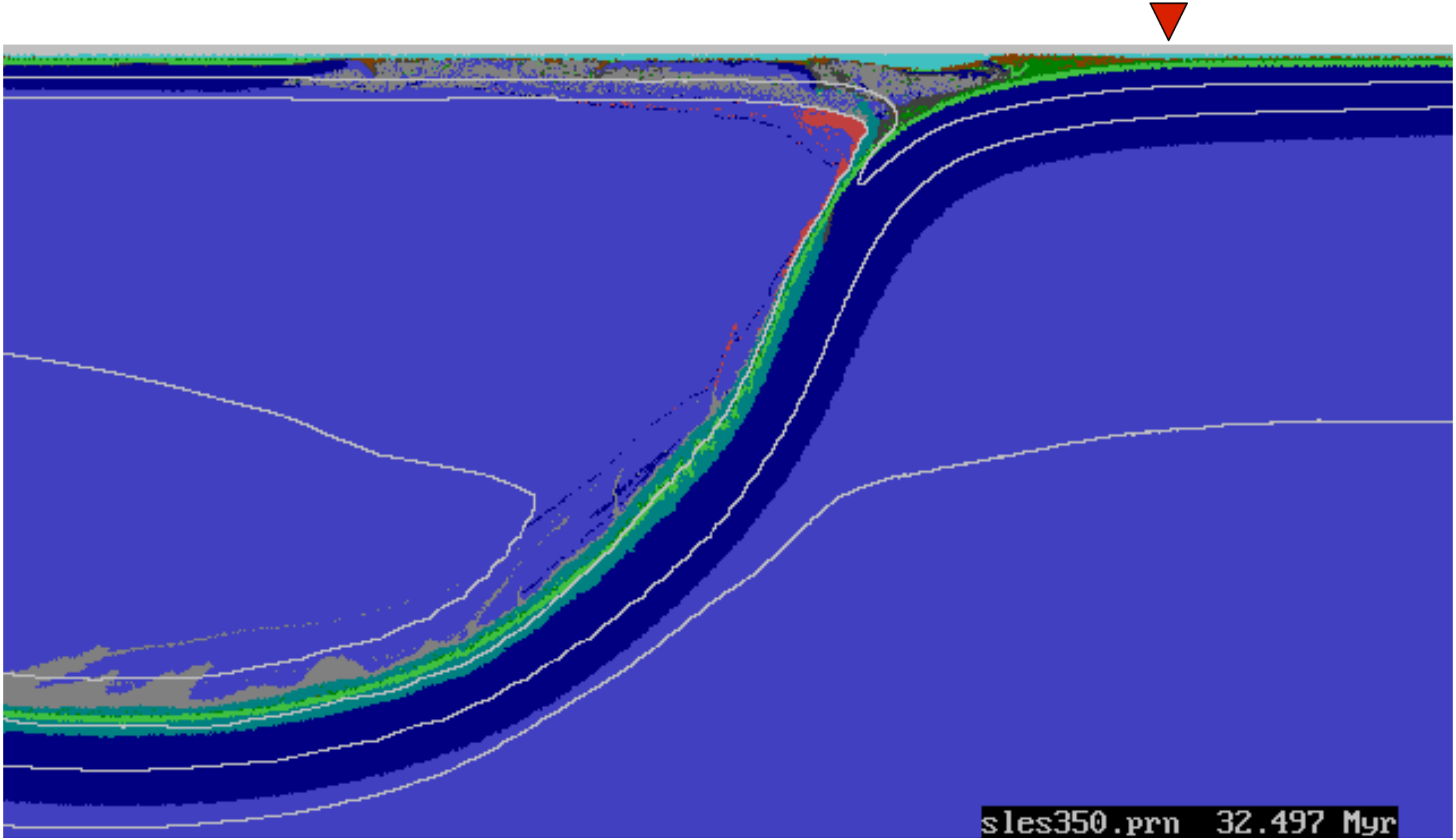
sles350.prn 32.497 Myr

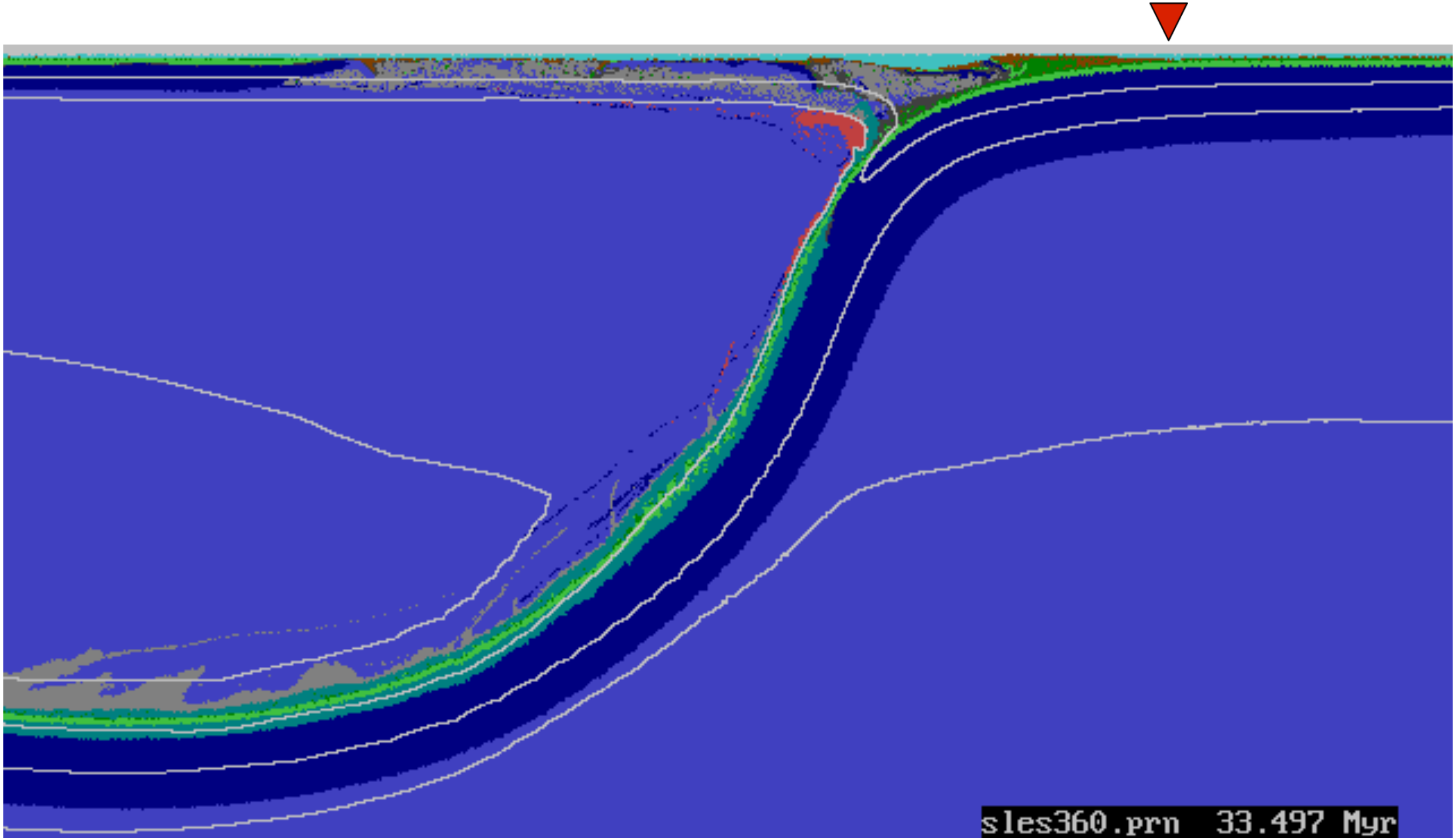
sles360.prn 33.497 Myr

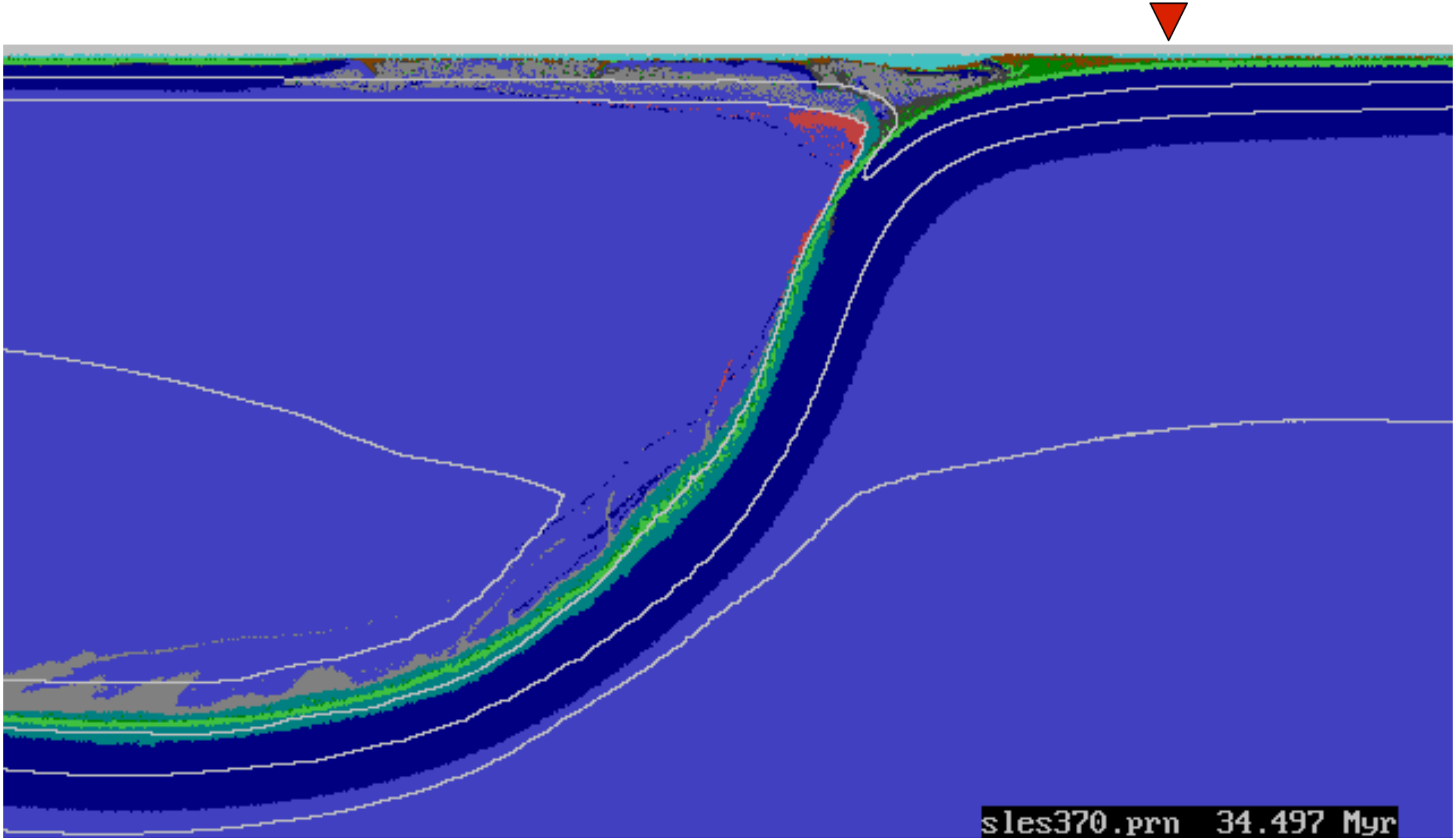

sles370.prn 34.497 Myr

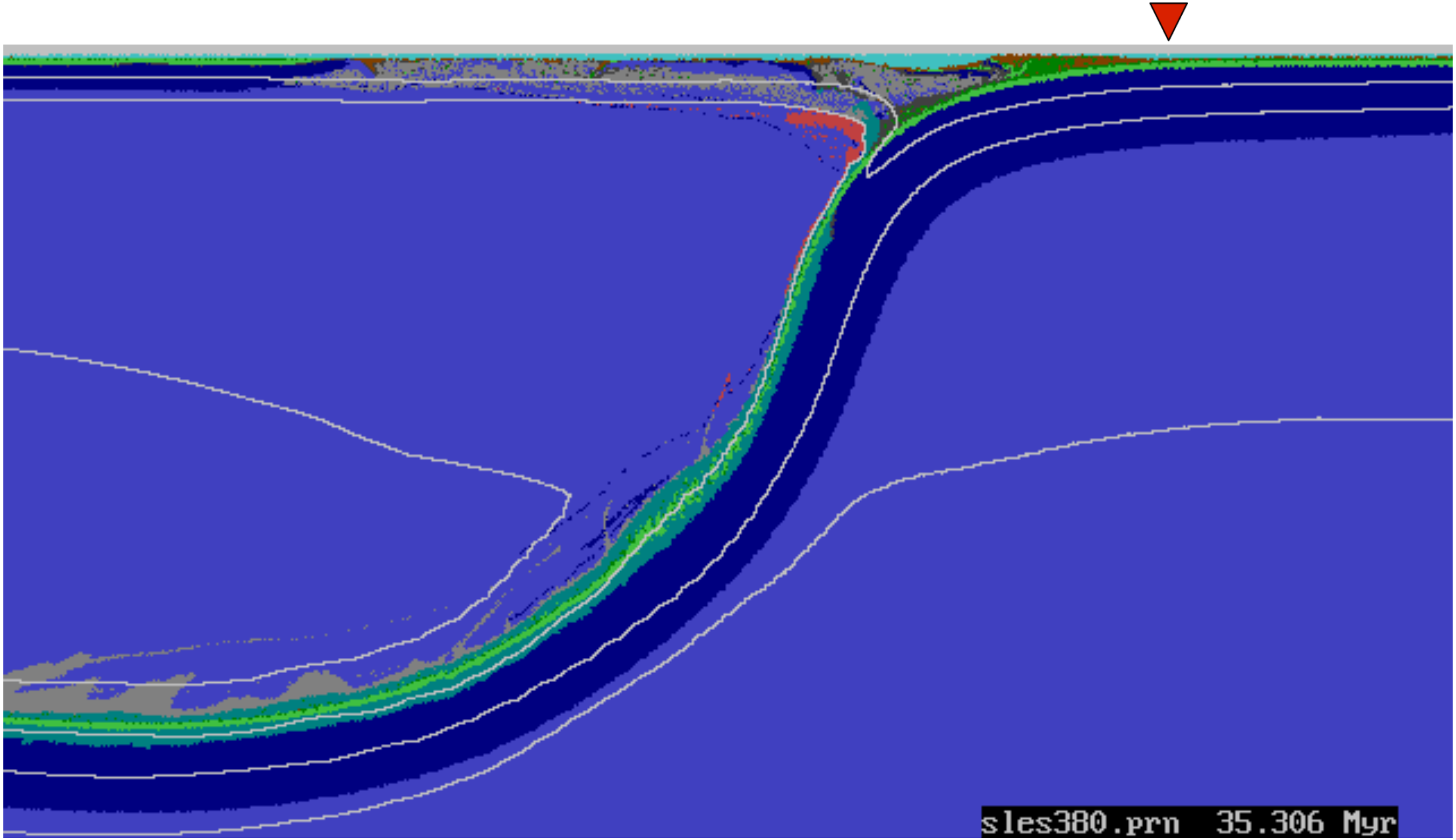
sles380.prn 35.306 Myr

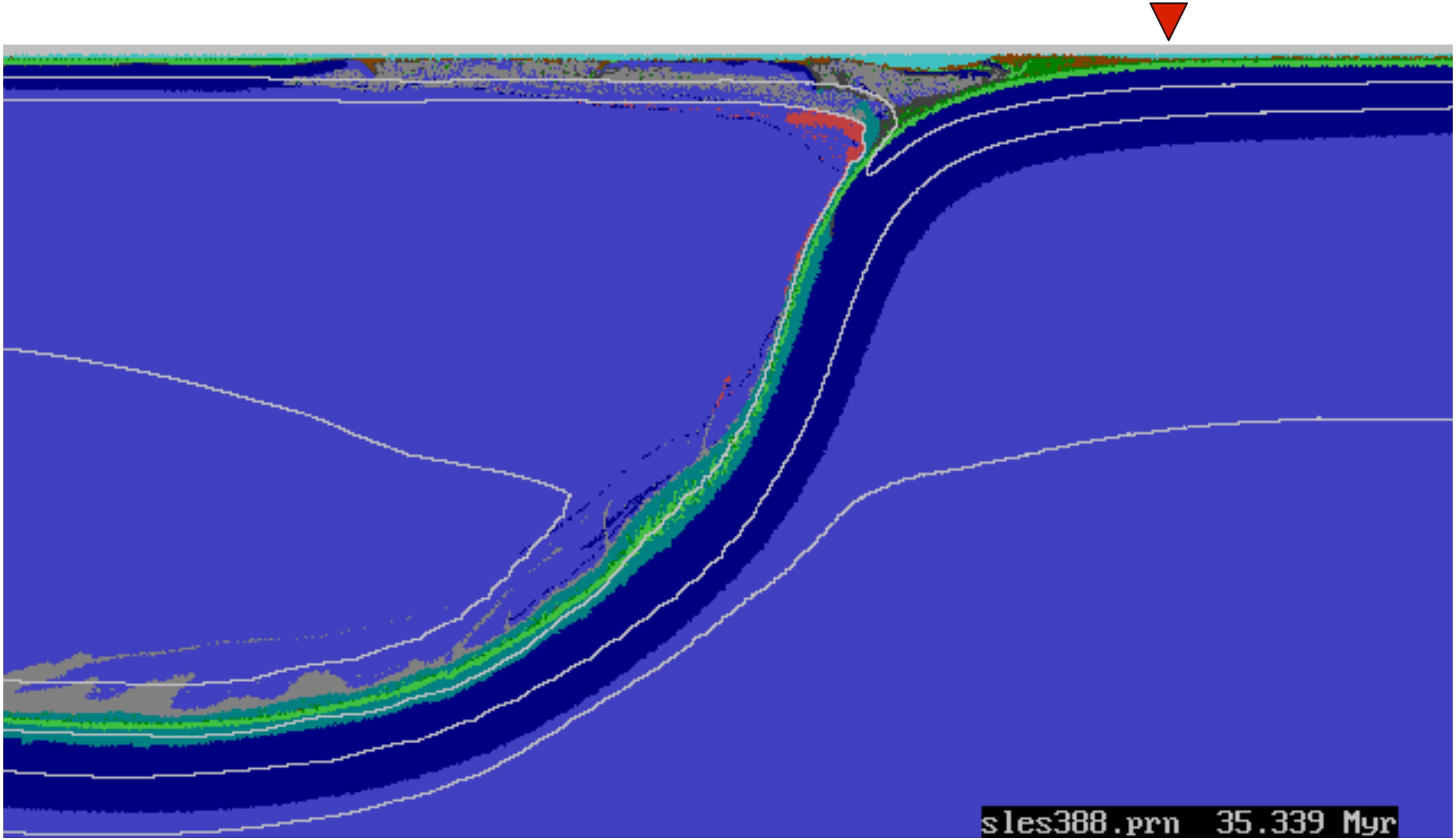
sles388.prn 35.339 Myr

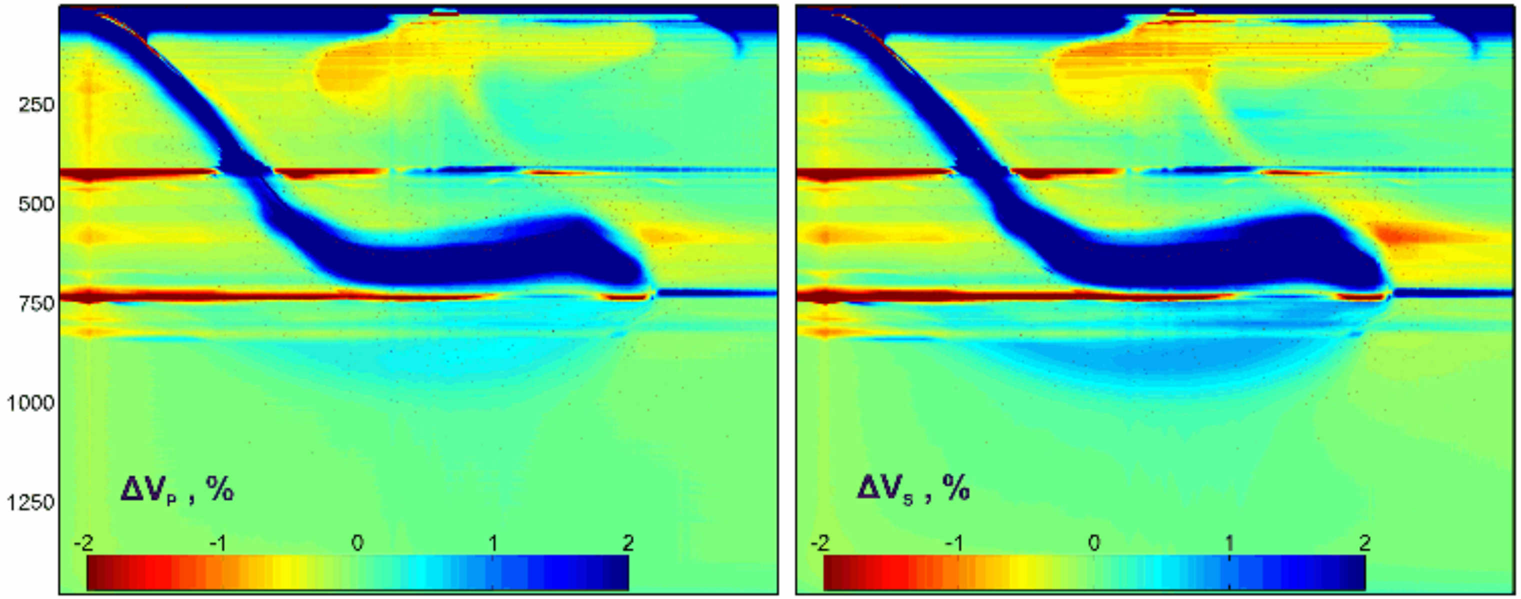

Mishin et al. (2008)

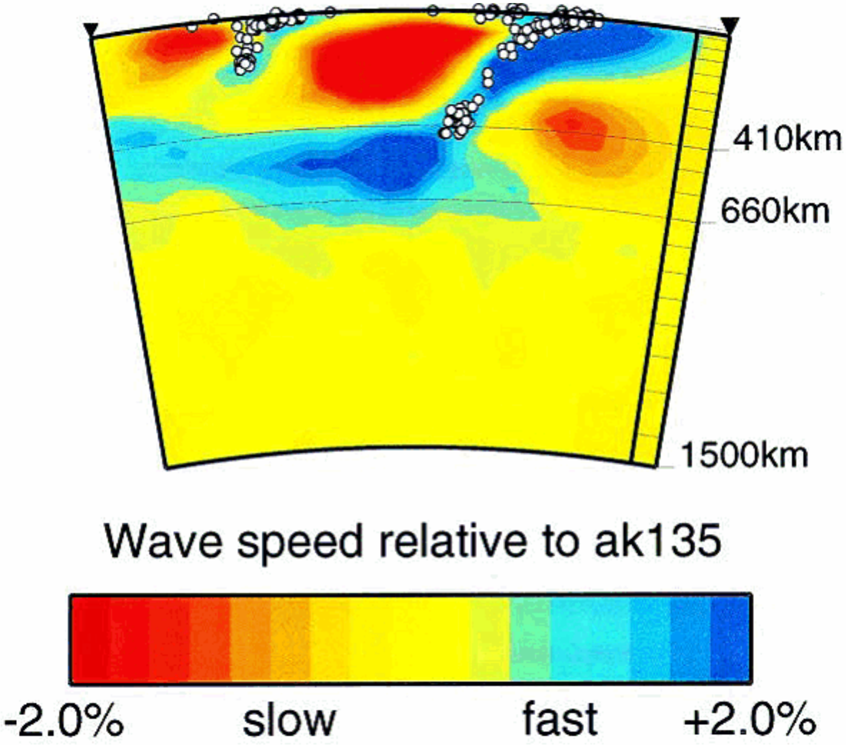

Widiyantoro et al. (1999)

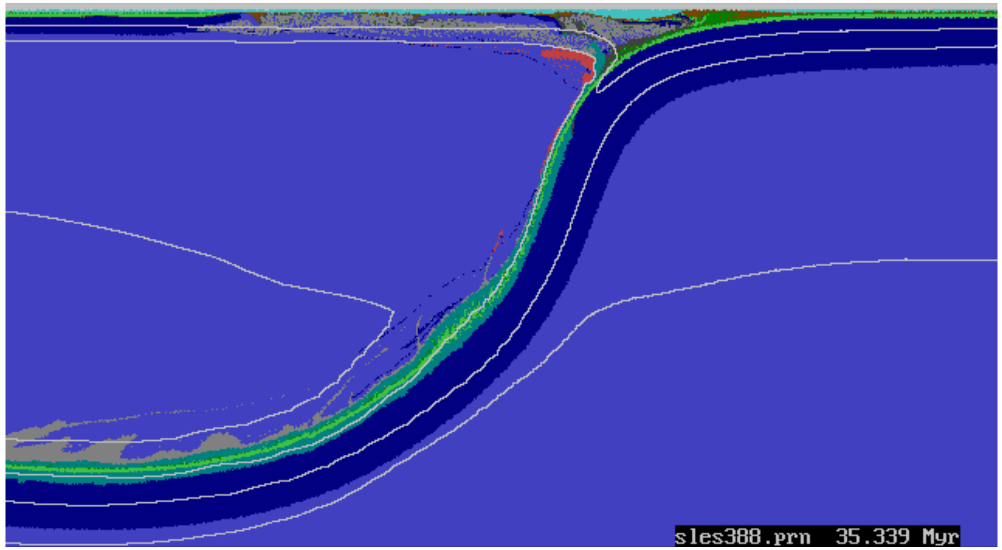

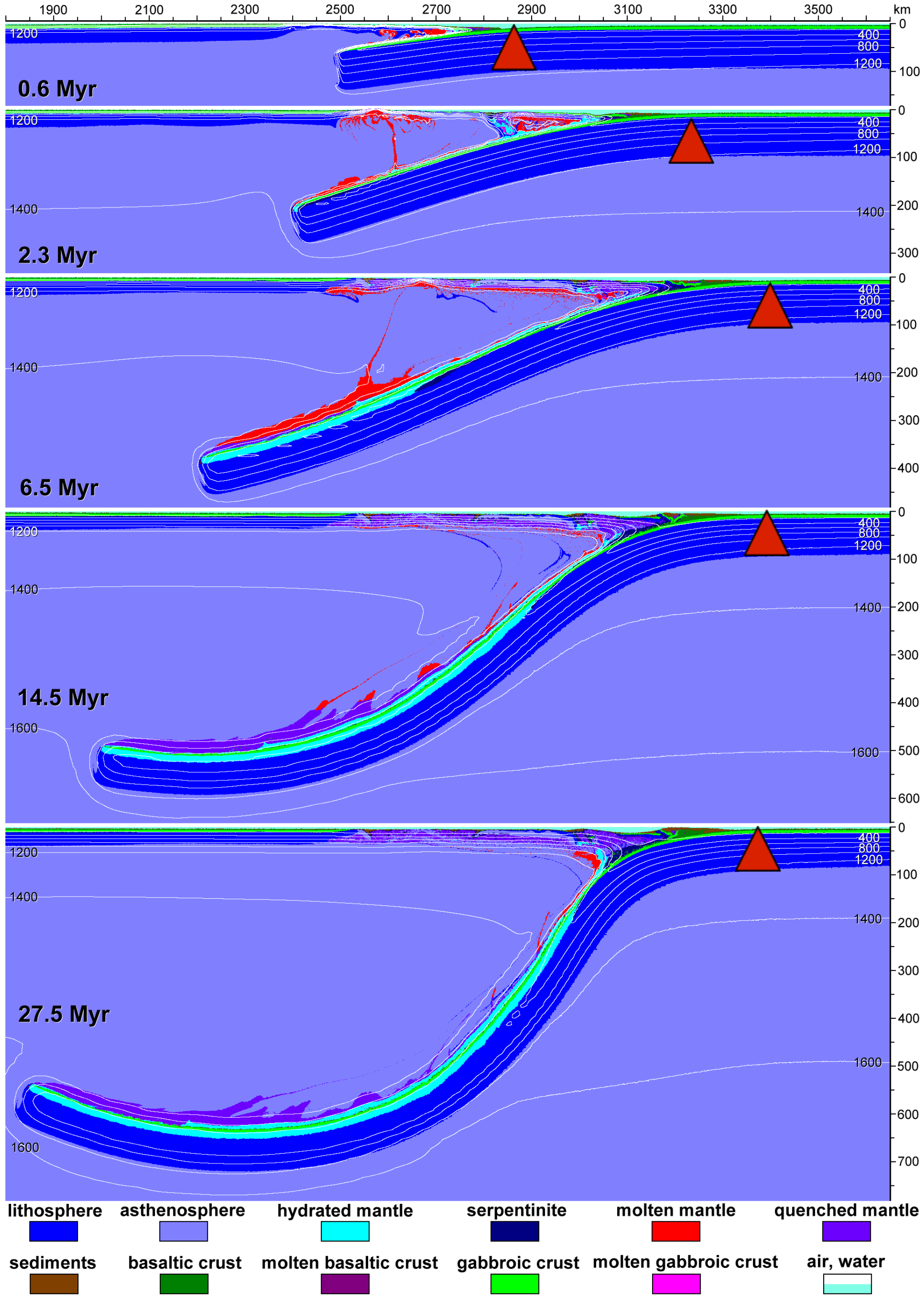

Intesity of slab bending changes with time

Turcotte & Schubert (1982)

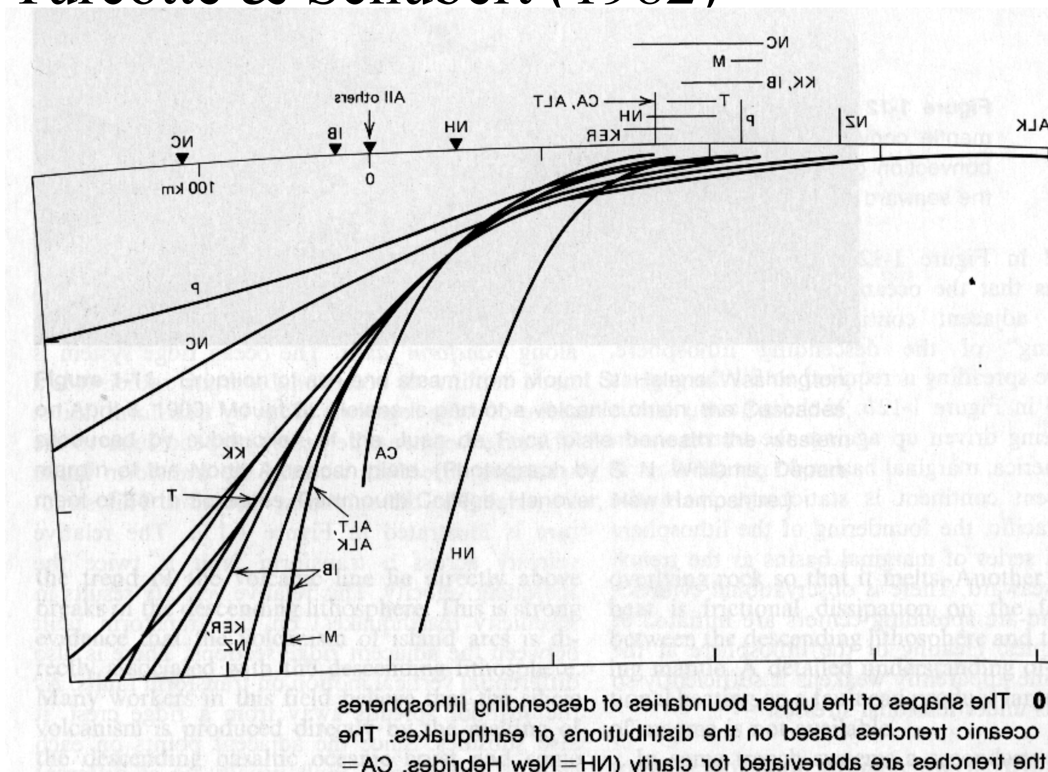

Why is it so easy to bend slabs?

Because bending is natural !

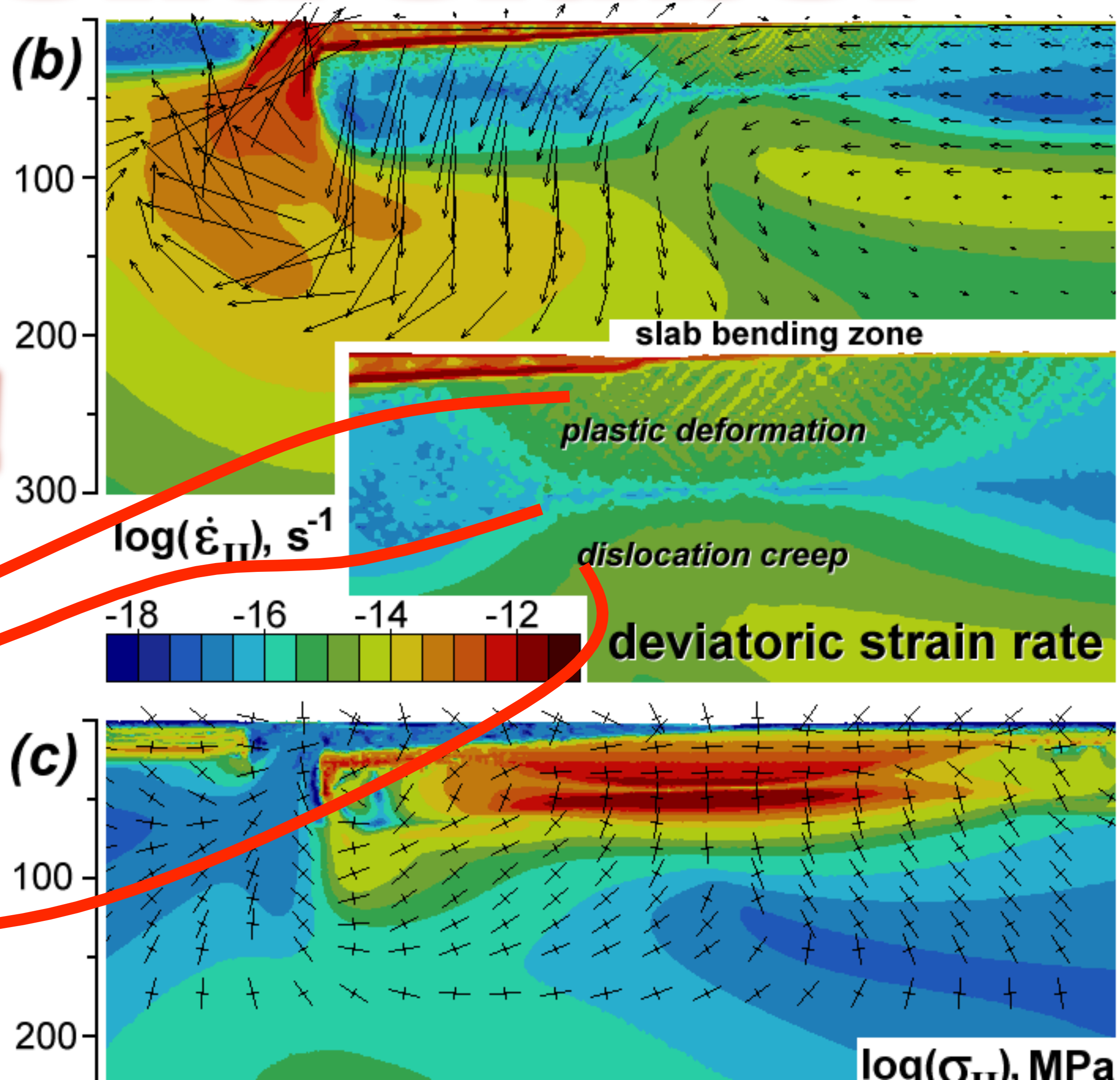

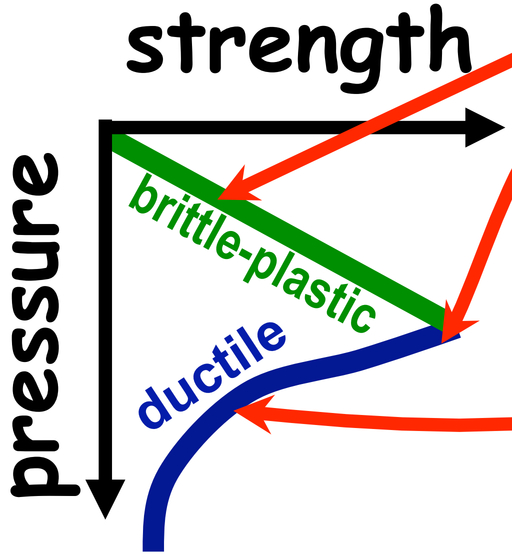

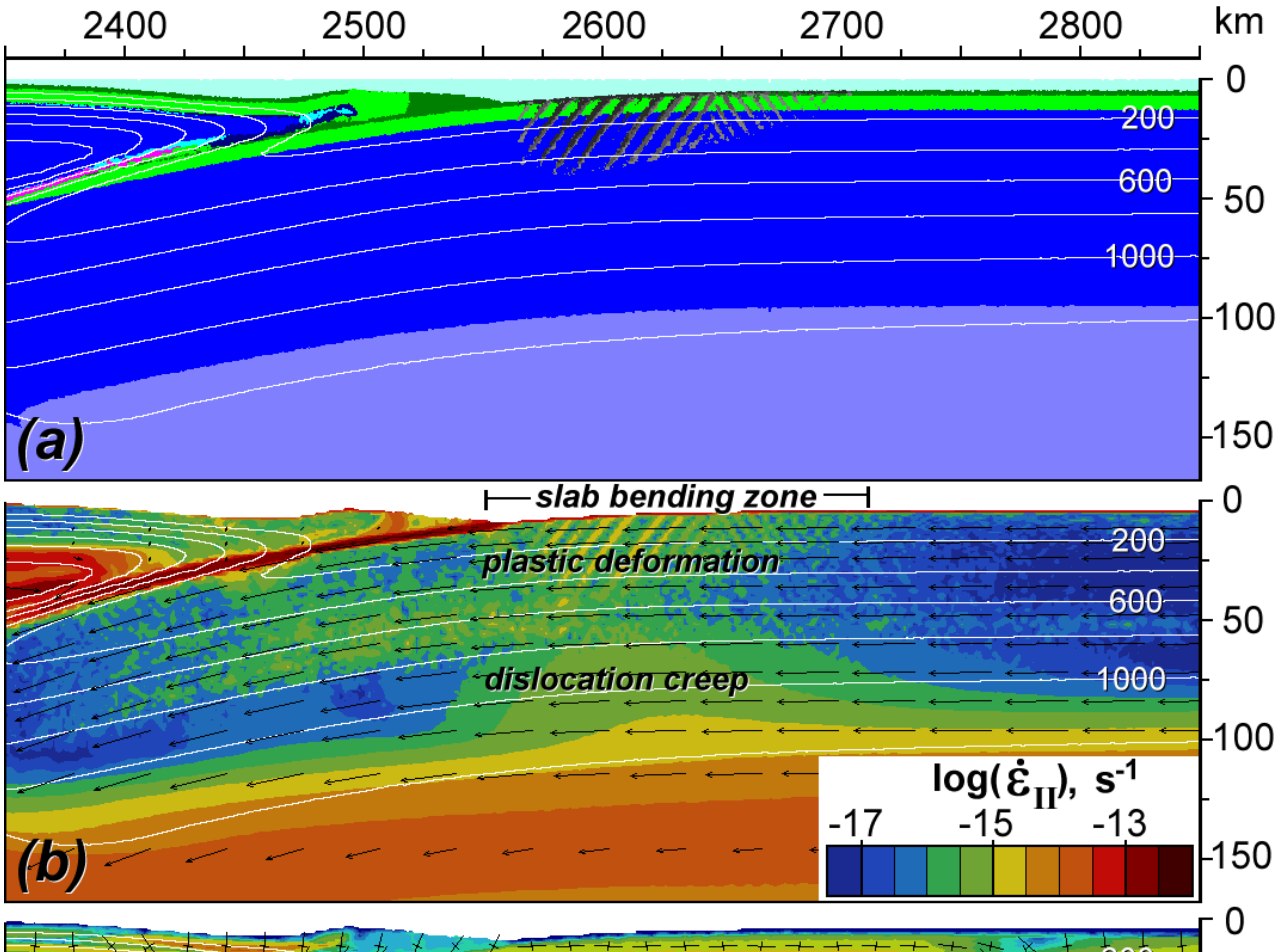
2400
2500
2600
2700
2800
km
0
200
600
50
1000
100
150
(a)
slab bending zone
0
plastic deformation
200
600
50
dislocation creep
1000
100
$\log(\dot{\varepsilon}_{II})$, s^{-1}
-17
-15
-13
150
(b)
0

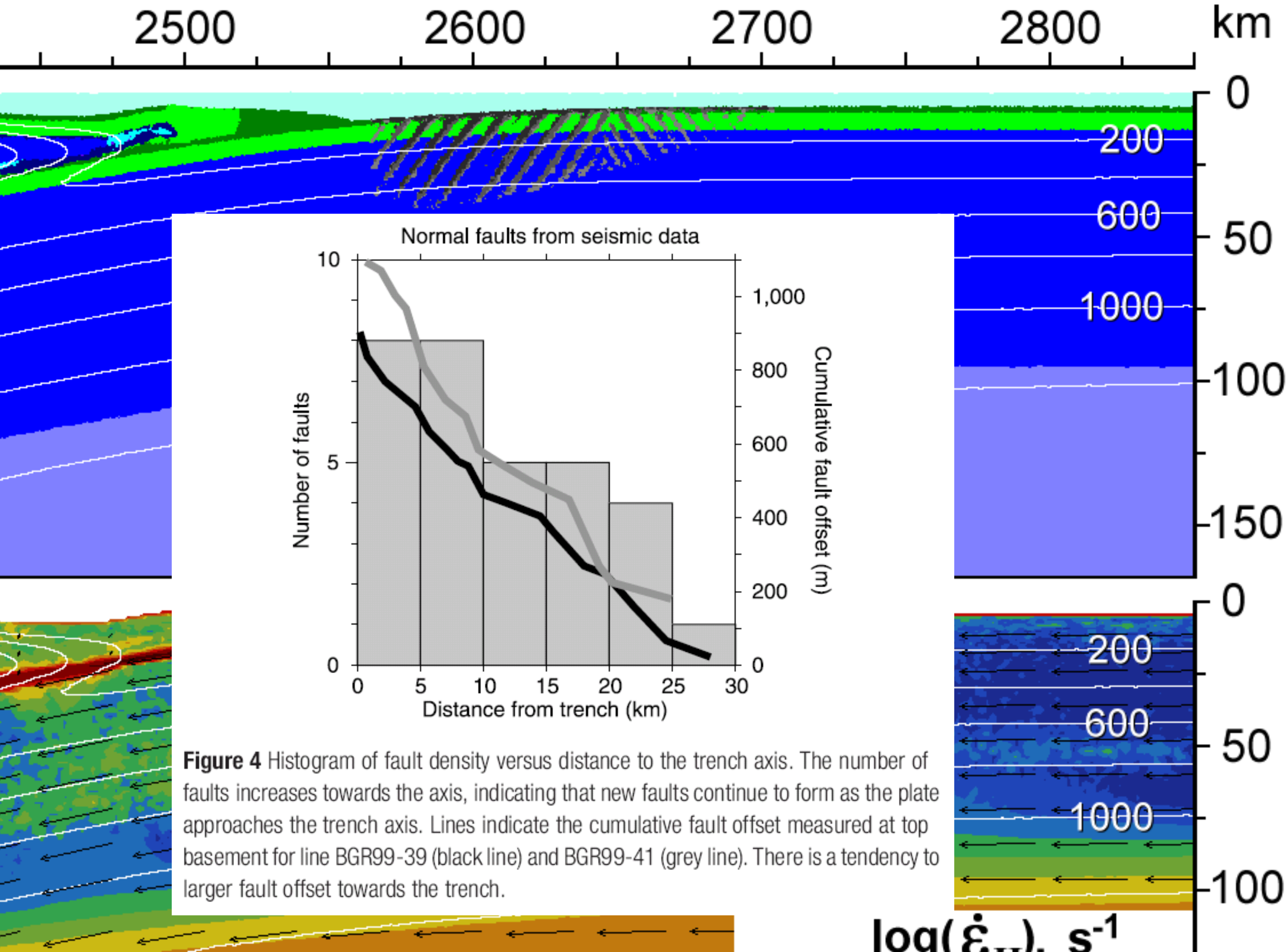

Figure 4 Histogram of fault density versus distance to the trench axis. The number of faults increases towards the axis, indicating that new faults continue to form as the plate approaches the trench axis. Lines indicate the cumulative fault offset measured at top basement for line BGR99-39 (black line) and BGR99-41 (grey line). There is a tendency to larger fault offset towards the trench.

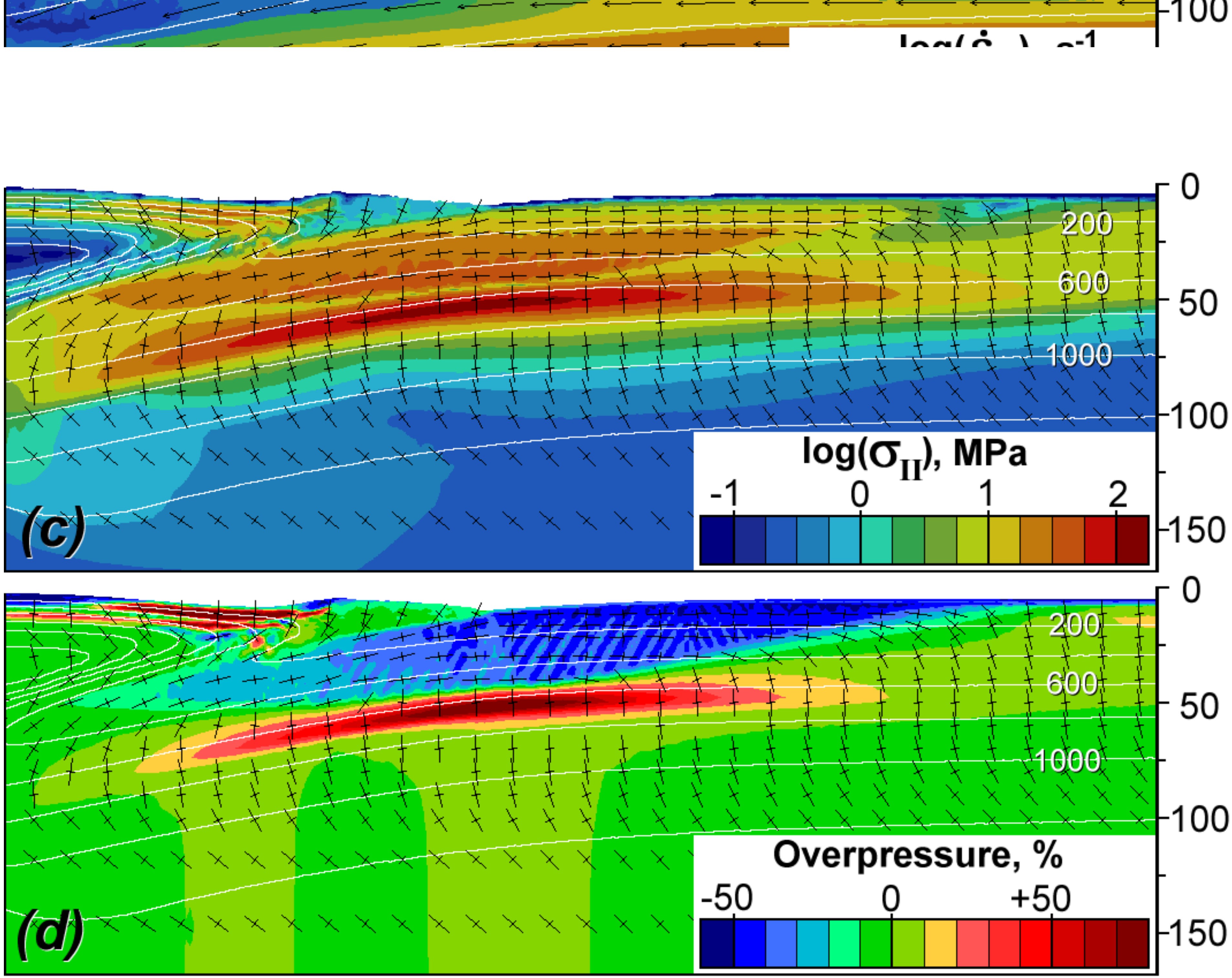
100
0
200
600
50
1000
100
150
log(σII), MPa
-1
0
1
2
(c)
0
200
600
50
1000
100
150
Overpressure, %
-50
0
+50
(d)

Ranero et al (2007)

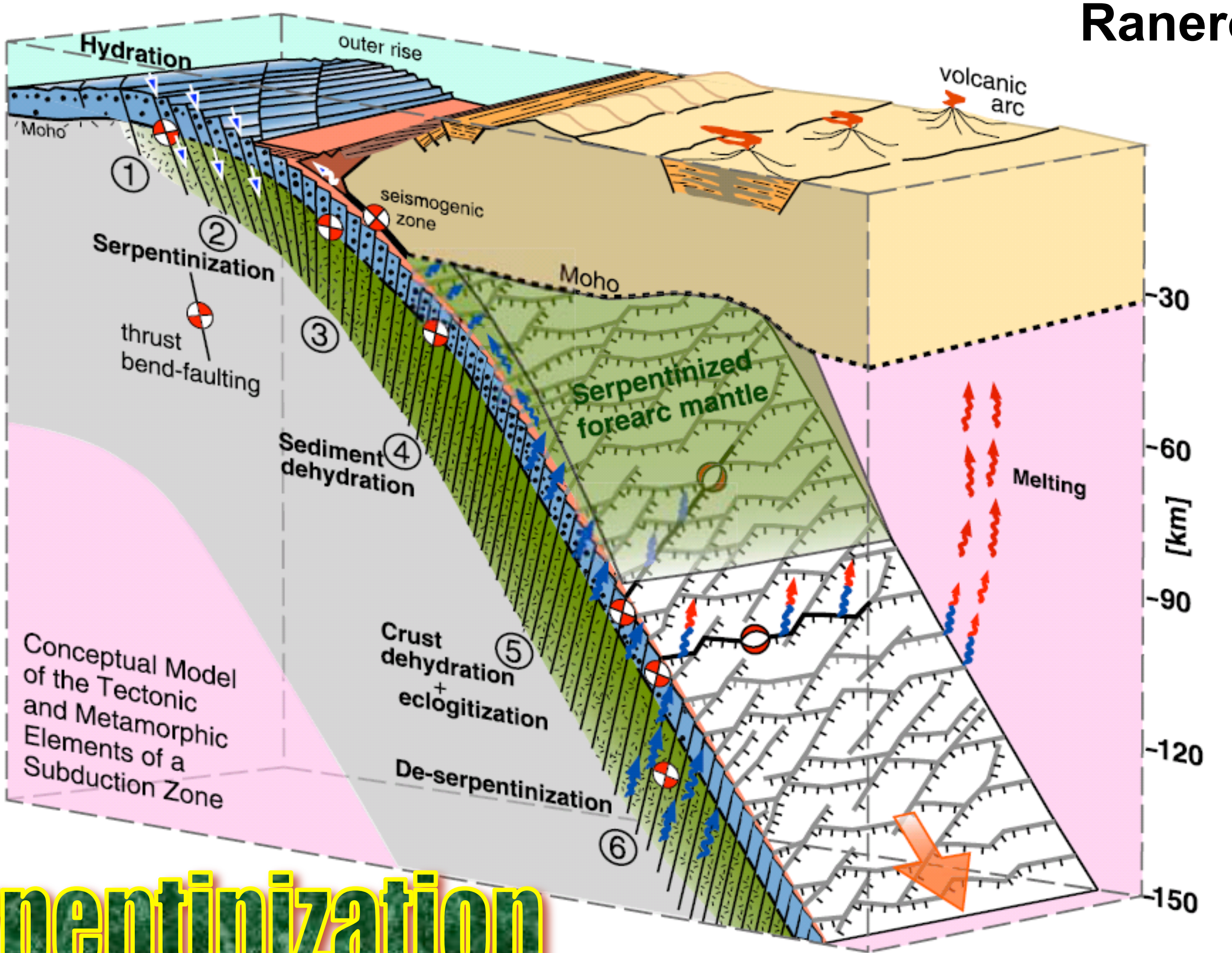

Slab serpentinization

Figure 13. Cartoon showing a conceptual model of the structure and metamorphic evolution of subducting lithosphere formed at a fast spreading center. The topography of the plate in the outer-rise/trench region has been exaggerated to show better the deformation associated to plate bending. Scale is approximate everywhere else. Fault plane solutions of earthquakes are projected into the top of the slab and the plane of the cross section. Black filled circles in oceanic crust indicate hydration. See section 6 for discussion of model.

Serpentinized normal faults

Faccenda et al (2008, Nature)

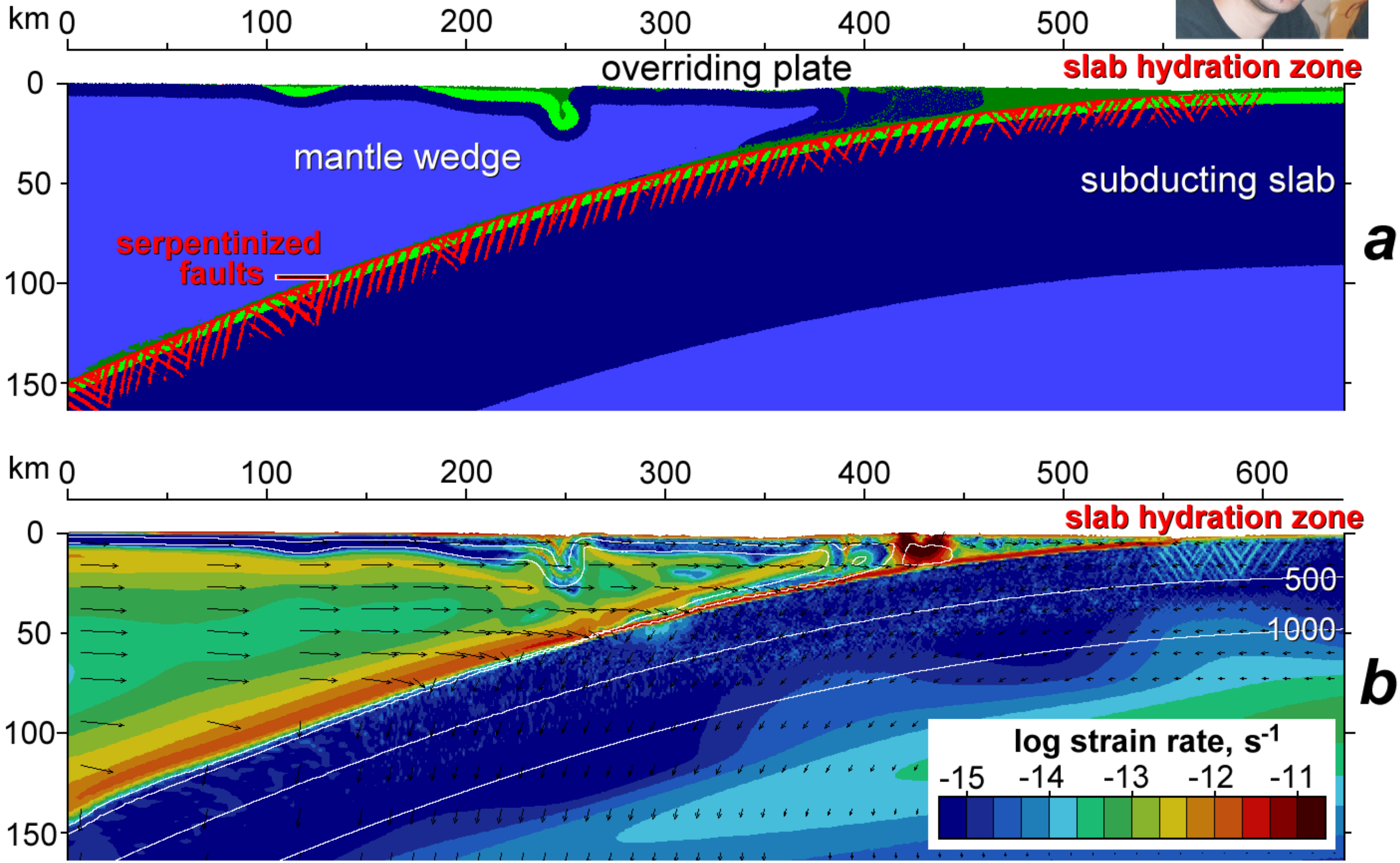

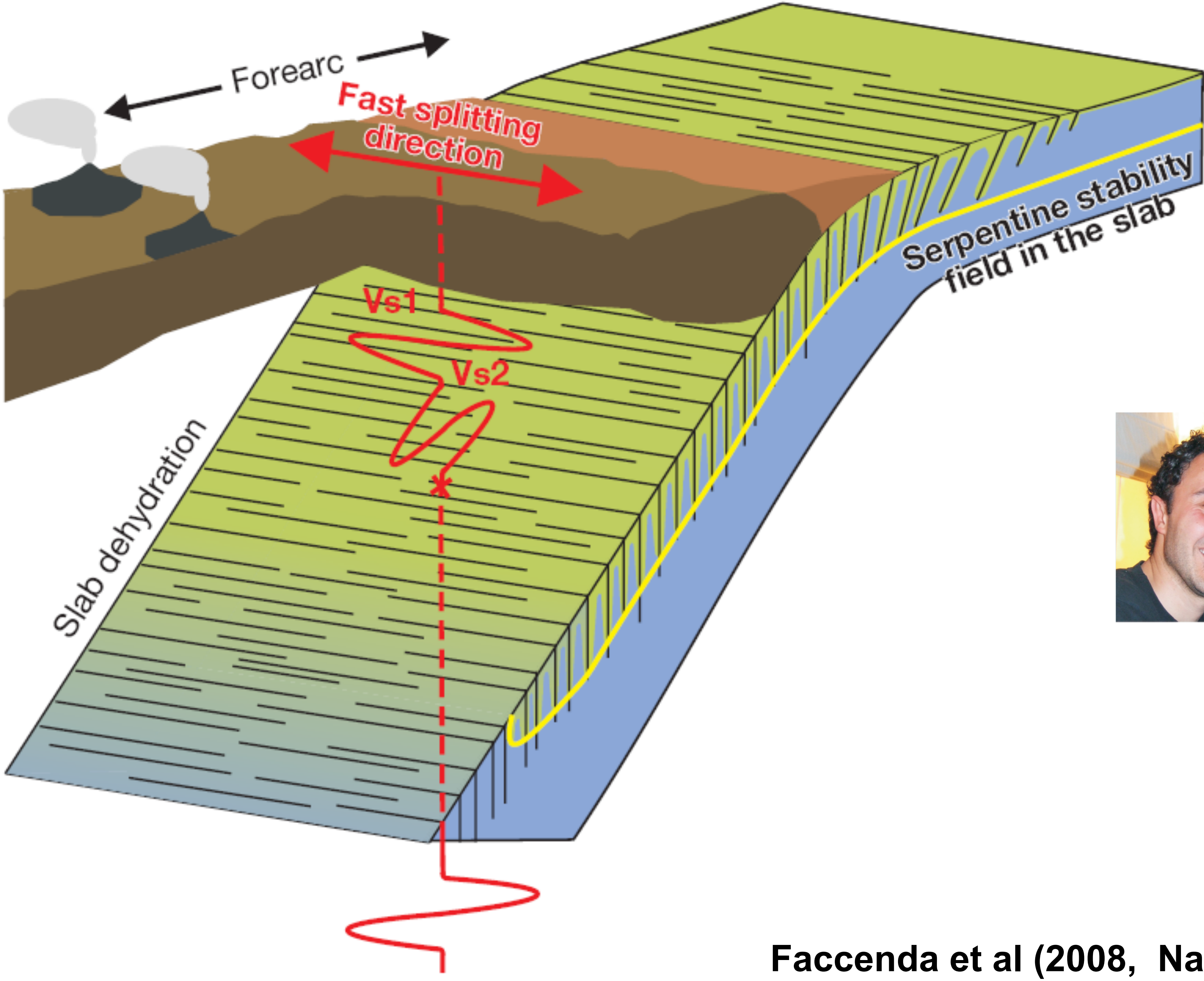

Faccenda et al (2008, Nature)

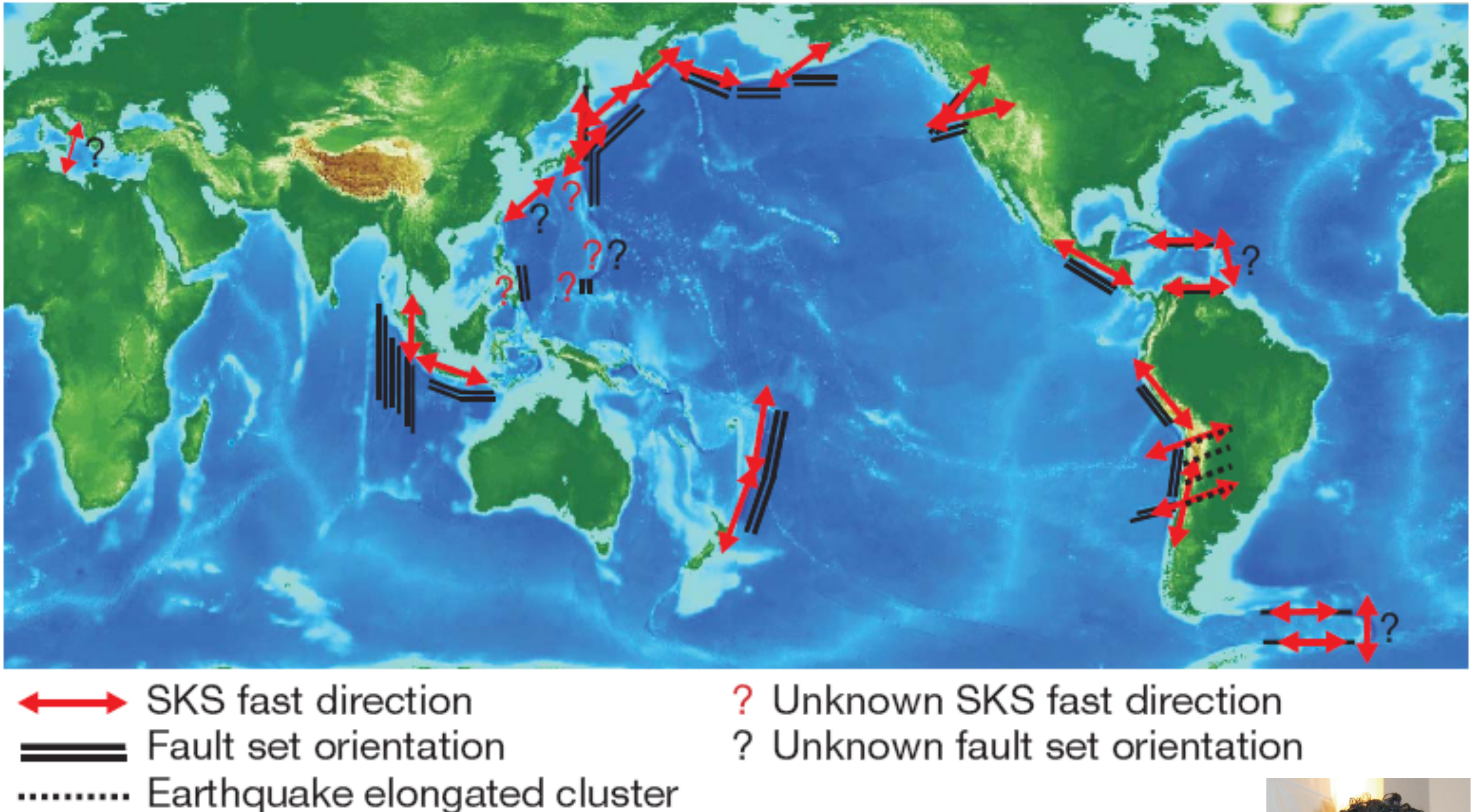

Faccenda et al (2008, Nature)

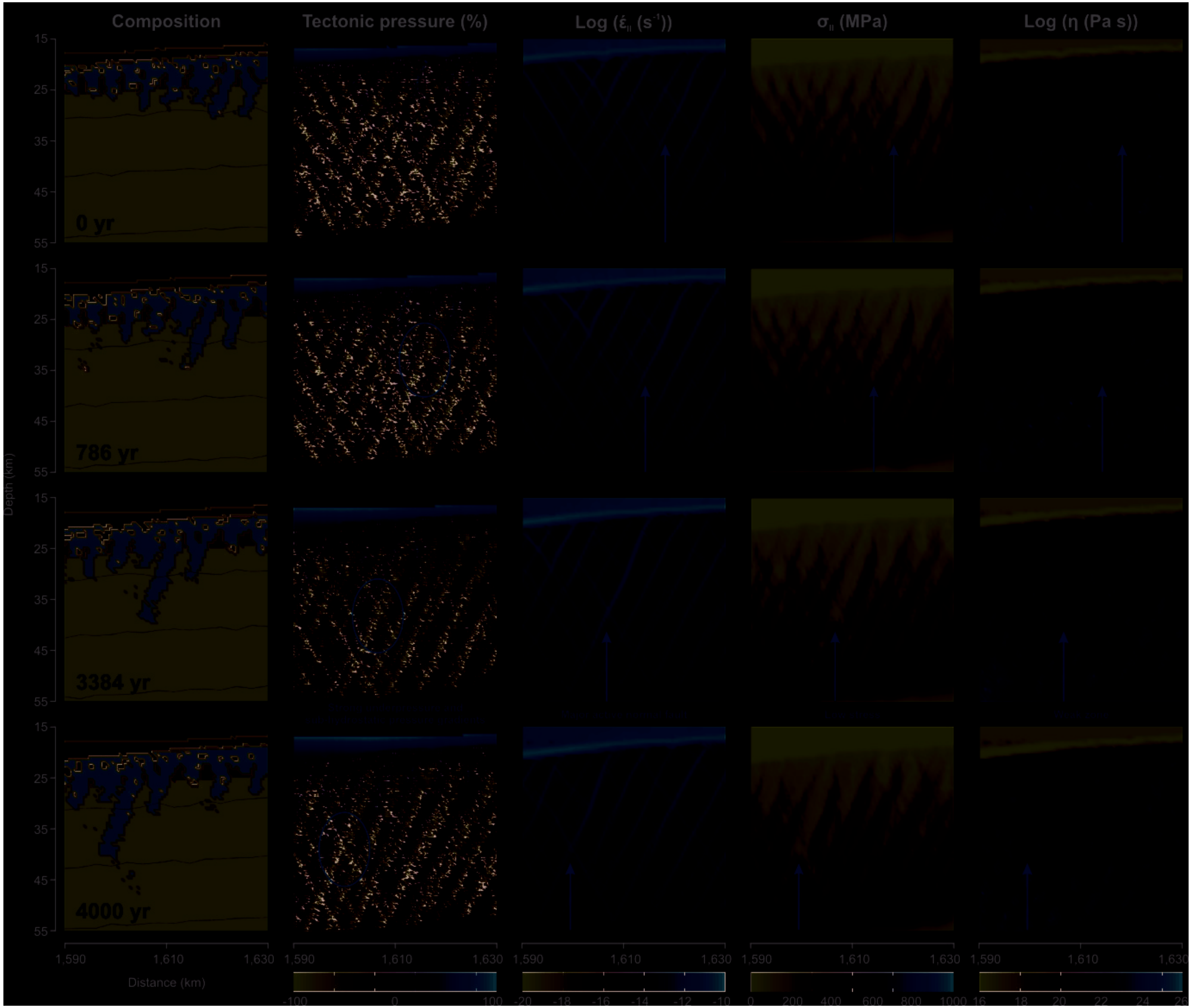

Faccenda et al (2009, accepted to Nature Geosciences)

Can plumes rising in the mantle wedge be cold ?

?

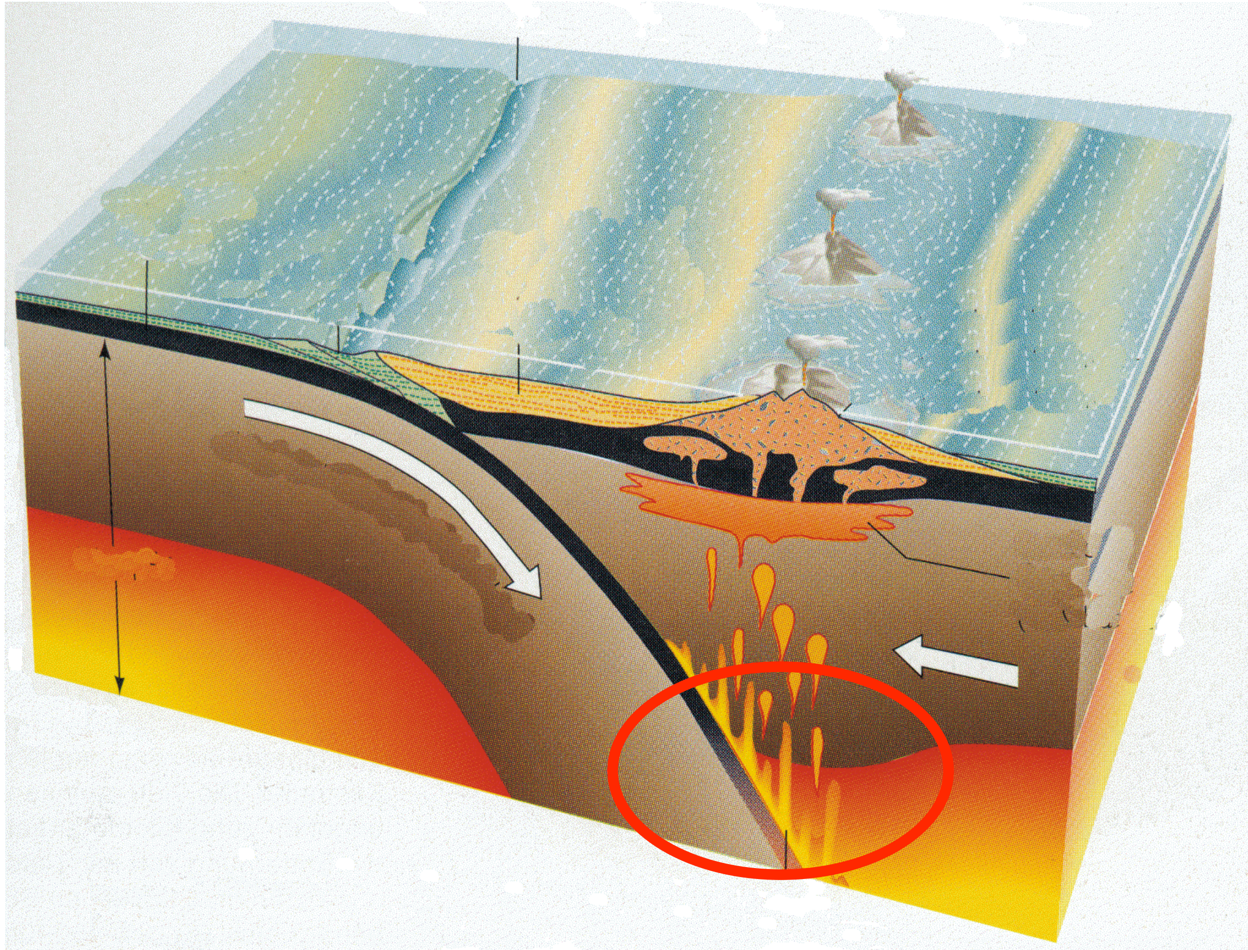

No exceptions?!

Thermal norm:

rising ***plumes*** are ***hotter*** then their ***environment***

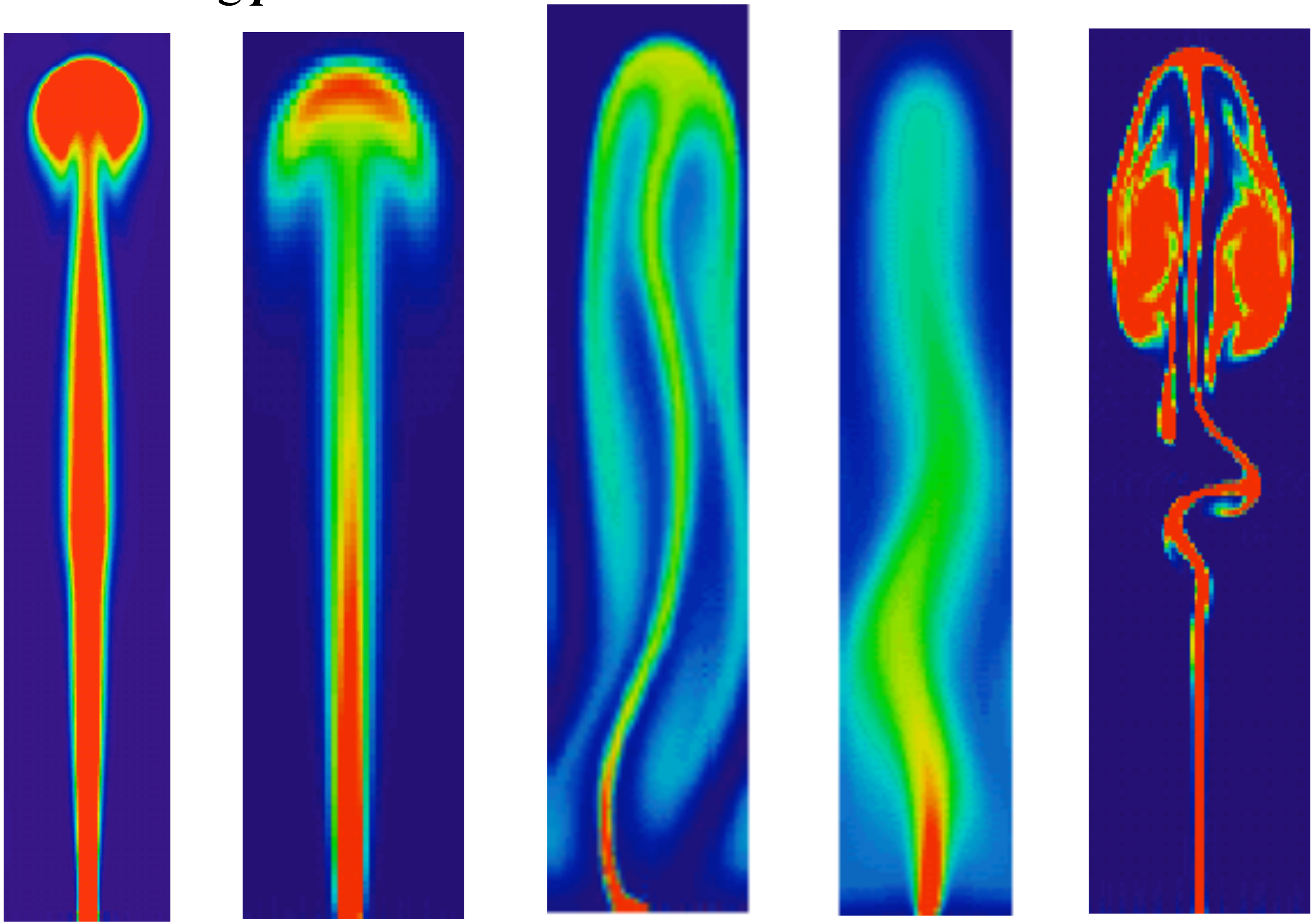

Typical thermal structures of mantle plumes (Hier Majumder et al., 2002)

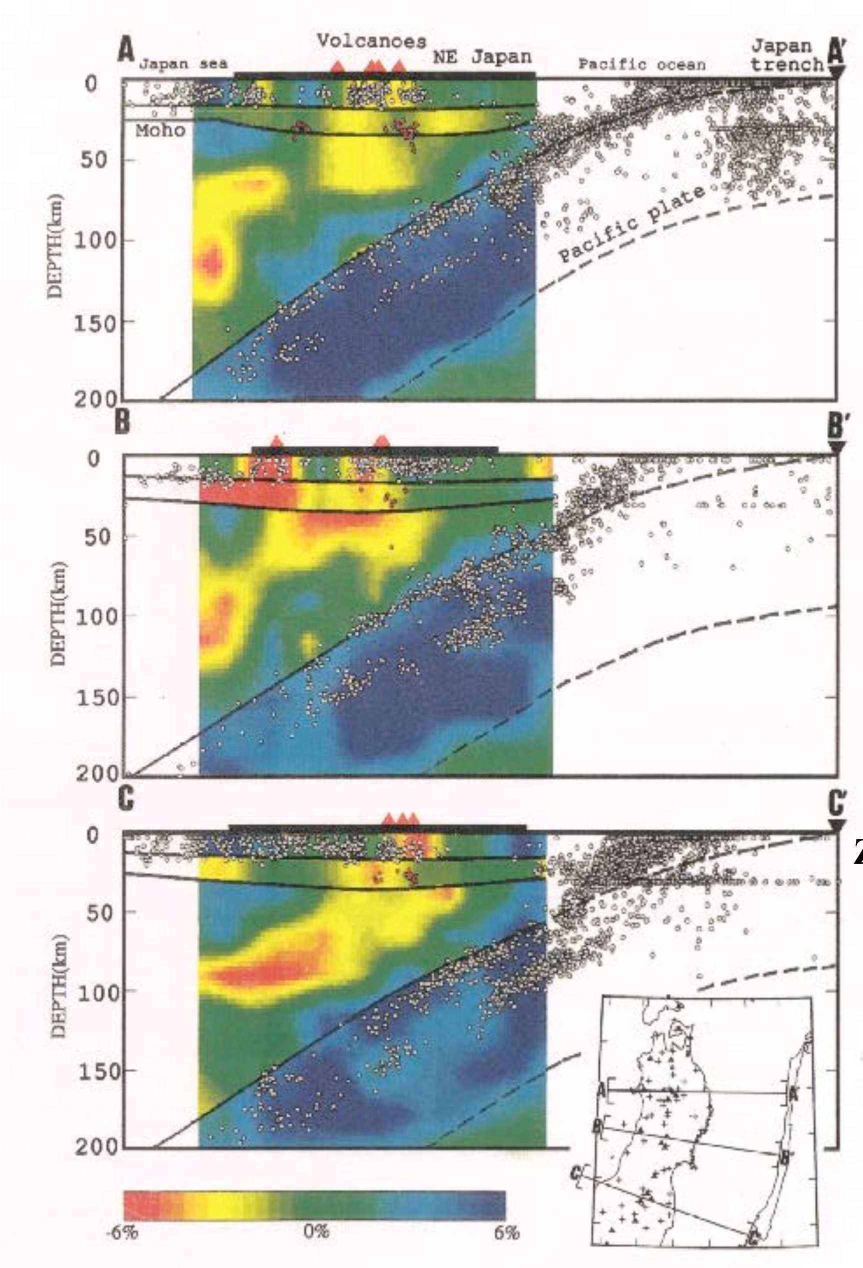

Zhao et al. (1992)

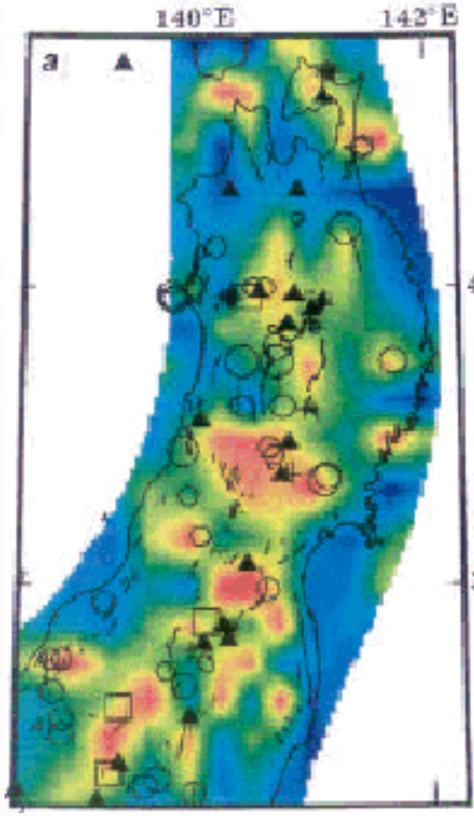

Zhao & Kayal, (2000)

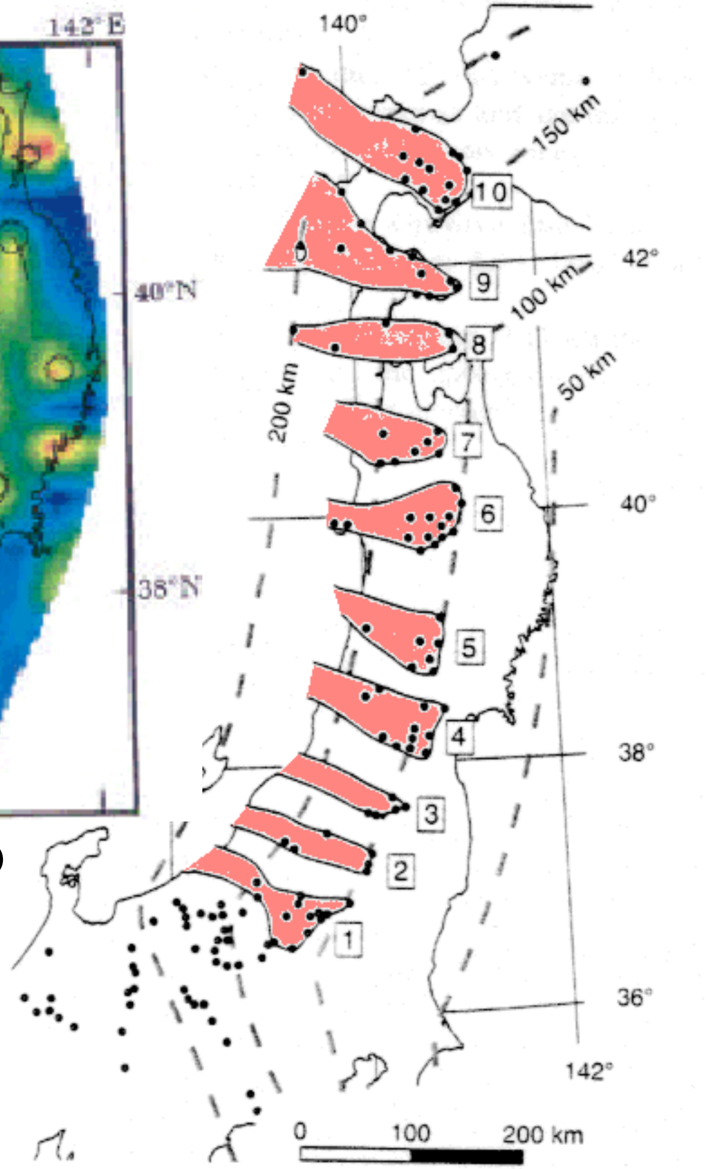

Fig. 9. Hot fingers in the mantle wedge beneath Northeast Japan. Dashed lines show depth contours to the surface of the dipping seismic zones. Quaternary volcanoes lie above the hot mantle fingers.

Tamura et al., (2002)

Seismic tomography of Japan trench region

Animation
“Cold plumes
&
Cold waves”

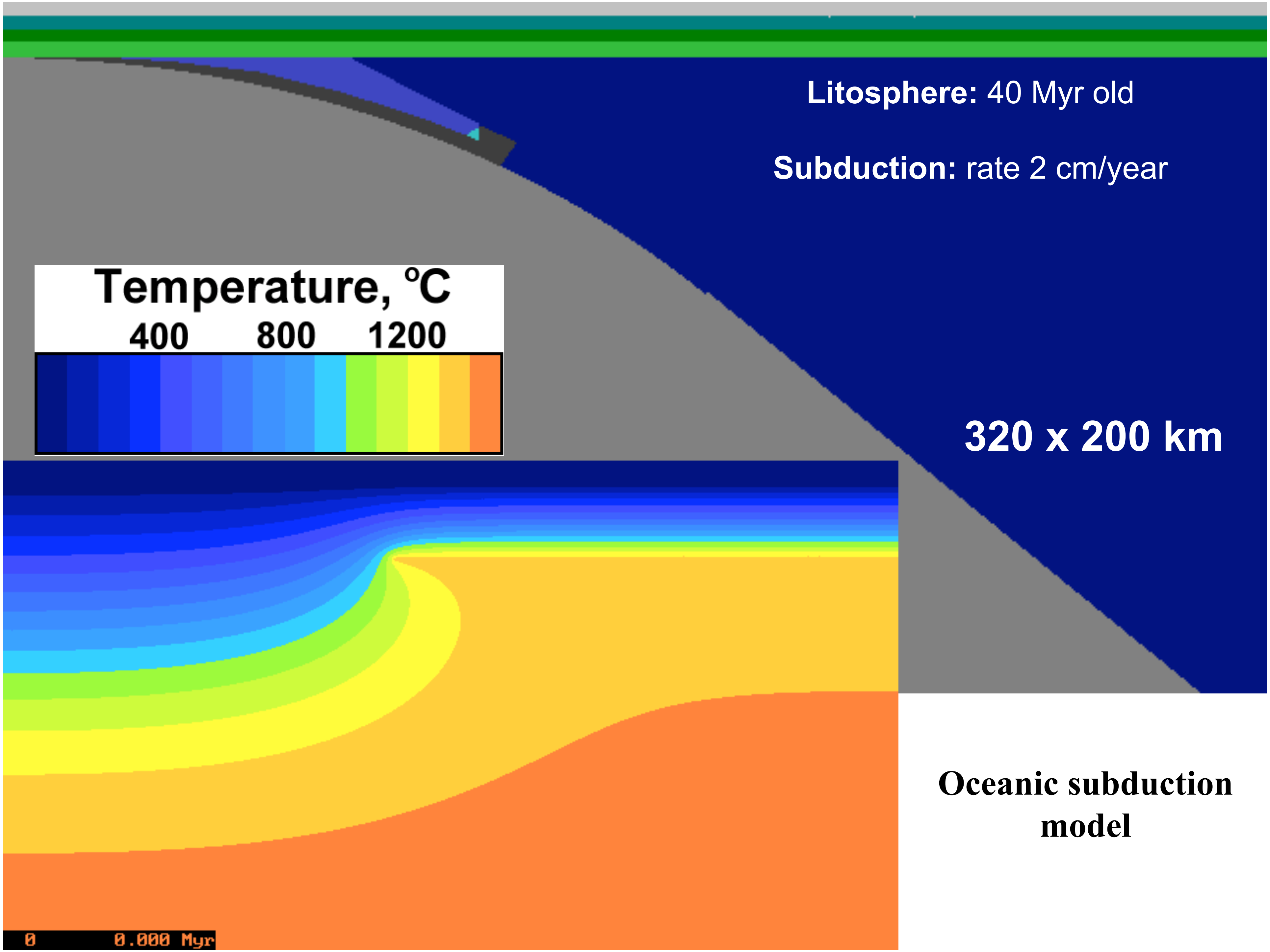

Oceanic subduction model

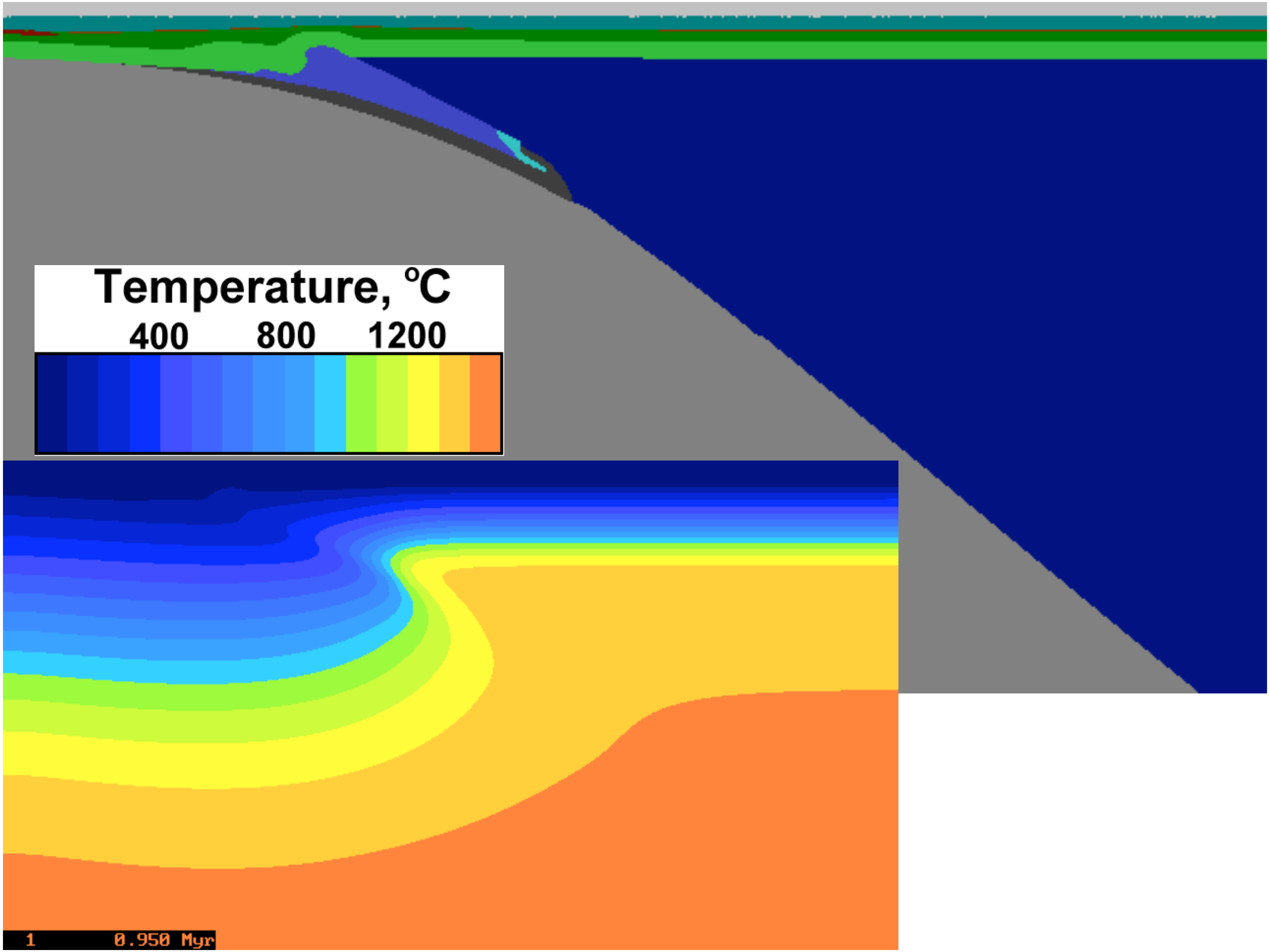
Temperature, °C
400
800
1200
1 0.950 Myr

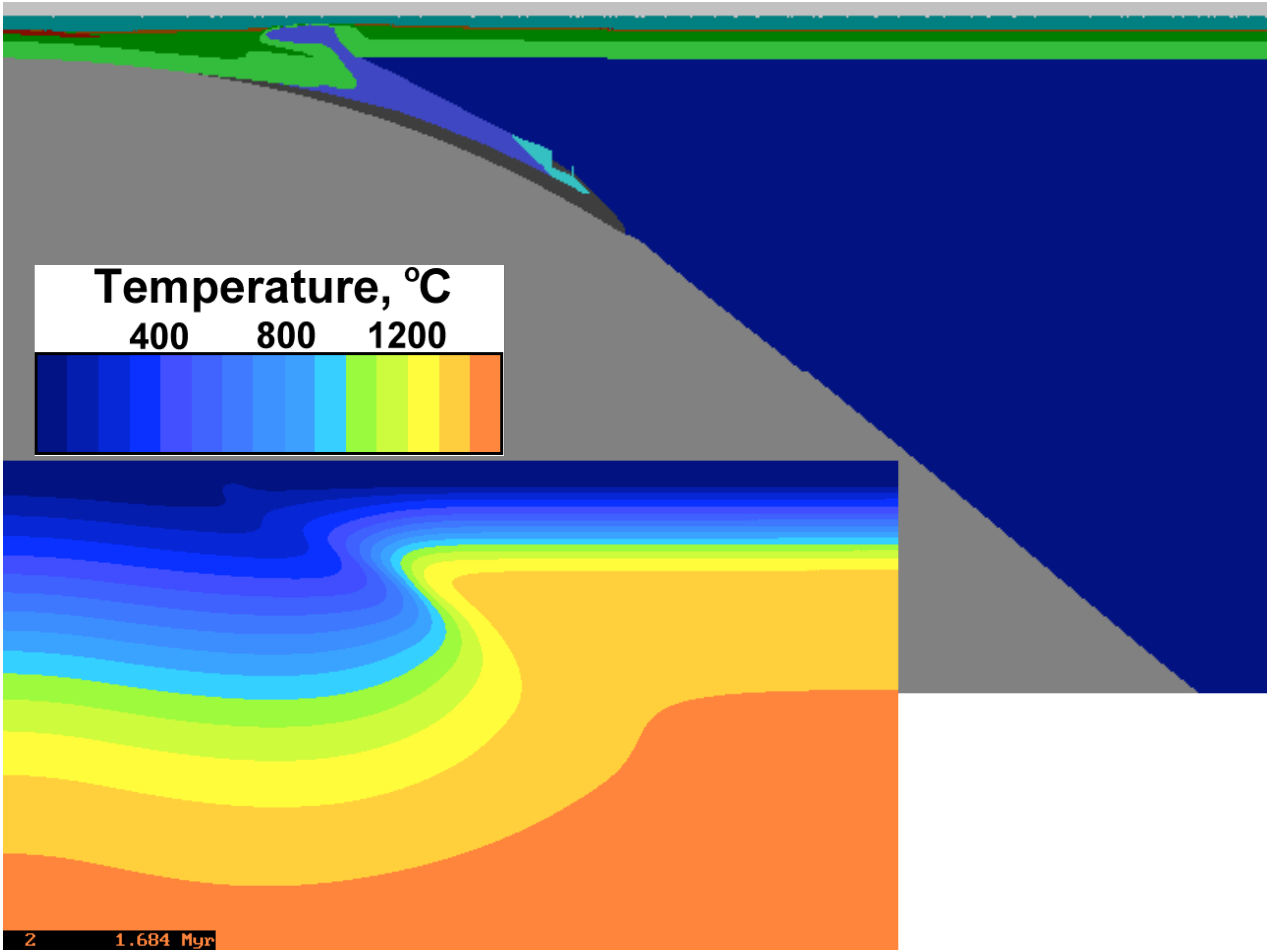
Temperature, ºC
400 800 1200
2 1.684 Myr

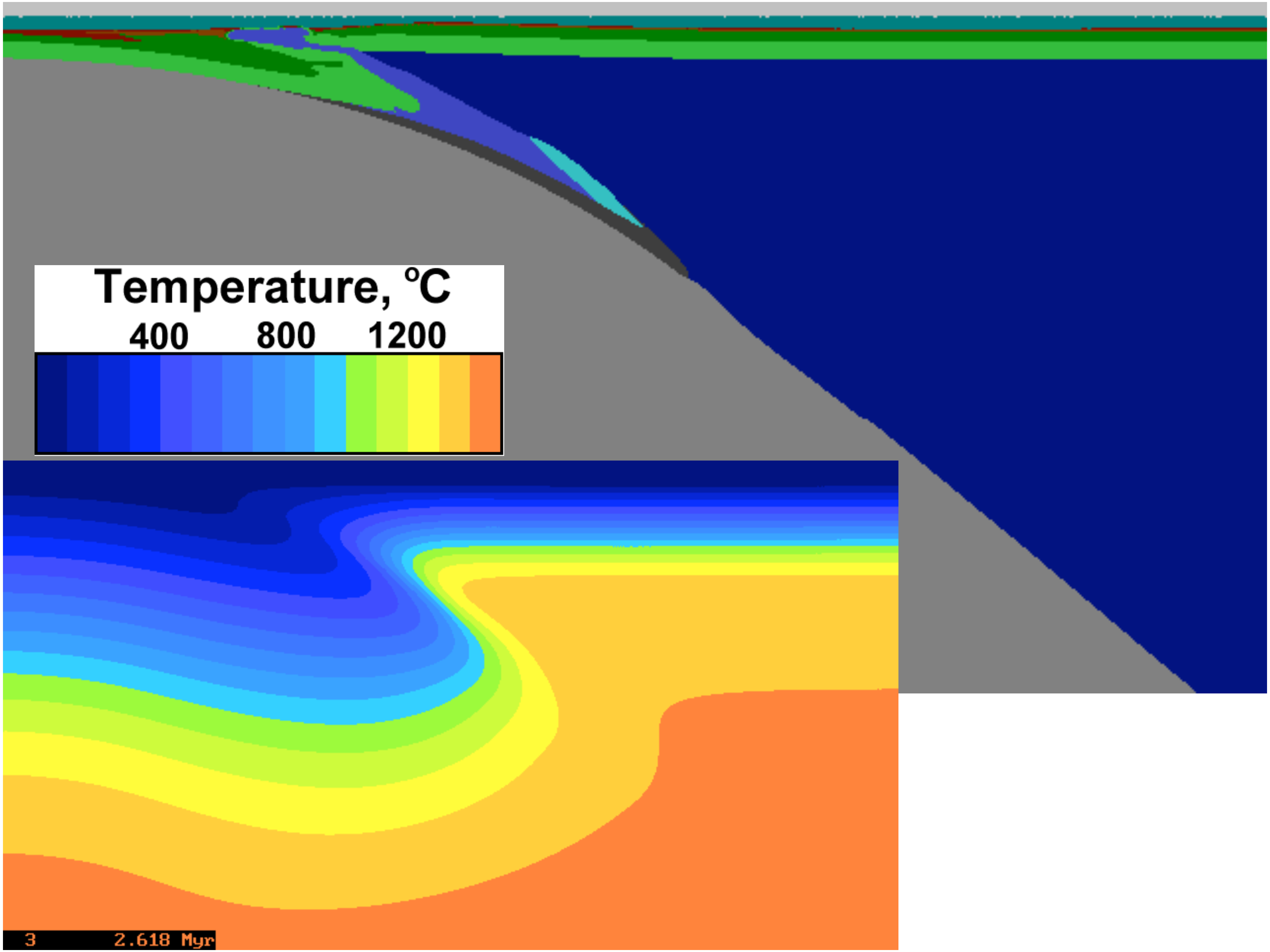
Temperature, °C
400
800
1200
3 2.618 Myr

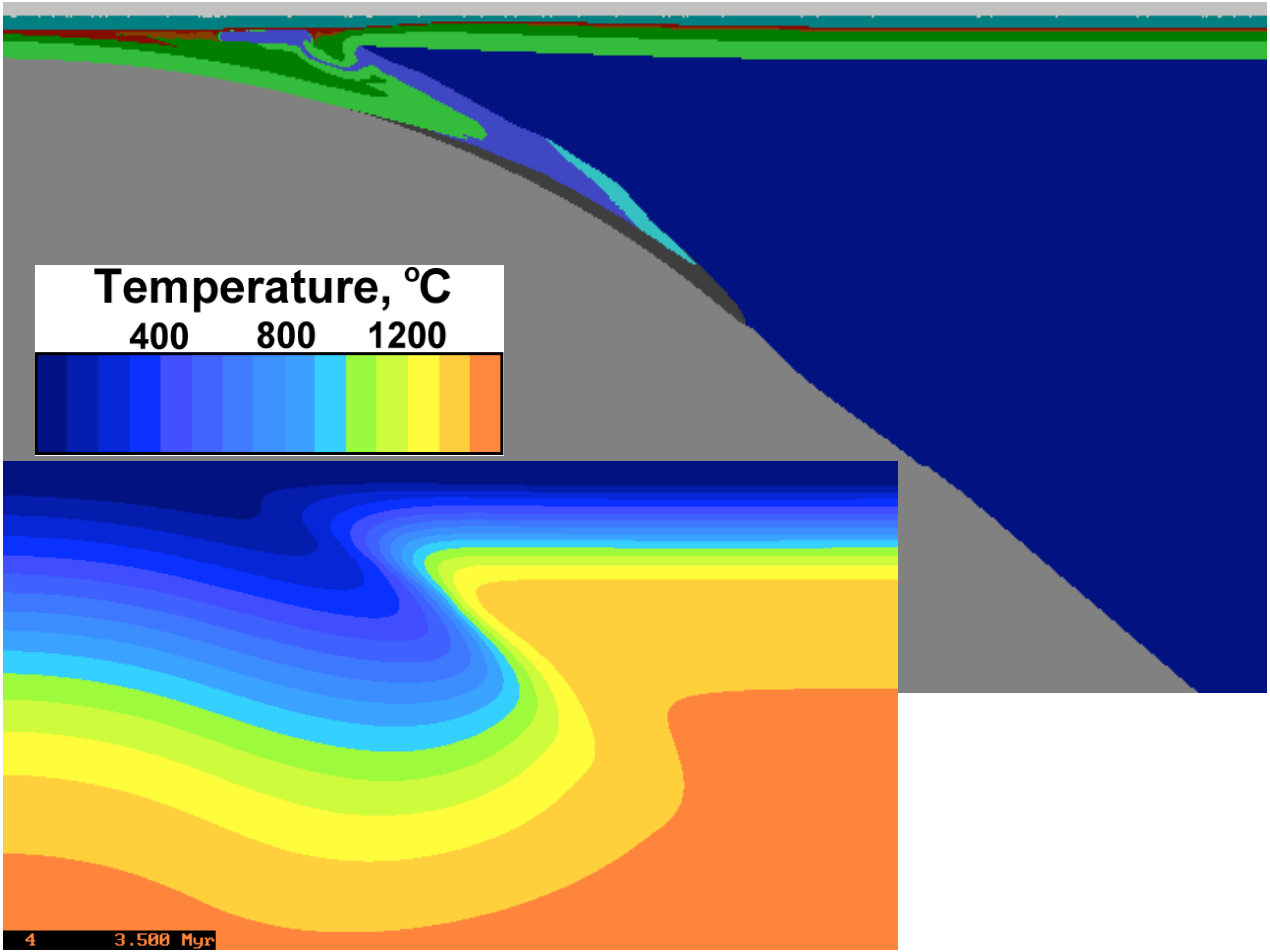

Temperature, °C
400 800 1200
4 3.500 Myr

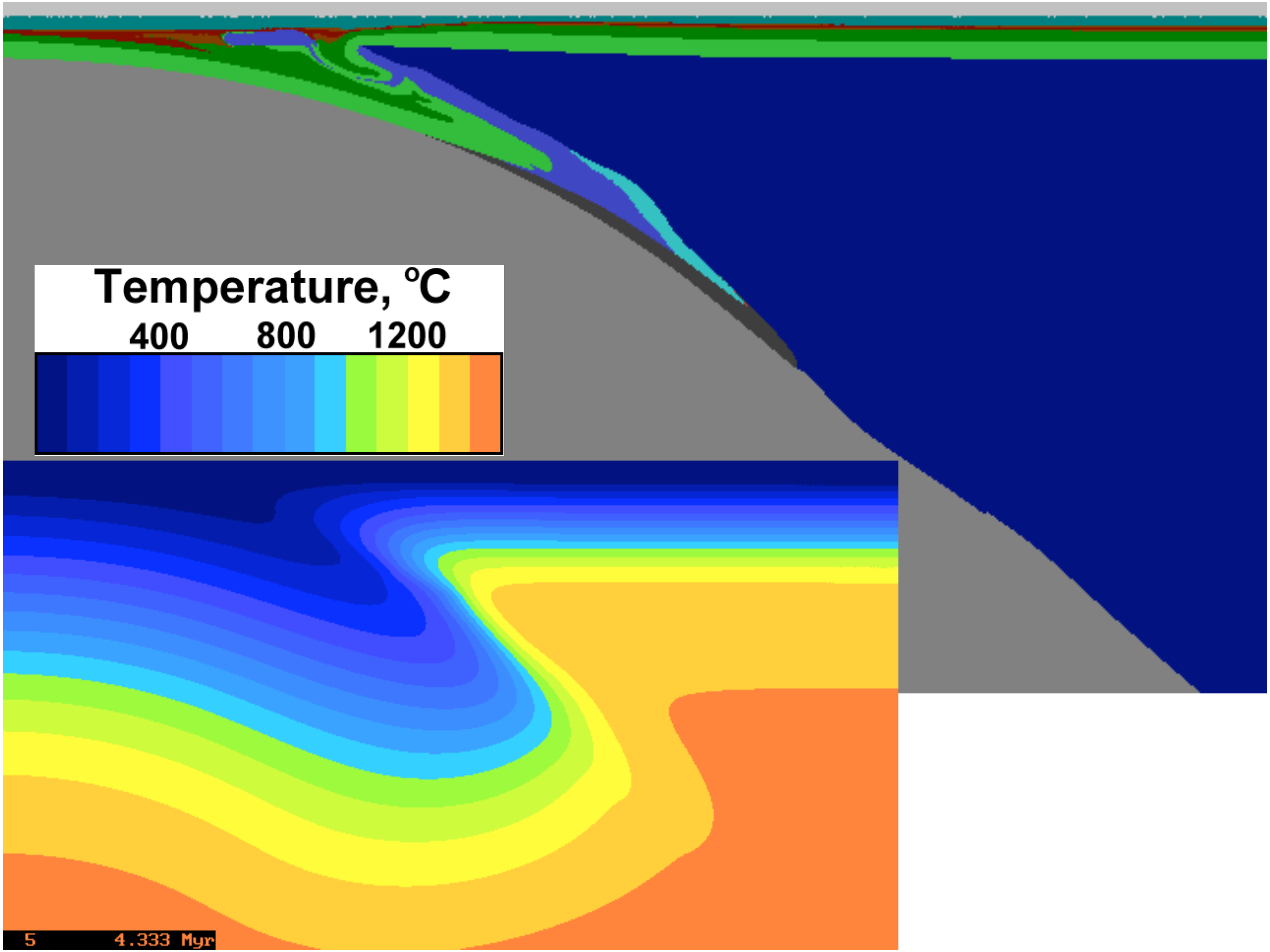
Temperature, °C
400
800
1200
5
4.333 Myr

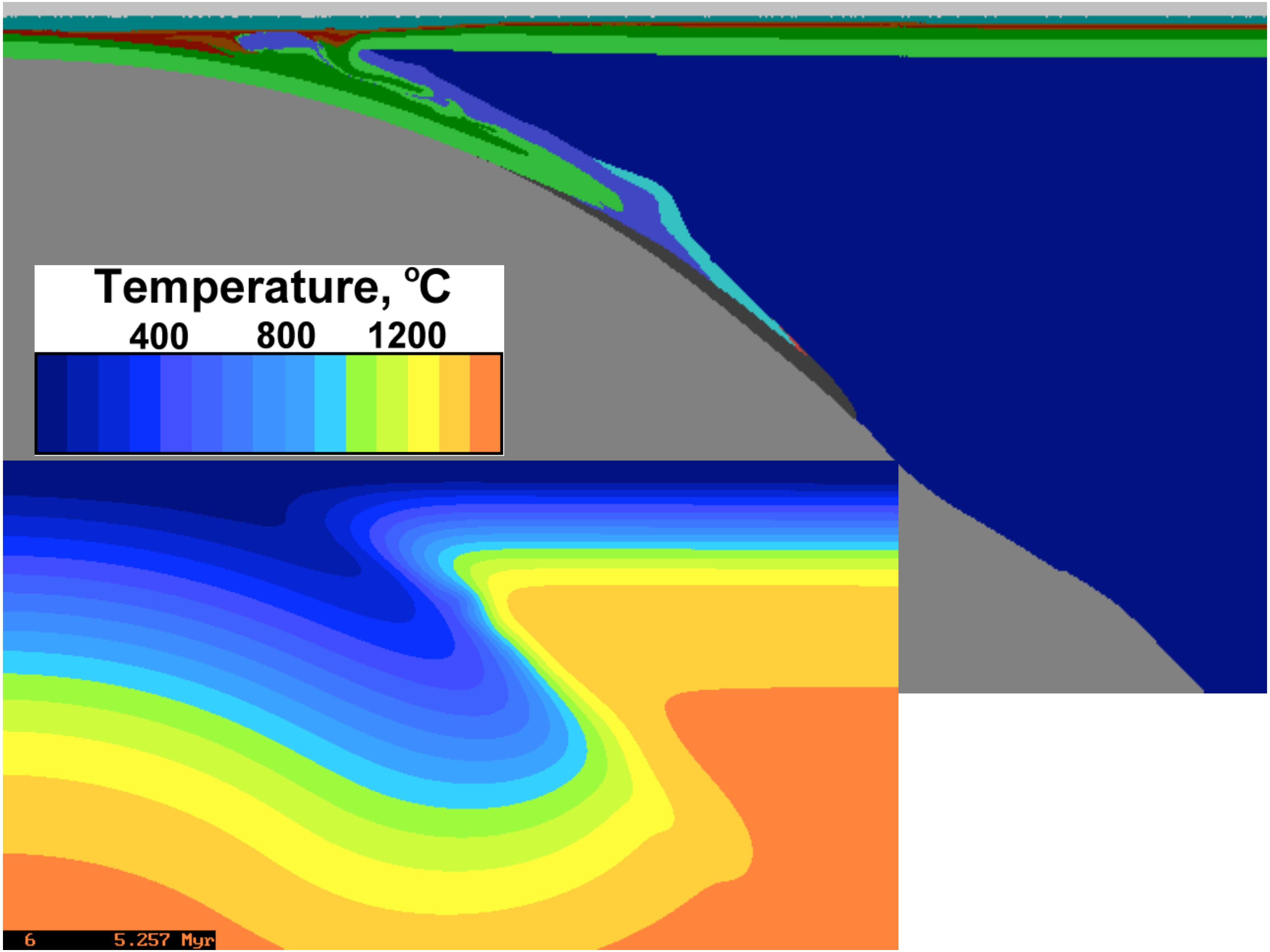

Temperature, °C
400
800
1200
6
5.257 Myr

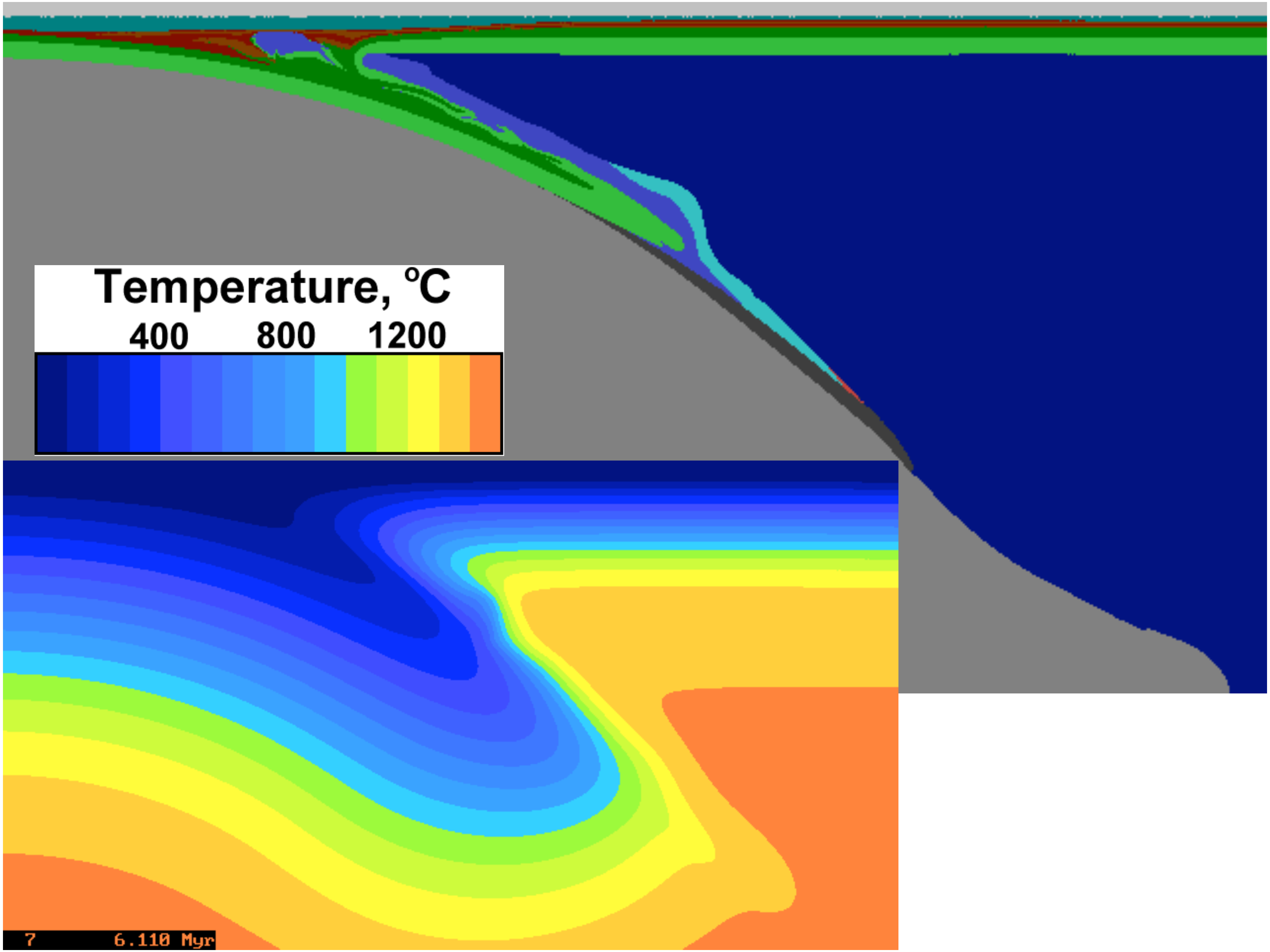
Temperature, °C
400
800
1200
7
6.110 Myr

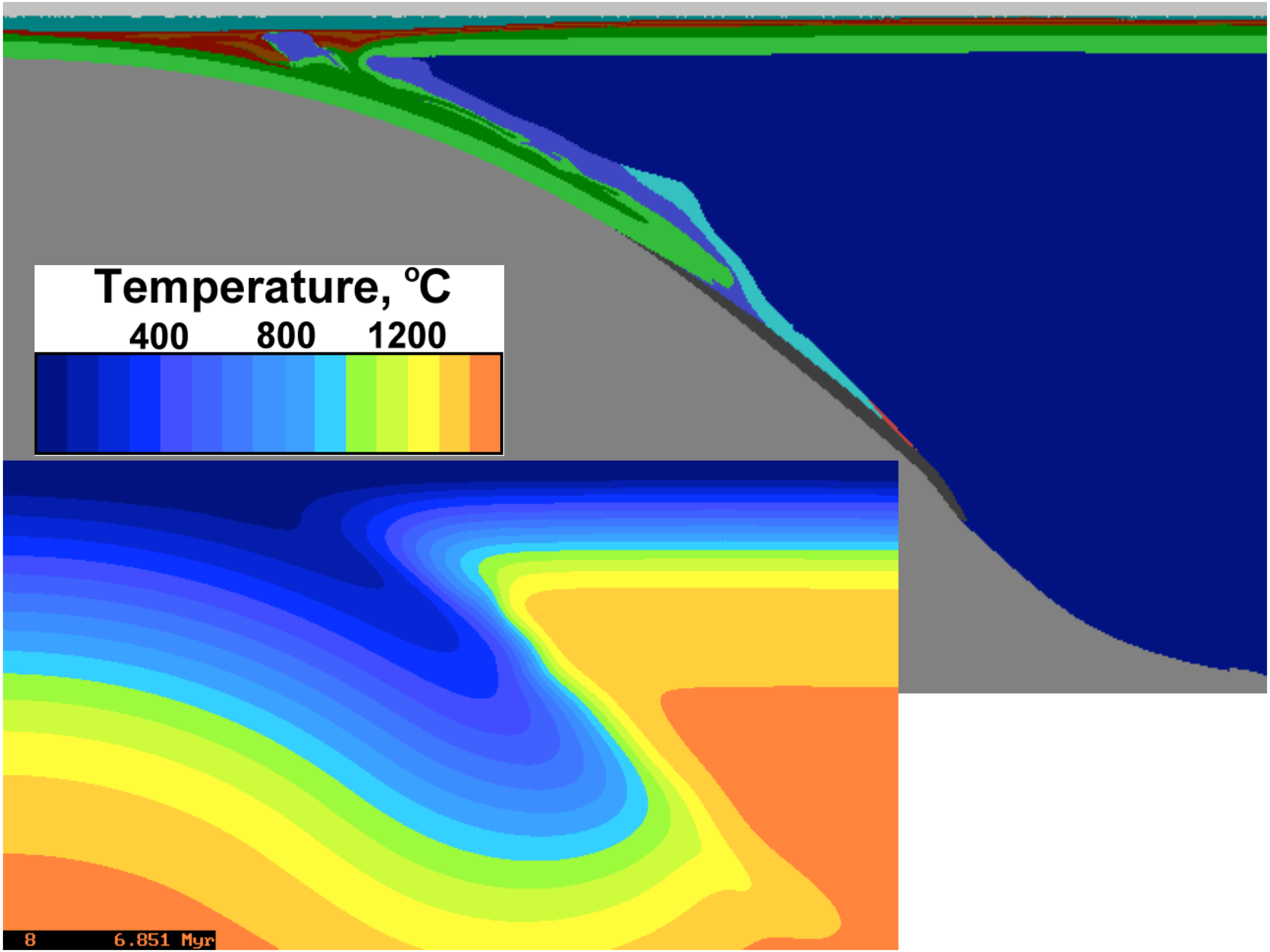

Temperature, °C
400
800
1200
8
6.851 Myr

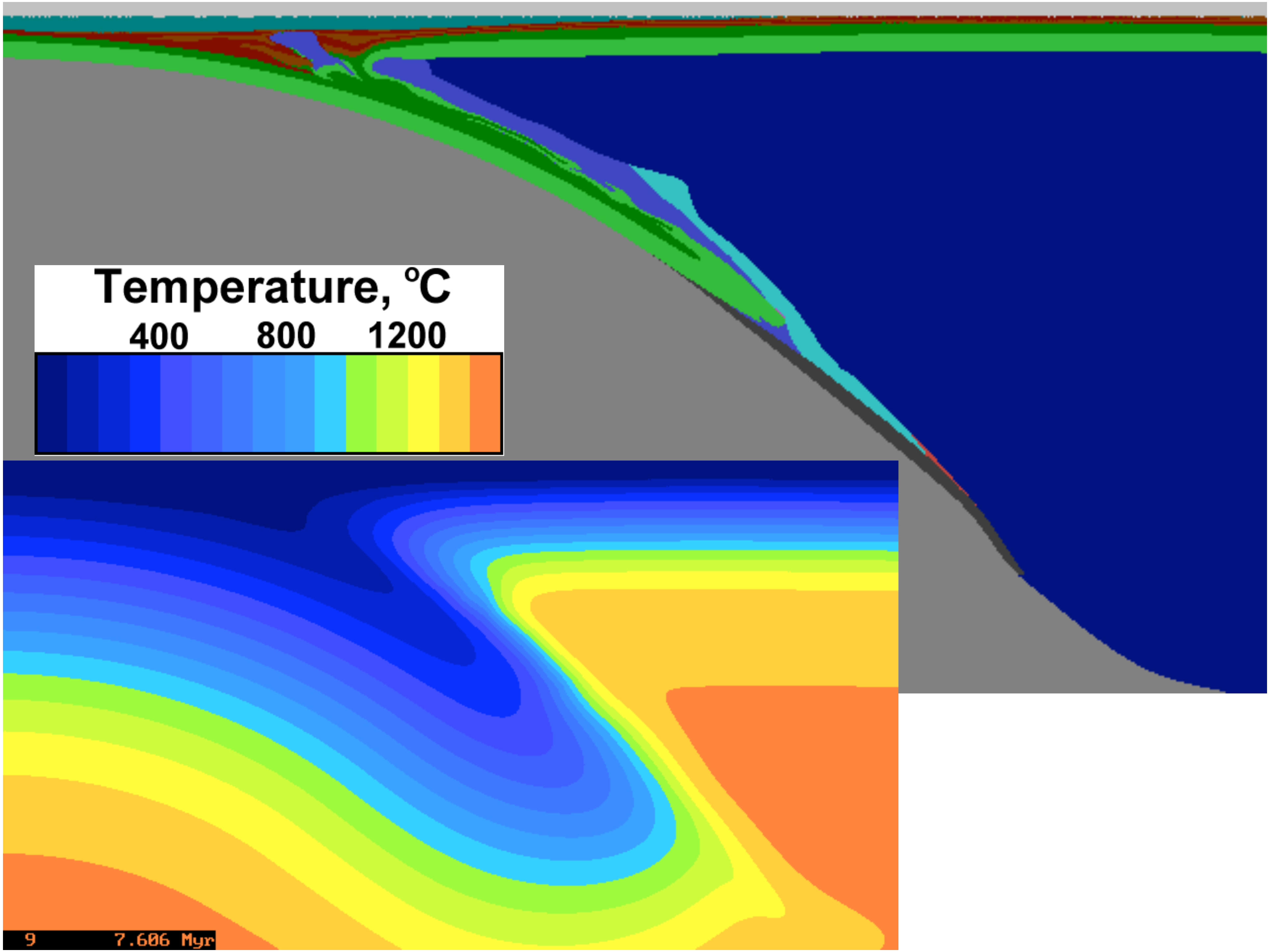

Temperature, °C
400
800
1200
9
7.606 Myr

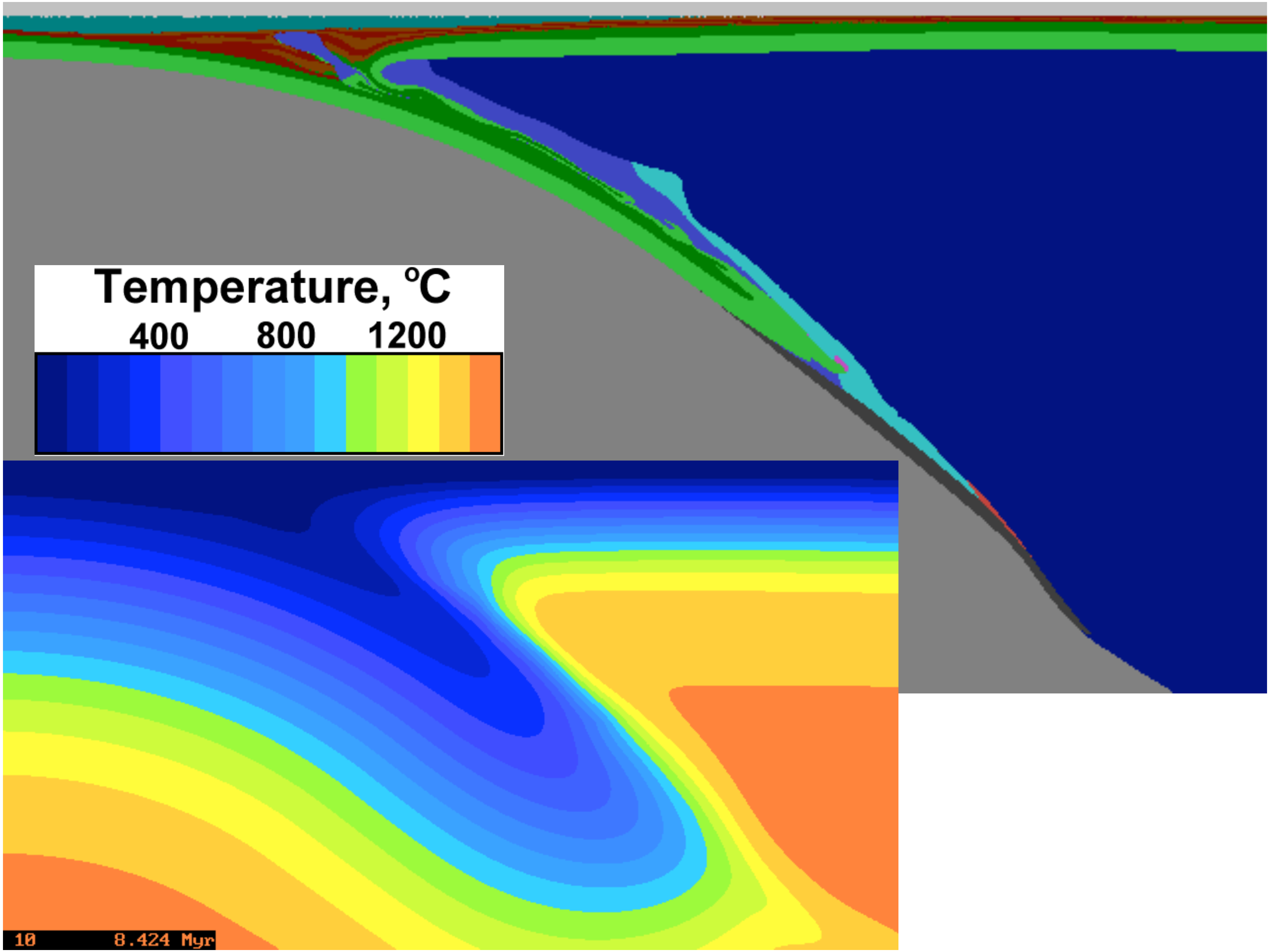
Temperature, °C
400
800
1200
10
8.424 Myr

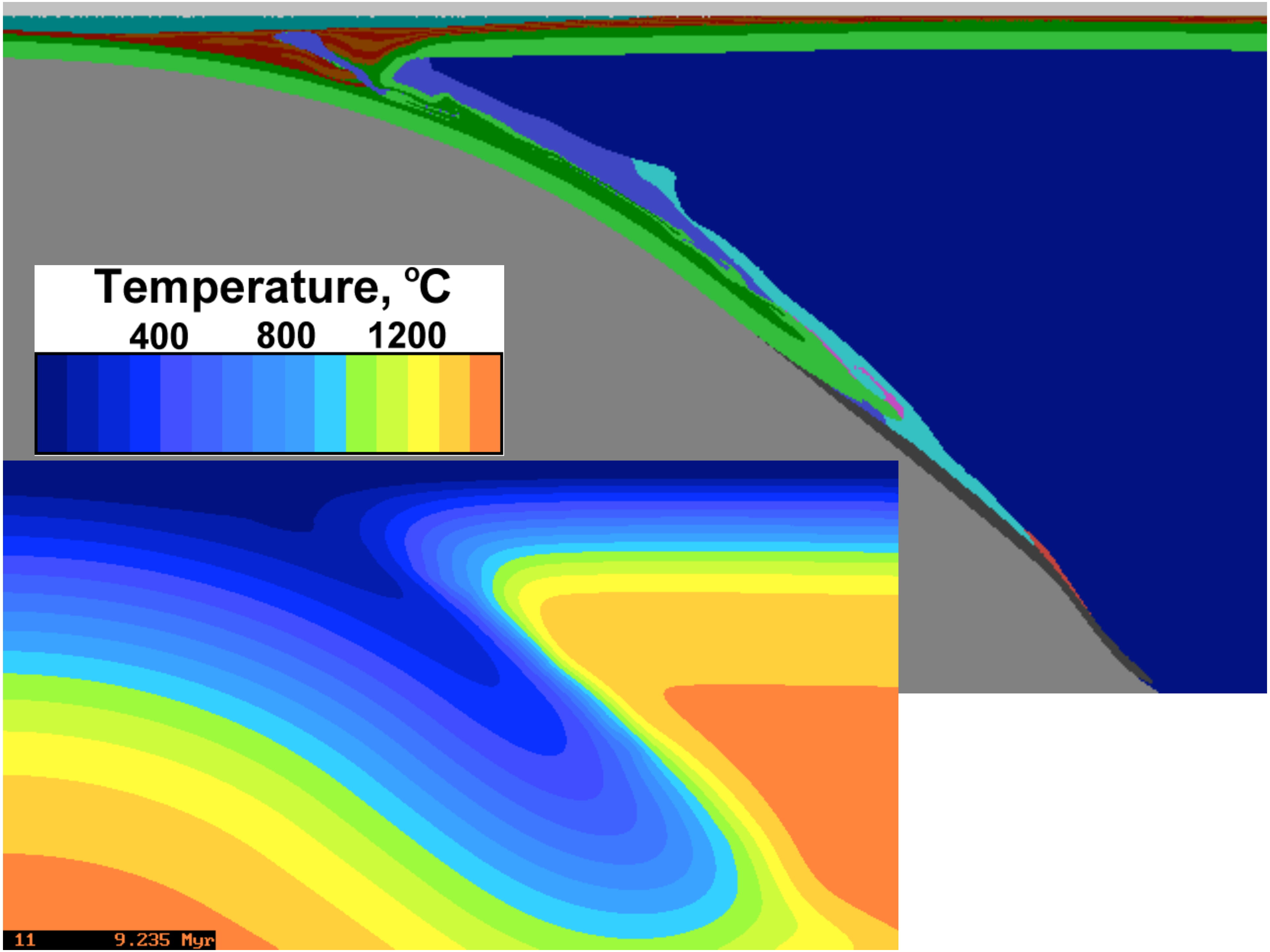

Temperature, °C
400
800
1200
11 9.235 Myr

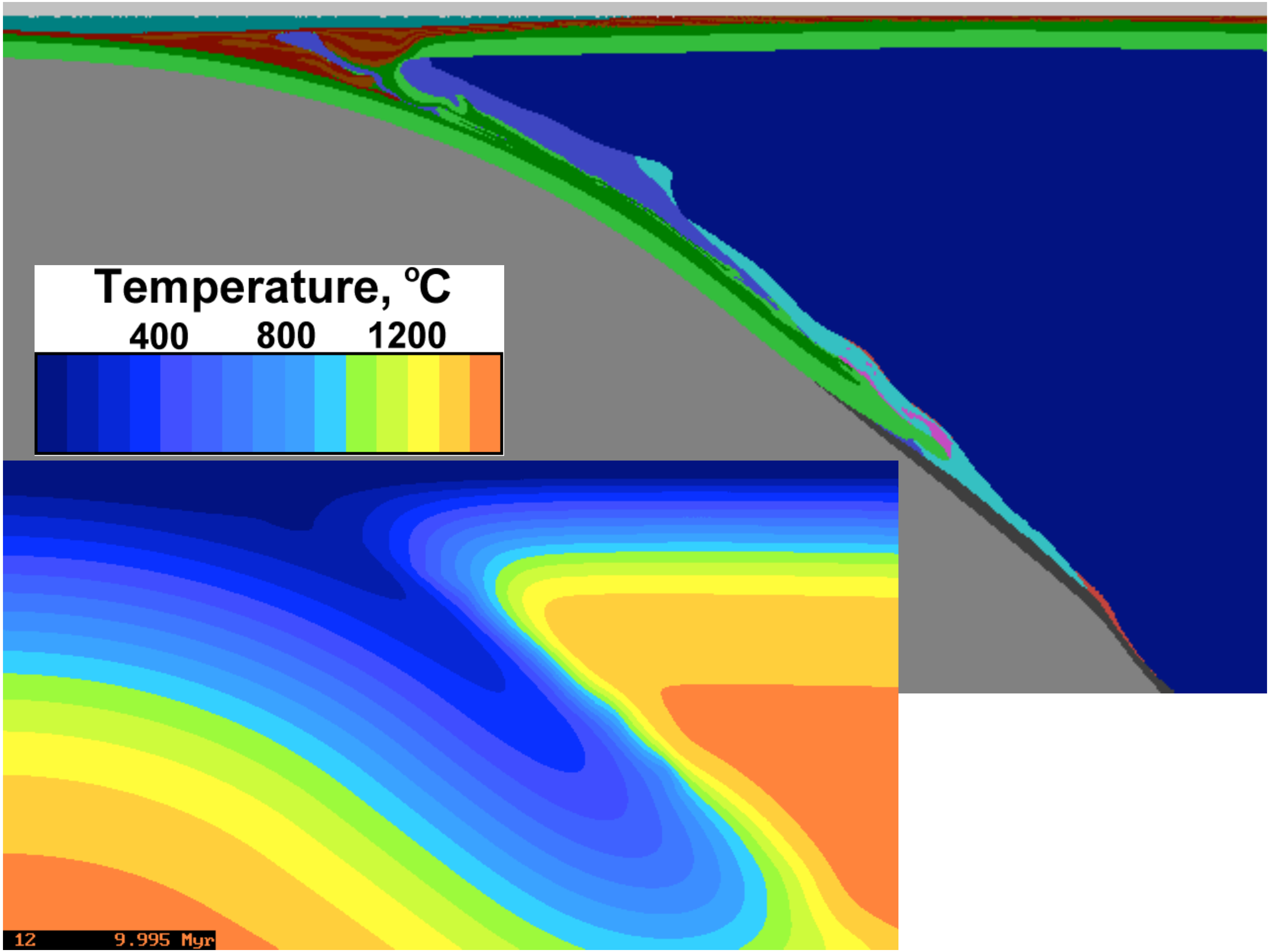
Temperature, °C
400
800
1200
12
9.995 Myr

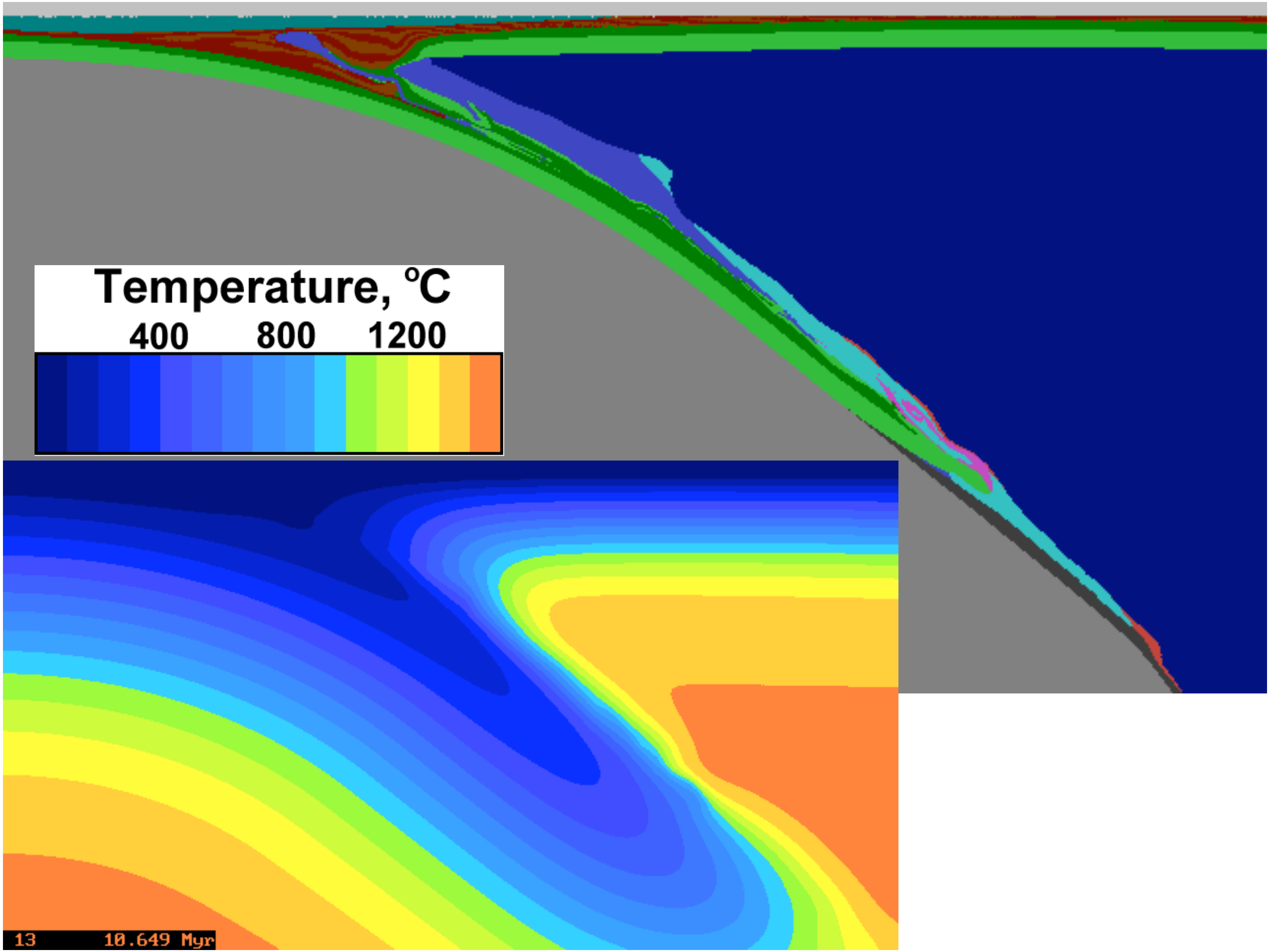

Temperature, °C
400
800
1200
13 10.649 Myr

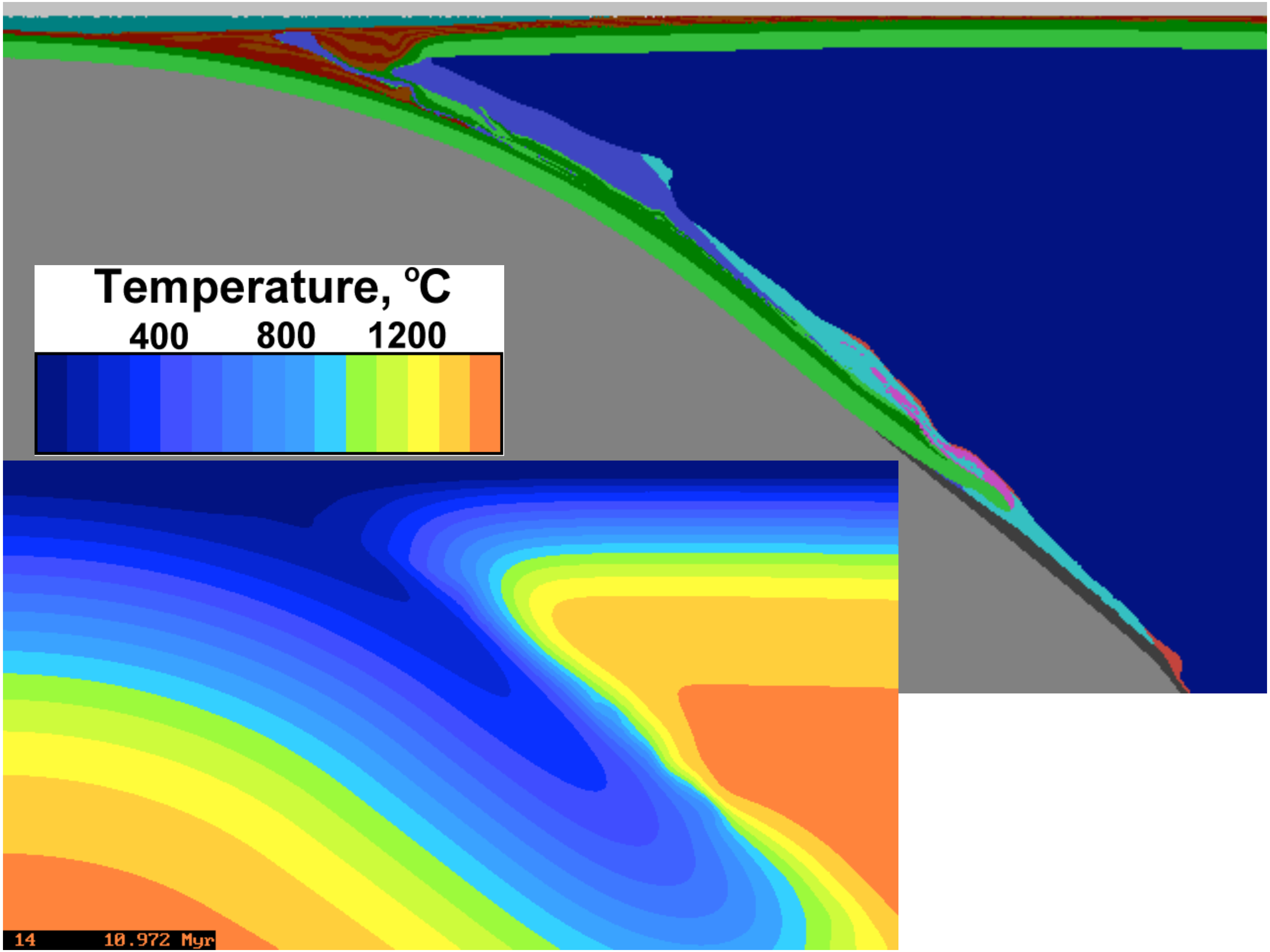

Temperature, °C
400
800
1200
14
10.972 Myr

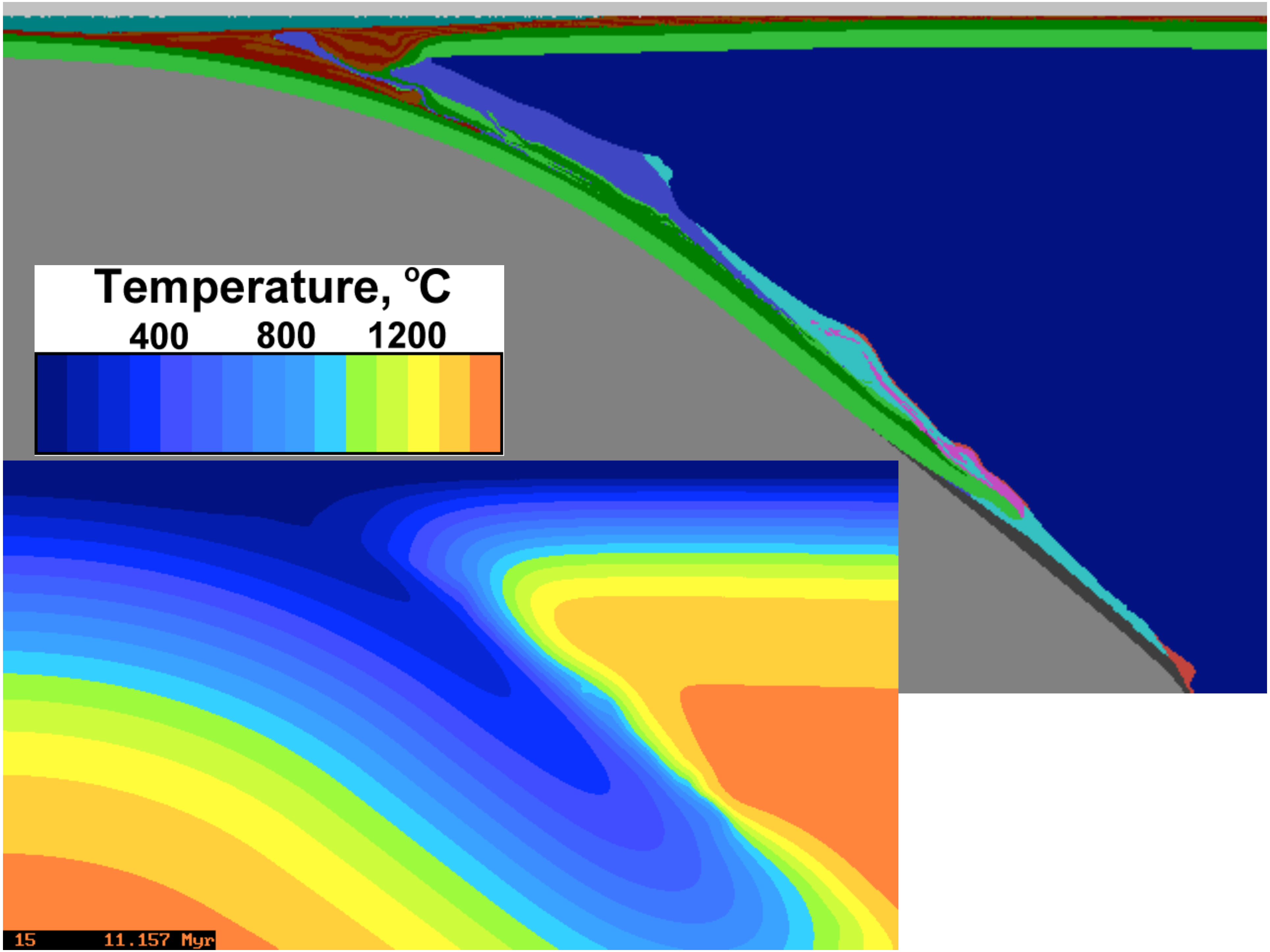
Temperature, °C
400
800
1200
15
11.157 Myr

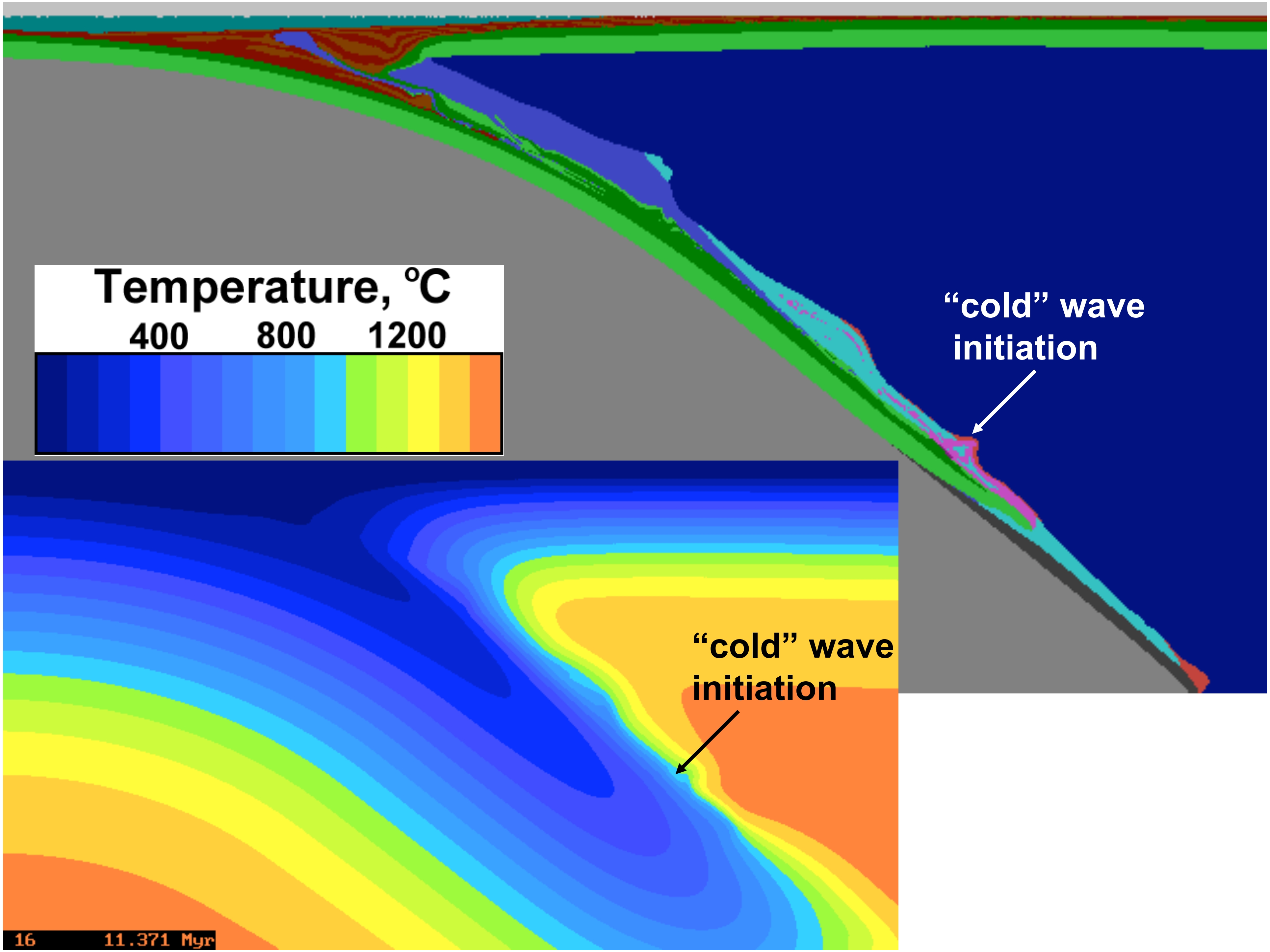
Temperature, °C
400
800
1200
"cold" wave
initiation
"cold" wave
initiation
16 11.371 Myr

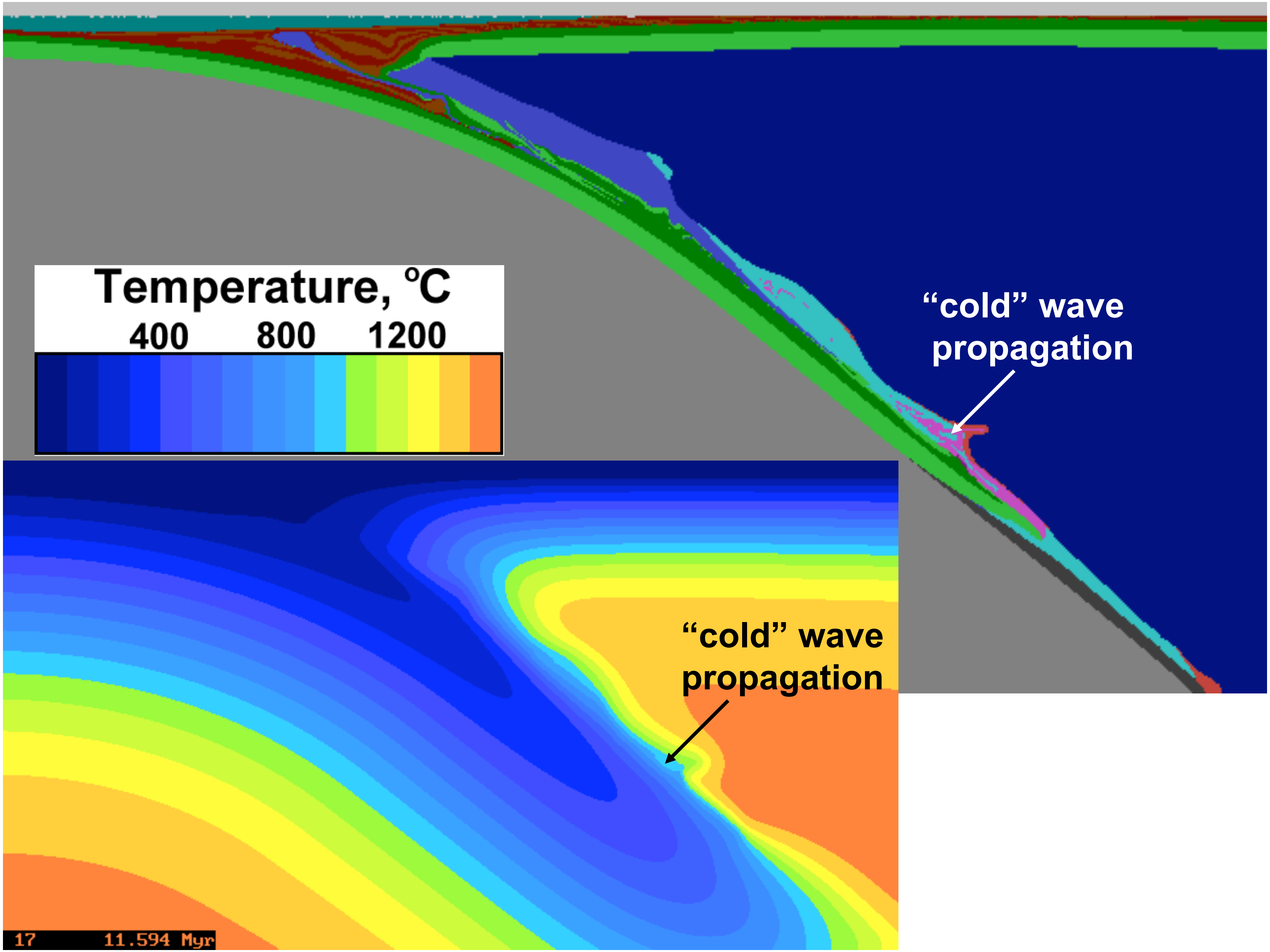
Temperature, °C
400
800
1200
"cold" wave
propagation
"cold" wave
propagation
17
11.594 Myr

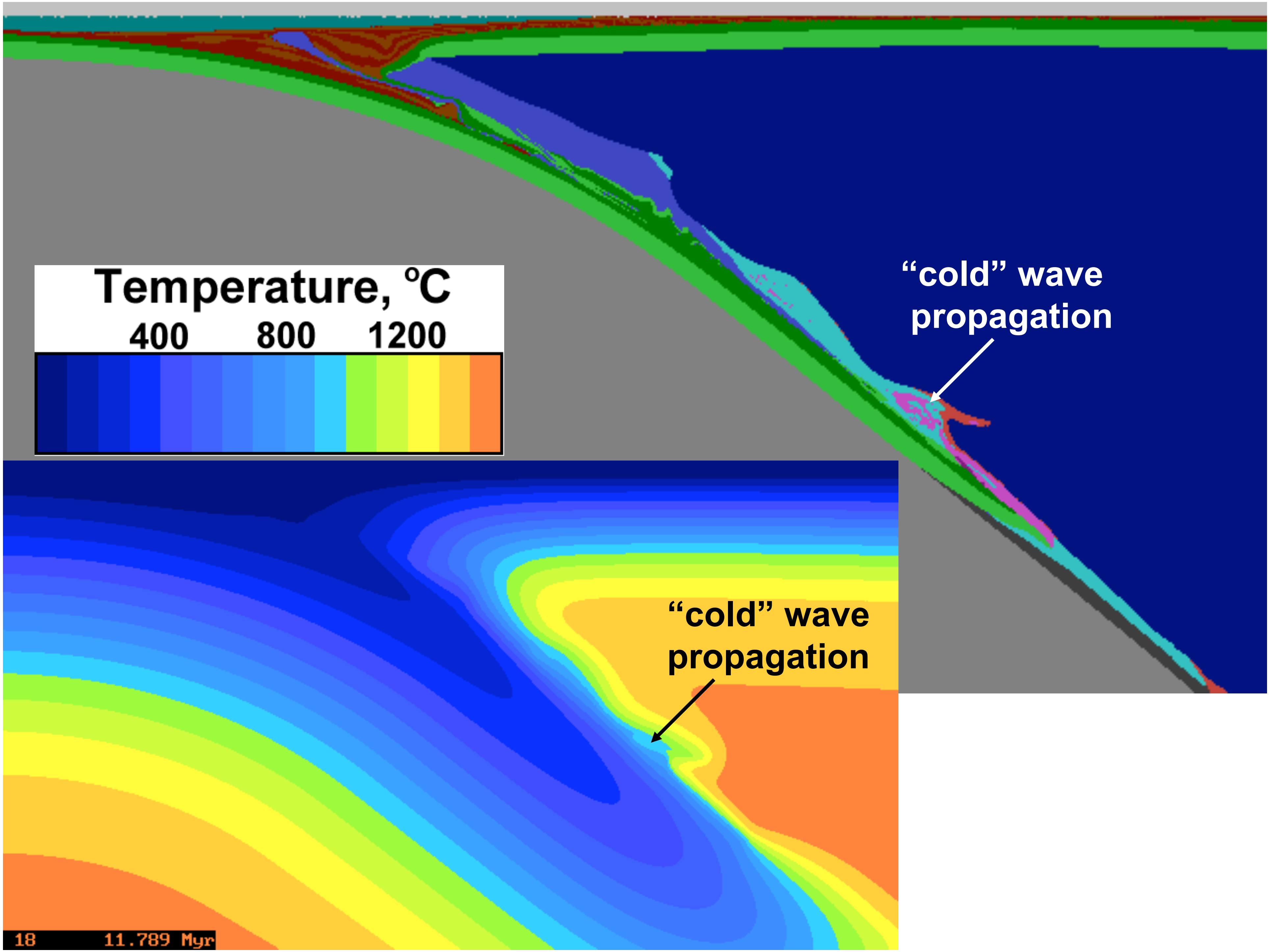

Temperature, ºC
400
800
1200
"cold" wave
propagation
"cold" wave
propagation
18
11.789 Myr

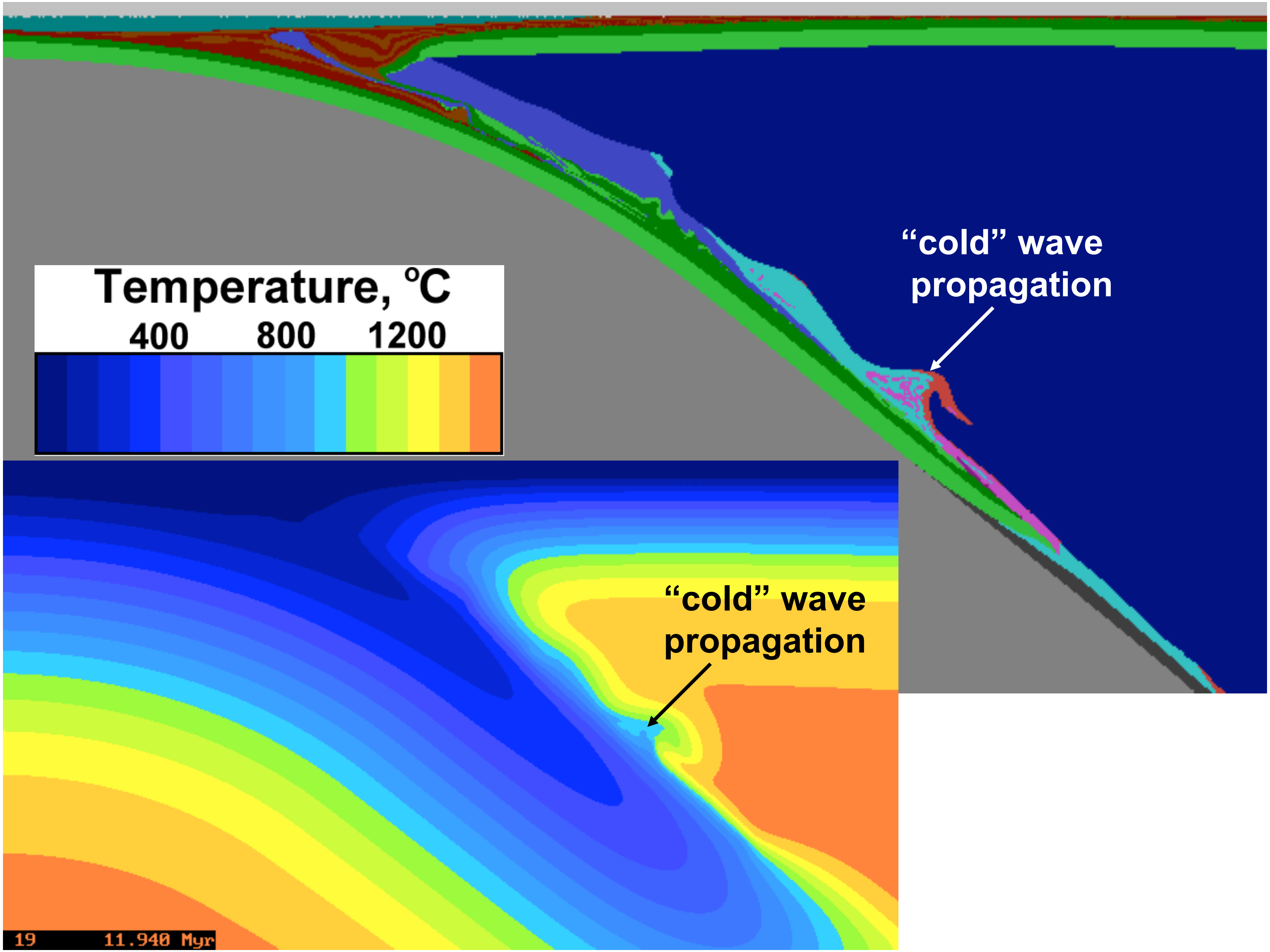

Temperature, °C
400
800
1200
"cold" wave propagation
"cold" wave propagation
19 11.940 Myr

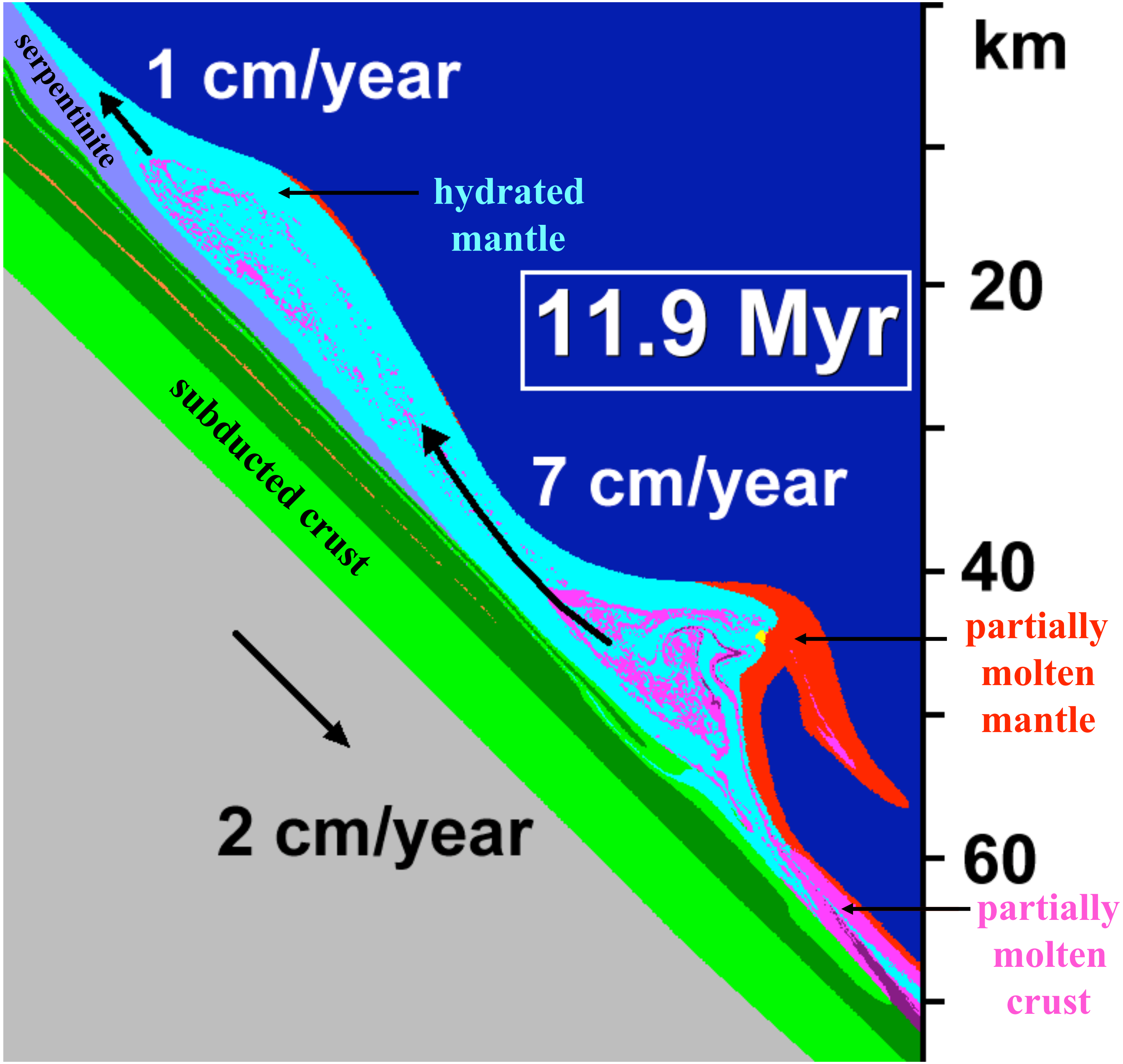

serpentinite
1 cm/year
hydrated mantle
km
20
11.9 Myr
subducted crust
7 cm/year
40
partially molten mantle
60
partially molten crust
2 cm/year

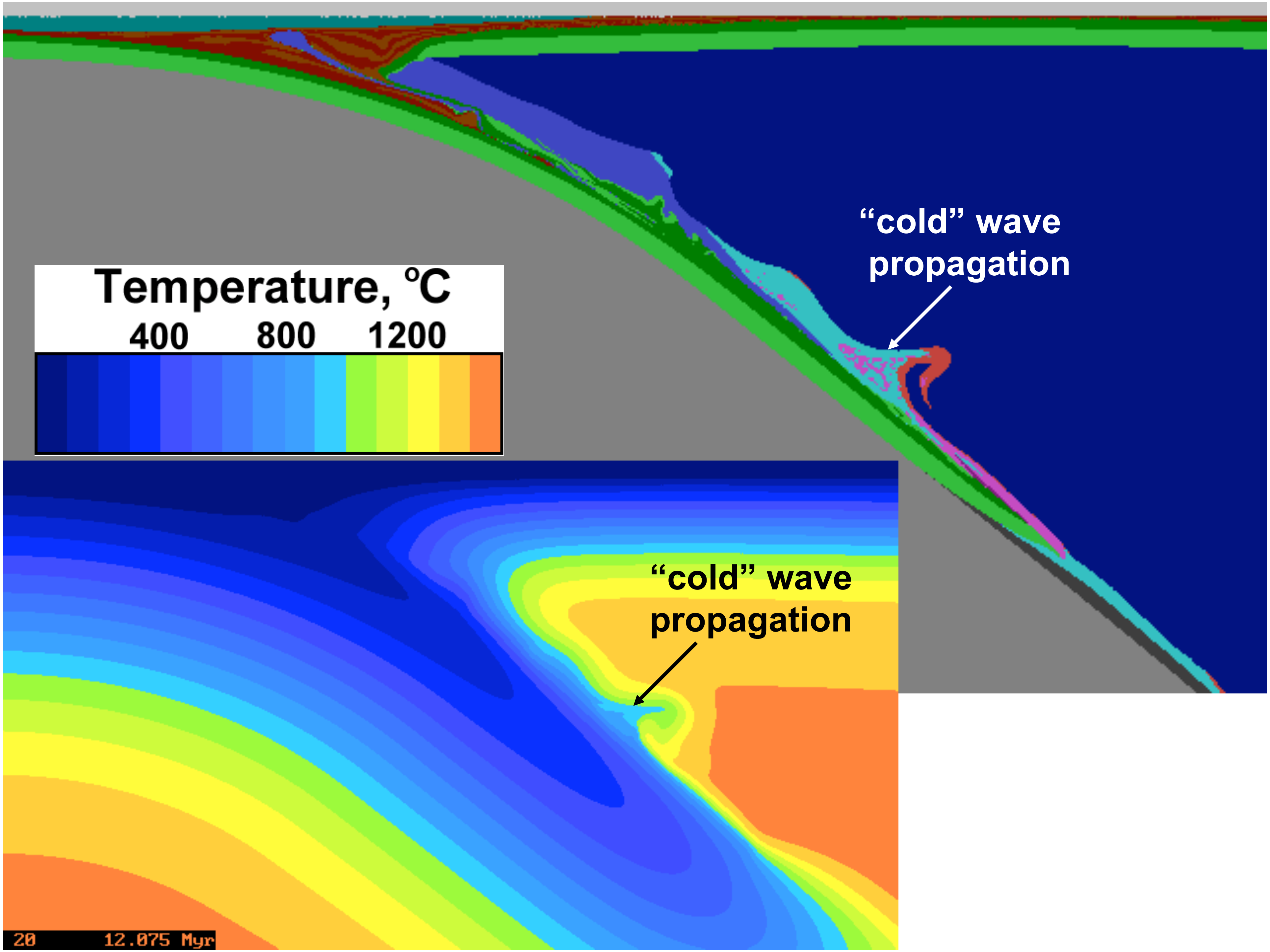

“cold” wave propagation
Temperature, ºC
400 800 1200
“cold” wave propagation
20 12.075 Myr

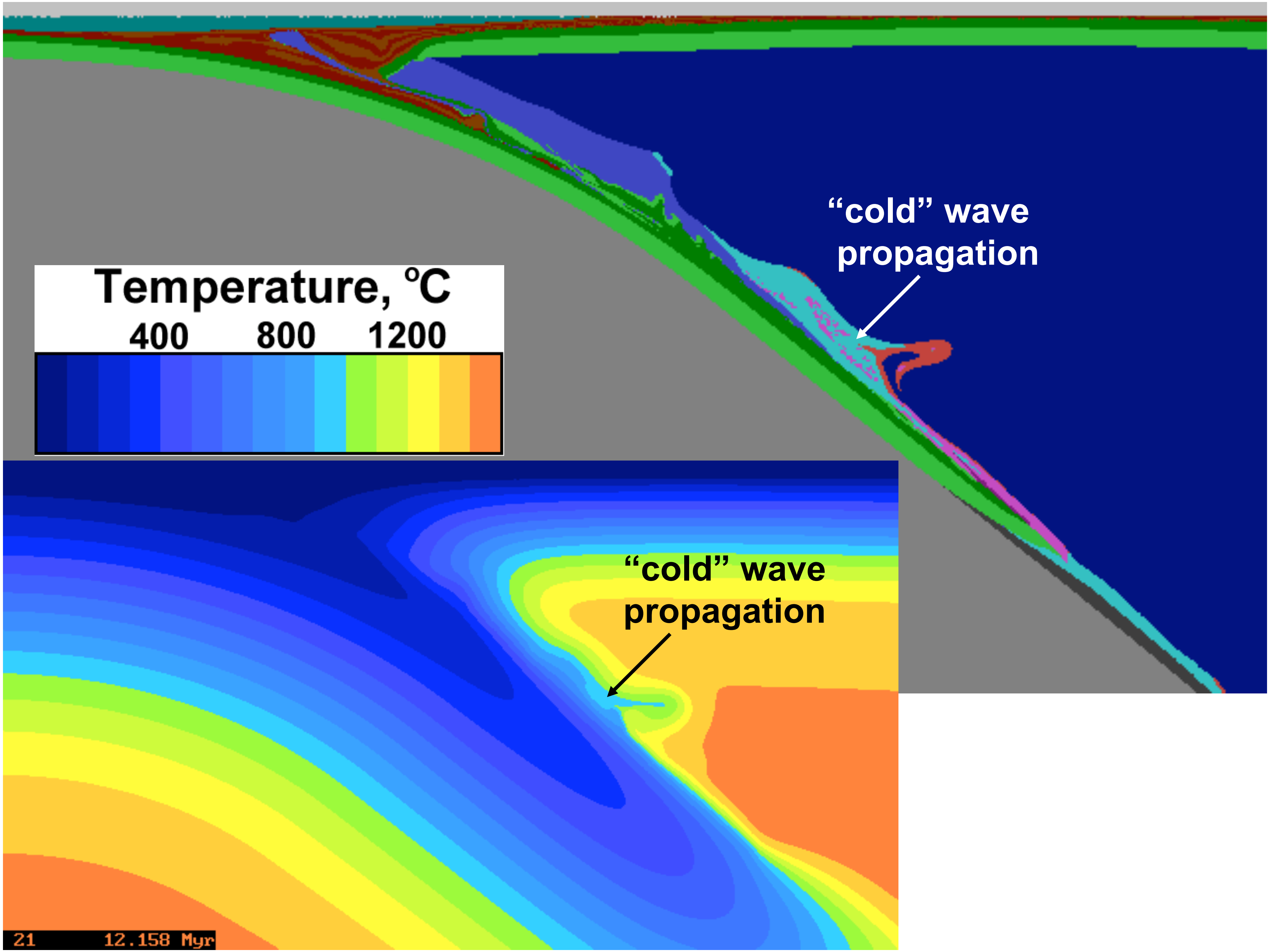

Temperature, °C
400
800
1200
"cold" wave propagation
"cold" wave propagation
21 12.158 Myr

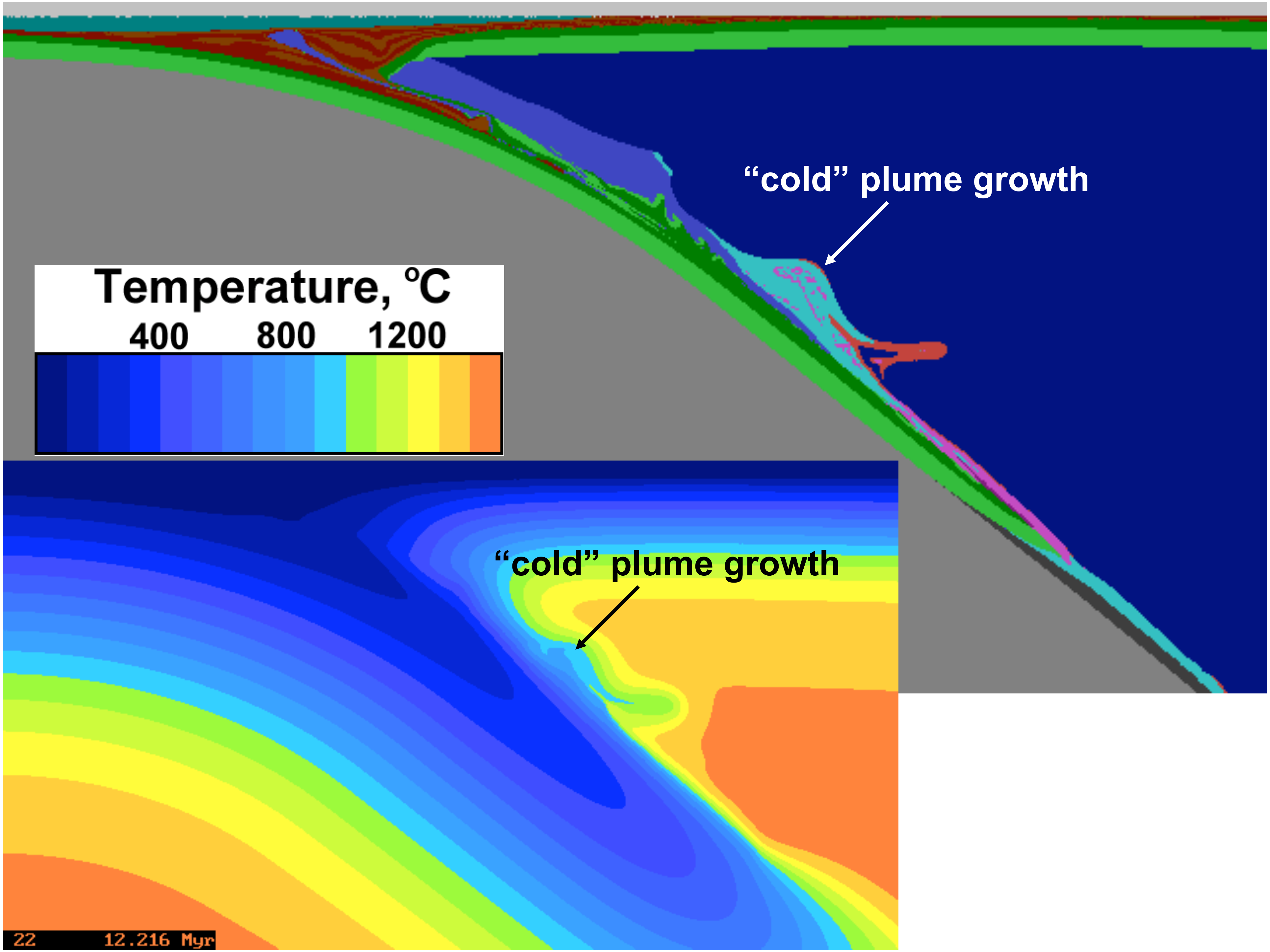
"cold" plume growth
Temperature, °C
400 800 1200
"cold" plume growth
22 12.216 Myr

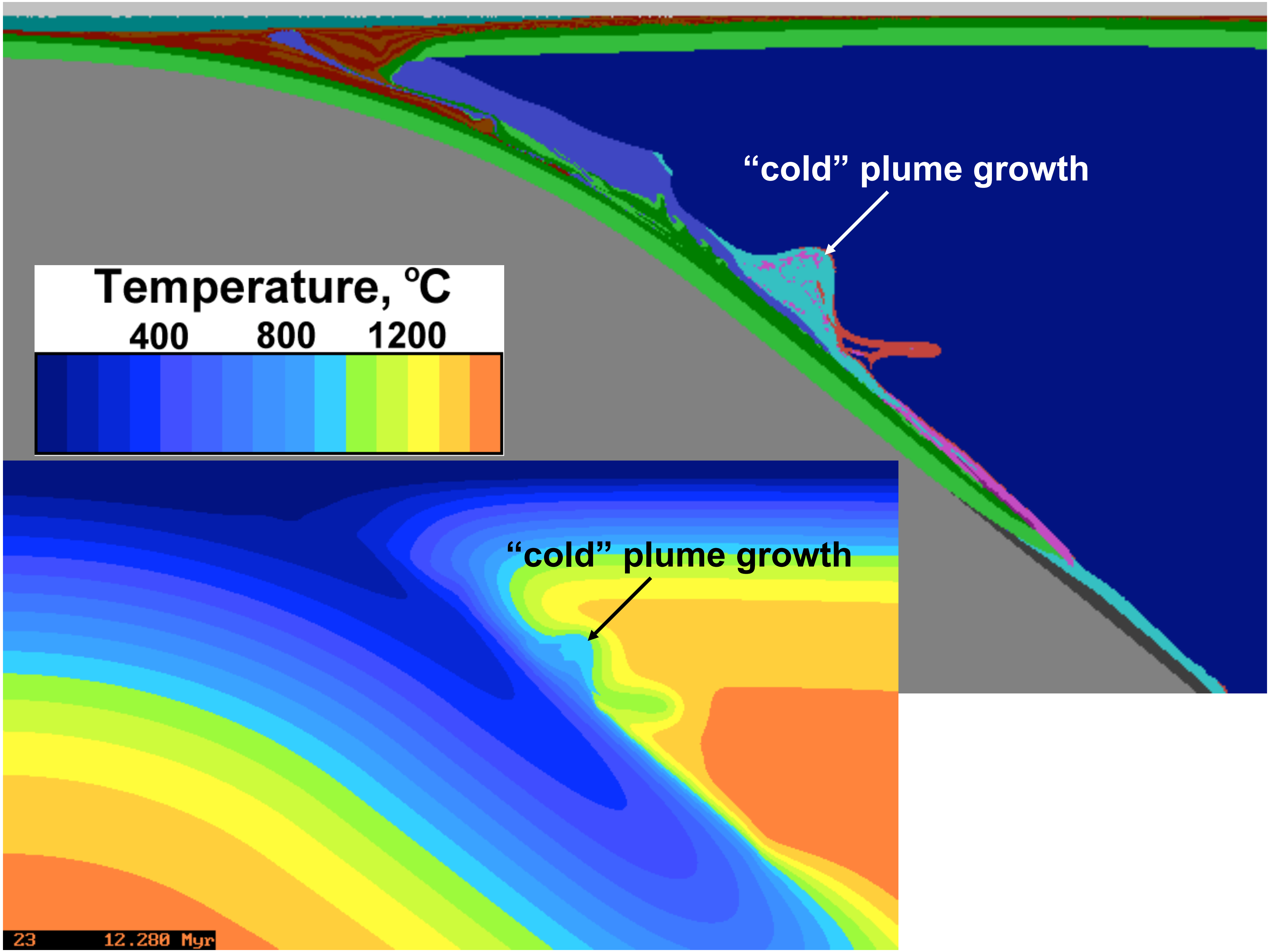

"cold" plume growth
Temperature, °C
400
800
1200
"cold" plume growth
23
12.280 Myr

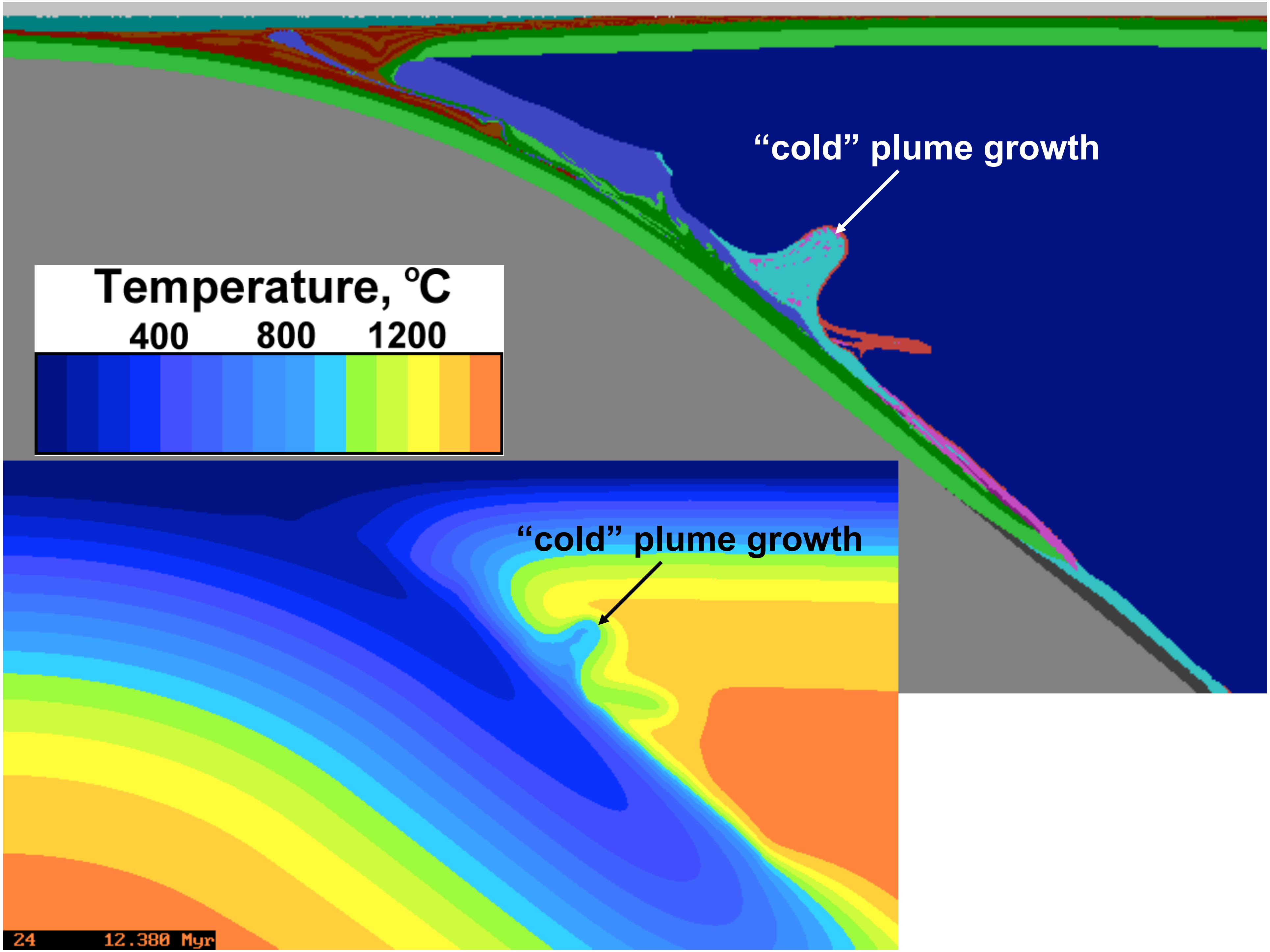
"cold" plume growth
Temperature, °C
400
800
1200
"cold" plume growth
24
12.380 Myr

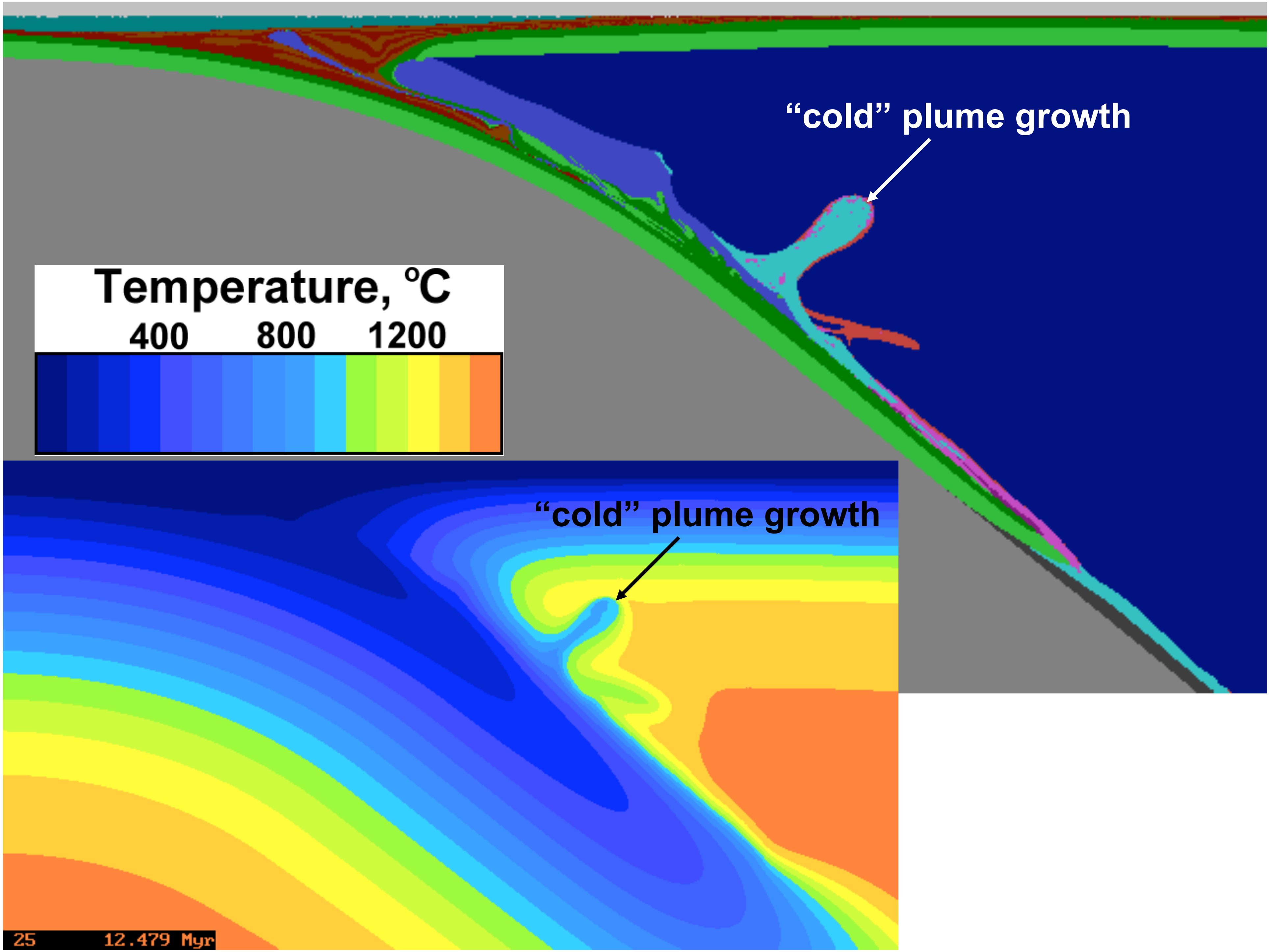
"cold" plume growth
Temperature, ºC
400
800
1200
"cold" plume growth
25
12.479 Myr

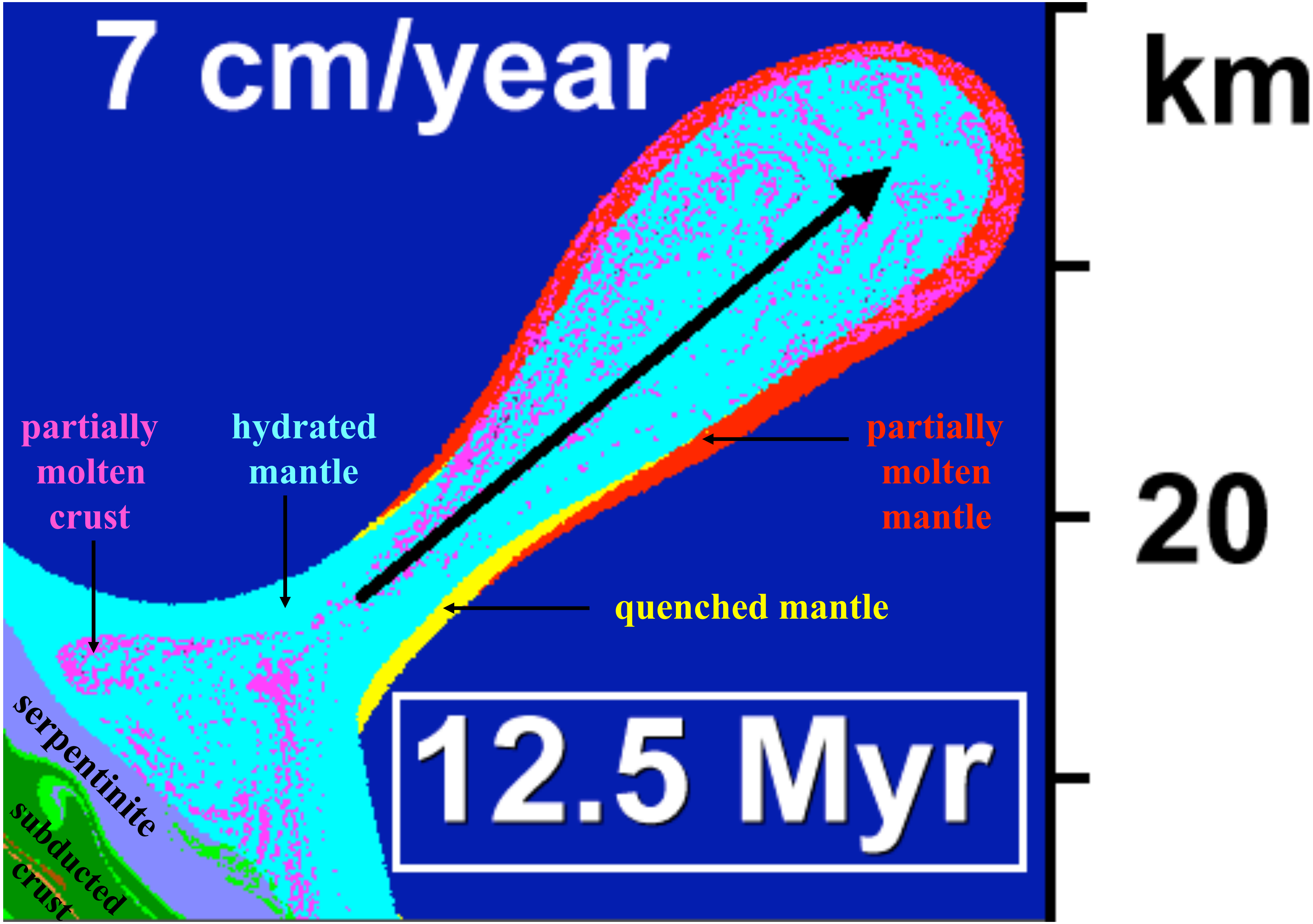

Gerya et al. (2004)

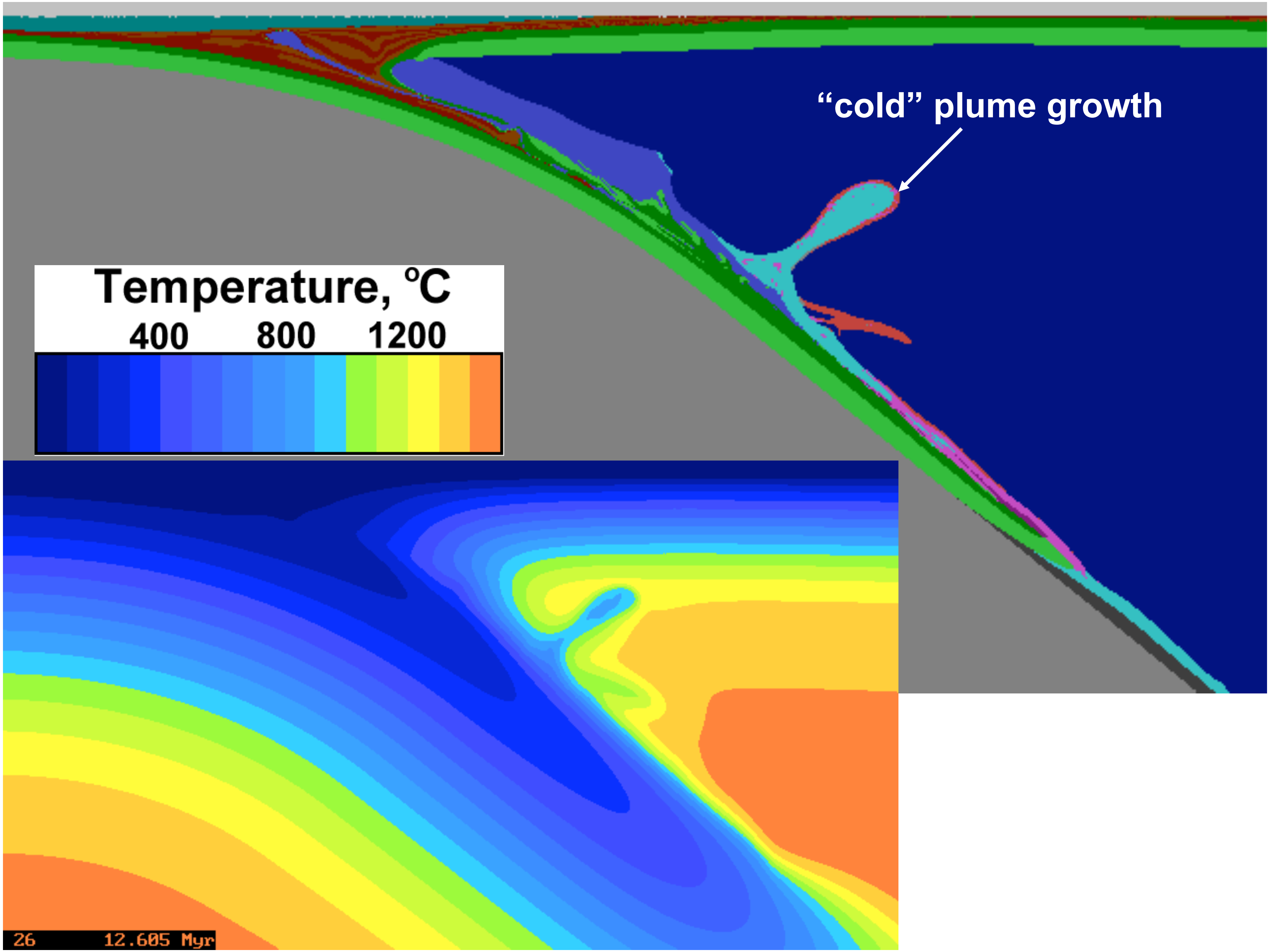

"cold" plume growth
Temperature, °C
400
800
1200
26
12.605 Myr

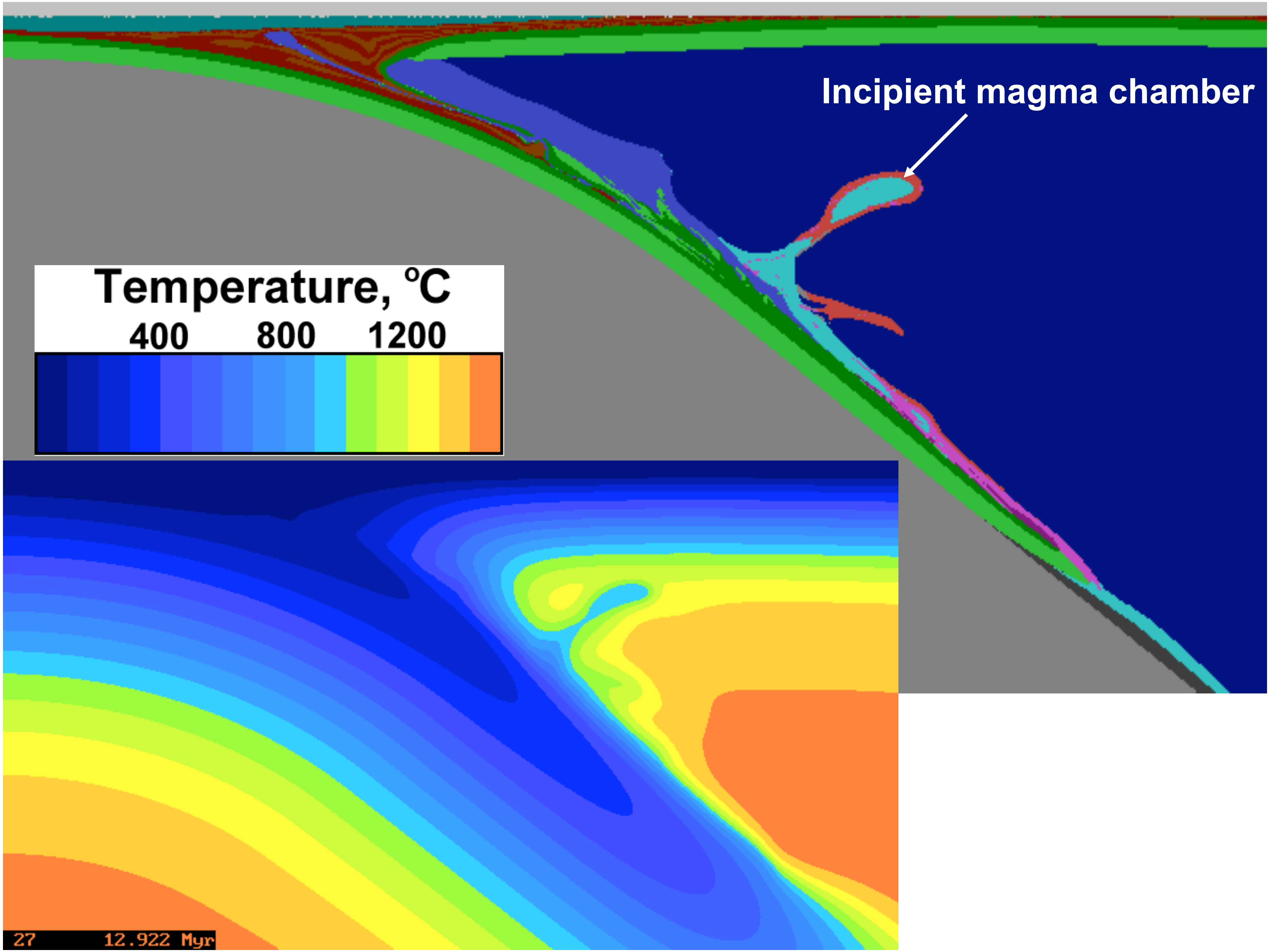

Incipient magma chamber
Temperature, °C
400
800
1200
27
12.922 Myr

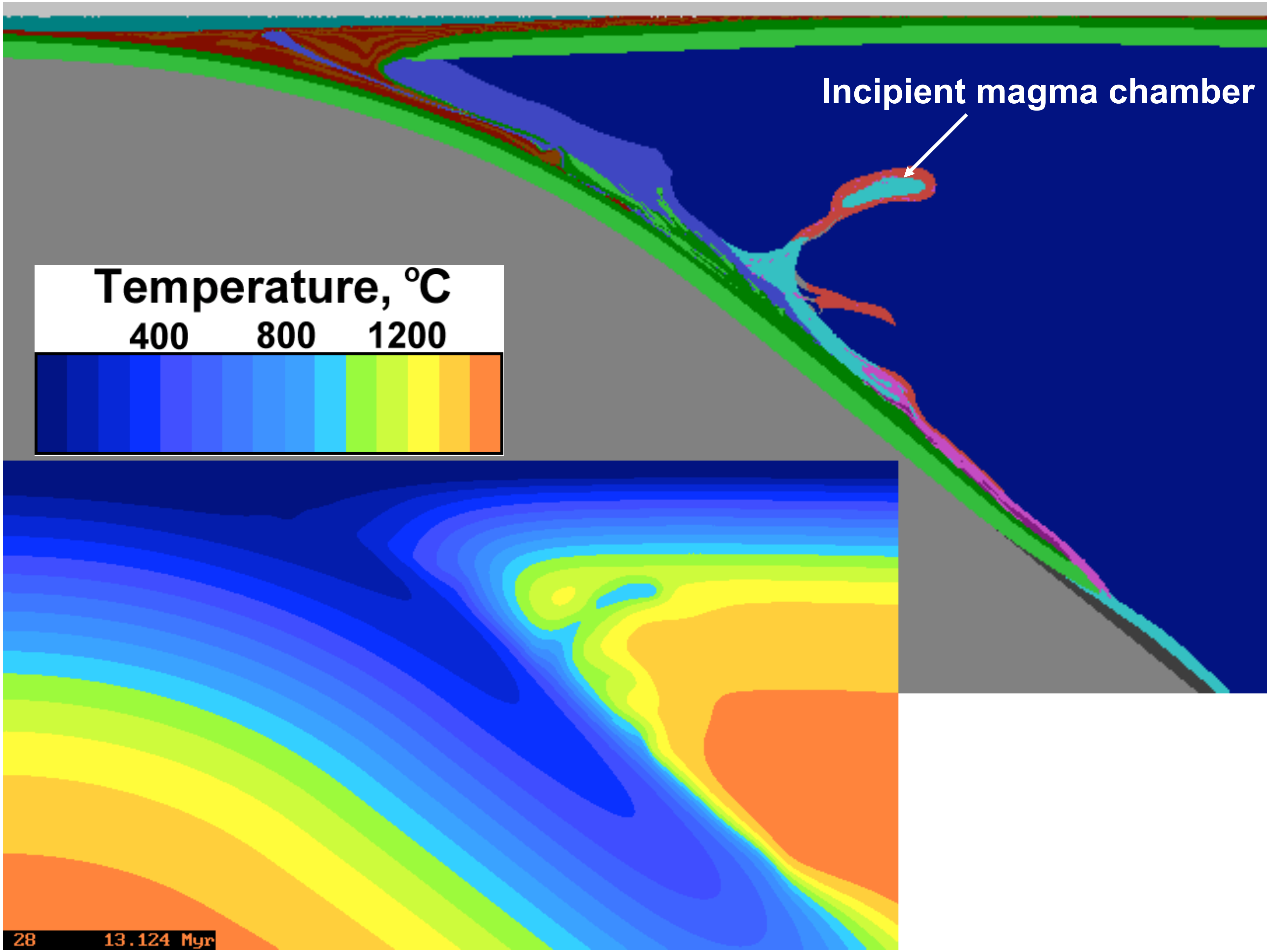

Incipient magma chamber
Temperature, °C
400
800
1200
28
13.124 Myr

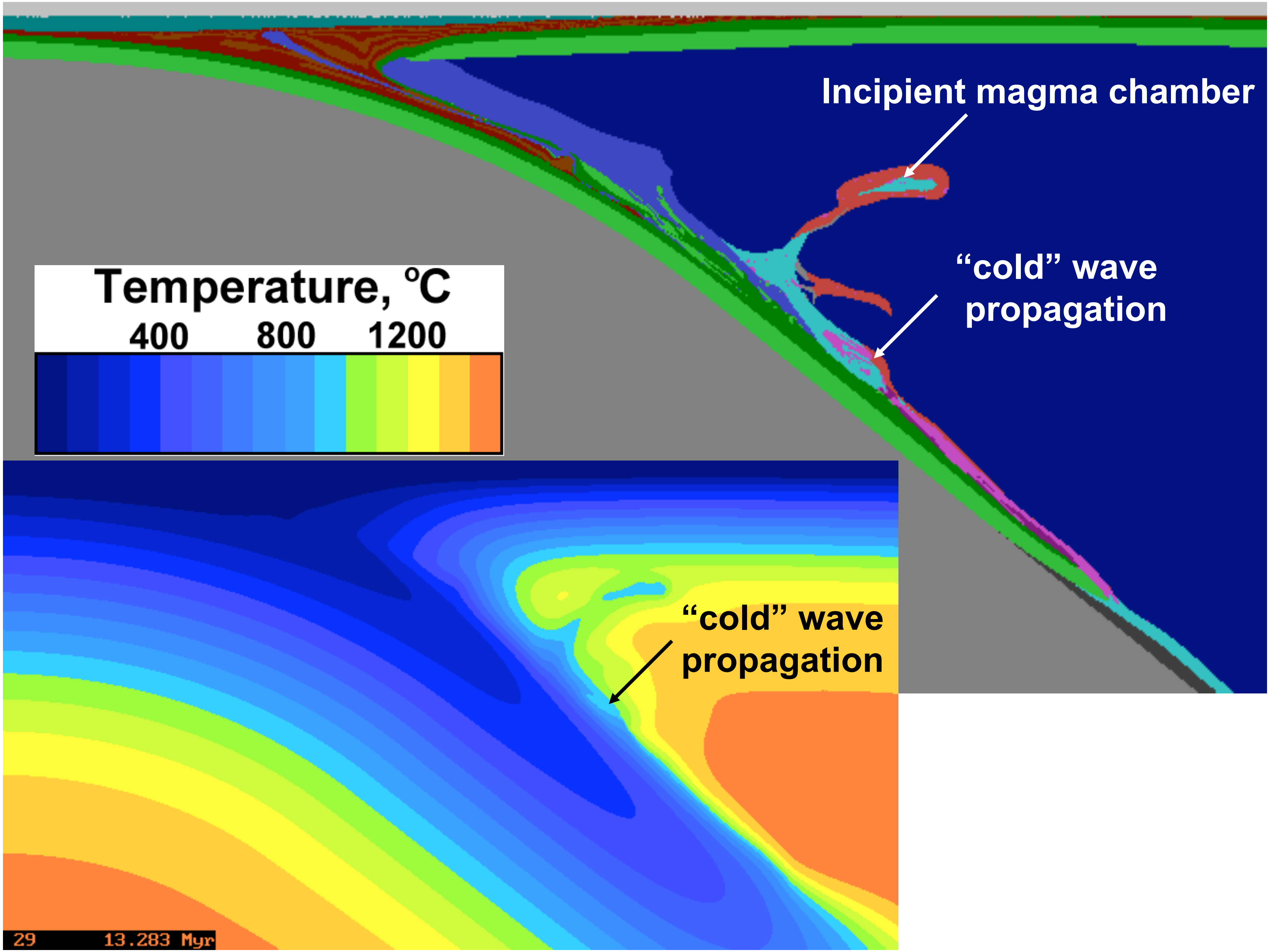
Incipient magma chamber
"cold" wave propagation
Temperature, ºC
400 800 1200
"cold" wave propagation
29 13.283 Myr

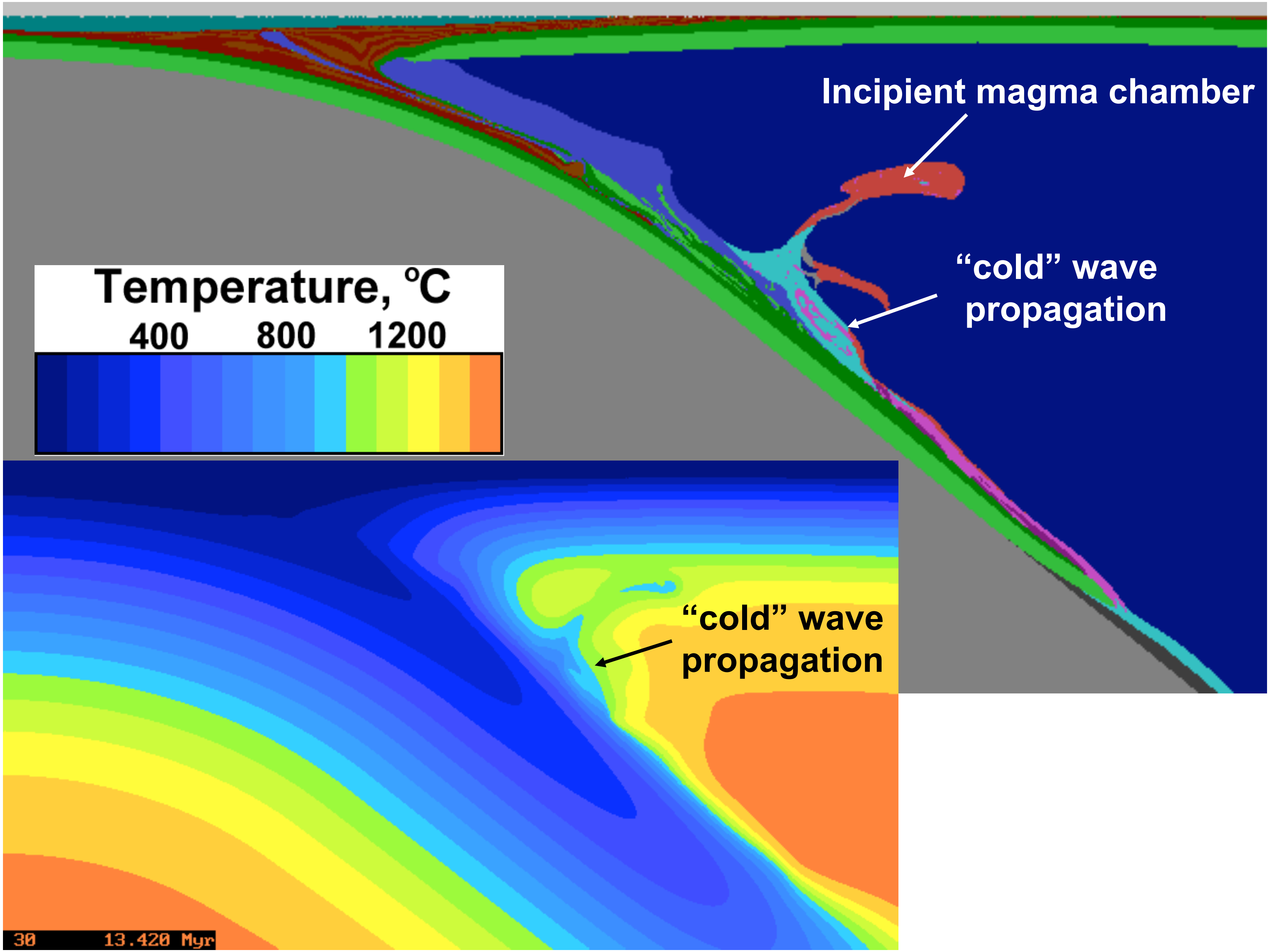
Incipient magma chamber
"cold" wave propagation
Temperature, °C
400
800
1200
"cold" wave propagation
30 13.420 Myr

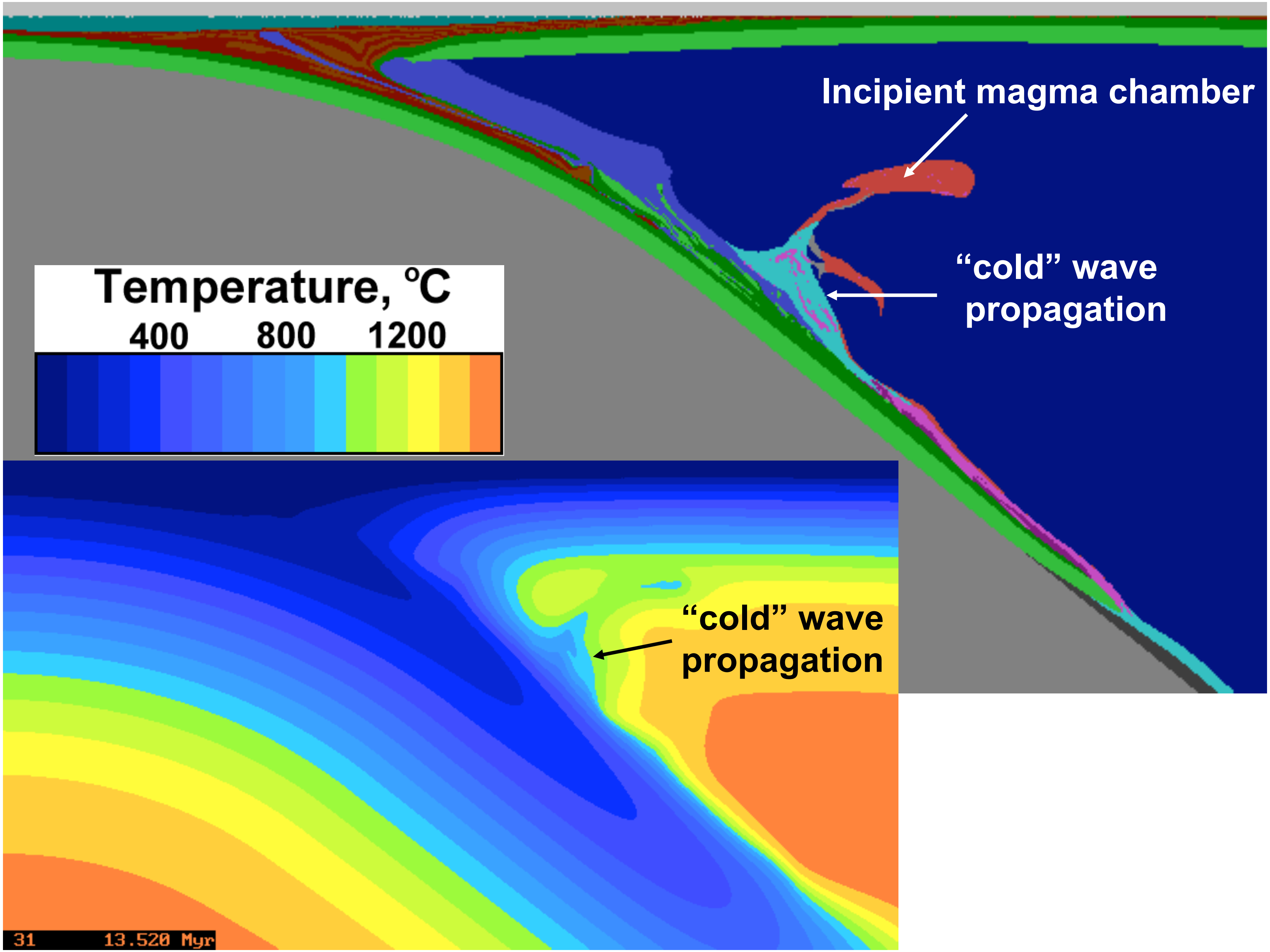

Incipient magma chamber
“cold” wave propagation
Temperature, °C
400
800
1200
“cold” wave propagation
31
13.520 Myr

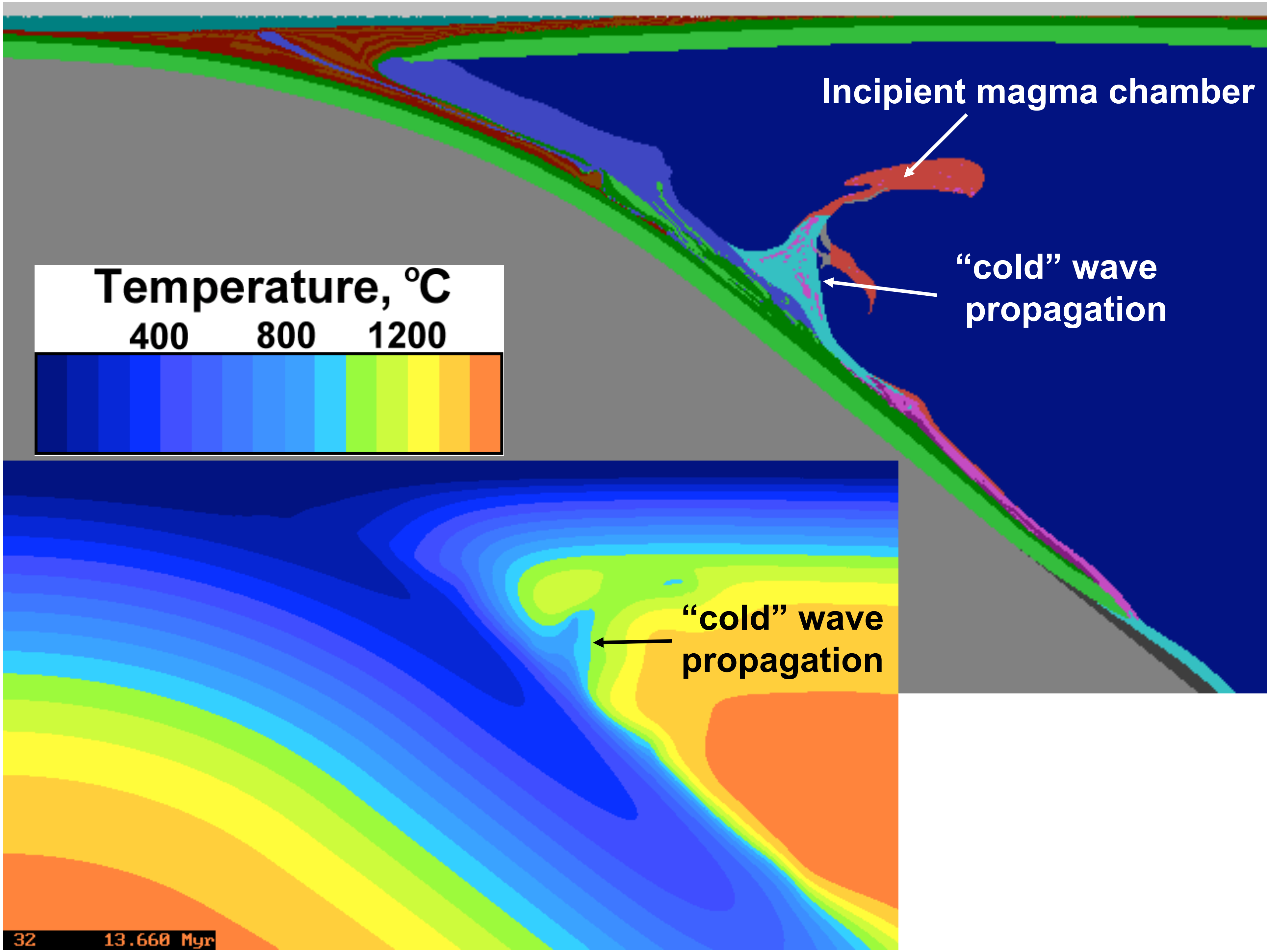
Incipient magma chamber
"cold" wave propagation
Temperature, °C
400 800 1200
"cold" wave propagation
32 13.660 Myr

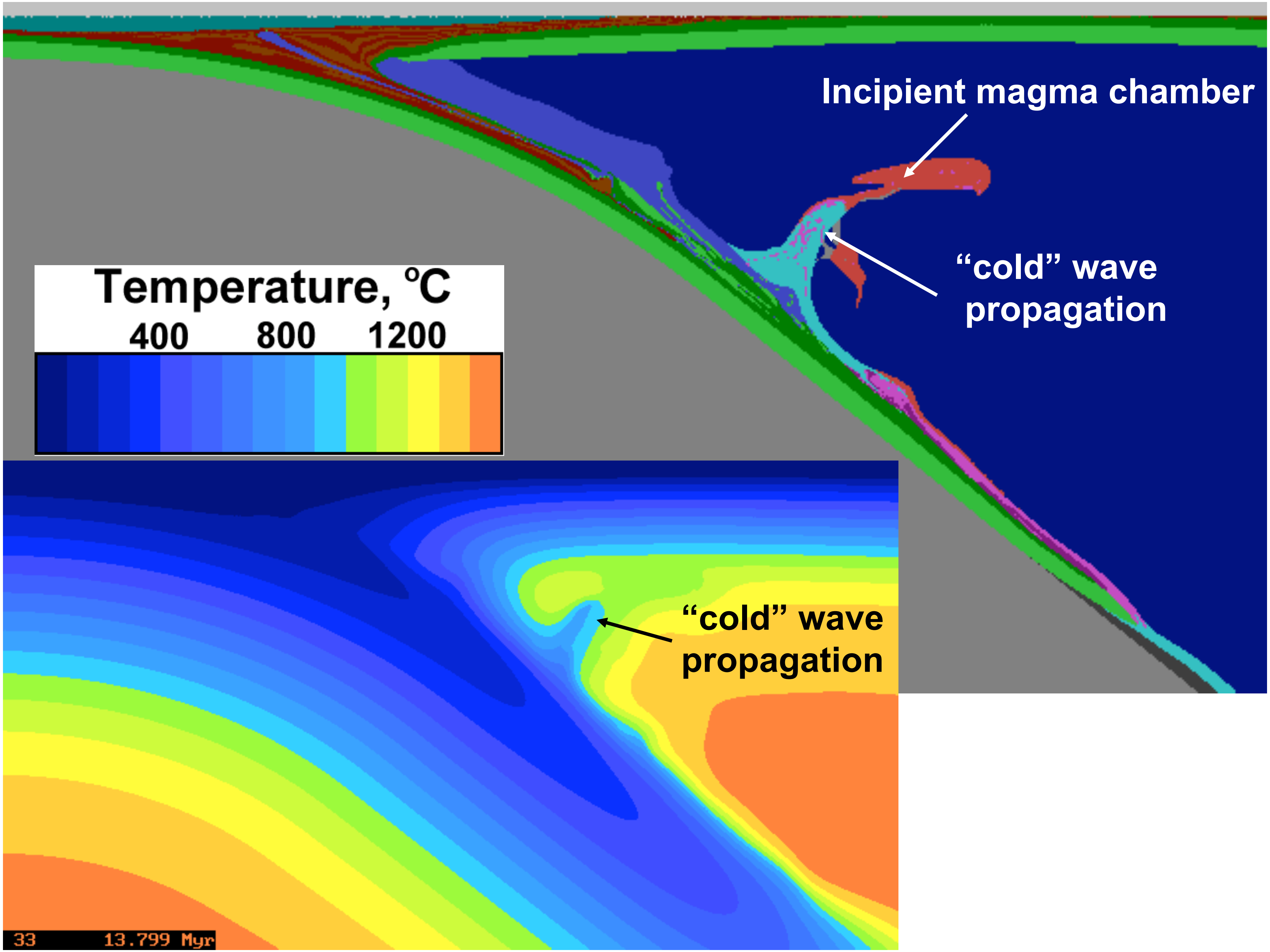
Incipient magma chamber
"cold" wave propagation
Temperature, °C
400
800
1200
"cold" wave propagation
33
13.799 Myr

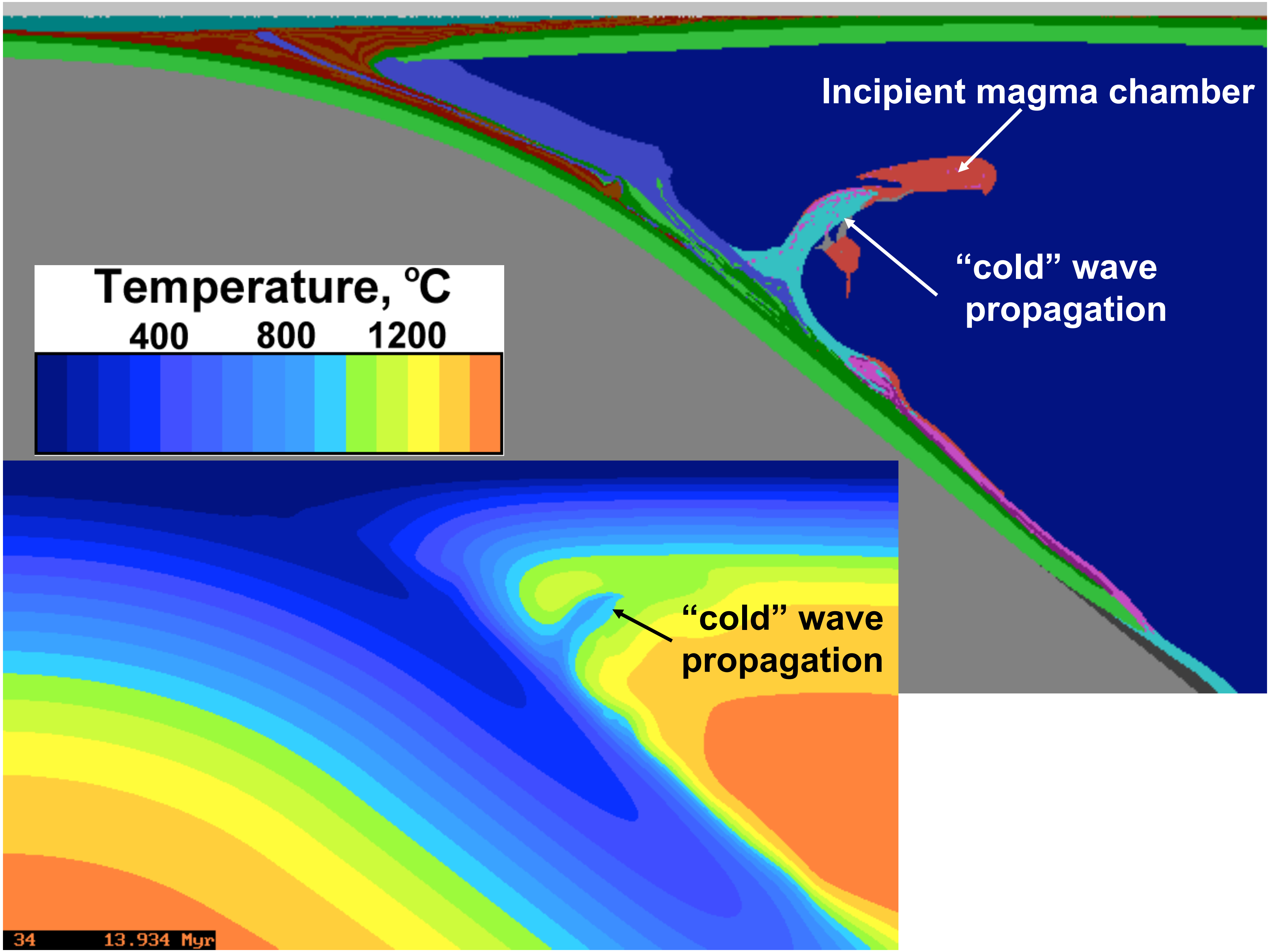

Incipient magma chamber
"cold" wave propagation
Temperature, °C
400
800
1200
"cold" wave propagation
34 13.934 Myr

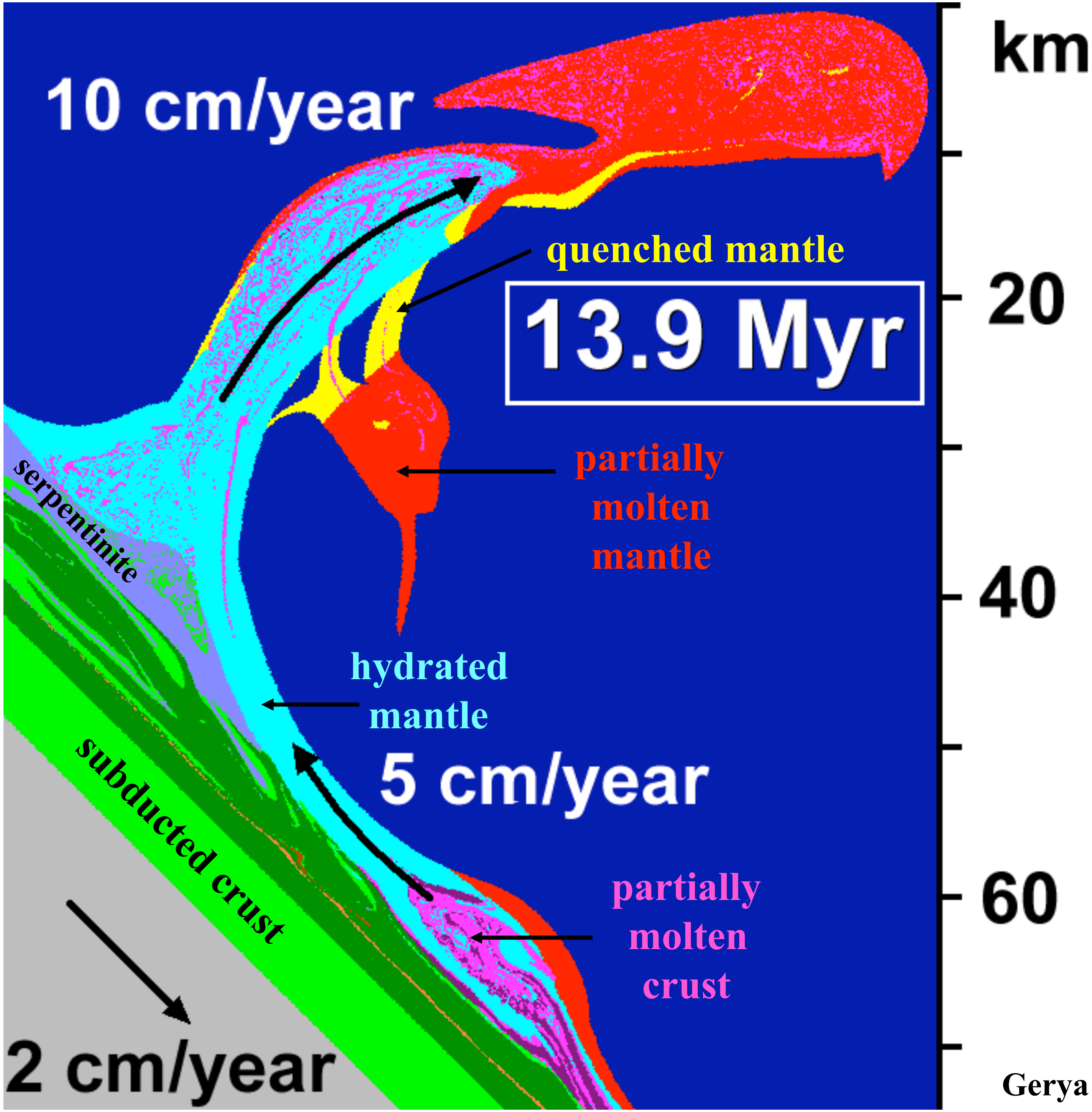

Gerya et al. (2004)

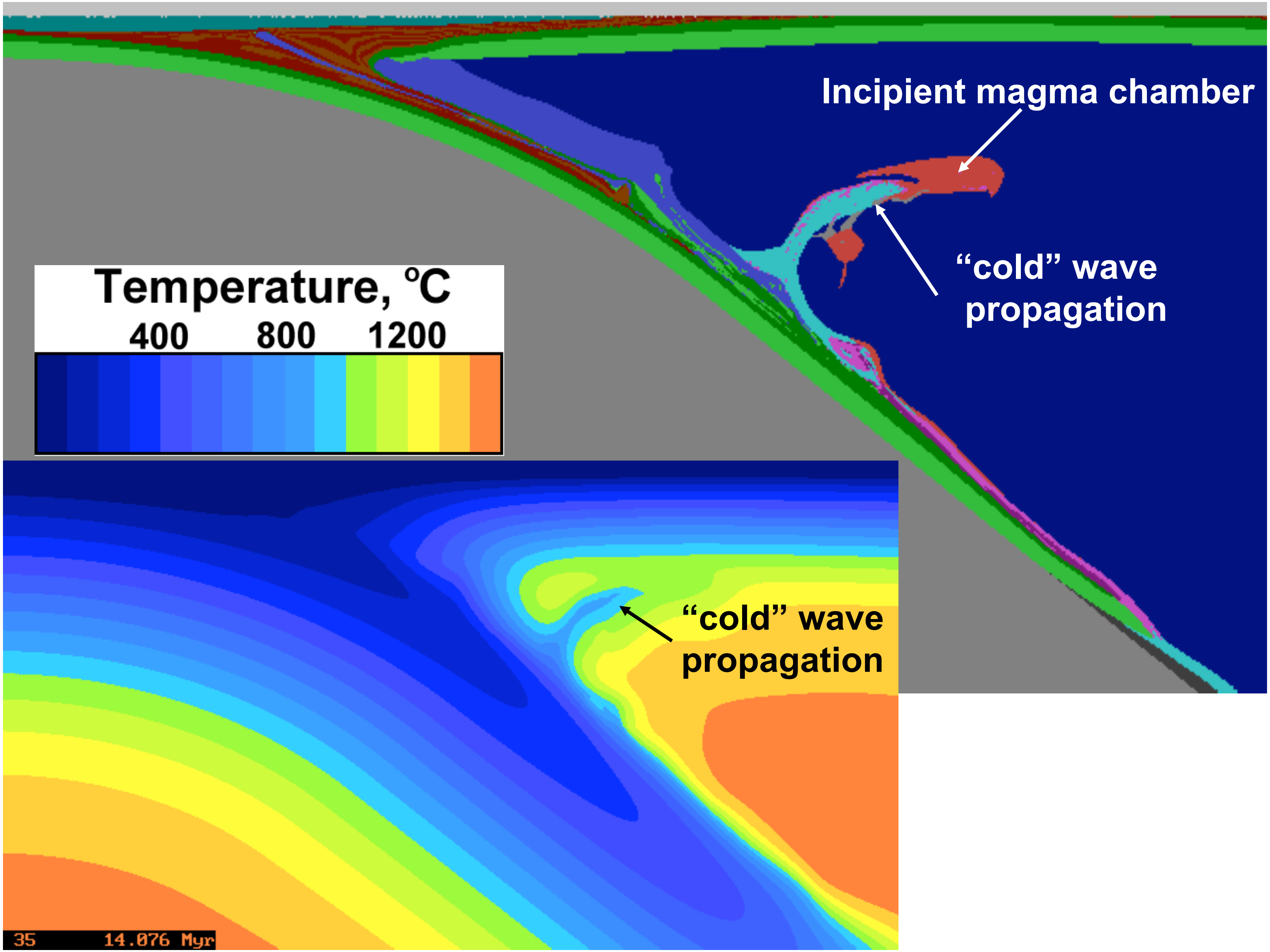

Incipient magma chamber
"cold" wave propagation
Temperature, ºC
400 800 1200
"cold" wave propagation
35 14.076 Myr

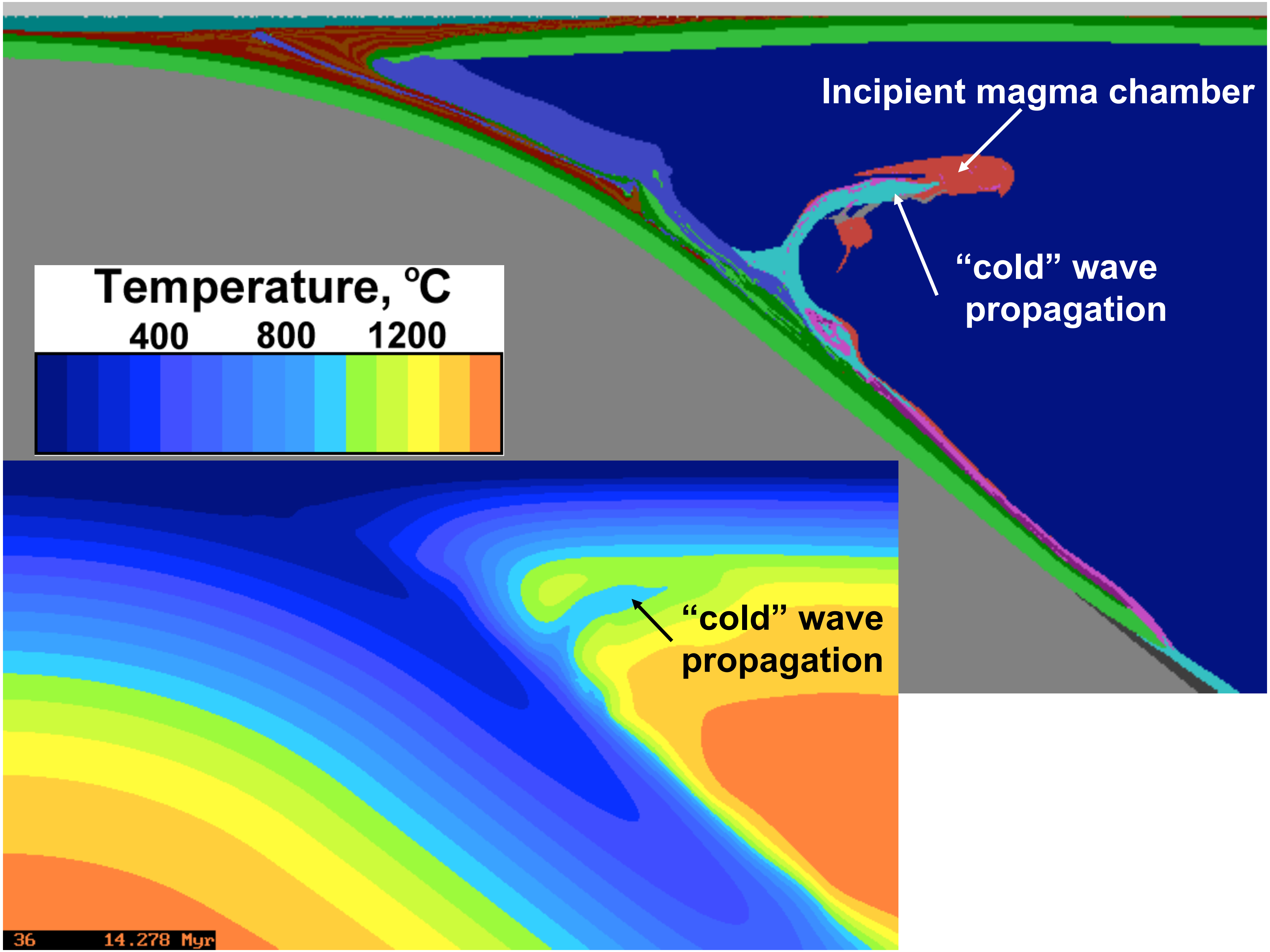
Incipient magma chamber
"cold" wave propagation
Temperature, °C
400
800
1200
"cold" wave propagation
36
14.278 Myr

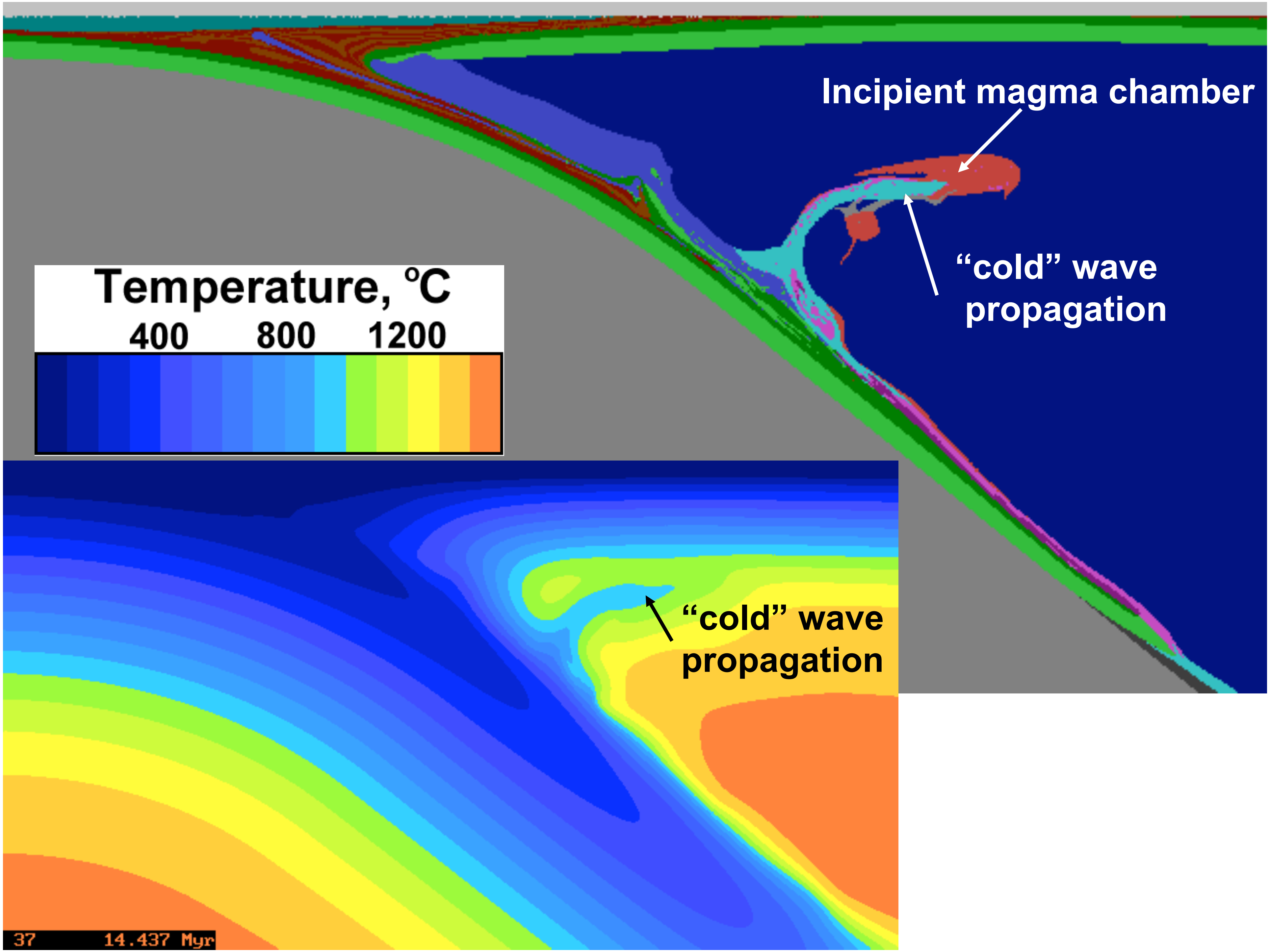
Incipient magma chamber
"cold" wave propagation
Temperature, ºC
400
800
1200
"cold" wave propagation
37
14.437 Myr

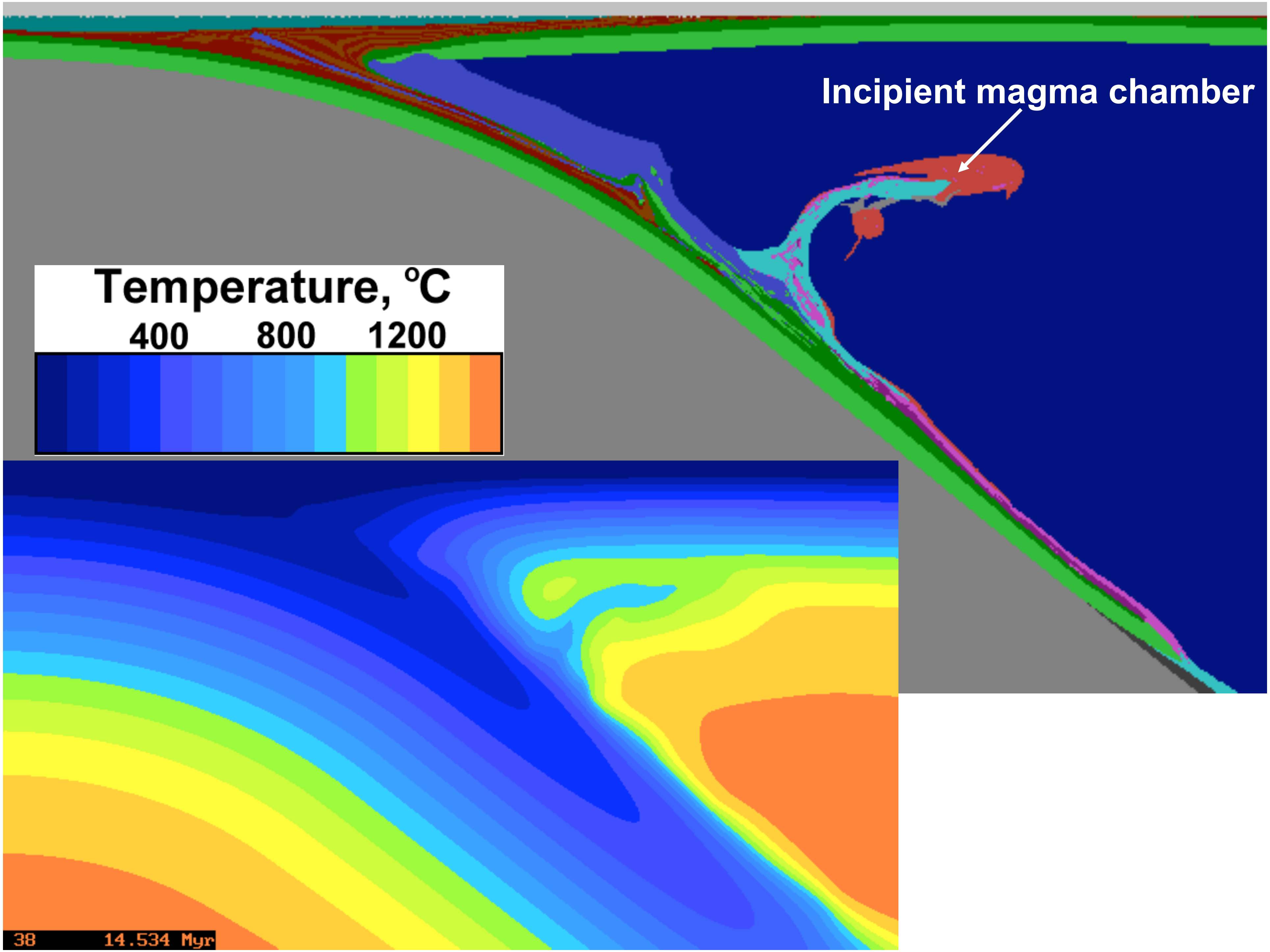

Incipient magma chamber
Temperature, ºC
400
800
1200
38
14.534 Myr

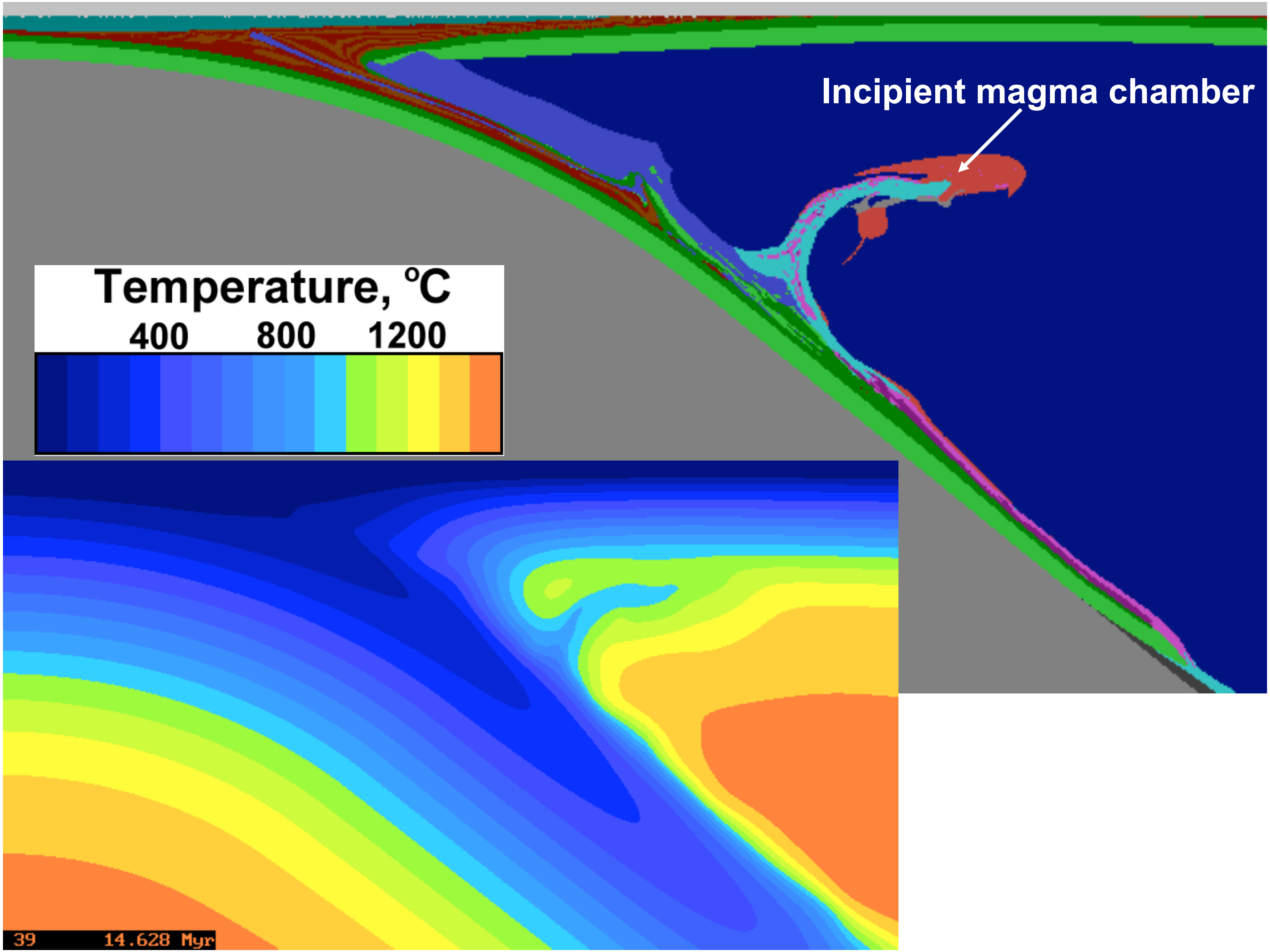
Incipient magma chamber
Temperature, °C
400
800
1200
39
14.628 Myr

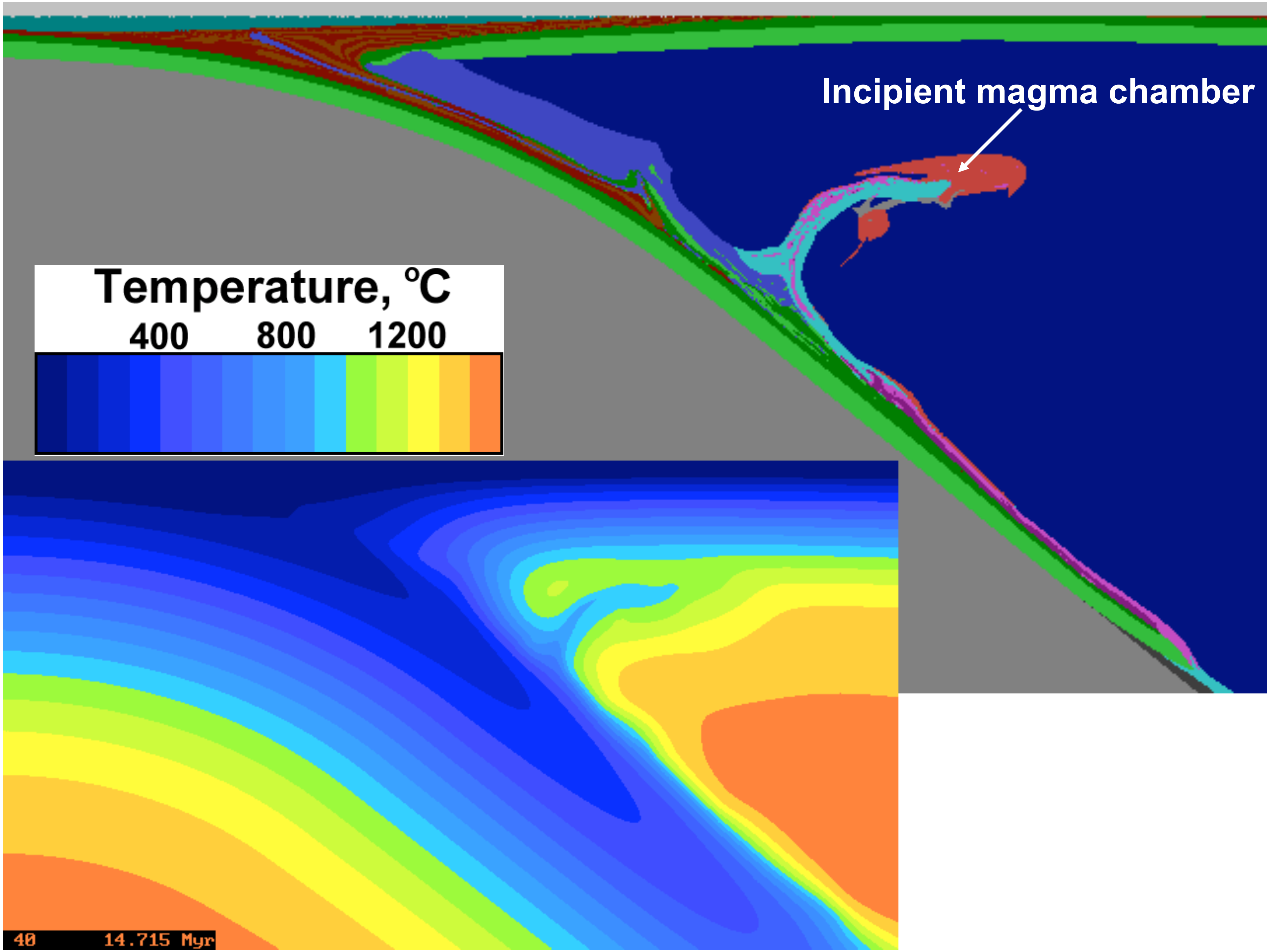
Incipient magma chamber
Temperature, °C
400
800
1200
40
14.715 Myr

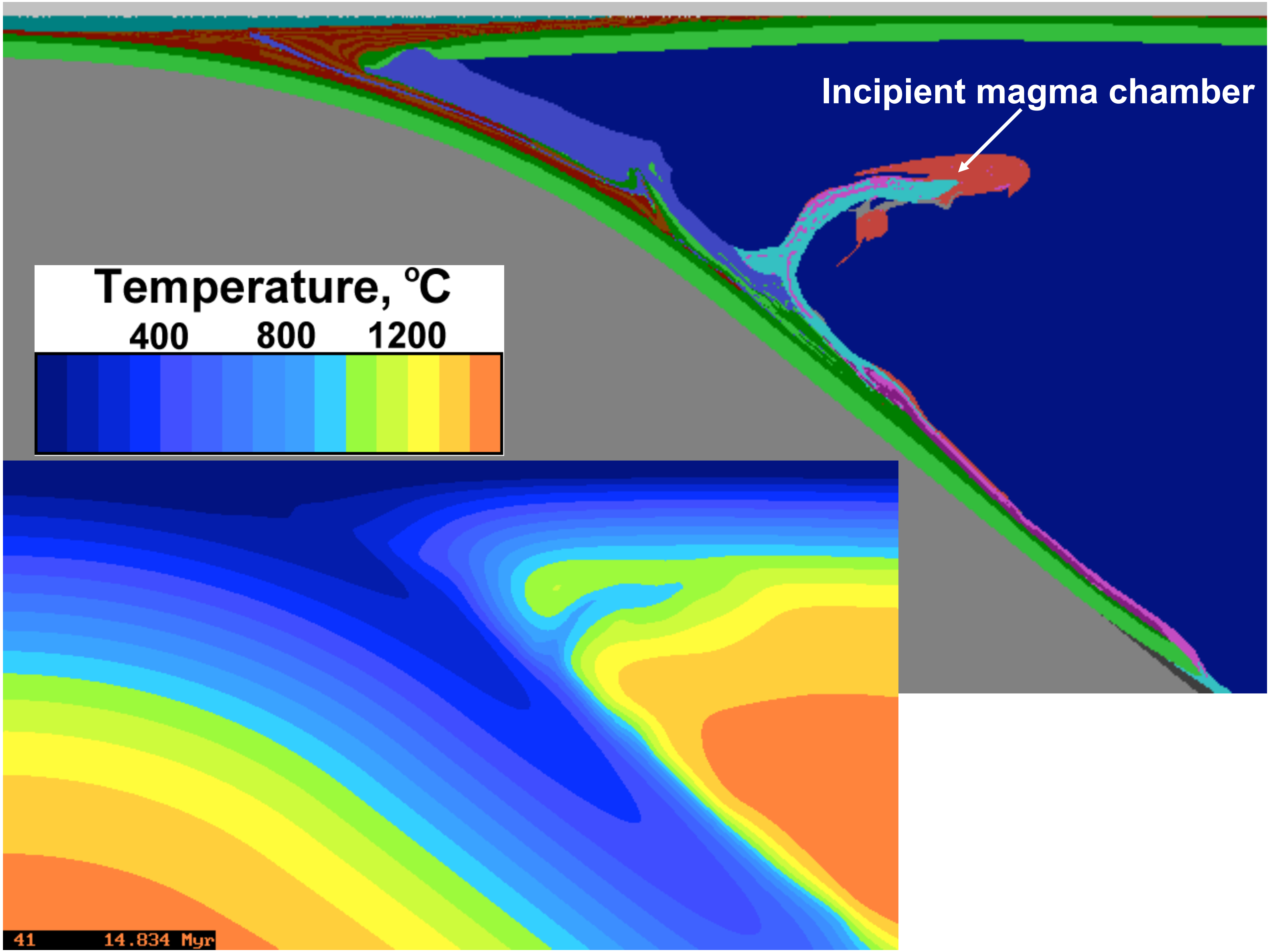

Incipient magma chamber
Temperature, °C
400
800
1200
41
14.834 Myr

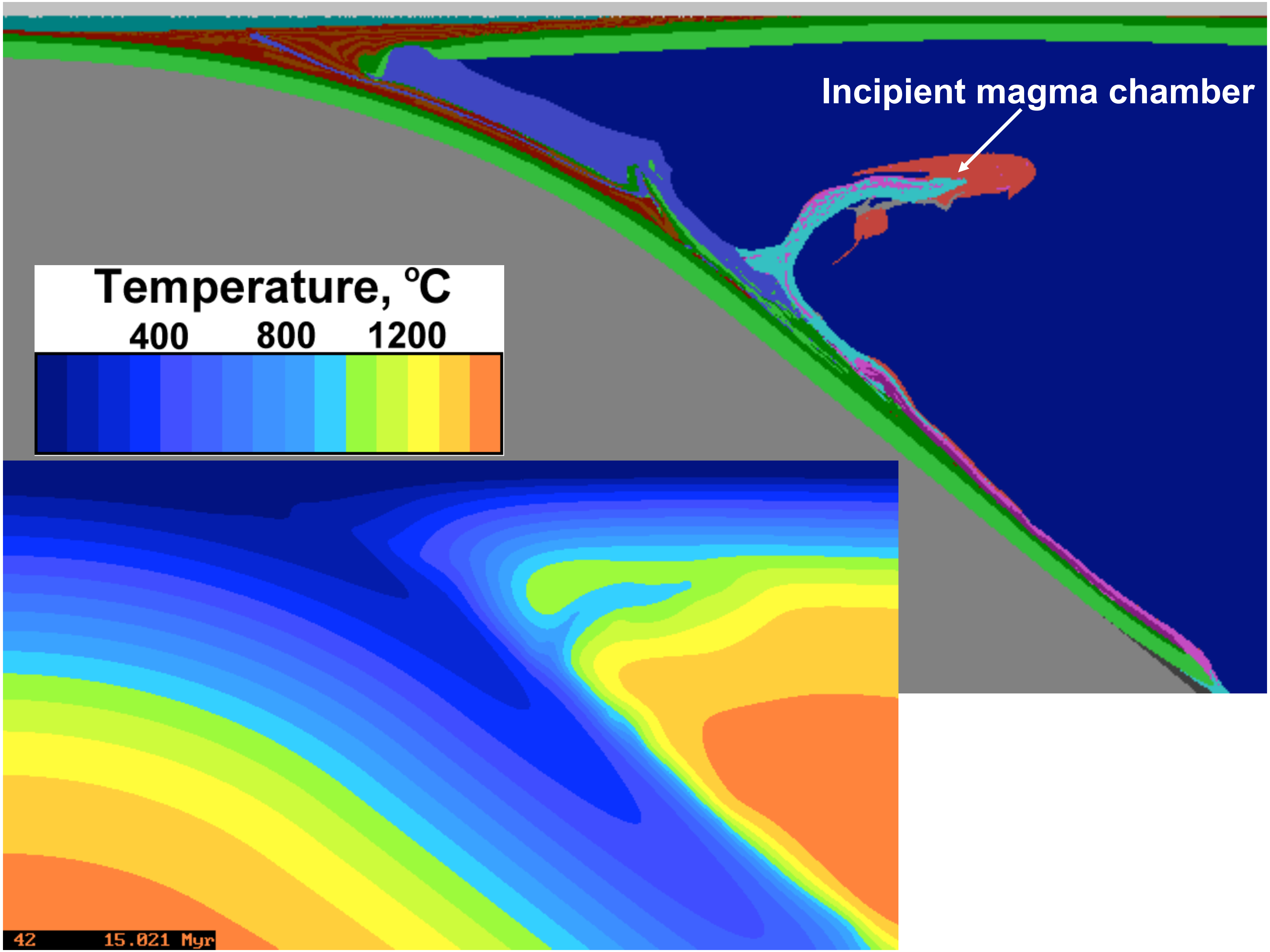
Incipient magma chamber
Temperature, °C
400
800
1200
42
15.021 Myr

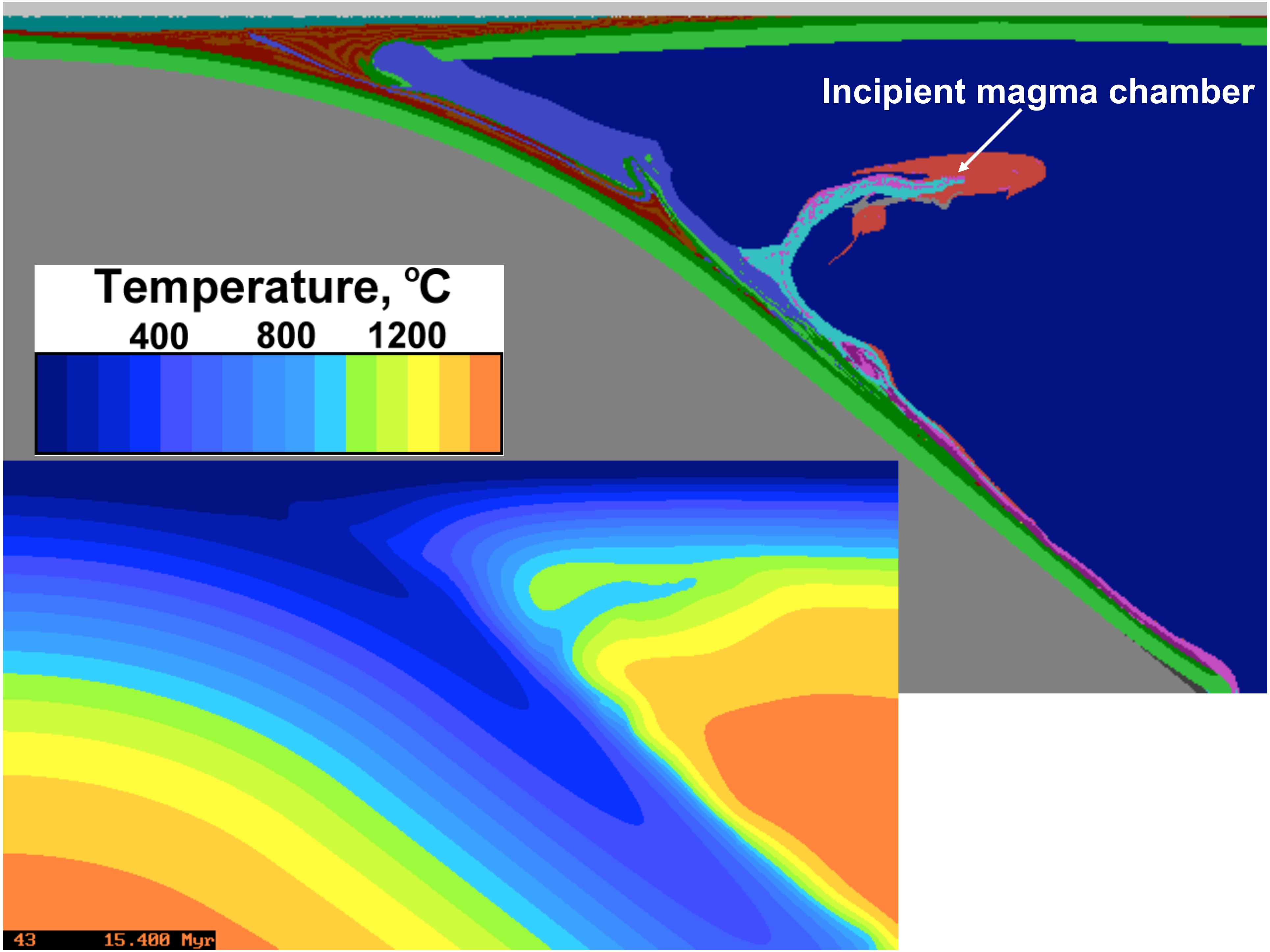

Incipient magma chamber
Temperature, °C
400
800
1200
43
15.400 Myr

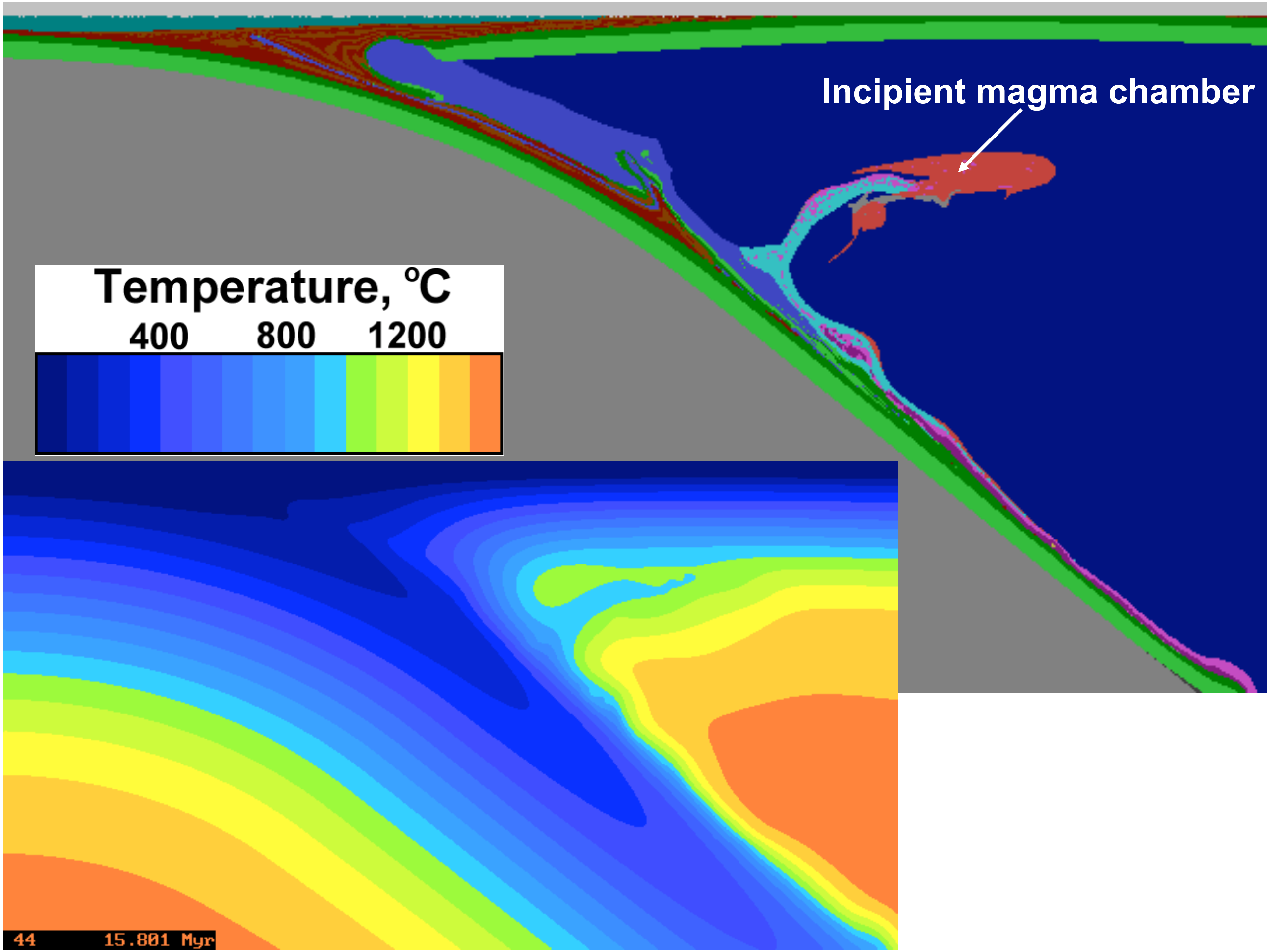
Incipient magma chamber
Temperature, °C
400
800
1200
44 15.801 Myr

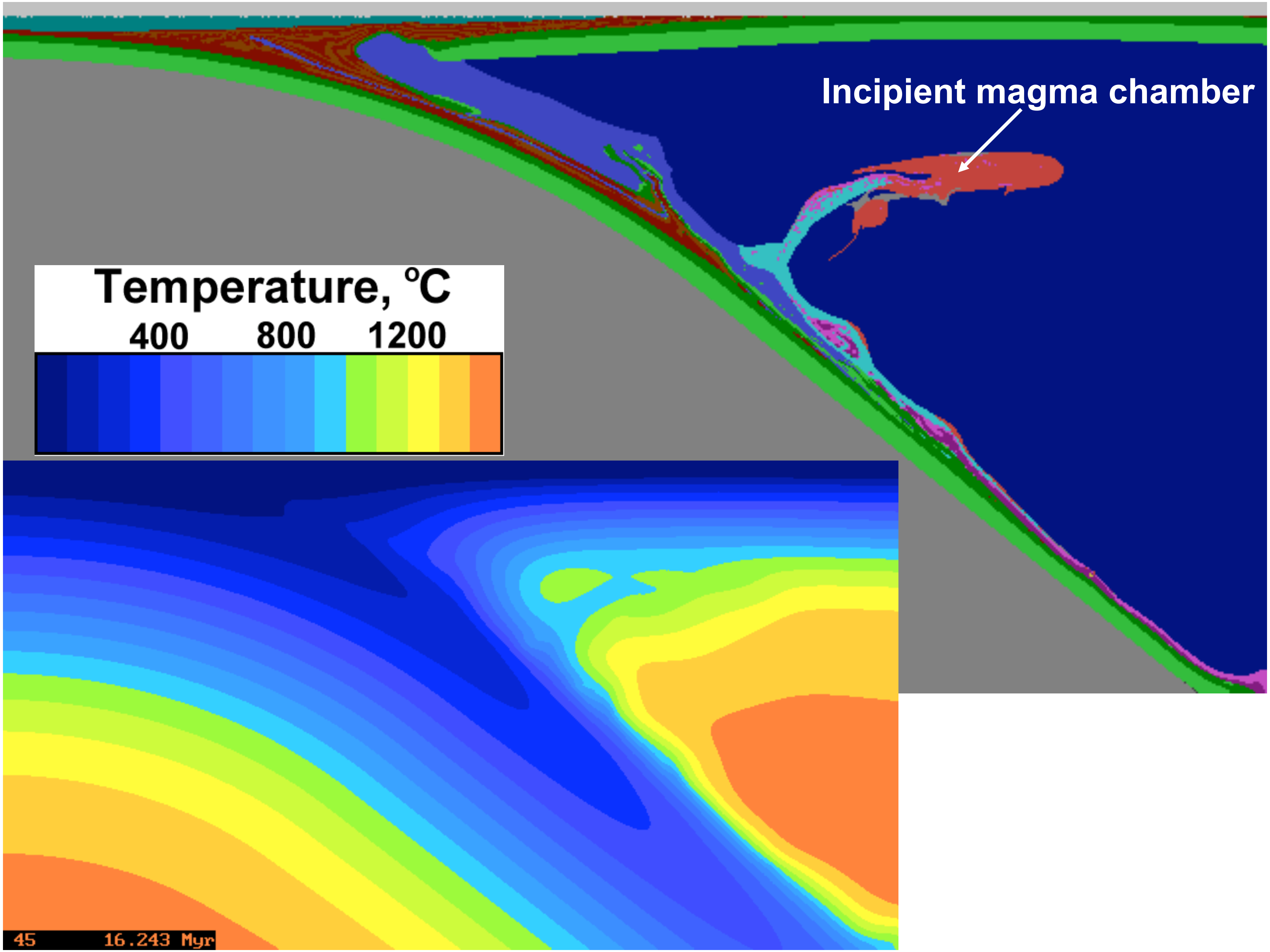

Incipient magma chamber
Temperature, °C
400 800 1200
45 16.243 Myr

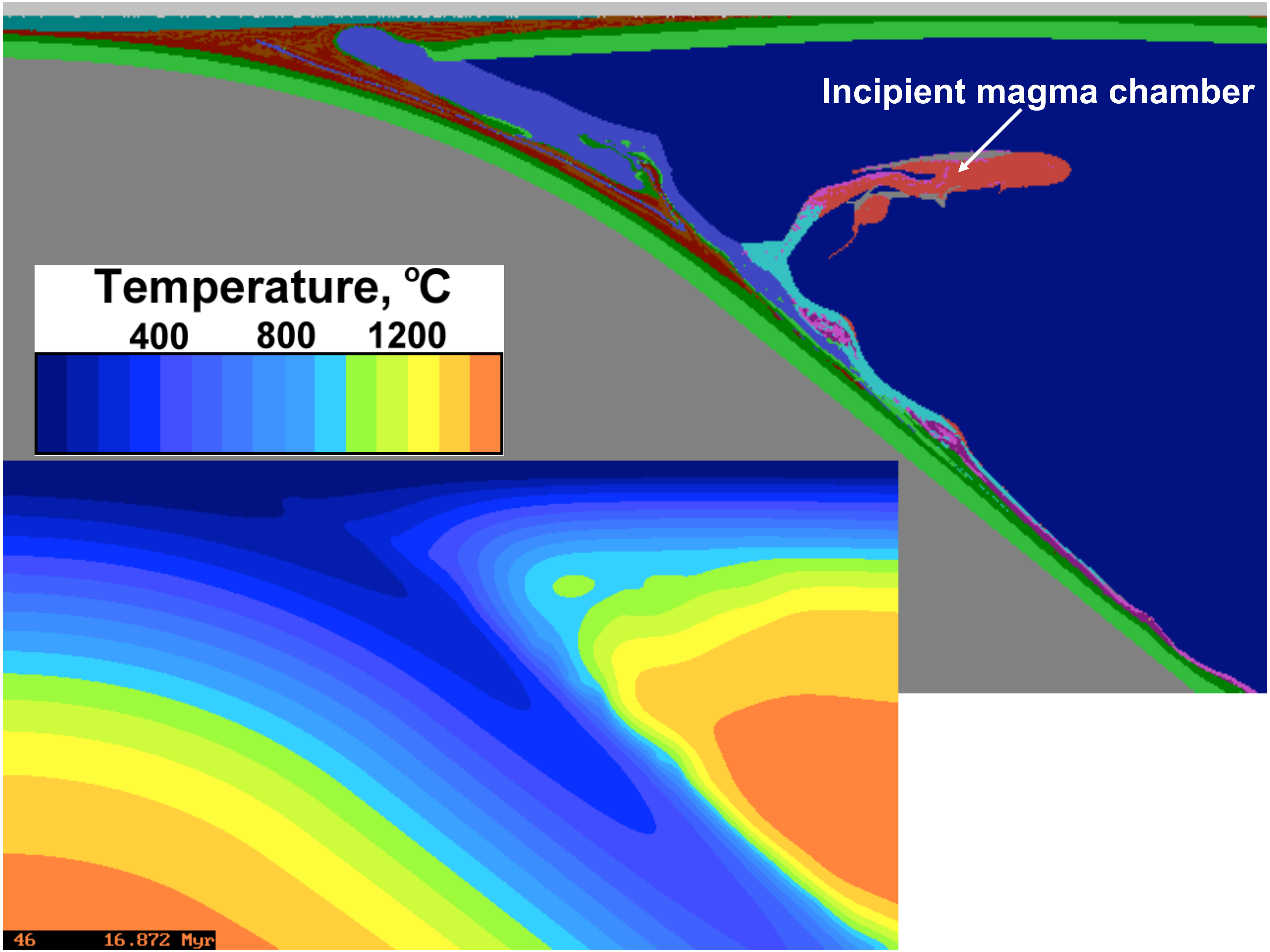
Incipient magma chamber
Temperature, °C
400
800
1200
46 16.872 Myr

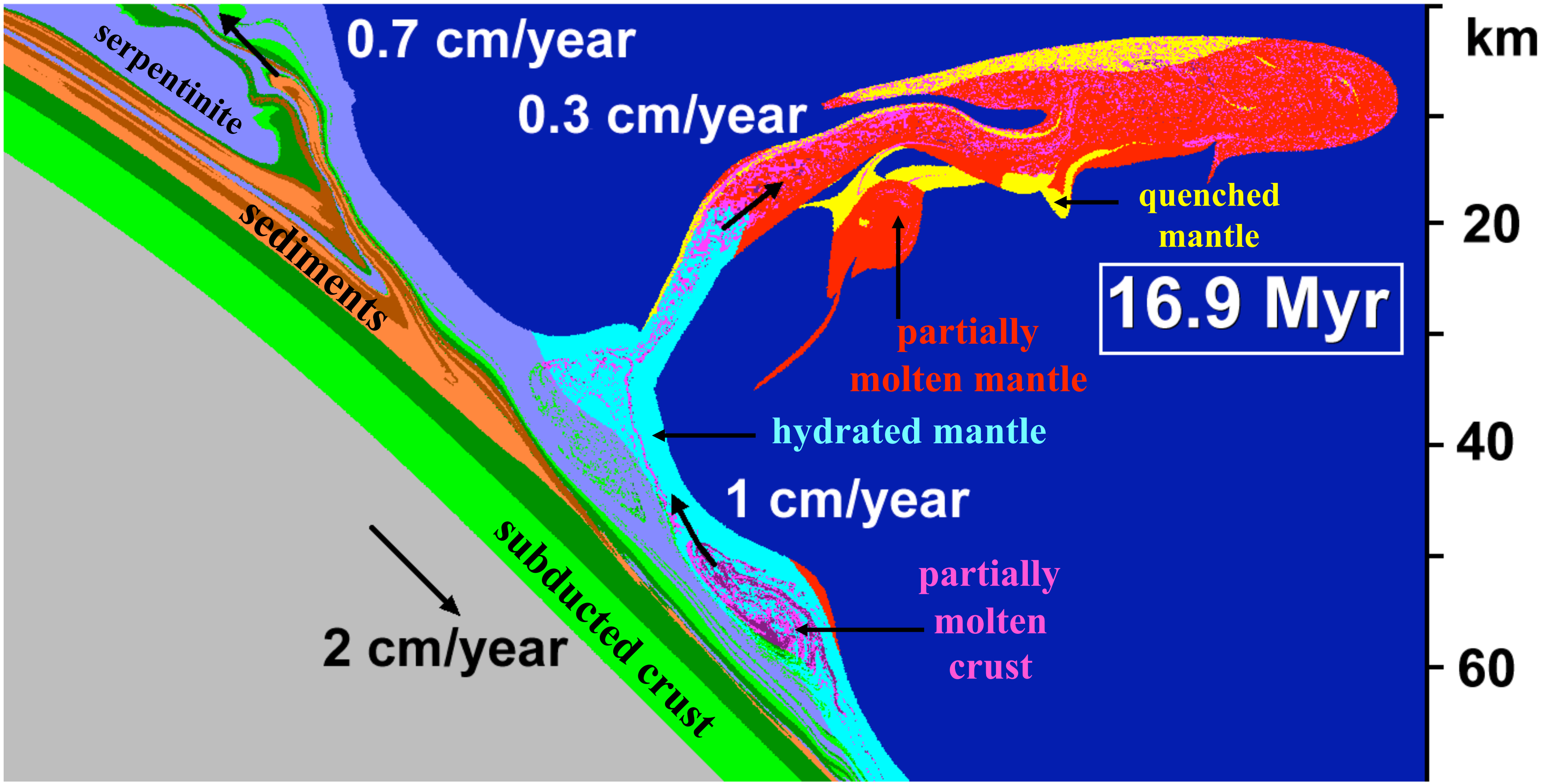

(Gerya et al., 2004)

Mixed and unmixed cold plumes

10 million markers

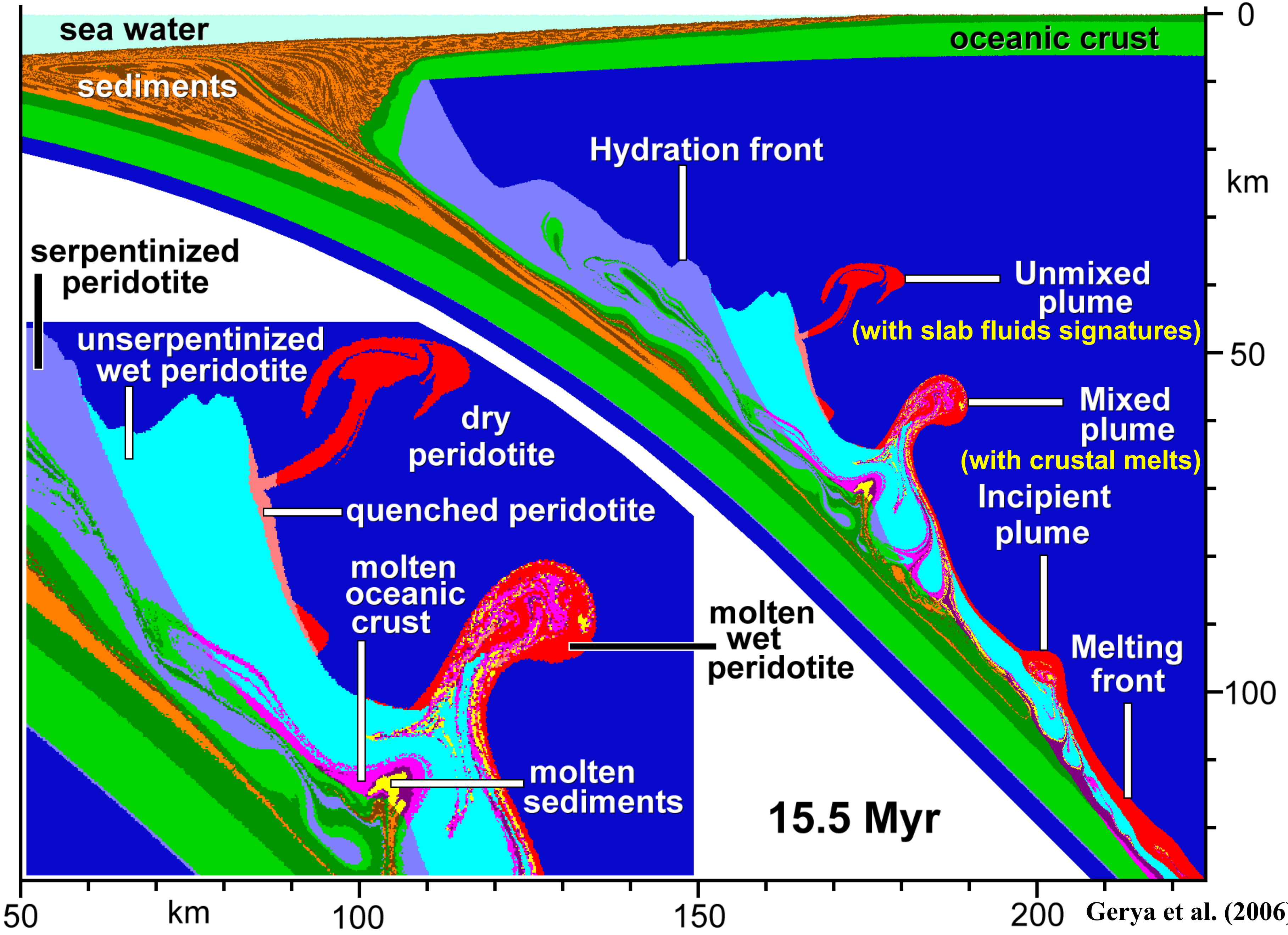

Gerya et al. (2006)

3D cold plumes

Guizhi
Zhu

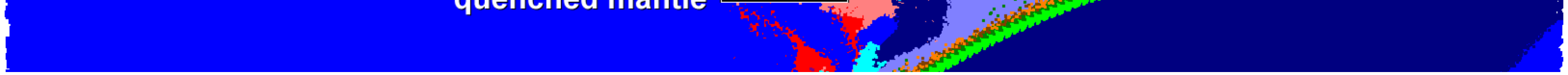

High-resolution 3D subduction models

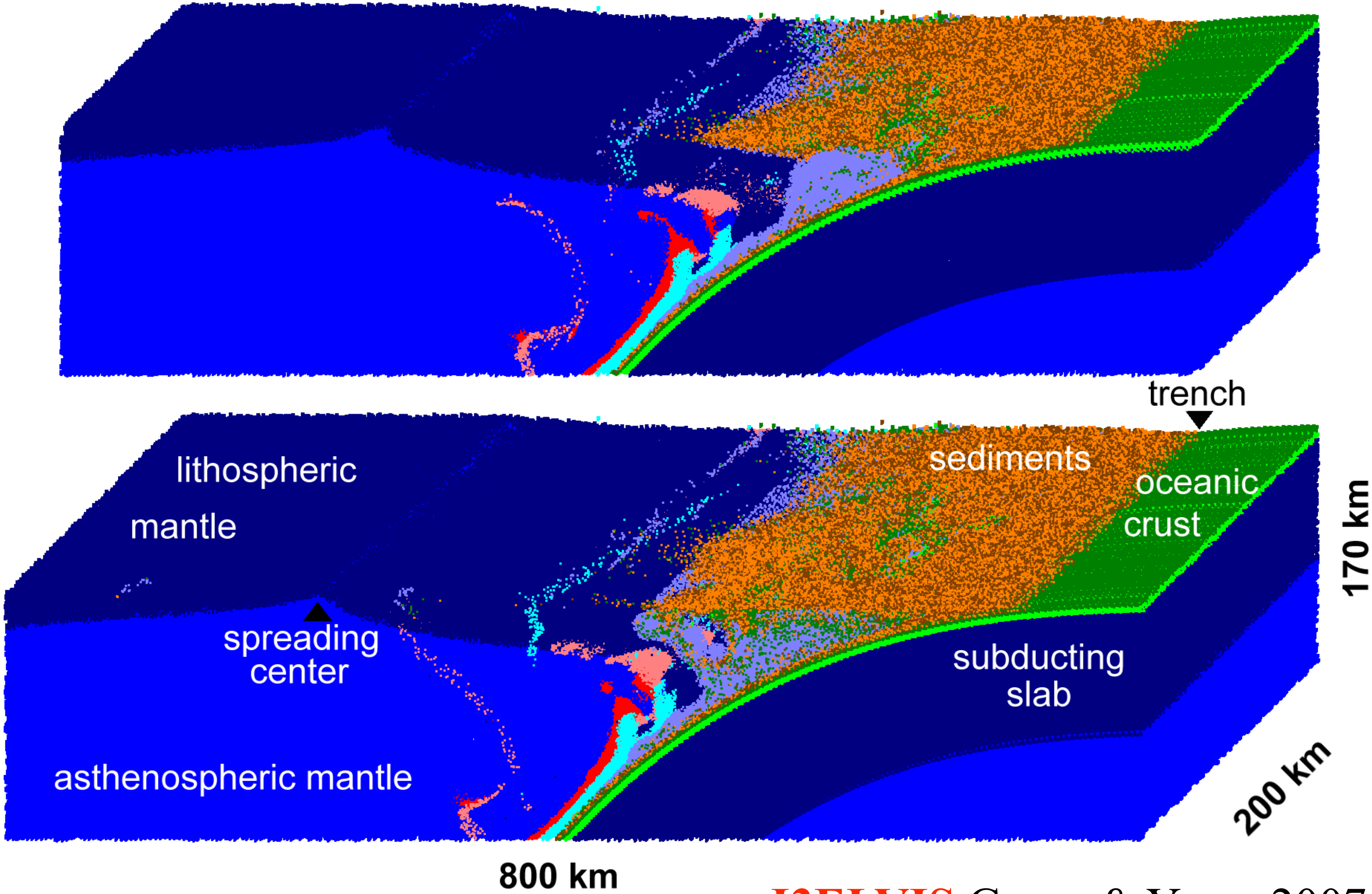

I3ELVIS Gerya & Yuen, 2007

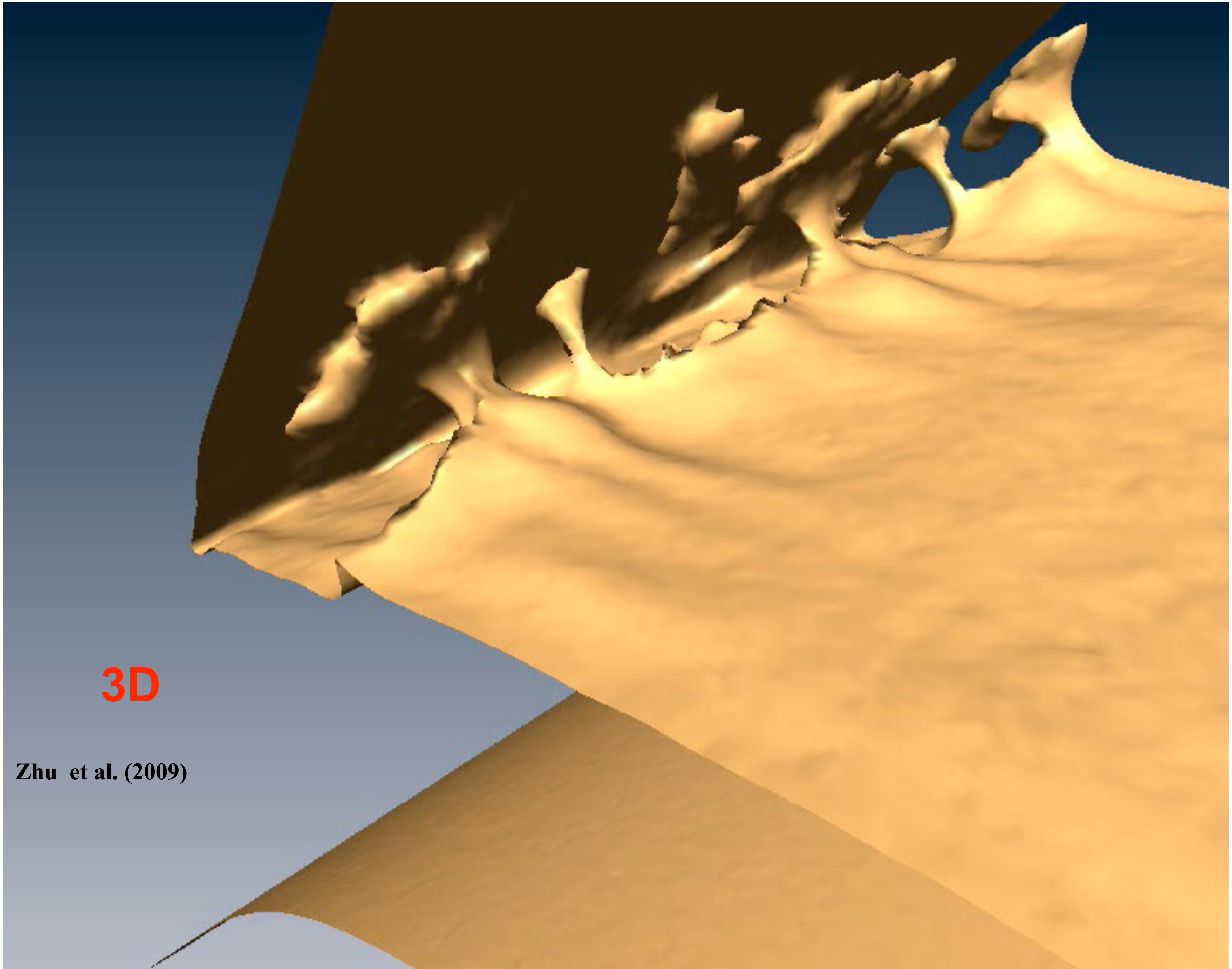
3D
Zhu et al. (2009)

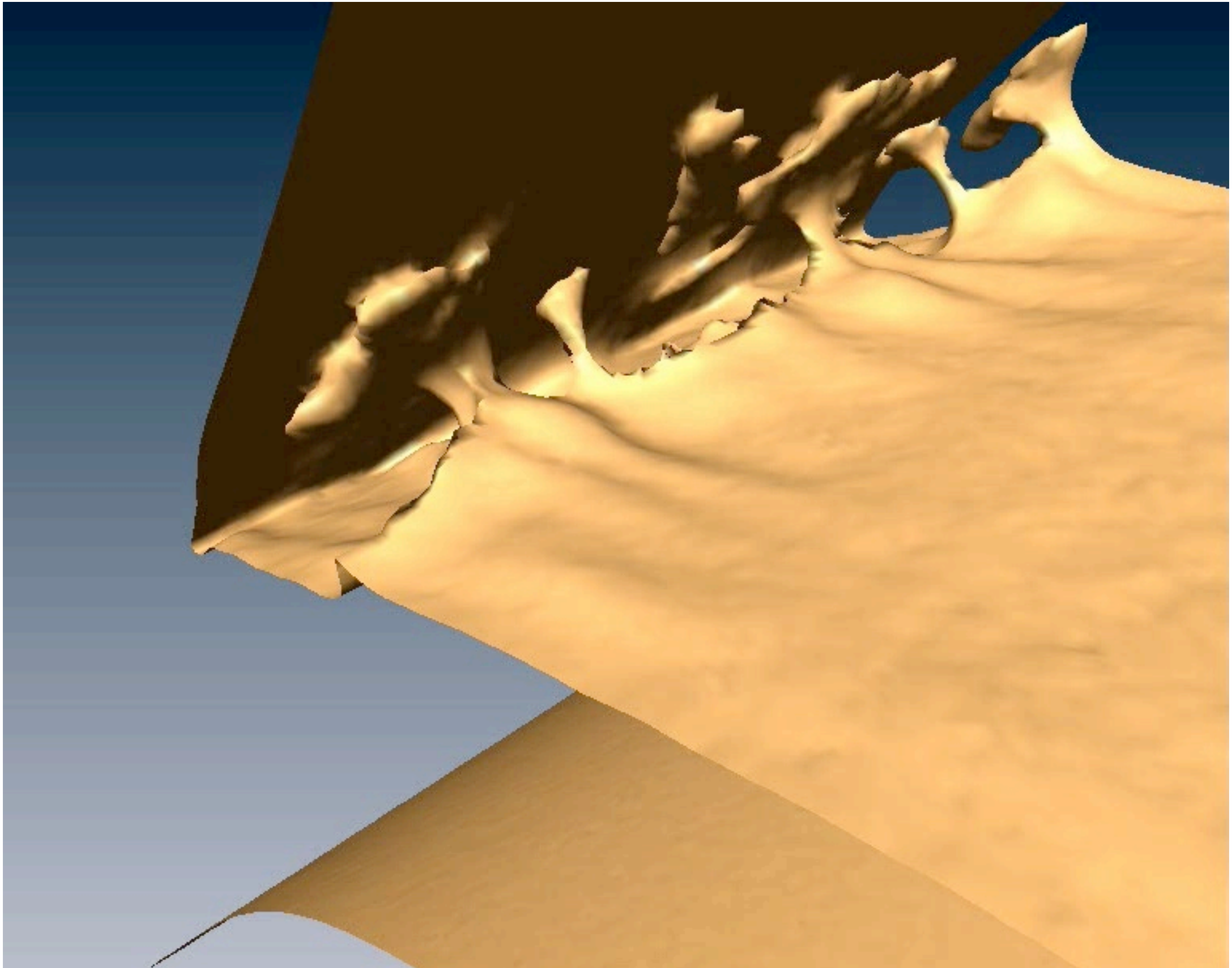

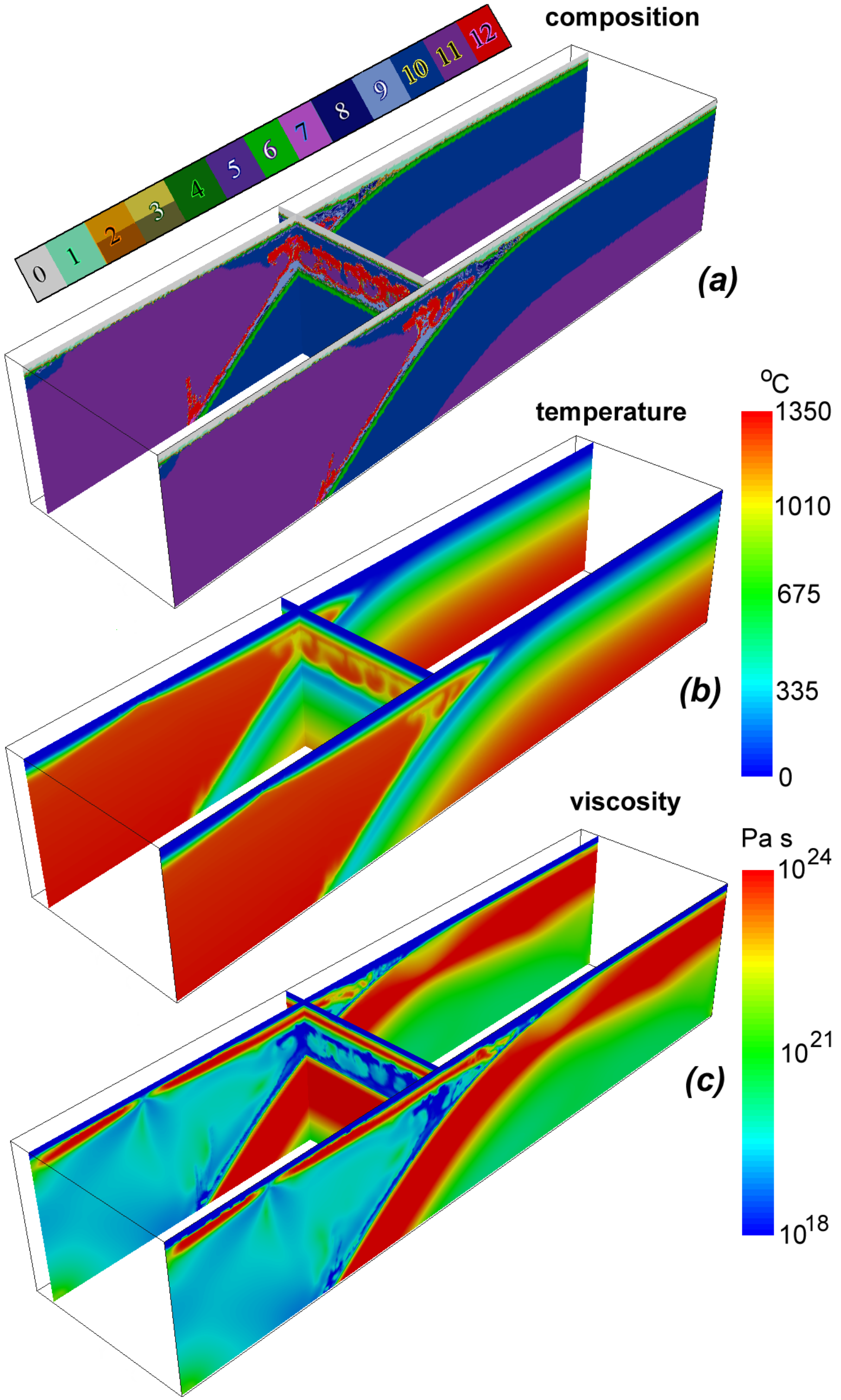

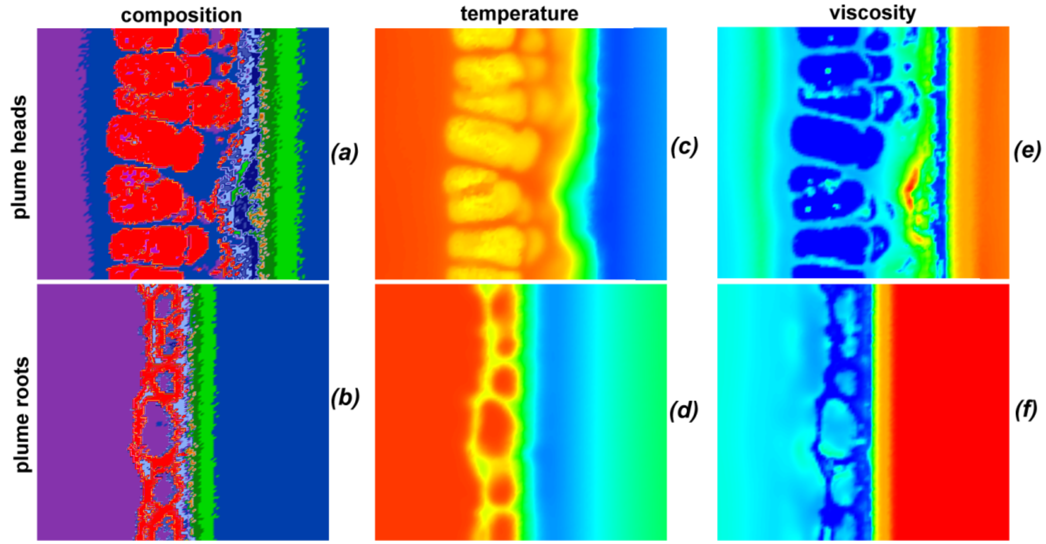

Zhu et al. (2009)

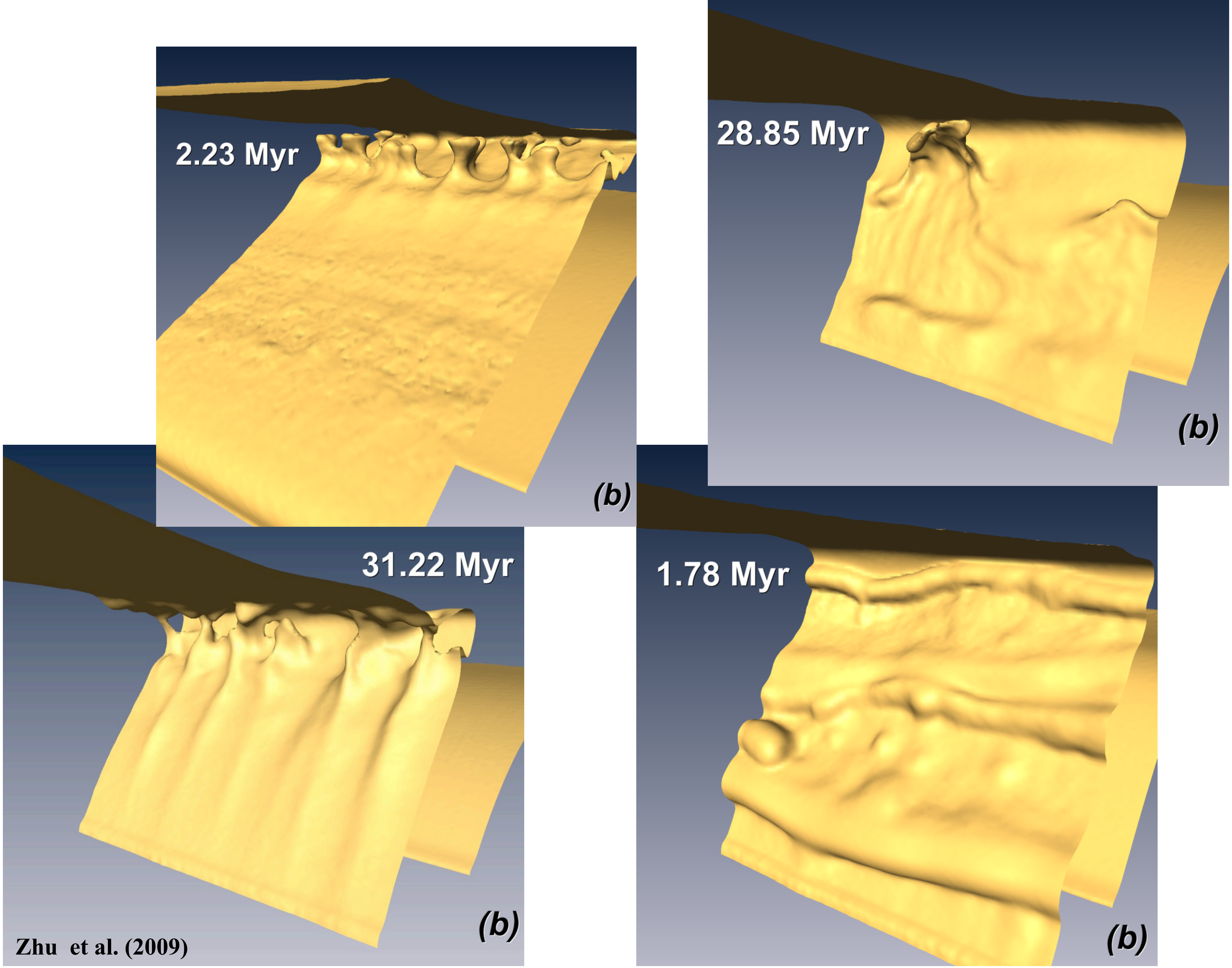
2.23 Myr
(b)
28.85 Myr
(b)
31.22 Myr
(b)
Zhu et al. (2009)
1.78 Myr
(b)

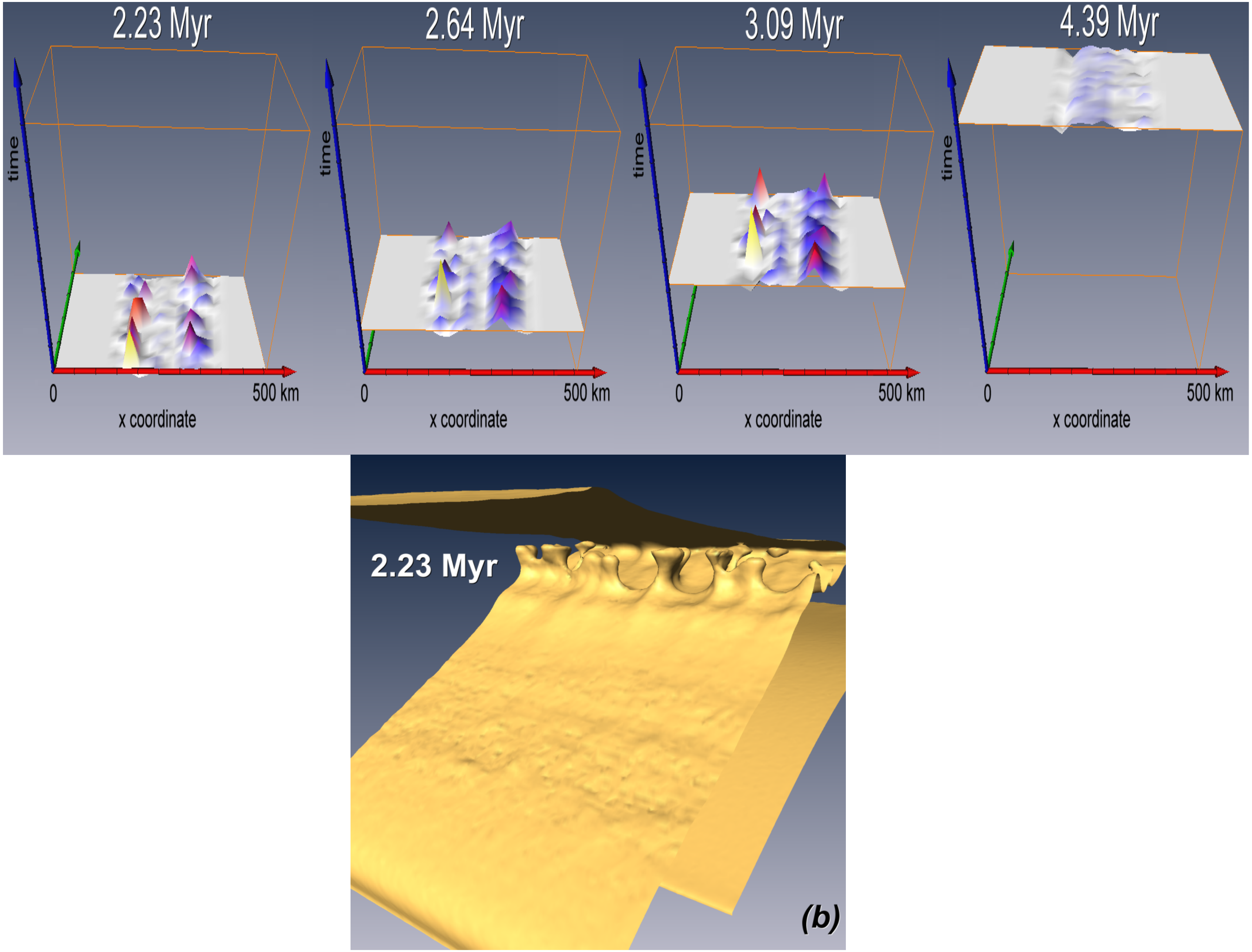
2.23 Myr
2.64 Myr
3.09 Myr
4.39 Myr
time
0
500 km
x coordinate
2.23 Myr
(b)

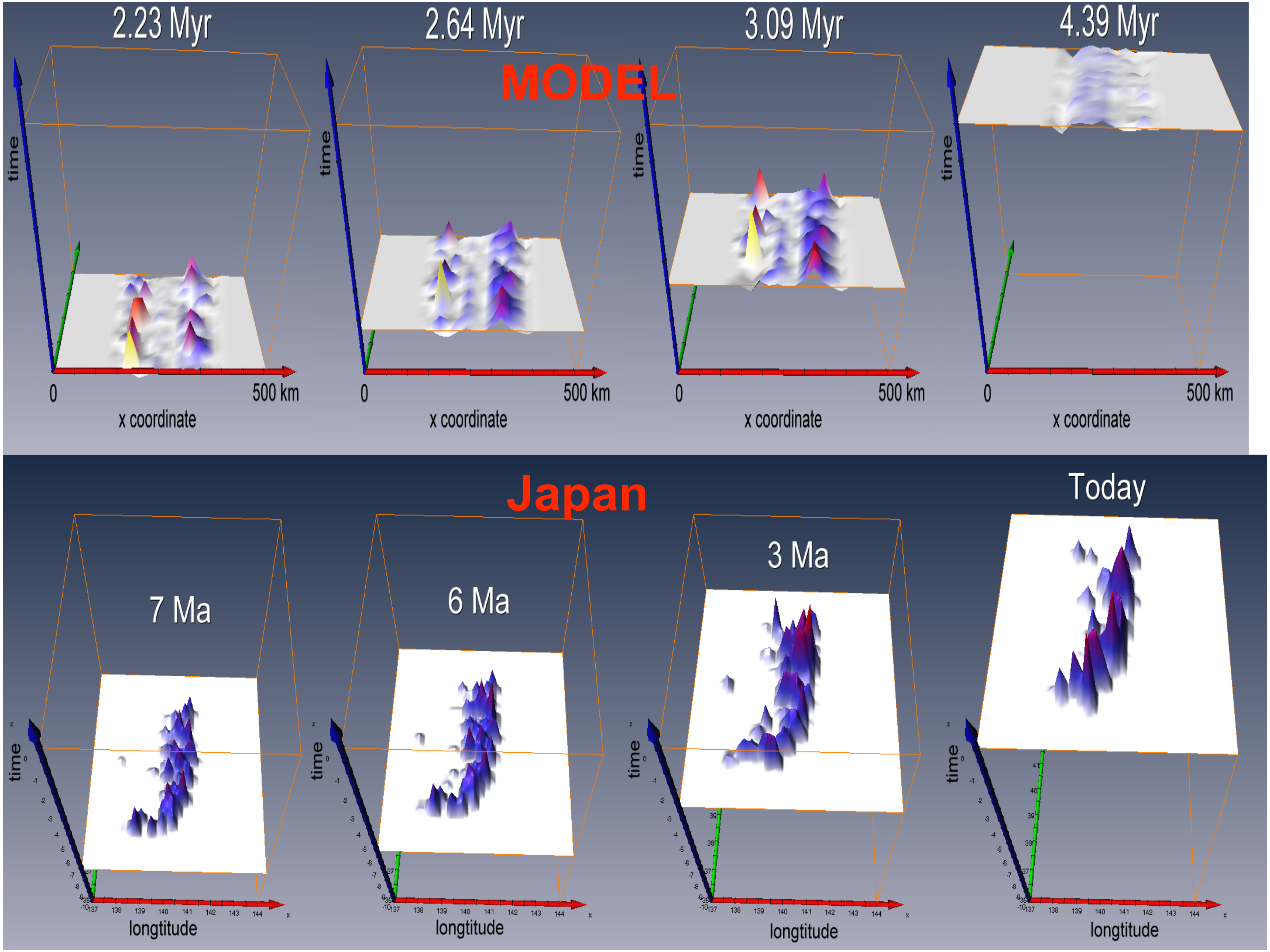

MODEL
2.23 Myr
2.64 Myr
3.09 Myr
4.39 Myr
time
0
500 km
x coordinate
Japan
7 Ma
6 Ma
3 Ma
Today
time
longtitude

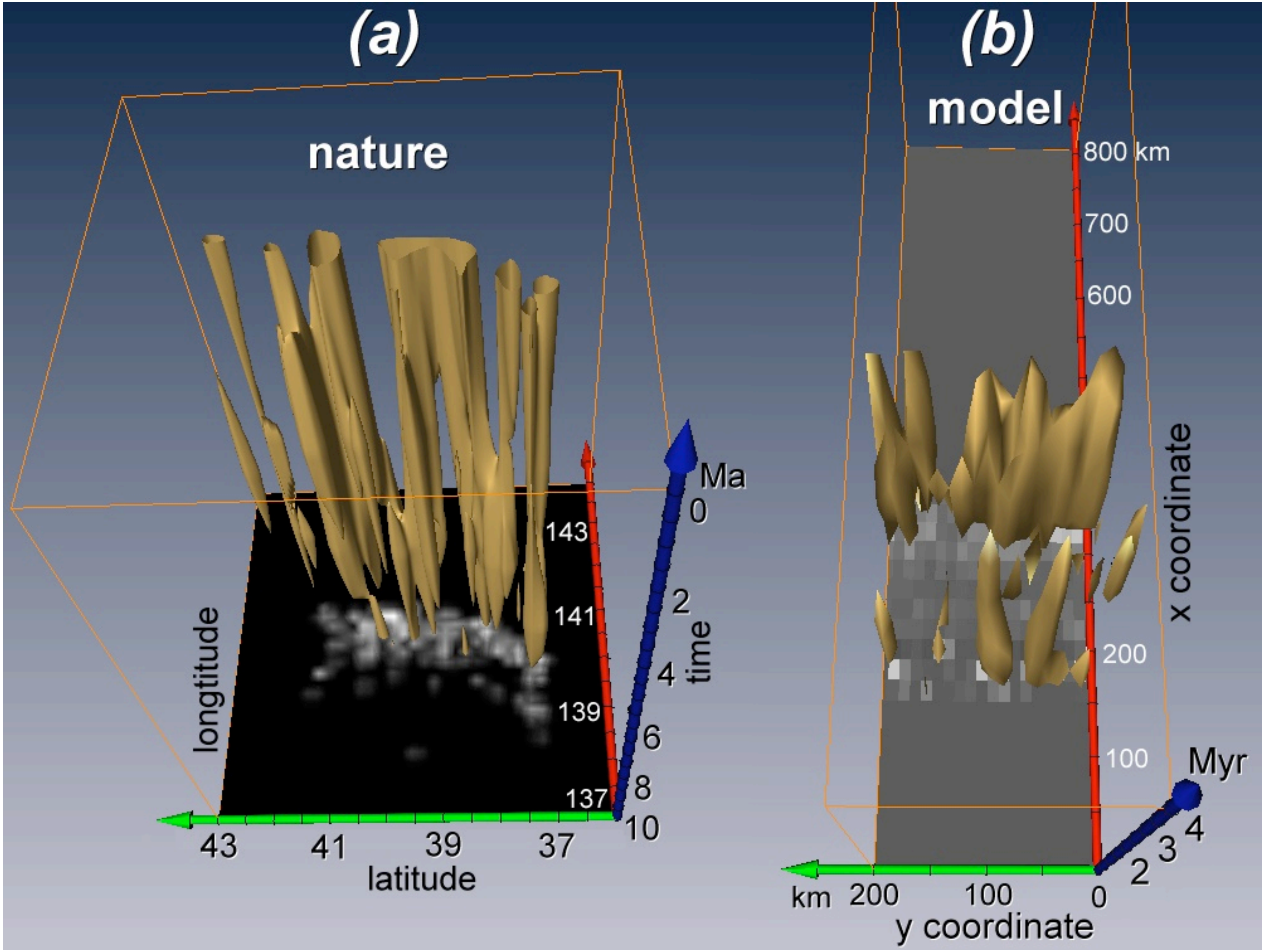
(a)
nature
Ma
0
2
4
6
8
10
time
143
141
139
137
longtitude
43
41
39
37
latitude
(b)
model
800 km
700
600
200
100
x coordinate
Myr
2
3
4
km
200
100
0
y coordinate

Can numerical modelling predict new subduction related phenomena?

?

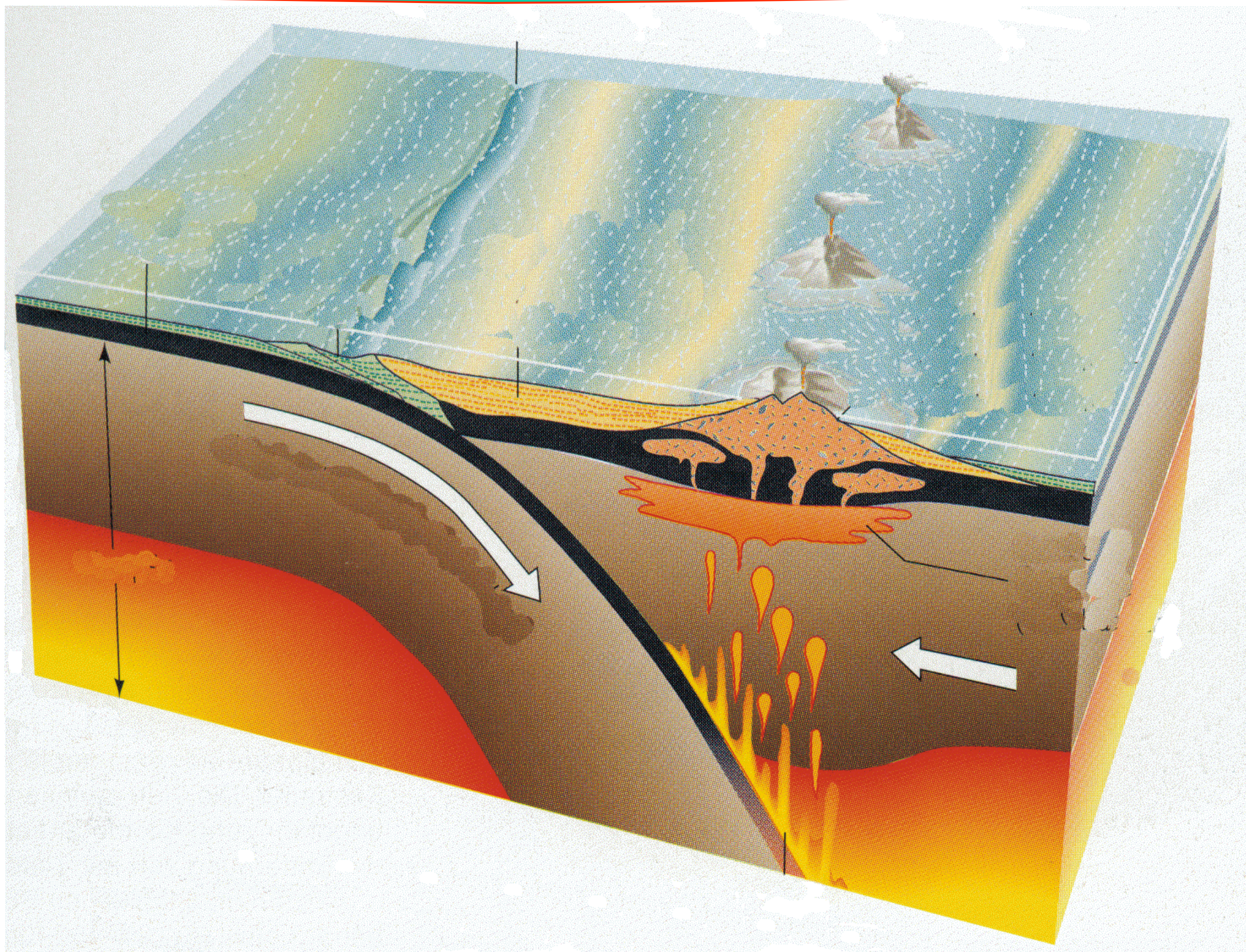

Gorczyk et al. (2006)

Inventing of subduction wheel

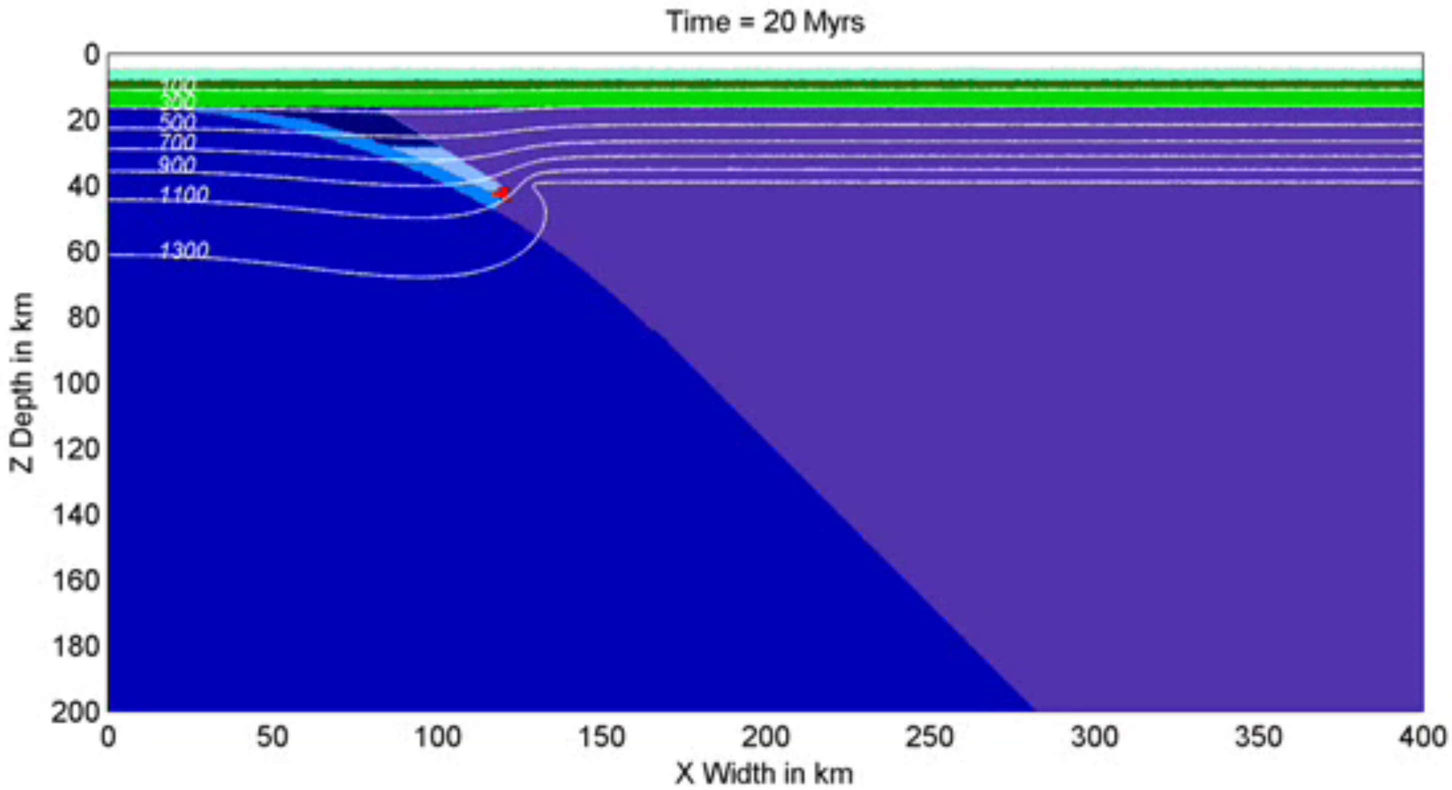
Time = 20 Myrs
0
20
40
60
80
100
120
140
160
180
200
Z Depth in km
100
300
500
700
900
1100
1300
0
50
100
150
200
250
300
350
400
X Width in km

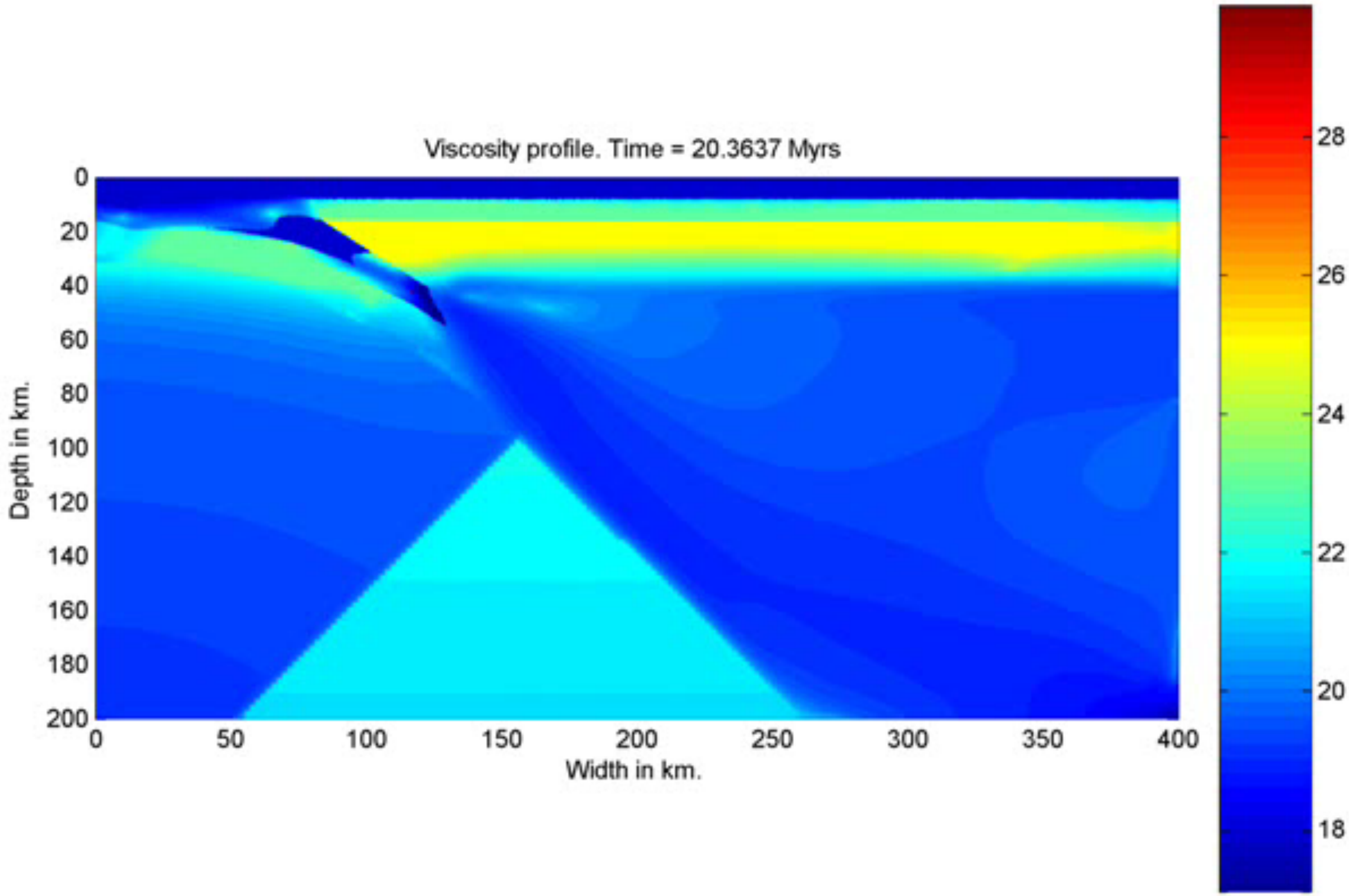

Viscosity profile. Time = 20.3637 Myrs
Depth in km.
0
20
40
60
80
100
120
140
160
180
200
0
50
100
150
200
250
300
350
400
Width in km.
28
26
24
22
20
18

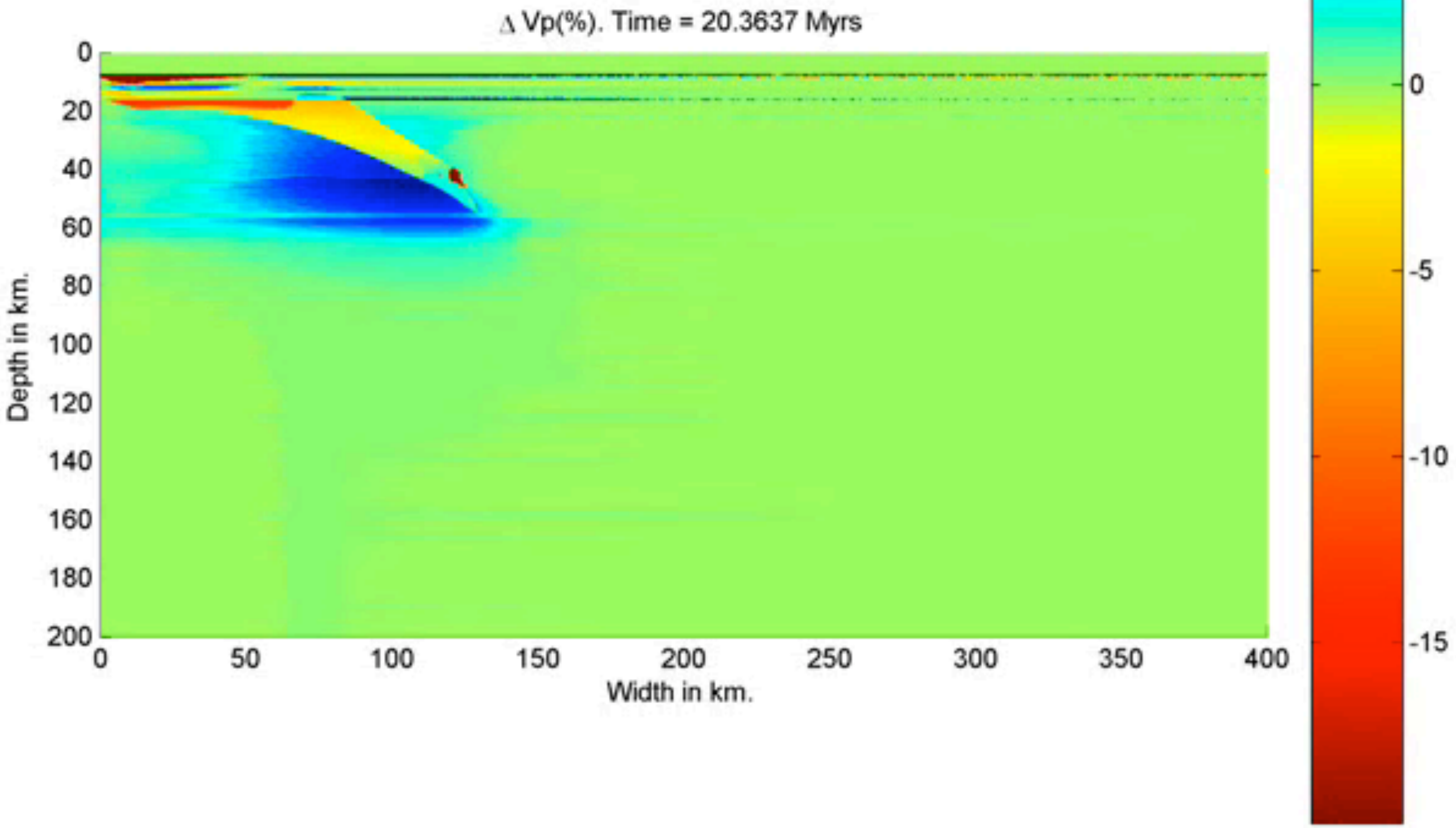
Δ Vp(%). Time = 20.3637 Myrs
Depth in km.
0
20
40
60
80
100
120
140
160
180
200
0
50
100
150
200
250
300
350
400
Width in km.
5
0
-5
-10
-15

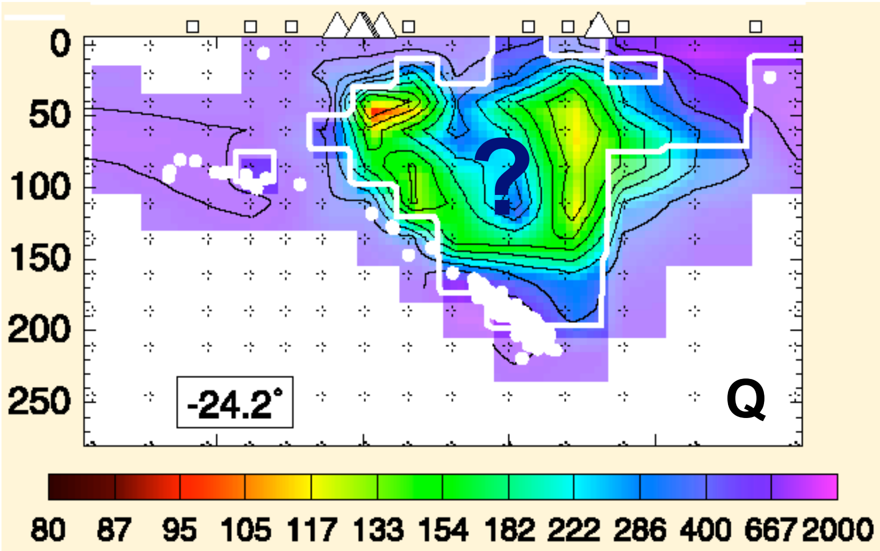

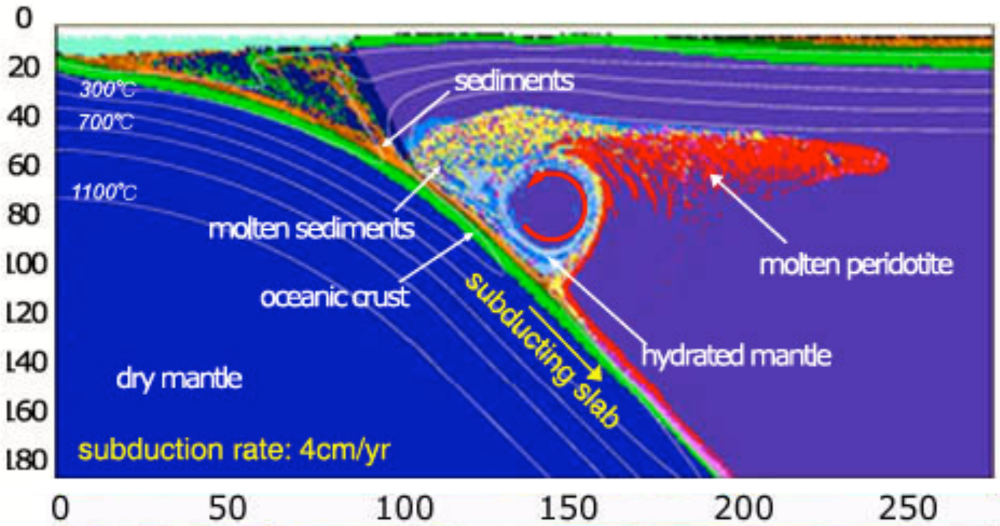

B. Schurr et al. / Earth and Planetary Science Letters 215 (2003) 105–119

Gorczyk et al. (2006)

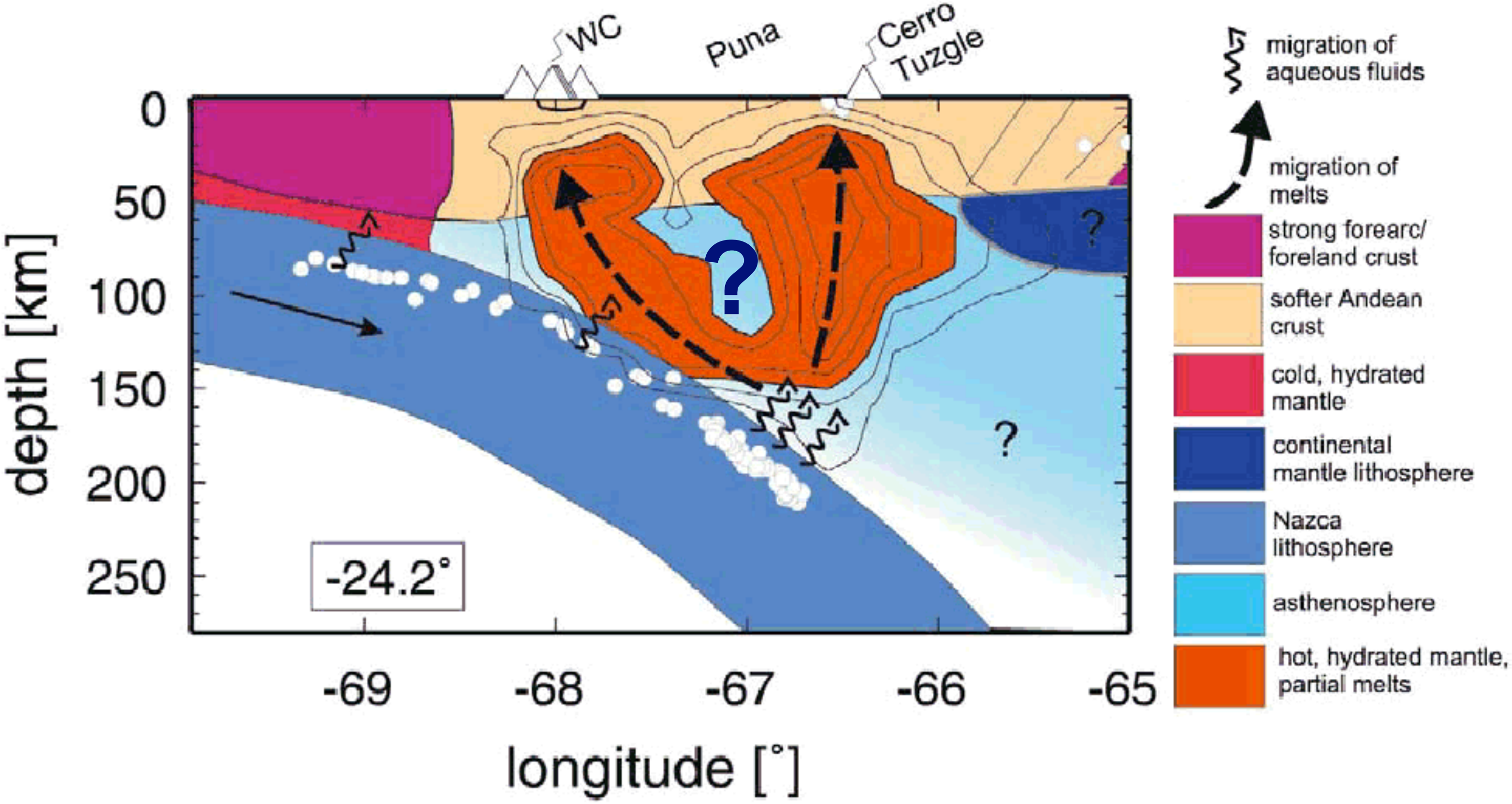

What are physical controls

of magmatic productivity in volcanic arcs

?

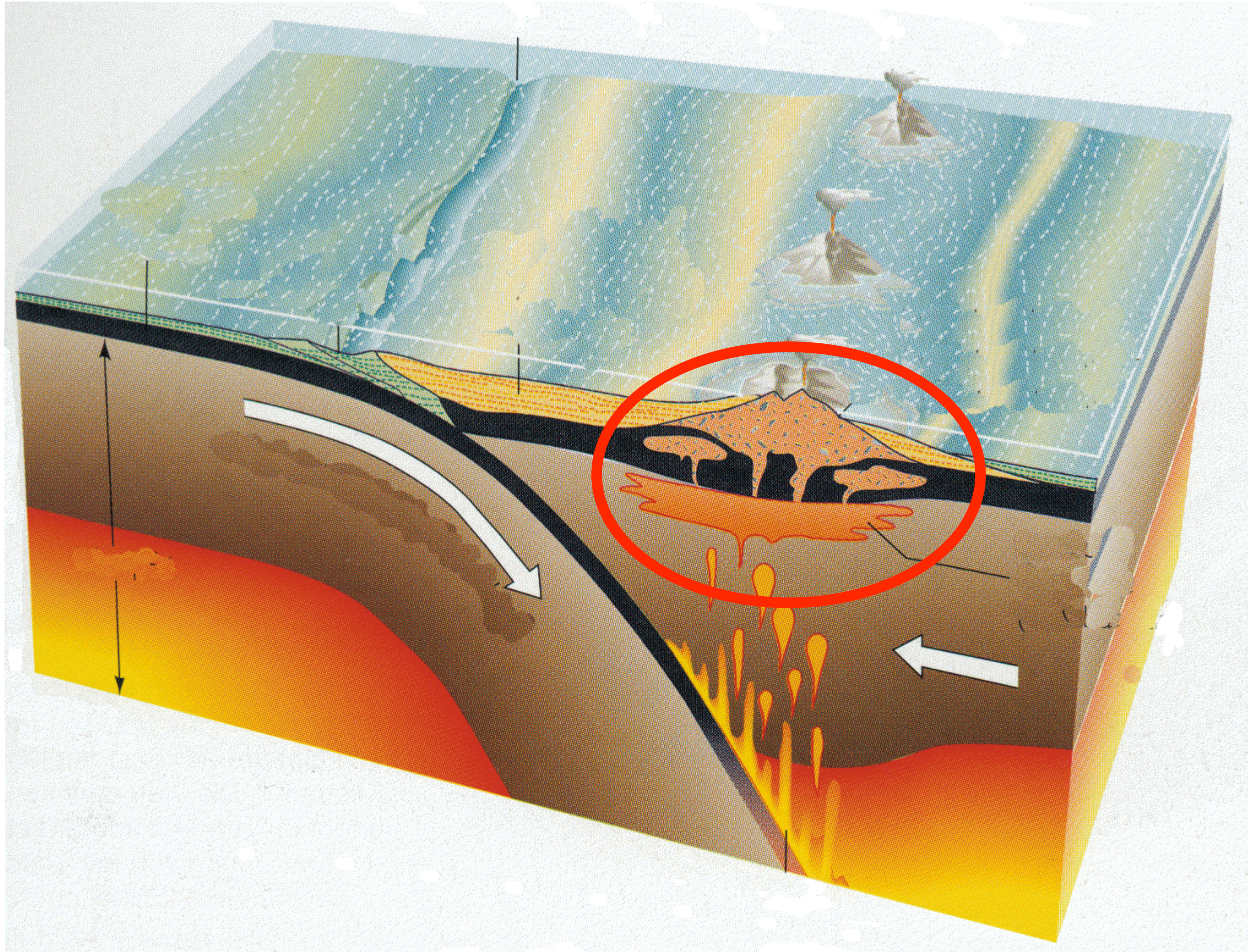

active margin

Gerya and Löw (in preparation)

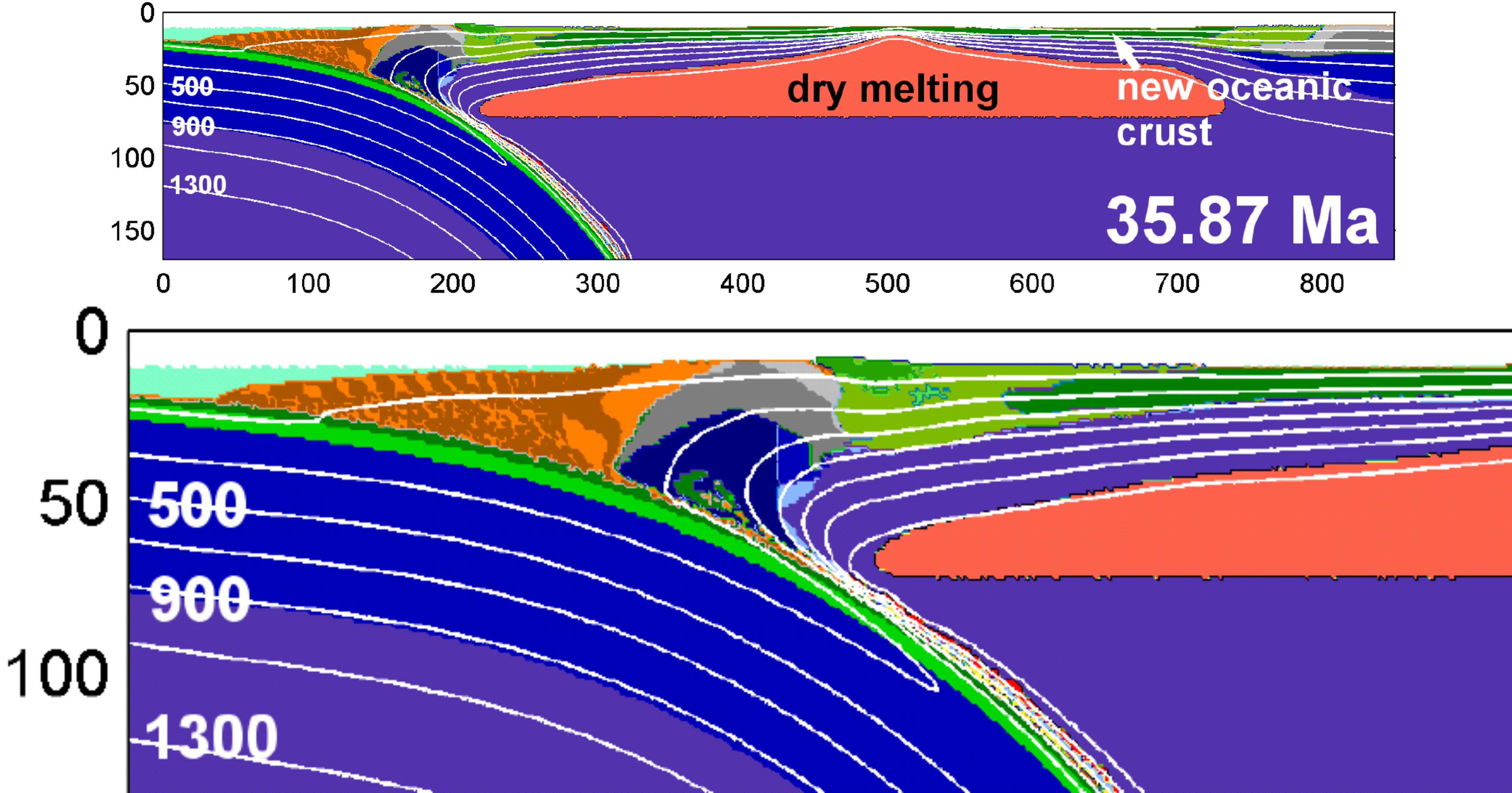

What is important ?

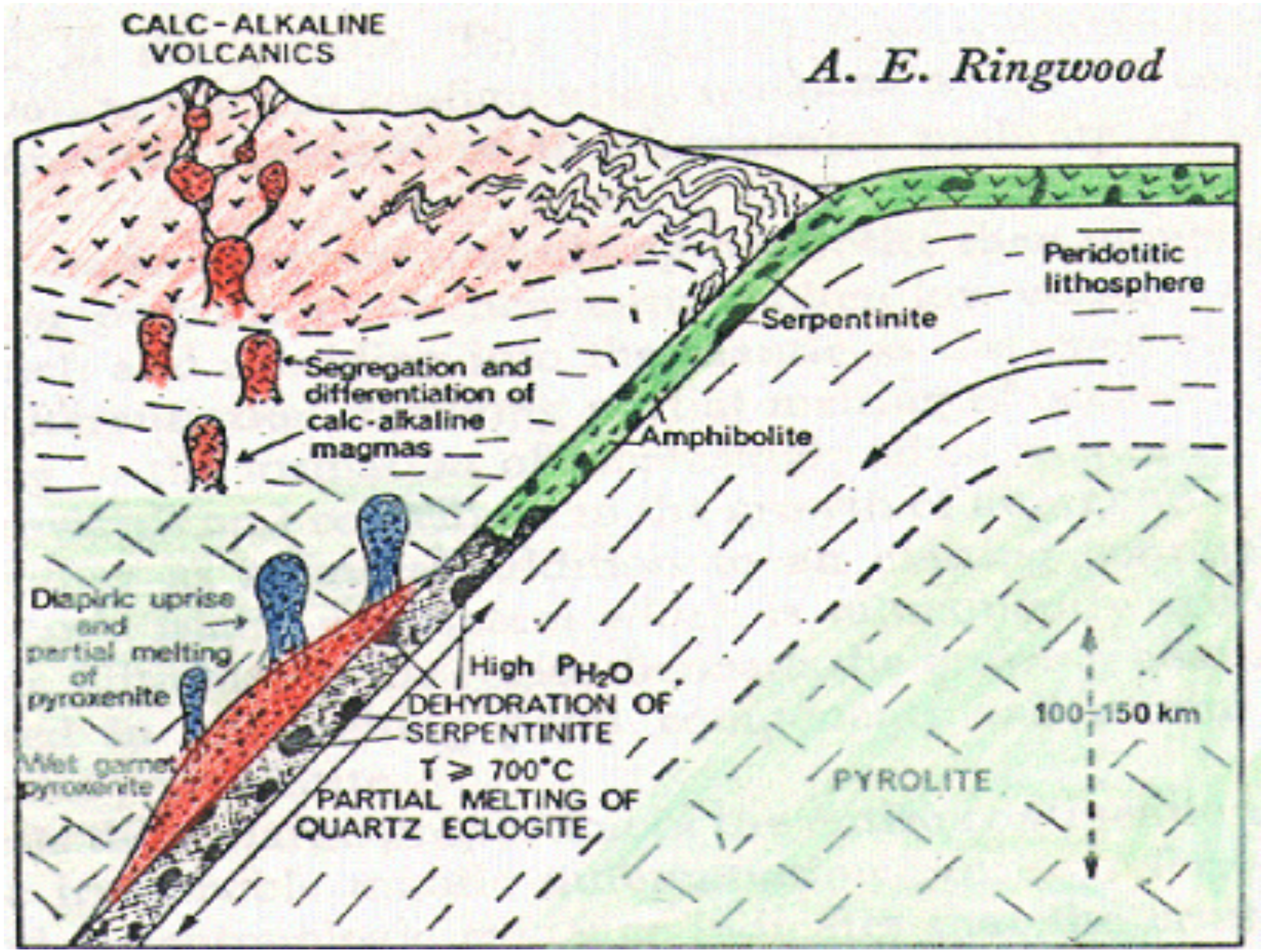

Effects of moving fluids and melt on rock rheoogy

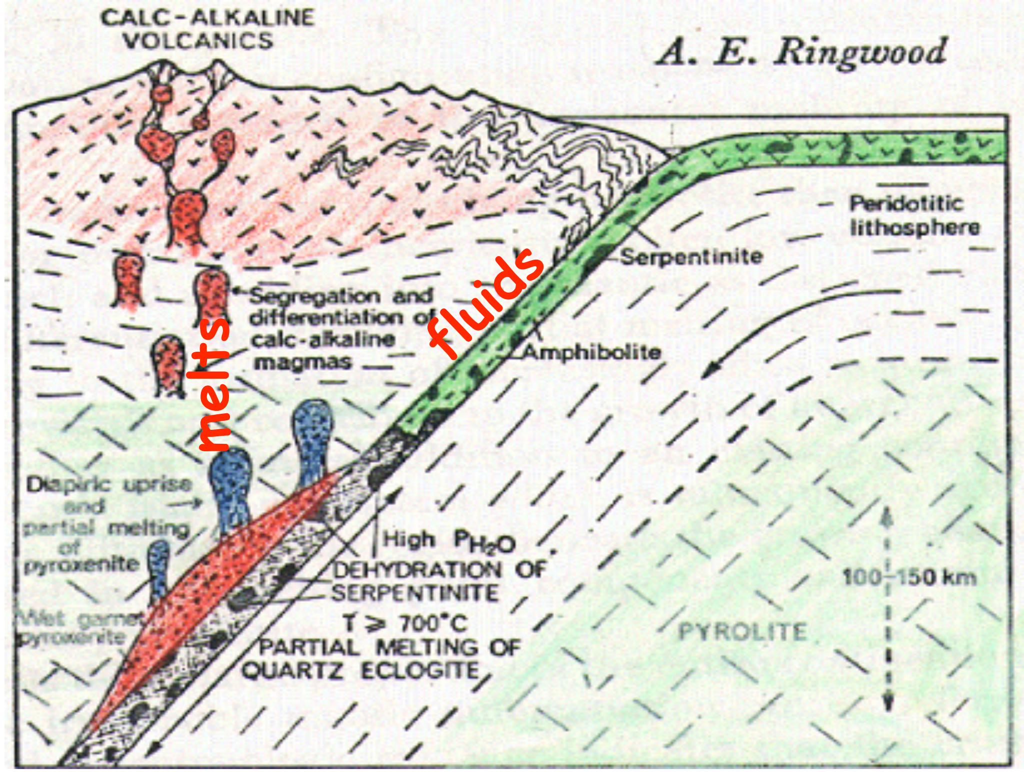

Fluids and melts

We explored two weakening parameters:

λ_{fluid} λ_{melt}

Plastic strength of rocks decreases with increasing pore fluid/melt pressure

$$\sigma_{yield} = c + p \cdot \sin(\psi_{dry}) \cdot \lambda$$

σ_{yield}	yield strength	c	cohesion
p	pressure	ψ	friction angle

$$\lambda_{fluid} = 1 - \frac{P_{fluid}}{P_{solid}}$$

$$\lambda_{melt} = 1 - \frac{P_{melt}}{P_{solid}}$$

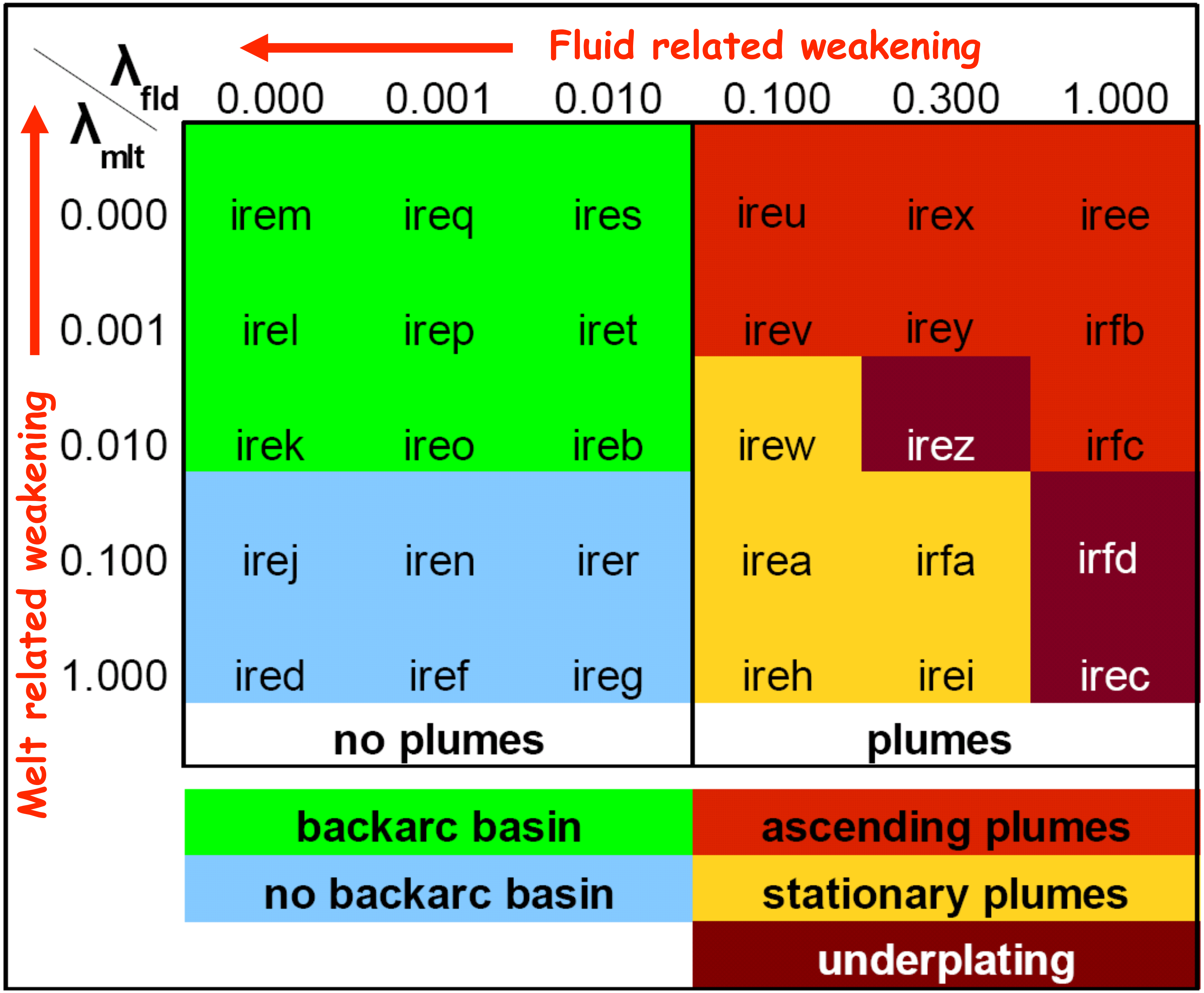

Fluid related weakening
λ_{fld}
λ_{mlt}
0.000
0.001
0.010
0.100
0.300
1.000
Melt related weakening
0.000
0.001
0.010
0.100
1.000
irem
ireq
ires
ireu
irex
iree
irel
irep
iret
irev
irey
irfb
irek
ireo
ireb
irew
irez
irfc
irej
iren
irer
irea
irfa
irfd
ired
iref
ireg
ireh
irei
irec
no plumes
plumes
backarc basin
ascending plumes
no backarc basin
stationary plumes
underplating

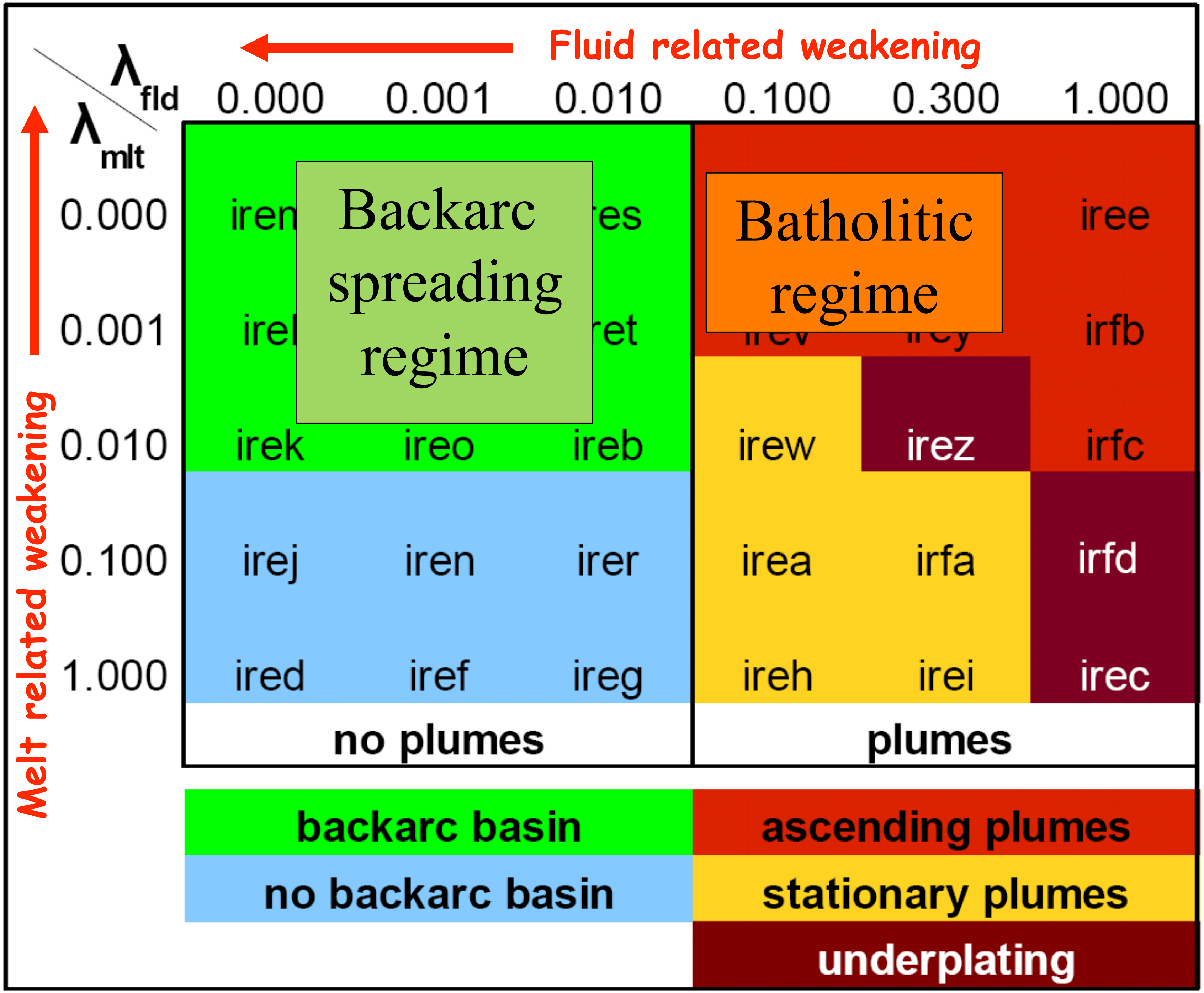

Fluid related weakening
λfld
λmlt
0.000
0.001
0.010
0.100
0.300
1.000
Melt related weakening
0.000
0.001
0.010
0.100
1.000
Backarc spreading regime
Batholitic regime
iree
irfb
irek
ireo
ireb
irew
irez
irfc
irej
iren
irer
irea
irfa
irfd
ired
iref
ireg
ireh
irei
irec
no plumes
plumes
backarc basin
no backarc basin
ascending plumes
stationary plumes
underplating

backarc spreading regime

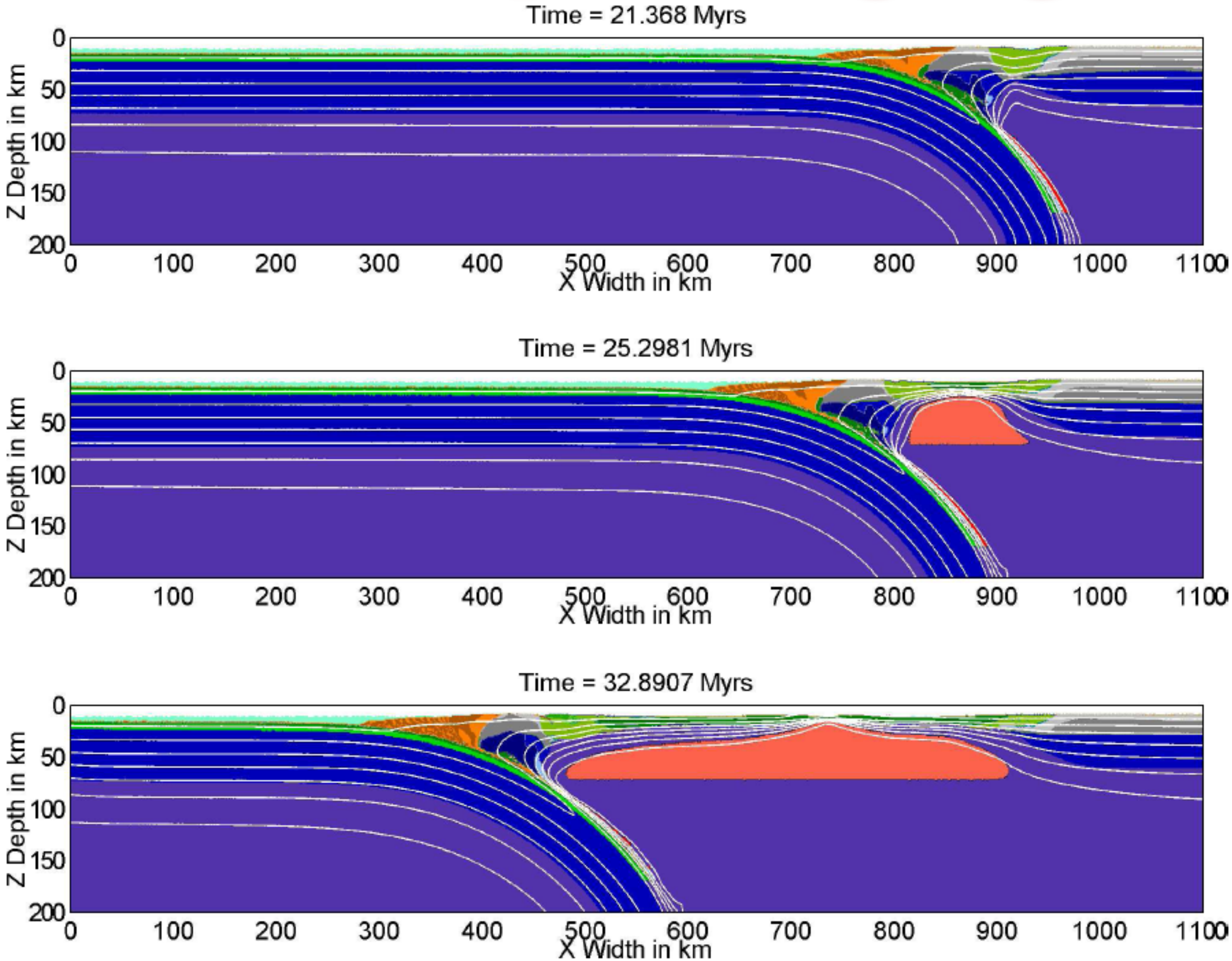

backarc spreading regime

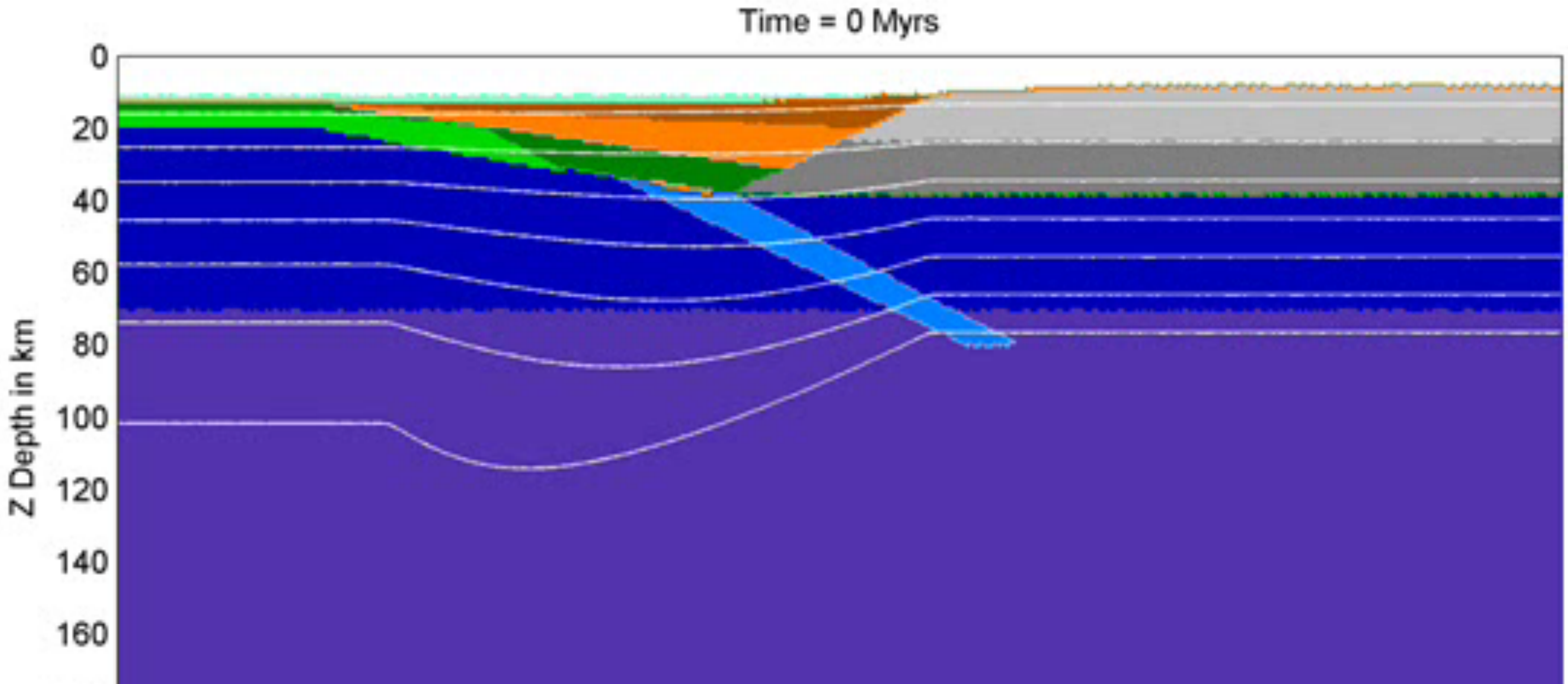

backarc spreading regime

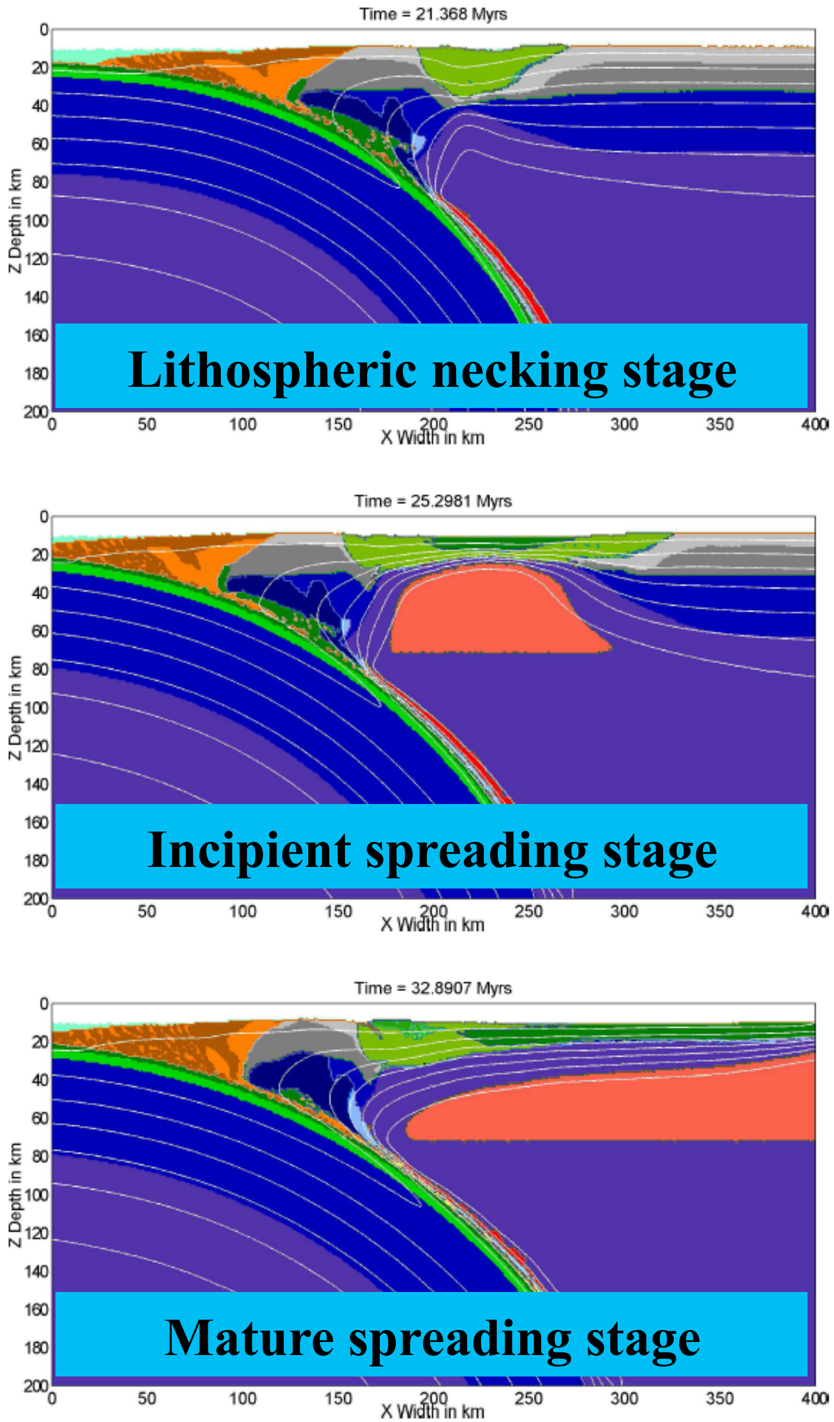

Crustal growth rate

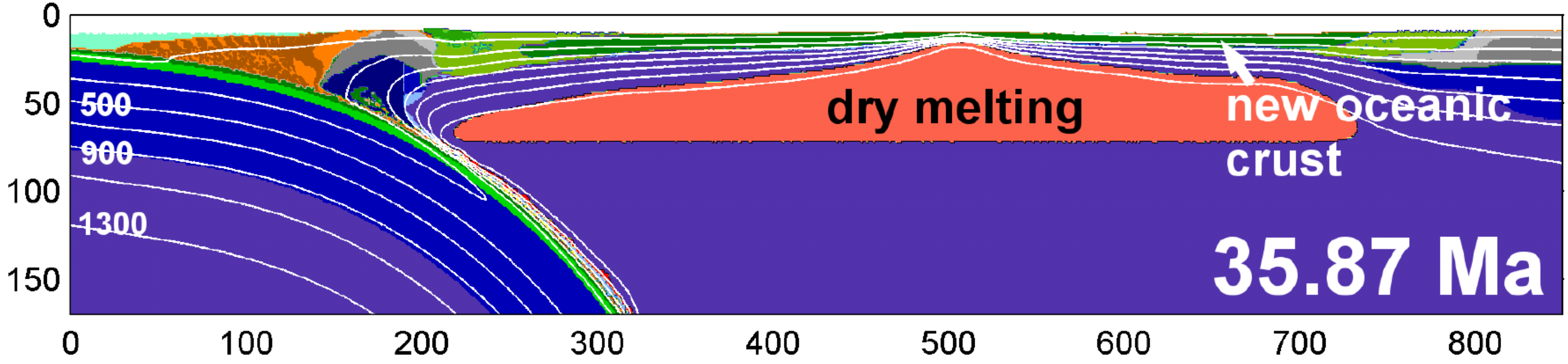

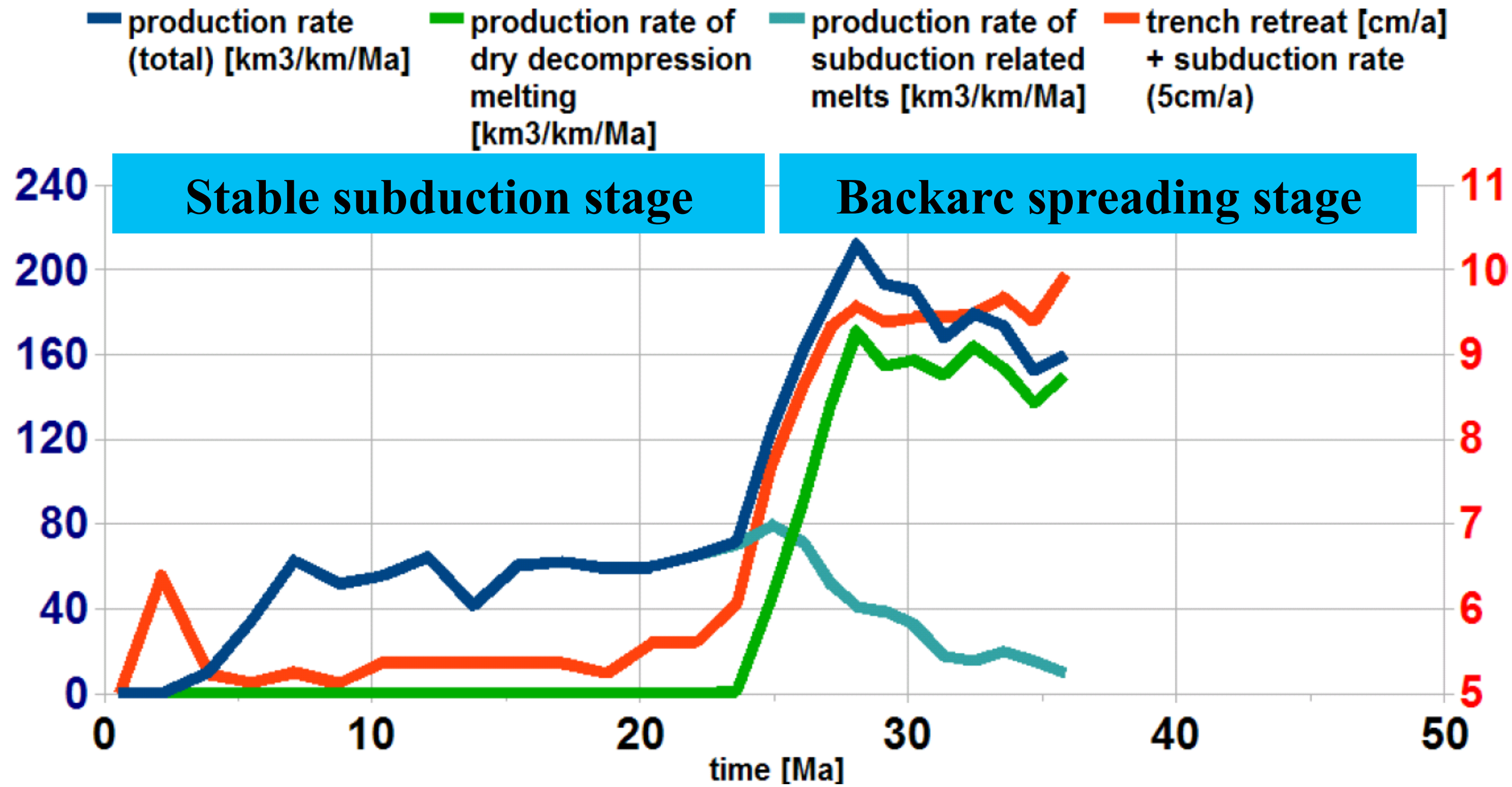

batholitic regime

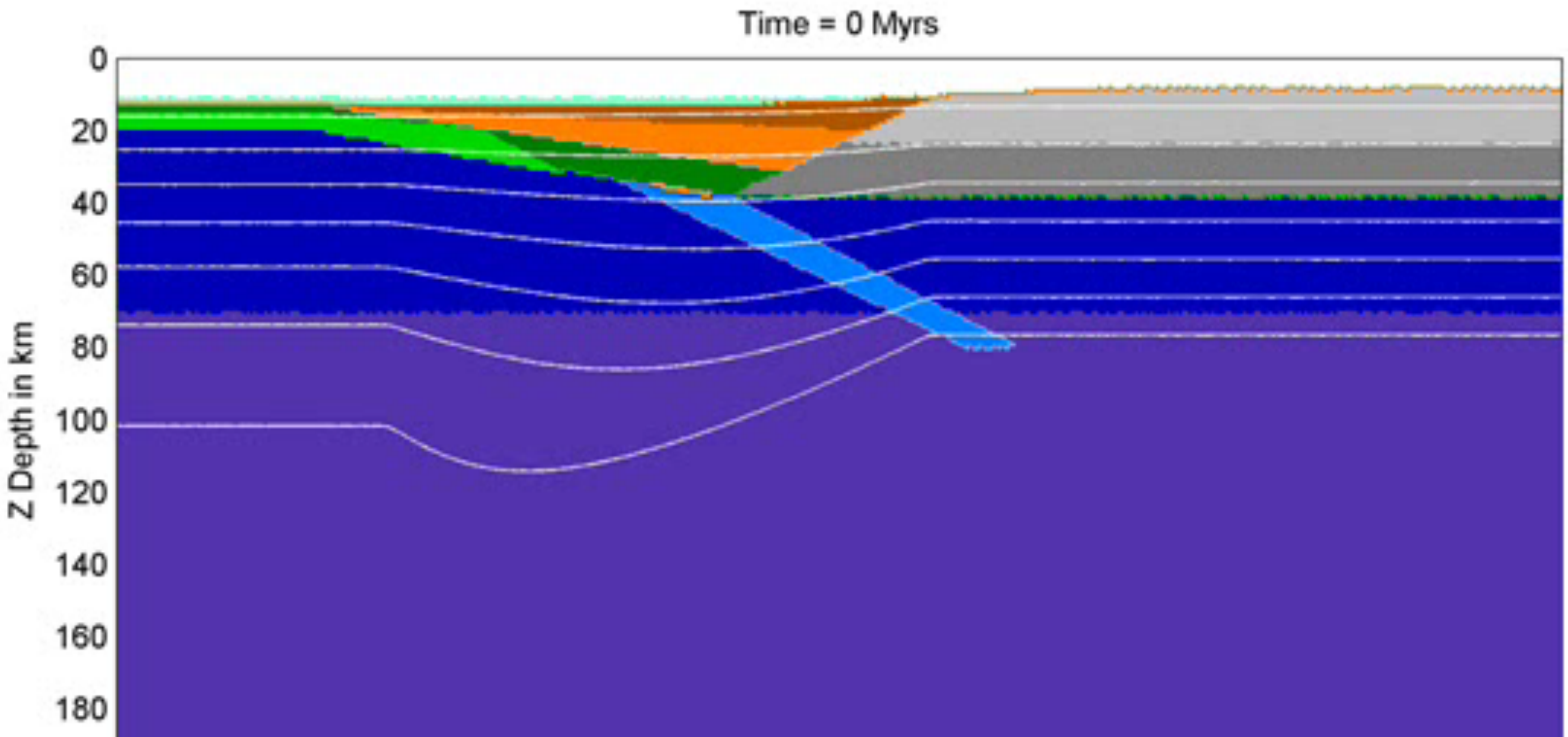

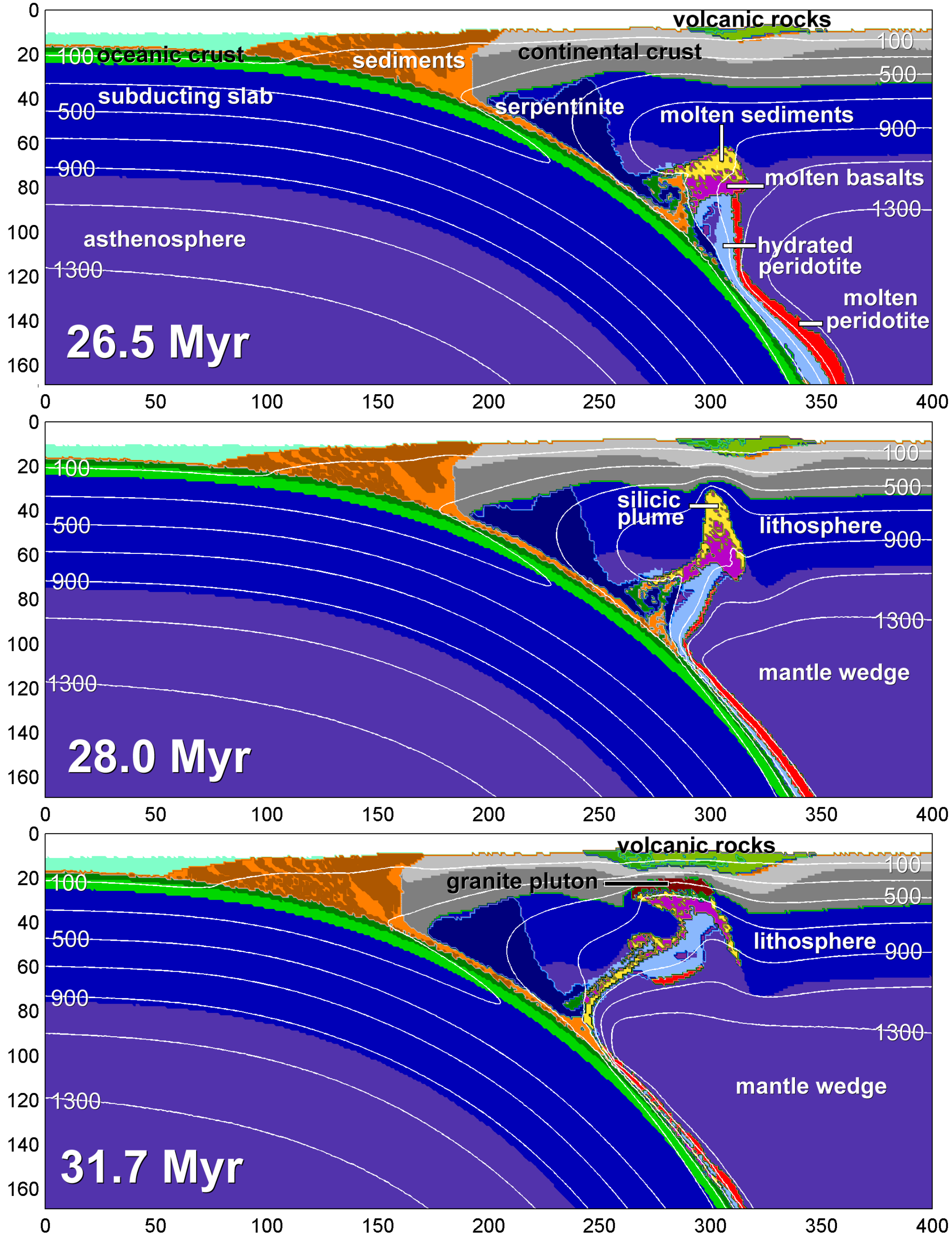

Prediction: batholits should grow from thermal-chemical sublithospheric plumes

Castro et al. (2009)

What was with subduction in the early Earth

Sizova et al. (2009)

Subduction under active margin

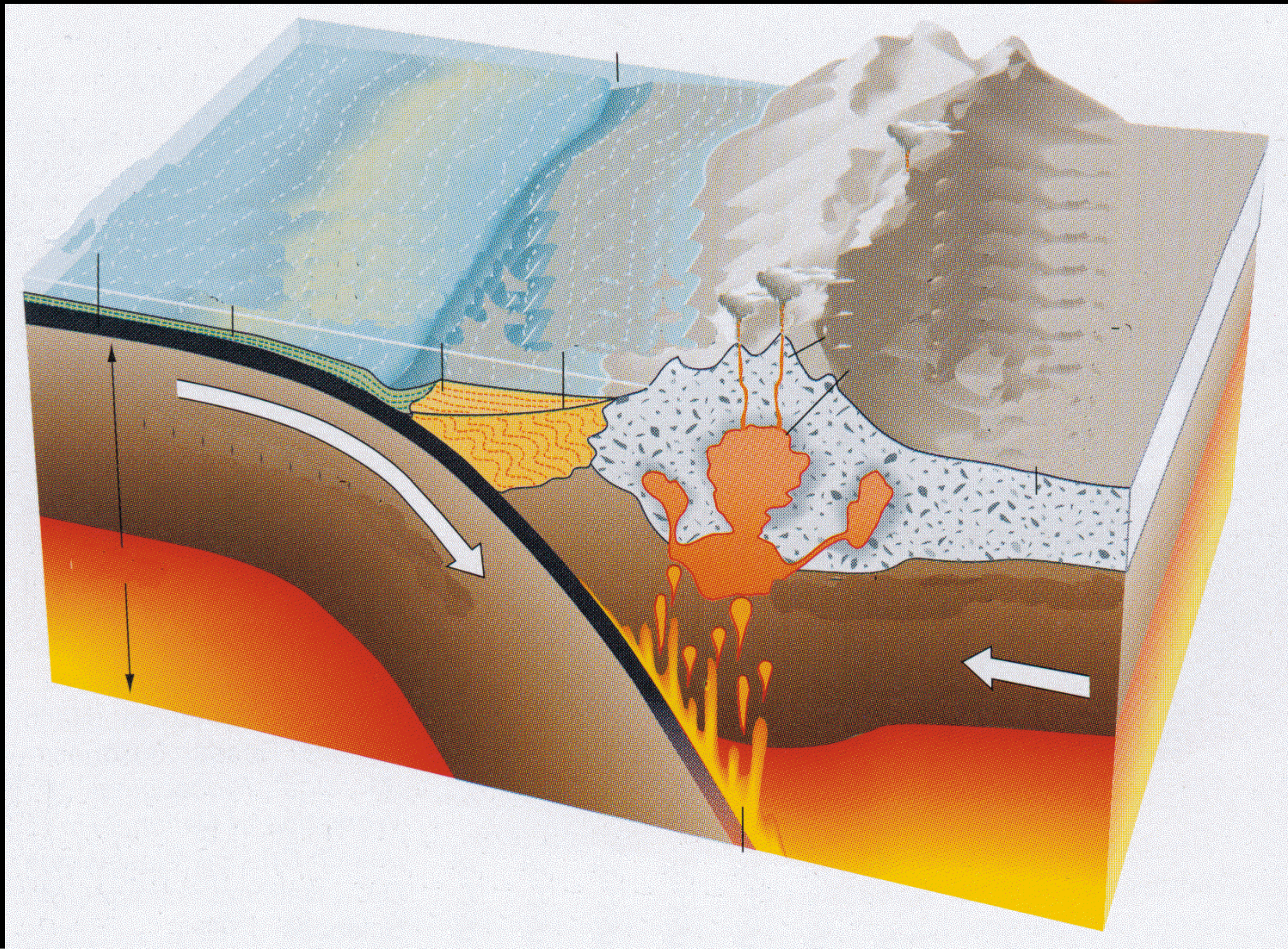

Numerical experiments (different mantle temperature and radiogenic hating)

present day

	ΔT=0°C	ΔT=50°C	ΔT=100°C	ΔT=150°C	ΔT=160°C	ΔT=175°C	ΔT=200°C	ΔT=250°C
H	normal subduction	normal subduction	normal subduction	normal subduction	normal subduction	underthrusting	underthrusting	no subduction
Hx1.5	normal subduction	normal subduction	normal subduction	normal subduction	normal subduction	underthrusting	underthrusting	no subduction
Hx2	normal subduction	normal subduction	normal subduction	normal subduction	normal subduction	underthrusting	underthrusting	no subduction
Hx2.5	normal subduction	normal subduction	normal subduction	normal subduction	normal subduction	underthrusting	underthrusting	no subduction
Hx3	normal subduction	normal subduction	normal subduction	normal subduction	normal subduction	underthrusting	underthrusting	no subduction
Hx5	normal subduction	normal subduction	normal subduction	normal subduction	normal subduction	underthrusting	underthrusting	no subduction

"normal subduction" regime

"pre-subduction" regime

"no subduction" regime

ΔT = Tm – Tm^0; Tm^0=1360°C (present mantle temperature at 70 km)

H – radiogenic heating (present day)

Numerical experiments (different mantle temperature and radiogenic hating)

present day

	ΔT=0°C	ΔT=50°C	ΔT=100°C	ΔT=150°C	ΔT=160°C	ΔT=175°C	ΔT=200°C	ΔT=250°C
H	normal subduction	normal subduction	normal subduction	normal subduction	normal subduction	underthrusting	underthrusting	no subduction
H	normal	normal	normal	normal	normal subduction	underthrusting	underthrusting	no subduction
H					normal subduction	underthrusting	underthrusting	no subduction
H					normal subduction	underthrusting	underthrusting	no subduction
Hx3						underthrusting	underthrusting	no subduction
Hx5						underthrusting	underthrusting	no subduction

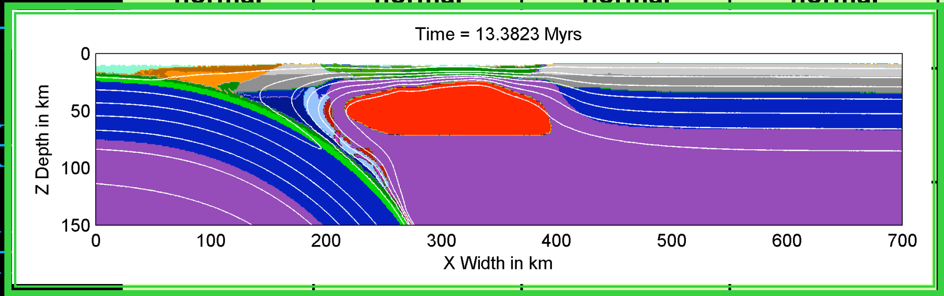

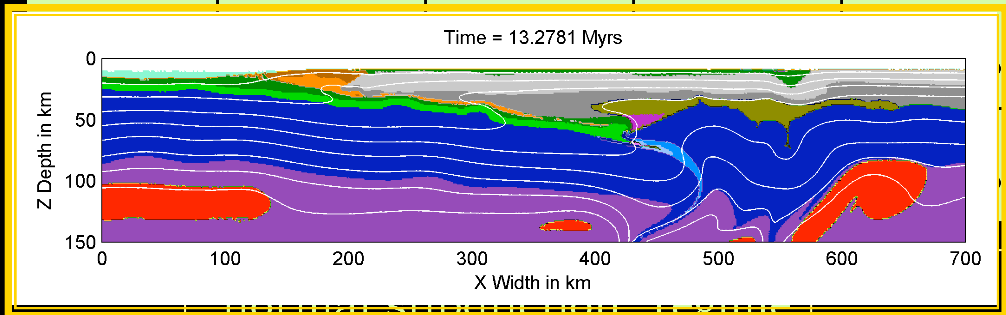

"pre-subduction"

"no

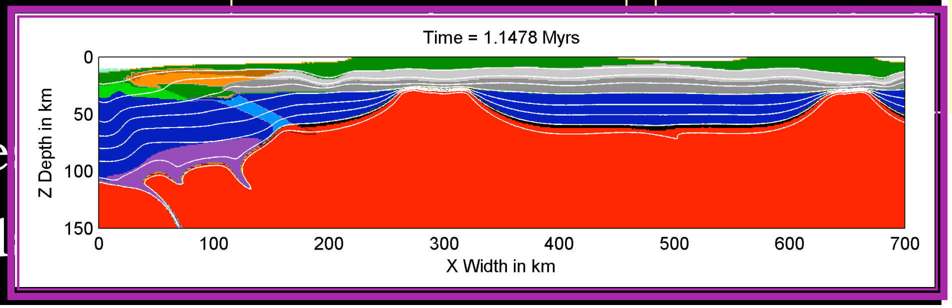

ΔT = Tm – Tm^0; Tm^0=1360°C (pre

H – radiogenic heating (present d

Normal subduction

ΔT = 0 – 175 °C

Initial experiment
(present day)

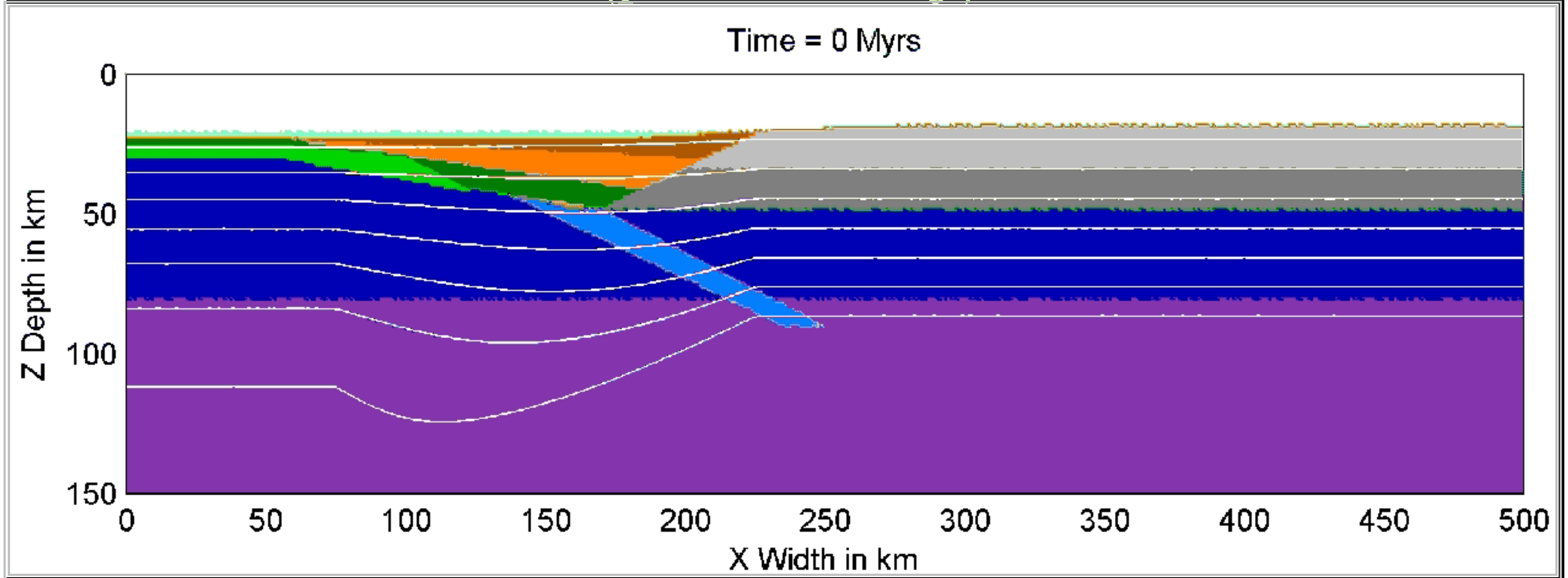

Formation of mantle wedge, arc, backarc basin

Underthrusting ("pre-subduction" regime) ΔT = 175 – 250 °C

Hx2.5

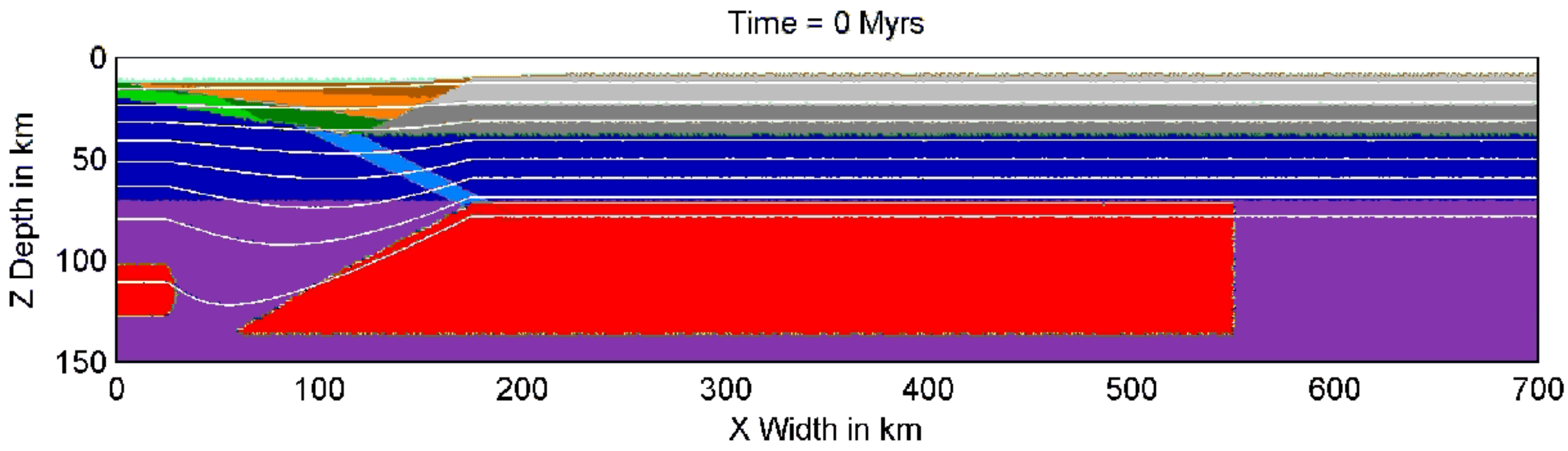

Plates are very weak.
They have strong tendency of horizontal buckling.
Both slab and lower continental crust start to melt.
No mantle wedge, no arc, no backarc basin.

"No subduction" regime

ΔT > 250 °C

Hx3

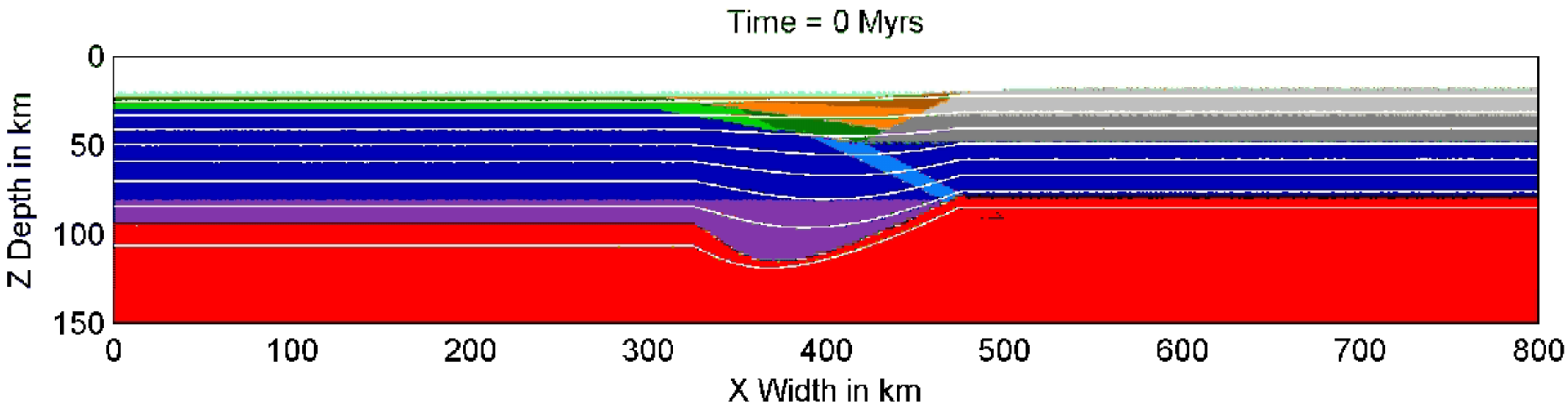

Only horizontal movements

Prediction: three regimes for the Earth

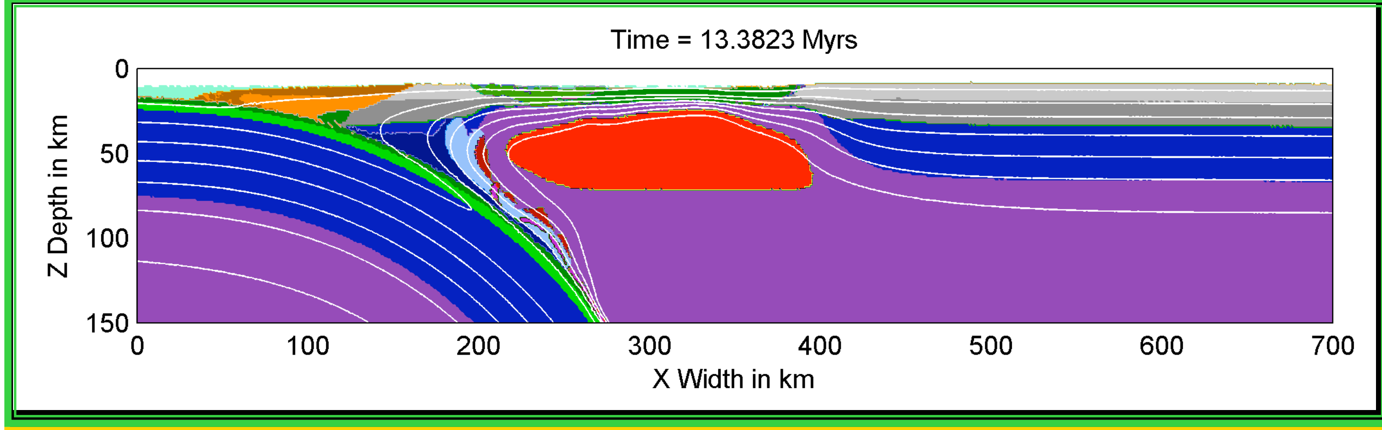

"normal subduction" regime

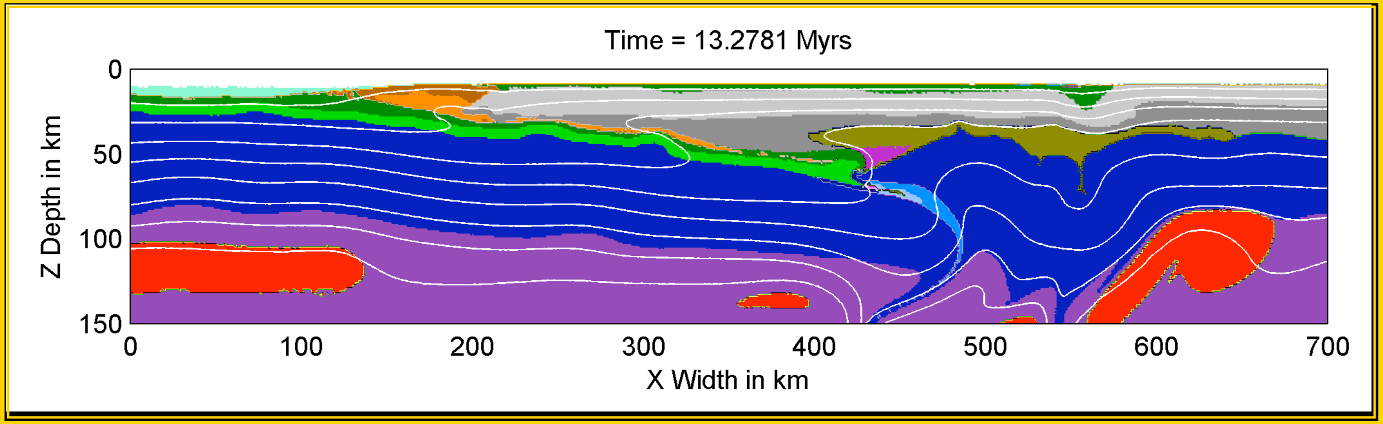

"pre-subduction" regime

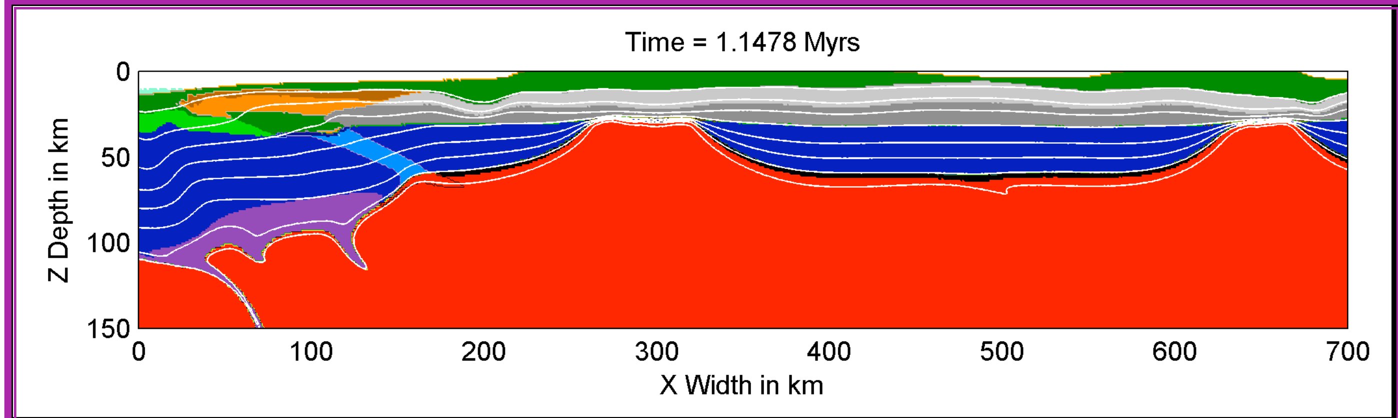

"no subduction" regime

Sizova et al. (2009)

Transitions from numerical experiments

ΔT=160°C	ΔT=175°C ΔT=200°C	ΔT=250°C
"normal subduction" regime	"pre-subduction" regime H > Hx1.5	"no subduction" regime

?

Petrological data:

Neoarchean time (2.5-3Ga):

ΔT = 100 - 200°C

(Grove, Parman, 2004; Komia et.al., 1999)

H: Hx2 – Hx3

(Chacko, 2003; Hynes, 2001; Davies, 1992)

Evolving tectonic regimes

Kent C. Condie

Presentation on Geological Society of America
Penrose Conference

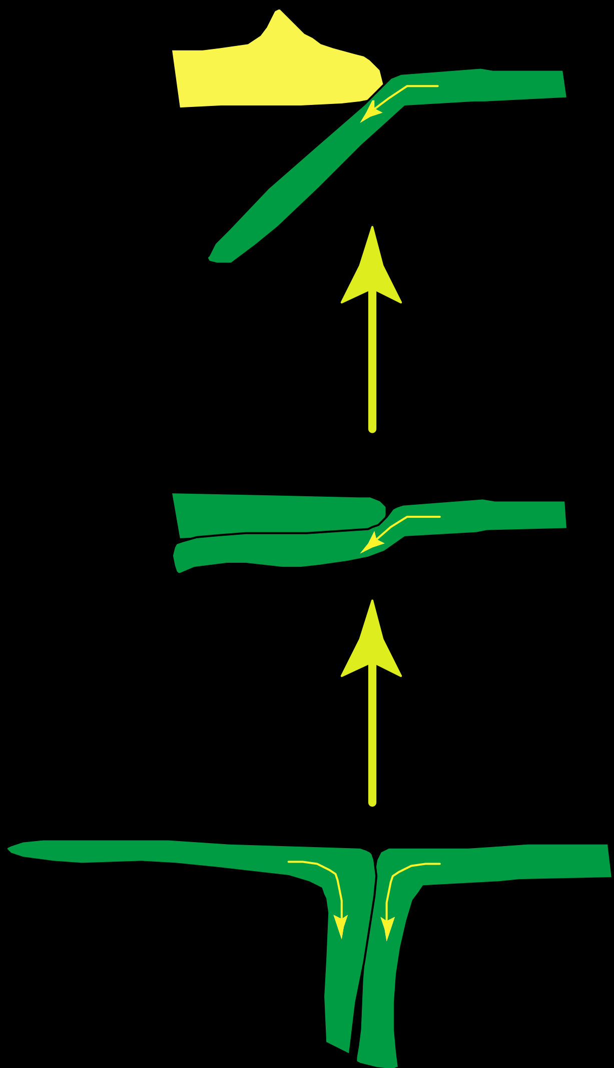

Steep Subduction

3.0 - 2.5 Ga

Flat Subduction

4.5 - 3.0 Ga

Symmetric Subduction

> 4.5 Ga ?

What factors control

subduction initiation at passive margins?

?

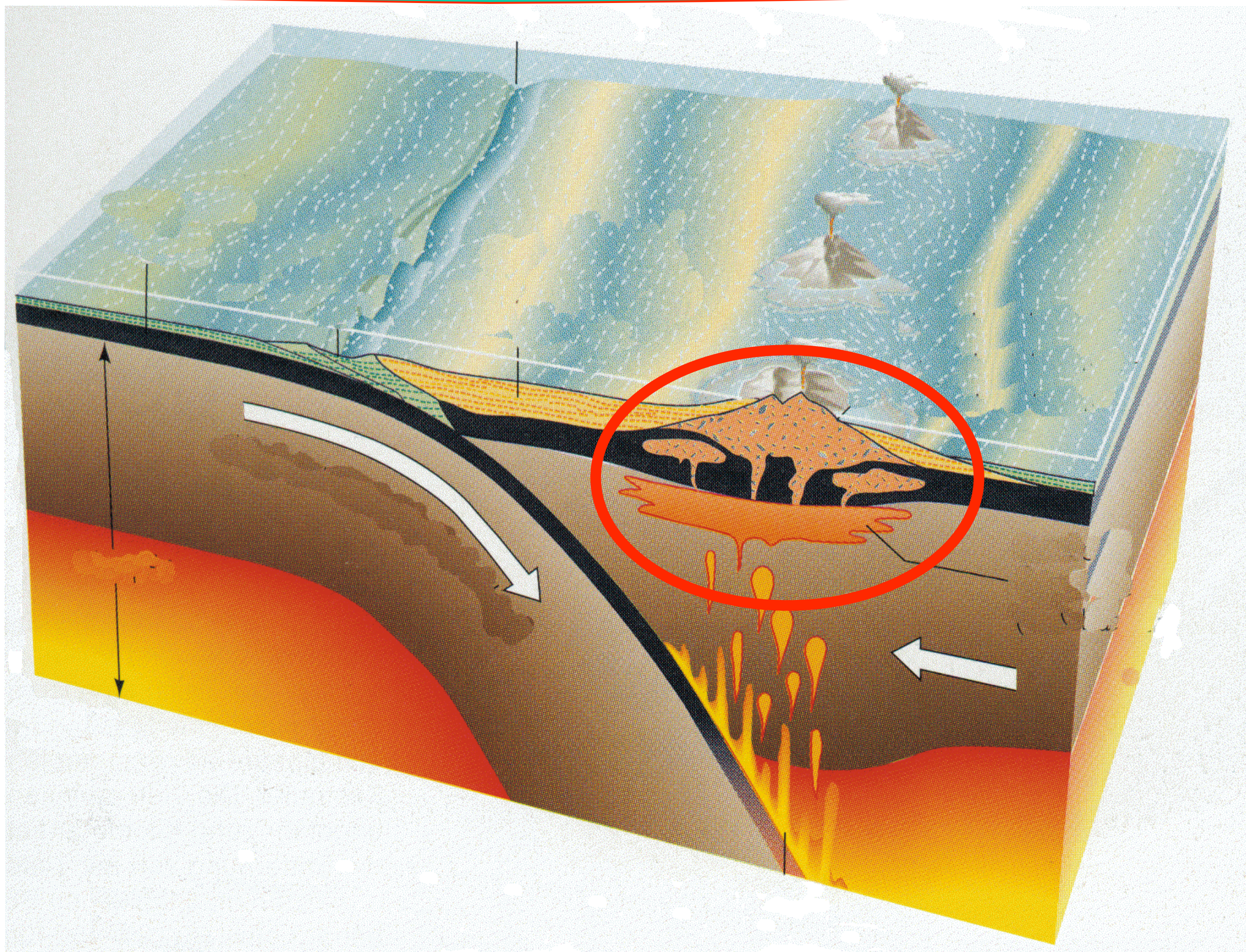

Subduction initiation controversy

A combination of **slab pull** (mostly) and **ridge-push** has been shown to be the dominant driving mechanism of plate tectonics (e.g. Elsasser, 1967; McKenzie, 1969; Forsyth and Uyeda, 1975). It is also known that an oceanic lithosphere older than 20-50 Ma becomes denser than the underlying asthenosphere. However, McKenzie (1977) showed that, despite the favourable gravitational instability and ridge-push, **elastic and frictional forces prevent subduction from arising spontaneously**.

Therefore the twofold question: **what forces can trigger subduction** (other than negative buoyancy and ridge-push), and **where can it nucleate**? Several mechanisms have been proposed to try and answer this double question:

(1)plate rupture within an oceanic plate or at a passive margin (e.g. McKenzie, 1977; Dickinson and Seely, 1979; Mitchell, 1984; Müeller and Phillips, 1991).

(2)Reversal of the polarity of an existing subduction zone (e.g. Dickinson and Seely, 1979; Mitchell, 1984).

(3) Change of transform faults into trenches (e.g. Uyeda and Ben-Avraham, 1972; Hilde et al., 1976; Cooper et al., 1977; Karson and Dewey, 1978; Casey and Dewey, 1984; Müeller and Phillips, 1991).

(4)Sediment loading at passive margins of old or young lithosphere (e.g. Dewey, 1969; Fyfe and Leonardos, 1977; Karig, 1982; Cloetingh et al., 1982; Erickson, 1993; Regenauer-Lieb et al., 2001).

(5) Forced convergence at oceanic fracture zones (e.g. Mueller and Phillips, 1991; Toth and Gurnis, 1998; Doin and Henry, 2001; Hall et al., 2003; Gurnis et al., 2004).

(6)Tensile decoupling of the continental and oceanic lithosphere due to rifting (Kemp and Stevenson, 1996).

(7) Lateral compositional buoyancy contrast within the lithosphere (Niu et al., 2003).

(8)Addition of water (Regenauer-Lieb et al., 2001).

(9)Small-scale convection in the sub-lithospheric mantle (Solomatov, 2004).

(10) Thermal-chemical plumes (Ueda et al., 2008).

(11) **Spontaneous thrusting of the buoyant continental crust over the oceanic (Mart et al., 2005).**

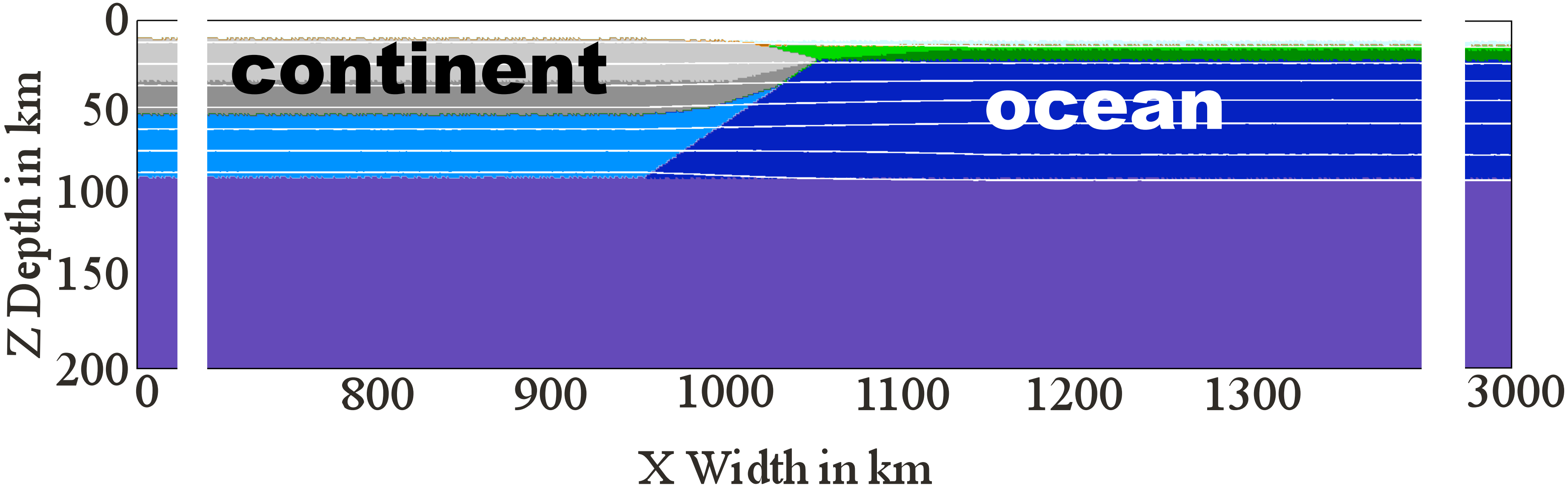

Nikolaeva et al. (in revision)

3 geodynamic regimes

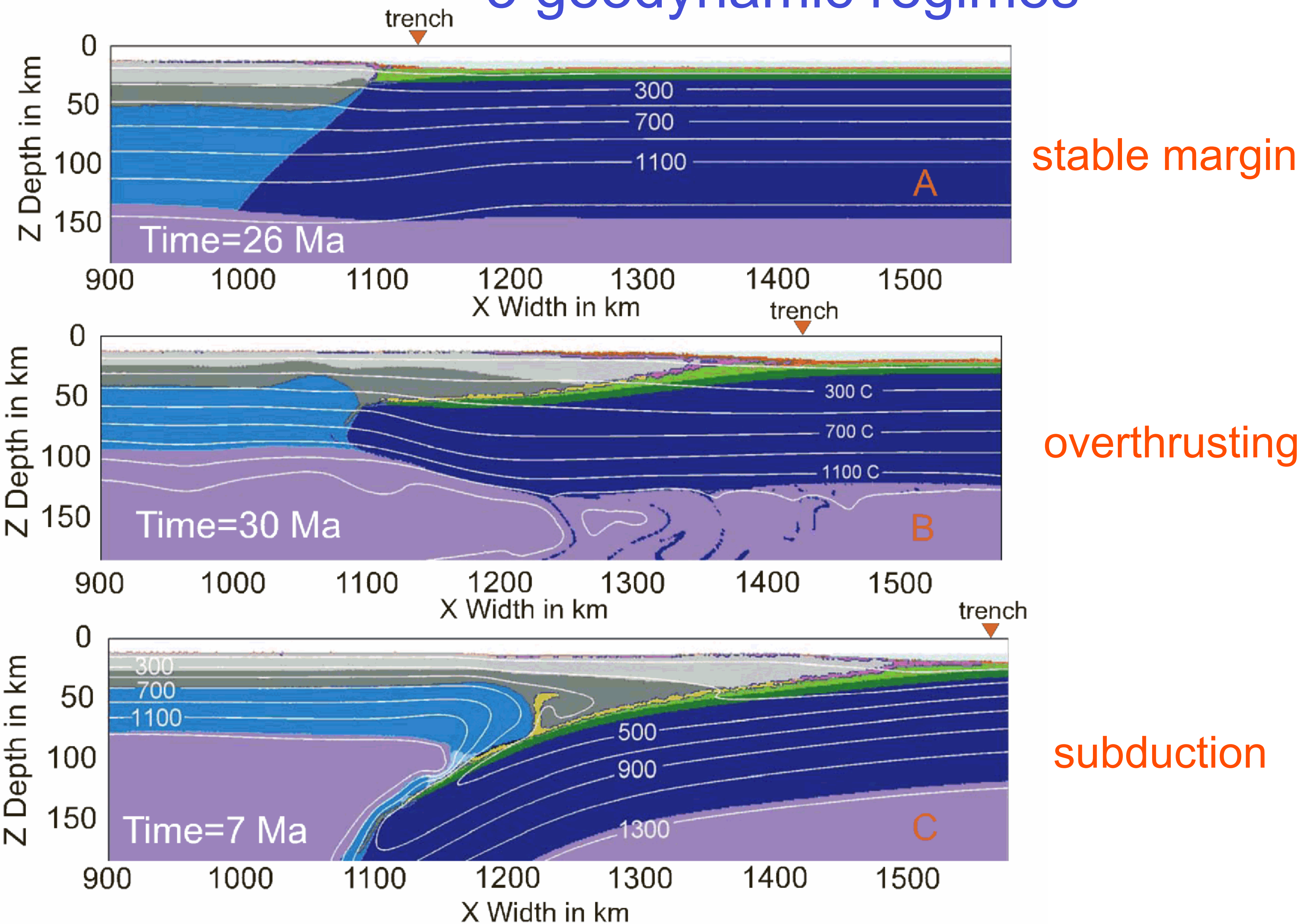

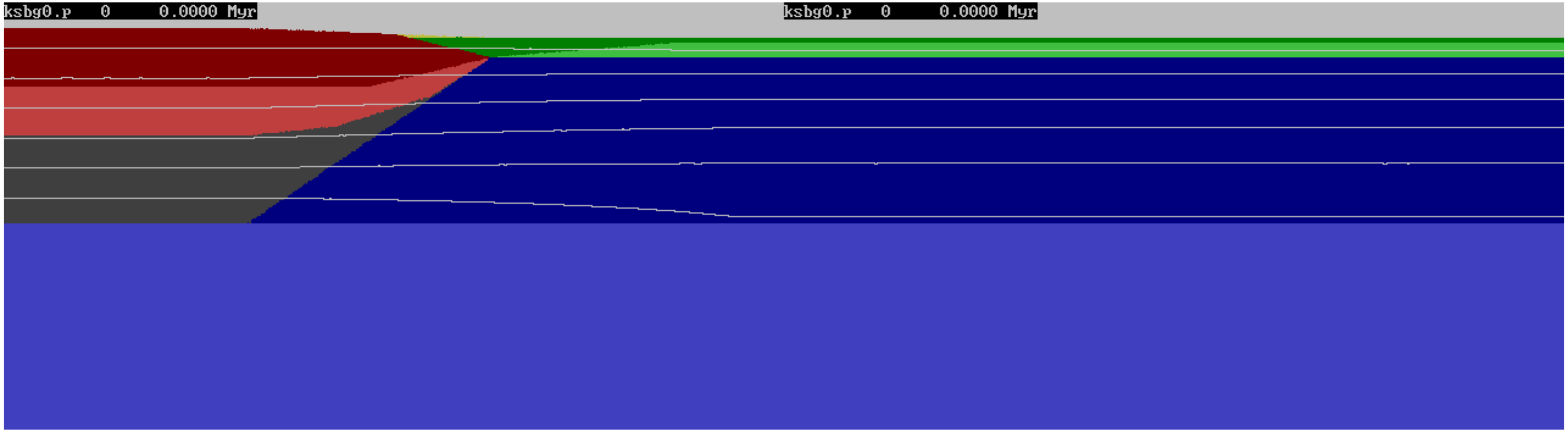

subduction regime

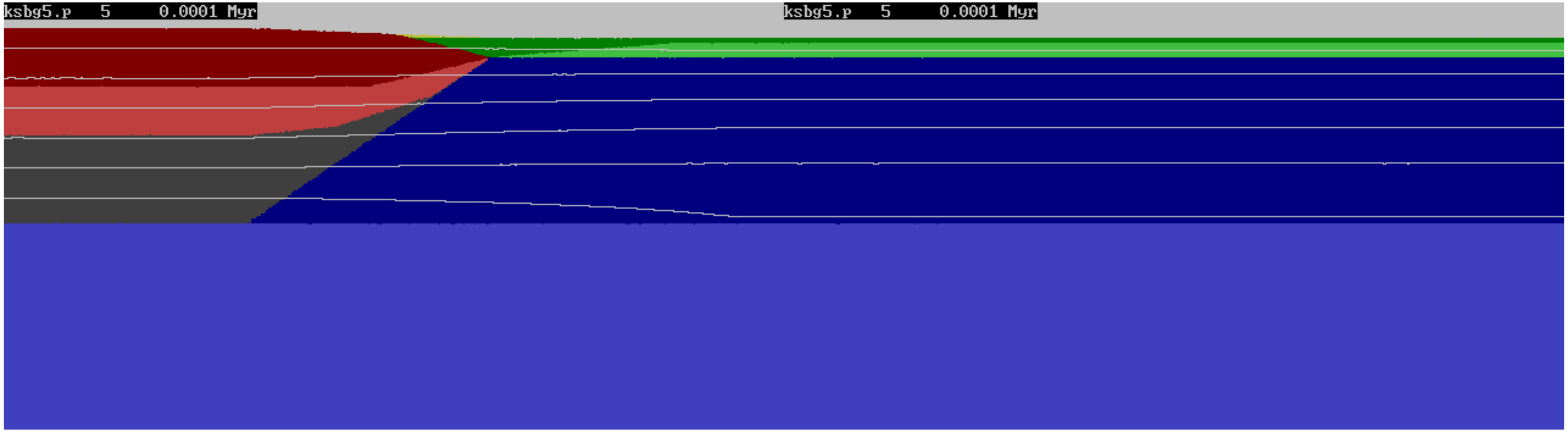

subduction regime

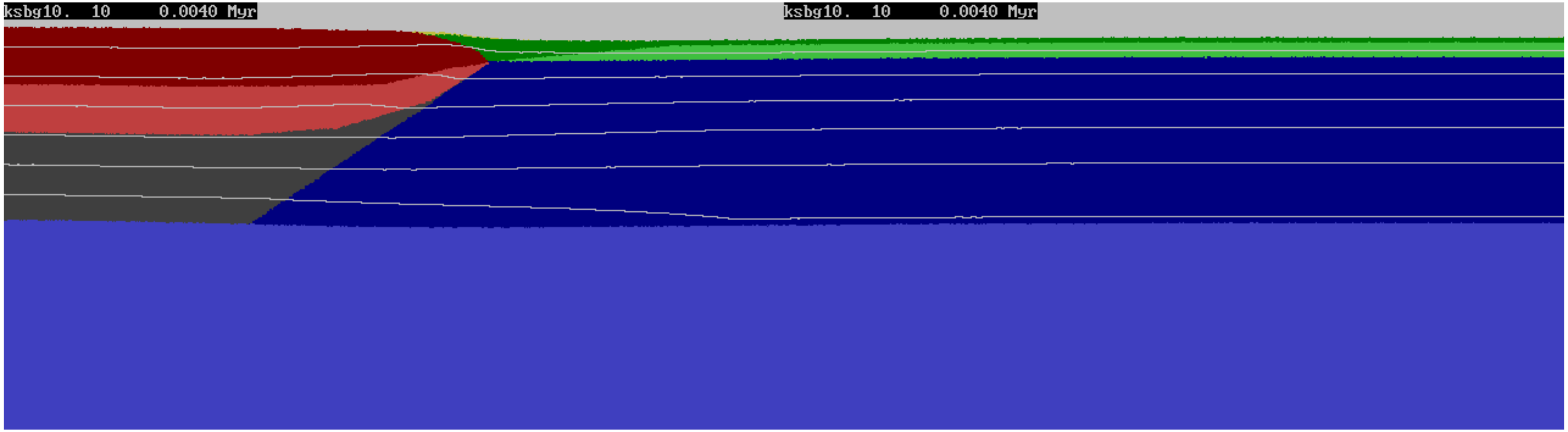

subduction regime

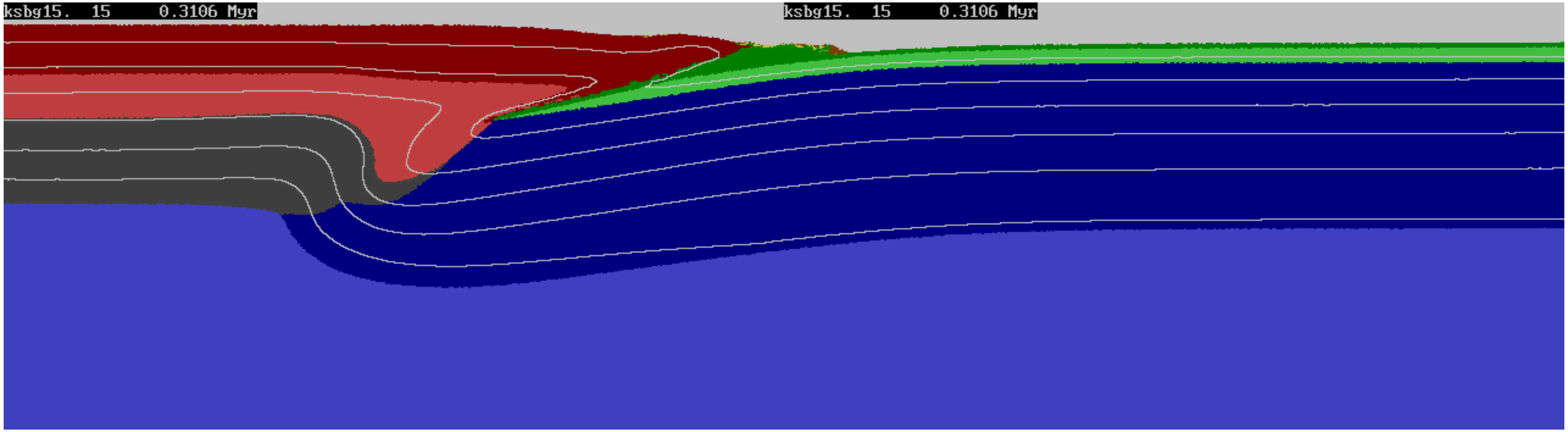

subduction regime

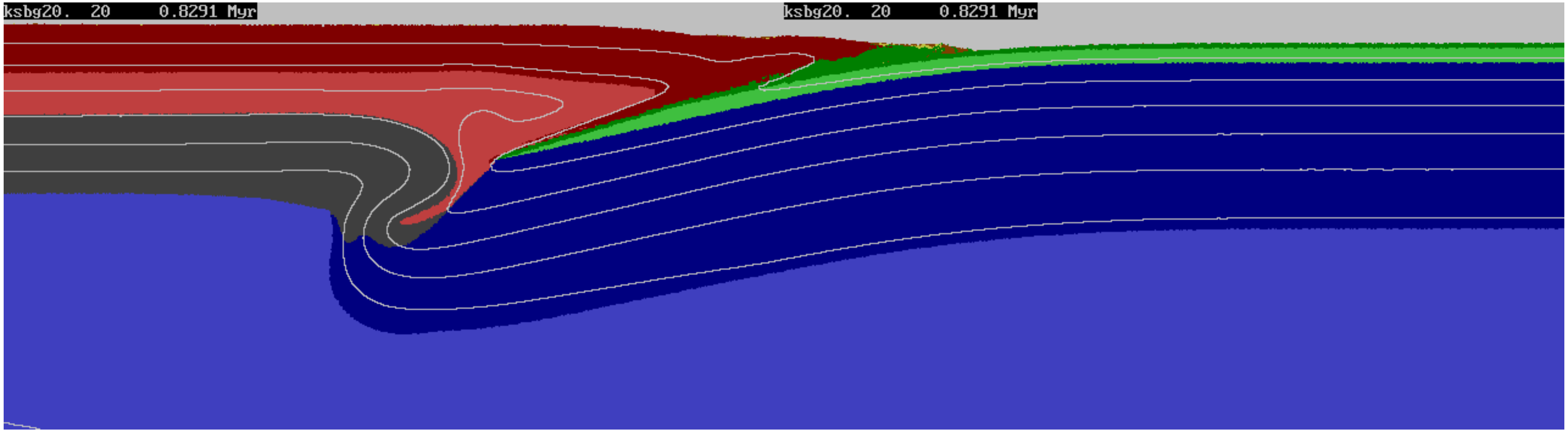

subduction regime

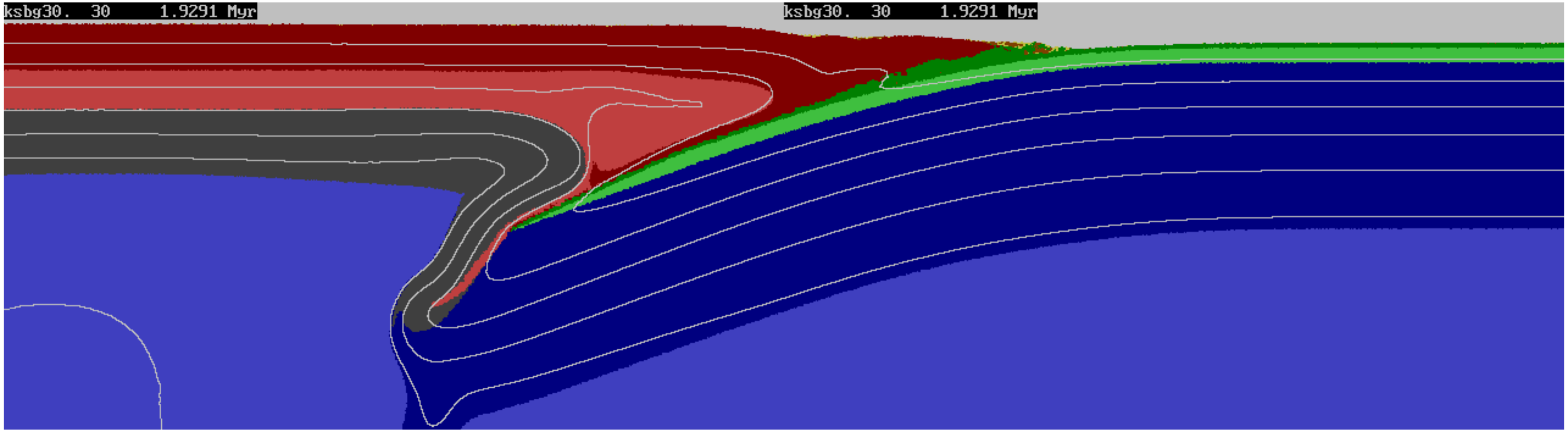

subduction regime

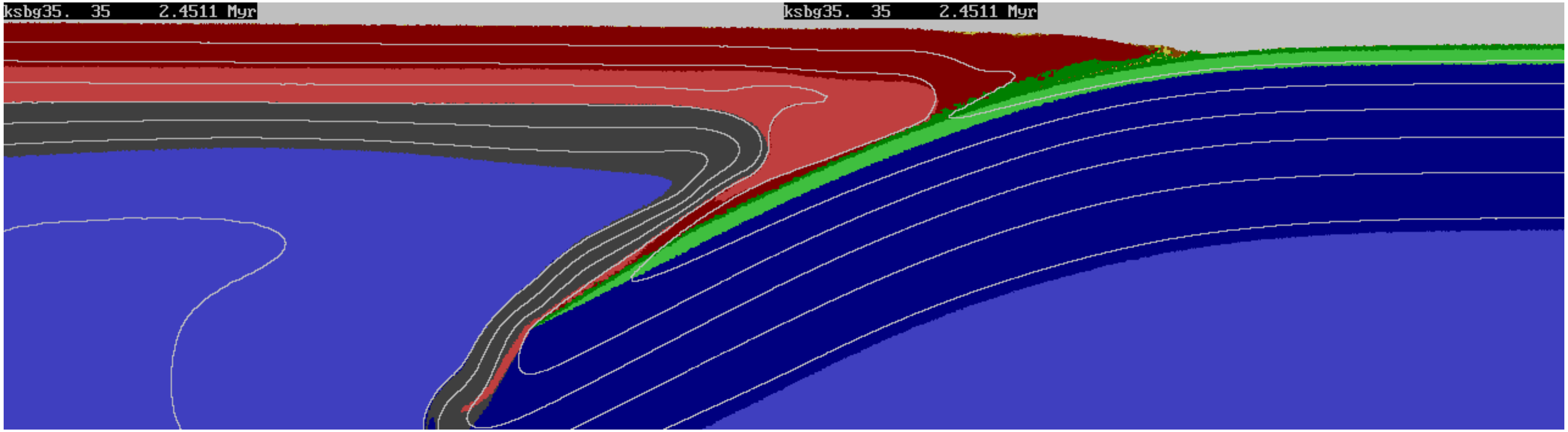

subduction regime

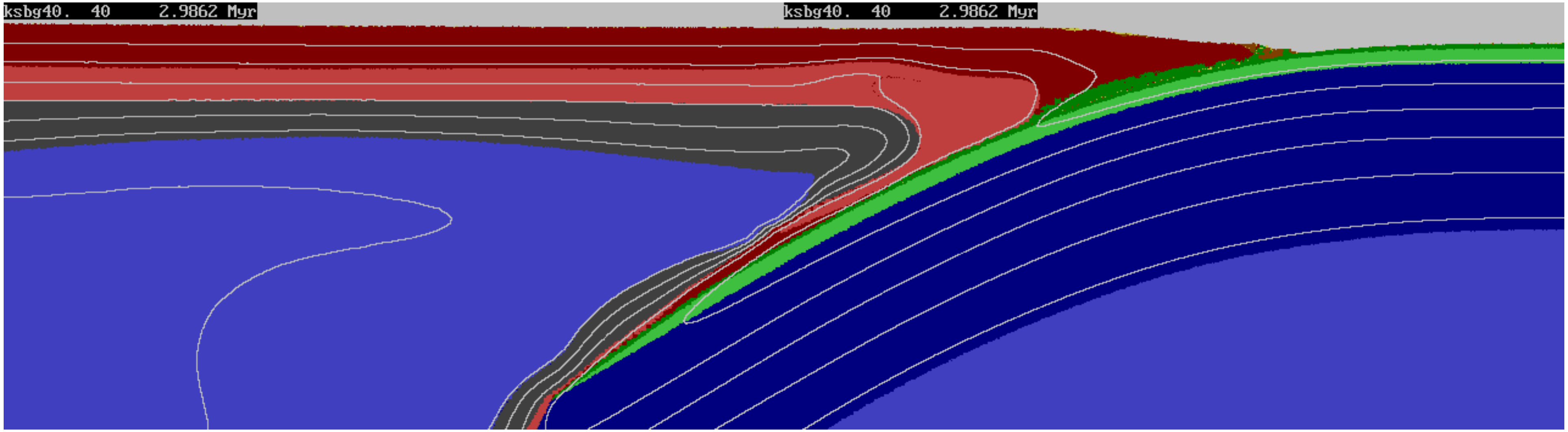

subduction regime

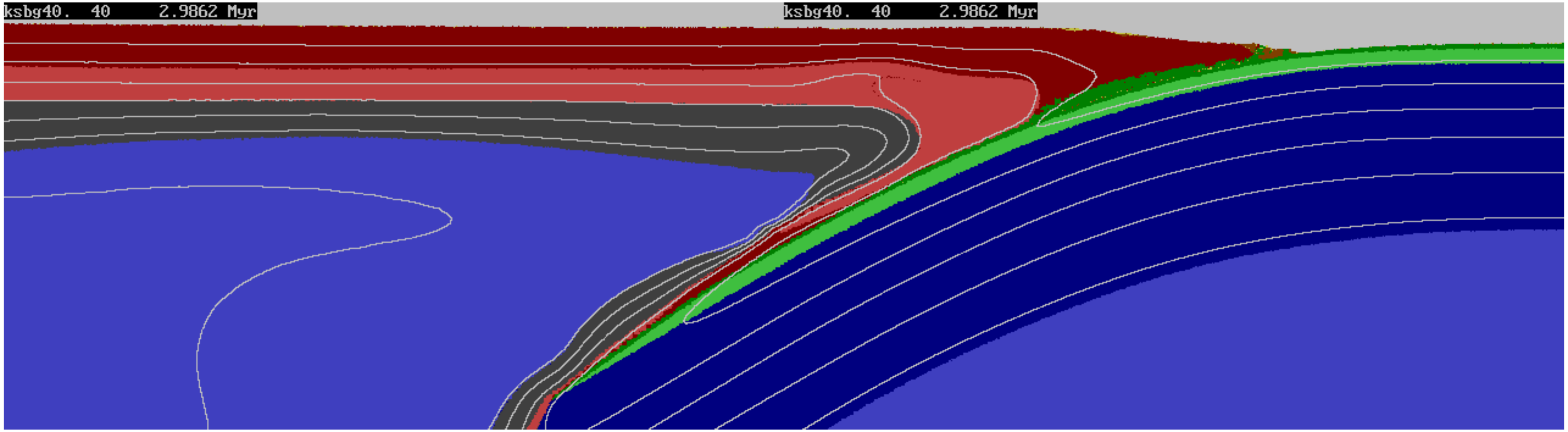

subduction regime

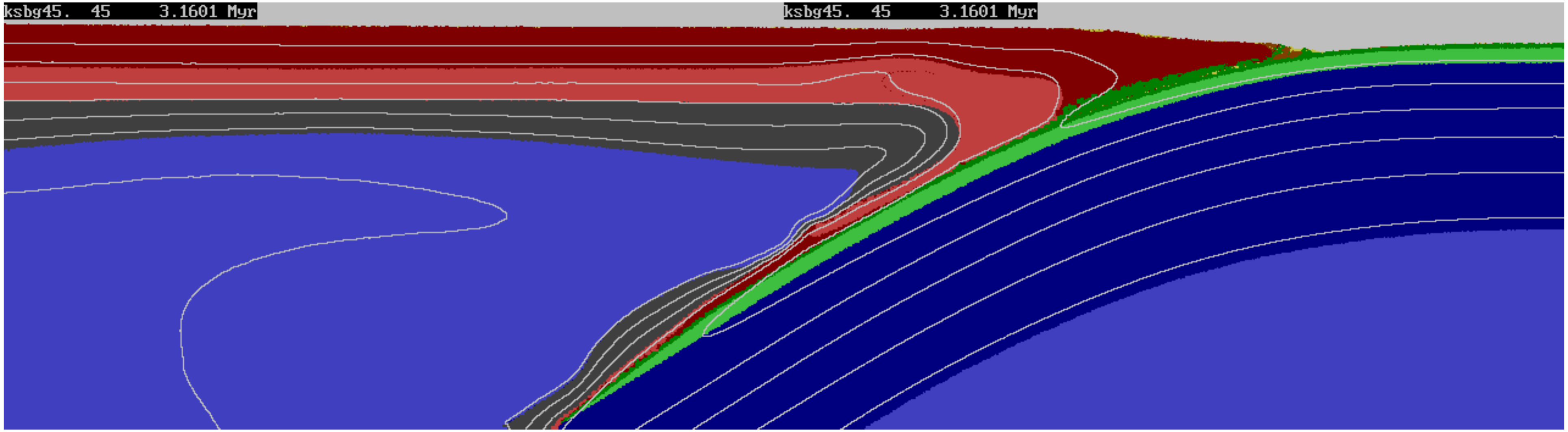

ksbg45. 45 3.1601 Myr

subduction regime

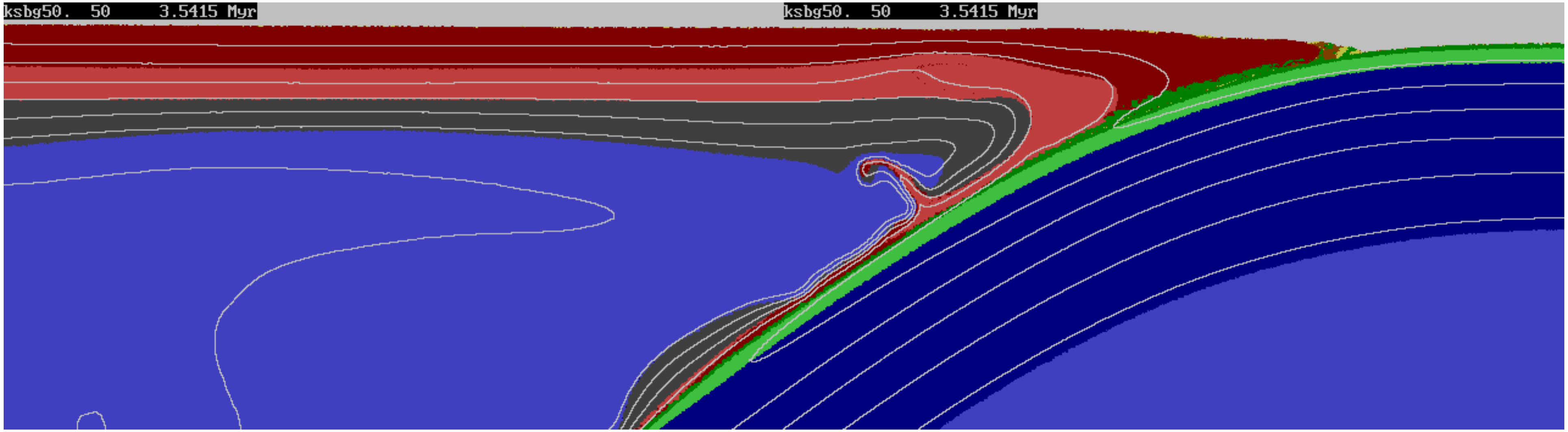

subduction regime

Nikolaeva et al.(in revision)

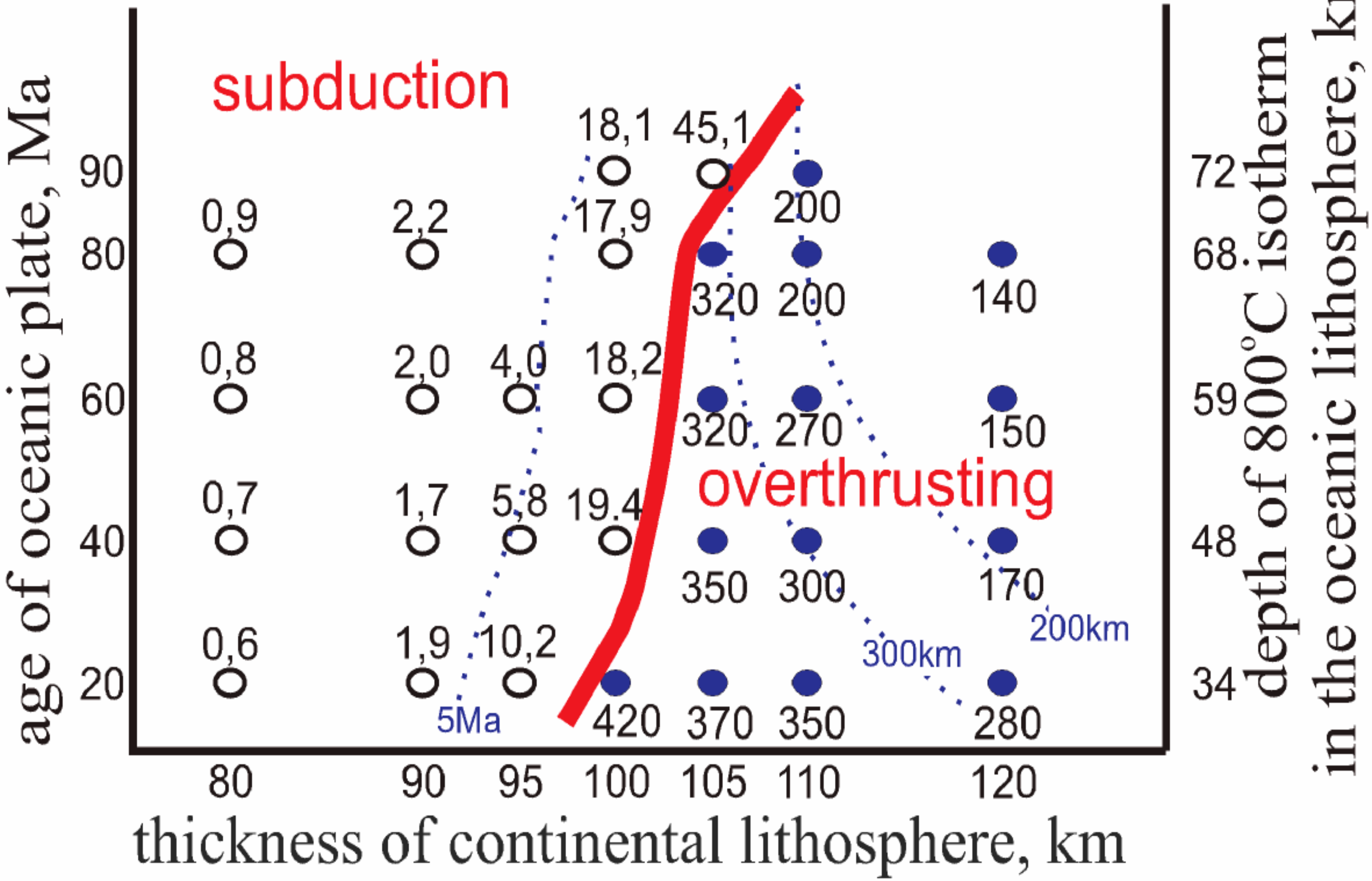

The age of the oceanic plate

does not play a major role !

Nikolaeva et al.
(in revision)

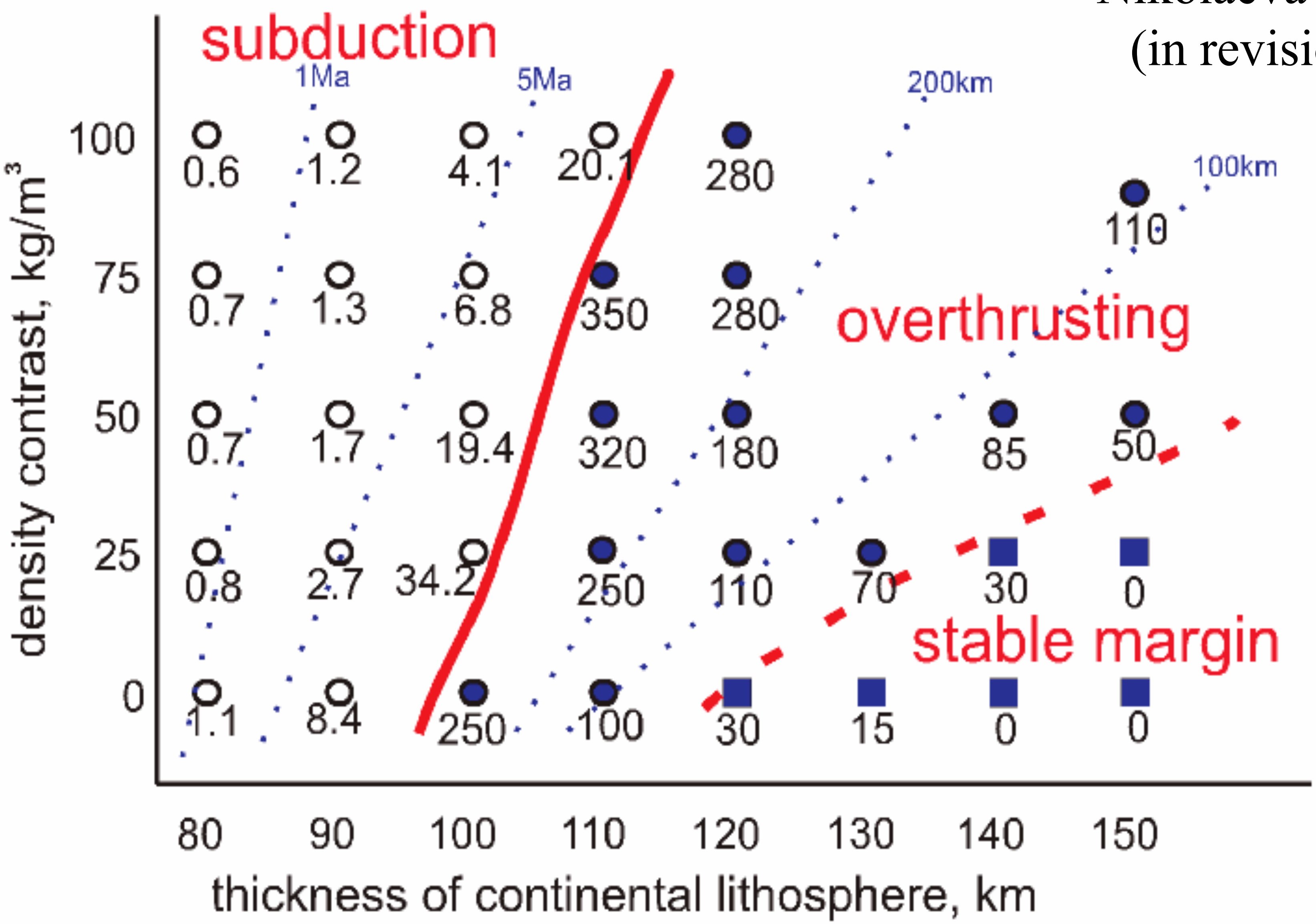

Thin continental lithosphere and
large chemical density contrast between oceanic and continental mantle
favor and speed-up subduction initiation

Chemical density contrast

Chemical density contrast between subcontinental lithospheric mantle (SCLM) and Primitive Mantle after Poudjom Djomani et al., 2001, Earth Planet. Sci. Lett., 184, 605-621:

for Archean age of SCLM ~ **80** kg/m^3,

for Proterozoic age of SCLM ~ **40** kg/m^3,

for Phanerozoic age of SCLM ~ **30** kg/m^3.

Prediction:
subduction should start
on rifted margins of old continents

Nikolaeva et al. (submitted)

Challenges

1. Geochemistry
2. Two-phase flow
3. 3D modeling
4. Reaction kinetics

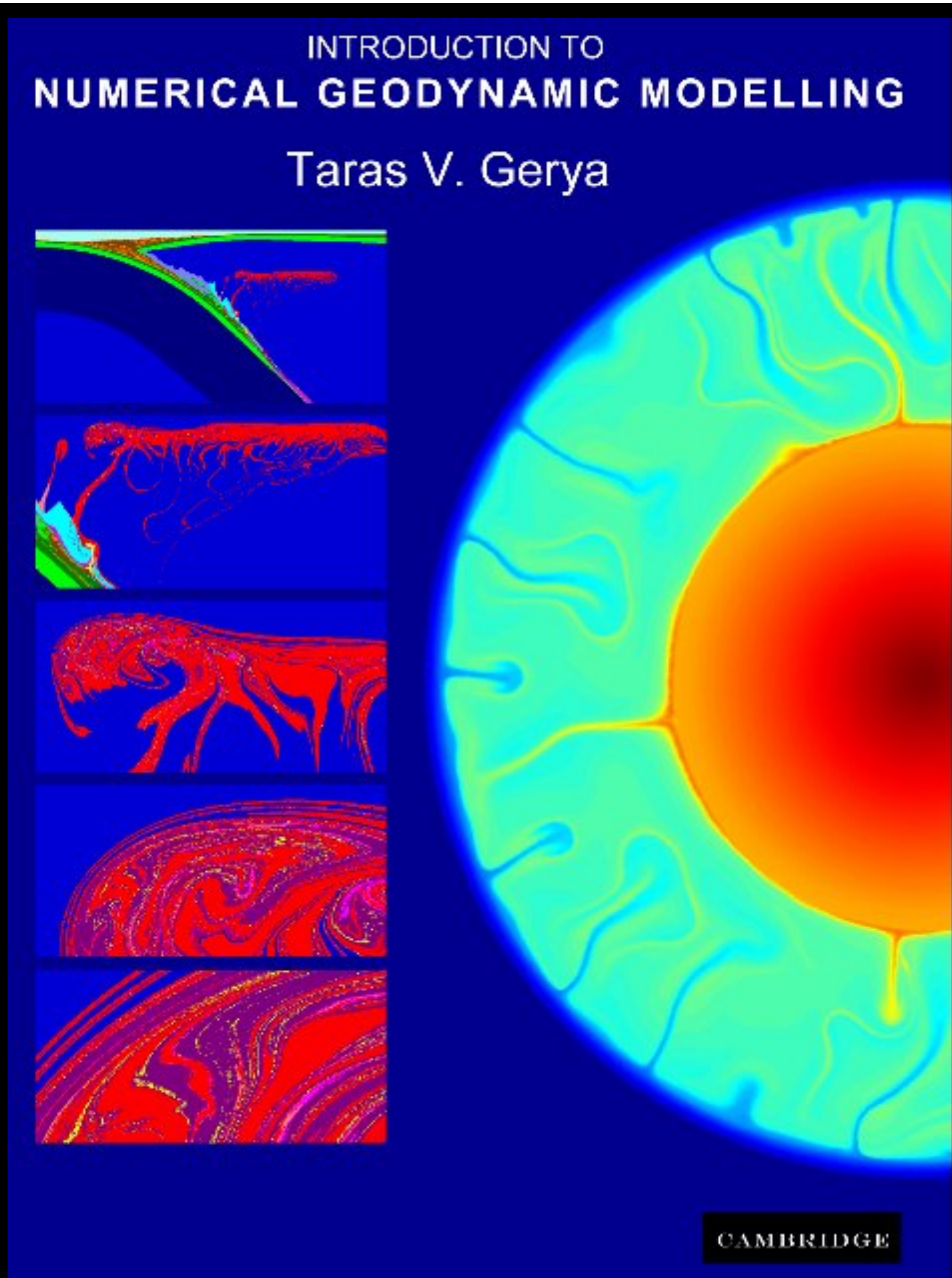

December 2009, Cambridge University Press